

Charles University in Prague
Faculty of Science

Program: Biomedicine
Cell and developmental biology



Marián Hruška-Plochán, M.Sc.

**HUNTINGTON'S DISEASE MODELING AND STEM CELL THERAPY
IN SPINAL CORD DISORDERS AND INJURY**

Ph.D. Thesis

Advisor: Motlík Jan, Prof., DVM, Ph.D., D.Sc.

Consultant: Maršala Martin, Prof., MD.

Prague, 2013

Declaration:

I hereby declare that this thesis or its substantial proportion has not been used to accept the same or any other degree or diploma at the Charles University or any other educational institution. All used literature and information sources were properly cited.

I produced this thesis independently at the Institute of Animal Physiology and Genetics, Academy of Sciences of the Czech Republic, v.v.i. and at the University of California San Diego, CA, USA.

San Diego, April 30 2013



Marián Hruška-Plochán

ACKNOWLEDGMENTS

First of all, I would like to thank my thesis advisor Prof. Jan Motlik for the opportunity to join his laboratory, for the many helpful and inspiring discussions, for his endless support and motivation, for his insights into developmental biology and neuroscience and for all the great times we had in the lab and “on the road”. I would like to thank Prof. Martin Marsala, who as my consultant and also my advisor helped me in any way he could. Thanks to his exceptional knowledge of neuroscience and his advices, I was able to solve every obstacle which came into my way.

I am especially grateful to Dr. Stefan Juhas and Dr. Jana Juhasova for all the exciting experiments we have done together and for all the fun we had in the lab every day. I would like to thank to all my colleagues at the Institute of Animal Physiology and Genetics, Academy of Sciences of the Czech Republic, v.v.i. and to the whole lab of Dr. Marsala at the University of California San Diego.

I also want to thank Prof. Marian DiFiglia and Prof. Elena Cattaneo for the many, many scientific discussions and advices that greatly helped me during the course of my studies.

Last but definitely not least I would like to thank my family and especially my wife Dagmar for all the patience and love. I am also thankful to all my friends for their support.

This work was supported by Institutional research concept RVO 67985904, grants from CHDI Foundation (ID 1035), California Institute for Regenerative Medicine (CIRM), Grantové Agentury University Karlovy (GAUK) no. 18410, and by EMBO Short-Term Fellowship Award - fellowship no. ASTF 308-2009.

ABSTRACT

Neurological disorders affect more than 14% of the population worldwide and together with traumatic brain and spinal cord injuries represent major health, public and economic burden of the society. Incidence of inherited and idiopathic neurodegenerative disorders and acute CNS injuries is growing globally while neuroscience society is being challenged by numerous unanswered questions. Therefore, research of the CNS disorders is essential. Since animal models of the CNS diseases and injuries represent the key step in the conversion of the basic research to the clinics, we focused our work on generation of new animal models and on their use in pre-clinical research. We generated and characterized transgenic minipig model of Huntington's disease (HD) which represents the only successful establishment of a transgenic model of HD in minipig which should be valuable for testing of long term safety of HD therapeutics. Next, we crossed the well characterized R6/2 mouse HD model with the *gad* mouse model which lacks the expression of UCHL1 which led to results that support the theory of "protective" role of mutant huntingtin aggregates and suggest that UCHL1 function(s) may be affected in HD disturbing certain branches of Ubiquitin Proteasome System. Traumatic spinal cord injury and Amyotrophic Lateral Sclerosis (ALS) are the two most severe and common disorders of the spinal cord in humans. Thus, the two animal models we used in our human neural stem cells (HSSC) grafting experiments were: i) mutant SOD1^{G93A} transgenic rat model of ALS (SOD1 rat) and ii) the rat model of acute lumbar (L3) compression injury developed in our lab. Intraspinal grafting of clinical grade HSSC used in our experiments led to local protection of α -motoneurons residing in the close proximity of the grafted cells in immunosuppressed SOD1 rats and demonstrated progressive and significant improvement in motor and sensory function in immunosuppressed rats with previous L3 contusion injury. Our numerous xenogeneic grafting experiments led us to the development of new immunosuppressive tacrolimus-loaded pellets which are now commercially available and provide steady drug release for up to 3 months, making delivery labor efficient, minimally invasive, and producing stabilized blood concentration levels. Our work resulted in generation of one of the first large animal models of Huntington's disease, revealed the possible role of UCHL1 in HD and demonstrated the therapeutic potential of neural stem cell therapy in spinal cord disorders. These results were already successfully applied in experimental and human clinical settings and we believe that will further stimulate and accelerate translational research of CNS disorders.

ABSTRAKT

Neurologické poruchy postihují více než 14 % světové populace a společně s traumatickým poškozením mozku a míchy představují významnou zdravotní a socioekonomickou zátěž. Výskyt dědičných a idiopatických neurodegenerativních poruch a akutních poškození CNS navíc zaznamenává globální nárůst a neurovědecká komunita je proto stavěna před množstvím nezodpovězených otázek. To je důvodem, proč lze pokládat výzkum poruch CNS za klíčový. Vzhledem k tomu, že zvířecí modely nemocí a traumatických poškození CNS mají nepostradatelnou úlohu v projekci výsledků základního výzkumu do klinické praxe, tato práce je zaměřena na vytvoření nových zvířecích modelů a jejich využití v preklinickém výzkumu. Vytvořili a charakterizovali jsme transgenní model miniaturního prasete pro Huntingtonovu chorobu, jenž je doposud jediným prasečím modelem a představuje velice hodnotný subjekt pro dlouhodobé testování bezpečnosti léčby. Dále jsme zkřížili již charakterizovaný myší model Huntingtonovy choroby s myším modelem *gad* postrádajícím expresi UCHL1 s výsledky, které potvrzují teorii o “ochranné” funkci agregátů mutovaného huntingtinu a vedou k předpokladu, že funkce UCHL1 v ubiquitin proteazomového systému mohou být v Huntingtonově chorobě narušené. Traumatické poškození a amyotrofická laterální skleróza (ALS) jsou dvěma nejzávažnějšími a nejčastějšími poruchami míchy u lidí. K experimentům s transplantací lidských nervových kmenových buněk byly využity dva potkaní modely, transgenní model s ALS (SOD1^{G93A}) a model akutního poškození míchy způsobeného kompresí. Intraspinální transplantace u imunosuprimovaných SOD1 ALS transgenních potkanů vedla k lokální ochraně α -motoneuronů a dále k výraznému zlepšení motorických a senzorických funkcí imunosuprimovaných potkanů s akutním poškozením míchy. Početné xenogenní transplantační experimenty vedly k vývoji nových pelet s imunosupresivy, které jsou nyní již komerčně dostupné a zajišťují řízené uvolňování léčiva až po dobu tří měsíců, přičemž způsob podání je velice efektivní, minimálně invazivní a umožňuje udržení stabilní hladiny v krvi. Naše práce vedla ke vzniku jednoho z prvních velkých zvířecích modelů Huntingtonovy choroby, odhalila u tohoto onemocnění úlohu UCHL1 a rovněž terapeutický potenciál nervových kmenových buněk v léčbě poruch a poškození míchy. Výsledky této práce již byly úspěšně aplikovány v experimentálních podmínkách a též v klinické praxi. Pevně věříme, že naše práce bude dále stimulovat translační výzkum poruch CNS.

CONTENTS

1. Chapter 1 Huntington's disease	4
1.1. Huntington's disease	5
1.1.1. History	6
1.1.2. Clinical presentation of HD	7
1.1.3. Neuropathology	8
1.2. Huntingtin protein	9
1.2.1. Wild-type huntingtin	10
1.2.2. Huntingtin functions	11
1.2.3. Loss of function and gain of function	12
1.3. Molecular mechanisms of huntingtin neuropathology	13
1.3.1. Excitotoxicity	13
1.3.2. Mitochondrial dysfunctions	14
1.3.3. Transcriptional dysregulation	14
1.3.4. Proteolysis	15
1.3.5. UPS dysfunction in HD	15
1.3.6. Autophagy in HD	17
1.3.7. Misfolding and aggregation	17
1.4. Current treatments	20
1.5. Transgenic animal models of HD	21
2. Chapter 2 (Neural) Stem cell therapy in spinal cord disorders and injury	24
2.1. (Neural) Stem cell therapy in spinal cord introduction.....	25
2.2. Amyotrophic lateral sclerosis	26
2.2.1. Clinical presentation of ALS	27
2.2.2. Neuropathology in ALS	29
2.2.3. SALS vs FALS	32
2.2.4. Animal models of ALS	32
2.2.4.1. SOD1 models of ALS	32
2.2.5. SOD1 mutations	34
2.2.5.1. SOD1 pathology	35
2.2.6. TDP-43 mutations	35
2.2.7. FUS/TLS mutations	37
2.2.8. C9ORF72 mutations	37
2.2.9. Pathological mechanisms in ALS	38

2.2.9.1.	Oxidative stress	38
2.2.9.2.	Mitochondrial dysfunction	38
2.2.9.3.	Apoptosis	39
2.2.9.4.	Glutamate excitotoxicity	39
2.2.9.5.	Protein aggregation	40
2.2.9.6.	Neuroinflammation	40
2.2.9.7.	Endoplasmic reticulum stress	40
2.2.9.8.	Impaired axonal transport	41
2.2.9.9.	Glial Cell Pathology	41
2.2.9.10.	Dysregulated transcription and RNA processing	42
2.2.10.	Therapies in ALS	42
2.2.10.1.	Neural Stem cell therapy in ALS	43
2.3.	(Neural) Stem cell therapy in spinal cord injury	45
2.3.1.	Spinal cord injury	45
2.3.2.	SCI therapy	46
2.3.2.1.	(Neural) Stem cell therapy in SCI	47
2.4.	Immunosuppression in spinal cord stem cell transplantation experiments	50
3.	Aims of the thesis	52
4.	Materials and methods	53
4.1.	Animals and surgery	53
4.2.	Construction and production of the HIV1-HD-548aaHTT-145Q vector and verification of vectors in vitro	54
4.3.	Transgenesis	54
4.4.	Cell derivation and preparation	55
4.5.	Cell grafting	56
4.6.	Immunosuppression	56
4.7.	Electrophysiology	56
4.8.	Biochemical assays	57
4.9.	Immunofluorescence and immunohistochemistry stainings	58
4.10.	Statistical analyses	58
5	Results	60
5.1.	Generation and characterization of Huntington's disease transgenic minipig	60
5.2.	Evaluation of possible functions of UCHL1 in Ubiquitin Proteasome System Impairment in Huntington's disease	82

5.3.	Evaluation of neural stem cell replacement in SOD1 ^{G93A} rat model of ALS	106
5.4.	Evaluation of neural stem cell replacement therapy in a rat model of acute lumbar spinal cord injury	121
5.5.	Evaluation of Tacrolimus-loaded releasable pellets as an alternative and effective Immunosuppression protocol in rat spinal cord transplantation studies	180
6.	Discussion	220
6.1.	<i>In vivo</i> modeling of Huntington's disease	220
6.1.1.	UCHL1 in HD	220
6.1.2.	tgHD minipig	223
6.1.3.	HD summary	227
6.2.	(Neural) Stem cell therapy in spinal cord disorders and injury	227
6.2.1.	Rationale for spinal cell-replacement therapy after spinal trauma and in ALS	227
6.2.2.	Cell survival and differentiation	228
6.2.3.	Effect of spinal grafting of HSSC on the recovery of motor function and muscle spasticity	230
6.2.4.	Grafted HSSCs into lumbar cord offered no effect on survival of SOD1 rats	231
6.2.5.	Effect of spinal grafting of HSSC on the recovery of sensory function	231
6.2.6.	Mechanism of HSSC-mediated therapeutic action in SCI and ALS	233
6.2.7.	Defining the optimal TAC immunosuppressive regimen to permit long-term survival and maturation of spinally grafted human neural precursors in rats.....	234
6.2.8.	(Neural) stem cell therapy in spinal cord summary	235
6.3.	General conclusion	236
7.	References	237
8.	List of abbreviations	267
9.	Author's publications	271
9.1.	Publications in Scientific Journals with IF with relation to Ph.D. thesis	271
9.2.	Publications in Scientific Journals without IF with relation to Ph.D. thesis	271
9.3.	Publications in Scientific Journals with IF without relation to Ph.D. thesis	272
9.4.	Poster presentations	272
10.	Curriculum vitae	273

CHAPTER 1

Huntington's disease

Huntington's disease transgenic minipig

UCHL1 in Huntington's disease

1.1. HUNTINGTON'S DISEASE

Huntington's disease (HD) is fatal autosomal dominant hereditary neurodegenerative disorder clinically characterized by progressive motor dysfunction, cognitive decline, and psychiatric disturbance (Ross and Tabrizi 2011). Causative mutation of HD is an expansion of the polyglutamine (CAG) repeat sequence in the coding region of exon 1 of the huntingtin gene localized on chromosome 4 (HTT; IT-15) leading to expression of mutant huntingtin protein with expanded poly-glutamine (polyQ) tract (1993) which induces progressive and devastating neurodegenerative changes in the whole brain with striatum, cerebral cortex (Vonsattel and DiFiglia 1998) and white matter (Dumas et al. 2012; Tabrizi et al. 2012) being the most affected regions.

Prevalence of the mutation/disease is about 4–10 per 100 000 in populations of Western European and North American descent, with many more at risk of the disease (having inherited the mutant gene) (Vonsattel and DiFiglia 1998; Tabrizi et al. 2011). Prevalence is much lower in Asian (Pringsheim et al. 2012) and African (Sturrock and Leavitt 2010) populations. CAG repeats longer than 40 are associated with nearly full penetrance by age 65 years (Langbehn et al. 2004; Ross and Tabrizi 2011). Longer CAG repeats predict earlier onset of the disease (Langbehn et al. 2004) (Fig. 1) accounting for up to 50–70% of variance in age of onset (Ross and Tabrizi 2011), with the remaining variance most likely to be attributed to modifying genes (40% of remainder) and the environment (60% of remainder) (Wexler and Res 2004). Individuals with less than 35 CAG repeats will not develop HD, those with 36 to 39 may or may not develop HD, and those with 40 or more will develop the disease (Vonsattel and DiFiglia 1998; Langbehn et al. 2004). An intermediate CAG repeat length between 29 and 35 does not cause the disease but may expand into the pathogenic range in future generations (Novak and Tabrizi 2010).

Most HD patients have expansions ranging from 40–55 CAG repeats (Vonsattel and DiFiglia 1998; Langbehn et al. 2004) leading to the onset of the disease symptoms in the middle age (40 years in average) while juvenile onset (under the age of 20) is associated with CAG repeats 60 or longer (Langbehn et al. 2004). Disease progresses over 15-20 years from onset and culminates in death (Novak and Tabrizi 2010). Diagnosis of Huntington's disease is formally made on the extrapyramidal motor signs of chorea, dystonia, bradykinesia, or incoordination in an individual at risk. However, many patients have substantial cognitive or behavioural disturbances before onset of diagnostic motor signs (Ross and Tabrizi 2011). The motor phenotype can be assessed in manifest HD patients using the motor component of the Unified Huntington Disease Rating Scale (UHDRS). The UHDRS is a widely used clinical and research tool developed by the Huntington Study Group (HSG) (1996) for the measurement of the motor, cognitive, psychiatric, and functional performance in HD (Sturrock and Leavitt 2010).

HD gene was cloned 20 years ago and important advances have been made in the clinical, genetic, pathological, and biochemical understanding of this disease yet there is no effective treatment for Huntington's disease available. Most drugs currently used in HD are designed to attenuate the symptoms of the disease and improve quality of life including psychiatric agents for the control of behavioral symptoms, motor sedatives, cognitive enhancers, and

neuroprotective agents (Frank and Jankovic 2010; Novak and Tabrizi 2010; Zuccato et al. 2010). Nonetheless, promising disease modifying and/or delaying treatments are currently being tested in animal models (Zuccato et al. 2010) with huntingtin lowering approaches being the most promising ones (Johnson and Davidson 2010; Sah and Aronin 2011; Kordasiewicz et al. 2012; Southwell et al. 2012). Moreover, recent research revealed broad spectra of potential biomarkers which could be used in future clinical trials to better assess their potential (Hersch and Rosas 2011; Weir et al. 2011).

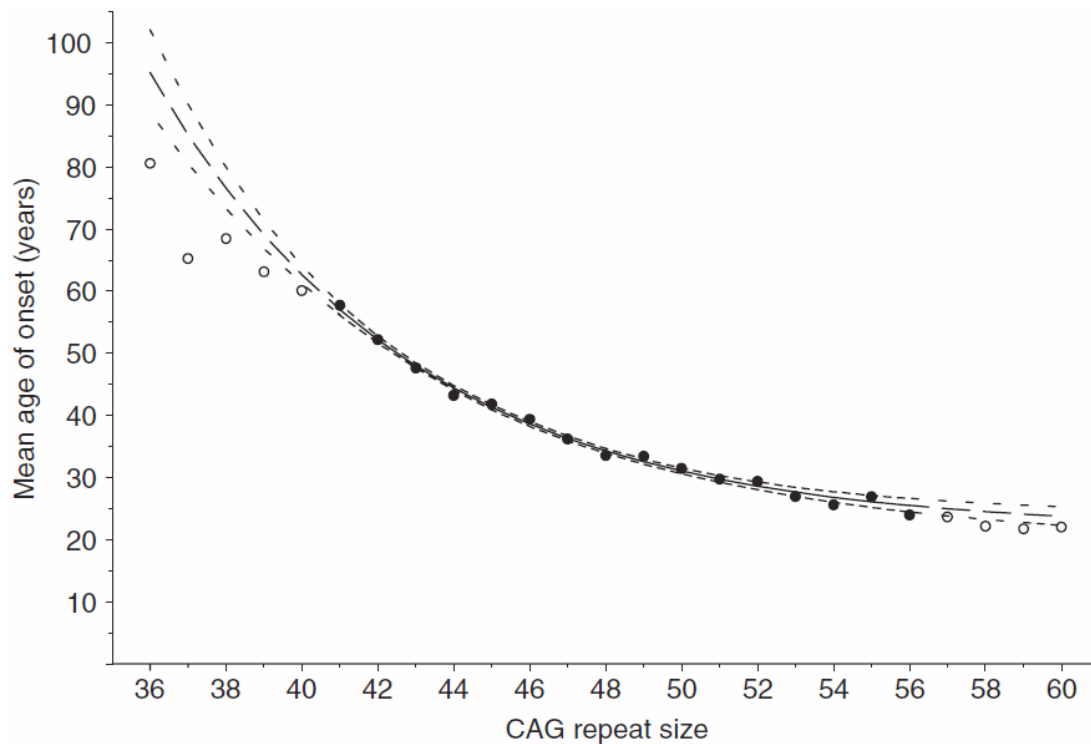


Fig. Population estimates of the mean age of onset of HD for CAG repeat lengths 36–60.

The ● symbols and solid line indicate the range of data that was used to fit the exponential curves. The ○ symbols and long dashed lines indicate CAG lengths for which the model's predictions were extrapolated. Small dashed lines indicate 95% confidence intervals, larger spaces between dashes indicate the region where the model's predictions were extrapolated. (Taken from Langbehn et al. 2004).

1.1.1. History

Huntington's disease is also known as Huntington's chorea. It was first described as an epidemic of dancing mania in 1374 and it was Paracelsus who first used the term chorea suggesting its origin in central nervous system (CNS). In 17th century, English colonists used the name "that disorder" or "San Vitus" dance to refer to HD. In those days, people with chorea, because of the involuntary muscle jerks and twitches characteristic of HD, were often thought to be possessed by the devil (Zuccato et al. 2010). The first accurate description of the disease was written by young American doctor George Huntington in 1872 after whom was this disorder originally named Huntington's chorea. The name has later changed to

Huntington's disease to reflect the fact that chorea is not the only important manifestation of the disease (Novak and Tabrizi 2010).

After the rediscovery of Gregor Mendel's theory in 1900, the British geneticist William Bateson established definitively (in 1909) that Huntington's chorea was inherited as a Mendelian autosomal dominant disease (Wexler 2010). Then in an era when eugenics attracted scientists, physicians, and intellectuals of all political stripes a Connecticut psychiatrist Percy R Vessie introduced prejudice and misunderstanding that characterized families affected by HD in early 20th century. Vessie portrayed HD individuals more as villains than as victims and later called for their "rigid sterilization" (Wexler 2010).

Fortunately, later in the 1950s, Dr. Amerigo Negrette diagnosed HD in a large community of people living around Lake Maracaibo in Venezuela which 20 years later became the center of discovery of the HD gene, made possible thanks to the remarkable efforts of Nancy Wexler (Zuccato et al. 2010). The gene responsible for HD was mapped to the short arm of chromosome 4 in 1983 (Gusella et al. 1983) and 10 years later, IT15 gene comprised of 67 exons and containing expanded CAG trinucleotide repeat was located on 4p16.3 (1993).

1.1.2. Clinical presentation of Huntington's disease

Characteristic symptoms of HD are often described as adult-onset triad of motor, cognitive and psychiatric changes (Novak and Tabrizi 2010). The onset of the disease is currently defined as the point at which characteristic motor signs develop as assessed by the motor component of the Unified Huntington Disease Rating Scale (UHDRS) (1996) which was updated and expanded in 1999 (UHDRS '99) enhancing all of the components of the UHDRS (group 1999). This is when the patient is diagnosed as having "manifest" HD. However, most patients develop "soft" motor, cognitive or psychiatric symptoms during the prodromal ("pre-manifest") period, often many years before any motor signs are seen (Novak and Tabrizi 2010; Sturrock and Leavitt 2010).

Typical age of adult onset of HD is between 35 and 50 years (Zuccato et al. 2010). HD can be characterized as a movement, cognitive, psychiatric and metabolic disorder (for review see (Novak and Tabrizi 2010; Sturrock and Leavitt 2010). Early stages of HD are associated with progressive movement, psychiatric and cognitive disturbances. Motor impairments in HD can be typically divided into two categories: involuntary movements such as chorea (rapid, random and uncontrollable movements), and impaired voluntary movements, which cause limb incoordination and impaired hand function (Novak and Tabrizi 2010). Motor symptoms change over the course of the disease progression with declining chorea being replaced by dystonia (involuntary muscle contractions that cause slow repetitive movements or abnormal postures), rigidity and bradykinesia (decrease of movement speed) (Ross and Tabrizi 2011). Typical cognitive deficits including subtle personality changes, slow speed of cognitive processing, olfaction, and memory recall can be detected some 15 years prior the motor symptoms are diagnosed (Paulsen 2011). Depression, irritability, anxiety, apathy are the most frequent psychiatric signs in HD (Duff et al. 2007). Obsessive compulsive and aggressive behaviors, psychotic symptoms occur less often (van Duijn et al. 2007) and alterations in sexual behavior are also common (Rosenblatt 2007). Early occurring sleep disturbances,

catabolic weight loss are also present and together with alternation in sexual behavior can be partially explained by hypothalamic dysfunction (Politis et al. 2008). Subtle psychiatric symptoms can be observed as early as 10 years before the first motor changes (Duff et al. 2007).

Two CAG-length dependent variant forms of HD exist. Juvenile HD, which is characterized by early disease onset (within the first two decades) and which accounts to about 5-10% of all HD. Juvenile HD is associated with 60 or more CAG repeats (Sturrock and Leavitt 2010) and is generally inherited from the father as the instability of CAG repeat tracts during male gametogenesis is much greater than in females (Ranen et al. 1995). In addition to early onset, juvenile HD is more severe and rapidly progressing (mean survival of between 8 and 9.3 years). Senile chorea or more precisely late-onset HD represents 25% of all HD cases. Patients present their initial symptoms after age 50 and onset at age 80 or above may occur (Sturrock and Leavitt 2010). The clinical features of late-onset HD resemble those of mid-life HD, but the illness progresses more slowly and is usually less functionally disabling than adult-onset disorder (Britton et al. 1995).

Because of progressive motor dysfunction, dementia and psychiatric disturbances, HD patients become unable to walk, perform daily tasks including planning and organization, have dietary problems and eventually will become unable to take care of themselves and will require long-term 24 hour institutional care (Zuccato et al. 2010). Emergencies in HD generally involve life threatening complications which may result from injuries related to falls (trauma), pneumonia and choking, nutritional deficiency, infection or sepsis. 15-20 years after the disease onset most HD patients eventually die due to aspiration pneumonia and poor nutrition because of swallowing difficulties (Lanska et al. 1988; Sorensen and Fenger 1992).

1.1.3. Neuropathology

Despite the ubiquitous mutant huntingtin (mHTT) expression HD pathology is remarkably brain specific with the most prominent neuronal cell loss and brain atrophy in the striatum and cerebral cortex (Vonsattel and DiFiglia 1998) and severe loss of white matter as recently discovered using new imaging techniques (Dumas et al. 2012; Tabrizi et al. 2012). Total brain weight can be reduced by 200 – 300g (see Fig. 3 for comparison of HD and normal brain) (Vonsattel et al. 1985). The first and most commonly used grading system for neuropathological classification of HD was developed by Jean Paul Vonsattel in 1985 (Vonsattel et al. 1985). This grading system was developed through examination of 238 post-mortem half-brain HD specimens and is based on the severity and pattern of striatal (mainly caudate nucleus) degeneration. Vonsattel and colleagues distinguished 5 grades of neuropathological severity in HD (0-4). Grade 0: Gross examination shows features appear indistinguishable from normal brains after gross examination (Vonsattel et al. 1985) but 30-40% neuronal loss can be detected in the head of caudate nucleus without reactive astrogliosis (Vonsattel and DiFiglia 1998). Grade 1 shows atrophy, neuronal loss and astrogliosis of the tail, head and in some cases body of the caudate nucleus. Cell counts show 50% or greater neuronal loss in the head of caudate nucleus. Gross striatal atrophy is mild to moderate in

Grade 2 and severe in Grade 3. The microscopical changes are more severe than in Grade 1. In Grade 4, striatum is severely atrophic showing 95% or higher neuronal loss (Vonsattel and DiFiglia 1998) (see Fig. 2 for gross anatomy pictures of Vonsattel grades).

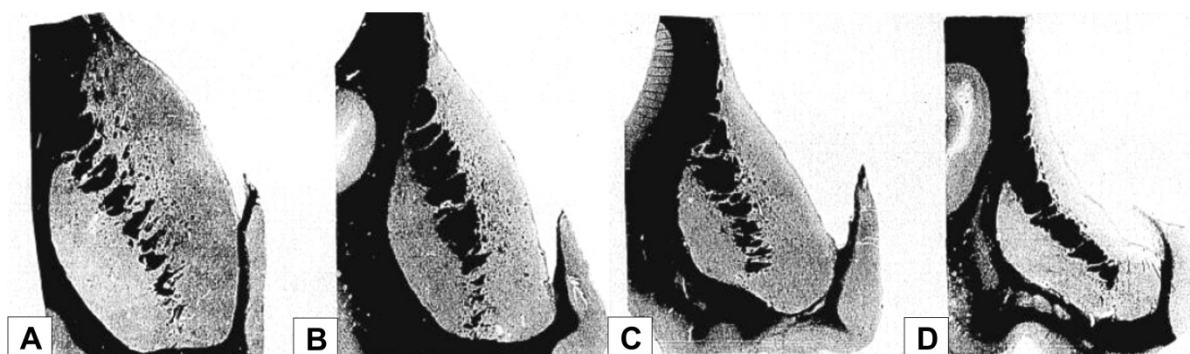


Fig. 2 Vonsattel HD grades. Luxol fast-blue hematoxylin and eosin stain. A) Control, and grades 0 and 1. No abnormality on gross examination. B) Grade 2. The caudate nucleus is atrophic, but maintains its convex medial outline. C) Grade 3. The striatal atrophy is moderate to severe and the medial outline of the caudate nucleus is no flat, forming a nearly straight line. The cross-section outline of the anterior limb of the internal capsule has likewise lost its medial convexity. The putamen is atrophic. D. Grade 4. Very severe atrophy of the caudate nucleus and putamen, with markedly concave medial outline of both caudate nucleus and internal capsule. Taken and modified from Vonsattel et al. 1985.

Further histological examination of the HD brains revealed that striatal neuronal degeneration is relatively selective for GABAergic medium size spiny neurons (MSNs) which represent up to 90% neurons of the striatum and which represent the output neurons of the striatum projecting to substantia nigra pars reticulata and to globus pallidus (Shoulson and Young 2011). On the contrary, interneurons expressing Somatostatin/neuropeptideY/NADPH diaphorase/NO synthetase (Ferrante et al. 1985) and large aspiny cholinergic neurons (AChE and ChAT+) are relatively spared (Ferrante et al. 1987) and without the presence of mHTT aggregates (Davies et al. 1997). First neurons which degenerate in early and middle stages of HD are those MSNs expressing GABA/enkephalin and projecting to the external globus pallidus (these are more vulnerable than GABA/Substance P+ MSNs projecting to internal pallidal segment) (Reiner et al. 1988; Albin et al. 1992). The loss of these neurons most likely leads to development of chorea (Reiner et al. 1988; Shoulson and Young 2011). MSNs expressing GABA/substance P and projecting to substantia nigra pars reticulata die later and are more vulnerable than MSNs expressing GABA/substance P and projecting to substantia nigra pars compacta (Reiner et al. 1988). Loss of GABA/Substance P (direct pathway) MSNs then causes motor incoordination (Shoulson and Young 2011). In addition to the striatum cerebral cortex (mainly layers III, V and VI), globus pallidus, thalamus, subthalamic nucleus, substantia nigra, cerebellum and white matter are affected (Vonsattel and DiFiglia 1998).

Development of imaging techniques revealed that the hypothalamus is also atrophied in HD (Politis et al. 2008). Recent results of the TRACK-HD MRI study showed that whole brain atrophy, ventricular expansion, caudate, putamen, and overall white and grey matter atrophy had statistically significantly greater mean annual change in early HD patients

(including pre-manifest individuals) and thus brain imaging could potentially serve as biomarker in HD (Tabrizi et al. 2011; Tabrizi et al. 2012).

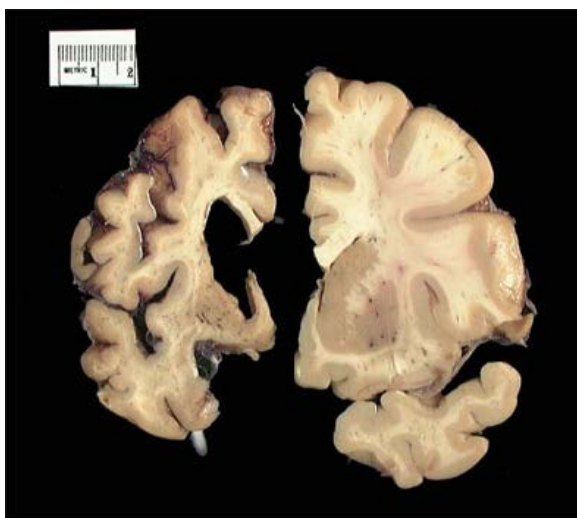


Fig. 3 Comparison of normal brain (right) to a brain of a late stage Huntington's Disease patients (left). Atrophy of the HD brain is visible in all brain areas with the most severe atrophy apparent in the striatum. Photo courtesy of the Harvard Brain Tissue Resource Center.

1.2. Huntingtin protein

1.2.1. Wild-type huntingtin

Wild-type (WT) huntingtin is a 3144 amino acids, 348-kDa large soluble protein (see Fig. 4 for schematic diagram) with no sequence homology with other proteins which is ubiquitously expressed in human and rodents (Cattaneo et al. 2005), with highest expression levels the CNS neurons and the testes (Van Raamsdonk et al. 2006; Van Raamsdonk et al. 2007). Huntingtin is particularly enriched in cortical pyramidal neurons in layers III and V that project to the striatal neurons (Fusco et al. 1999). Subcellularly, mammalian huntingtin is associated with most of the organelles including the nucleus (Kegel et al. 2002), endoplasmic reticulum, Golgi complex (Hilditch-Maguire et al. 2000) and the mitochondrion (Rockabrand et al. 2007; Orr et al. 2008). Huntingtin is also localized within synaptic vesicles (DiFiglia et al. 1995) and associated with microtubules (Hoffner et al. 2002). Because of its large size (348-kDa), huntingtin crystallization is hampered and thus, there are no clear data on the structure of the protein (Zuccato et al. 2010). Recently, crystals of both wild-type (Kim et al. 2009) and mutant N-terminal fragments (Kim 2013) were analyzed confirming the previous predictions that the expanded mHTT polyQ region adopts a β -sheet structure (Kim 2013).

Huntingtin contain multiple important sites including its polyQ site which begins at the 18th amino acid. Huntingtin orthologs multialignment revealed that the polyQ is an ancient acquisition of huntingtin and it has been postulated that at the base of protostome-deuterostome divergence, the huntingtin ancestor possesses a huntingtin protein with a single Q or no Q in the corresponding position. The polyQ has then expanded gradually in mammals to become the longest and most polymorphic polyQ in humans with rodents show a shorter polyQ (7 and 8 Q in mouse and rat, respectively) inverting the evolutionary trend (Tartari et al. 2008; Zuccato et al. 2010). Recent findings suggest that anti-apoptosis may have been one of huntingtin ancestral function(s), and that in deuterostomes, huntingtin evolved to acquire a

unique regulatory activity for controlling interactions between neuroepithelial cells by regulating a critical cell-cell adhesion pathway involving ADAM10 and Ncadherin activities, with implications for brain evolution and development (Lo Sardo et al. 2012).

Downstream to the polyQ, huntingtin contains 36 HEAT domains organized in 3 main clusters (Takano and Gusella 2002; MacDonald 2003). HEAT domain consist of a series of three amino acids which are repeated ~10 times along a 37-47 amino acid stretch and are involved in protein-protein interactions (Neuwald and Hirano 2000). C-terminus of huntingtin contains nuclear export signal (NES) sequence and a less active nuclear localization signal (NLS) which might indicate that huntingtin (or a part of it) is involved in transporting molecules from the nucleus to the cytoplasm (Xia et al. 2003).

Huntingtin contains multiple cleavage sites for caspases, calpain, and aspartyl proteases generating a wide range of fragments (Goldberg et al. 1996; Wellington et al. 1998; Wellington et al. 2000; Gafni and Ellerby 2002; Wellington et al. 2002; Gafni et al. 2004) but the exact contribution of huntingtin proteolysis to cell functioning is unclear. Huntingtin is modified by numerous posttranslational modifications including ubiquitination of N-terminal lysines K6, K9 and K15 which target huntingtin to the proteasome and which is affected when polyQ is expanded (Kalchman et al. 1996; DiFiglia et al. 1997). Huntingtin is phosphorylated on multiple serine residues and phosphorylation on S536 inhibited calpain-mediated cleavage and reduced toxicity of mutant huntingtin (Schilling et al. 2006). Furthermore, IkappaB kinase (IKK) complex phosphorylates huntingtin on S13 and may activate S16 phosphorylation which promotes modification of the adjacent lysine residues and target wild-type huntingtin clearance by the proteasome and the lysosome (Thompson et al. 2009). When S13 and S16 were mutated to aspartate in full length BACHD mice, disease pathogenesis was abolished (Gu et al. 2009). Sumoylation of the first 17 amino acids modulates its subcellular localization, activity, and stability (Steffan et al. 2004) and palmitoylation at cysteine 214 is consistent with huntingtin role in regulation of vesicular trafficking and is decreased by expanded polyQ in mutant huntingtin which contributes to formation of neuronal inclusions and toxicity (Huang et al. 2004; Yanai et al. 2006). Lysine residue 444 is acetylated and is required to target huntingtin to macroautophagy pathway (Jeong et al. 2009). Huntingtin interacts with many proteins and most of the interactions are associated with its N-terminal domain and some interactions were proven to be affected by polyQ expansion in mutant huntingtin.

1.2.2. Huntingtin functions

Wild-type huntingtin has numerous functions which are important for normal embryonic development and neurogenesis (Cattaneo et al. 2005; Lo Sardo et al. 2012). It was shown that huntingtin has anti-apoptotic functions and that this function is contained within the 548 N-terminal amino acids (Rigamonti et al. 2000; Leavitt et al. 2006).

Brain derived neurotrophic factor (BDNF) which in adult brain, is mainly produced by the cerebral cortex and thus is particularly important for the survival of striatal neurons and the activity of cortico-striatal synapses (Cattaneo et al. 2005). It has been demonstrated that wild-type but not mutant huntingtin stimulates the expression of BDNF by regulation of BDNF promoter (Zuccato et al. 2001; Zuccato et al. 2003) and in addition, wild-type huntingtin

specifically enhances the vesicular transport of BDNF along microtubules (Gauthier et al. 2004) suggesting that the striatal support of BDNF is mostly dependent on wild-type huntingtin function. Further research revealed that *bdnf* transcription is regulated by Repressor element 1 (RE1; also known as the neuronrestrictive silencer element, NRSE) which is recognized by the RE1-silencing transcription factor (REST; also known as neuronal restrictive silencing factor, NRSF) transcriptional regulator and which acts as a transcriptional silencer of large number of neuronal gene containing RE1/NRSE sequences (Zuccato et al. 2003). Wild-type huntingtin sequesters the available REST/NRSF in the cytoplasm preventing it from forming the nuclear co-repressor complex at the RE1/NRSE nuclear site and allowing gene transcription of *bdnf* and other genes (Zuccato et al. 2003). It was therefore hypothesized that huntingtin might act in the nervous system as a general facilitator of neuronal gene transcription (Zuccato et al. 2003; Cattaneo et al. 2005).

Reduction of wild-type huntingtin also cause mitochondria immobilization and disrupts axonal transport (Trushina et al. 2004). Wild-type huntingtin directly binds on of the key molecules in synaptic transmission, e.g. on the postsynaptic density protein 95 (PSD95) that binds the NMDA and kainate receptors at the postsynaptic density (Smith et al. 2005). A decreased interaction of mutant huntingtin with PSD95 has been described in HD, suggesting that more PSD95 is released in HD, thus affecting the activity of NMDA receptors, and possibly leading to their overactivation/sensitization and to excitotoxicity (Sun et al. 2001).

1.2.3. Loss of function and gain of function

Despite the fact that huntingtin is essential for life and development, it is clear that just a simple loss of its function(s) cannot lead to HD. Nevertheless, the CAG expansion in the HD gene is responsible for changes in huntingtin posttranslational modifications and most likely for changes in its structure leading to its altered protein-protein interactions which ultimately cause impairment of biological mechanisms where wild-type huntingtin plays crucial role (because WT huntingtin lost its function). But based on genetic experiments using mouse models of HD (Duyao et al. 1995; Zeitlin et al. 1995; Mangiarini et al. 1996; Reddy et al. 1998; Hodgson et al. 1999; Hurlbert et al. 1999; Shelbourne et al. 1999; Graham et al. 2006) and non-specific huntingtin silencing experiments (Harper et al. 2005; Wang et al. 2005b; Machida et al. 2006; DiFiglia et al. 2007), it is evident that mutant huntingtin retains some of its “wild-type” functions and that mutant huntingtin is required to evoke HD pathology and symptoms.

Moreover, it has been previously demonstrated that the most toxic fragment of mutant huntingtin is the exon 1 containing an expanded polyQ tract (E1mHTT) (Miller et al. 2011). Recent discovery of the critical role of CAG repeat length-dependent aberrant splicing of mutant huntingtin gene which results in E1mHTT expression suggests that the pathology in all knock-in HD mouse models as well as in human HD could be driven by that very same exon 1 fragment of mutant huntingtin (Sathasivam et al. 2013). This breakthrough finding could represent the primary cause of huntingtin pathology in HD.

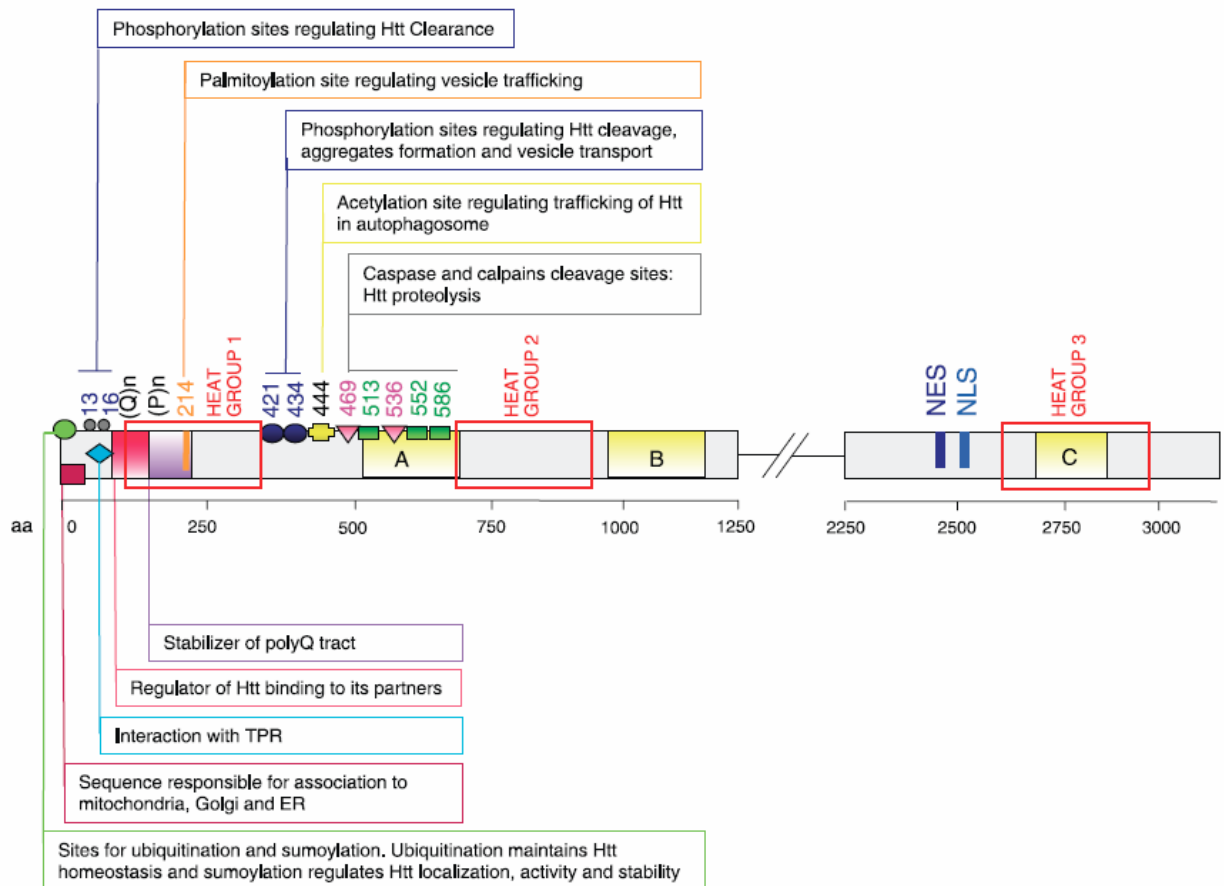


Fig. 4 Schematic diagram of the huntingtin amino acid sequence. (Q)*n* indicates the polyglutamine tract, which is followed by the polyproline sequence (P)*n*; the red emptied rectangles indicate the three main groups of HEAT repeats (HEAT group 1, 2, 3). The small green rectangles indicate the caspase cleavage sites and their amino acid position (513, 552, 586), while the small pink triangles indicate the calpain cleavage sites and their amino acid positions (469, 536). Boxes in yellow: B, regions cleaved preferentially in the cerebral cortex; C, regions of the protein cleaved mainly in the striatum; A, regions cleaved in both. Posttranslational modifications: ubiquitination (UBI) and/or sumoylation (SUMO) sites (green); palmitoylation site (orange); phosphorylation at serines 13, 16, 421, and 434 (blue); acetylation at lysine 444 (yellow). NES is the nuclear export signal while NLS is the nuclear localization signal. The nuclear pore protein translocated promoter region (TPR, azure) is necessary for nuclear export. Htt, huntingtin. ER, endoplasmic reticulum. (Taken from Zuccato C et al. 2010).

1.3. Molecular mechanisms of mutant huntingtin neuropathology

As we already described earlier, wild-type huntingtin has a lot of crucial functions which, when huntingtin is mutated, are lost and which lead to severe impairment of the systems involved but which are not the source of HD pathology. We therefore further describe just the mutant huntingtin associated pathology (see Fig. 5 for schematic illustration).

1.3.1. Excitotoxicity

Excitotoxicity was the first identified pathogenic mechanism in HD and results in dysfunction in corticostriatal synapses (Zuccato et al. 2010). Early data showed that in HD, glutamate receptors are lost and that there is a significant decrease of NMDA receptor

(NMDAR) binding at pre- and early symptomatic stages in the human HD (London et al. 1981; Young et al. 1988; DiFiglia 1990; Dure et al. 1991). Glial cells may play a role in HD as GLT1 (EAAT2), the Na⁺ dependent glial transporter of glutamate is downregulated in some mouse HD models and in human postmortem HD brains evidenced by impaired clearance of glutamate (Lievens et al. 2001; Behrens et al. 2002; Estrada-Sanchez et al. 2009). Enhanced NMDAR sensitivity to NMDA and increased NMDA evoked currents leading to impaired synaptic plasticity were detected in striatal neurons from HD mouse (Fan and Raymond 2007). It has also been shown that NR2B subunit of NMDAR was reduced in the HD striatum (Zeron et al. 2002). As mentioned before, mutation of huntingtin causes loss of its interaction with PSD95 which then oversensitize NMDA receptors (Sun et al. 2001).

1.3.2. Mitochondrial dysfunctions

It has been shown that huntingtin binds directly to mitochondria (Choo et al. 2004) altering their metabolic activity and motility within the cells (Trushina et al. 2004; Orr et al. 2008). Increased mtDNA mutations and deletions have also been detected in neurons of the cerebral cortex of HD patients (Horton et al. 1995; Cantuti-Castelvetri et al. 2005). Using the 1H-magnetic resonance spectroscopy (1H-MRS), decrease of N-acetylaspartate in basal ganglia and thalamus (Jenkins et al. 1993; Moffett et al. 2007) and increase of production of lactate in the cerebral cortex and basal ganglia (Jenkins et al. 1993; Koroshetz et al. 1997) of HD patients has been demonstrated. Biochemical studies of brain and peripheral tissues from HD patients and HD animal models revealed decreased activity of several enzymes involved in oxidative phosphorylation such as complex I, II, III, and IV (Gu et al. 1996; Arenas et al. 1998; Sawa et al. 1999; Tabrizi et al. 1999; Saft et al. 2005; Benchoua et al. 2006; Benchoua et al. 2008; Jeong et al. 2009). Impaired calcium handling has been found in the mitochondria isolated from HD patients (Panov et al. 2002) and when NMDA receptors were transiently activated in primary striatal neurons from YAC128 transgenic mice, these cells failed to reestablish calcium homeostasis in higher proportion compared with neurons from wild-type littermates (Oliveira et al. 2006). Mutant huntingtin was found to bind p53 and increase p53 levels and transcriptional activity, leading to the upregulation of two proapoptotic downstream players, Bcl2-associated X protein (BAX) and p53-upregulated modulator of apoptosis (PUMA) (Bae et al. 2005). Mutant huntingtin also represses transcription of PGC-1 α , a gene encoding for a transcriptional coactivator that regulates expression of genes involved in mitochondrial biogenesis and respiration (Cui et al. 2006). The expression of these genes is severely impaired in the disease (Cui et al. 2006).

1.3.3. Transcriptional dysregulation

DNA microarrays showed a large number of gene expression changes in cellular and mouse models of HD (Chan et al. 2002; Fossale et al. 2002; Luthi-Carter et al. 2002a; Luthi-Carter et al. 2002b; Sipione et al. 2002; Cha 2007). They indicate also that gene dysregulation occurs before the onset of symptoms, suggesting that transcriptional dysregulation is an important causative factor in the disease (Cha 2007). A large set of data also indicates that there is no single transcriptional regulator in HD and rather demonstrates the involvement of

multiple transcription factors and DNA target sequences and some critical pathways in HD, such as the GC-box/Sp1-mediated, the CRE/CREB regulation systems, and the REST/NRSF (Cha 2007; Johnson and Buckley 2009) (Fig. 4).

Mutant huntingtin reduces the transcription of many genes involved in the cholesterol biosynthesis pathway (Sipione et al. 2002). Subsequent *in vivo* studies validated these results with the observation of reduced expression of some key cholesterologenic genes in brain tissues from HD mice and human samples (Sipione et al. 2002). Expanded polyQ has been found to directly bind the acetyltransferase domain of CBP and p300/CBP associated factor (P/CAF), blocking their acetyltransferase activity (Steffan et al. 2001). This causes a condensed chromatin state and reduced gene transcription (Steffan et al. 2001). Furthermore, hypoacetylation of histone H3 in HD associates with downregulated genes (Sadri-Vakili et al. 2007).

1.3.4. Proteolysis

As mentioned above, huntingtin contains multiple cleavage sites for caspases, calpain, and aspartyl proteases generating a wide range of fragments (Goldberg et al. 1996; Wellington et al. 1998; Wellington et al. 2000; Gafni and Ellerby 2002; Wellington et al. 2002; Gafni et al. 2004), but the exact contribution of huntingtin proteolysis to cell functioning and pathology is still not completely understood. Caspase fragments of huntingtin were observed in HD mice and in post mortem brain tissue from HD patients (Kim et al. 2001; Wellington et al. 2002). Moreover, it has been proposed that a crucial proteolytic cleavage event in HD is mediated by caspase-6 (Graham et al. 2006). More recent findings, however, suggest that mutant huntingtin cleavage by caspase-6 is not necessary for the production of N-terminal toxic fragments (Gafni et al. 2012; Landles et al. 2012).

1.3.5. UPS dysfunction in HD

Early studies of the UPS impairment in HD suggested that polyQ aggregates could directly inhibit the function of 26S proteasome (Bence et al. 2001), that the degradation of polyQ proteins is inefficient (Holmberg et al. 2004) and that the eukaryotic proteasome is not able to digest polyQ sequences of polyQ-containing proteins (Venkatraman et al. 2004). In more recent studies, conflicting results showed that the proteasome is fully capable to degrade the expanded polyQ proteins (Michalik and Van Broeckhoven 2004), that the UPS impairment is not caused by direct choking of purified proteasomes but revealed that the UPS impairment is most likely global (Bennett et al. 2005).

Bennett et al (Bennett et al. 2007) supported the idea of global UPS impairment in *in vivo* studies by observation of elevated levels of polyUb chains in R6/2 and *Hdh*^{Q150/Q150} mouse models and human post-mortem HD brains (Bennett et al. 2007). In early studies of UPS activity in HD, artificial reporters of UPS activity based on destabilized GFP were successfully applied in *in vitro* cellular HD models (Bence et al. 2001; Bennett et al. 2005) but when translated into *in vivo* studies using R6/2 mouse model, these reporters failed to

accumulate and thus failed to confirm global UPS impairment *in vivo* (Bett et al. 2009; Maynard et al. 2009).

However, when the UPS GFPu reporters were fused to either postsynaptic PSD95 or presynaptic SNAP25 proteins, increased levels of GFPu reporters were observed in the synapses of R6/2 and *Hdh*^{Q150} HD mouse models (Wang et al. 2008). These observations suggest that the malfunction of UPS in HD could be region-specific rather than global.

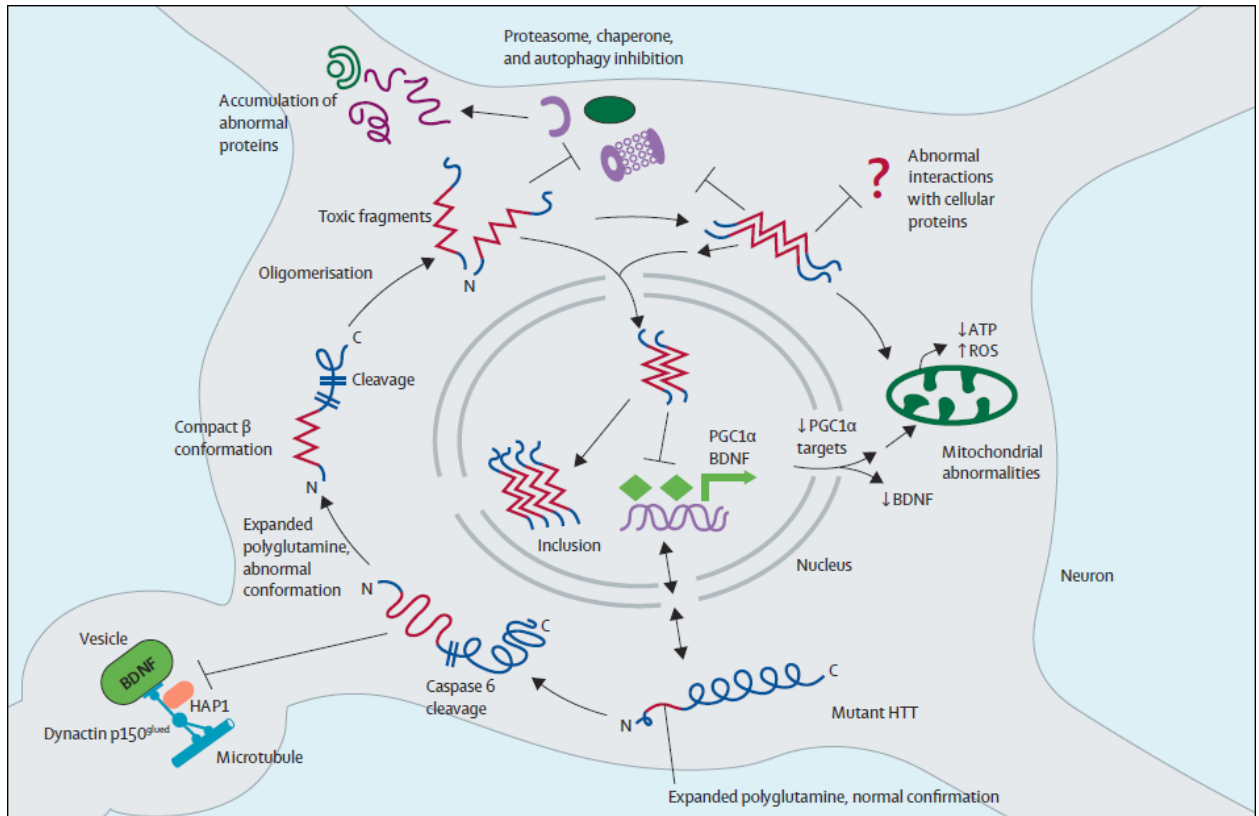


Fig. 5 Postulated intracellular pathogenesis of Huntington's disease. Mutant HTT (shown as a blue helical structure) with an expanded polyglutamine repeat (shown in red) undergoes a conformational change and interferes with cellular trafficking, especially of BDNF. Mutant HTT is cleaved at several points to generate toxic fragments with abnormal compact β conformation. Pathogenic species can be monomeric or, more likely (and as shown), form small oligomers. Toxic effects in the cytoplasm include inhibition of chaperones, proteasomes, and autophagy, which can cause accumulation of abnormally folded proteins and other cellular constituents. There may be direct interactions between mutant HTT and mitochondria. Other interactions between mutant HTT and cellular proteins in the cytoplasm are still poorly understood. Pathognomonic inclusion bodies are found in the nucleus (and small inclusions are also found in cytoplasmic regions). However, inclusions are not the primary pathogenic species. A major action of mutant HTT is interference with gene transcription, in part via PGC1 α , leading to decreased transcription of BDNF and nuclear-encoded mitochondrial proteins. ROS=reactive oxygen species. Taken from Ross and Tabrizi 2011).

1.3.6. Autophagy in HD

Increase of autophagosome-like structures has been shown in the brains of HD patients (Sapp et al. 1997; Kegel et al. 2000; Petersen et al. 2001). Recent studies revealed that mTOR, the negative regulator of the autophagic pathway, is sequestered into polyQ huntingtin aggregates in HD cell models, transgenic mice, and HD patient brain (Ravikumar et al. 2004). This ultimately leads to the induction of autophagy and clearance of mutant huntingtin fragments, which protects cells from death (Ravikumar et al. 2004). In addition, administration of chemical activators of autophagy or overexpression of genes implicated in autophagy enhance the clearance of mutant huntingtin, reduce aggregate formation, and improve the behavioral phenotype in HD mice (Ho et al. 2001; Ravikumar et al. 2002; Ravikumar et al. 2004; Yamamoto et al. 2006; Sarkar and Rubinsztein 2008). Recent findings suggest that huntingtin clearance by the lysosome depends on LAMP-2A, the integral membrane receptor protein that can directly import proteins across the lysosomal membrane (Thompson et al. 2009). It has also been shown that acetylation of lysine residue 444 is required to target huntingtin to macroautophagy pathway (Jeong et al. 2009). Recently, Li et al (2010) suggested that the clearance of soluble N-terminal mutant huntingtin is more dependent on the function of the UPS and that autophagy could function as a backup system to clear mutant huntingtin or is more efficient to remove aggregated forms of huntingtin (Li et al. 2010).

1.3.7. Misfolding and aggregation

HD onset and severity is polyQ-length-dependent and is characterized histopathologically by the presence of mutant huntingtin protein aggregates and inclusion bodies (IBs) found in affected neurons as it was first detected in HD mouse (Mangiarini et al. 1996) and human HD patients (DiFiglia et al. 1997) (see Fig. 6 for mHTT aggregates). Intensive research revealed that many factors influence the incidence of aggregated mutant huntingtin including levels of mutant protein expression, polyglutamine length, the length of the mutant huntingtin fragment, and age of the animal (Hackam et al. 1998; Li and Li 1998; Chen et al. 2002). Indeed, the frequency of aggregates formation is higher in the presence of short N-terminal mutant huntingtin fragments (Hackam et al. 1998). Biochemical analyses of nuclear and cytoplasmic inclusions showed that nuclear aggregates are composed mostly by the N-terminal fragments (Cooper et al. 1998; Hackam et al. 1998; Martindale et al. 1998).

Long polyglutamine repeats can adopt a polar zipper conformation that is stabilized by hydrogen bonds between the amides (Perutz et al. 1994). The newly formed polar zipper conformation results in a cylindrical, parallel β -sheet structure with one helical turn requiring 20 glutamines while a helix containing 40 or more glutamines displays two successive turns which enable hydrogen bond formation between the two turns leading to greatly enhanced overall stability (Perutz et al. 2002). This polyQ-dependent aggregation displays kinetics of nucleated-growth polymerization with a prolonged lag phase required for forming an aggregation nucleus, followed by a fast extension phase during which additional polyglutamine monomers rapidly join the growing aggregate (Wanker 2000; Bates 2003).

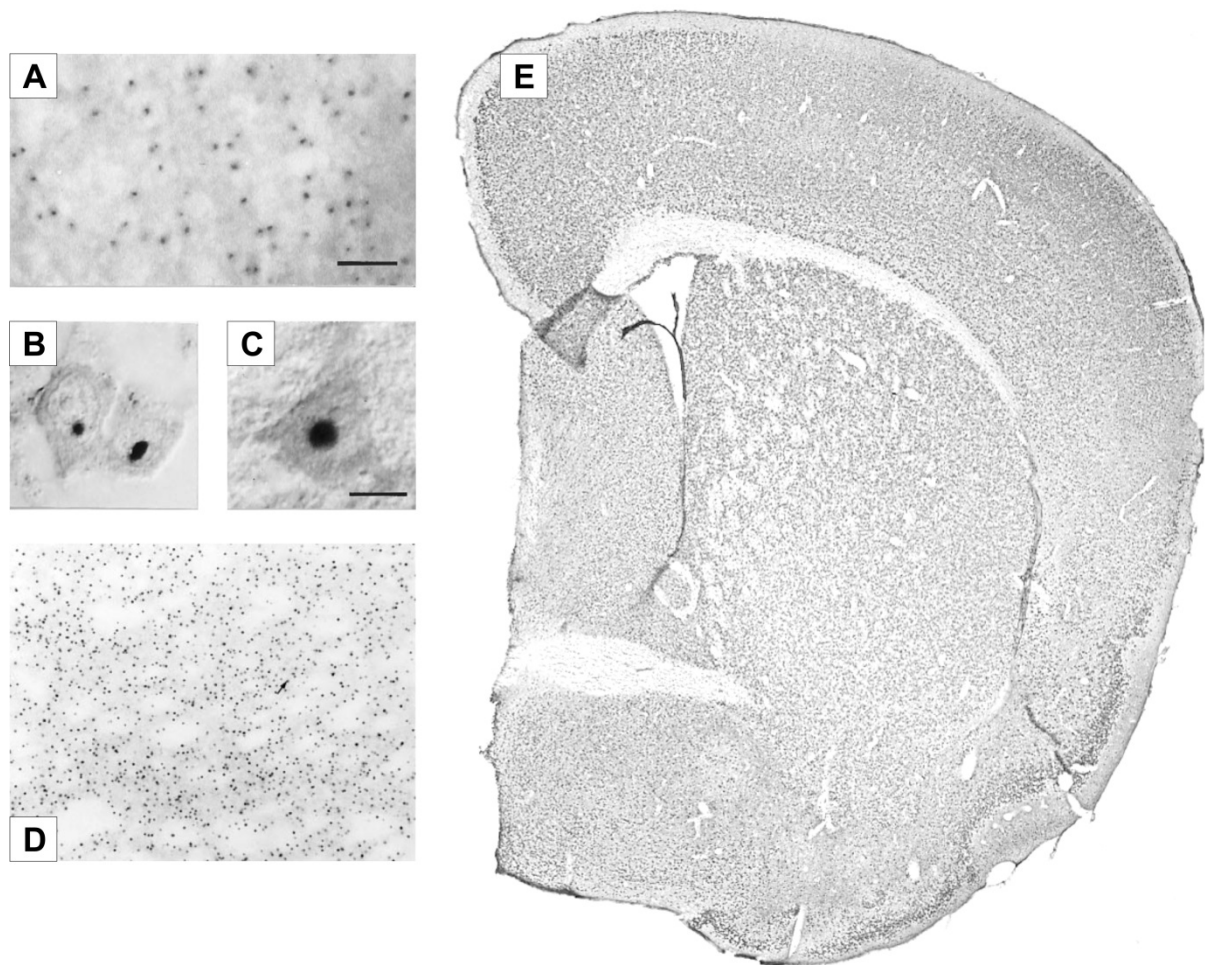


Fig. 6 Mutant huntingtin aggregates in mouse and human brain.

First demonstration of mHTT aggregates in human cortex (A, C) and striatum (B) and in striatum of the first HD transgenic mouse model R6/2 as evidenced by staining with the AB1 antibody (D). E) Represents coronal section at the level of anterior commissure (one hemisphere) of R6/2 brain mouse stained with mHTT aggregate-specific mEM48 antibody showing mHTT aggregate formation in virtually every single neuron. A, B and C taken from DiFiglia et al. 1997, D from Davies et al. 1997 and E is author's original work.

Another mutant huntingtin aggregation pathway depends on the first 17 N-terminal amino acids. First observed are the oligomers having the first 17 amino acids of the protein in its core and polyQ sequences exposed on the surface. As the polyQ increases, the structure decompacts and oligomers and/or protofibrils rearrange into amyloid-like structures capable of rapidly propagating via monomer addition (Thakur et al. 2009) (see Fig. 7 for schematic drawings of mHTT aggregation pathways).

It has also been demonstrated that the initial aggregation of mutant huntingtin is independent of its ubiquitination and that ubiquitination of mutant huntingtin aggregates represents their secondary growth phase (Gong et al. 2012; Skibinski and Boyd 2012).

It has been shown that that full length mutant huntingtin has to be cleaved in order to undergo the aggregation steps (Scherzinger et al. 1997; Cooper et al. 1998; Lunkes et al. 2002; Graham et al. 2006) as it is hypothesized that uncleaved mutant huntingtin is prevented from fibrillar polymerization because of steric interference resulting from the size of the full length protein. Therefore, cleavage of mutant huntingtin appears to be the rate limiting step in

aggregate formation (Woodman et al. 2007). However, recent discovery of a critical role of CAG Repeat Length–Dependent aberrant splicing of mutant huntingtin gene which results in exon 1 mHTT protein expression suggests that the pathology in all knock-in HD mouse models and human HD could be driven by the expression of the same exon 1 mHTT which is expressed in R6/2 mouse (Sathasivam et al. 2013).

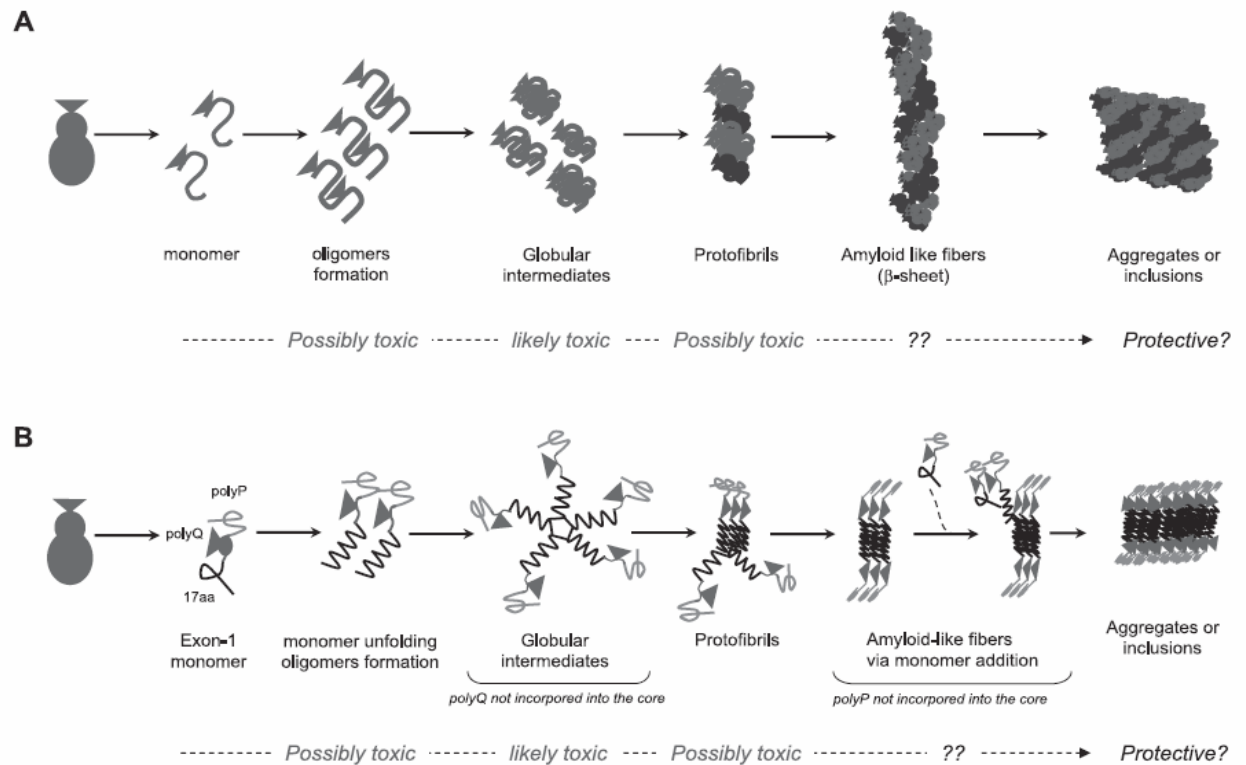


Fig. 7 The process of aggregate formation. Two major aggregation pathways are in competition with each other and explain how the polyQ expansion can facilitate aggregation. A) in the first pathway, mutant huntingtin undergoes covalent modifications (posttranslational modification or cleavage), determining the conversion of the protein to an abnormal conformation. The mutant protein forms oligomer intermediates that then give rise to globular intermediates from which protofibrils are generated. Protofibril intermediates associate to produce amyloid like structures, resulting in aggregates or inclusions. B) in the second pathway, oligomers having the first 17 amino acids of the protein in its core and polyQ sequences exposed on the surface are formed. As the polyQ increases, the structure decompacts and oligomers or protofibrils rearrange into amyloid-like structures capable of rapidly propagating via monomer addition and producing aggregates. Taken from Zuccato et al.

While the aggregation of mutant huntingtin is often described as a pathological hallmark of HD, recent data show that even though the pathological aggregation of mutant huntingtin is associated with certain pathological mechanisms in HD (reviewed in (Zuccato et al. 2010), the formation of aggregates could represent a cell disease-coping response to the most toxic fragments of mutant huntingtin (Arrasate et al. 2004; Miller et al. 2011). These new data demonstrate that: i) that the presence of soluble monomeric E1mhtt strongly predicts neuronal death (Miller et al. 2011), ii) that neurons which develop IBs show improved survival and decreased levels of diffuse forms of mHTT (Arrasate et al. 2004), iii) the already mentioned

critical role of CAG Repeat Length–Dependent aberrant splicing of mutant HTT gene which results in E1mHTT protein expression (Sathasivam et al. 2013) and that iv) downregulation of the E1mHTT expression by antisense oligonucleotide infusion in the R6/2 mouse led to prevention of brain atrophy, improved neuronal survival and suppression of new mhtt synthesis, however it did not significantly alter mhtt aggregation, suggesting that disease progression is probably independent of mhtt aggregate formation (Kordasiewicz et al. 2012). Clearly, the aggregation of mutant huntingtin has implications in normal protein turnover by UPS and autophagy (Sarkar and Rubinsztein 2008; Wang et al. 2008; Li et al. 2010) (discussed above).

1.4. Current treatments

Regrettably, there is no cure for HD (Novak and Tabrizi 2010). Currently, there are several potential therapeutic agents (memantine, tetrabenazine, minocycline, trehalose, C2–8, creatine, coenzyme Q10, ethyl- EPA, cysteamine, HDAC inhibitors, mitramycin) mostly acting on the downstream targets that have shown improvement of motor and/or cognitive dysfunction mostly in the R6/2 and N171–82Q mouse lines. Seven compounds have been systematically tested in HD patients at different stages of the disease (Zuccato et al. 2010). Unfortunately, only a few drugs have been tested in HD patients with some benefits. Only one is now available in several countries (tetrabenazine) (Frank and Jankovic 2010). Tetrabenazine has the best evidence of efficacy in Huntington’s disease and has been shown to reduce chorea (Novak and Tabrizi 2010).

One possible explanation why the drugs successfully tested in mice models of HD failed in humans can be found in the discrepancies existing between mouse HD models and human disease (Zuccato et al. 2010; Morton and Howland 2013). These discrepancies highlight the difficulty in predicting the efficacy of new drugs in humans based on animal models of HD (Zuccato et al. 2010) and demonstrate the need of large animal model of HD which will better simulate the human HD (Morton and Howland 2013). Given the multiple pathogenic mechanisms involved in HD, it is expected that a compound targeting one pathological mechanism may not be effective alone. Combinations of therapeutic agents that target different pathogenic mechanisms should have greater efficacy. Thus, recent discovery work for therapeutics have been expanded to include potential therapies which influence the misfolding, clearance or lowering of mutant huntingtin expression modifying the upstream events leading to HD (Yamamoto et al. 2006; Perrin et al. 2007; Kordasiewicz et al. 2012). Huntingtin lowering approaches are the most promising ones employing antisense oligonucleotides and siRNA strategies targeting either both alleles or just the mutant one (Johnson and Davidson 2010; Sah and Aronin 2011; Kordasiewicz et al. 2012; Southwell et al. 2012). Moreover, recent research revealed broad spectra of potential biomarkers which could be used in future clinical trials to better assess potential of the therapeutics (Hersch and Rosas 2011; Weir et al. 2011).

Cell replacement therapies in HD patients led to somehow mixed results, but with little evidence to date that it produces long-term benefits in the majority of patients. This, coupled to the emerging post-mortem data in some of these patients, suggests that this approach may

not be the optimal therapeutic strategy for treating HD. However, until clear evidence emerges of disease modifying therapies for HD, it remains one possible strategy and could even be used in conjunction with such treatments as a way of repairing and retarding the disease (reviewed in (Wijeyekoon and Barker 2011)). The potential of the cell replacement therapies in HD, however, was demonstrated in several animal models where neural stem/progenitor cells could survive and differentiated into replacement striatal neurons following transplantation into the brain resulting in an improvement of motor and cognitive functions (reviewed in (Maucksch et al. 2013)).

Currently, the aim of treatment is to manage symptoms and improve quality of life. No current treatments can slow disease progression (Handley et al. 2006; Imarisio et al. 2008; Novak and Tabrizi 2010). There are many effective options for symptomatic management, both drug and non-drug based (Phillips et al. 2008; Mestre et al. 2009).

1.5. Transgenic animal models of HD

A wide array of transgenic animals have been produced following the identification of the HD gene mutation in 1993 (1993) (see Table 1 for the list of most commonly used mouse HD models). Commonly used is the R6/2 mouse expressing exon 1, with 144 CAG repeats, of the human *htt* gene under the control of the human huntingtin promoter (Mangiarini et al. 1996). Neuropathologic analyses show progressive reduction in neostriatal volume, brain weight, and striatal neuron number with the presence of mHTT aggregates that increase in size and number over the lifespan of the animal (Stack et al. 2005). R6/1 strain mice were produced soon after with the intent of producing a milder HD phenotype employing the same exon 1 mHTT fragment with 116 CAG repeats. Relative expression levels of the human mHTT transgene to the 2 endogenous mouse HTT genes was decreased in comparison to the R6/2 line at 31% and 75% of endogenous, respectively. Hallmark intracellular inclusions are formed in a similar pattern as seen in R6/2 mice. Dopamine and cyclic adenosine monophosphate-regulated phosphoprotein (DARPP32) immunostaining, a marker for striatal GABAergic neuronal pools, is decreased (van Dellen et al. 2000), though striatal neuron number has not been shown to decrease over the lifespan of the animal (Naver et al. 2003). Yeast artificial chromosome (YAC) and prion promoter driven human HTT N171-82Q transgenic animals are also commonly employed models. YAC mice carry the full length human HTT gene under the control of the human HTT promoter including either 72 or 128 CAG repeats (Hodgson et al. 1999). Striatal neurons have been shown to be reduced in number by as much as 18% in this model (Slow et al. 2003). N171-82Q transgenic animals develop HTT intranuclear inclusions and neuritic aggregates (Schilling et al. 1999) in striatal, cortical and hippocampal brain areas and exhibit neuronal loss by as much as 25% (McBride et al. 2006).

Two HD transgenic rat models have been produced in recent years by the Olaf Riess' group at the University of Tübingen. Von Horsten et al. used a human derived 51 CAG sequence inserted into a 1962 bp rat HTT fragment under the control of the endogenous rat promoter (von Horsten et al. 2003) and more recently, Yu et al. generated BACHD transgenic rats which express full-length mutant human huntingtin with 97CAA/CAG repeats under control of the human huntingtin promoter and all regulatory elements (Yu et al. 2011). tgHD

rat model exhibit adult-onset neurological phenotypes with reduced anxiety, cognitive impairments, and slowly progressive motor dysfunction as well as typical histopathological alterations in the form of neuronal nuclear inclusions in the brain (von Horsten et al. 2003). On the other hand, BACHD rat model exhibited an obvious delay in reversal learning during Skinner box tests as early as at 3 months of age and immunohistological staining with anti-DARPP32 revealed neurodegeneration and neuronal atrophy in the lateral striatum at 12 months of age (Yu et al. 2011).

Despite the fact that transgenic animals generated invaluable data and revealed many molecular mechanisms underlying Huntington's disease pathology, this technology suffers by specific limitations which are attributed to the nature of how the transgene is incorporated into the genome. In classical transgenesis, the exogenous huntingtin gene is inserted randomly and therefore could affect the activity of other HD-non-related genes. In many cases, the expression of the transgenic huntingtin is driven by artificial promoters leading to non-physiological protein expression (Zuccato et al. 2010). To overcome these limitations, a variety of knock-in mouse HD models was generated providing the HD research community with genetically precise replicas of HD. Knock-in mouse HD models were generated in two different ways: i) first being the introduction of the pathogenic CAG repeats into the endogenous mouse huntingtin gene (Shelbourne et al. 1999; Lin et al. 2001), ii) replacing mouse exon 1 with human exon 1 carrying expanded CAG repeats (CAG range from 48 to 200) while keeping the mouse *Hdh* promoter (Wheeler et al. 1999; Ishiguro et al. 2001; Menalled et al. 2003; Heng et al. 2010). Knock-in models with shorter polyCAG repeats exhibited just modest neurodegenerative changes (Zuccato et al. 2010; Bowles et al. 2011) while models carrying ~100 and more CAG repeats (namely *HdhQ92*, *HdhQ94*, *HdhQ111*, *HdhQ140*, *HdhQ150* and *HdhQ200*) showed mHTT inclusion formation, neuronal dysfunctions, striatal gliosis and progressive motor deficits in a CAG length-dependent fashion (Wheeler et al. 2000; Lin et al. 2001; Menalled et al. 2002; Menalled et al. 2003; Heng et al. 2008; Hickey et al. 2008; Heng et al. 2010; Zuccato et al. 2010; Bowles et al. 2011). The homozygous KI models exhibited an even more pronounced HD phenotype (Heng et al. 2007; Woodman et al. 2007; Heng et al. 2008; Moffitt et al. 2009; Heng et al. 2010). The *HdhQ140* knock-in model showed striatal atrophy and neuronal loss at 2 years of age (Hickey et al. 2008). At about the same age (100 weeks), *HdhQ150* KI mice demonstrated approximately 50% loss of neurons in heterozygous and homozygous mice, though only the homozygous *HdhQ150* mice exhibited loss of striatal volume (Heng et al. 2007; Heng et al. 2008).

A transgenic non-human primate model (Yang et al. 2008) was generated using a lentiviral construct expressing exon 1 of the human HTT gene with 84 CAG repeats. Five HD transgenic macaques were generated exhibiting HD neuropathology with rapid onset of an HD like phenotype, though only 2/5 animals survived past 6 months. Two other large animal models were generated in the past years – HD transgenic sheep carrying full-length human HTT with 73 polyglutamine repeats under the control of the human HTT promoter (Jacobsen et al. 2010) and HD transgenic minipig expressing the 548aa N-terminal fragment of human htt with a 124 polyQ repeats generated by our group (Baxa et al. 2013). This transgenic minipig is described in greater details in the results and discussion sections. Another cloned transgenic HD minipigs bearing N-terminal mutant HTT (208 amino acids and 105 Q) have

been generated via somatic cell nuclear transfer technology (Yang et al. 2010), but the extreme high expression levels of the transgene led to premature (3 days old) death of three of the 5 born piglets, fourth lived for only 25 days and the fifth founder was still viable at the beginning of 2013 (Morton and Howland 2013).

Strain Name	Transgenic or Knockin	Gene Characteristics	Promoter	Repeat Length	Motor Symptom Onset	Lifespan	Background Strain(s)	References
R6/2	Transgenic fragment	Exon 1 of human HTT gene	1 kb of Human	~150	6 weeks	10-13 wks	C57BL/6xCBA	(Mangiarini et al. 1996)
R6/1	Transgenic fragment	Exon 1 of human HTT gene	1 kb of Human	116	18 weeks	32-40 wks	C57BL/6xCBA or C57BL/6	(Mangiarini et al. 1996)
N171-82Q	Transgenic fragment	First 171 AA of human HTT (exons	Prnp	82	3 months	16-22 wks	C57BL/6xC3H/He	(Schilling et al. 1999)
Tg100	Transgenic fragment	First ~3 kb of human HTT cDNA	Rat NSE	100	3 months (nonspecific)	Normal	C57BL/6xSJL	(Laforet et al. 2001)
HD94	Transgenic fragment	Chimeric human/mouse HTT	TetO + tTA	94	4-8 weeks (claspings)	Normal	C57BL/6xCBA	(Yamamoto et al. 2000)
YAC72	Transgenic full-length	Full length human HTT gene	Human HTT	72	16 months	Normal	FVB/N	(Hodgson et al. 1999)
YAC128	Transgenic full-length	Full length human HTT gene	Human HTT	120	6 months	Normal	FVB/N	(Slow et al. 2003)
BACHD	Transgenic full-length	Full length human HTT gene (floxed	Human HTT	97 (mixed)	2 months	Normal	FVB/N	(Gray et al. 2008)
HdhQ72, Q80	Knockin	Endogenous murine Htt gene, expanded	Mouse Htt	72, 80	12 months	Normal	Mixed 129Sv, C57BL/6	(Shelbourne et al. 1999)
HdhQ111	Knockin	Endogenous murine Htt gene, chimeric	Mouse Htt	109	24 months (gait)	Normal	Mixed 129Sv, CD1	(Wheeler et al. 1999)
HdhQ94	Knockin	Endogenous murine Htt gene, chimeric	Mouse Htt	94	2 months (rearing)	Normal	Mixed 129Sv, C57BL/6	(Levine et al. 1999)
HdhQ140	Knockin	Endogenous murine Htt gene, chimeric	Mouse Htt	140	4 months	Normal	Mixed 129Sv, C57BL/6	(Menalled et al. 2003)
HdhQ150	Knockin	Endogenous murine Htt gene, expanded	Mouse Htt	150	100 weeks	Normal	Mixed 129Ola, C57BL/6	(Lin et al. 2001)

Table 1. Commonly Used Mouse Models of HD. Taken and modified from Crook and Housman 2011.

CHAPTER 2

(Neural) Stem cell therapy in spinal cord disorders and injury

ALS

(Neural) Stem cell therapy in spinal cord injury

Immunosuppression in stem cell transplantation

2.1. (NEURAL) STEM CELL THERAPY IN SPINAL CORD

Most tissues are composed of a variety of differentiated cells of different lineages and it is still poorly understood how their numbers are maintained in adult tissues during homeostasis and in response to injury. The adult central nervous system has always been considered to be a relatively static tissue with little cell turnover (Barnabe-Heider et al. 2010). However, discoveries throughout the past two decades demonstrated that there is more plasticity than previously believed and that new neurons are produced continuously from stem cells in the subventricular zone of the lateral ventricles and the dentate gyrus of the hippocampus (Zhao et al. 2008). In most parts of the central nervous system, however, neurons are not added in adulthood and there is limited cell turnover (Barnabe-Heider et al. 2010).

The spinal cord does not possess a clear neurogenic niche (Kim et al. 2007; Sahni and Kessler 2010) and/or is not favorable for neural differentiation of ependymal-derived endogenous progenitors (Sabelstrom et al. 2013) as the spinal cord ependymal cell and astrocyte proliferation is restricted to self-duplication to maintain their populations in the uninjured spinal cord, whereas oligodendrocyte progenitors self-renew and give rise to an increasing number of mature oligodendrocytes (Barnabe-Heider et al. 2010). Nonetheless, it has been recently showed that the cell turnover after spinal cord injury significantly accelerates the delivery of new glial cells derived from ependymal cells (39%), followed by astrocytes (by duplication) (34%) and oligodendrocytes (by self-renewal of oligodendrocyte progenitors) (27%) (Barnabe-Heider et al. 2010) (see Fig. 8 D-F for schematic drawings).

It has been therefore postulated that the presence of resident cells in the adult spinal cord capable to promote functional recovery after injury could be used to develop pharmacological strategies to modulate endogenous spinal cord stem cells in situ (Barnabe-Heider et al. 2010; Sabelstrom et al. 2013). While these ideas remain to be challenged by numerous experiments, the already available data from multiple laboratories suggests that the transplantation of neuronal stem cells into the injured cord represent potential therapeutic intervention leading to improvement of both sensory and motor functions (Cummings et al. 2005; Faulkner and Keirstead 2005; Iwanami et al. 2005; Keirstead et al. 2005; Cloutier et al. 2006; Cizkova et al. 2007; Erceg et al. 2010; Salazar et al. 2010; Sharp et al. 2010; Usvald et al. 2010; Davies et al. 2011; All et al. 2012; Lu et al. 2012) (van Gorp et al. 2013).

Uninjured spinal cord disturbed by wide spread disease pathology which is affecting vast majority of its cell types, like in ALS, represent another challenge which can be addressed by stem cell therapy either by replacing diseased cell populations directly or by introducing a cell population (like astrocytes) that can be supportive to the motor neurons affected by the disease process (Clement et al. 2003; Vargas and Johnson 2010; Lunn et al. 2011). It is now well established that the astrocyte actively and/or passively promote α -motoneuronal degeneration in ALS (Nagai et al. 2007; Vargas and Johnson 2010; Ince et al. 2011) and because in cell replacement therapies, the intrinsic complications of replacing highly specialized cells, such as motor neurons, make astrocytes an ideal target (Vargas and Johnson 2010). Human spinal cord-derived stem cells (HSSCs) are neural progenitor cells isolated from the cervico-thoracic spinal cord of an 8-week gestation fetus (Guo et al. 2010). In our experiments, these cells have shown therapeutic benefit when grafted into the ventral horn of spinal cord of the rat

SOD1^{G93A} model of ALS (Hefferan et al. 2012), in a rat model of ischemic spinal cord injury (Cizkova et al. 2007), or in the rat with lumbar contusion injury (van Gorp et al. 2013). Histological analyses showed that vast majority of the transplanted cells differentiated into neurons and that the astrocyte and oligodendrocyte differentiation was limited (Cizkova et al. 2007; Hefferan et al. 2012), (van Gorp et al. 2013 in press).

Since a large number of previous experiments from different laboratories demonstrated the promising potential of human neural stem therapy in spinal cord disorders and injuries and also showed the proliferative potential of spinal cord stem cells, the future research will most likely include transplantation of more specific neural progenitors together with modulation of the plasticity of the cells residing in the adult spinal cord which will come together with specific trophic support of both the endogenous and transplanted cells and which could be further combined and thus supported by specific gene (silencing) therapy.

2.2. AMYOTROPHIC LATERAL SCLEROSIS

Amyotrophic lateral sclerosis (ALS; also known as Lou Gehrig's disease (USA) and motor neuron disease (UK)) is a late onset, progressive and fatal neurodegenerative disease characterized by loss of upper motor neurons in the motor cortex and lower motor neurons in the brain stem and spinal cord. Loss of the motor neurons leads to muscle atrophy, weakness, fasciculation and spasticity later followed by paralysis and ultimately results in death due to respiratory failure.

First described in 1869 by Jean-Martin Charcot (therefore initially known as a Charcot's disease), ALS was named based on his observations of distinct loss of axons in the lateral aspect of the spinal cord (Boillee et al. 2006a). Typical onset of the disease is usually in midlife (45-60 years) with a relentlessly progressive disease course of 3 to 5 years but the variability is very high (Robberecht and Philips 2013). Worldwide incidence and prevalence of ALS are 1–2 and 4–6 per 100,000 each year, respectively, with a lifetime ALS risk of 1/350 to 1/1000 (Pasinelli and Brown 2006; Kiernan et al. 2011) and incidence peak (10–15/100,000/year) between ages 60 and 79 (Logroscino et al. 2005).

Approximately 90% of all cases are classified as sporadic (SALS), defined as having no family history of the disease. The remaining cases are inherited in a dominant fashion i.e. familial (FALS) of which 20% are associated with mutations within copper/zinc superoxide dismutase 1 (SOD1) (Haidet-Phillips et al. 2011). Mutations in at least 15 genes can cause FALS, and the genetic basis of many FALS cases remains to be found (Ferraiuolo et al. 2011). ALS causing SOD1 mutations were discovered in 1993 (Rosen et al. 1993) and for a long time, most of the research of ALS pathogenesis has been focused on SOD1 (Lagier-Tourenne and Cleveland 2009). Recent identification of 43 kDa TAR DNA-binding protein (TDP-43; (Arai et al. 2006; Neumann et al. 2006) and FUS/TLS (Kwiatkowski et al. 2009; Vance et al. 2009) causative mutations which are both involved in pre-mRNA splicing, RNA transport and RNA translation, led to the idea that aberrant RNA metabolism contributes to ALS pathogenesis (Lagier-Tourenne et al. 2010; Polymenidou et al. 2012; Robberecht and Philips 2013). More recent finding of the chromosome 9 open reading frame 72 (C9ORF72) mutation (DeJesus-Hernandez et al. 2011; Renton et al. 2011) led to confirmation that ALS and

Frontotemporal lobe degeneration (FTLD) are two ends of the spectrum of one disease (Robberecht and Philips 2013) what was previously suggested by clinical (Lillo and Hodges 2009) and pathological observations (Burrell et al. 2011) (see Fig. 9 for detailed graphical demonstration).

Despite the intensive research and growing scientific and clinical interest, no cure for ALS exists. Current clinical therapy is limited to symptomatic treatment such as respiratory and nutritional management (Ikeda 2013) and to riluzole, the only FDA-approved drug that has been shown to have a modest effect on prolonging survival in ALS patients for ALS (Bensimon et al. 1994; Lacomblez et al. 1996b). Just very recently, 1st phase of ALS clinical trial with neural stem cells was successfully completed (Glass et al. 2012) and at the time of writing of this thesis, positive results of the first antisense oligonucleotide (ASO) ALS clinical trial where the ASOs against SOD1 were delivered intrathecally in patients with SOD1 ALS were published (Miller et al. 2013). These promising results are, however, just preliminary and therefore it is very important to further accelerate the research of ALS.

2.2.1. Clinical presentation of ALS

The clinical features of ALS are a direct consequence of the progressive loss of upper (UMN) and lower motor neurons (LMN), with secondary denervation and subsequent reinnervation of muscles. This causes that even with the disease already ongoing, the clinical symptoms are not detectable (Nefussy and Drory 2010). As the disease progresses, this compensatory mechanism fails and only at this stage of axonal degeneration and dysfunction the neuronal body becomes abnormal and die (Robberecht and Philips 2013) and as their number begins to decrease, one of the earliest symptoms of ALS may be increased fatigue. As the number of motor units innervating a muscle decreases further, permanent weakness develops and the affected muscles gradually undergo atrophy (Nefussy and Drory 2010).

ALS has multiple presentations and these are indicative of the loss of neurons across the whole motor system (Mitchell and Borasio 2007). Identification of the specific phenotypes is very important for prognosis and survival of the patient (Kiernan et al. 2011) as large differences in survival and age at disease onset exist even between individuals from one family, even if ALS is caused by exactly the same mutation (Robberecht and Philips 2013).

The main presentations of ALS include: 1) limb-onset ALS (about 70%). This include: i) Cervical-onset with upper-limb symptoms, either bilateral or unilateral. Upper limb signs might be upper motor neuron (involving the limbs leads to spasticity, weakness, and brisk deep tendon reflexes), lower motor neuron (fasciculations, wasting, and weakness), or both. ii) Lumbar onset which indicates degeneration of the ventral horn α -motoneurons (α MN) of the lumbar enlargement and is associated with lower motor neuron symptoms (fasciculations, wasting, and weakness) and signs in the legs; 2) bulbar onset ALS (25%) with speech (dysarthria) and swallowing difficulties (dysphagia), and with limb features developing later in the course of the disease; 3) primary lateral sclerosis with pure UMN involvement which is less common; and 4) progressive muscular atrophy with pure LMN involvement (Mitchell and Borasio 2007; Kiernan et al. 2011).

The overall population-based lifetime risk of ALS is 1:400 for women and 1:350 for men. Peak age at onset is 58–63 years for sporadic disease and 47–52 years for familial disease (Kiernan et al. 2011). Because of the variety of ALS forms/presentations reflexing differential involvement of motor centers, the prognosis is highly related to the symptoms observed. Reduced survival is associated with older age at onset, early respiratory problems and bulbar-onset of the disease. Younger age at onset and limb-onset of the disease predict longer survival. Nonetheless, ALS is uncompromisingly progressive and 50% of patients die within 30 months of symptom onset and about 20% patient survive between 5-10 years after the onset (Talbot 2009).

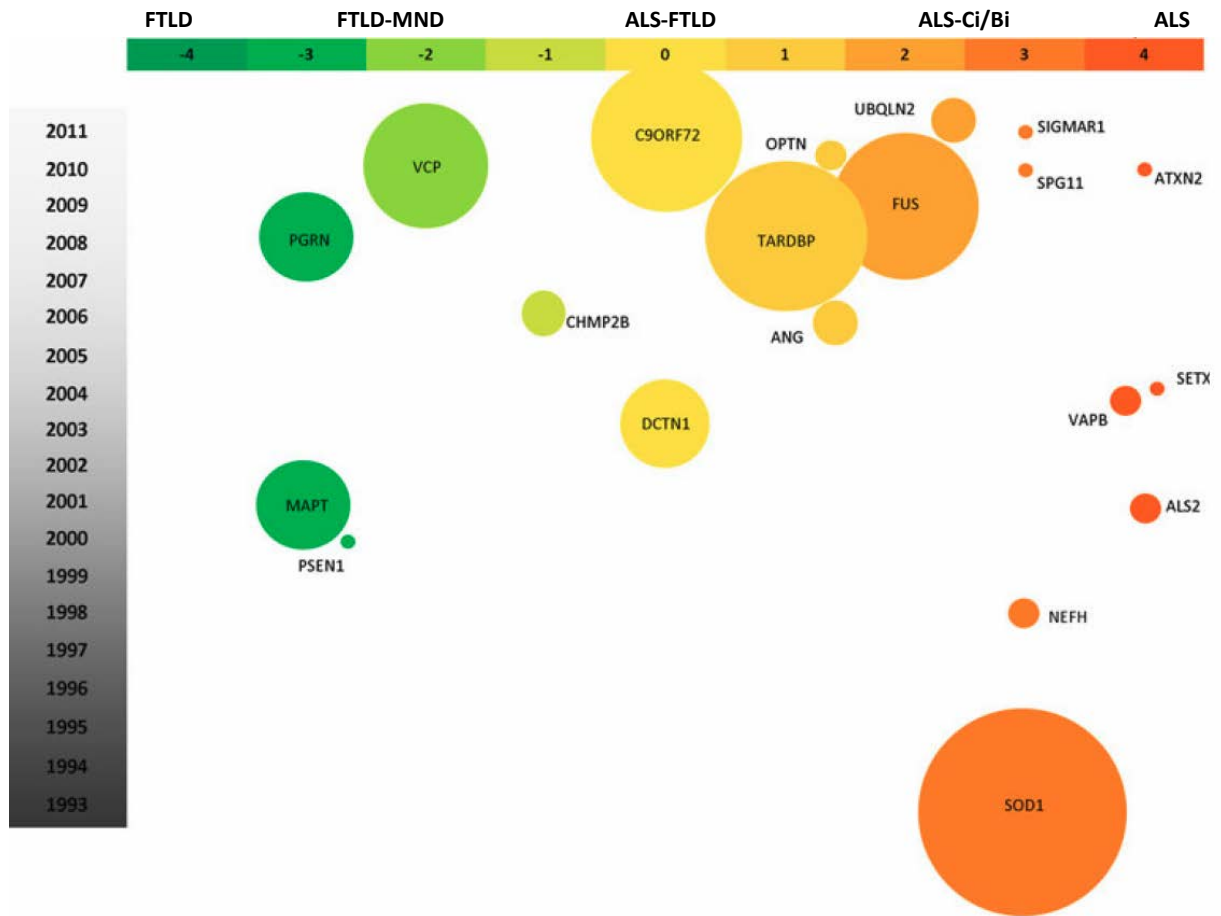


Fig. 9. ALS-FTLD genes plotted to show phenotype, year of discovery and importance gauged by research outputs.

The X axis is a score representing the involvement of each gene in ALS or FTLD (-4 being FTLD, 0 being ALS-FTLD, and +4 ALS/MND based on evidence from the ALSod database (<http://alsod.iop.kcl.ac.uk>), PubMed, peer-reviewed publications and case studies. The Y axis represents year of mutation identification. The circle size represents the level of research on each gene scaled by the logarithm of the number of articles from PubMed retrieved by the search command ((\GENE[[Title/Abstract]) AND amyotrophic lateral sclerosis[Title/Abstract]) AND frontotemporal dementia[Title/ Abstract]) AND genetics[MeSH Subheading]. Taken and modified from Al-Chalabi et al. 2012 and further modified according to Robberecht and Philips 2013.

15% ALS patients have also frontotemporal dementia (FTD; behavioral variant of frontotemporal lobe degeneration (FTLD)) (Ringholz et al. 2005; Lillo and Hodges 2009) with TDP-43 positive inclusions in cortical neurons (Neumann et al. 2006; Davidson et al. 2007; Mackenzie et al. 2007) (whereas at least 50% ALS patients have evidence for more subtle cognitive and/or behavioral dysfunction (Ringholz et al. 2005)) and 15% of the patients with FTLD have also ALS and many more FTLD patient have evidence of lower motor neuron involvement (Lomen-Hoerth et al. 2002; Burrell et al. 2011). This suggests that ALS and FTLD are two ends of the spectrum of one disease (Kiernan et al. 2011; Robberecht and Philips 2013). FUS-positive inclusions have been recently identified in FTLD patients with ubiquitin-positive, TDP43-negative FTLD and in patients with FALS caused by mutations in FUS (Neumann et al. 2009a) further emphasizing the pathological overlap between ALS and FTD. Finally, the identification of a common cause for ALS and FTLD — the chromosome 9 open reading frame 72 (C9ORF72) mutation (DeJesus-Hernandez et al. 2011; Renton et al. 2011) — confirmed this clinical and pathological concept. Patients for which there is clinical evidence for both disorders are said to have ALS-FTLD. Many patients with ALS show some cognitive or behavioural changes but do not meet the criteria for FTLD: they are said to have ALS-Ci/Bi (ALS with cognitive or behavioral impairment). Patients with FTLD can similarly show evidence of mild motor neuron involvement (clinically or on electromyographs) without developing ALS: they are said to have FTLD-MND. Some patients have pure ALS or FTLD (Robberecht and Philips 2013) (Fig. 9).

2.2.2. Neuropathology in ALS

The pathophysiological mechanisms underlying the development of ALS seem to be multifactorial with evidence of a complex interaction between genetic and molecular pathways (Kiernan et al. 2011) but the causes of most cases of ALS remain undefined (Pasinelli and Brown 2006). The pathological hallmark of ALS is the degeneration of upper and lower motor neurons. As it was first depicted by Jean-Martin Charcot involvement of the upper motor neurons results in axonal degeneration and secondary loss of myelin in the lateral spinal cord (=Amyotrophic lateral sclerosis). However, not all motor neurons are affected. Oculomotor neurons and neurons in Onuf's nucleus (sacral motor neurons innervating sphincter muscles of the anus and urethra in humans) are unaffected in ALS (Kanning et al. 2010). It has also been noted that large motor neurons are more vulnerable than smaller ones (Frey et al. 2000). These large motor neurons with fast type axons/synapses/motor units (FF; fast-fatiguable) have large fields of innervation and limited sprouting capacity. On the other hand, small slow-fatiguable (SF or S) tonic motor neurons innervating small neuromuscular fields with notable sprouting capacity are most resistant in ALS and survive until end-stage in the mutant SOD1^{G93A} mouse (Pun et al. 2006).

Degenerating neurons in ALS were found to contain various inclusion bodies and/or protein aggregates: i) ubiquitinated Lewy body-like or Skein-like inclusions (Leigh et al. 1991) are generally considered as a hallmark of pathology in ALS (Al-Chalabi et al. 2012); ii) Bunina bodies (cystatin C-containing inclusion) (Okamoto et al. 2008), and iii) accumulation

of phosphorylated neurofilaments (Pasinelli and Brown 2006). New discovered mutations in the genes coding TDP-43 and FUS/TLS lead to more or less ubiquitin positive cytoplasmic inclusions which are SOD1 negative (Arai et al. 2006; Neumann et al. 2006; Igaz et al. 2008; Kwiatkowski et al. 2009; Munoz et al. 2009; Neumann et al. 2009a; Vance et al. 2009; Tateishi et al. 2010). Interestingly, FUS/TLS are not TDP43 positive (Vance et al. 2009; Tateishi et al. 2010) (see Fig. 10 for aggregation in ALS). Another apparent pathological feature of ALS is fragmentation of Golgi apparatus (Okamoto et al. 2010).

In addition, it is now well established that reactive astrogliosis (Vargas and Johnson 2010) and microglia (Boillee et al. 2006b) and impaired functions of glial cells in general (Neusch et al. 2007), as well as active secretion of yet unknown toxic agents from astrocytes contributes to ALS pathology (Nagai et al. 2007; Haidet-Phillips et al. 2011). Schwann cells were also shown to be involved (Lobsiger et al. 2009) and recent data about oligodendrocyte dysfunction in ALS (Kang et al. 2013; Philips et al. 2013) just underlined that the ALS is complex and systemic disease affecting every single cell type in the CNS and beyond.

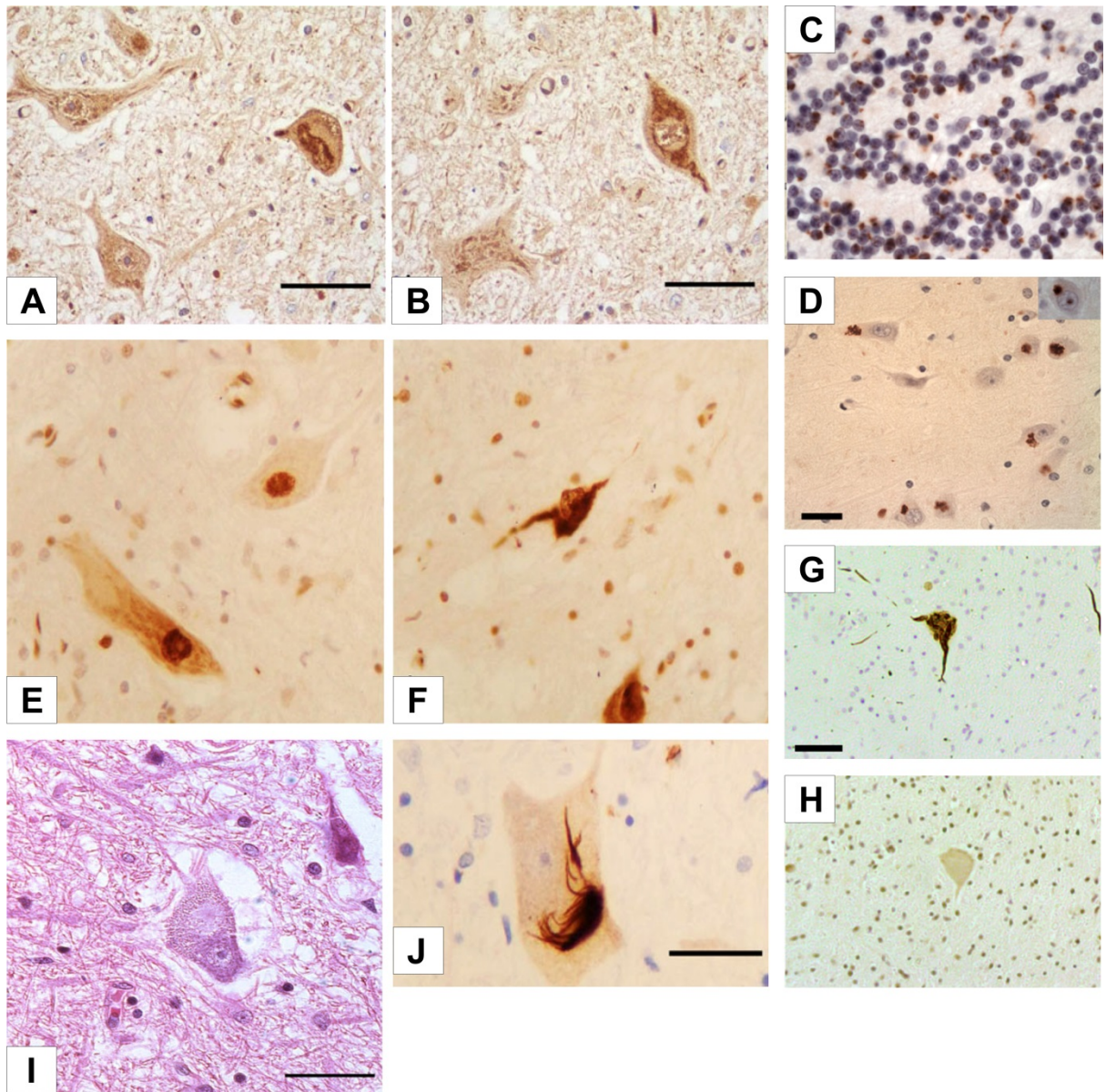


Fig. 10 Aggregation in ALS. (A, B) Ubiquitin staining of spinal motor neurons from a case of SOD1 FALS due to the G85R mutation. The lesions resemble skein-type neuronal cytoplasmic inclusions rather than neurofilament conglomerates and were negative for neurofilament staining (bar 50 μ m). (C, D) ALS patient with C9orf72 repeat expansion showing D) the CA4 region of the hippocampus with numerous p62 positive (TDP-43 negative) star-like neuronal cytoplasmic inclusions and an intranuclear inclusion (inset); C) Numerous p62 positive (TDP-43 negative) neuronal cytoplasmic inclusions are seen in the granular layer of the cerebellum (anti-p62) (scale bar (D) 40 μ m). (E, F) FUS immunostaining of spinal ventral horn showing normal nuclear staining (E) and a cell containing cytoplasmic accumulation of FUS (F) (bar 50 μ m). (G, H) SOD1 pathology. Anterior horn neuron in the spinal cord of a woman with SOD-1 mutation showing cytoplasmic immunopositivity for p62 (G) and immunonegativity for TDP-43 (H) in the same neuron (anti-p62 and TDP-43) (scale bar 40 μ m). I) ‘‘Lewy-like hyaline inclusion’’ body in a spinal motor neuron. Despite the superficial resemblance to a Lewy body such lesions are immunoreactive to TDP-43 and not to a-synuclein. (bar 50 μ m). J) Spinal ventral horn in ALS/MND p62 staining of a skein type inclusion (bar 50 μ m). Taken and modified from Ince et al. 2011; and from Al-Chalabi et al. 2012.

2.2.3. SALS vs FALS

Based on the genetic background of the disease, ALS can be classified into two categories: familial ALS (FALS) and sporadic ALS (SALS) which are clinically very similar (Rothstein 2009). Most of the ALS cases (classic adult-onset) occur as SALS and only about 10% of patients are diagnosed as having FALS (Rothstein 2009; Nefussy and Drory 2010; Haidet-Phillips et al. 2011) which is probably overestimation as it was revealed by a recent meta-analysis which showed that FALS represent approx. 5% of the case (Byrne et al. 2011). SALS is defined as having no family history of the disease (Robberecht and Philips 2013). ALS is considered to be familiar if one or more relatives are diagnosed by ALS (Sabatelli et al. 2013), but no consensus exists on standard definition criteria for FALS (Byrne et al. 2012).

FALS is mostly hereditary (Table 2) and almost always autosomal dominant with rare occurrence of X-linked or recessive disease (Ince et al. 2011). The most common mutations causing FALS are found in the genes coding i) copper/zinc superoxide dismutase 1 (SOD1) which represents approx. 20% of FALS cases, ii) TAR DNA-binding protein 43 (TDP-43) responsible for ~1-5%, iii) FUS (fused in sarcoma) or TLS (translocation in liposarcoma) (FUS/TLS) for ~1-5% and the mutation in iv) Chromosome 9 open reading frame 72 (C9ORF72) is the cause of FALS in about 40-50% cases (Robberecht and Philips 2013). All these four mutations are, to some extent, also known to be responsible for SALS (McGoldrick et al. 2013). Incomplete family history, *de novo* mutations and incomplete penetrance are some of the common reasons for misclassification between SALS and FALS but as all genes mutated in FALS have also been found mutated in patients without a family history, it is worth considering if the classification of sporadic versus familial disease is biologically justified (Nefussy 2013).

2.2.4. Animal models of ALS

Taking into account the historical sequence of the discovery of major FALS causing mutations, SOD1 animal models are the most commonly used models in ALS research and drug discovery (Turner and Talbot 2008; McGoldrick et al. 2013). The subsequent identification of mutations in TDP-43 and FUS/TLS genes led to recent generation of a great battery of novel ALS rodent models (McGoldrick et al. 2013), however, the validity of these models for ALS research remains to be demonstrated (Robberecht and Philips 2013). Because our work was primarily focused on stem cell-based therapy in SOD1^{G93A} rat, just short description of mouse models is provided with the greatest emphasis on SOD1^{G93A} animal models. Detailed description of ALS animal models can be found elsewhere (Turner and Talbot 2008; Kanning et al. 2010; McGoldrick et al. 2013).

2.2.4.1. SOD1 models of ALS

Soon after the discovery of SOD1 mutations (chromosome 21q22.11) in FALS (Rosen et al. 1993) first transgenic animal (mouse) model of ALS (SOD1^{G93A}) was generated (Gurney et al. 1994). This mouse expresses human SOD1 promoter driven SOD1^{G93A} (approx. 20-24 copies) (Gurney et al. 1994). About 21 SOD1 rodent models were developed to date

(McGoldrick et al. 2013). Despite vast differences in transgene copy number, steady-state transcript and protein levels, dismutase activity and neuropathology, the introduced mutations induce fatal-ALS like symptoms with different disease latencies and progression rates (Turner and Talbot 2008). Transgenic SOD1^{G93A} mice (see Fig. 11 for detailed course of the disease) are the most frequently used mouse ALS models followed by SOD1^{G37R}, SOD1^{G85R} and SOD1^{G86R} mice (see Table 2 for list of the SOD1 ALS mouse models). Similarly, SOD1^{G93A} rats are the most employed rat ALS models (Turner and Talbot 2008). SOD1^{WT} mouse models and SOD1 KO&null models were also generated and these models showed that i) overexpression of wild-type SOD1 leads to axonal loss and motor neuron degeneration in spinal cord of aged animals (Jaarsma et al. 2000; Jonsson et al. 2006) and that ii) KO of wild-type SOD1 in SOD1 null mice causes striking age-dependent denervation of hind limb muscles (Fischer and Glass 2007) and skeletal muscle atrophy (Muller et al. 2006).

SOD1 transgenic rat models were generated relatively recently and provide obvious advantage of the body and mainly CNS size. Two different human SOD1 mutations (SOD1^{G93A} and SOD1^{H46R}) induced ALS-like phenotypes (Nagai et al. 2001; Howland et al. 2002). Transgenic rat were generated by two different groups of Yasuto Itoyama at Tohoku University in Japan (Nagai et al. 2001) and Don W. Cleveland at UCSD (Howland et al. 2002). Rats from these two groups express different levels of mutant SOD1 protein and therefore display different phenotypes.

ALS-like phenotype of the Cleveland's SOD1^{G93A} (L26H) ALS transgenic rat can be shortly described as follows: i) in presymptomatic stage, no overt motor neuron loss is evident; ii) the appearance of vacuoles in lumbar motor neurons as well as gliosis precede both motor neuron loss and clinical signs of disease in rats (Howland et al. 2002); iii) our group recently discovered that the appearance of first muscle fibrillations (indicator of muscle denervation) in electromyography measurements (EMG) of gastrocnemius muscle precedes the 10% body weight loss time point (commonly used as a disease onset point in studies using this ALS rat model) by approx. 14 days and provide a highly sensitive and early index of disease onset and is defined by the presence of both spinally mediated hyper-reflexia and muscle denervation and corresponds with a significant loss of spinal interneurons and α -motoneurons (10% loss) (Hruska-Plochan et al. manuscript in prep); iv) ongoing rapid decrease of α -motoneuron numbers which at 10% body weight loss reach 70% and which is accompanied by axon degeneration, myelin ovoids, macrophage infiltration, ubiquitin and mSOD1 aggregates, aberrant accumulation of neurofilaments and loss of EAAT2 in ventral horn gray matter astrocytes (Howland et al. 2002); v) rapid decline and muscle atrophy leading to hindlimb (later also forelimb) paralysis, respiration difficulties and death (Howland et al. 2002). This rapid progression and severity of the disease phenotype is in contrast to the slower progression of disease and higher levels of mutant SOD1 protein observed in SOD1^{G93A} transgenic mice (G1H and G1L) where disease duration approached 60–70 days (Gurney et al. 1994; Dal Canto and Gurney 1995; Dal Canto and Gurney 1997). Thus, the rapid progression of disease in the SOD1^{G93A} transgenic rats seems not to be just a simple function of expression levels but rather may be characteristic of a species difference in the presentation of clinical phenotype (Howland et al. 2002).

SOD1 mutant	SOD1 activity (fold)	Disease onset (months)	Disease duration	Reference
SOD1 ^{A4Va}	nd	8	3	(Deng et al. 2006)
SOD1 ^{G37R}	14.5	4-6	nd	(Wong et al. 1995)
SOD1 ^{H46R}	nd	5	1	(Chang-Hong et al.
SOD1 ^{H46R/H48Q}	0	4-6	nd	(Wang et al. 2002)
SOD1 ^{H46R/H48Q/H63G/H120G}	0	8-12	nd	(Wang et al. 2003)
SOD1 ^{L84V}	nd	5-6	1	(Tobisawa et al. 2003)
SOD1 ^{G85R}	0	8-14	0.5	(Bruijn et al. 1997b)
SOD1 ^{G86Rb}	0	3-4	1	(Ripps et al. 1995)
SOD1 ^{D90A}	6-8	12	2	(Jonsson et al. 2006)
SOD1 ^{G93A}	11	3-4	1-2	(Gurney et al. 1994)
SOD1 ^{I113T}	nd	12	2	(Kikugawa 2000)
SOD1 ^{L126X}	nd	7-9	nd	(Wang et al. 2005a)
	nd	11	0.75	(Deng et al. 2006)
SOD1 ^{L126delTT}	0	15	1	(Watanabe et al. 2005)
SOD1 ^{G127X}	0	8	0.25	(Jonsson et al. 2004)

Table 2. Transgenic mutant SOD mouse models. Taken and modified from Turner and Talbot 2008
nd: not described; a Double transgenic for SOD1^{WT}. b Murine transgene.

However, even after 20 years of intensive research using the great spectrum of SOD1 rodent models, understanding of how SOD1 mutations lead to selective premature death of motor neurons remains vague (Lagier-Tourenne and Cleveland 2009; McGoldrick et al. 2013).

Because of the large number of mutations responsible for FALS and in some instances SALS, we had primarily focused on the description of pathology which is associated with mutant SOD1 as i) the SOD1 mutations were the first identified cause of FALS and thus the majority of ALS research was done in SOD1 animal models and ii) ALS research in our lab is mainly performed on SOD1^{G93A} transgenic rats. We also describe some other mutations with major contributions to FALS and SALS.

2.2.5. SOD1 mutations

11 missense mutations in the Cu⁺²/Zn⁺² superoxide dismutase 1 (SOD1) gene were first described in 1993 (Rosen et al. 1993). Mutations in this antioxidant gene are associated with about 20% of FALS (Boillee et al. 2006a). SOD1 is an enzyme composed of 153 amino acids, encoded by 5 exons and is involved in free radical scavenging, in which more than 150 different mutations (almost all dominant) have been reported to be pathogenic (Robberecht and Philips 2013). The mutations encompass all coding regions of the gene affecting over 70 positions with preponderance for exons 4 and 5. One zinc and two copper binding residues are targeted by the mutations, in addition to all four cysteines. Interestingly, glycine-93 appears particularly vulnerable, since it is point mutated to all six possible residues in FALS (Turner and Talbot 2008). Most are missense mutations, but a few truncation mutations at the very C-terminal part of the protein have been reported, suggesting that most of the molecule must be present for it to have its pathogenic effect (Robberecht and Philips 2013).

SOD1-linked FALS is clinically heterogeneous both within and between affected families, hampering efforts to correlate disease onset and severity with mutation. However, the most severe and prevalent mutation in America, A4V, reliably predicts short survival (Cudkowicz et al. 1997), while D90A, the most common SOD1 mutation worldwide and in the sporadic population, correlates with non-penetrant, recessive or slowly progressive disease (Andersen et al. 1995; Hand et al. 2001). Some SOD1 mutations do not cause ALS and carriers can remain asymptomatic throughout life, suggesting that not all SOD1 mutations cause ALS and some are rather polymorphisms (Turner and Talbot 2008).

2.2.5.1. SOD1 pathology

SOD1 is an ubiquitous homodimer which becomes misfolded when mutated and is primarily found in motor neurons and glial cells of the spinal cord (Pasinelli and Brown 2006; Nagai et al. 2007; Al-Chalabi et al. 2012). Its main physiological function is to protect cells from oxidative damage by metabolizing superoxide radicals (Gurney et al. 1994) but it also has additional enzymatic functions including peroxidation, nitration, copper buffering, phosphatase activation, zinc homeostasis, thioloxidation and immunomodulation (reviewed in (Turner and Talbot 2008).

Wild-type SOD1 that is oxidized also misfolds, it is aggregation-prone (Rakhit et al. 2002) and toxic to motor neurons (Ezzi et al. 2007) which suggest a role for wild-type SOD1 in SALS, possibly after secondary (oxidative) modification (Robberecht and Philips 2013).

Mutant SOD1 misfolds and is targeted for degradation through ubiquitination and seems to have toxic effects on the cell proteostasis machinery, impairing its two major components: the UPS and autophagy (Bendotti et al. 2012; Chen et al. 2012). Increase in autophagosomes has been detected in motor neurons in the spinal cord of patients with ALS and of rodent models (Morimoto et al. 2007; Sasaki 2011). Mutant SOD1 accumulates as oligomers and later as aggregates which are ubiquitinated, which lead to a stress response (Robberecht and Philips 2013) in both SALS and FALS (Rothstein 2009). Intracellular aggregates may mediate motor neuron degeneration through several mechanisms, including sequestration of essential cellular components (Bruijn et al. 1998), reduced chaperone activity (Bruening et al. 1999) and impaired capacity of the UPS (Niwa et al. 2002) (see Fig. 12 for SOD1 ALS pathogenesis). Furthermore, recent findings suggest that mutant misfolded SOD1 may trigger prion-like aggregation of normal wild-type SOD1 (Polymenidou and Cleveland 2011).

2.2.6. TDP-43 mutations

In 2006, 43 kDa TAR DNA-binding protein (TDP-43) was identified as a major component of ubiquitinated protein aggregates found in the in the cytoplasm and nucleus of both neurons and glial cells in many patients with sporadic ALS and/or FTLD (Arai et al. 2006; Neumann et al. 2006). Identification of dominant mutations in the TDP-43 coding gene TARDBP as a primary cause of ALS provided evidence that aberrant TDP-43 can directly cause neurodegeneration (Kabashi et al. 2008; Rutherford et al. 2008; Sreedharan et al. 2008; Van Deerlin et al. 2008; Yokoseki et al. 2008). All the mutations are dominant missense

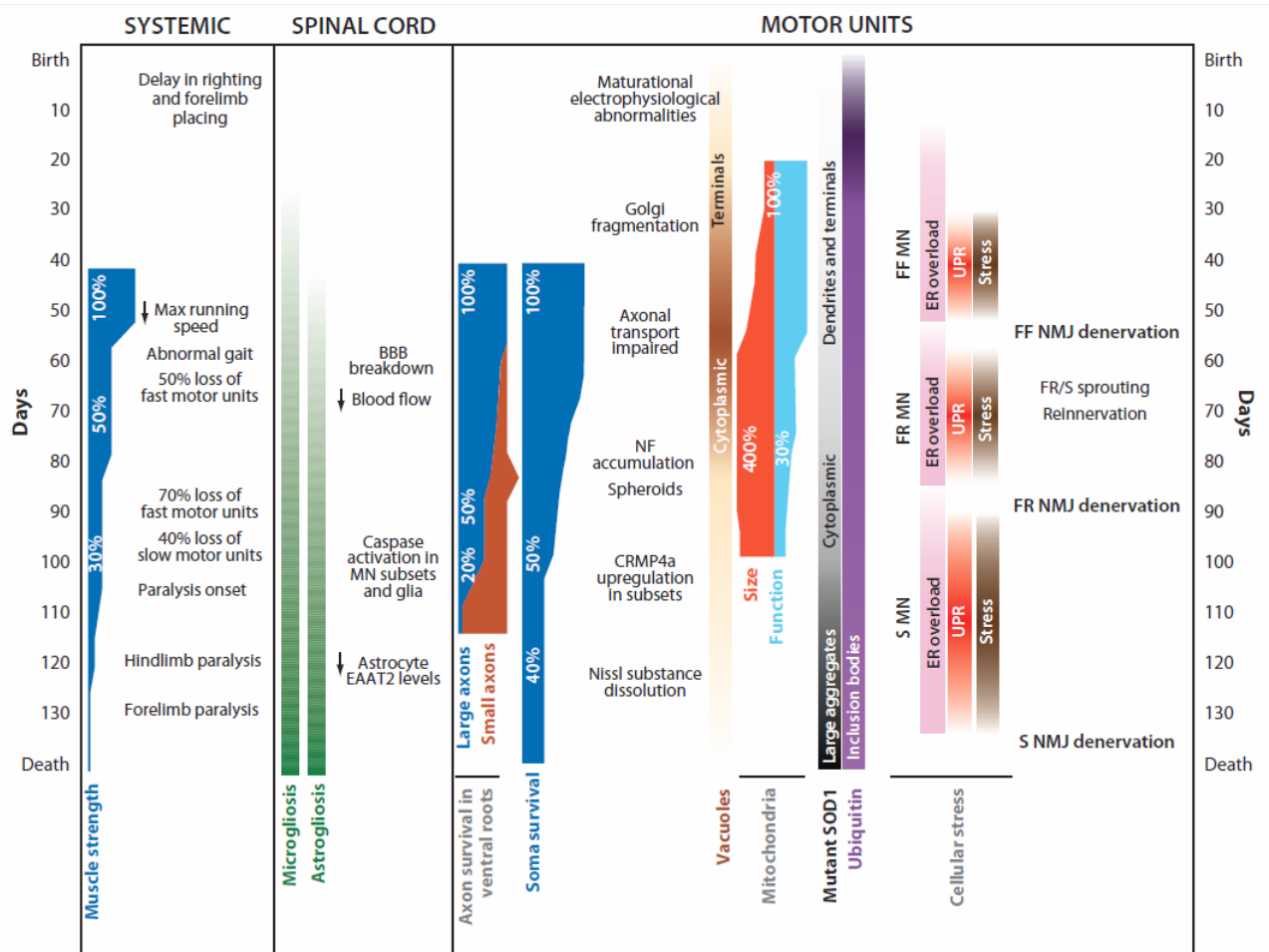


Fig. 11 Time course of neurodegeneration in the *SOD1^{G93A}* mouse model of amyotrophic lateral sclerosis (ALS). The diagram provides an overview of the complex ballet of cellular and molecular mechanisms that lead over six months to the death of this severe model of ALS. Many changes occur before muscle strength is reduced by half, including initial alterations in electrophysiology and behavior followed by ubiquitination and ER stress in susceptible FF motor neurons leading to axonal dieback and microgliosis and astrogliosis in the spinal cord. These are accompanied by subcellular changes such as Golgi fragmentation and mitochondrial swelling. During the following months, these changes become exacerbated and generalized to other motor units, leading to extensive motor neuron loss and muscle paralysis. Indicated stages (scale in days) represent those in the *G93A* high-expressor line. Some parameters have not been studied at earlier stages, so the indicated dates represent the latest possible onset. The overall layout progresses from systemic and behavioral changes on the left toward molecular and cellular changes in motor units on the right. Taken from Kanning et al. 2010.

changes with the exception of a truncating mutation at the extreme C-terminal of the protein (Y374X) (Daoud et al. 2009). Abnormal accumulation of hyperphosphorylated, ubiquitinated and N-terminally truncated TDP-43 missing their nuclear targeting domain is the pathological hallmark in most familial and sporadic forms of ALS and FTL-D-U (Neumann et al. 2009a).

As under normal conditions, TDP-32 is mainly localized within the nucleus, partial clearance of TDP-43 from the nuclei of neurons containing cytoplasmic aggregates suggest that the pathogenesis could be a result of loss of function of TDP43 (Lagier-Tourenne et al. 2010). TDP-43 inclusions are not restricted to motor neurons but can be widespread in brain in ALS patients with or without dementia (Geser et al. 2008; Van Deerlin et al. 2008; Yokoseki

et al. 2008) and interestingly, the composition of TDP-43 inclusions seems to differ between cortical brain and spinal cord in ALS patients (Igaz et al. 2008; Neumann et al. 2009a).

2.2.7. FUS/TLS mutations

Mutations in another RNA/DNA binding protein, FUS/TLS (fused in sarcoma/translocated in liposarcoma), were discovered 3 years later and were identified as a primary cause of familial ALS (Kwiatkowski et al. 2009; Vance et al. 2009). Most are missense mutations with a few exceptions (Belzil et al. 2009; Kwiatkowski et al. 2009; DeJesus-Hernandez et al. 2010). The inheritance pattern is dominant except for one recessive mutation (H517Q) (Kwiatkowski et al. 2009). The site and age of disease onset are variable within families and incomplete penetrance of several FUS/TLS mutations (Kwiatkowski et al. 2009; Blair et al. 2010; Groen et al. 2010; Hewitt et al. 2010) may help to explain the absence of family history in sporadic patients (Belzil et al. 2009; Corrado et al. 2010; Lai et al. 2011; Sproviero et al. 2012) as well as *de novo* mutations (Zou et al. 2013).

Similar to TDP43, FUS/TLS is mainly nuclear, with lower levels of cytoplasmic accumulation detected in most cell types (Andersson et al. 2008). Brains and spinal cord from patients with FUS/TLS mutations revealed abnormal FUS/TLS cytoplasmic inclusions in neurons and glial cells (Kwiatkowski et al. 2009; Vance et al. 2009; Tateishi et al. 2010) which are immunoreactive for FUS/TLS and ubiquitin but strikingly not for TDP-43 (Vance et al. 2009; Tateishi et al. 2010). FUS/TLS and ubiquitin positive and TDP-43 negative inclusions were later identified in different in FTLN and ALS patients (Munoz et al. 2009; Neumann et al. 2009b; Woulfe et al. 2010). FUS/TLS nuclear staining was occasionally reduced in neurons bearing cytoplasmic inclusions, but this pattern was less obvious than in TDP-43 proteinopathies (Vance et al. 2009; Tateishi et al. 2010).

TDP-43 and FUS/TLS mislocalizations and/or aggregations have now been observed in a large number of disorders, leading to a new nomenclature for such diseases: TDP-43 and FUS/TLS proteinopathies (Lagier-Tourenne et al. 2010). They are both structurally close to the family of heterogeneous ribonucleoproteins (hnRNPs) and have been involved in multiple levels of RNA processing including transcription, splicing, transport and translation (Lagier-Tourenne et al. 2010; Robberecht and Philips 2013).

2.2.8. C9ORF72 mutations

ALS-causing nucleotide repeat expansion mutations of the chromosome 9 open reading frame 72 (C9ORF72) were recently identified (DeJesus-Hernandez et al. 2011; Renton et al. 2011). C9ORF72 contains a GGGGCC hexanucleotide (G4C2) sequence that is located between two transcription initiation sites. In most normal individuals, the G4C2 sequence is repeated mostly two-to-five times. An abnormal expansion of this sequence is found in about 40% of families with ALS and in about 7% of patients with supposed SALS (Majounie et al. 2012; Mok et al. 2012). The length of the expanded repeat is still uncertain but may consist of several hundreds or even thousands of repeats. This expansion is also found in patients with FTLN without ALS (DeJesus-Hernandez et al. 2011; Renton et al. 2011; Majounie et al. 2012). The penetrance of the mutation is probably 50% around the age of 60 years and nearly

100% above the age of 80 years (Majounie et al. 2012). The normal function of the presumably cytoplasmic protein C9ORF72 is unknown (Robberecht and Philips 2013).

2.2.9. Pathological mechanisms in ALS

The pathogenic mechanisms in ALS are multifactorial and still not fully determined. As vast majority of the research conducted over the past 20 years was predominantly performed on the models expressing mutant SOD1, this short overview is accordingly focused on disease caused by mutant SOD1 (Fig. 12). Detailed time course of neurodegeneration in the SOD1^{G93A} mouse model is shown in Fig. 11.

2.2.9.1. Oxidative stress

Oxidative stress causes structural damage and changes in redox-sensitive signaling. It's caused by an imbalance between the generation and removal of reactive oxygen species (ROS), and/or by a reduction in the ability of the biological system to remove or repair ROS-induced damage. It was proposed that the mutant SOD1 toxicity is mediated by oxidative damage as mutation-induced structural changes in the mutant SOD1 protein could expose the active copper site to aberrant substrates (Beckman et al. 1993). The peroxidase hypothesis suggested that mutations in SOD1 catalyzed copper-mediated conversion of hydrogen peroxide to reactive hydroxyl radicals, promoting further oxidative damage (Wiedau-Pazos et al. 1996). Peroxynitrite was also supposed to be a substrate candidate for mutant SOD1 as increased levels of 3-nitrotyrosine, a marker for peroxynitrite-mediated oxidative damage, have been reported in SOD1 mice and in ALS patients (Beal et al. 1997; Bruijn et al. 1997a; Ferrante et al. 1997). Moreover, elevated levels of oxidative damage to proteins, lipids and DNA (Shaw et al. 1995; Fitzmaurice et al. 1996; Shibata et al. 2001) have been found in postmortem tissue from SALS and SOD1 FALS cases. Mutant SOD1 in microglia increases NADPH oxidase (NOX)-mediated superoxide resulting in prolongation of ROS production (Harraz et al. 2008). NOX2 expression is increased in mutant SOD1 mice and in the CNS of patients with ALS, and survival of SOD1^{G93A} mice is extended by knockout of *Nox1* or *Nox2* (Wu et al. 2006; Marden et al. 2007; Carter et al. 2009).

2.2.9.2. Mitochondrial dysfunction

Mitochondria have a central role in intracellular energy production, calcium homeostasis and control of apoptosis. Defective respiratory chain function associated with oxidative damage to mitochondrial proteins and lipids has been found in tissue from patients with ALS and in mutant SOD1 models (Mattiazzi et al. 2002; Wiedemann et al. 2002). In SOD1 mice, the mutant protein aggregates in vacuoles in the mitochondrial intermembrane space (Wong et al. 1995) and it has been shown that calcium buffering is impaired in mitochondria purified from the CNS (Damiano et al. 2006). Furthermore, mutant SOD1 mitochondrial morphology has been observed in skeletal muscle and spinal motor neurons from patients with ALS (Sasaki and Iwata 2007). Axonal transport of mitochondria is impaired in experimental models of ALS which most likely leads to dying back axonopathy in ALS (De Vos et al. 2008). As

creatine in SOD1^{G93A} mice delayed the onset of motor deficits and increased survival of motor neurons (Klivenyi et al. 1999), dysregulated energy metabolism is likely to contribute to motor neuron dysfunction in ALS. Involvement of mitochondria in apoptotic pathway is described below.

2.2.9.3. Apoptosis

It has been shown that the programmed cell death in mutant SOD1 ALS mouse models is executed via the intrinsic (mitochondrial) apoptotic pathway (Mu et al. 1996; Ekegren et al. 1999; Martin 1999; Vukosavic et al. 1999; Guegan et al. 2001). The extrinsic pathway is also involved as it crosstalk with the intrinsic pathway through the proteolysis of the BID (BH-3 only protein BCL-2 family protein) and this proteolysis is initially mediated by caspase-1 and not by caspase-8 (Guegan et al. 2002). The FADD/caspase-8 pathway is indeed involved in Fas-triggered motoneuron death, since cell death can be prevented by the caspase-8 inhibitor peptide IETD and considerably reduced by overexpression of a dominant-negative form of FADD (Raoul et al. 2002). Moreover, another novel Fas/Daxx/Ask/p38/nNOS pathway, which probably plays important role in the SOD1 ALS apoptotic induced death of α -motoneurons, was discovered (Raoul et al. 2002; Wengenack et al. 2004). mSOD1 astrocytes from the mouse ALS models and astrocytes from familial and sporadic ALS patients are toxic to motoneurons (Nagai et al. 2007; Haidet-Phillips et al. 2011) and this effect is in part mediated by soluble toxic factor(s) through a BAX-dependent mechanism (Nagai et al. 2007).

Genetic experiments demonstrated that i) overexpression of the Bcl-2 (BCL-2 family protein) showed therapeutic effect in mouse mSOD1 ALS models by delaying the onset of the disease and prolonging the lifespan (Kostic et al. 1997; Vukosavic et al. 2000); ii) deletion of PUMA (BH-3 only BCL-2 family protein) delayed motoneuron degeneration and disease progression in a mouse SOD1 ALS model (Kieran et al. 2007); iii) deletion of the BAX alone in the mouse SOD1 ALS model prolongs animal survival, blocks α -motoneuron degeneration and reactive gliosis and delays neuromuscular denervation (Gould et al. 2006) and that iv) combined BAX and BAK deletion halts neuronal loss, prevents axonal degeneration, symptom onset, weight loss, and paralysis and extends survival by approximately 21% in the mouse SOD1 ALS model (Reyes et al. 2010). Therefore, proteins upstream to caspases represent potential therapeutic targets.

2.2.9.4. Glutamate excitotoxicity

Glutamate is the main excitatory neurotransmitter in the CNS. Excitotoxicity, the neuronal injury resulting from excessive activation of glutamate receptors, may be caused by increased synaptic levels of glutamate, or by increased sensitivity of the postsynaptic neuron to glutamate, resulting from alterations in neuronal energy homeostasis or glutamate receptor expression (Van Damme et al. 2005). Disruption of intracellular calcium homeostasis, with secondary activation of proteolytic and ROS-generating enzyme systems, perturbation of mitochondrial function and ATP production are the key components of excitotoxicity (Arundine and Tymianski 2003). Several other findings in the mSOD1 model also point towards a role for excitotoxicity in ALS pathology, including altered electrophysiological

properties and increased sensitivity of motor neurons to excitotoxicity (Meehan et al. 2010), altered AMPA receptor subunit expression, reduced expression and activity of EAAT2 (Howland et al. 2002; Boston-Howes et al. 2006) and increased glutamate efflux from spinal cord nerve terminals (Milanese et al. 2011). Ameliorating excitotoxicity by the drug riluzole, which has several effects including inhibition of presynaptic glutamate release, is the only strategy that has so far slowed disease progression in ALS (Bensimon et al. 1994; Lacomblez et al. 1996a; Lacomblez et al. 1996b; Cheah et al. 2010).

2.2.9.5. Protein aggregation

As we have described before, mutations in several genes in ALS (mainly in SOD1, TDP-43 and FUS coding genes) lead to expression of misfolded proteins which aggregate and are most of the times polyubiquitinated and thus form distinctive inclusions in the ALS brain and spinal cord. Proteins found in aggregates in ALS provide several important clues about the disease pathogenesis. Loss of nuclear TDP-43 and/or aggregation of the protein in cytoplasmic inclusions may be key pathogenic processes in both SALS and FALS (Robberecht and Philips 2013). The neurofilamentous pathology suggests that neurofilament dysfunction is important in some forms of ALS. The increase in phosphorylated neurofilament epitopes in motor neuron perikarya may contribute to the observed slowing of axonal neurofilament transport (Ackerley et al. 2003).

2.2.9.6. Neuroinflammation

Activated microglia and infiltrating lymphocytes indicate an inflammatory component in the CNS pathology of ALS (Henkel et al. 2004). Proinflammatory mediators including monocyte chemoattractant protein 1 and IL-8126 are present in the CSF of patients with ALS, and biochemical indicators of immune-response activation are present in the blood (Mantovani et al. 2009). In ALS there is a complex interplay between microglia and T cells that modify the rate of disease progression in a way that is not seen in other neurodegenerative disorders (Lewis et al. 2012; Gentleman 2013). Reduced counts of CD4+CD25+ regulatory T (TREG) cells and monocytes (CD14+ cells) are detected early in ALS, suggesting recruitment of these cells to the CNS early in the neurodegenerative process. TREG cells interact with microglia, attenuating neuroinflammation by stimulating secretion of anti-inflammatory cytokines (Kipnis et al. 2004). Correspondingly, microglia isolated from the mutant SOD1 mouse had a neuroprotective phenotype at disease onset whereas those isolated from end-stage disease animals had a classical neuroinflammatory phenotype (Liao et al. 2012). Astrocyte activation plays a central part in inflammation, and mutant SOD1 astrocytes secrete inflammatory mediators, including prostaglandin E2, leukotriene B4, and nitric oxide under both basal and activated conditions (Hensley et al. 2006).

2.2.9.7. Endoplasmic reticulum stress

It is believed that some misfolded proteins, such as mutant SOD1, are sent to the endoplasmic reticulum (ER), even though they lack the proper signal peptide for the

translocation. The excess of misfolded proteins in the ER may cause an ER-associated protein degradation response, which leads to ER-stress. This stress, in turn, may activate ER stress-related cell death signaling pathways, including apoptosis (Kikuchi et al., 2006). Consistent with these findings, an up-regulation of ER stress-related genes in vulnerable motor neurons of presymptomatic transgenic mutant SOD1 mice has been found (Saxena et al., 2009).

2.2.9.8. Impaired axonal transport

Neurofilaments are the most abundant cytoskeletal proteins in motor neurons and play a key role in stimulating axonal growth and in determining axonal diameter (Rothstein 2009). Aberrant accumulation of neurofilaments in the cell body and proximal axons of motor neurons is described as a hallmark of ALS (Xu et al. 1993). Importantly, neurofilament accumulation was increased in motor neuron cell bodies and decreased in axons. Thus, perikaryal accumulation of neurofilaments may counterbalance mutant SOD1 toxicity by buffering against damaging intracellular events, such as excessive calcium levels (Couillard-Despres et al. 1998) or hyperphosphorylation of neuronal substrates by cyclin-dependent kinase 5 (Nguyen et al. 2001).

2.2.9.9. Glial Cell Pathology

Growing number of studies support the hypothesis that selective degeneration of motor neurons in ALS is not a cell-autonomous process (Di Giorgio et al. 2007; Nagai et al. 2007; Di Giorgio et al. 2008; Marchetto et al. 2008; Ferraiuolo et al. 2011; Robberecht and Philips 2013). First, defects in astroglia-specific glutamate transporters were identified in a large percentage of sporadic ALS patients (Rothstein et al. 1995) and later in all SOD1 rodent models (Howland et al. 2002). Astrocytic inclusions are early indicators of SOD1 mutant toxicity, preceding symptom onset and increasing with disease progression (Bruijn et al. 1997b). Mutant SOD1 astrocytes from the mouse ALS models and astrocytes from familial and sporadic ALS patients are toxic to motoneurons (Nagai et al. 2007; Haidet-Phillips et al. 2011) and removal of mutant SOD1 protein from astrocytes markedly delayed disease progression (Yamanaka et al. 2008a), indicating that non-neuronal cells are major contributors to disease progression (Rothstein 2009).

Damage within more than one cell type appears to be required, because restricted expression of mutant SOD1 in astrocytes (Gong et al. 2000) or motor neurons (Pramatarova et al. 2001) alone failed to induce motor deficits in SOD1 mice. Interestingly, when the expression of mutant SOD1 was active in all neurons, the ALS symptoms developed in the neuron specific SOD1 mouse (Jaarsma et al. 2008). The involvement of multiple cell types in ALS pathogenesis is supported by analysis of chimeric mice made of mixtures of wild-type and SOD1 mutant expressing cells (Boillee et al. 2006b; Julien 2007; Yamanaka et al. 2008a; Yamanaka et al. 2008b). In addition, Schwann cells were also shown to be involved (Lobsiger et al. 2009) and recent data about oligodendrocyte dysfunction in ALS (Kang et al. 2013; Philips et al. 2013) just underlined that the ALS is complex and systemic disease affecting every single cell type in the CNS and beyond.

2.2.9.10. Dysregulated transcription and RNA processing

TDP-43 and FUS/TLS are genes that encode RNA processing proteins (Lagier-Tourenne and Cleveland 2009; Vance et al. 2009; Lagier-Tourenne et al. 2010). Patients with the FUS/TLS mutations have cytoplasmic inclusions containing FUS/TLS but not TDP-43 (Robberecht and Philips 2013). Although TDP-43 inclusions are not observed in FUS mutant cases, FUS is an RNA-binding protein that is found in complexes together with TDP-43, and ALS-associated TARDBP mutations promote the interaction between TDP43 and FUS (Ling et al. 2010). TDP-43 and FUS/TLS have striking structural and functional similarities, implicating alterations in processing of RNA and microRNA as a key event in ALS pathogenesis, although the underlying functional mechanisms remain unknown (Lagier-Tourenne et al. 2010; Nefussy 2013). It has been recently shown that abundance of only 45 RNAs is reduced after depletion of either TDP-43 or FUS/TLS from mouse brain, but that among these are mRNAs that were transcribed from genes with exceptionally long introns and that encode proteins that are essential for neuronal integrity. Expression levels of a subset of these were lowered after TDP-43 or FUS/TLS depletion in stem cell-derived human neurons and in TDP-43 aggregate-containing motor neurons in sporadic ALS, supporting a common loss-of-function pathway as one component underlying motor neuron death from misregulation of TDP-43 or FUS/TLS (Lagier-Tourenne et al. 2012). Furthermore, another ALS causing mutation, the hexanucleotide repeat expansion of the gene C9ORF72, leads to the loss of one alternatively spliced C9ORF72 transcript and to the formation of nuclear RNA foci (DeJesus-Hernandez et al. 2011).

2.2.10. Therapies in ALS

The current management of ALS is based on the recognition of the importance of multidisciplinary care (Nefussy 2013). Regrettably, even after more than a century of ALS research and a great number of experimental therapies tested on rodent models (Turner and Talbot 2008; McGoldrick et al. 2013), there is no cure for the disease (Nefussy 2013; Robberecht and Philips 2013). However, many of the symptoms that develop during the course of the disease are treatable and the improvement in symptomatic care of the patients during the last decade led to an improved rate of survival (Qureshi et al. 2009). Symptomatic treatment is mainly focused on respiratory management by either invasive or noninvasive ventilator support (Bourke et al. 2006; Heffernan et al. 2006) or by diaphragm pacing in ALS patients who still have some preservation of diaphragm muscle fibers (Onders et al. 2009). Nutritional management is also very important in management of ALS and early initiation of enteral tube feeding stabilizes body weight and can improve survival (Miller et al. 2009). Recognition of the role of glutamate excitotoxicity in sporadic disease and in animal models led to the development of riluzole, the only treatment to date that has been shown to ameliorate the course of sporadic ALS (Bensimon et al. 1994; Lacomblez et al. 1996a; Lacomblez et al. 1996b).

2.2.10.1. Neural Stem cell therapy in ALS

As mentioned earlier, there is good evidence that the ALS motoneuron pathology could be triggered by a non-cell autonomous process. Problems with glutamate excitotoxicity and astrocyte mediated toxicity together with obviously challenging replacement of host neurons, neural stem cells, particularly astrocytes precursors, appear to be the ideal source for cell-replacement therapies in ALS.

Accordingly, recent *in vivo* spinal cell grafting data provided evidence that local segmental enrichment with wild-type neural or astrocyte precursors leads to a certain degree of neuroprotection. Focal enrichment of normal astrocytes, by transplantation of fetal rat spinal cord-derived lineage-restricted astrocyte precursors, produced significant benefit in a rat SOD1^{G93A} ALS model (Lepore et al. 2008). It was hypothesized that neuroprotection was mediated in part by the primary astrocyte glutamate transporter EAAT2 (GLT1 in rodents) which was over-expressed in grafted cells (Lepore et al. 2008). Using lumbar spinal grafting of human spinal neural stem cells (HSSCs), Xu et al. (2006) previously reported significantly higher number of persisting lumbar α -motoneurons found in treated animals (Xu et al. 2006). More recently, Xu et al. (2011) reported a lifespan extension of SOD1^{G93A} rats by 17 days after dual cervical (C4–C5) and lumbar (L4–L5) transplantation of HSSCs (Xu et al. 2009) and finally, our own HSSCs cell replacement studies in the same ALS rat model confirmed the therapeutic potential of this approach (Hefferan et al. 2012). Just very recently, 1st phase of ALS clinical trial with the same neural stem cells used in previous pre-clinical studies (Xu et al. 2009; Hefferan et al. 2012), was successfully completed (Glass et al. 2012).

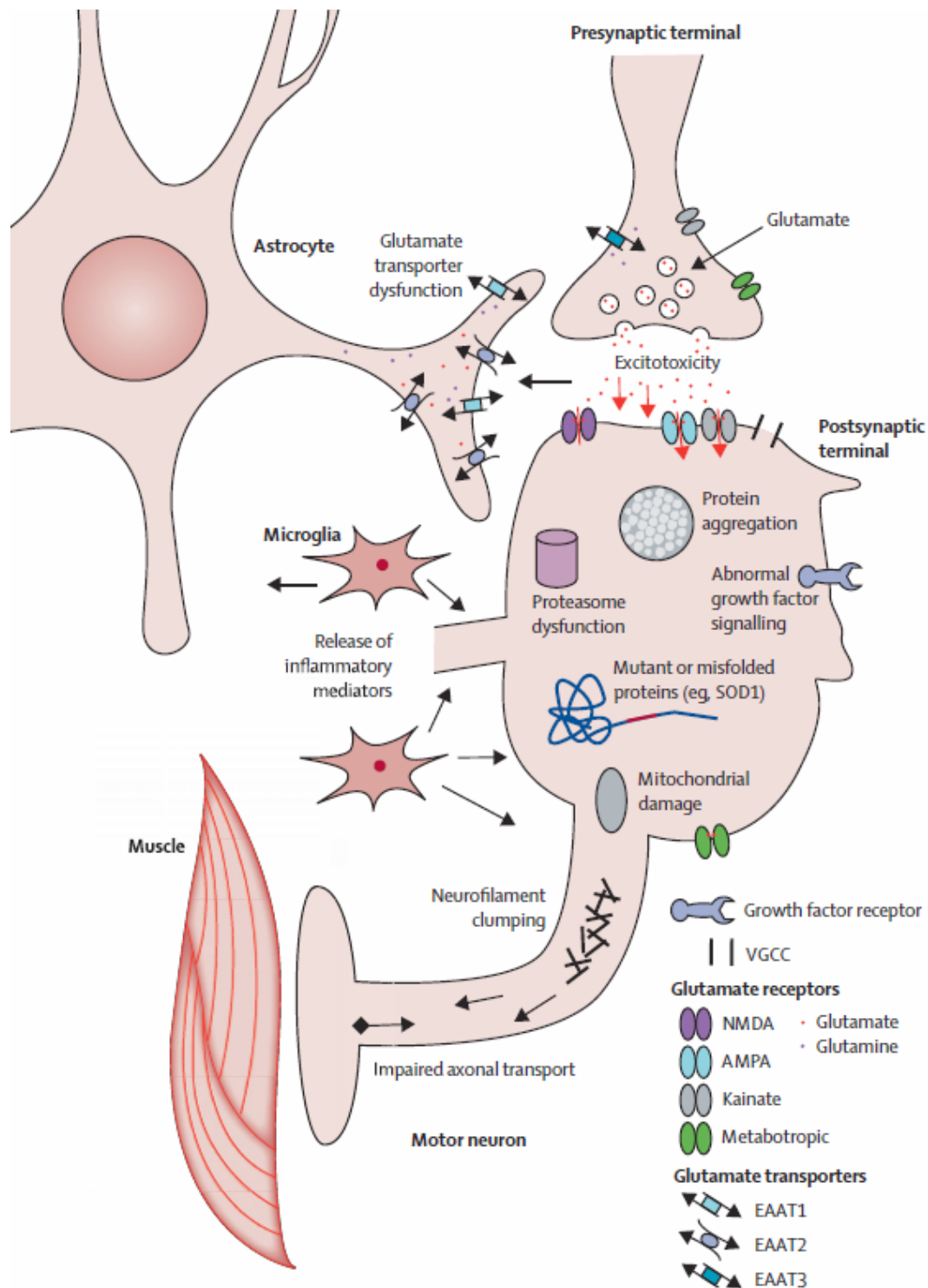


Fig. 12 The main current concepts in the pathogenesis of amyotrophic lateral sclerosis (SOD1 related). The main pathogenic mechanisms occur in the motor neurons, at the neuromuscular junction, and in surrounding cells. Themes include glutamate-mediated excitotoxicity through upstream neuronal stimulation, possibly modulated by neighbouring astrocytes. In addition, there is evidence of protein misaggregation and mitochondrial dysfunction within the motor neuron cell body. Downstream axonal transport might be primarily impaired, ultimately leading to a loss of neuromuscular connectivity and muscle atrophy. External neuroinflammatory (microglial) processes can be secondary, in response to motor neuron injury, or can have a primary pathogenic role. EAAT=excitatory amino acid transporter. SOD1=superoxide dismutase. VGCC=voltage-gated calcium channel. Taken from (Turner et al. 2009).

2.3. (NEURAL) STEM CELL THERAPY IN SPINAL CORD INJURY

2.3.1. Spinal cord injury

Spinal cord injury (SCI) and the consequent disabilities represent a great burden to the affected patients, their family, medical system and to society as whole. Neurological deficits after the injury are often life-long and are associated with severe disabilities.

Reported worldwide traumatic SCI annual incidence rates are between 8 to 59 cases per million, with motor vehicle collisions (MVC), falls, violence and sports activities as a leading causes (Lin and Bono 2010; Sahni and Kessler 2010; van den Berg et al. 2010; Devivo 2012). The most recent report estimate that in 2007, the world-wide incidence was about 23 traumatic SCI cases per million (Lee et al. 2013). These data, however, substantially underestimate the prevalence and societal impact of SCI as a 2004 study sponsored by the Christopher and Dana reeve Foundation revealed that 1,275,000 people in the US have some form of SCI with costs to the health system estimated to be US\$40.5 billion annually (Sahni and Kessler 2010). The notably higher incidence in the USA (25-59 cases depending on the sate) compared to Europe can be explained by very high rate of injuries caused by the act of violence in the USA (total 24.1% of SCI in the USA) while in other counties injuries caused by violence are rare (Lin and Bono 2010). The age distribution in traumatic SCI is bimodal with a first peak for young adults attributable to MVC, and a second peak in elderly people aged 65 and older that can be mainly credited to falls (Lin and Bono 2010; van den Berg et al. 2010; Devivo 2012). According to the 2002 report of WHO, number of SCI caused by MVC is progressively rising and the cost of head and spinal cord injury is by far the largest (medical cost including post injury care), exceeding the combined cost per unit of all other injuries, including fatalities (WHO 2002).

Clinical and experimental data on SCI show that the damage to the spinal cord which results in clinically defined loss of neurological function can be in general divided into two categories. Pathology and corresponding functional loss directly caused by the mechanical injury of axons and neurons at the site of injury fall into the first category, whereas the other category represents secondary changes induced by the injury (local edema, hematoma, ischemia, excitotoxicity, inflammation, demyelation and secondary axonal degeneration and dieback) which can develop over hours to weeks after the initial damage of the cord (for detailed review see (Hagg and Oudega 2006).

Direct traumatic impact to the spinal cord causes immediate death of cells in the vicinity of the injury site and includes neurons, astrocytes, oligodendrocytes and endothelial cells. Stretching of axons can cause membrane damage and may later contribute to progressive axon degeneration followed by dieback of the neurons (Shi and Pryor 2002). Soon after the injury, damage to local blood vessels results in hemorrhage and within few hours, injury site is massively infiltrated by neutrophils which together with hemorrhage lead to edema (Maier and Schwab 2006; Yoon and Tuszynski 2012). Cells at the injury site continue to die and increase level of glutamate which contributes to excitotoxicity (Park et al. 2004) as well as the increase of free radicals (Hagg and Oudega 2006). Local and distal microglia becomes activated (Emery et al. 1998; Nakamura et al. 2003; Hagg and Oudega 2006; Yoon and Tuszynski 2012)

and oligodendrocytes further die in apoptosis (Crowe et al. 1997; Casha et al. 2001). During the first week, monocytes, macrophages, and T-lymphocytes start to invade the damaged area and their accumulation worsens necrotic events (Popovich et al. 1997; Popovich 2000; Bareyre and Schwab 2003).

Scar consisting of type A pericytes-derived stromal cells (fibroblasts) (Goritz et al. 2011), surviving proliferating astrocytes as well as new ependymal-derived astrocytes (Meletis et al. 2008; Barnabe-Heider et al. 2010) is formed at the injury/impact site (Goritz et al. 2011) and the progressive loss of the tissue leads to formation of fluid-filled cysts (syringomyelia) (Fitch et al. 1999; Hagg and Oudega 2006; Yoon and Tuszynski 2012) (see Fig. 8). Wide spread secondary damage to the spinal cord further continues for months or even years (Hagg and Oudega 2006) and includes apoptotic death of the cells close and distant to injury (Emery et al. 1998), including oligodendrocytes (Crowe et al. 1997; Casha et al. 2001), which leads to demyelination resulting in axonal degeneration and dieback of the neurons (Kim et al. 2007; Meletis et al. 2008; Barnabe-Heider et al. 2010) which then ultimately leads to progressive atrophy of the spinal cord and formation of new and expansion of fluid-filled cysts (Hagg and Oudega 2006). Scar at the impact site remains present and its residing reactive astrocytes express extracellular axonal growth-inhibitory proteoglycans which limits potential plasticity (Morgenstern et al. 2002; Rhodes and Fawcett 2004; Maier and Schwab 2006; Meletis et al. 2008). However, astrocytes shield the intact tissue from further damage and limit the infiltration of inflammatory cells and further demyelination (Faulkner et al. 2004). Thus, the large number of astrocytes at the injury site appears important to limit and restrain the inflammatory response, but this may be at the expense of axonal regrowth (Barnabe-Heider et al. 2010) (see Fig. 8). Neurological function later spontaneously recovers as a result of plasticity (Rosenzweig et al. 2010) and proliferation of ependymal-derived oligodendrocytes leading to remyelination (Meletis et al. 2008; Sabelstrom et al. 2013) to a level that depends on the severity of the injury.

2.3.2. SCI therapy

Based on the current knowledge of the neuropathological mechanisms behind the neurological dysfunction in SCI patients, the current experimental and clinical treatment strategies are focused on: i) improvement of local metabolism and blood flow (e.g., through decompression therapy and hypothermia (both regional and systemic) (Batchelor et al. 2010; Cappuccino et al. 2010; Dietrich et al. 2011a; Dietrich et al. 2011b; Dietrich 2012; Jones et al. 2012; Oudega 2012), and ii) modulation of local inflammatory response (e.g., with methylprednisolone) (Fleming et al. 2006; Ankeny and Popovich 2009; Cappuccino et al. 2010; David and Kroner 2011; Bracken 2012). These two strategies are commonly used in the clinics and showed more or less positive results (Hawryluk et al. 2008; Dietrich et al. 2011b).

The other two therapeutic strategies are still mostly experimental with several clinical trials already performed and are aimed at improving the local neurotropic activity at and around the injury epicenter with the primary goal of increasing the survival of partially injured axons and/or neurons (Kim et al. 2007; Sahni and Kessler 2010; Yoon and Tuszynski 2012). These treatment strategies include iii) therapy based on the use of locally delivered trophic

factors (such as BDNF-, GDNF-, and FGF-peptides or growth factors-gene-encoding vectors) which can be combined or comes together with iv) fetal or embryonic stem cell-derived neuronal and/or glial precursors (Llado et al. 2004; Cao et al. 2005; Lu and Tuszynski 2008; Sahni and Kessler 2010; Yoon and Tuszynski 2012).

2.3.2.1. (Neural) Stem cell therapy in SCI

Therapeutic strategies involving transplantation of stem cells after SCI focus on the replacement of lost or damaged cells (mainly neurons and oligodendrocytes), provision of trophic support for neurons, or manipulation of the environment within the damaged spinal cord (trophic factors, prevention of scar and cyst formation) to facilitate axon regeneration. It is clear that this task is extremely challenging but, especially in the case of spinal cord, is of extreme importance as unlike other regions in the adult mammalian nervous system, the spinal cord does not possess a neurogenic niche (Kim et al. 2007; Sahni and Kessler 2010) and/or is not favorable for neural differentiation of ependymal-derived endogenous progenitors (Sabelstrom et al. 2013).

In addition, the use of neuronal precursors for spinal grafting which leads to development of functional synapses between grafted neurons and the neurons of the host can serve to create a functional “relay” system throughout the injured spinal cord region as it has been demonstrated that acute grafting of fetal rat spinal cord-derived neuronal and glial-restricted precursors into a site of cervical dorsal column lesion leads to formation of functional ascending spinal relays *in vivo* (White et al. 2010; Bonner et al. 2011). Consistent with histologically and electrophysiologically validated maturation and functional incorporation of grafted neural cells in previously trauma-injured or chemically-lesioned spinal cord, a beneficial behavioral effect was also noted in several experimental studies. Acute spinal grafting of mouse neural precursors into the epicenter of L2 spinal cord compression injury improved hind-limb motor and sensory function in mice (Boido et al. 2011).

Similarly, acutely grafted human embryonic stem cell-derived oligodendrocyte (hES-OPCs) progenitors and/or motoneuron progenitors into a complete thoracic transection model resulted in partial restoration of hind-limb locomotor function and motor evoked potentials in rats (Erceg et al. 2010). hES-OPCs were successfully used in numerous studies of contusion injured rats (Faulkner and Keirstead 2005; Keirstead et al. 2005; Cloutier et al. 2006; Sharp et al. 2010; All et al. 2012). Acutely (2 hours) (All et al. 2012) or early after SCI (7days) (Faulkner and Keirstead 2005; Keirstead et al. 2005; Cloutier et al. 2006; Sharp et al. 2010) transplanted hES-OPCs survived, extensively migrated and led to robust remyelination (Cloutier et al. 2006) of surviving axons which resulted in significant improvement in locomotor function (Faulkner and Keirstead 2005; Keirstead et al. 2005; Sharp et al. 2010; All et al. 2012) whereas if transplanted 10 months after the injury, hES-OPCs survived and integrated into the host tissue but the cells failed to remyelinate spared axons and accordingly did not show any locomotor improvement (Faulkner and Keirstead 2005) suggesting that early cell grafting after the SCI is crucial. Another study demonstrated the potential of human astrocytes in a rat model of unilateral transections of the right-side dorso-lateral funiculus where transplanted human astrocytes (generated from human fetal glial precursor cells)

provided extensive benefit, including robust protection of spinal cord neurons, increased support of axon growth and locomotor recovery and also demonstrated the importance of astrocyte subpopulations (Davies et al. 2011).

Human neural stem cells isolated from fetal brains grown as neurospheres (hCNS-SCns) (Cummings et al. 2005; Salazar et al. 2010) were transplanted into the injury site of contusion injured mice 7 days (Cummings et al. 2005) or 30 days post SCI (Salazar et al. 2010) and exhibited long-term engraftment, migration, limited proliferation, and differentiation predominantly to oligodendrocytes and neurons and provided remyelination and locomotor recovery in both cases (Cummings et al. 2005; Salazar et al. 2010). Non-human primates with contusive SCI grafted with human fetal spinal cord-derived neural stem/progenitor cells (NSPCs) cultured as neurospheres survived in the host and differentiated into neurons, astrocytes, and oligodendrocytes, and partially filled cavities. Moreover, the bar grip power and the spontaneous motor activity of the transplanted animals were significantly higher than those of sham-operated control animals (Iwanami et al. 2005).

In our transplantational studies in SCI, we have extensively characterized the *in vivo* therapeutic effect after spinal grafting of cGMP-grade human fetal spinal cord-derived stem cells grown in monolayer (NSI-566RSCs line) using a rat spinal ischemia model and rat L3 compression injury model. We have shown that: i) grafting of NSI-566RSCs into lumbar spinal cord of adult Sprague-Dawley (SD) rats with previous spinal ischemic injury is associated with a progressive improvement of ambulatory function which correlates with long-term grafted cell survival and extensive neuronal differentiation (Cizkova et al. 2007) and ii) grafting of the same human GMP-grade fetal spinal stem cells (NSI-566RSCs) in immunosuppressed SD rats with L3 compression injury provided functionally-defined treatment effect. This treatment effect was expressed as a significant improvement in motor and sensory function (gait/paw placement, stretch-induced spinal hyperreflexia, and, mechanical and thermal sensitivity). In addition, an effective filling of trauma-induced spinal cavity with grafted cells was seen in HSSC-treated animals at 2 months after grafting (van Gorp et al. 2013 in press) (Fig. 8 B, C and Fig. 17). Using the same cell line, we have also demonstrated the optimal dosing protocol and safety after grafting into the lumbar spinal cord of immunosuppressed minipigs (Usvald et al. 2010). The dosing design defined in this pre-clinical minipig study was then subsequently used in a recently completed Phase I human clinical trial in ALS patients receiving lumbar and cervical grafts of NSI-566RSCs (Glass et al. 2012). In a recent study using an immunodeficient rat model of complete spinal cord Th3 transection, it was shown that NSI-566RSCs or rat embryonic neural precursor cells, embedded in a fibrin matrix with trophic factors and grafted one week after injury, were able to form functional relays. The formation of functional relays was validated behaviorally (BBB locomotor score), electrophysiologically (spinal cord evoked potentials), and histologically (host on graft and graft on host synapses) (Lu et al. 2012). Together, these data demonstrate that the use of this clinical grade NSI-566RSC cell line with already established favorable clinical safety profile represent a potential cell candidate for cell replacement therapy in patients with previous SCI. Furthermore, based on these results (Cizkova et al. 2007; Usvald et al. 2010; Lu et al. 2012) (van Gorp et al. 2013 in press), FDA recently approved clinical trial where NSI-566RSC cell line will be tested in chronic SCI (NIH 2013).

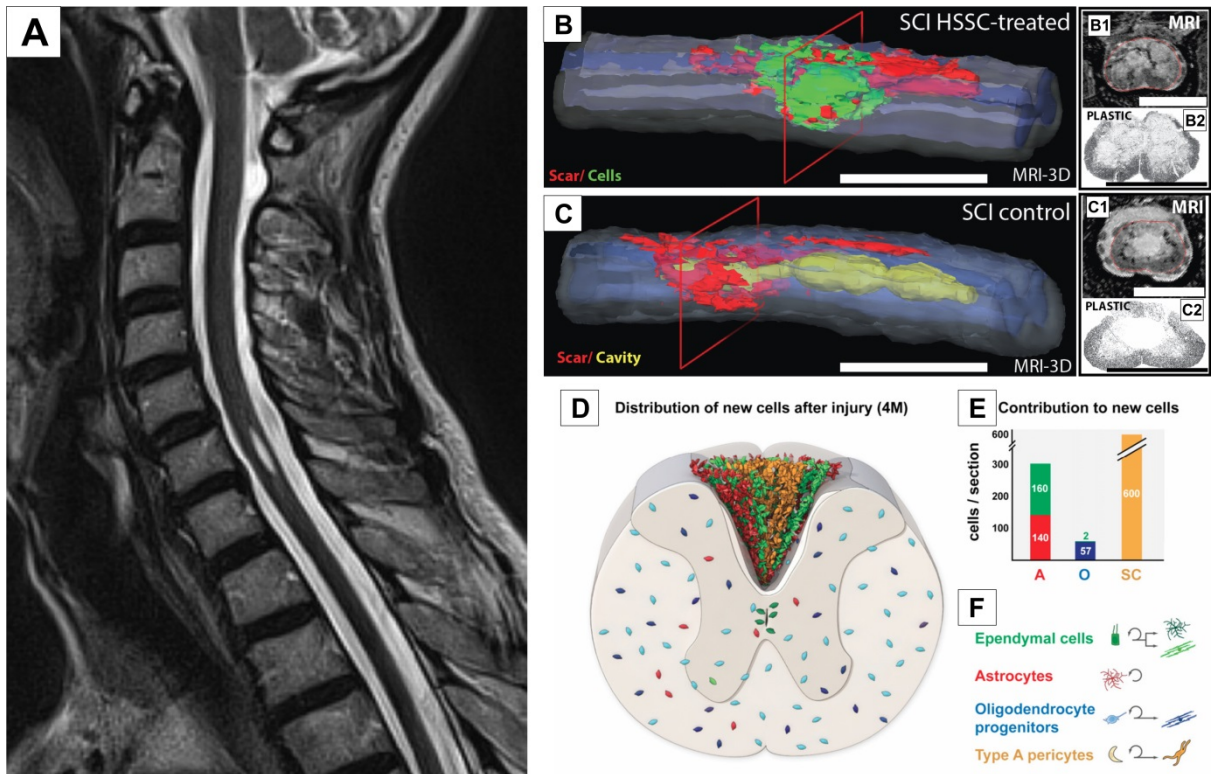


Fig. 8 Spinal cord injury, endogenous stem cell proliferation, scar and cyst formation. A) Syringomyelia in human patient as seen by MRI (arrow) (Fellner et al. 2010). B) 3D MRI reconstruction of the HSSCs grafted rat spinal cord with previous L3 contusion injury and (C) control SCI rat injected with media only clearly demonstrate the potential of the grafted neural stem cells in filling up the cavity and preventing the scar formation. (D–F) Distribution of the injury-induced generation of progeny from ependymal cells (green), astrocytes (red), oligodendrocyte progenitors (blue), type A pericytes (orange), and their progeny 4 months after a dorsal funiculus incision (A). B) Origin of new astrocytes (A), oligodendrocytes (O) and stromal cells (SC) 4 months after injury. Colors of the bars indicate cell fate according to the color scheme in (C). C) Schematic depiction showing the fate of ependymal cells, astrocytes, oligodendrocyte progenitors, and type A pericytes in the injured spinal cord. A) Taken from Fellner et al. 2010, B and C is Fig. 4 A-B from author's publication *Amelioration of motor/sensory dysfunction and spasticity in a rat model of acute lumbar spinal cord injury by human neural stem cell transplantation*. (D-F) Taken from Sabelström et al. 2013.

2.4. IMMUNOSUPPRESSION IN SPINAL CORD STEM CELL TRANSPLANTATION EXPERIMENTS

As we have stated before, transplantation of neural stem cells into the injured and/or diseased spinal cord may lead to the replacement of lost or damaged cells (mainly neurons and oligodendrocytes), provision of trophic support for neurons, or manipulation of the environment within the damaged spinal cord to facilitate axon regeneration, which, in the case of spinal cord, is extremely important as the spinal cord does not possess a neurogenic niche (Kim et al. 2007; Sahni and Kessler 2010) and/or is not favorable for neural differentiation of ependymal-derived endogenous progenitors (Sabelstrom et al. 2013). However, in order to achieve sufficient differentiation and demonstrate promising therapeutic potential, extended graft survival (4-6+ weeks) is necessary (Kakinohana et al. 2012b). Numerous previous experimental animal and clinical data showed that xenogeneic neural grafts are rapidly rejected (via lymphocyte infiltration of the graft) in non-immunosuppressed animals and/or human patients (Deacon et al. 1997; Barker et al. 2000; Brevig et al. 2000) which clearly demonstrated that the immunosuppression in xenogeneic neural grafts is essential.

Extended graft survival involves the use of immunosuppressants to effectively block the host's acquired immune response to allogeneic or xenogeneic cell grafts. Existing clinical and experimental immunosuppression protocols normally use single or combination of immunosuppressants delivered orally (especially in humans), intraperitoneally, intravenously or subcutaneously in a single or multiple daily doses (reviewed in (MacGregor and Bradley 1995; Halloran 1996; Wentz et al. 2006; Barraclough et al. 2011).

Clinical grade immunosuppressants used in transplantation experiments include cyclosporines, mycophenolate mofetil (MFF), rapamycin or prednisolone, TAC (tacrolimus, FK-506, fujimycin, Prograf) (Lama et al. 2003; Su et al. 2011). TAC is often used in experimental settings as a solo therapy or in combination with other immunosuppressive drugs (i.e., MFF) with doses ranging from 0.05-3 mg/kg/24 hrs (Reis et al. 1998; Xu et al. 2010; Hefferan et al. 2011b), because is particularly effective due to its mechanism of action: TAC couples with immunophilins (FK-506 binding proteins; FKBP) (Siekierka et al. 1989; Liu et al. 1991; Thomson et al. 1995). The resulting formation of a pentameric complex of TAC, FKBP, calcineurins A and B and calmodulin results in the inhibition of the phosphatase activity of calcineurin (McKeon 1991; Halloran 1996) thus inhibiting activity of transcription factors requiring dephosphorylation for transport to the nucleus which leads to suppression of T-cell proliferation and function (i.e. IL-2 transcription) (Liu et al. 1991; Thomson et al. 1995; Minguillon et al. 2005). MFF is used to inhibit inosine monophosphate dehydrogenase, an enzyme needed for the proliferation of B and T lymphocytes (Fulton and Markham 1996). The importance of T-lymphocytes in rejection of neural grafts is demonstrated by the long-term survival of transplanted human spinal cord-derived neural stem cells in athymic rats (Yan et al. 2007) (van Gorp et al. 2013 in press).

However, despite the use of such aggressive immunosuppressive protocols, experimental xenograft studies are frequently hampered by inconsistent graft survival particularly seen in long-term survival studies or when used in disease animal models (Klein et al. 2005; Suzuki et al. 2007). It is believed that the oscillation in plasma drug concentrations and/or insufficient

target plasma levels may in part account for inconsistent graft survival (Hefferan et al. 2011b). Even though we successfully used combinatory immunosuppression protocol which included Prograf (FK506; Astellas Pharma) in combination with Cellcept (mycophenolate mofetil (MFF); Roche Pharmaceuticals) in all our previous xenografting studies (Cizkova et al. 2007; Usvald et al. 2010; Hefferan et al. 2011b; Hefferan et al. 2012; Kakinohana et al. 2012b) (van Gorp et al. 2013 in press), the requirements of BID injections in order to achieve satisfactory TAC levels and to minimize toxicity make this approach i) labor intensive, ii) frequently associated with side effects resulting from repetitive animal injections (such as local inflammatory changes and infection), and iii) associated with systemic side effects such as nephrotoxicity and hepatotoxicity (reviewed in (Finn 1999; Gijzen et al. 2012).

Therefore we have sought for an optimized immunosuppression protocol which will provide long-term effective and stable delivery of immunosuppressant without the need of daily injection.

To extend the half-life of administered drugs in general, long-releasing formulations were previously developed. i) TAC-loaded liposomes that have been shown to provide moderate prolongation of the TAC half-life in the whole blood of naïve rats in comparison with conventional i.v. injections of TAC diluted in saline (Ko et al. 1994; Dutta et al. 1998; McAlister 1998). ii) Biodegradable microspheres were shown to provide a relatively stable level of TAC in whole blood for up to 10-21 days after single s.c. administration (Miyamoto et al. 2004; Wang et al. 2004). As the use of implantable biodegradable pellets has been successfully used to deliver a variety of synthetic drugs or hormones in human patients and in animal experimental models and showed up to 3-6 months of stable drug release after a single pellet implantation (Studd and Magos 1987; Packard 1992; Jockenhovel et al. 1996; Srinivasan et al. 2002), we decided to prepare TAC-loaded pellets for the use in experimental allo- and xenografting in rodents or minipig. To our knowledge, no immunosuppressive pellet formulation has been reported to be successfully used in rodent or other animal models of xenogeneic neural precursor transplantation (Sevc et al, 2013 in revision). TAC pellets are now commercially available and provide steady drug release for up to 3 months, making delivery labor efficient, minimally invasive, and producing stabilized blood concentration levels (Sevc et al, 2013 in revision).

3. AIMS OF THE THESIS

The main goal of our studies was to **generate and characterize new large animal model of Huntington's disease** which will contribute to the development of new disease modifying therapies and to resolve the **question of mutant huntingtin aggregation and disturbed protein homeostasis** in Huntington's disease. We aimed at:

- *Generation and characterization of transgenic minipig of Huntington's disease.*
- *Study of the potential role of UCHL1 in ubiquitin proteasome system impairment in Huntington's disease.*

The next specific aim of our studies was to test the **therapeutic potential of neural stem cell transplantation in spinal cord disorders and injury**. We mainly focused our effort on:

- *Test of the potential therapeutic effect of the spinal grafted human neural stem cells on the disease progression in the SOD1^{G93A} ALS rat model.*
- *Amelioration of motor and/or sensory dysfunction and spasticity in a rat model of acute lumbar spinal cord injury by human neural stem cell transplantation.*
- *Development of more reliable and less labor intensive immunosuppression protocol for xenogeneic neural stem cell transplantation experiments in rat.*

4. MATERIALS AND METHODS

In order to proceed with our complex *in vivo* studies, involvement of large scale of methods beginning with molecular biology through *in vitro* experiments and biochemical methods to animal surgery and the use of sophisticated clinical instruments was prerequisite. Majority of the work was conducted at the Institute of Animal Physiology and Genetics, AS CR, Libechev, Czech Republic and/or at the Neuroregeneration laboratory at UCSD, CA, USA. Multiple other laboratories from Czech Republic, Slovakia, Italy, Switzerland and USA also participated in the studies. The complete materials and methods used in our experiments can be found in the author's publications which are included in the results section of this Ph.D. thesis. We list and describe here just those methods which ultimately led to development of the new animal models and those which were used in their characterization and in evaluation of therapeutic intervention.

4.1. Animals and surgery

To pursue our studies, we have used three different species of laboratory animals. In order to generate Huntington's disease transgenic minipigs, wild-type Libechev minipigs (Vodicka et al. 2005) were used. In our UCHL1 studies, we have used the R6/2 HD mouse (Mangiarini et al. 1996) (B6CBA-Tg(HDexon1)62Gpb/1J ovary transplanted females which are essentially wild-type mice with the ovaries of the R6/2 mice) obtained from The Jackson Laboratory and the *gad* mutant mouse (Saigoh et al. 1999) was obtained and used with permission from Dr. Keiji Wada, National Institute of Neuroscience, Tokyo, Japan. For our transplantation and immunosuppression studies, we have used (L26H) SOD1^{G93A} transgenic ALS rats from Dr. Don W Cleveland colony at UCSD, San Diego, USA (Howland et al. 2002) and Sprague-Dawley albino rats (Velaz Praha, Czech Republic and Harlan Industries, Indianapolis, USA). All components of our studies were carried out in accordance with the Institutional Animal Care and Use Committee of Institute of Animal Physiology and Genetics, v.v.i. and conducted according to current Czech regulations and guidelines for animal welfare and with approval by the State Veterinary Administration of the Czech Republic and/or were approved by the University of California, San Diego Institutional Animal Care and Use Committee.

Minipigs. In our study, as is standard practice, the gilts (sexually mature, regularly estrous cycling minipig females) and weaned sows were housed in groups of 3 – 4 minipigs, and boars were kept individually. The regular estrous cycle (20 days) facilitated reproductive experiments. The ample body size of the minipigs made feasible all surgical and laparoscopic approaches and their execution in a timely way. General anesthesia of minipigs was induced by TKX mixture (Tiletaminum 250 mg, Zolazepamum 250 mg, Ketamine 10 % 3 ml, Xylazine 2 % 3 ml) in a dose of 1 ml per 10 kg of body weight for experimental procedures including embryo transfer and oocyte collection. All surgery was conducted under sterile conditions in a standard surgical room. Postoperative care included treatment with analgesics and antibiotics. Animals were housed separately during recovery from anesthesia and then returned to the animal colony. Profound barbiturate anesthesia (Thiopental Valeant, 1 g, i.v.) was used for transcardial perfusions.

Mouse. In order to generate genetic cross-breed for our UCHL1 studies, heterozygous *gad* males were crossed with R6/2 OT females to generate progeny of three genotypes used in this study: wild type (WT), R6/2 and R6/2x*gad*. All mice were weighted at the day of perfusion (at 6 or 10 weeks). The mice were anesthetized by mixture of ketamine (Narketan 10) and xylazine (Rometar 2%) and transcardially perfused with either just ice-cold PBS or the PBS perfusion was followed by perfusion with 4% PFA.

Rats. Compression model: Twelve-week-old Female Sprague-Dawley rats were anesthetized with isoflurane (5% induction, 1.5-2% maintenance; in room air) and placed into a Lab Standard Stereotaxic frame (Stoelting, Cat# 51600, Wood Dale, IL, USA). Wide Th13 laminectomy was performed using an air-powered dental drill and binocular microscope (exposing the dorsal surface of spinal segment L3). An acrylic rod (\varnothing 2.9 mm, length 15 cm; 35 g) was then slowly lowered on the exposed L3 segment until it slightly touched the spinal cord but without inducing any compression. The rod was kept in place for 15 min, while both temperatures (systemic and the temperature of the exposed cord) were maintained at $37 \pm 0.3^\circ\text{C}$. After spinal compression, the rod and mineral oil was removed and the wound sutured in anatomical layers.

ALS model: (L26H) SOD1^{G93A} transgenic rats (Howland et al. 2002) were randomly divided into 3 experimental groups – no treatment (untreated SOD1^{G93A}), media-treated SOD1^{G93A}, and cell-grafted SOD1^{G93A}; non-transgenic littermates were used as control animals and received no treatment. Both rat models were also used in our TAC-pellet study.

4.2. Construction and production of the HIV1-HD-548aaHTT-145Q vector and verification of vectors *in vitro*

The lentiviral vector for the generation of tgHD minipig was constructed at UCSD and subsequently tested and used in transgenesis at IAPG. N-terminal truncated form of human huntingtin was created from the plasmid pFLmixQ145 comprising human full-length HTT cDNA with 145 CAG/CAA repeats (obtained from Coriell Cell Repositories, Camden, NJ). The first 548aa of huntingtin (ending with residues AVPSDPAM) and including 145 Q was ligated with the HD promoter and inserted into the backbone plasmid pHIV7, which contained cPPT and WPRE cis-enhancing elements. Lentiviral vectors were produced by transient co-transfection of HEK293T cells. HIV1-CMV-EGFP vector (1×10^9 IU/ml) was used as the standard. Transgene expression was tested on porcine differentiated neural stem cells. Subsequently, transduction potential of lentiviral vectors was evaluated using porcine zygotes. Matured porcine oocytes were laparoscopically aspirated from pre-ovulatory follicles. After IVF, embryos at pronuclear stage were microinjected with 10 – 20 pl of HIV1-CMV-EGFP construct into the perivitelline space and cultured into the blastocyst.

4.3. Transgenesis

In order to collect necessary oocytes for transgenesis, adult female minipigs were synchronized by Regumate (Jenssen Pharmaceuticals) (5 donors and 3 recipients per experiment). Donor females were superovulated by administration of pregnant mare's serum

gonadotropin (PMSG) (Intervet International B.V.) and ovulation was induced by gnRH (Intervet International B.V.). After mating with the boars, pronuclear stage embryos were flushed from oviducts and microinjected into the perivitelline space with HIV1-HD-548aaHTT-145Q lentiviral vector (50 – 100 viral particles per zygote). The injected embryos were laparoscopically transferred into the fallopian tubes of recipients.

In order to confirm the presence of the transgene in the minipig genome, we have used the following techniques. **Genotyping:** Biopsies of porcine skin were used to obtain DNA which was purified using DNeasy Blood & Tissue kit (Qiagen). The presence of the transgene was determined by PCR amplification of the region containing the WPRE coding sequence within the transgene (254 bp amplicon). SELK gene (360 bp amplicon) was used as an endogenous control. **Fluorescent in situ hybridization and karyotyping:** The localization of transgenes within the porcine genome was detected by Fluorescence in situ hybridization (FISH) analysis (Trask 1991). Mutant HTT sequence from the recombinant plasmid (HIV1-HD-548aaHTT-145Q) was labeled with biotin-16-dUTP (Roche Diagnostics GmbH) using a nick transcription kit (Abbott). The resulting probe did not detect the endogenous porcine HTT gene. Immunodetection and amplification were performed using avidin-FITC and anti-avidin-biotin. Chromosomes were counterstained with propidium iodide and DAPI. Karyotyping was determined using image analysis of reverse DAPI banding.

4.4. Cell derivation and preparation

The cells, named “NSI-566RSC”, were produced by Neuralstem Inc. (Rockville, MD, USA), as described before (Johe et al. 1996; Hefferan et al. 2011b). Briefly, human spinal cord neural precursors (HSSCs) were prepared from the cervical-upper thoracic region obtained from a single eight week fetus. Meninges and dorsal root ganglia were removed and dissociated into a single cell suspension by mechanical trituration in serum-free, modified N2 media (human plasma apo-transferrin, recombinant human insulin, glucose, progesterone, putrescine, and sodium selenite in DMEM/F12). For growth of the HSSCs, 10 ng/ml basic fibroblast growth factor (bFGF) was added to the modified N2 media and expanded serially as a monolayer culture on poly-D-lysine and fibronectin (Johe et al. 1996). Approximately 6.1×10^6 total cells were obtained upon the initial dissociation of the spinal cord tissue. The growth medium was changed every other day. The first passage was conducted 16 days after plating. At this point, the culture was composed mostly of post-mitotic neurons and mitotic HSSCs. Mainly the mitotic cells were harvested through brief treatment with trypsin and subsequent use of soybean trypsin inhibitor. The cells were harvested at approximately 75% confluence, which occurred every 5-6 days (20 passages). At various passages, the cells were frozen in the growth medium plus 10% dimethyl sulfoxide at $5-10 \times 10^6-10$ cells/ml. The frozen cells were stored in liquid nitrogen. Upon thawing, the overall viability and recovery was typically 80-95%. A cell bank of passage 16 cells was prepared and used for this study. One day prior to each grafting day, one cryopreserved vial of the previously prepared cells was thawed, washed, concentrated in hibernation buffer, and shipped from the cell preparation site (Neuralstem, Inc., Rockville, MD, USA) to the surgery site (University of California, San

Diego, CA, USA) at 2-8°C by overnight delivery. Upon receipt the following day, the cells were used directly for implantation without further manipulation. Before and after implantation, the viability of cells was measured with trypan blue (0.4%; Sigma). Typically, a >85% viability rate was recorded.

4.5. Cell grafting

In our cell transplantation studies, cells were grafted via intraparenchymal injections. The animals were placed in the stereotactic frame and the L3 spinal cord (i.e., the dura mater) was then re-exposed at the previous laminectomy site in case of SCI rat and a partial T12–L1 laminectomy was performed using a dental drill (exposing the dorsal surface of L2–L6 segments) in 60–65 d old SOD1 rats. Injections were performed using a 33 gauge beveled needle and 100 µL Nanofil syringe (World Precision Instruments, Cat# NF33BV & Nanofil-100, Sarasota, FL, USA) connected to a microinjection unit (Kopf Instruments, Cat# 5000 & 5001, Tujunga, CA, USA) in SCI rats and using glass capillary (tip diameter 80–100 µm) in SOD1 rats. The duration of each injection was 45-60 sec followed by a ≥ 30 sec pause before slow needle/glass capillary withdrawal. The center of the injection was targeted intermediate of the ventral and dorsal horn and close to the lateral funiculus (distance from the dorsal surface of the spinal cord at L3 level: 0.80 mm). Twelve injections (20,000 cells/µL) were done; four injections (0.5 µL each, 0.8-1.0 mm apart, rostrocaudally) at each lateral boundary of the injury (8 in total), plus two (bilateral) injections (0.5 µL each) 1.5 mm caudal from the previous, most caudal injections, and two injections at the core of the epicenter (1 µL at each side of the dorsal vein, bilaterally). In SOD1 rats, injections of 0.5µl (10000 cells per injection) were made every 700–900 µm, rostro-caudally, on each side of the lumbar spinal cord targeting L2–L5 segments. The total number of injections ranged between 9–13 injections per side. After the injections, the incision was cleaned with penicillin-streptomycin solution and sutured in two layers.

4.6. Immunosuppression

In order to achieve sufficient differentiation and demonstrate promising therapeutic potential immunosuppression started typically one day before grafting, methylprednisolone acetate (Depo-Medrol, 10 mg/kg, i.m.) was given, which was repeated thereafter 3 times with 1 mg/kg/week i.m. Starting directly after grafting, all animals received 3 mg/kg/BID s.c. of Tacrolimus (Prograf/FK506, Astellas, Deerfield, IL, USA) until the end of the study. For post-transplant days 0-10, the animals also received 30 mg/kg/day s.c. of Mycophenolate mofetil (CellCept, Genentech, CA, USA). Immunosuppression was also given to the non-grafted Sprague-Dawley or SOD1 rats (i.e., the naïve, sham operated, and all control animals).

4.7. Electrophysiology

Electrophysiology measurements were used in order to investigate the potential functional beneficial effect of the transplanted cells on the host neuronal circuits in the diseased/injured spinal cord. **Measurement of muscle spasticity in SCI rats:** At 1.5 weeks and 2 months post-

injury, the presence of muscle spasticity in the lower extremities was measured using a previously described system (Marsala et al. 2005). Briefly, animals were placed in a restrainer and a hindpaw was taped to a rotational metal plate driven by a computer-controlled stepping motor. The metal plate is interconnected loosely to the “bridging” digital force transducer (LCL454G, 0–454 g range; Omega, Stamford, CT, USA). The resistance of the ankle to dorsiflexion was measured during stepping motor-driven ankle dorsiflexion (40°; MDrive 34 with onboard electronics; microstep resolution to 256 microsteps/full step; Intelligent Motion Systems, Marlborough, CT, USA) at 3 different ankle-rotational velocities (40, 60 or 80°/sec). The EMG signal was recorded from the ipsilateral gastrocnemius muscle during the same time frame. To record EMG activity, a pair of tungsten electrodes was inserted percutaneously into the gastrocnemius muscle 1 cm apart. EMG signals were bandpass filtered (100 Hz to 10 kHz) and recorded before, during, and after ankle dorsiflexion. EMG responses were recorded with an alternating current-coupled differential amplifier (model DB4; World Precision Instruments, Sarasota, FL, USA). EMG was recorded concurrently with ankle resistance measurements, both with a sample rate of 1 kHz. Both muscle resistance and EMG data were collected directly to the computer using custom software (Spasticity version 2.01; Ellipse, Kosice, Slovak Republic). **Hoffmann reflex recordings** (H-reflex) in SOD1 rats: Animals were anesthetized with ketamine (100 mg/kg, i.m.). For stimulation of the H-reflex, a pair of needle electrodes was transcutaneously inserted into the vicinity of the tibial nerve. For recording, a pair of silver needle electrodes was placed into the right foot muscles. The tibial nerve was stimulated with increasing stimulus intensity (0.1–10 mA in 0.5 mA increments, 0.1 Hz, 0.2ms; WPI; Isostim A320). The threshold for both the M and H waves was determined and Hmax/Mmax ratio calculated. Recordings were made before and at 15-min intervals after drug treatment (i.e. baclofen or nipecotic acid).

4.8. Biochemical assays

In our HD experiments, we have used a combination of biochemical methods to identify the soluble mutant human and aggregated huntingtin as well as the wild-type mouse and porcine huntingtin and other proteins. Prior brain removal from the skull, animals were always transcardially perfused with ice-cold sterile PBS in order to remove blood from vessels and to slow-down post-mortem enzymatic changes during the brain removal. Reproducibility of western blotting of high molecular weight wild-type huntingtin and posttranslationally modified soluble mutant huntingtin with expanded polyQ tract as well as polyubiquitin species was improved by using iBlot gel transfer device (LifeTech # IB301001) with appropriate set of membranes and buffers. Autoradiographic film (GE Healthcare #28906839) was chosen for signal detection.

Primary antibodies used were selected based our previous experience and available published data. In addition to western blots, three high sensitive biochemical assays were used for detection of aggregated mutant huntingtin. As mutant huntingtin aggregates are insoluble and resistant to chemical extractions they can be poorly determined by polyacrylamide gel electrophoresis because they are retained in the loading wells (Hazeki et al. 2000). Therefore, SDS-agarose gel electrophoresis for resolving aggregates (AGERA) with subsequent western

blot analysis was employed as it represent a simple and sensitive biochemical detection method for quantitative and qualitative investigations of aggregate formation. Even though detailed investigation of aggregate growth or of aggregate composition depending on size is impossible by the filter-trap assay for aggregates (Scherzinger et al.1997) due to indiscriminate retention of all protein inclusions larger than the filter pores of the cellulose acetate membrane, we have used this assay as an mutant huntingtin aggregate screening method. Using highly specific antibodies which bind the human huntingtin (and wild-type huntingtins of other species) discriminating its wild-type or mutant origin (based on the fact that mutant huntingtin contain polyQ stretch) with special europium cryptate and D2 fluorophores (these fluorophores enables the use of FRET in high-throughput screenings) (Weiss et al. 2009; Baldo et al. 2012), we performed TR-FRET quantitative analysis of soluble mutant human, wild-type porcine and mouse and aggregated human huntingtin. In order to keep the reproducibility and consistency, the protein lysates from all brain tissues were prepared in a way which was suitable for all biochemical analyses used and indeed, the same lysates (after the lysis was performed, the lysates were aliquoted and aliquots were sent to different labs) were used in all biochemical analyses in different laboratories which resulted in high correlation of achieved results.

4.9. Immunofluorescence and immunohistochemistry stainings

Immunohistochemical (or fluorescent) methods were used in all our studies. The use of great spectrum of specific primary antibodies allowed us to visualize (and thus to quantify in some instances) the presence of the mutant huntingtin and its possible interacting partners in mouse and brain tissues, to assess the pathology of the striatum, to discriminate specific endogenous cell types in brain and spinal cord, to evaluate the degree of survival of the transplanted HSSCs in the rat spinal cord, to inspect the HSSCs differentiation and formation of functional synapses with host neurons *in vivo*, to assess the degree of injured tissue regeneration (cell replacement) in the injured spinal cord and to evaluate the therapeutic effect of transplanted HSSCs in SOD1 rats as expressed by quantification of surviving α -motoneurons in ventral horns of spinal cord. Antibodies specific for lymphocytes surface markers were used in the immunosuppressive study where we used these antibodies to demonstrate the presence or absence of the immune cells in the vicinity of the grafted cells in the spinal cord. The use of these methods was essential especially in cell grafting experiments where the visualization of the tissue containing the grafted cells is the only method which can directly show the survival, differentiation and integration of the transplanted cells in the host tissue.

4.10. Statistical analyses

Two-way comparisons were performed by student t-test. Multiple comparisons were performed using one-way analysis of variance (ANOVA) followed by Student-Newman-Keuls or two-way group \times time repeated measures, using a fixed-effect model, and a Bonferroni *post hoc* test was used in the case of multiple comparisons. All results are shown as mean \pm standard error of mean (SEM) unless indicated. $P < 0.05$ was considered to be

statistically significant. All statistical analyses were done using GraphPad Prism (La Jolla, CA, USA), SPSS statistics 17 (for K-Means clustering; IBM, Armonk, NY, USA), or STATA 12 (StataCorp LP, College Station, TX, USA) and performed one or two-tailed.

5. RESULTS

5.1. Generation and characterization of Huntington's disease transgenic minipig

in publication

A Transgenic Minipig Model of Huntington's Disease

Baxa M, **Hruska-Plochan M**, Juhas S, Vodicka V, Pavlok A, Juhasova J, Miyanohara A, Nejime T, Klima J, Macakova M, Marsala S, Weiss A, Kubickova S, Musilova P, Vrtel R, Sontag EM, Thompson EM, Schier J, Hansikova H, Howland DS, Cattaneo E, Difiglia M, Marsala M, Motlik J.

Journal of Huntington's Disease 2 (2013) 47–68. DOI 10.3233/JHD-130001 (first two authors are joint first authors)

Journal launched in June 2012 and thus does not have an IF yet

Declaration of co-authors

“I hereby declare that Marián Hruška-Plochán was adequately involved (30%) in the study design, experiments, interpretation of results and writing of this manuscript.”

Prague, April 30 2013

Motlík Jan, Prof., DVM, Ph.D., D.Sc.

Research Report

A Transgenic Minipig Model of Huntington's Disease

Monika Baxa^{a,b,1}, Marian Hruska-Plochan^{a,b,c,d,1}, Stefan Juhas^a, Petr Vodicka^{a,p}, Antonin Pavlok^a, Jana Juhasova^a, Atsushi Miyanochara^e, Tetsuya Nejime^c, Jiri Klima^a, Monika Macakova^{a,b}, Silvia Marsala^{c,d}, Andreas Weiss^{f,r}, Svatava Kubickova^g, Petra Musilova^g, Radek Vrtel^h, Emily M. Sontag^{i,j}, Leslie M. Thompson^{i,j,k}, Jan Schier^l, Hana Hansikova^m, David S. Howlandⁿ, Elena Cattaneo^o, Marian DiFiglia^p, Martin Marsala^{c,d,q} and Jan Motlik^{a,*}

^aLaboratory of Cell Regeneration and Plasticity, Institute of Animal Physiology and Genetics, v.v.i., AS CR, Libechev, Czech Republic

^bFaculty of Science, Department of Cell Biology, Charles University in Prague, Prague, Czech Republic

^cNeuroregeneration Laboratory, Department of Anesthesiology, University of California, San Diego, La Jolla, CA, USA

^dSanford Consortium for Regenerative Medicine, San Diego, La Jolla, CA, USA

^eVector Development Laboratory, Human Gene Therapy Program, Department of Pediatrics, University of California, San Diego, La Jolla, CA, USA

^fNovartis Institutes for Biomedical Research, Neuroscience Discovery, Basel, Switzerland

^gDepartment of Genetics and Reproduction, Veterinary Research Institute, Brno, Czech Republic

^hDepartment of Clinical Genetics and Fetal Medicine, Palacky University, University Hospital Olomouc, Olomouc, Czech Republic

ⁱDepartment of Biological Chemistry, University of California, Irvine, CA, USA

^jDepartment of Psychiatry and Human Behavior, University of California, Irvine, CA, USA

^kDepartment of Neurobiology and Behavior University of California, Irvine, CA, USA

^lInstitute of Information Theory and Automation v.v.i., AS CR, Prague, Czech Republic

^mLaboratory for Study of Mitochondrial Disorders, First Faculty of Medicine, Department of Pediatrics and Adolescent Medicine, Charles University and General University Hospital in Prague, Prague, Czech Republic

ⁿCHDI Foundation, Princeton, NY, USA

^oDepartment of Pharmacological Sciences and Centre for Stem Cell Research, Università degli Studi di Milano, Milan, Italy

^pDepartment of Neurology, Massachusetts General Hospital, Boston, MA, USA

^qInstitute of Neurobiology, Slovak Academy of Sciences, Kosice, Slovak Republic

^rIRBM Promidis, Pomezia, Italy

¹The first two authors contributed equally to this work.

*Correspondence to: Jan Motlik, Institute of Animal Physiology and Genetics, v.v.i., Laboratory of Cell Regeneration and Plasticity, Rumburska 89, 27721 Libechev, Czech Republic. Tel: +420 315639560; Fax: +420 315639510; E-mail: motlik@iapg.cas.cz.

Abstract.

Background: Some promising treatments for Huntington's disease (HD) may require pre-clinical testing in large animals. Minipig is a suitable species because of its large gyrencephalic brain and long lifespan.

Objective: To generate HD transgenic (TgHD) minipigs encoding huntingtin (HTT)^{1–548} under the control of human HTT promoter.

Methods: Transgenesis was achieved by lentiviral infection of porcine embryos. PCR assessment of gene transfer, observations of behavior, and postmortem biochemical and immunohistochemical studies were conducted.

Results: One copy of the human HTT transgene encoding 124 glutamines integrated into chromosome 1 q24–q25 and successful germ line transmission occurred through successive generations (F0, F1, F2 and F3 generations). No developmental or gross motor deficits were noted up to 40 months of age. Mutant HTT mRNA and protein fragment were detected in brain and peripheral tissues. No aggregate formation in brain up to 16 months was seen by AGERA and filter retardation or by immunostaining. DARPP32 labeling in WT and TgHD minipig neostriatum was patchy. Analysis of 16 month old siblings showed reduced intensity of DARPP32 immunoreactivity in neostriatal TgHD neurons compared to those of WT. Compared to WT, TgHD boars by one year had reduced fertility and fewer spermatozoa per ejaculate. *In vitro* analysis revealed a significant decline in the number of WT minipig oocytes penetrated by TgHD spermatozoa.

Conclusions: The findings demonstrate successful establishment of a transgenic model of HD in minipig that should be valuable for testing long term safety of HD therapeutics. The emergence of HD-like phenotypes in the TgHD minipigs will require more study.

Keywords: Huntington's disease, mutant huntingtin, minipigs, large animal model, lentiviral transgenesis, FISH analysis, mRNA and protein expression, immunohistochemistry, DARPP32, AGERA assay, TR-FRET assay, spermatozoa

ABBREVIATIONS

AGERA	Agarose gel electrophoresis for resolving aggregates
HD	Huntington's disease
HTT	Huntingtin
TgHD	Transgenic HD
TR-FRET	Time-Resolved Förster Resonance Energy Transfer

INTRODUCTION

Huntington's disease (HD) is an inherited autosomal dominant neurodegenerative disorder with a worldwide prevalence of 3–10 affected individuals per 100,000 persons in Western Europe and North America [1, 2]. Progressive impairment of motor, emotional and cognitive functions [3, 4] is a consequence of the expansion of the CAG repeat stretch in exon 1 of the gene encoding huntingtin (HTT) protein [5]. The onset and the severity of HD correlates inversely with CAG repeat number [6]. The current pharmacotherapy of HD provides improvement of symptoms but no treatment is available to stop disease progression [7, 8].

Animal models are important tools to evaluate therapies for neurodegenerative disorders. Models of HD in rodent, *Drosophila*, *C. elegans*, and non-human primate have been generated. In general, each of these models shows some biochemical and neuronal features similar to HD in humans [2, 3]. Rodent and fly mod-

els of HD have been very useful for understanding the molecular basis for behavioral and neuronal abnormalities [2]. Although rodent models of HD that express either truncated [9–11] or full-length [12, 13] human mutant HTT display differences in onset and severity of phenotypes, these models collectively have provided valuable information related to target validation and drug therapy. However, the rodent's small brain size and differences in neuroarchitecture to humans limits their use for detailed neuroanatomic characterization associated with HD [14–17] and for adapting methods such as non-invasive imaging that are used in human clinics [18–20]. Large HD genetic models such as sheep [21] and the non-human primate [22] have been generated to help address these problems.

Pigs, and mainly minipigs, represent an optimal model for preclinical drug trials and long-term safety studies [20, 23–26]. This species has a physiology resembling in several aspects that of humans [27–29]. The large size of the pig brain permits detailed identification of brain structures by imaging techniques such as PET [30–32] and MRI [33–39]. There has been recent progress in defining the porcine genome [40–43], porcine single nucleotide polymorphisms [44], microRNAome [45–47], and improved techniques for genetic modification of pigs [48–51]. The porcine homologue of the huntingtin gene has a large ORF of 9417 nucleotides encoding 3139 amino acids with a predicted size of 345 kDa (GenBank, Accession No. AB016793). There is a 96% similarity between

the porcine and human huntingtin genes (GenBank, Accession No. AB016794). The number of CAG repeats in the porcine HTT gene is polymorphic, ranging from 8 to 14 units, and falls within the range of the normal human huntingtin gene [52]. Similar to humans, miniature pig possesses two HTT transcripts of approximately 11 and 13 kb [52, 53]. The similarities between porcine and human huntingtin genes and proteins have provided further impetus to use the pig as a model of HD [20, 54].

Recently, a cloning strategy was used to generate a transgenic HD minipig. Unfortunately, this porcine model suffered frequent perinatal mortality for reasons that are unclear [55]. Here we used a strategy based on lentiviral infection of porcine embryos and report the successful germ line transmission through successive generations (F0, F1, F2 and F3 generations) of a HD transgene encoding the first 548 aa of HTT with 124 glutamines under the control of human HTT promoter. Mutant protein expression is detected in both CNS and non-CNS tissues and in brain is comparable to the endogenous huntingtin. DARPP32 immunoreactivity in a 16 month old TgHD minipig was reduced compared to a WT sibling. At about one year of age, sperm number and oocyte penetration were severely affected in TgHD minipigs. These findings suggest that we have in hand a suitable large animal model for evaluating potential HD therapeutics.

MATERIALS AND METHODS

Supplementary data

Supplementary Data (S1–S8) are placed on the website of The Institute of Animal Physiology and Genetics, v.v.i.: www.iapg.cas.cz/CentrumPIGMOD/JHD

Minipigs

The Institute of Animal Physiology and Genetics in Libečov imported the first miniature pigs in 1967 from the Hormel Institute, University of Minnesota (two boars and three sows) and from the Institute for Animal Breeding and Genetics, University of Göttingen, Germany (two boars and four sows). Since then breeding, animal health and body shape have been thoroughly controlled and outbreeding conditions maintained by import of several additional boars from Göttingen [29]. Through continuous selection there has been an increase in the average litter size (now about 6–8 piglets) and maintenance of a white color, which has enabled the study of epidermal stem cells [56].

The animals were bred beginning at about 5 months of age when they reach sexual maturity. At this stage they weigh about 12–15 kg. In our minipig colony longevity is unknown because animals are housed for a maximum of about 8 years. However, the survival of parental minipig breeds (Hormel and Göttingen) has been reported to be 12 to 20 years. In this study, as is standard practice, the gilts (sexually mature, regularly estrous cycling minipig females) and weaned sows were housed in groups of 3–4 minipigs, and boars were kept individually. The regular estrous cycle (20 days) facilitated reproductive experiments.

All components of this study were carried out in accordance with the Institutional Animal Care and Use Committee of Institute of Animal Physiology and Genetics, v.v.i. and conducted according to current Czech regulations and guidelines for animal welfare and with approval by the State Veterinary Administration of the Czech Republic. The ample body size of the minipigs made feasible all surgical and laparoscopic approaches and their execution in a timely way. General anesthesia of minipigs was induced by TKX mixture (Tiletaminum 250 mg, Zolazepamum 250 mg, Ketamine 10% 3 ml, Xylazine 2% 3 ml) in a dose of 1 ml per 10 kg of body weight for experimental procedures including embryo transfer and oocyte collection. All surgery was conducted under sterile conditions in a standard surgical room. Postoperative care included treatment with analgesics and antibiotics. Animals were housed separately during recovery from anesthesia and then returned to the animal colony. Profound barbiturate anesthesia (Thiopental Valeant, 1g, i.v.) was used for transcatheter perfusions.

Construction and production of the HIV1-HD-548aaHTT-145Q vector and verification of vectors in vitro

N-terminal truncated form of human huntingtin was created from the plasmid pFLmixQ145 comprising human full-length HTT cDNA with 145 CAG/CAA repeats (obtained from Coriell Cell Repositories, Camden, NJ). The first 548 aa of huntingtin (ending with residues AVPSDPAM) and including 145 Q was ligated with the HD promoter and inserted into the backbone plasmid pHIV7, which contained cPPT and WPRE cis-enhancing elements. Lentiviral vectors were produced by transient cotransfection of HEK293T cells. HIV1-CMV-EGFP vector (1×10^9 IU/ml) was used as the standard (See Supplementary Data S1 for details). Transgene expression was tested on porcine differentiated neural stem

cells. Subsequently, transduction potential of lentiviral vectors was evaluated using porcine zygotes. Matured porcine oocytes were laparoscopically aspirated from pre-ovulatory follicles. After IVF, embryos at pronuclear stage were microinjected with 10–20 pl of HIV1-CMV-EGFP construct into the perivitelline space and cultured into the blastocyst stage *in vitro* (See Supplementary Data S2 for details).

Transgenesis

Gilts were synchronized by Regumate (Jenssen Pharmaceuticals) (5 donors and 3 recipients per experiment). Donor females were superovulated by administration of pregnant mare's serum gonadotropin (PMSG) (Intervet International B.V.) and ovulation was induced by GnRH (Intervet International B.V.). After mating with the boars, pronuclear stage embryos were flushed from oviducts and microinjected into the perivitelline space with HIV1-HD-548aaHTT-145Q lentiviral vector (50–100 viral particles per zygote). The injected embryos were laparoscopically transferred into the fallopian tubes of recipients (See Supplementary Data S3 and S4 for details).

Genotyping

Biopsies of porcine skin were used to obtain DNA which was purified using DNeasy Blood & Tissue kit (Qiagen). The presence of the transgene was determined by PCR amplification of the region containing the WPRE coding sequence within the transgene (254 bp amplicon). Each PCR reaction contained 0.75 ng/ μ l of purified gDNA in 20 μ l of reaction mixture and underwent 32 cycles of amplification (94°C for 30 s, 56°C for 40 s, 72°C for 40 s) following an initial 3 min denaturation period. SELK gene (360 bp amplicon) was used as an endogenous control. Primer sequences:

WPRE Fwd: 5' GAGGAGTTGTGGCCCGTTG
TCAGGCAACG 3'
WPRE Rev: 5' AGGCGAGCAGCCAAGGAAA
GGACGATG 3'
SELK Fwd: 5' ACAGGCCCAAATAAAGAG
3'
SELK Rev: 5' CAAATTTGGAGCCTTTTGT 3'

Fluorescent *in situ* hybridization

The localization of transgenes within the porcine genome was detected by Fluorescence *in situ* hybridization (FISH) analysis [57]. Mutant HTT

sequence from the recombinant plasmid (HIV1-HD-548aaHTT-145Q) was labeled with biotin-16-dUTP (Roche Diagnostics GmbH) using a nick transcription kit (Abbott). The resulting probe did not detect the endogenous porcine HTT gene. Immunodetection and amplification were performed using avidin-FITC and anti-avidin-biotin. Chromosomes were counterstained with propidium iodide and DAPI. Karyotyping was determined using image analysis of reverse DAPI banding.

Microdissection of chromosomes and analysis of copy number variation

The incorporation of transgenic HTT into the q arm of chromosome 1 was confirmed by microdissection of q arms of both chromosomes 1 followed with a non-specific degenerate oligonucleotide-primed (DOP) PCR. 2 μ l of DOP PCR amplification product were used as a template to carry out PCR amplification of the transgene.

Primer sequences:

MDS Fwd: 5' TTCATAGCGAACCTGAAGTC 3'
MDS Rev: 5' TTGTGTCCTTGACCTGCTGC 3'

The number of copies of the transgenes integrated into the porcine genome was determined using relative comparison of quantitative DNA amplification between the endogenous porcine HTT and the transgenic human HTT. HTT primers and probe 6-carboxyfluorescein, (6-FAM, TaqMan Probe, Applied Biosystems) were designed to detect HTT of both species. ACTB (VIC, TaqMan Probe, Applied Biosystems) was used as a reference gene. Each multiplex qPCR reaction was performed in a reaction volume of 20 μ l using TaqMan Gene Expression chemistry (ROX passive reference, Applied Biosystems) using 75 cycles of amplification (30 s at 94°C, 30 s at 51.1°C, 30 s at 72°C) following an initial 3 min denaturation period. The qPCR data were analyzed using LinReg-PCR software [58].

The sequences of the oligonucleotides:

HTT TaqMan MGB Probe: 6-FAM-TCTGCGTC
ATCACTGC-MGBNFQ
HTT Primer Fwd: 5' CTTCTGGGCATCGCTATG
3'
HTT Primer Rev: 5' CATTTCGTAGCCACCATC
3'
ACTB TaqMan MGB Probe: VIC-AGTCCCTG
CCTTCCCAA-MGBNFQ

ACTB Primer Fwd: 5' GTCATTCCAAGTATCAT
GAGATG 3'
ACTB Primer Rev: 5' TGGAGTACATAATTTA
CACTAAAGC 3'

Determination of glutamine number in human mutant huntingtin

The number of glutamines in human mutant HTT was determined by PCR using primer pairs that flanked the region of the CAG/CAA repeat. The length of the PCR fluorescently labeled product was detected using Fragment analysis on an Applied Biosystems 3130 Genetic Analyzer. Samples were separated in gel polymer POP-7 gel at 60°C using LIZ 600 size standard. Data analysis was performed by GeneMapper® software.

Primer sequences:

HD1: 5' ATGAAGGCCTTCGAGTCCCTCAAGT
CCTTC 3' (6-FAM)
HD3pig: 5' CGGCGGCGGTGGCGGTTGCTGT
TGCTGCTG 3'

PCR protocol: 95°C for 5 min, followed by 40 cycles of denaturation at 94°C for 30 s, annealing at 70°C for 30 s and elongation at 72°C for 30 s with a final extension of 3 min.

Detection of mRNA expression of mutant human HTT

Purified RNA was obtained from cultured porcine skin fibroblasts using RNeasy Plus minikit (Qiagen). RT PCR amplification was performed in a reaction mixture containing 2.0 ng/μl of total RNA with reaction volume of 20 μl. The primer set for RNA huntingtin insert (1446 bp amplicon) was designed using Beacon Designer. ACTB (~100 bp amplicon, PrimerDesign Ltd) was used as a reference gene. The HTT amplification was performed in one step starting with reverse transcription at 50°C for 30 min and denaturation at 95°C for 15 min, followed by 50 cycles of denaturation at 94°C for 45 s, annealing at 56°C for 45 s and elongation at 72°C for 95 s with the final extension of 2 min. The amplification of ACTB reference gene was performed in a one-step reaction (50°C for 30 min, 95°C for 15 min, followed by 35 cycles of amplification at 94°C for 45 s, 61°C for 30 s and 72°C for 30 s with the final extension of 3 min. Reaction mixtures missing reverse transcriptase were included for each animal sample to exclude the possibility of contamination with genomic DNA.

Primer sequences:

HTT RNA Fwd: 5' GAAACTTCTGGGCATCGC
TATG 3'
HTT RNA Rev: 5' GAAAGCCATACGGGAAG
CAATAG 3'

Biochemical assays

Eight minipigs at the age of 4 ($N=4$), 10 ($N=2$) and 16 months ($N=2$) from F2 generation (4 TgHD+4 WT) were perfused under deep anesthesia with ice-cold PBS. The left hemisphere of each perfused brain was dissected and used in biochemical assays (SDS-PAGE and Western blot and TR-FRET). Brain and tissue biopsies were stored at -80°C.

15 μg of total protein from crude homogenates of TgHD minipig and WT littermates samples were diluted by NuPage 4× LDS sample buffer (LifeTech #NP0007) and 0.1 M DTT. Samples were loaded onto 3–8% Tris-acetate (LifeTech #EA03755) gel and run at 125 V in Tris-Acetate SDS Running Buffer (LifeTech #LA0041) until the 30 kDa band of Novex Sharp protein standard (LifeTech #LC5800) had migrated to the end of the gel. Gels were then immersed in transfer buffer containing 1% SDS and 20% MeOH for 8 minutes and then transferred onto nitrocellulose membrane (LifeTech #IB301001) using an iBlot gel transfer device (LifeTech #IB1001) P3 for 8 minutes. Membranes were blocked with 5% milk for 30 min at RT (BioRad #170-6404) and probed with anti-HTT antibody (Ab1, 1:1,000; [59]) overnight at 4°C. Membranes were then incubated for 1 h at RT in a 1:5,000 dilution of Peroxidase-conjugated Donkey Anti-Rabbit secondary antibody (Jackson ImmunoResearch #711-035-152); followed by 5 min incubation in Supersignal West Pico (Pierce #3408). Signal was detected on autoradiographic film (GE Healthcare #28906839). Membranes were stripped by Re-Blot Plus Strong Solution (10×) (Millipore #92590) for 15 minutes at RT, blocked by 5% milk and re-probed with anti-actin antibody in a 1:500 dilution (Sigma #A4700). After 1 h incubation at RT in secondary Donkey anti-Mouse antibody (Jackson ImmunoResearch #715-0350150), detection was performed as described above.

SDS-agarose gel electrophoresis for resolving aggregates (AGERA) and Western blot analysis

The analysis of mutant HTT oligomers by SDS-AGE and Western analysis was performed as described previously [60–63]. 50 μg of total protein from

tions were finally mounted with DePeX (Sigma). Analysis was performed using a confocal microscope equipped with 4 lasers (405, Argon, 561 and 633 nm lasers) (SP5, Leica Microsystems), virtual microscopy scanners (VS110[®]-5, Olympus, NanoZoomer 2.0-HT, Hamamatsu) and a light microscope (Primo Star, Zeiss).

Determination of the number and intensity of DARPP32 + neurons

Images of regions of caudate and putamen were obtained using the confocal microscope and a HCX PL APO lambda blue 63.0 × 1.40 OIL UV objective to detect DAPI staining. PMT setup, pinhole sizes (1 Airy) and contrast values were kept constant across different sessions. The number of coronal sections analyzed per caudate nucleus and putamen ranged from 3–5 and 25 areas were scanned in each section. Areas of analysis were sectioned in the *z* plane in 1-micron optical sections (13–20 μm) using Fiji software (<http://fiji.sc>) and only cells confirmed to include the entire DAPI stained nucleus were included in the analysis. This sampling method is an optical dissector technique and minimizes sampling errors (due to partial cells) and stereological concerns, as minor variations in cell volumes do not influence sampling frequencies [68, 69]. The DAPI staining in DARPP32 labeled cells revealed nuclei of two distinct morphologies—large grainy nuclei mainly in the caudate nucleus and smaller compact nuclei mainly in putamen. Only cells with DARPP32 labeling and these nuclear features were included in the analysis. A total of 5,256 neurons in TgHD minipig and 3,644 neurons in WT minipig were counted. All values were reported as the number of neurons positive for immunoreactive DARPP32 per mm³ tissue. In the same scanned areas used for the cell based analysis the overall intensity of DARPP32 signal was also measured. The average signal intensity was determined for all images in a stack and expressed as the mean intensity.

Semen collection and penetration test

Semen samples from 2 transgenic boars of F1 generation (G117 and G118) and 3 wild type boars (F808, F630, F719) were collected starting at age 12 months and periodically over 14 months. Five and 18 samples were taken for the WT and 16 and 18 for the TgHD minipigs. Total number of spermatozoa per ejaculate was estimated by Sperm Class Analyzer (Microptic, Spain). Differences in the number of sper-

matozoa between individual boars were analyzed using Kruskal-Wallis test followed by Mann-Whitney U test for the *post hoc* comparison. Values of $p < 0.05$ were considered significant. The spermatozoa were prepared for *in vitro* penetration test by double centrifugation (20 min/600 g, 10 min/600 g) and the following swim-up procedure [70] provided about 1×10^6 cells for *in vitro* fertilization. The cycling minipig gilts were synchronized by Regumate (Jenssen Pharmaceuticals) and superovulated by administration of PMSG (Intervet International B.V.). Ovulation was induced by GnRH (Intervet International B.V.). The oocyte-cumulus complexes were isolated from large antral follicles 72 h after PMSG injection at the germinal vesicle stage and they were cultured for 40–44 h up to metaphase II with the first polar body [70]. In 13 independent experiments, oocytes with intact zona pellucida were used. In some experiments, the zona pellucida was removed by incubation with 0.25% pronase. After 24 h of incubation with spermatozoa, oocytes were mounted on slides, fixed in acetic-alcohol, stained with acetic-orcein and examined with phase contrast microscopy. The penetration rate into matured pig oocytes was recorded. Differences among individuals in penetration rate were analyzed using Kruskal-Wallis test followed by Mann-Whitney U test used for the *post hoc* comparison between individual boars and values of $p < 0.05$ were considered significant.

RESULTS

Generation and characterization of TgHD minipig

The HIV1 backbone plasmid pHIV7, which contains cPPT and WPRE cis-enhancing elements (Supplementary Data S1), was used for the construction of a lentiviral vector carrying the sequence of the first 548 amino acids of human HTT protein containing 145 glutamines under the control of human HD promoter (Fig. 1A). The transduction potential of the lentiviral construct was verified on porcine zygotes using the HIV1-CMV-EGFP construct. Efficient transduction of porcine embryos was confirmed by the presence of EGFP fluorescence in embryoblasts and trophoblasts (Supplementary Data S2).

The TgHD minipigs were generated by using microinjection of HIV1-HD-548aaHTT-145Q construct into the perivitelline space of the one-cell stage porcine embryos (Supplementary Data S3). Twenty-nine injected zygotes were transferred to recipient sows via laparoscopy (Supplementary Data S4). After standard duration of gravidity (115 days), the first

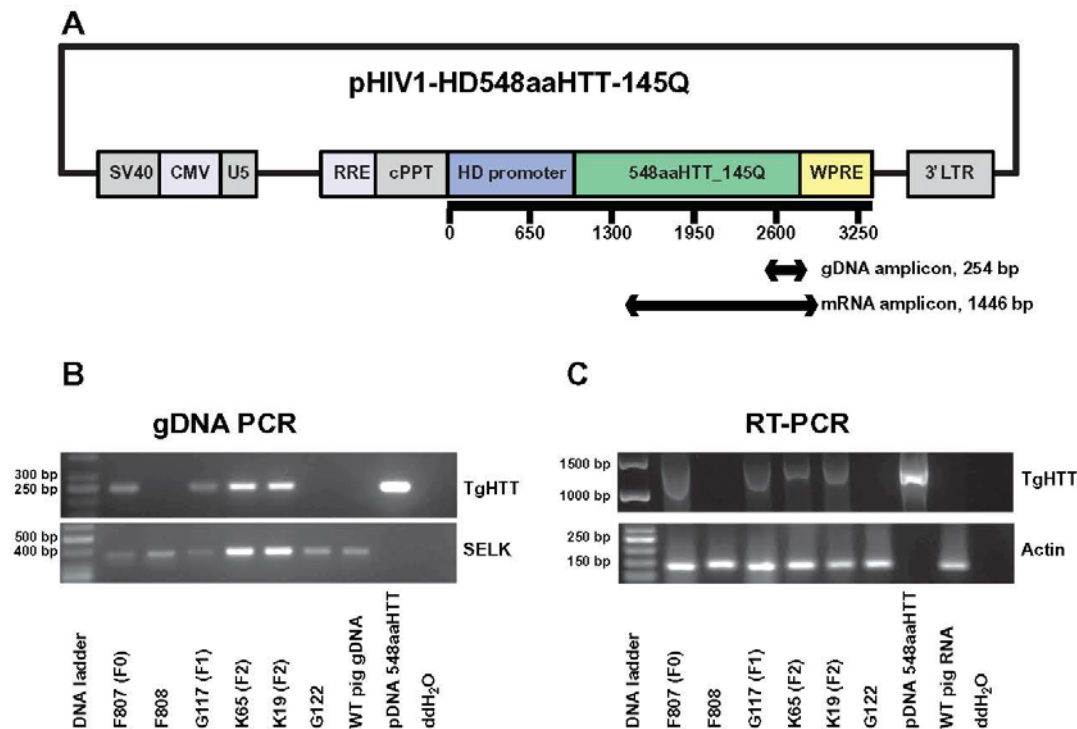


Fig. 1. Molecular characterization of TgHD minipigs. (A) Schematic of the first 548aa of human HTT cDNA fragment with the stretch of 145 glutamines ligated to human HTT promoter in the pHIV7 backbone. WPRE primer set (gDNA amplicon) was used for genotyping the animals. 548aaHTT primer set (mRNA amplicon) was used for confirmation of mRNA expression. (B) PCR of the human HTT and WPRE region (TgHTT) shows presence of transgene in porcine DNA. Amplification of SELK gene (360 bp amplicon) was used as control for the quality of DNA. (C) Expression of mRNA by RT PCR amplification of 1446 bp long amplicon spanning the region encoding human HTT and WPRE region. Amplification of actin mRNA (ACTB) was used as a control for RNA quality. Reaction mixtures without reverse transcriptase were included for each animal sample to exclude the possibility of genomic contamination (data not shown). Plasmid DNA with 548aaHTT-145Q construct was used as a positive control. WT pig genomic DNA and mRNA and ddH₂O were used as negative controls. Generation (F0, F1, F2) is indicated just for TgHD animals.

HIV1-HD-548aaHTT-145Q manipulated piglets were born. One gilt (F807) in a litter of 6 live newborns was transgenic. Two non-transgenic piglets died within 48 hours after birth (Fig. 2). The number of transgenic animals when expressed as a proportion of the number of live births or as a proportion of microinjected zygotes was 16.7% or 3.5%, respectively.

The F0 transgenic gilt was mated with its non-transgenic littermate to produce F1 generation. In the two litters of 17 newborns, five piglets were transgenic (Fig. 2). Germ line transmission to the F1 generation was 29.4%. F1 transgenic boars were sexually mature at the expected age of five months and they successfully produced offspring.

Of 92 F2 piglets born from seventeen litters – 73 survived (20.7% perinatal mortality) and 37 of these were transgenic (TgHD, black symbols, Supplemen-

tary Data S5) resulting in a 40.2% F2 generation transgenesis rate per born piglet. The number of piglets in a litter and newborn mortality was comparable between offspring of TgHD and WT animals (Supplementary Data S6). The proportion of TgHD and WT piglets in F2 generation were comparable, enabling creation of optimal experimental groups (TgHD vs. WT animals).

Five transgenic boars and one TgHD female of the F2 generation were bred and a total of 51 live WT and 30 live TgHD piglets were obtained from 23 litters. The incidence of perinatal mortality in F3 generation was 14.2% and the rate of transgenesis was 34.9%.

The F0 transgenic sow was also mated with an F1 transgenic boar. Four transgenic piglets were born in two litters (Supplementary Data S5). No homozygote TgHD transgenic offspring were obtained.

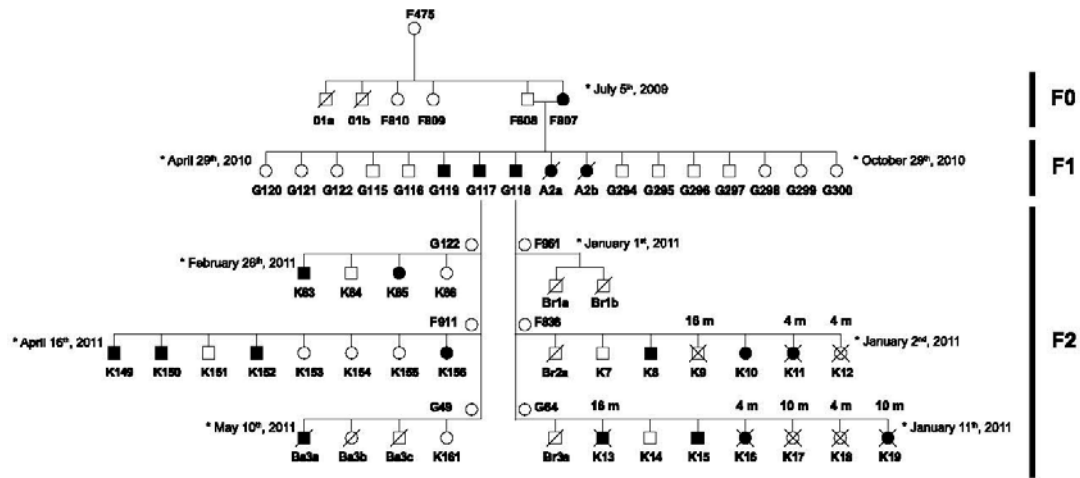


Fig. 2. Breeding and pedigrees of TgHD minipigs. Black boxes (males) and black circles (females) represent animals positively tested for the transgene in DNA extracted from biopsy of ear tissue. "F" denotes a dead minipig within the first 48 hours; "X" indicates an animal sacrificed for biochemical and microscopic studies. The F0 minipig gave birth to 5 TgHD piglets in two litters. Mendelian inheritance is indicated in the F2 generation.

DNA and RNA analysis

Genotyping was performed using PCR as described in Methods. Figure 1B demonstrates TgHD minipigs in F0, F1 and F2 generations. Expression of mRNA was confirmed by RT-PCR amplification of the region encoding human HTT and WPRE region (Fig. 1C). To confirm mRNA expression of the full insert, primers were designed for amplification of the 1446 bp product from the 548aa HTT transgene. mRNA of mutant huntingtin was transcribed in all TgHD minipigs. Mutant HTT gene was detected by FISH analysis on chromosome 1 (1q24-q25) in animals from the first three generations (Fig. 3A). Microdissection of q arms of chromosomes 1 followed with non-specific DOP-PCR confirmed the presence of the transgene in chromosome 1. Chromosomes 6 and 13 were used as negative controls (Fig. 3B).

Quantitative PCR was used to detect the presence of both endogenous wild type HTT gene and the mutant HTT transgene in the porcine genome. Assuming the presence of the two endogenous porcine HTT alleles, all the transgenic animals integrated 1 copy of the transgene in their genome (Fig. 3C). Furthermore, fragment analysis of the PCR amplicons of the DNA fragment containing CAG/CAA sequence showed that the integrated transgene was in frame and consisted of 124 CAG/CAA instead of the original 145 (Fig. 3D).

Development and behavior of TgHD minipigs

The development and behavior of the TgHD minipigs from F0, F1, F2 and F3 generations appeared comparable to WT. TgHD piglets looked normal at birth, were able to stand within a few minutes and their size was similar to each other and to WT. Social dominance relationships among the WT and HD littermates began forming two days after birth and as expected, changed as a consequence of weaning and sexual maturity. TgHD and WT animals of both sexes became sexually mature at the expected age of 5 months and were able to produce offspring. We noticed a decline in the fertility of the F1 generation TgHD boars beginning at about 12 months (see below). Motor deficits characteristic of HD were not evident in the TgHD animals. Lateral eye movements were smooth and vertical gaze movement was similar to WT minipigs. Saccades were not slow, facial praxis was normal, and vocalization had a normal rhythm. No involuntary movements were observed. A qualitative rating scale was developed to evaluate stance, gait, and ability to cross a barrier in TgHD and WT animals starting at age 3 months and at monthly intervals up to 30 and 40 months of age. A rating of 0 was normal and 3 was the most impaired (see Supplementary Data S7 for details). Using this rating scale, there was no difference in score for standing, gait, or crossing a barrier between WT (score = 0) and F0 TgHD minipigs (F807) up to 40 months and F1

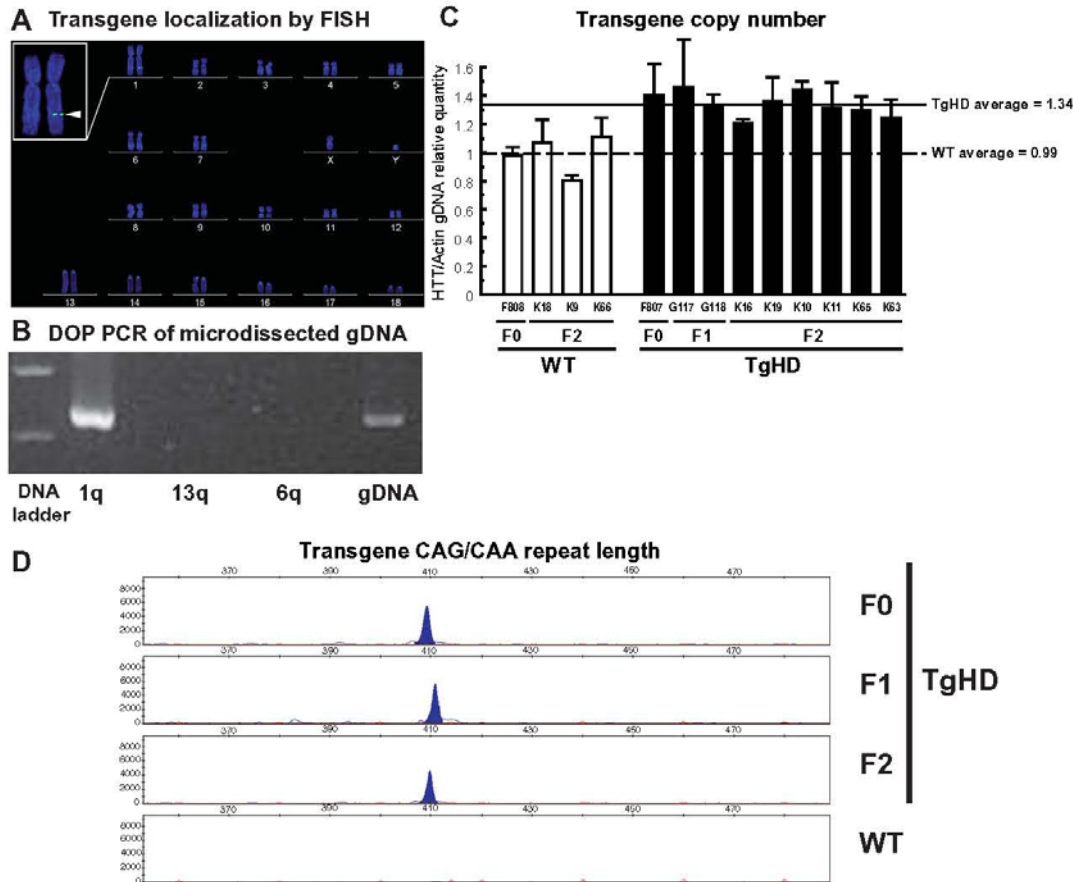


Fig. 3. Localization and copy number of mutant HTT and length of CAG/CAA repeat in TgHD minipig. (A) Incorporation of mutant HTT into the porcine genome. FISH technique shows the localization of the transgene on chromosome 1 (1q24-q25) (inset, arrowhead) of F1 TgHD male. (B) Microdissection of q arms of chromosome 1 followed by non-specific degenerate oligonucleotide primed (DOP) PCR confirms the presence of the transgene on chromosome 1 but not chromosomes 6 and 13. Genomic DNA from TgHD minipig was used as a positive control. (C) Bar graph shows quantity of HTT gDNA (both endogenous porcine HTT and human HTT transgene) in WT and TgHD animals relative to endogenous actin gDNA. Lines indicate mean values for the WT (dashed line) and transgenic animals (full line). Copy number of the transgene was determined by comparing its mean value to that of the WT. (D) The result of analysis of fragment length electrophoresis is shown. PCR amplification with primers specific for transgene shows a peak of 410bp in TgHD animals but not in the WT. 410bp fragment encodes both primer sequence and CAG/CAA repeat sequence encoding 124 glutamines in all three generations. CAG/CAA repeat number was similar in different porcine tissues (data not shown).

generation minipigs (G117, G118, and G122) up to 30 months of age (Scores = 0).

Expression of mutant huntingtin protein

Brain lysates were obtained from two 4 month old F2 TgHD minipigs and two WT minipigs. SDS-PAGE and Western blot analysis was performed as described in methods using antibody Ab1 to detect HTT. Mutant HTT protein fragment was detected in all regions of the

CNS examined including motor cortex, putamen, caudate nucleus, hippocampus, hypothalamus, thalamus, cerebellum, and spinal cord (Fig. 4A top for one WT and one TgHD). Mutant HTT fragment migrated at the expected size of 120 kDa. Peripheral tissues including small intestine, lung, liver, kidney, ovaries and skin also expressed the TgHD protein whereas little or no transgenic HTT was present in stomach, heart, skeletal muscle and spleen (Fig. 4A bottom). With some exceptions (for example, hypothalamus), the densitometry

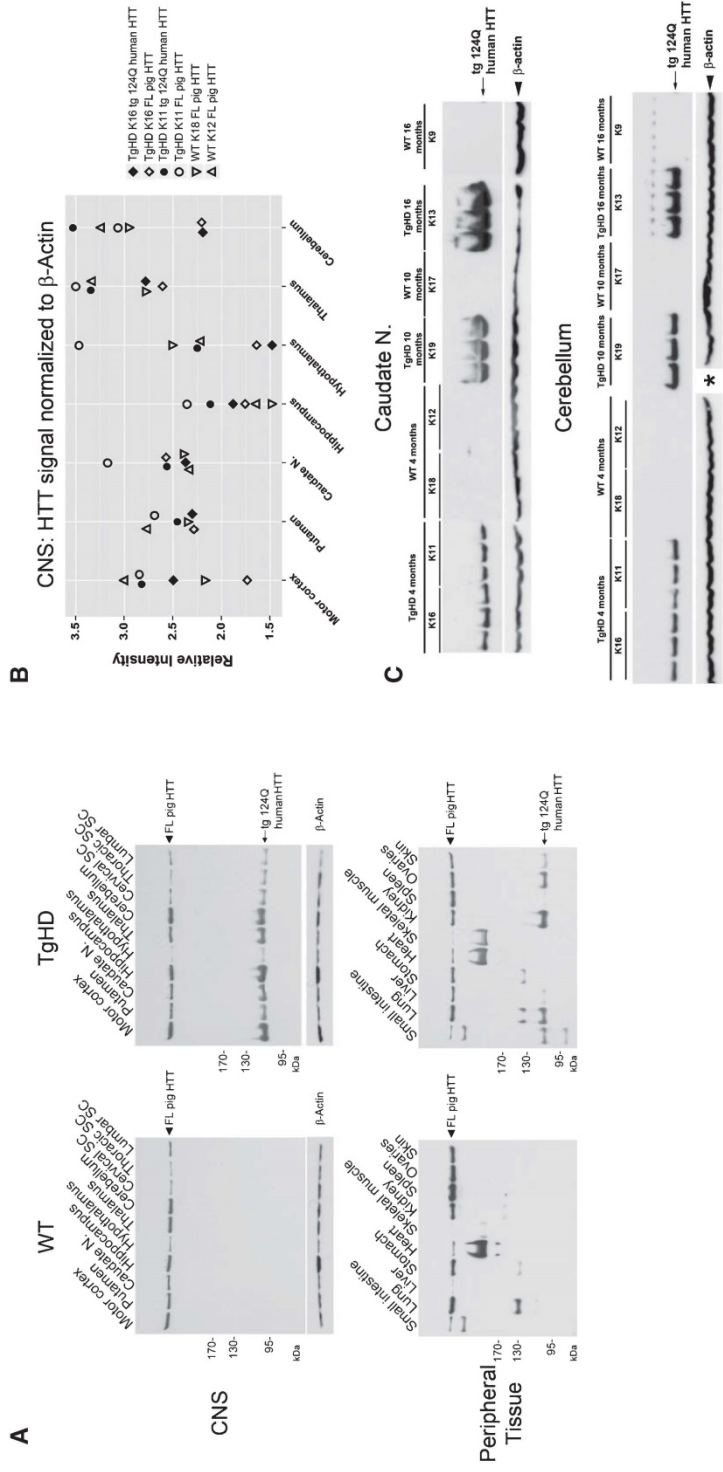


Fig. 4. Western blot analysis of mutant HTT protein in F2 WT and TgHD minipig. (A) Western blot immunoprobed with the anti-HTT1-17 antibody Ab1 shows expression of the porcine WT (FL-HTT) and human HTT transgenic protein fragment (tg 124 Q human HTT) in different CNS and peripheral tissues of 4 month old minipigs. (B) Scatterplot of signal intensity values for pig huntingtin and mutant HTT relative to beta actin levels in different brain regions for WT and TgHD minipigs. (C) Western blot analysis of caudate nucleus and cerebellum from F2 - 4, 10 and 16 month old WT and TgHD minipigs. Samples of each animal are shown in triplicate. Actin is shown as loading control. Asterisk denotes missing actin band for one of triplicates of K19 cerebellum sample.

analysis showed that the levels of mutant HTT fragment in different brain regions were comparable to the levels of the endogenous porcine huntingtin seen on the same blots (see scatterplot, Fig. 4B). Further Western blot analysis of caudate nucleus and cerebellum was performed in frozen samples of brain from 8 minipigs (4 TgHD and 4 WT) ages 4, 10 and 16 months. Results showed that the mutant protein fragment was detected in the TgHD minipigs at all ages. The signals for the mutant protein migrated more broadly in SDS-PAGE in the caudate and cerebellum of the 10 and 16 months old minipigs than in the samples from the 4 month old minipig (Fig. 4C). Whether this characteristic of migration is related to an altered property of mutant HTT is unclear.

We quantified the levels of soluble mutant HTT in CNS and peripheral tissues of two sibling pairs of TgHD and WT minipigs using TR-FRET as described in Methods. Results in all brain and spinal cord regions and some peripheral tissues (lung, spleen, kidney, ovaries) showed robust HTT signal in TgHD animals compared to WT minipigs suggesting the assay was detecting mutant HTT (Fig. 5). To determine the presence of aggregated mutant HTT in TgHD minipig brain, AGERA and filter retardation assays were applied. Homogenates from motor cortex, putamen, caudate nucleus and cerebellum of WT and TgHD 16 month old minipigs were tested with mEM48 antibody. Based on these assays, aggregated mutant HTT was not

present in the brain of TgHD minipig but was detected as expected in the brain of the R6/2 HD mouse (Fig. 6).

Immunohistochemistry of WT and TgHD brains

HTT immunoreactivity was examined by the immunoperoxidase method in the 4 month old minipig brain at the levels of the neostriatum using anti-HTT antibody Ab1 which detects HTT1–17. The cortex, caudate nucleus and putamen showed HTT immunoreactivity. Within these regions the gray matter was more strongly labeled than the white matter (Fig. 7). Consistent with findings in mice and human brain [71], endogenous HTT in WT minipig strongly localized to somatodendritic regions of cortical neurons and to cell bodies of neostriatal neurons. Neuropil of cortex and neostriatum was also strongly labeled. The other anti-HTT antibody which detected endogenous huntingtin in WT minipig was AB585, which was made to HTT585–725 [59]. There was no difference in the intensity of staining for HTT in TgHD minipig compared to WT minipig with anti-HTT Ab1. No nuclear inclusions were detected in the TgHD brain even though Ab1 antibody detects nuclear inclusions in the human HD cortex [72]. Antibodies MW8 and mEM48 are known to detect nuclear aggregates in other HD animal models but did not produce any staining in the TgHD minipig. Similarly no labeling was detected with MW8 in the 16 month old TgHD pigs.

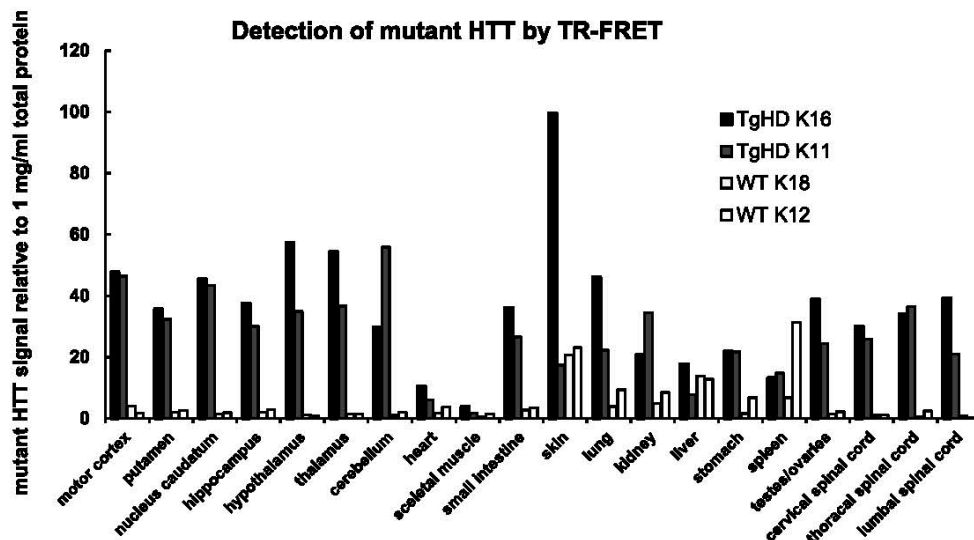


Fig. 5. TR-FRET analysis of soluble HTT protein in F2 WT and TgHD minipig. Bar graph shows results of TR-FRET analysis of soluble mutant HTT protein in TgHD and WT tissue samples (isolated from 4 month old minipigs) expressed as mutant HTT signal per 1 mg/ml total protein. Results of TR-FRET quantitative analysis correlated with western blot analysis shown in Fig. 4B.

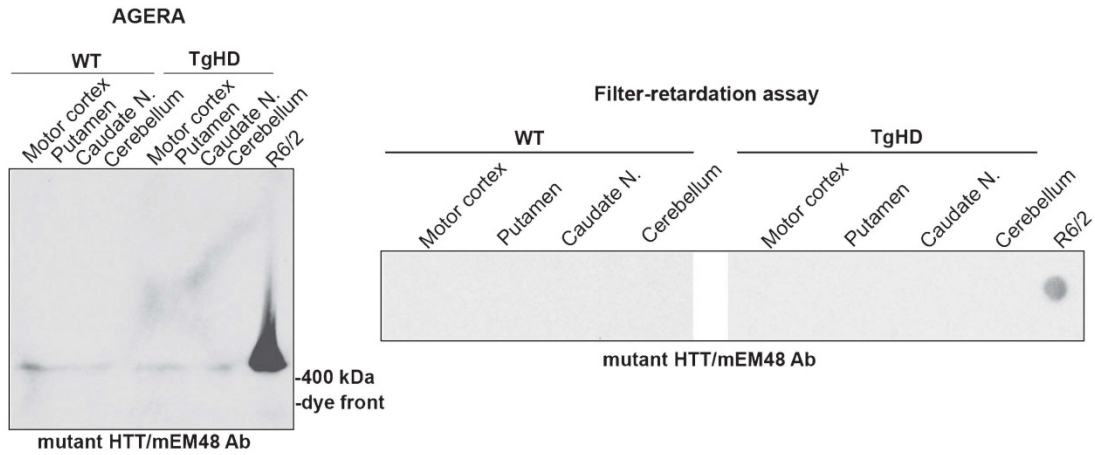


Fig. 6. Biochemical assays for detection of aggregated mutant HTT. AGERA and Filter retardation assays were performed as described in Methods using tissue from different brain regions of WT and TgHD minipig and R6/2 HD mouse. Membranes were probed with mEM48 antibody. Only R6/2 sample shows signal in both assays.

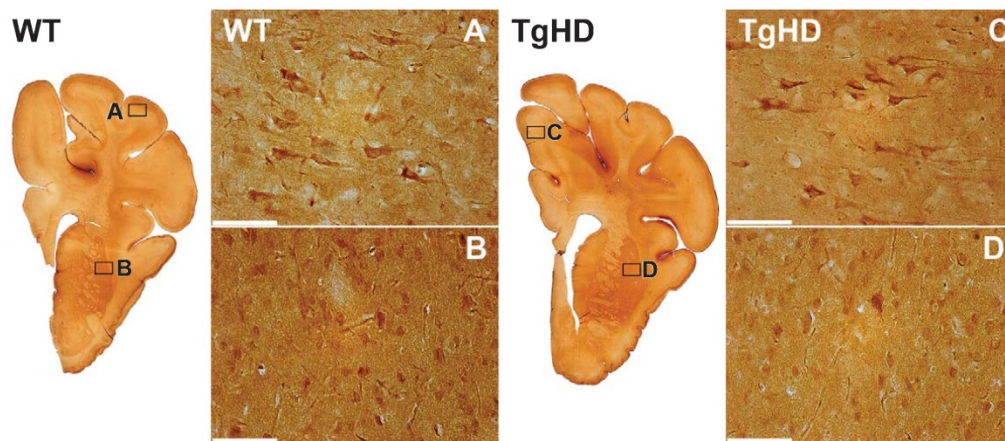


Fig. 7. HTT localization in the brain of WT and TgHD minipig. Shown are coronal sections of 4 month old WT minipig brain on the left and TgHD minipig brain on the right labeled using the immunoperoxidase method to detect HTT with anti-HTT1–17 (Ab1). Boxed regions of the cingulate cortex and the putamen are shown in images to the right of each section. HTT immunoreactivity has a strong somatodendritic localization in WT and TgHD cortex and in somata of medium sized neostriatal neurons. There is no obvious difference in labeling between WT and TgHD neurons. Scale bars 100 μ m.

DARPP32 is highly localized to neuronal cell bodies and processes of the normal rodent and human neostriatum. A decline in DARPP32 immunoreactivity in the neostriatum is characteristic of HD mice [73, 74]. Immunoperoxidase labeling for DARPP32 in the neostriatum of F2 generation 16 month old WT and TgHD minipigs showed intense labeling in neuronal cell bodies and neuropil (Fig. 8A–D). Some areas of less intense DARPP32 neuropil staining were present and may be striosomes, which have been described using other neuronal markers in rodent and human striatum

[75, 76] (Fig. 8B, D). Immunofluorescence analysis of caudate and putamen of F2 WT and TgHD minipigs at ages 4, 10 and 16 months also showed DARPP32 robustly expressed in neostriatal neurons and neuropil (Fig. 9A–C, shown for 16 months). A quantitative stereology analysis was performed in the sibling pair of 16 month old minipigs. Results showed that the median number of DARPP32+ neurons per mm^3 in caudate and putamen of the TgHD minipig was slightly lower compared to the WT (TgHD: 24,781 caudate neurons and 22,351 putamen neurons, and WT: 26,846 caudate

neurons and 23,863 putamen neurons) (Fig. 9C). In the TgHD brain there were reduced signal intensities for DARPP32 labeling in the caudate nucleus (11.3% reduction) and putamen (31.7% reduction) compared to the WT sibling. Although these data are highly preliminary and need confirmation in additional minipigs, the results suggest that by 16 months of age the levels of DARPP32 in TgHD minipig start to decline.

Analysis of reproductive capacity in TgHD boars

The number of spermatozoa per ejaculate was systematically evaluated in the transgenic boars from the age of 13 months to 26 months. There was a significant decline in the median number of spermatozoa in TgHD minipigs ($2.45\text{--}3.65 \times 10^9$ of spermatozoa) compared to WT ($8.15\text{--}12.48 \times 10^9$ of spermatozoa) (Fig. 10A, Kruskal-Wallis test $p < 0.001$ followed by *post-hoc* Mann-Whitney U, $p < 0.01$). These data suggest an impairment of spermatogenic production of the testes of TgHD minipigs. A time course analysis of

the TgHD sperm samples showed that sperm number was reduced at 13 months and remained low up to 26 months (Supplementary Data S8). IVF assay showed that in WT oocytes with zona pellucida intact, the number of TgHD spermatozoa that penetrated the oocyte was lower than for the WT spermatozoa (Fig. 10B). The median percentage of WT oocytes that were penetrated by TgHD spermatozoa was significantly lower than WT oocytes penetrated by WT spermatozoa (Kruskal-Wallis test $p < 0.001$ followed by *post-hoc* Mann-Whitney U, $p < 0.05$) (Fig. 10C). These results indicated that the penetration activity of spermatozoa in TgHD boars was impaired compared to those of WT spermatozoa. To investigate the basis for the impaired penetration rate in TgHD, WT oocytes with zona pellucida removed were used for further analysis. Removing the zona pellucida markedly increased penetration rate in the WT and TgHD groups to 100% level (Fig. 10D). These findings suggest that the presence of the HTT gene interferes with the penetration of TgHD spermatozoa through the zona pellucida but does not

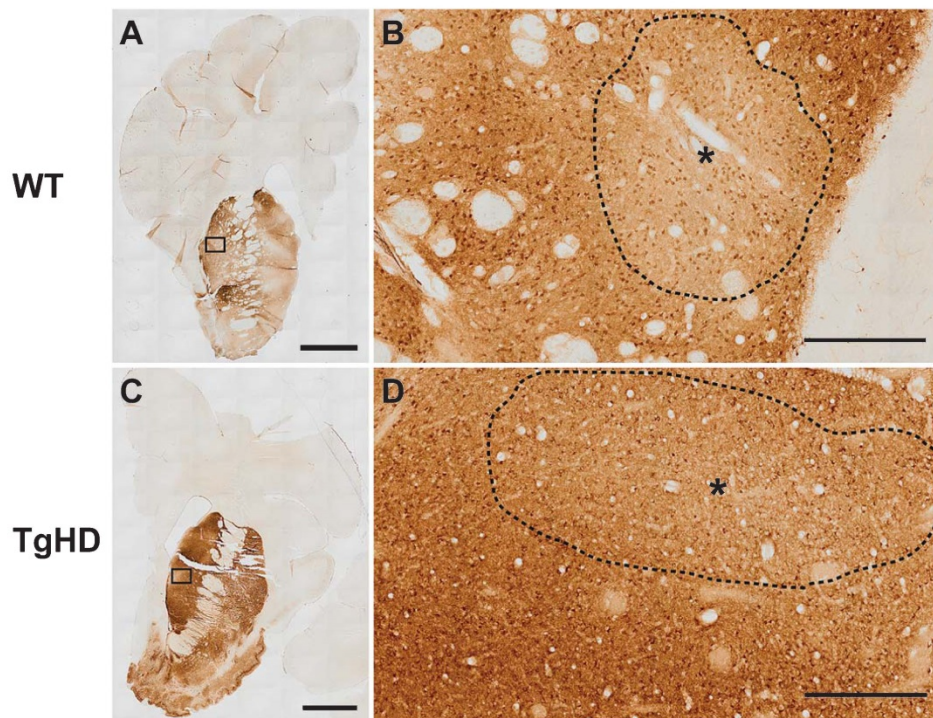


Fig. 8. DARPP32 immunoreactivity with immunoperoxidase method in 16 month old F2 WT and TgHD minipig brain. (A and C) Coronal sections through the neostriatum of WT (A) and TgHD (C) minipig show intense labeling for DARPP32 in the caudate nucleus and putamen and in the basal forebrain. Boxed areas are shown at higher magnification in B and D. (B and D) Higher magnification images show the intense labeling of neuropil and cell bodies. Areas of weaker neuropil labeling are demarcated by a dashed line and asterisk in the center and may represent striosomes. Scale bars in A and C are 5 mm and in B and D are 500 μm .

interfere with fusion of the post-acrosomal spermatozoa membrane and the cytoplasmic membrane of oocytes.

DISCUSSION

Rodent models of HD including transgenic mice expressing N-terminal fragments of mutant HTT have been very important for understanding disease mechanisms, validating targets, and testing candidate therapies, but have some limitations for modeling the human disease [2, 17]. The miniature pig (*Sus scrofa*) has similarities to humans in anatomy, physiology, and metabolism [20, 28, 29]. The size and structure of pig brain makes it amenable to neurosurgical procedures and non-invasive high resolution neuroimaging methods similar to those performed in humans [30, 34, 77]. The lifespan of minipigs and their sophisticated cognitive and motor abilities also make them useful for long-term studies of learning, memory and behavior [28, 78, 79]. In this study we show successful establishment of a transgenic minipig stably expressing N-truncated human mutant huntingtin 1–548 with 124 glutamines through multiple generations.

Transgenic HD minipigs were generated using lentiviral transduction of porcine zygotes in syngamy, at the onset of embryonic DNA synthesis. The precise timing of lentiviral transduction enhances incorporation of the transgene cDNA into embryos. The lentiviral delivery did not cause mosaicism, since the mutant HTT was revealed in all tissues tested in F1 and F2 TgHD minipigs and maintained the same number of glutamines. We found an in-frame deletion of the expanded CAG/CAA tract such that the integrated transgene encoded 124 glutamines instead of the original 145 glutamines. Similar contraction of the polyglutamine repeat has been observed in human HD [80]. The rates of transgenesis and viability of offspring in pig were higher with lentiviral delivery than with a cloning strategy reported previously [55, 81, 82]. In our experiments, the lentiviral construct that was used to transduce the minipig genome did not influence survival or normal development through multiple generations. The total neonatal mortality of our TgHD minipigs was 17.2%, which is in the range of the WT strain (16.4%, Supplementary Data S6). In contrast, the transgenic HD pigs, generated via a cloning strategy and bearing N-terminal mutant HTT (208 amino acids and 105 Q), showed a severe chorea phenotype before death and the presence of apoptotic cells in brain [55].

Both female and male transmissions of the HD transgene were confirmed in our TgHD minipigs. Two litters of F1 generation minipigs were born with a rate of transgenesis of 29.4%. The litters of F2 and F3 generations had a Mendelian inheritance of the transgene of 40.2% and 34.9%, respectively. Importantly, one single copy of exogenous HTT was found in chromosome 1 (1q24-q25) where it was maintained in F1 and F2 offspring. The TgHD minipigs of F0–F2 generations had two alleles coding endogenous pig HTT and one allele for the N-terminal human mutant HTT. No homozygote TgHD minipigs were generated with heterozygote TgHD matings. The site of insertion of the transgene may have disrupted some essential genetic sequence that caused lethality of progeny homozygous for the HD transgene [83]. More detailed information on the exact site of insertion of the transgene in chromosome 1 may reveal more insights about potential homozygote lethality.

Mutant HTT protein expression was detected in different brain regions including cortex, caudate nucleus and putamen and in a variety of peripheral tissues and confirmed by both Western Blot analysis and TR-FRET. With one exception (hypothalamus in one of the TgHD minipigs), the data from WB and TR-FRET biochemical assays showed a good correspondence for the relative distribution of human mutant HTT in different brain regions and peripheral tissues. The expression of the transgenic protein was not confirmed in heart, stomach, spleen and skeletal muscle. *Trottier et al.* [84] determined the presence of HTT protein also in heart. Discrepancies in observed distribution of huntingtin in tissues can be influenced by the preparation of protein lysates [85]. In “bloody” tissues (liver, spleen), red color of analyte is known to artificially increase background in TR-FRET readout thus higher mutant HTT background signals in these WT tissues were likely due to this effect. The variations in the expression level of protein were expected in skin tissue due to insufficient homogenization.

Midbrain dopaminergic neurons play a critical role in basal ganglia circuitry and function including coordination of movement. Protein phosphatase 1 regulatory subunit 1B, also known as dopamine- and cAMP-regulated neuronal phosphoprotein (DARPP32), is highly expressed in caudate-putamen medium-sized spiny neurons [73, 86]. Dopamine D1 receptor stimulation enhances cyclic AMP formation, resulting in the phosphorylation of DARPP32 [86] at Thr34 by PKA [87]. A loss of DARPP32 levels in medium-sized spiny striatal neurons was observed in several rodent models of HD [74, 88], and in the globus pallidus and putamen

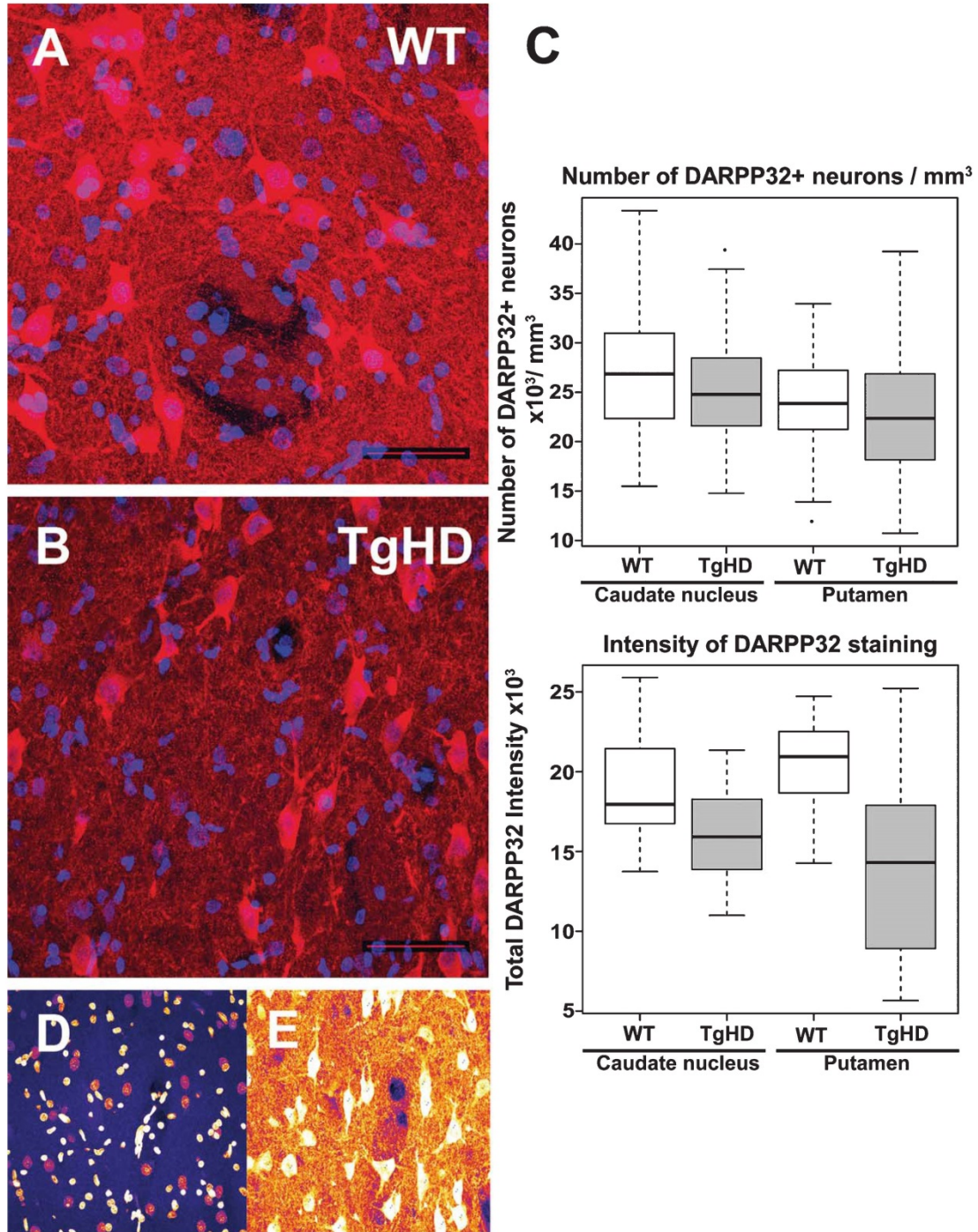


Fig. 9.

of 7 month old HD sheep [21]. A 16 month old TgHD minipig brain had a reduction compared to WT in the intensity of neuronal labeling for DARPP32 in the caudate nucleus and putamen. Clearly these findings, which are based on a detailed quantitative analysis of only one sibling pair of WT and TgHD minipigs, need to be confirmed in more animals. Nevertheless, the data suggest that changes in DARPP32 may begin in the TgHD minipig brain at around 16 months of age.

The formation of aggregates is a hallmark of HD pathology. Nuclear and cytoplasmic inclusions of mutant HTT are seen in human postmortem HD brain and in mouse models of HD [9, 72]. There was no evidence of aggregates of mutant HTT protein in the TgHD minipig up to 16 months of age based on biochemical (AGERA, filter retardation) and immunohistochemical assays with antibody to anti-HTT1-17. This antibody detects mutant HTT inclusions in the human HD brain. Other antibodies commonly used to detect nuclear inclusions of human HTT fragments in HD mice including MW8 and EM48 produced no staining in the TgHD minipigs. The absence of nuclear inclusions in the TgHD minipigs was consistent with the negative results for aggregation observed using the AGERA and filter retardations assays. Clearly study of brains from older TgHD minipigs will be needed to determine onset of aggregate formation. Many factors influence the incidence of aggregated mutant HTT including levels of mutant protein expression, polyglutamine length, the length of the mutant HTT fragment, and age of the animal [89–91]. It is noteworthy that a well studied HD mouse model BACHD which expresses full length mutant HTT with 97 glutamines encoded by CAG/CAA repeats [92] develops brain pathology and progressive motor deficits but lacks obvious intranuclear mutant HTT aggregates [93]. Some neuropil aggregates appeared in late stages (12–18 months BACHD) and were more prominent when aggressive antigen retrieval and anti-HTT antibody 3B5H10 were used in the brain sections [94], suggesting that epitopes for detecting mutant HTT aggregates may be masked. As with BACHD, the polyglutamine tract in our TgHD minipig has a mix of CAG/CAA repeats. It is possible that CAG/CAA sequence generates protein

conformations that are unfavorable for immunodetection of aggregates.

A surprising finding was evidence for a decline in fertility in F1 boars caused by reduced sperm number and penetration rate. This phenotype can be easily monitored in the TgHD minipigs and therefore represents a biomarker that can be suitable for therapeutics. From 13–26 months the decline in sperm function was constant. Analysis of earlier ages might reveal a period of progressive decline that could also be a useful index for analysis of therapeutics. As only 2 F1 transgenic boars were available for detailed analysis, these findings must be considered preliminary and we are currently investigating reproductive competence in a larger cohort of F2 animals. Pathology in the germinal epithelium has been documented in human HD and YAC 128 HD mouse on histological sections where a decreased number of germ cells and reduced seminiferous tubule cross-sectional area have been observed [95]. The testicular pathology in humans was related to the presence of mutant HTT since severity was greater in patients with longer CAG repeats and testicular pathology was not present in a patient with amyotrophic lateral sclerosis. The YAC 128 HD mouse develops testicular pathology between 9 and 12 months prior to significant reduction in testosterone or GnRH levels but coinciding with changes in the brain and the appearance of motor deficits. Unlike the TgHD minipigs, problems with sperm quality and fertility have not been reported in HD patients.

No evident changes in motor function were observed in a F0 TgHD minipig up to the age of 40 months. However, only 4 animals (3 TG vs. 1 WT) were subjected to the study. A systematic quantitative study focusing on changes in motor and cognitive functions in TgHD minipigs is underway (Dr. R. Reilmann, unpublished data). In contrast to our TgHD minipigs, the short-lived transgenic piglets produced by a cloning strategy showed dyskinesia and chorea-like movements before death [55].

In summary we have developed a heterozygote TgHD minipig that expresses a human mutant HTT fragment throughout the CNS and peripheral tissues in a stable fashion through multiple generations. The TgHD minipig is healthy at birth and through early

Fig. 9. Immunofluorescence labeling of DARPP32 in WT and TgHD minipig neostriatum. (A and B) Shown are images of microscopic fields from the putamen of 16 month old WT (A) and TgHD sibling minipig (B). DARPP32 labeling in the cytoplasm is red and DAPI staining in the nucleus is in blue. (C) Upper boxplot shows median numbers of DARPP32+ neurons (mm^{-3}) in caudate nucleus and putamen of WT and TgHD minipigs. Lower box plots shows median intensity of DARPP32 staining determined as described in Methods. (D) and (E) are pseudo-color images of DAPI stained nuclei and DARPP32 stained neurons respectively in WT putamen obtained using fire view in Fiji software as part of thresholding for the neuronal counting procedure. Scale bar 50 μm . (Colours are visible in the online version of the article; <http://dx.doi.org/10.3233/JHD-130001>)

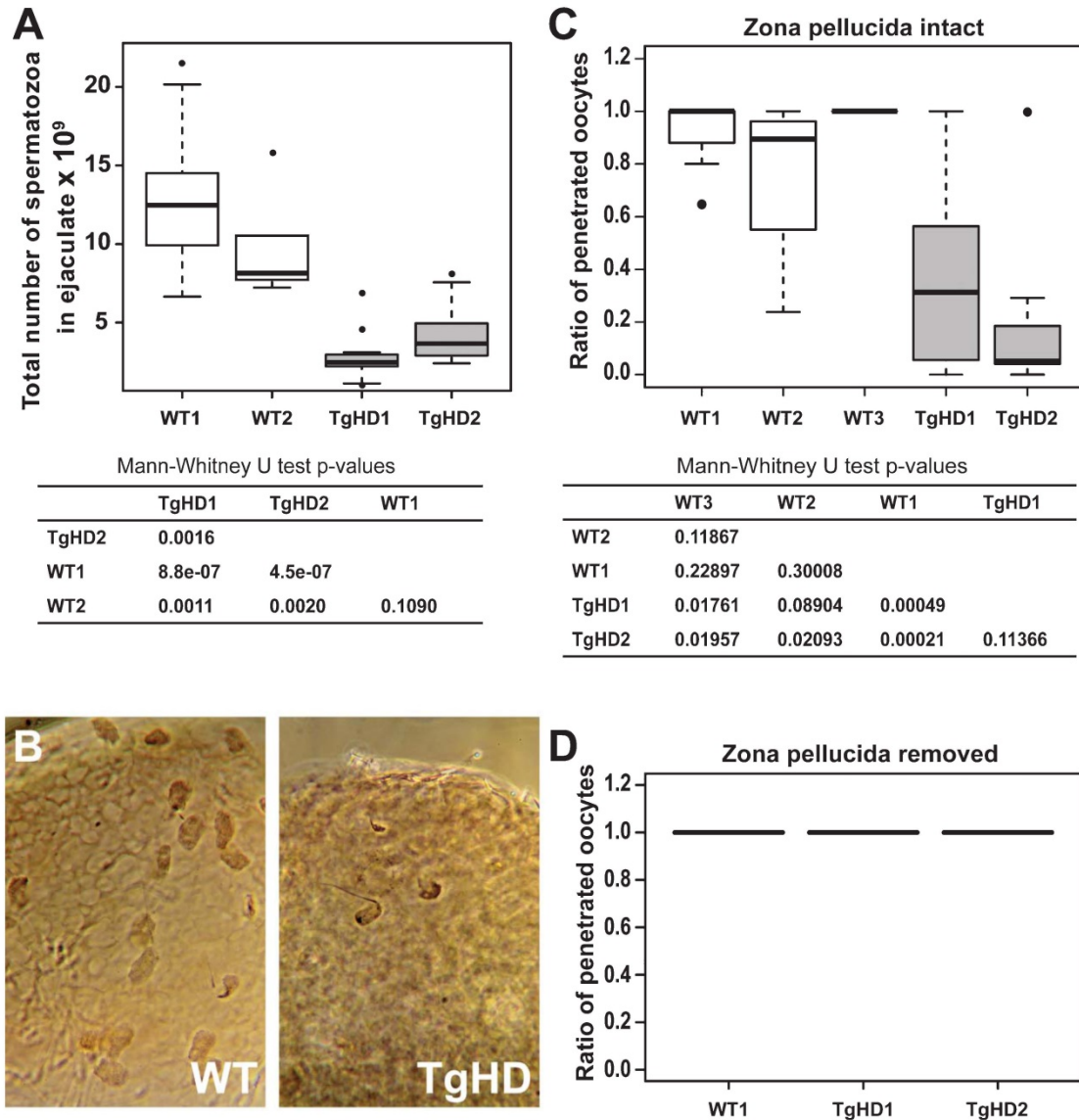


Fig. 10. Failure of reproductive capacity in TgHD boars. (A) Boxplots show number of spermatozoa per ejaculate in two WT boars and in 2 TgHD minipig boars of similar age (see methods for details). The median number of spermatozoa is reduced in TgHD minipigs compared to WT minipigs, *p*-values for all pairwise comparisons (Mann-Whitney U test) are shown in the table. (B) Left: Image of WT oocyte fertilized with WT spermatozoa *in vitro*: Note the large number of penetrated, partly de-condensed spermatozoa that are visible in intact oocyte *in vitro* fertilized with WT spermatozoa. Right: Image of WT oocyte fertilized with TgHD spermatozoa *in vitro*. Note the small number of spermatozoa. The syngamy of male and female pronuclei is visible and only one supernumerary penetrated sperm is evident. (C) Boxplots show the median ratio of intact WT oocytes (including zona pellucida) penetrated by WT or TgHD spermatozoa as determined by IVF. *P*-values for all pairwise comparisons (Mann-Whitney U test) are shown in the table below. (D) Boxplots show the median ratio of WT oocytes with zona pellucida removed penetrated by WT or TgHD spermatozoa as determined by IVF.

development and does not exhibit obvious signs of abnormal movement up to 40 months of age. However, a decline is evident at 16 months in DARPP32 immunoreactivity in the neostriatum, the region most

affected in HD, as well as a decline in sperm number and penetration rate beginning at about 13 months. Formal testing of the TgHD minipigs in a battery of motor tasks is now underway.

ACKNOWLEDGMENTS

We would like to thank Patricia Jandurova, Irena Deylova and Stepan Hladky for the excellent technical assistance. We are grateful to Professor Jindrich Martinek for his help with the immunohistochemistry and virtual microscopy. We thank Jiri Jarkovsky, Institute of Biostatistics, Masaryk University, Brno, Czech Republic for advice on statistics. This work was supported by the CHDI Foundation (ID 1035), The Technical Agency of the Czech Republic (TA01011466), the project EXAM from European Regional Development Fund CZ.1.05/2.1.00/03.0124, The Grant Agency of the Charles University - Project No. 589412 and RVO 67985904.

CONFLICT OF INTEREST

One of the authors, Dr. David S. Howland is employed by CHDI Inc. which supported this research.

REFERENCES

- [1] Gil JM, Rego AC. Mechanisms of neurodegeneration in Huntington's disease. *The European Journal of Neuroscience*. 2008;27(11):2803-20. PubMed PMID: 18588526. Epub 2008/07/01. eng.
- [2] Zuccato C, Valenza M, Cattaneo E. Molecular mechanisms and potential therapeutical targets in Huntington's disease. *Physiological Reviews*. 2010;90(3):905-81. PubMed PMID: 20664076. Epub 2010/07/29. eng.
- [3] Perez-De La Cruz V, Santamaria A. Integrative hypothesis for Huntington's disease: A brief review of experimental evidence. *Physiological Research/Academia Scientiarum Bohemoslovaca*. 2007;56(5):513-26. PubMed PMID: 17184144. Epub 2006/12/23. eng.
- [4] Walker FO. Huntington's disease. *Lancet*. 2007;369(9557):218-28. PubMed PMID: 17240289. Epub 2007/01/24. eng.
- [5] The Huntington's Disease Collaborative Research Group. A novel gene containing a trinucleotide repeat that is expanded and unstable on Huntington's disease chromosomes. *Cell*. 1993;72(6):971-83. PubMed PMID: 8458085. Epub 1993/03/26. eng.
- [6] Brinkman RR, Mezei MM, Theilmann J, Almqvist E, Hayden MR. The likelihood of being affected with Huntington disease by a particular age, for a specific CAG size. *American Journal of Human Genetics*. 1997;60(5):1202-10. PubMed PMID: 9150168. Pubmed Central PMCID: 1712445. Epub 1997/05/01. eng.
- [7] Dunnett SB, Rosser AE. Cell transplantation for Huntington's disease Should we continue? *Brain Research Bulletin*. 2007;72(2-3):132-47. PubMed PMID: 17352937. Epub 2007/03/14. eng.
- [8] Lee ST, Kim M. Aging and neurodegeneration. Molecular mechanisms of neuronal loss in Huntington's disease. *Mechanisms of Ageing and Development*. 2006;127(5):432-5. PubMed PMID: 16527334. Epub 2006/03/11. eng.
- [9] Davies SW, Turmaine M, Cozens BA, DiFiglia M, Sharp AH, Ross CA, et al. Formation of neuronal intranuclear inclusions underlies the neurological dysfunction in mice transgenic for the HD mutation. *Cell*. 1997;90(3):537-48. PubMed PMID: 9267033. Epub 1997/08/08. eng.
- [10] Mangiarini L, Sathasivam K, Seller M, Cozens B, Harper A, Hetherington C, et al. Exon 1 of the HD gene with an expanded CAG repeat is sufficient to cause a progressive neurological phenotype in transgenic mice. *Cell*. 1996;87(3):493-506. PubMed PMID: 8898202. Epub 1996/11/01. eng.
- [11] Schilling G, Becher MW, Sharp AH, Jinnah HA, Duan K, Kotzuk JA, et al. Intranuclear inclusions and neuritic aggregates in transgenic mice expressing a mutant N-terminal fragment of huntingtin. *Human Molecular Genetics*. 1999; 8(3):397-407. PubMed PMID: 9949199. Epub 1999/02/09. eng.
- [12] Reddy PH, Williams M, Charles V, Garrett L, Pike-Buchanan L, Whetsell WO, Jr., et al. Behavioural abnormalities and selective neuronal loss in HD transgenic mice expressing mutated full-length HD cDNA. *Nature Genetics*. 1998; 20(2):198-202. PubMed PMID: 9771716. Epub 1998/10/15. eng.
- [13] Van Raamsdonk JM, Murphy Z, Slow EJ, Leavitt BR, Hayden MR. Selective degeneration and nuclear localization of mutant huntingtin in the YAC128 mouse model of Huntington disease. *Human molecular genetics*. 2005;14(24):3283-35. PubMed PMID: 16278236. Epub 2005/11/10. eng.
- [14] Ariano MA, Aronin N, DiFiglia M, Tagle DA, Sibley DR, Leavitt BR, et al. Striatal neurochemical changes in transgenic models of Huntington's disease. *Journal of Neuroscience Research*. 2002;68(6):716-29. PubMed PMID: 12111832. Epub 2002/07/12. eng.
- [15] Reynolds GP, Dalton CF, Tillery CL, Mangiarini L, Davies SW, Bates GP. Brain neurotransmitter deficits in mice transgenic for the Huntington's disease mutation. *Journal of Neurochemistry*. 1999;72(4):1773-6. PubMed PMID: 10098889. Epub 1999/03/31. eng.
- [16] Van Raamsdonk JM, Pearson J, Slow EJ, Hossain SM, Leavitt BR, Hayden MR. Cognitive dysfunction precedes neuropathology and motor abnormalities in the YAC128 mouse model of Huntington's disease. *The Journal of Neuroscience : The Official Journal of the Society for Neuroscience*. 2005;25(16):4169-80. PubMed PMID: 15843620. Epub 2005/04/22. eng.
- [17] Yang SH, Chan AW. Transgenic animal models of huntington's disease. *Current Topics in Behavioral Neurosciences*. 2011;7:61-85. PubMed PMID: 21225414. Epub 2011/01/13. eng.
- [18] Bendixen E, Danielsen M, Larsen K, Bendixen C. Advances in porcine genomics and proteomics—a toolbox for developing the pig as a model organism for molecular biomedical research. *Briefings in Functional Genomics*. 2010;9(3):208-19. PubMed PMID: 20495211. Epub 2010/05/25. eng.
- [19] Casal M, Haskins M. Large animal models and gene therapy. *Eur J Hum Genet*. 2006;14(3):266-72. PubMed PMID: 16333317. Epub 2005/12/08. eng.
- [20] Swindle MM, Makin A, Herron AJ, Clubb FJ, Jr., Frazier KS. Swine as models in biomedical research and toxicology testing. *Vet Pathol*. 2012;49(2):344-56. PubMed PMID: 21441112. Epub 2011/03/29. eng.
- [21] Jacobsen JC, Bawden CS, Rudiger SR, McLaughlan CJ, Reid SJ, Waldvogel HJ, et al. An ovine transgenic Huntington's disease model. *Human Molecular Genetics*. 2010; 19(10):1873-82. PubMed PMID: 20154343. Pubmed Central PMCID: 2860888. Epub 2010/02/16. eng.
- [22] Yang SH, Cheng PH, Banta H, Piotrowska-Nitsche K, Yang JJ, Cheng EC, et al. Towards a transgenic model

- of Huntington's disease in a non-human primate. *Nature*. 2008;453(7197):921-4. PubMed PMID: 18488016. Pubmed Central PMCID: 2652570. Epub 2008/05/20. eng.
- [23] Bjarkam CR, Jorgensen RL, Jensen KN, Sunde NA, Sorensen JC. Deep brain stimulation electrode anchoring using BioGlue(R), a protective electrode covering, and a titanium microplate. *Journal of Neuroscience Methods*. 2008; 168(1):151-5. PubMed PMID: 17953993. Epub 2007/10/24. eng.
- [24] Ettrup KS, Sorensen JC, Rodell A, Alstrup AK, Bjarkam CR. Hypothalamic deep brain stimulation influences autonomic and limbic circuitry involved in the regulation of aggression and cardiocerebrovascular control in the Gottingen minipig. *Stereotactic and Functional Neurosurgery*. 2012;90(5):281-91. PubMed PMID: 22797692. Epub 2012/07/17. eng.
- [25] Fjord-Larsen L, Kusk P, Tornoe J, Juliusson B, Torp M, Bjarkam CR, et al. Long-term delivery of nerve growth factor by encapsulated cell biodelivery in the Gottingen minipig basal forebrain. *Molecular Therapy: The Journal of the American Society of Gene Therapy*. 2010;18(12):2164-72. PubMed PMID: 20664524. Pubmed Central PMCID: 2997581. Epub 2010/07/29. eng.
- [26] Jensen KN, Deding D, Sorensen JC, Bjarkam CR. Long-term implantation of deep brain stimulation electrodes in the pontine micturition centre of the Gottingen minipig. *Acta Neurochirurgica*. 2009;151(7):785-94; discussion 94. PubMed PMID: 19404572. Epub 2009/05/01. eng.
- [27] Lind NM, Moustgaard A, Jelsing J, Vajta G, Cumming P, Hansen AK. The use of pigs in neuroscience: Modeling brain disorders. *Neuroscience and Biobehavioral Reviews*. 2007; 31(5):728-51. PubMed PMID: 17445892. Epub 2007/04/21. eng.
- [28] Lunney JK. Advances in swine biomedical model genomics. *International Journal of Biological Sciences*. 2007;3(3):179-84. PubMed PMID: 17384736. Pubmed Central PMCID: 1802015. Epub 2007/03/27. eng.
- [29] Vodicka P, Smetana K, Jr., Dvorankova B, Emerick T, Xu YZ, Ourednik J, et al. The miniature pig as an animal model in biomedical research. *Annals of the New York Academy of Sciences*. 2005;1049:161-71. PubMed PMID: 15965115. Epub 2005/06/21. eng.
- [30] Ishizu K, Smith DF, Bender D, Danielsen E, Hansen SB, Wong DF, et al. Positron emission tomography of radioligand binding in porcine striatum *in vivo*: Haloperidol inhibition linked to endogenous ligand release. *Synapse*. 2000; 38(1):87-101. PubMed PMID: 10941144. Epub 2000/08/15. eng.
- [31] Rosa-Neto P, Doudet DJ, Cumming P. Gradients of dopamine D1- and D2/3-binding sites in the basal ganglia of pig and monkey measured by PET. *NeuroImage*. 2004;22(3):1076-83. PubMed PMID: 15219579. Epub 2004/06/29. eng.
- [32] Andersen F, Watanabe H, Bjarkam C, Danielsen EH, Cumming P, DaNe XSG. Pig brain stereotaxic standard space: Mapping of cerebral blood flow normative values and effect of MPTP-lesioning. *Brain Research Bulletin*. 2005;66(1):17-29. PubMed PMID: 15925140. Epub 2005/06/01. eng.
- [33] Duhaime AC, Saykin AJ, McDonald BC, Dodge CP, Eskey CJ, Darcey TM, et al. Functional magnetic resonance imaging of the primary somatosensory cortex in piglets. *Journal of Neurosurgery*. 2006;104(4 Suppl):259-64. PubMed PMID: 16619637. Epub 2006/04/20. eng.
- [34] Gizewski ER, Schanze T, Bolle I, de Greiff A, Forsting M, Laube T. Visualization of the visual cortex in minipigs using fMRI. *Research in Veterinary Science*. 2007;82(3):281-6. PubMed PMID: 17064742. Epub 2006/10/27. eng.
- [35] Watanabe H, Andersen F, Simonsen CZ, Evans SM, Gjedde A, Cumming P, et al. MR-based statistical atlas of the Gottingen minipig brain. *NeuroImage*. 2001;14(5):1089-96. PubMed PMID: 11697940. Epub 2001/11/08. eng.
- [36] Bjarkam CR, Cancian G, Larsen M, Rosendahl F, Ettrup KS, Zeidler D, et al. A MRI-compatible stereotaxic localizer box enables high-precision stereotaxic procedures in pigs. *Journal of Neuroscience Methods*. 2004;139(2):293-8. PubMed PMID: 15488243. Epub 2004/10/19. eng.
- [37] Rosendahl F, Chakravarty MM, Sunde N, Rodell A, Jonsdottir KY, Pedersen M, et al. Defining the intercommissural plane and stereotaxic coordinates for the Basal Ganglia in the Gottingen minipig brain. *Stereotactic and Functional Neurosurgery*. 2010;88(3):138-46. PubMed PMID: 20357521. Epub 2010/04/02. eng.
- [38] Rosendahl F, Frandsen J, Chakravarty MM, Bjarkam CR, Pedersen M, Sangill R, et al. New surgical technique reduces the susceptibility artefact at air-tissue interfaces on *in vivo* cerebral MRI in the Gottingen minipig. *Brain Research Bulletin*. 2009;80(6):403-7. PubMed PMID: 19712728. Epub 2009/08/29. eng.
- [39] Rosendahl F, Pedersen M, Sangill R, Stodkilde-Jorgensen H, Nielsen MS, Bjarkam CR, et al. MRI protocol for *in vivo* visualization of the Gottingen minipig brain improves targeting in experimental functional neurosurgery. *Brain Research Bulletin*. 2009;79(1):41-5. PubMed PMID: 19185604. Epub 2009/02/03. eng.
- [40] Archibald AL, Bolund L, Churcher C, Fredholm M, Groenen MA, Harlizius B, et al. Pig genome sequence-analysis and publication strategy. *BMC Genomics*. 2010;11:438. PubMed PMID: 20642822. Pubmed Central PMCID: 3017778. Epub 2010/07/21. eng.
- [41] Jiang Z, Rothschild MF. Swine genome science comes of age. *International Journal of Biological Sciences*. 2007;3(3):129-31. PubMed PMID: 17384732. Pubmed Central PMCID: 1802017. Epub 2007/03/27. eng.
- [42] Jorgensen FG, Hobolth A, Hornshøj H, Bendixen C, Fredholm M, Schierup MH. Comparative analysis of protein coding sequences from human, mouse and the domesticated pig. *BMC Biology*. 2005;3:2. PubMed PMID: 15679890. Pubmed Central PMCID: 549206. Epub 2005/02/01. eng.
- [43] Wernersson R, Schierup MH, Jorgensen FG, Gorodkin J, Panitz F, Staerfeldt HH, et al. Pigs in sequence space: A 0.66X coverage pig genome survey based on shotgun sequencing. *BMC Genomics*. 2005;6:70. PubMed PMID: 15885146. Pubmed Central PMCID: 1142312. Epub 2005/05/12. eng.
- [44] Ramos AM, Crooijmans RP, Affara NA, Amaral AJ, Archibald AL, Beever JE, et al. Design of a high density SNP genotyping assay in the pig using SNPs identified and characterized by next generation sequencing technology. *PLoS One*. 2009;4(8):e6524. PubMed PMID: 19654876. Pubmed Central PMCID: 2716536. Epub 2009/08/06. eng.
- [45] Kim J, Cho IS, Hong JS, Choi YK, Kim H, Lee YS. Identification and characterization of new microRNAs from pig. *Mammalian Genome: Official Journal of the International Mammalian Genome Society*. 2008;19(7-8):570-80. PubMed PMID: 18548309. Epub 2008/06/13. eng.
- [46] Li M, Xia Y, Gu Y, Zhang K, Lang Q, Chen L, et al. MicroRNAome of porcine pre- and postnatal development. *PLoS One*. 2010;5(7):e11541. PubMed PMID: 20634961. Pubmed Central PMCID: 2902522. Epub 2010/07/17. eng.
- [47] Reddy AM, Zheng Y, Jagadeeswaran G, Macmill SL, Graham WB, Roe BA, et al. Cloning, characterization and

- expression analysis of porcine microRNAs. *BMC Genomics*. 2009;10:65. PubMed PMID: 19196471. Pubmed Central PMCID: 2644714. Epub 2009/02/07. eng.
- [48] Hofmann A, Kessler B, Ewerling S, Weppert M, Vogg B, Ludwig H, et al. Efficient transgenesis in farm animals by lentiviral vectors. *EMBO Reports*. 2003;4(11):1054-60. PubMed PMID: 14566324. Pubmed Central PMCID: 1326377. Epub 2003/10/21. eng.
- [49] Nagashima H, Fujimura T, Takahagi Y, Kurome M, Wako N, Ochiai T, et al. Development of efficient strategies for the production of genetically modified pigs. *Theriogenology*. 2003;59(1):95-106. PubMed PMID: 12499021. Epub 2002/12/25. eng.
- [50] Kurome M, Ueda H, Tomii R, Naruse K, Nagashima H. Production of transgenic-clone pigs by the combination of ICSI-mediated gene transfer with somatic cell nuclear transfer. *Transgenic Research*. 2006;15(2):229-40. PubMed PMID: 16604463. Epub 2006/04/11. eng.
- [51] Lavitrano M, Busnelli M, Cerito MG, Giovannoni R, Manzini S, Vargiolu A. Sperm-mediated gene transfer. *Reproduction, Fertility, and Development*. 2006;18(1-2):19-23. PubMed PMID: 16478599. Epub 2006/02/16. eng.
- [52] Matsuyama N, Hadano S, Onoe K, Osuga H, Showguchi-Miyata J, Gondo Y, et al. Identification and characterization of the miniature pig Huntington's disease gene homolog: Evidence for conservation and polymorphism in the CAG triplet repeat. *Genomics*. 2000;69(1):72-85. PubMed PMID: 11013077. Epub 2000/10/03. eng.
- [53] Lin B, Rommens JM, Graham RK, Kalchman M, MacDonald H, Nasir J, et al. Differential 3' polyadenylation of the Huntington disease gene results in two mRNA species with variable tissue expression. *Human Molecular Genetics*. 1993;2(10):1541-5. PubMed PMID: 7903579. Epub 1993/10/01. eng.
- [54] Aigner B, Renner S, Kessler B, Klymiuk N, Kurome M, Wunsch A, et al. Transgenic pigs as models for translational biomedical research. *Journal of Molecular Medicine*. 2010;88(7):653-64. PubMed PMID: 20339830. Epub 2010/03/27. eng.
- [55] Yang D, Wang CE, Zhao B, Li W, Ouyang Z, Liu Z, et al. Expression of Huntington's disease protein results in apoptotic neurons in the brains of cloned transgenic pigs. *Human Molecular Genetics*. 2010;19(20):3983-94. PubMed PMID: 20660116. Pubmed Central PMCID: 2947404. Epub 2010/07/28. eng.
- [56] Modlik J, Klima J, Dvorankova B, Smetana K, Jr. Porcine epidermal stem cells as a biomedical model for wound healing and normal/malignant epithelial cell propagation. *Theriogenology*. 2007;67(1):105-11. PubMed PMID: 17055565. Epub 2006/10/24. eng.
- [57] Trask BJ. DNA sequence localization in metaphase and interphase cells by fluorescence *in situ* hybridization. *Methods in Cell Biology*. 1991;35:3-35. PubMed PMID: 1779860. Epub 1991/01/01. eng.
- [58] Ruijter JM, Ramakers C, Hoogaars WM, Karlen Y, Bakker O, van den Hoff MJ, et al. Amplification efficiency: Linking baseline and bias in the analysis of quantitative PCR data. *Nucleic Acids Research*. 2009;37(6):e45. PubMed PMID: 19237396. Pubmed Central PMCID: 2665230. Epub 2009/02/25. eng.
- [59] DiFiglia M, Sapp E, Chase K, Schwarz C, Meloni A, Young C, et al. Huntingtin is a cytoplasmic protein associated with vesicles in human and rat brain neurons. *Neuron*. 1995;14(5):1075-81. PubMed PMID: 7748555. Epub 1995/05/01. eng.
- [60] Weiss A, Klein C, Woodman B, Sathasivam K, Bibbel M, Regulier E, et al. Sensitive biochemical aggregate detection reveals aggregation onset before symptom development in cellular and murine models of Huntington's disease. *Journal of Neurochemistry*. 2008;104(3):846-58. PubMed PMID: 17986219. Epub 2007/11/08. eng.
- [61] Legleiter J, Mitchell E, Lotz GP, Sapp E, Ng C, DiFiglia M, et al. Mutant huntingtin fragments form oligomers in a polyglutamine length-dependent manner *in vitro* and *in vivo*. *The Journal of Biological Chemistry*. 2010;285(19):14777-90. PubMed PMID: 20220138. Pubmed Central PMCID: 2863238. Epub 2010/03/12. eng.
- [62] Sontag EM, Lotz GP, Agrawal N, Tran A, Aron R, Yang G, et al. Methylene blue modulates huntingtin aggregation intermediates and is protective in Huntington's disease models. *The Journal of Neuroscience : The Official Journal of the Society for Neuroscience*. 2012;32(32):11109-19. PubMed PMID: 22875942. Epub 2012/08/10. eng.
- [63] Sontag EM, Lotz GP, Yang G, Sontag CJ, Cummings BJ, Glabe CG, et al. Detection of mutant huntingtin aggregation conformers and modulation of SDS-soluble fibrillar oligomers by small molecules. *Journal of Huntington's Disease*. 2012;1(1):127-40.
- [64] Scherzinger E, Lurz R, Turnaine M, Mangiarini L, Hollenbach B, Hasenbank R, et al. Huntingtin-encoded polyglutamine expansions form amyloid-like protein aggregates *in vitro* and *in vivo*. *Cell*. 1997;90(3):549-58. PubMed PMID: 9267034. Epub 1997/08/08. eng.
- [65] Weiss A, Abramowski D, Bibbel M, Bodner R, Chopra V, DiFiglia M, et al. Single-step detection of mutant huntingtin in animal and human tissues: A bioassay for Huntington's disease. *Analytical Biochemistry*. 2009;395(1):8-15. PubMed PMID: 19664996. Epub 2009/08/12. eng.
- [66] Bjarkam CR, Pedersen M, Sorensen JC. New strategies for embedding, orientation and sectioning of small brain specimens enable direct correlation to MR-images, brain atlases, or use of unbiased stereology. *Journal of Neuroscience Methods*. 2001;108(2):153-9. PubMed PMID: 11478974. Epub 2001/08/02. eng.
- [67] Sorensen JC, Bjarkam CR, Danielsen EH, Simonsen CZ, Geneser FA. Oriented sectioning of irregular tissue blocks in relation to computerized scanning modalities: Results from the domestic pig brain. *Journal of Neuroscience Methods*. 2000;104(1):93-8. PubMed PMID: 11163415. Epub 2001/02/13. eng.
- [68] Guzowski JF, McNaughton BL, Barnes CA, Worley PF. Environment-specific expression of the immediate-early gene Arc in hippocampal neuronal ensembles. *Nature Neuroscience*. 1999;2(12):1120-4. PubMed PMID: 10570490. Epub 1999/11/26. eng.
- [69] West MJ. Design-based stereological methods for counting neurons. *Progress in Brain Research*. 2002;135:43-51. PubMed PMID: 12143362. Epub 2002/07/30. eng.
- [70] Rath D, Niemann H. *In vitro* fertilization of porcine oocytes with fresh and frozen-thawed ejaculated or frozen-thawed epididymal semen obtained from identical boars. *Theriogenology*. 1997;47(4):785-93. PubMed PMID: 16728028. Epub 1997/03/01. eng.
- [71] Bhide PG, Day M, Sapp E, Schwarz C, Sheth A, Kim J, et al. Expression of normal and mutant huntingtin in the developing brain. *The Journal of Neuroscience : The Official Journal of the Society for Neuroscience*. 1996;16(17):5523-35. PubMed PMID: 8757264. Epub 1996/09/01. eng.
- [72] DiFiglia M, Sapp E, Chase KO, Davies SW, Bates GP, Vonsattel JP, et al. Aggregation of huntingtin in neuronal

- intranuclear inclusions and dystrophic neurites in brain. *Science*. 1997;266(5334):1990-3. PubMed PMID: 9302293. Epub 1997/09/26. eng.
- [73] Ouimet CC, Greengard P. Distribution of DARPP-32 in the basal ganglia: An electron microscopic study. *Journal of Neurocytology*. 1990;19(1):39-52. PubMed PMID: 2191086. Epub 1990/02/01. eng.
- [74] van Dellen A, Welch J, Dixon RM, Cordery P, York D, Styles P, et al. N-Acetylaspartate and DARPP-32 levels decrease in the corpus striatum of Huntington's disease mice. *Neuroreport*. 2000;11(17):3751-7. PubMed PMID: 11117485. Epub 2000/12/16. eng.
- [75] Tippett LJ, Waldvogel HJ, Thomas SJ, Hogg VM, van Roon-Mom W, Synek BJ, et al. Striosomes and mood dysfunction in Huntington's disease. *Brain : A Journal of Neurology*. 2007;130(Pt 1):206-21. PubMed PMID: 17040921.
- [76] Crittenden JR, Graybiel AM. Basal Ganglia disorders associated with imbalances in the striatal striosome and matrix compartments. *Frontiers in Neuroanatomy*. 2011;5:59. PubMed PMID: 21941467. Pubmed Central PMCID: 3171104.
- [77] Keereman V, Fierens Y, Broux T, De Deene Y, Lonnew M, Vandenbergh S. MRI-based attenuation correction for PET/MRI using ultrashort echo time sequences. *J Nucl Med*. 2010;51(5):812-8. PubMed PMID: 20439508. Epub 2010/05/05. eng.
- [78] Gieling ET, Nordquist RE, van der Staay FJ. Assessing learning and memory in pigs. *Anim Cogn*. 2011;14(2):151-73. PubMed PMID: 21203792. Pubmed Central PMCID: 3040303. Epub 2011/01/05. eng.
- [79] Gieling ET, Schuurman T, Nordquist RE, van der Staay FJ. The pig as a model animal for studying cognition and neurobehavioral disorders. *Current Topics in Behavioral Neurosciences*. 2011;7:359-83. PubMed PMID: 21287323. Epub 2011/02/03. eng.
- [80] Wheeler VC, Persichetti F, McNeil SM, Mysore JS, Mysore SS, MacDonald ME, et al. Factors associated with HD CAG repeat instability in Huntington disease. *Journal of Medical Genetics*. 2007;44(11):695-701. PubMed PMID: 17660463. Epub 2007/07/31. eng.
- [81] Lai L, Prather RS. Creating genetically modified pigs by using nuclear transfer. *Reproductive Biology and Endocrinology : RB&E*. 2003;1:82. PubMed PMID: 14613542. Pubmed Central PMCID: 280726. Epub 2003/11/14. eng.
- [82] Polejaeva IA, Chen SH, Vaught TD, Page RL, Mullins J, Ball S, et al. Cloned pigs produced by nuclear transfer from adult somatic cells. *Nature*. 2000;407(6800):86-90. PubMed PMID: 10993078. Epub 2000/09/19. eng.
- [83] Park F. Lentiviral vectors: Are they the future of animal transgenesis? *Physiol Genomics*. 2007;31(2):159-73. PubMed PMID: 17684037. Epub 2007/08/09. eng.
- [84] Trottier Y, Devys D, Imbert G, Saudou F, An I, Lutz Y, et al. Cellular localization of the Huntington's disease protein and discrimination of the normal and mutated form. *Nature Genetics*. 1995;10(1):104-10. PubMed PMID: 7647777. Epub 1995/05/01. eng.
- [85] Wood JD, MacMillan JC, Harper PS, Lowenstein PR, Jones AL. Partial characterisation of murine huntingtin and apparent variations in the subcellular localisation of huntingtin in human, mouse and rat brain. *Human Molecular Genetics*. 1996;5(4):481-7. PubMed PMID: 8845840. Epub 1996/04/01. eng.
- [86] Walaas SI, Greengard P. DARPP-32, a dopamine- and adenosine 3':5'-monophosphate-regulated phosphoprotein enriched in dopamine-innervated brain regions. I. Regional and cellular distribution in the rat brain. *The Journal of Neuroscience : The Official Journal of the Society for Neuroscience*. 1984;4(1):84-98. PubMed PMID: 6319627. Epub 1984/01/01. eng.
- [87] Hemmings HC, Jr., Greengard P, Tung HY, Cohen P. DARPP-32, a dopamine-regulated neuronal phosphoprotein, is a potent inhibitor of protein phosphatase-1. *Nature*. 1984;310(5977):503-5. PubMed PMID: 6087160. Epub 1984/08/09. eng.
- [88] Bibb JA, Yan Z, Svenningsson P, Snyder GL, Pieribone VA, Horiuchi A, et al. Severe deficiencies in dopamine signaling in presymptomatic Huntington's disease mice. *Proceedings of the National Academy of Sciences of the United States of America*. 2000;97(12):6809-14. PubMed PMID: 10829080. Pubmed Central PMCID: 18747. Epub 2000/06/01. eng.
- [89] Hackam AS, Singaraja R, Wellington CL, Metzler M, McCutcheon K, Zhang T, et al. The influence of huntingtin protein size on nuclear localization and cellular toxicity. *The Journal of Cell Biology*. 1998;141(5):1097-105. PubMed PMID: 9606203. Pubmed Central PMCID: 2137174. Epub 1998/06/12. eng.
- [90] Chen S, Bertheliev V, Hamilton JB, O'Nuallain B, Wetzel R. Amyloid-like features of polyglutamine aggregates and their assembly kinetics. *Biochemistry*. 2002;41(23):7391-9. PubMed PMID: 12044172. Epub 2002/06/05. eng.
- [91] Li SH, Li XJ. Aggregation of N-terminal huntingtin is dependent on the length of its glutamine repeats. *Human Molecular Genetics*. 1998;7(5):777-82. PubMed PMID: 9536080. Epub 1998/05/23. eng.
- [92] Gray M, Shirasaki DI, Cepeda C, Andre VM, Wilburn B, Lu XH, et al. Full-length human mutant huntingtin with a stable polyglutamine repeat can elicit progressive and selective neuropathogenesis in BACHD mice. *The Journal of Neuroscience : The Official Journal of the Society for Neuroscience*. 2008;28(24):6182-95. PubMed PMID: 18550760. Pubmed Central PMCID: 2630800. Epub 2008/06/14. eng.
- [93] Pouladi MA, Stanek LM, Xie Y, Franciosi S, Southwell AL, Deng Y, et al. Marked differences in neurochemistry and aggregates despite similar behavioural and neuropathological features of Huntington disease in the full-length BACHD and YAC128 mice. *Human Molecular Genetics*. 2012;21(10):2219-32. PubMed PMID: 22328089.
- [94] Miller J, Arrasate M, Brooks E, Libeu CP, Legleiter J, Hatters D, et al. Identifying polyglutamine protein species *in situ* that best predict neurodegeneration. *Nature Chemical Biology*. 2011;7(12):925-34. PubMed PMID: 22037470. Pubmed Central PMCID: 3271120. Epub 2011/11/01. eng.
- [95] Van Raamsdonk JM, Murphy Z, Selva DM, Hamidzadeh R, Pearson J, Petersen A, et al. Testicular degeneration in Huntington disease. *Neurobiology of Disease*. 2007;26(3):512-20. PubMed PMID: 17433700. Epub 2007/04/17. eng.

5.2. Evaluation of possible functions of UCHL1 in Ubiquitin Proteasome System Impairment in Huntington's disease

in publication

Partial UCHL1 depletion in R6/2 mouse model of Huntington's Disease accelerates mutant huntingtin aggregation

Hruska-Plochan M, Juhas S, Juhasova J, Wu S, Dumpi J, Weiss A, Marsala M, Motlik J.

NeuroReport (submitted)

IF (2012): 1.656; 5-year IF (2012): 1.989

Declaration of co-authors

“I hereby declare that Marián Hruška-Plochán was adequately involved (70%) in the study design, experiments, interpretation of results and writing of this manuscript.”

Prague, April 30 2013

Motlík Jan, Prof., DVM, Ph.D., D.Sc.

Partial UCHL1 depletion in R6/2 mouse model of Huntington's Disease accelerates mutant huntingtin aggregation

Marian Hruska-Plochan^{1,2,3,*}, Stefan Juhas², Jana Juhasova², Stephanie Wu⁴, Jecedthel Dumpit¹, Andreas Weiss^{5,6}, Martin Marsala^{1,7} and Jan Motlik².

¹Neuroregeneration laboratory, Sanford Consortium for Regenerative Medicine, Department of Anesthesiology, University of California, San Diego, La Jolla, CA, USA;

²Laboratory of Cell Regeneration and Plasticity, Institute of Animal Physiology and Genetics, AS CR, Libečov, Czech Republic;

³Department of Cell Biology, Faculty of Science, Charles University in Prague, Prague, Czech Republic;

⁴Neuralstem Inc, Rockville, Maryland, USA;

⁵Novartis Institutes for Biomedical Research, Neuroscience Discovery, Basel, Switzerland;

⁶Present address: IRBM Promidis, Pomezia, Italy;

⁷Institute of Neurobiology, Slovak Academy of Sciences, Soltesovej 6, Kosice, Slovakia.

Running head: "UCHL1 downregulation in HD mouse model"

Number of figures: 6 (taking up 3/4 of a page)

Character count (including spaces and images): 14617

*Correspondence and reprint requests to: Marian Hruska-Plochan, Sanford Consortium for Regenerative Medicine, Department of Anesthesiology, University of California, San Diego, 2880 Torrey Pines Scenic Drive, Room 4113, La Jolla, CA 92037, USA. Tel: +1 858 534 7380; fax: +1 858 246 1483; email: mhruskaplochan@ucsd.edu

Conflict of interest statement

Authors declare no conflict of interest. AW is an employee of IRBM Promidis, Italy and SW is an employee of Neuralstem Inc, MD, USA.

Source of funding

This study was supported by the Charles University Grant Agency (GAUK) grant number 18410 to MHP and by Institutional research concept RVO 67985904.

Abstract

Huntington's disease is caused by an expansion of the polyglutamine-coding CAG triplet sequence in exon 1 of the huntingtin gene. This expansion leads to progressive and devastating neurodegenerative changes in the whole brain with the striatum and cerebral cortex being the regions most affected. The histological hallmark of the disease is the formation of neuronal inclusion bodies consisting of ubiquitinated aggregates of mutant huntingtin. Accordingly, the potential impairment of the Ubiquitin Proteasome System has long been speculated to play role in the development of mutant huntingtin-related pathology.

In the present study, we crossed the R6/2 Huntington's disease mouse model with the *gad* mouse model which lacks expression of deubiquitinating enzyme UCHL1, one of the most common proteins in the brain. The double mutant R6/2x*gad* mouse expresses exon 1 of human mutant huntingtin and one *gad* allele of UCHL1. We found that the reduction of UCHL1 in the R6/2 mouse significantly accelerated mutant huntingtin aggregation and increased the levels of polyubiquitin chains and polyubiquitinated proteins but it did not potentiate brain neuronal degeneration.

These results suggest that the Ubiquitin Proteasome System in Huntington's disease could be affected by inefficient recycling of monomeric ubiquitin by deubiquitinating enzymes, particularly by UCHL1. Our results also support the theory that the formation of inclusion bodies is a result of neuronal disease-coping response to a more toxic mutant huntingtin species.

Key words

R6/2 Huntington's disease mouse, Gracile axonal dystrophy (*gad*) mouse, ubiquitin proteasome system, ubiquitin carboxyl-terminal hydrolase L1 (UCHL1), ubiquitin homeostasis, mutant huntingtin, aggregation, TR-FRET, neurodegeneration

Introduction

Huntington's disease (HD) causative mutation (polyCAG repeat expansion in exon 1) leads to the expression of mutant huntingtin protein (mhtt) with expanded polyglutamine (polyQ) tract. Disease onset and severity is polyQ-length-dependent and is characterized morphologically by the presence of mhtt protein aggregates and inclusion bodies (IBs) found in affected neurons [1, 2]. However, the relationship between the appearance of mhtt aggregates and/or IBs and disease onset or progression is still not firmly established [2]. The IBs are ubiquitinated [1] suggesting that the formation of IBs in HD may be linked with aberrant Ubiquitin Proteasome System (UPS) activity [3]. However, involvement of mhtt and mhtt aggregation in UPS impairment in HD remains controversial [3-9].

Protein degradation via the UPS is a two-steps process: **1)** proteins are tagged by the covalent attachment of several ubiquitin molecules (mostly linked via Lys48) creating a polyubiquitin (polyUb) chain. **2)** the 26S proteasome recognizes polyUb tagged proteins and degrades them into short peptides. Deubiquitinating enzymes (DUBs) release free and reusable monoubiquitin [10].

The fact that the polyUb chains and high molecular polyUb protein complexes accumulate in the intracellular compartments in both *in vitro* and *in vivo* (mouse) HD models [3] but the GFP reporters of proteasome activity in R6 mouse models do not accumulate [6, 11], suggests a possible malfunction in DUBs activity. UCHL1 is a DUB with almost exclusive expression in nervous and reproductive systems [12] representing 1-2% of total soluble proteins in the brain [13]. UCHL1 also functions as an ubiquitin ligase and monoubiquitin stabilizer [13] and modulates synaptic function and structure [14]. Mutations of UCHL1 have been linked to several neurodegenerative diseases [13] and S18Y polymorphism in the UCHL1 gene was detected as a genetic-modifier in HD contributing to the variance in the age-at-onset of HD patients [15].

In the present study, we have crossed the transgenic R6/2 HD mouse model [16] with the mutant Gracile axonal dystrophy (*gad*) mouse which carries an in-frame deletion of exons 7 and 8 of UCHL1 gene resulting in a lack of UCHL1 expression. *Gad* mice exhibit autosomal recessively inherited neurodegenerative disorder which leads to “dying-back” axonal neurodegeneration and formation of A β , ubiquitin and proteasome subunits containing inclusions in axons of degenerating neurons [13, 17]. The goal of this study was to investigate the potential role of UCHL1 in UPS impairment in a well-established model of HD.

Methods

Animals

All experiments were carried out according to the guidelines for the care and use of experimental animals and approved by the State Veterinary Administration of the Czech Republic. B6CBA-Tg(HDexon1)62Gpb/1J ovary transplanted females (R6/2 OT; which are WT mice with the ovaries of the R6/2 mice) were obtained from The Jackson Laboratory. *Gad* mutant mice were obtained from Dr. Keiji Wada. Heterozygous *gad* males were crossed with R6/2 OT females to generate progeny of three genotypes: wild type (WT), R6/2 and R6/2x*gad*. The mice were anesthetized by mixture of ketamine (Narketan 10) and xylazine (Rometar 2%) and transcardially perfused with ice-cold PBS. Brain was removed, and immersed in 4% PFA fixative or stored frozen.

Western blot

20 μ g of total protein from crude homogenates of WT, R6/2 and R6/2x*gad* striatal and cortical samples were used. Membranes were incubated with primary antibodies overnight (ON) at 4°C.

Immunofluorescence

Brains were post-fixed in 4% PFA and cryopreserved by 30 % sucrose. Brains were then sectioned into 30 μ m thick free-floating sections. Sections were selected according to their A-P relation to the anterior commissure. Sections were incubated in primary antibodies at 4°C ON.

TR-FRET quantitative analysis

TR-FRET (Time-Resolved Förster Resonance Energy Transfer) detection of soluble mutant, wild-type and aggregated mutant huntingtin was performed by using 4 different antibody pairs (2B7+MW1; 2B7+MAB2166; 4C9+4C9 or MW8+MW8 [18]). For details see Table, Supplemental Digital Content 3, which shows detailed WB, IHC and TR-FRET methods and list of antibodies.

Quantification of DARPP32+ medium spiny neurons

Sections from 4 brains per genotype, 2 sections/animal were stained with DARPP32 antibody. Z-stack images of dorsomedial and central caudoputamen were acquired and DARPP32+ medium spiny neurons (MSNs) quantified in a blinded fashion using ImageJ software.

Immunofluorescence quantification of MW8+ mutant huntingtin aggregates

Sections from 4 brains per genotype, 3 sections/animal were stained with MW8 antibody specific for aggregated mhtt. Z-stack of images from primary motor cortex layer V (cortex) and dorsolateral caudoputamen (striatum) were analyzed with ImageJ software for the presence of particles with a size of 2-INF μ m² and a circularity of 0.5 to 1.0 with pixel threshold set: Striatum 457-MAX; Cortex 514-MAX.

Statistical analyses

DARPP32 MSN counts, brain and body weights were compared using ANOVA. To analyze the differences of mhtt aggregates between two groups we used Student's t-tests. For all statistical analyses a P value of 0.05 was considered significant. Results are expressed as means with the standard error of the mean (SEM). All statistical analyses were done using GraphPad Prism (La Jolla, CA, USA).

Results

Genetic cross of R6/2 transgenic HD mouse with mutant gad mouse

To test whether the UPS malfunction in HD is caused by the dysregulation of ubiquitin recycling we generated a genetic crossbreed of R6/2 [16] and *gad* mice [17]. Brains of 3 genotypes (wild type (WT), R6/2 and R6/2x*gad*) were harvested at 6 (R6/2 at early stage) or 10 weeks (R6/2 at advanced stage; *gad* at early stage) and 2-4 brains per genotypes were used in different assays.

Brain and body weight of R6/2x*gad* cross were similar to R6/2 (Fig. 1). Brain weight of both R6/2 and R6/2x*gad* was significantly reduced when compared to WT brains, which is consistent with previous reports [16, 19].

Numbers of DARPP32+ MSNs of R6/2xgad striatum are similar to those of R6/2

Dopamine- and cAMP-regulated neuronal phosphoprotein (DARPP32) is a well-established marker of striatal MSNs. The number of MSNs in the R6/2x*gad* striatum was similar to that in R6/2. When compared to WT striatum, both R6/2 and R6/2x*gad* striata exhibited a slight decreasing trend in MSNs numbers (Fig. 2). These data are consistent with previous reports that show only a modest decrease in MSNs numbers in R6/2 mice [16, 19].

Reduced UCHL1 expression in R6/2 x gad accelerated mhtt aggregation

TR-FRET quantitative assays of soluble mutant, wild-type and aggregated mutant huntingtin protein were performed (n=2 per genotype per time point) by using 4 different TR-FRET antibody pairs (Fig. 3a) to investigate the possible effect of UCHL1 downregulation on htt protein levels. Soluble mhtt species levels were lower and aggregated mhtt levels were higher in R6/2xgad brain at both time points and in both regions (with most apparent differences at 10 weeks) when compared to R6/2. These results were then confirmed by confocal analysis of MW8+ mhtt aggregates in brain sections from 10 week-old animals. We found that mhtt aggregates and IBs were significantly larger and more numerous in R6/2xgad striatum but not in cortex (Fig. 4). As the number of large prominent IBs per neuron was unchanged (Fig. 5e), the elevated numbers of MW8+ aggregates most likely represent neuropil mhtt aggregates in R6/2xgad striatum. Western blot analysis by AB1 antibody revealed that mhtt from R6/2xgad brain migrated faster in the gel suggesting that posttranslational change of mhtt had occurred (Fig. 3b).

UPS impairment in R6/2 mouse could be caused by altered ubiquitin recycling

Staining with polyUb antibody showed that the polyUb deposits in R6/2xgad mouse brain were larger and denser and that the MW8+ aggregates also contained polyUbK48 and 63 chains (see Figure, Supplemental Digital Content 1, which shows double stains). Western blot analysis of the whole cortical and striatal lysates using anti-polyUb antibody showed increased levels of polyUb chains and polyUb proteins in the R6/2xgad striatum, however this increase was not as clear in the cortex (Fig. 3c). MW8+ mhtt IBs contain UCHL1 protein and MW1+ soluble species of mhtt colocalize with UCHL1 (Fig. 6). Moreover,

expression of UCHL1 was higher in ChAT+ interneurons (Fig. 5a-d) than in MSNs (Fig. 2b,f,j).

Discussion

In the present study, we researched a potential role of mhtt in UPS impairment in HD by crossing the *gad* mutant mouse (to partially reduce the levels of UCHL1) with a well characterized R6/2 mouse model of HD.

It is becoming clear that the disease-causing and aggregation-prone agent in HD is the exon 1 containing an expanded polyQ tract (E1mhtt). These conclusions are based on findings that demonstrate: i) that the presence of soluble monomeric E1mhtt strongly predicts neuronal death [20], ii) that neurons which develop IBs show improved survival and decreased levels of diffuse forms of mhtt [21], iii) a critical role of CAG Repeat Length–Dependent aberrant splicing of mutant HTT gene which results in exon 1 mhtt protein expression. These findings suggest that the pathology in all knock-in HD mouse models and human HD could be driven by the same E1mhtt which is expressed in R6/2 mouse [22]. Furthermore, downregulation of the E1mhtt expression by antisense oligonucleotide infusion in the R6/2 mouse led to prevention of brain atrophy, improved neuronal survival and suppression of new mhtt synthesis, however it did not significantly alter mhtt aggregation, suggesting that disease progression is independent of mhtt aggregate formation [23].

Our current results agree with these observations as the accelerated aggregation of mhtt in R6/2x*gad* striatum correlated with an increased decline in soluble mhtt species (Fig. 3a) and did not enhance the loss of DARPP32+ MSNs (Fig. 2), nor did it affect brain or body weight (Fig. 1). In addition, we observed that UCHL1 expression is higher in ChAT+ cholinergic interneurons than in MSNs (Fig. 5a-d). This may help to explain selective

sparing and the lack of apparent IBs in these neurons (Fig. 5e) [19]. This is in agreement with the study of Lombardino et al [24] which suggested that larger neurons have higher UCHL1 expression and that the higher UCHL1 expression is associated with a reduced risk of neuronal death [24].

Because the IBs in HD are ubiquitinated formation of IBs has always been linked with UPS malfunction. Early studies of the UPS impairment in HD suggested that polyQ aggregates could directly inhibit the function of 26S proteasome [4] and that the eukaryotic proteasome is not able to process polyQ sequences of polyQ-containing proteins [8]. In recent studies, conflicting results showed that i) the proteasome remains functionally intact and can effectively degrade the expanded polyQ proteins [25], ii) the UPS impairment is not caused by direct "choking" of purified proteasomes, and iii) the UPS impairment in HD is global as it was shown *in vitro* [5] and *in vivo* in R6/2 and *Hdh*^{Q150/Q150} mice and human postmortem tissue [3]. Artificial reporters of UPS activity based on destabilized GFP were successfully applied in the UPS activity studies in HD cellular models [4, 5], but when translated into *in vivo* studies using R6 mice, these reporters failed to accumulate and thus failed to confirm global UPS impairment in HD [6, 11]. Nevertheless, fusing the UPS GFPu reporters to either postsynaptic PSD95 or presynaptic SNAP25 proteins revealed increased levels of GFPu reporters in the synapses of R6/2 and *Hdh*^{Q150} HD mouse models [9], suggesting that the malfunction of UPS in HD could be region-specific rather than global [3, 5].

It has been suggested that UCHL1 represents one of the major DUBs in the brain [14] as it is ubiquitously expressed in neurons and because it functions as a deubiquitinating enzyme, ubiquitin ligase and monoubiquitin stabilizer (for review see [13]). UCHL1 regulates synaptic function and structure and the main function of UCHL1 in synapses is most likely free mono-ubiquitin stabilization [14]. Our data showed that the reduced

UCHL1 expression in R6/2x*gad* striatum caused aggregates of mhtt to accumulate more in the neuropil of R6/2x*gad* mouse if compared to the R6/2 mouse (Fig. 4d). This suggests that the locally disturbed ubiquitin homeostasis in the synapses of HD models [9] could be caused by decreased monoUb-stabilizing and DUB activities of UCHL1 which, in turn may lead to the accumulation of polyUb chains and increased polyubiquitination of high molecular weight proteins as detected in previous works *in vivo* [3, 11] and in R6/2x*gad* striatum in our experiments (Fig. 3c). We found that mhtt from R6/2x*gad* brain lysates migrate faster in the gel (Fig. 3b) and we hypothesize that this may be caused by reduced mhtt ubiquitination. It is not clear, however, how mhtt alters UCHL1 function in HD.

In our experiments, we observed that UCHL1 co-localized with both soluble mhtt (Fig. 6f-i) and with aggregated mhtt (Fig. 6a-e). We hypothesize that abnormal interaction(s) of UCHL1 with mhtt could lead to impaired UCHL1 functioning or that the UCHL1 functions were compromised due to an ongoing clearance of mhtt by the UPS. It was shown that UCHL1 expression is regulated by the REST/NRSF (for review see [12]) and because mhtt causes a reduction in the transcription of RE1/NRSE neuron-linked genes (for review see [2]), mhtt could decrease the levels of UCHL1 indirectly. Another study showed that stimulation of NMDA receptors increases expression of UCHL1 [14] and because the NMDA receptors are over-activated in HD (for review see [2]), this could explain why we did not see decreased levels of UCHL1 protein in R6/2 brain (Fig. 3b).

Moreover, recent data suggests that oxidative modification of UCHL1 caused by oxidative stress in neurodegenerative diseases greatly affects UCHL1 activity (for review see [13]).

Conclusion

Our data showed that partial depletion of UCHL1 in R6/2x*gad* mice accelerated mhtt aggregation and increased the levels of polyUb chains and proteins in striatum but did not

result in increased degeneration of DARPP32+ MSNs. We also observed higher levels of UCHL1 in ChAT+ cholinergic interneurons and found that UCHL1 co-localized with mhtt in brain sections. Together, our data supports the theory of a “protective” role of mhtt IBs and suggests that UCHL1 function(s) may be affected in HD causing local dysregulation of ubiquitin homeostasis.

Acknowledgements

We would like thank Patricia Jandurova, Irena Deylova and Jitka Cervena for the excellent technical assistance, Ivana Hruskova for help with genotyping of mice, Dr. Marian DiFiglia for AB1 antibody and Dr. Keiji Wada for the *gad* mutant mice.

Author contributions

Conceived and designed the experiments: MHP and JM. Performed the experiments: MHP, SJ, JJ, SW, JD and AW. Analyzed the data: MHP and SJ. Wrote the paper: MHP and MM.

References

1. M DiFiglia, E Sapp, KO Chase, SW Davies, GP Bates, JP Vonsattel, et al. Aggregation of huntingtin in neuronal intranuclear inclusions and dystrophic neurites in brain. *Science* 1997, 277;1990-1993.
2. C Zuccato, M Valenza and E Cattaneo. Molecular mechanisms and potential therapeutical targets in Huntington's disease. *Physiol Rev* 2010, 90;905-981.
3. EJ Bennett, TA Shaler, B Woodman, KY Ryu, TS Zaitseva, CH Becker, et al. Global changes to the ubiquitin system in Huntington's disease. *Nature* 2007, 448;704-708.
4. NF Bence, RM Sampat and RR Kopito. Impairment of the ubiquitin-proteasome system by protein aggregation. *Science* 2001, 292;1552-1555.
5. EJ Bennett, NF Bence, R Jayakumar and RR Kopito. Global impairment of the ubiquitin-proteasome system by nuclear or cytoplasmic protein aggregates precedes inclusion body formation. *Mol Cell* 2005, 17;351-365.
6. JS Bett, C Cook, L Petrucelli and GP Bates. The ubiquitin-proteasome reporter GFPu does not accumulate in neurons of the R6/2 transgenic mouse model of Huntington's disease. *PLoS One* 2009, 4;e5128.
7. CI Holmberg, KE Staniszewski, KN Mensah, A Matouschek and RI Morimoto. Inefficient degradation of truncated polyglutamine proteins by the proteasome. *EMBO J* 2004, 23;4307-4318.
8. P Venkatraman, R Wetzell, M Tanaka, N Nukina and AL Goldberg. Eukaryotic proteasomes cannot digest polyglutamine sequences and release them during degradation of polyglutamine-containing proteins. *Mol Cell* 2004, 14;95-104.
9. J Wang, CE Wang, A Orr, S Tydlacka, SH Li and XJ Li. Impaired ubiquitin-proteasome system activity in the synapses of Huntington's disease mice. *J Cell Biol* 2008, 180;1177-1189.

10. A Ciechanover and P Brundin. The ubiquitin proteasome system in neurodegenerative diseases: sometimes the chicken, sometimes the egg. *Neuron* 2003, 40;427-446.
11. CJ Maynard, C Bottcher, Z Ortega, R Smith, BI Florea, M Diaz-Hernandez, et al. Accumulation of ubiquitin conjugates in a polyglutamine disease model occurs without global ubiquitin/proteasome system impairment. *Proc Natl Acad Sci U S A* 2009, 106;13986-13991.
12. IN Day and RJ Thompson. UCHL1 (PGP 9.5): neuronal biomarker and ubiquitin system protein. *Prog Neurobiol* 2010, 90;327-362.
13. R Setsuie and K Wada. The functions of UCH-L1 and its relation to neurodegenerative diseases. *Neurochem Int* 2007, 51;105-111.
14. AE Cartier, SN Djakovic, A Salehi, SM Wilson, E Masliah and GN Patrick. Regulation of synaptic structure by ubiquitin C-terminal hydrolase L1. *J Neurosci* 2009, 29;7857-7868.
15. S Metzger, P Bauer, J Tomiuk, F Laccone, S Didonato, C Gellera, et al. The S18Y polymorphism in the UCHL1 gene is a genetic modifier in Huntington's disease. *Neurogenetics* 2006, 7;27-30.
16. L Mangiarini, K Sathasivam, M Seller, B Cozens, A Harper, C Hetherington, et al. Exon 1 of the HD gene with an expanded CAG repeat is sufficient to cause a progressive neurological phenotype in transgenic mice. *Cell* 1996, 87;493-506.
17. K Saigoh, YL Wang, JG Suh, T Yamanishi, Y Sakai, H Kiyosawa, et al. Intragenic deletion in the gene encoding ubiquitin carboxy-terminal hydrolase in gad mice. *Nat Genet* 1999, 23;47-51.
18. B Baldo, P Paganetti, S Grueninger, D Marcellin, LS Kaltenbach, DC Lo, et al. TR-FRET-based duplex immunoassay reveals an inverse correlation of soluble and aggregated mutant huntingtin in huntington's disease. *Chem Biol* 2012, 19;264-275.

19. SW Davies, M Turmaine, BA Cozens, M DiFiglia, AH Sharp, CA Ross, et al. Formation of neuronal intranuclear inclusions underlies the neurological dysfunction in mice transgenic for the HD mutation. *Cell* 1997, 90;537-548.
20. J Miller, M Arrasate, E Brooks, CP Libeu, J Legleiter, D Hatters, et al. Identifying polyglutamine protein species in situ that best predict neurodegeneration. *Nat Chem Biol* 2011, 7;925-934.
21. M Arrasate, S Mitra, ES Schweitzer, MR Segal and S Finkbeiner. Inclusion body formation reduces levels of mutant huntingtin and the risk of neuronal death. *Nature* 2004, 431;805-810.
22. K Sathasivam, A Neueder, TA Gipson, C Landles, AC Benjamin, MK Bondulich, et al. Aberrant splicing of HTT generates the pathogenic exon 1 protein in Huntington disease. *Proc Natl Acad Sci U S A* 2013, 110;2366-2370.
23. HB Kordasiewicz, LM Stanek, EV Wancewicz, C Mazur, MM McAlonis, KA Pytel, et al. Sustained therapeutic reversal of Huntington's disease by transient repression of huntingtin synthesis. *Neuron* 2012, 74;1031-1044.
24. AJ Lombardino, XC Li, M Hertel and F Nottebohm. Replaceable neurons and neurodegenerative disease share depressed UCHL1 levels. *Proc Natl Acad Sci U S A* 2005, 102;8036-8041.
25. A Michalik and C Van Broeckhoven. Proteasome degrades soluble expanded polyglutamine completely and efficiently. *Neurobiol Dis* 2004, 16;202-211.

Figure legends

Figure 1. Brain and body weight. (A) Graph plot shows brain weight comparison. No difference was observed between R6/2 and R6/2x*gad* brains at both time points. (B) Body weight comparison. Again, no statistical difference was observed between R6/2 and R6/2x*gad* mice at both time points. (For both (A) and (B) all mice generated by R6/2 x *gad* crossing in our lab were included in statistical analysis but not all brains were used in the current study; n= 5 for WT and R6/2 6 weeks; n=16 for WT and R6/2 10 weeks; n= 11 for R6/2x*gad* 6 weeks and 10 weeks).

Figure 2. DARPP32+ medium spiny neuron quantification. Representative images of DARPP32-stained striatum of 10 weeks old WT (A), R6/2 (E) and R6/2x*gad* (I) mice. Images B, F and J show ImageJ unionjack LUT view of UCHL1 staining of the boxed regions in corresponding images A, E and I to better demonstrate the intensity values (with LUT scale at the bottom of the image). Note that the higher intensity of the UCHL1 staining is localized in DARPP32 negative (C, G, K) large neurons (B, F, J respectively). D, H and L show merged images of UCHL1 and DARPP32 staining. (M) Graph plot shows DARPP32+ MSN quantification. No significant difference between R6/2 and R6/2x*gad* striata was observed (n=4, for details see Methods). Scale bar represents 50µm.

Figure 3. TR-FRET and Western blot analysis of brain samples. (A) Table with LUT color code (warm colors lower signal, cold colors higher signal) shows results of TR-FRET analysis of soluble wild-type and mutant huntingtin and aggregated mutant huntingtin protein in WT, R6/2 and R6/2x*gad* brain samples expressed as % of htt signal over buffer background normalized to total protein as detected by 4 TR-FRET antibody pairs (2B7+MW1; 2B7+MAB2166; 4C9+4C9 or MW8+MW8 [18]). Note that R6/2x*gad* striatum

and cortex have higher levels of aggregated mhtt and lower levels of soluble mhtt at both time points with more apparent differences in 10 weeks (n=2 per time point per genotype). **(B)** Western blots of the same tissue used for TR-FRET analysis confirmed reduced UCHL1 expression in R6/2x*gad* mice brain (middle blot). Western blot immunoprobed with the anti-HTT1-17 antibody AB1 [1] revealed that the mhtt from R6/2x*gad* brain migrates faster in the gel (red arrow, upper blot). Lower blot is β -actin loading control blot. **(C)** Anti poly-ubiquitin antibody BML-PW0580 probed blots of the same tissues demonstrated elevated levels of the polyubiquitin chains and polyubiquitinated high molecular weight proteins in the R6/2x*gad* brain (upper blot). Lower blot is β -actin loading control blot. Two mice of each group were examined and blots were repeated two times for all samples.

Figure 4. Immunofluorescence quantification of mhtt aggregates. Graph plots show morphometric analysis of the size of MW8+ mhtt aggregates and IBs in **(A)** cortex or **(C)** striatum. Striatal but not cortical mhtt aggregates were significantly larger in R6/2x*gad* mice (Paired t-test, one tailed, $P < 0.05$, $n = 4$, for details see Methods). Quantitative analysis of MW8+ mhtt aggregates and IBs in cortex **(B)** and striatum **(D)**. There was significantly more mhtt aggregates in R6/2x*gad* mice striatum but not in cortex (Paired t-test, one tailed, $P < 0.05$, $n = 4$, for details see Methods). For more details, see Figure, Supplemental Digital Content 2, which demonstrates representative images used for quantification).

Figure 5. Confocal microscopy analysis of UCHL1 expression. **(A)** Representative image of 10 week-old WT striatum triple stained with UCHL1, DARPP32 and ChAT antibodies. Scale bare 25 μ m. **(B)** Image shows ImageJ unionjack LUT view of UCHL1 staining of the boxed region in **(A)** to better demonstrate the intensity values (with LUT scale at the bottom of the image). Note that the highest intensity of the UHCL1 staining is

localized in DARPP32 negative (C) but ChAT positive cholinergic interneuron (D). (E) Representative image of 10 week-old R6/2*xgad* striatum triple stained with MW8, DARPP32 and ChAT antibodies demonstrating that ChAT+ interneurons do not contain MW8+ mhtt aggregates and that the DARPP32+ MSNs do contain one prominent MW8+ IB per cell. Scale bare 10µm.

Figure 6. Confocal microscopy analysis of UCHL1 and mhtt. (A) Representative R6/2 cortical neuron stained with MW8 (B), UCHL1 (C) and NeuN (D) antibodies with orthogonal views constructed in ImageJ which demonstrates that MW8 mhtt aggregate-specific antibody [20] positive inclusion body contain UCHL1 protein. (E) Shows all three channels merged. Scale bar for A is 5µm. (F) Represents co-localized pixels of UCHL1 (G) and MW1 ((F); antibody specific for soluble mhtt species [20]) staining in R6/2 cortical neuron projected onto UCHL1 staining (reconstructed by ImageJ Colocalization Finder Plugin). (H) Is a merged image of F and G.

List of Supplemental Digital Content

Supplemental Digital Content 1. tiff

Supplemental Digital Content 2. tiff

Supplemental Digital Content 3. pdf

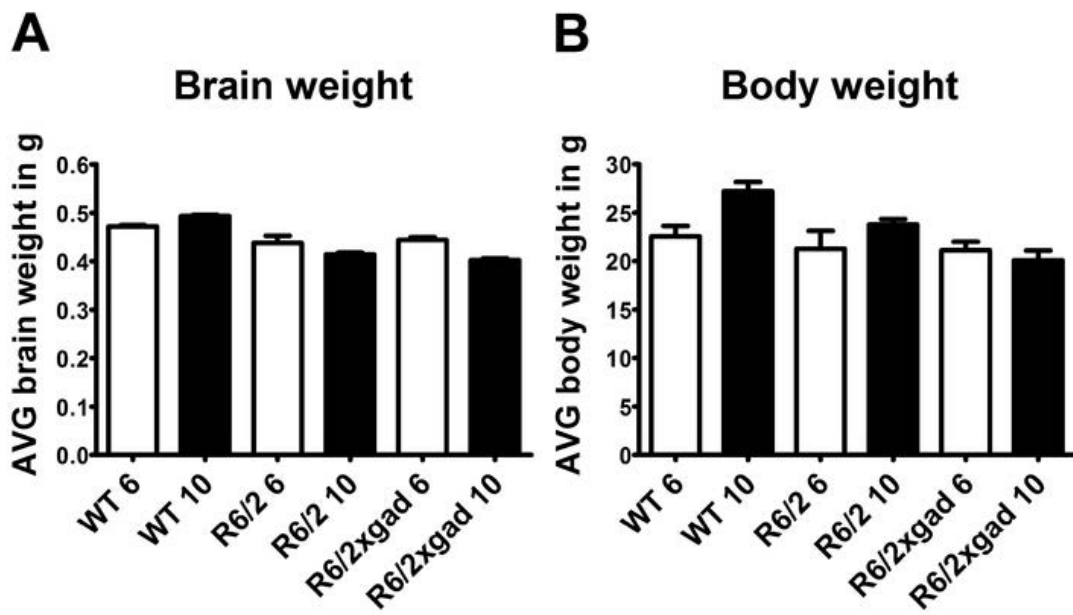


Fig. 1

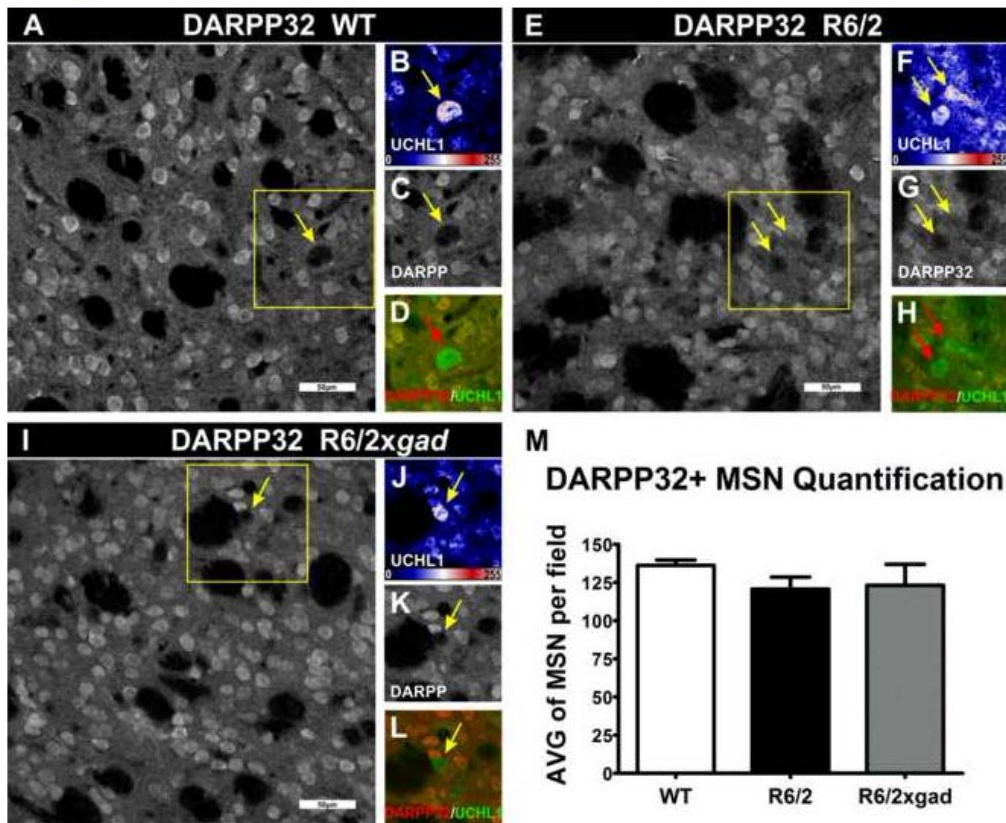


Fig. 2

Figure
[Click here to download high resolution image](#)

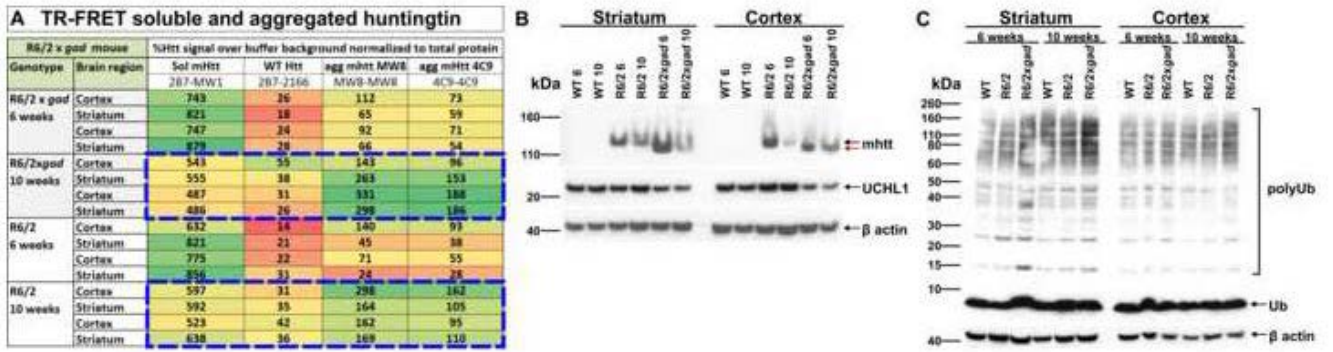


Fig. 3

Figure
[Click here to download high resolution image](#)

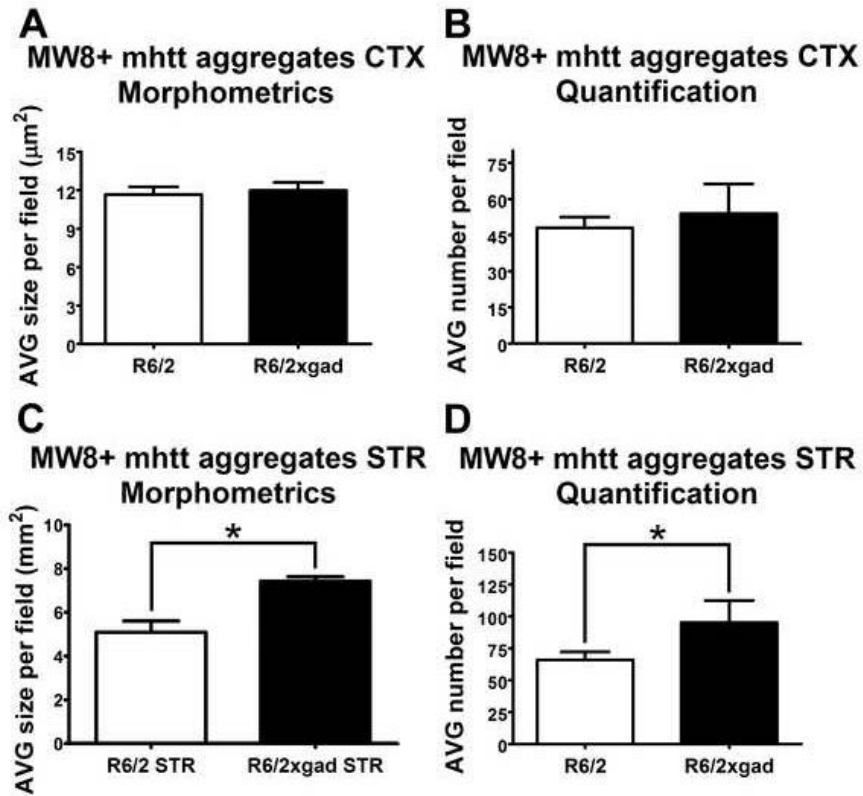


Fig. 4

Figure
[Click here to download high resolution image](#)

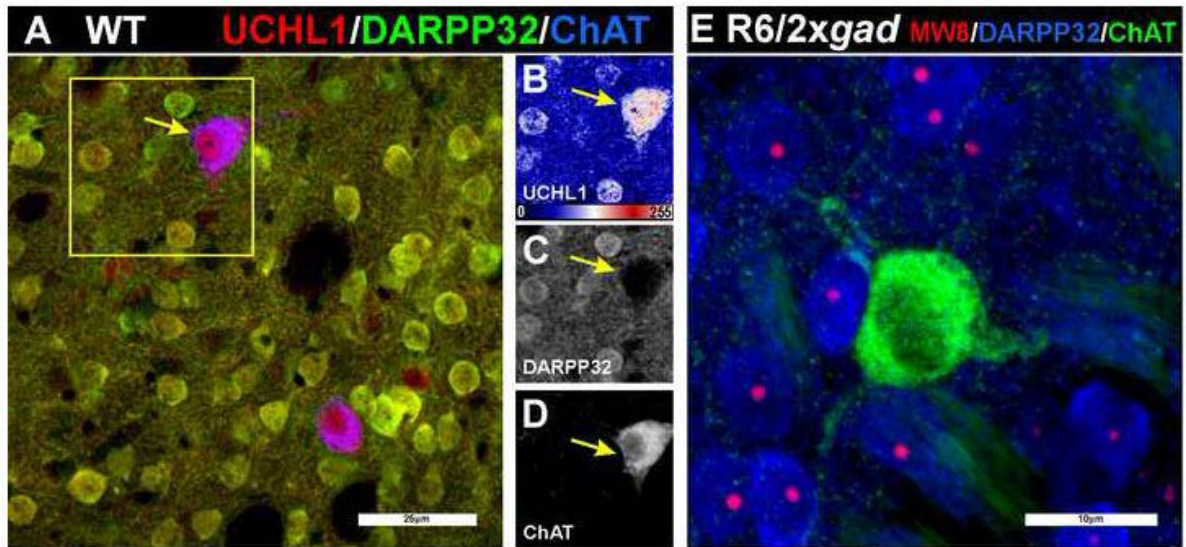


Fig. 5

Figure
[Click here to download high resolution image](#)

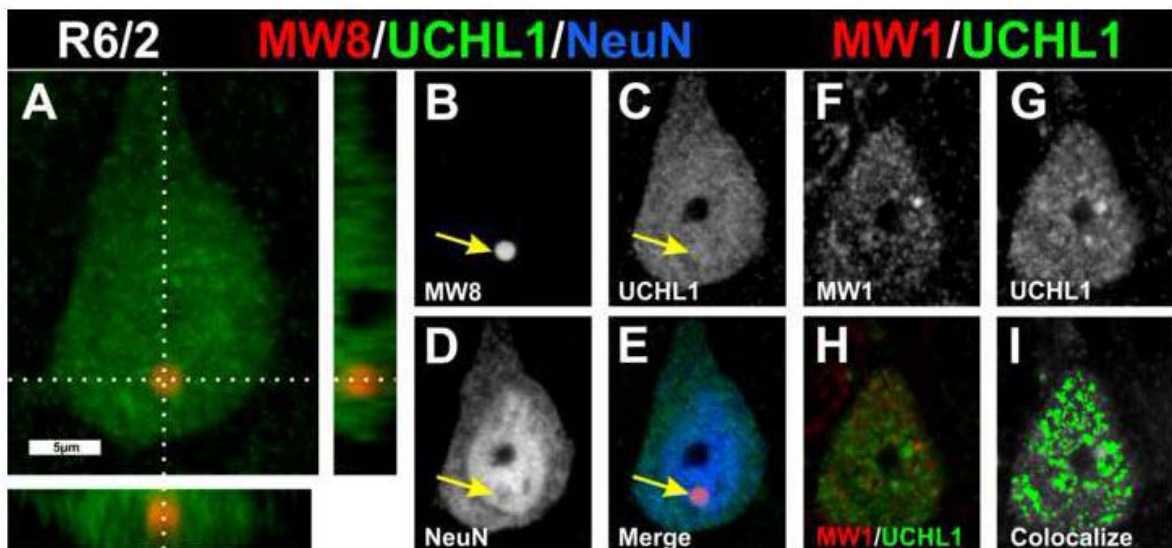


Fig. 6

Supplemental Digital Content 1.tiff

[Click here to download Supplemental Digital Content: SDC. 1.tif](#)

Supplemental Digital Content 2.tiff

[Click here to download Supplemental Digital Content: SDC. 2.tif](#)

tif

Supplemental Digital Content 3.pdf

[Click here to download Supplemental Digital Content: SDC. 3.pdf](#)

5.3. **Evaluation of neural stem cell replacement therapy in SOD1^{G93A} rat model of ALS**

in publication

Human Neural Stem Cell Replacement Therapy for Amyotrophic Lateral Sclerosis by Spinal Transplantation

Hefferan MP, Galik J, Kakinohana O, Sekerkova G, Santucci C, Marsala S, Navarro R, **Hruska-Plochan M**, Johe K, Feldman E, Cleveland DW, Marsala M.


PLoS ONE 7(8): e42614. doi:10.1371/journal.pone.0042614

IF (2012): 4,092; 5-year IF (2012): 4.537. Cited by 2 articles.

Declaration of co-authors

“I hereby declare that Marián Hruška-Plochán was adequately involved (30%) in the study design, experiments, interpretation of results and writing of this manuscript.”

San Diego, April 29 2013


Martin Maršala, Prof. MD.

Human Neural Stem Cell Replacement Therapy for Amyotrophic Lateral Sclerosis by Spinal Transplantation

Michael P. Hefferan¹, Jan Galik^{2,3}, Osamu Kakinohana¹, Gabriela Sekerkova⁴, Camila Santucci¹, Silvia Marsala¹, Roman Navarro¹, Marian Hruska-Plochan^{1,8,9}, Karl Johe⁵, Eva Feldman⁶, Don W. Cleveland⁷, Martin Marsala^{1,2*}

1 Neuroregeneration Laboratory, Department of Anesthesiology, University of California San Diego, La Jolla, California, United States of America, **2** Institute of Neurobiology, Slovak Academy of Sciences, Košice, Slovakia, **3** Institute of Biology and Ecology, Faculty of Science, Pavol Jozef Safarik University, Košice, Slovakia, **4** Department of Cell and Molecular Biology, Feinberg School of Medicine, Northwestern University, Chicago, Illinois, United States of America, **5** Neuralstem Inc, Rockville, Maryland, United States of America, **6** Department of Neurology, University of Michigan, Ann Arbor, Michigan, United States of America, **7** Ludwig Institute and Department of Cellular and Molecular Medicine, School of Medicine, University of California San Diego, La Jolla, California, United States of America, **8** Institute of Animal Physiology and Genetics, Academy of Sciences of the Czech Republic, Libečov, Czech Republic, **9** Department of Cell Biology, Faculty of Science, Charles University in Prague, Prague, Czech Republic

Abstract

Background: Mutation in the ubiquitously expressed cytoplasmic superoxide dismutase (SOD1) causes an inherited form of Amyotrophic Lateral Sclerosis (ALS). Mutant synthesis in motor neurons drives disease onset and early disease progression. Previous experimental studies have shown that spinal grafting of human fetal spinal neural stem cells (hNSCs) into the lumbar spinal cord of SOD1^{G93A} rats leads to a moderate therapeutical effect as evidenced by local α -motoneuron sparing and extension of lifespan. The aim of the present study was to analyze the degree of therapeutical effect of hNSCs once grafted into the lumbar spinal ventral horn in presymptomatic immunosuppressed SOD1^{G93A} rats and to assess the presence and functional integrity of the descending motor system in symptomatic SOD1^{G93A} animals.

Methods/Principal Findings: Presymptomatic SOD1^{G93A} rats (60–65 days old) received spinal lumbar injections of hNSCs. After cell grafting, disease onset, disease progression and lifespan were analyzed. In separate symptomatic SOD1^{G93A} rats, the presence and functional conductivity of descending motor tracts (corticospinal and rubrospinal) was analyzed by spinal surface recording electrodes after electrical stimulation of the motor cortex. Silver impregnation of lumbar spinal cord sections and descending motor axon counting in plastic spinal cord sections were used to validate morphologically the integrity of descending motor tracts. Grafting of hNSCs into the lumbar spinal cord of SOD1^{G93A} rats protected α -motoneurons in the vicinity of grafted cells, provided transient functional improvement, but offered no protection to α -motoneuron pools distant from grafted lumbar segments. Analysis of motor-evoked potentials recorded from the thoracic spinal cord of symptomatic SOD1^{G93A} rats showed a near complete loss of descending motor tract conduction, corresponding to a significant (50–65%) loss of large caliber descending motor axons.

Conclusions/Significance: These data demonstrate that in order to achieve a more clinically-adequate treatment, cell-replacement/gene therapy strategies will likely require both spinal and supraspinal targets.

Citation: Hefferan MP, Galik J, Kakinohana O, Sekerkova G, Santucci C, et al. (2012) Human Neural Stem Cell Replacement Therapy for Amyotrophic Lateral Sclerosis by Spinal Transplantation. PLoS ONE 7(8): e42614. doi:10.1371/journal.pone.0042614

Editor: Anthony E. Kincaid, Creighton University, United States of America

Received: December 31, 2011; **Accepted:** July 10, 2012; **Published:** August 20, 2012

Copyright: © 2012 Hefferan et al. This is an open-access article distributed under the terms of the Creative Commons Attribution License, which permits unrestricted use, distribution, and reproduction in any medium, provided the original author and source are credited.

Funding: Funding provided by Taubmann Foundation (EF, MM, MH) and California Institute of Regenerative Medicine (MM-RC1-00131-1). The funders had no role in study design, data collection and analysis, decision to publish, or preparation of the manuscript.

Competing Interests: KJ is employed by Neuralstem Inc. and has financial interest in the company. Neuralstem has patented technology of isolation and expansion of human fetal neural precursors and is currently conducting a clinical trial in ALS patients receiving spinal grafts of human spinal stem cells. This does not alter the authors' adherence to all the PLoS ONE policies on sharing data and materials, as detailed online in the guide for authors.

* E-mail: mmarsala@ucsd.edu

Introduction

Amyotrophic lateral sclerosis (ALS), also known as Lou Gehrig's disease, is characterized by the progressive development of motor dysfunction, α -motoneuron degeneration and death, in turn producing progressive fatal paralysis. Both inherited and sporadic instances of disease combine lower α -motoneuron degeneration and upper motor neuron lesion(s) [1,2]. Depending on the time course of α -motoneuron degeneration within spinal cord segments (cervical, lumbar or both), the early clinical manifestation of

disease typically presents as motor weakness with progressive loss of ambulatory and/or respiratory function. In addition to motor deficits, several other qualitatively distinct neurological symptoms including muscle spasticity and segmental hyper-reflexia are also frequently seen during disease progression [1].

While the pathological mechanisms leading to progressive neuronal degeneration are likely multi-factorial, there is converging evidence for the role of both motor neurons and astrocytes as key disease mediators. Early studies identified functional abnormalities in astroglial-specific glutamate transporters (EAAT2) in

both sporadic and familial ALS human tissues [3], as well as mutant SOD1 transgenic rodent models [4,5] Howlan}. The role of non-motor neurons in the evolution of α -motoneuron degeneration in ALS was initially validated by analysis of chimeric mouse models that were mixtures of normal and mutant SOD1 expressing cells. Those studies revealed that normal motor neurons within an ALS-causing mutant cell environment develop disease-related damage [6]. In addition, analysis of other chimeric mice in which 100% of motor neurons expressed high levels of a disease-causing ALS mutation in SOD1 demonstrated that the presence of normal non-neuronal cells could delay or eliminate disease [7]. Diminished mutant SOD1 synthesis from astrocytes strongly slowed the rate of disease progression [7]. Finally, *in vitro* studies have provided evidence that ALS glia isolated from mutant SOD1 transgenic mice release factors (not yet identified) that are sufficient to trigger human and rodent motor neuron degeneration *in vitro* [8–11]. Thus, the loss of astrocyte mediated glutamate buffering capacity and the secretion of toxic factors from local astrocytes may both contribute to neuronal degeneration in ALS.

Consistent with these mechanism-exploratory studies, which identified the role of mutated astrocytes in disease progression, recent *in vivo* spinal cell grafting data provided evidence that local segmental enrichment with wild-type neural or astrocyte precursors leads to a certain degree of neuroprotection. Focal enrichment of normal astrocytes, by transplantation of fetal rat spinal cord-derived, lineage-restricted astrocyte precursors (AP), produced significant benefit in a rat model that develops fatal motor neuron disease from expression of mutant SOD1^{G93A}. AP transplantation adjacent to cervical spinal cord respiratory motor neuron pools, the principal cells whose dysfunction leads to death in ALS, survived in diseased tissue, differentiated efficiently into astrocytes and reduced microglia in the cervical spinal cords of SOD1^{G93A} rats. Functionally, AP-grafted animals showed: i) extended survival and disease duration, ii) attenuated motor neuron loss, iii) slowed declines in forelimb motor performance, and iv) improved respiratory functions. It was hypothesized that neuroprotection was mediated in part by the primary astrocyte glutamate transporter EAAT2 expressed in grafted cells (called GLT1 in rodents) [12].

Mutant damage within motor neurons has also been demonstrated to play a central role in development of disease. In rodent models, diminishing mutant SOD1 synthesis within motor neurons (by selective transgene inactivation [7,13] or viral-mediated siRNA delivered by retrograde transport after intramuscular injection [14,15] can sharply delay disease onset. Spinal lumbar grafting of human fetal spinal neural stem cells (i.e., the same cells as used in our current study) in immunosuppressed SOD1^{G93A} rats has been reported to yield long-term graft survival (average 86 days) and formation of synapses with the host neurons. Grafted animals were reported to have disease onset delayed by 7 days and the age at which limb paralysis was reached was extended by 11 days [16,17].

The compelling evidence of non-cell autonomous contributions to disease in models of SOD1 mediated ALS makes cell replacement therapy an attractive option. We now report the long term survival and differentiation into neurons and astrocytes of human fetal spinal neural stem cells (hNSCs) after grafting into the vicinity of lumbar spinal α -motoneurons and a local transient functional benefit after grafting into immunosuppressed presymptomatic SOD1^{G93A} rats.

Results

Grafted human fetal spinal neural stem cells (hNSCs) show long term survival, develop neuronal morphologies and form synapses with host α -motoneurons

Twenty-four, SOD1^{G93A} rats (12 male, 12 female; 60–65 days old) received 10 bilateral injections of hNSCs targeted into ventral horn of L2–L5 spinal segments (Fig. 1A, B). Sixteen additional animals received media only. All animals survived until endstage disease, with the exception of one media- and two cell-treated animals which died perioperatively. Immunohistological examination of spinal cord tissue from animals at endstage using an antibody recognizing the human, but not rat, nuclear matrix protein (hNUMA) revealed identifiable human grafts in 18/22 animals. Four animals were graft-negative as indicated by injection tracks which were clearly visible, but with no human antigen detected (data not shown). hNUMA-immunoreactive cell grafts were found in the central and deep gray matter (laminae VII–IX) and sometimes extended into white matter (Fig. 1C). The overall appearance of spinal cords from cell-grafted animals was generally unremarkable, with only some examples of cell grafts extended into the white matter and slight enlargement of the spinal cord was then sometimes noted typically in the area closest to the graft. The pattern of engraftment identified by antibodies selective for human neuron-specific enolase (hNSE) (Fig. 1D) or doublecortin (DCX; Fig. 1E), an early postmitotic neuronal marker, closely matched that seen with hNUMA. Essentially all structures within the graft core labeled for both hNSE and doublecortin (Fig. 1F). Numerous individual doublecortin/hNUMA-immunopositive cells were readily found outside the graft core and had long neural-like processes with axonal varicosities (often more than 500 μ m in length; Fig. 1G).

Quantitative analyses showed that 78 \pm 6% of hNUMA-positive nuclei were surrounded by a doublecortin-positive cytoskeleton, suggesting that those cells were young, migrating, post-mitotic neurons. Likewise, no cells with doublecortin were found lacking an hNUMA-positive nucleus. Similar to the hNSE staining pattern, fibers with doublecortin were found extending >500 μ m radially from the graft core, sometimes crossing through/near lamina X to the opposite side. On average 12.5 \pm 1.2% of hNUMA-positive cells expressed the mature neuron marker NeuN (Fig. 1H). Graft cores identified with hNUMA were also intensely stained for the neuron-specific cytoskeletal protein β III tubulin (TUJ1; [18]; Fig. S1A–C) and GAP43 (Fig. S1D–G). Only 1.7 \pm 1.1% of hNUMA-positive cells appeared to be astrocytes with detectable GFAP filaments (Fig. 1I). Only 3.2 \pm 0.9% of hNUMA-positive cells reacted with the mature oligodendrocyte marker APC (not shown).

Examination of grafted spinal cord tissue revealed a dense fiber-like pattern of human-specific synaptophysin within the core and extending outward into the adjacent tissue (Fig. 1J, Fig. S2A–D). Persisting host motoneurons (α and γ) were frequently found to have human-specific synaptophysin-positive bouton-like structures adjacent to their cell body and associated processes. By examining specific neurotransmitter phenotype markers in 0.5 μ m-thick optical sections, 0.8 \pm 0.3% of human synaptophysin-positive structures were co-labeled with glutamate decarboxylase 65 (GAD65; Fig. 1K, Fig. S2E–H), a marker for γ -aminobutyric acid-producing neurons. Immunostaining for each of the three vesicular glutamate transporters known to exist in the spinal cord (VGluT 1, 2, and 3) revealed that 1.3 \pm 0.5% of boutons with human synaptophysin were glutamatergic (Fig. 1L; Fig. S2I–L). Glycinergic boutons, identified by immunostaining for a glycine transporter (GlyT2) represented 0.9 \pm 0.6% of these boutons (Fig.

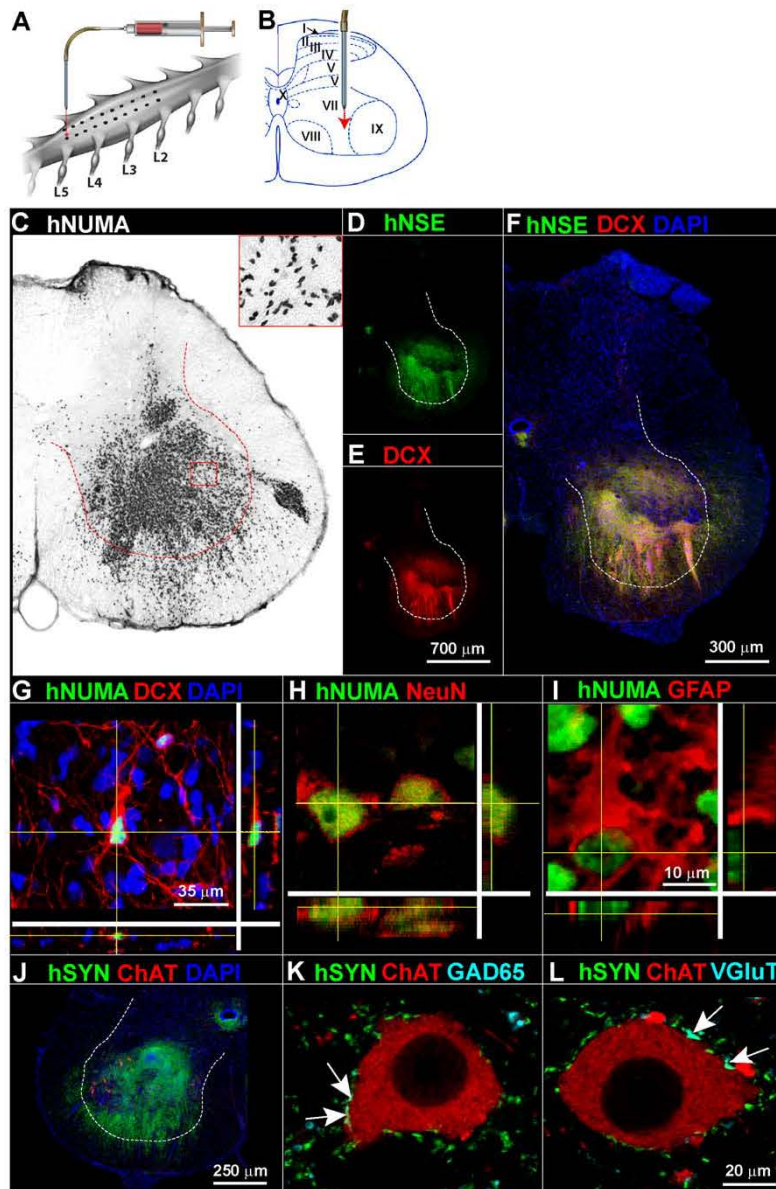


Figure 1. Human spinal neural stem cells grafted into lumbar spinal cord of $SOD1^{G93A}$ rats show long term survival and preferential neuronal differentiation. Using a glass capillary $SOD1^{G93A}$ rats (60–65 days old) received 10 bilateral injections of hNSCs targeted into the intermediate zone (lamina VII) and ventral horn (lamina VIII, IX) of L2–L5 spinal segments (A, B). Lumbar spinal cord sections from cell-grafted $SOD1^{G93A}$ animals immunostained for human nuclear matrix antigen (hNUMA) to identify all cells of human origin and developed by diaminobenzidine (C) shows a dense population of nucleus-like structures throughout the mid- and deep laminae (dashed line delineates the ventral horn) as well as more disperse nuclei outside the graft core and often into the white matter (inset). Neighboring sections revealed cell grafts that were strongly immunoreactive (IR) for human neuron-specific enolase (hNSE) and doublecortin (DCX; D–G). Other hNUMA-IR cells were found to react with the neuronal nuclear protein NeuN (H) and glial fibrillary acidic protein (GFAP; I). Human synaptophysin (hSYN) was detected throughout the cell grafts and was often found in the vicinity of persisting motoneurons (ChAT; choline acetyltransferase) in lamina IX and extending into the adjacent white matter (J). Single optical layer confocal images of surviving α -motoneurons show hSYN-IR bouton-like structures adjacent to the outer membrane of the soma (K, L). Only occasional hSYN-IR boutons co-stained with the GABA-ergic cell marker glutamate decarboxylase (GAD65; K); glutamatergic boutons were located by identifying specific glutamate vesicular transporters 1/2/3 (VGluT) and similarly showed only rare boutons also reactive for hSYN (L). Arrows show some examples of double-immunoreactive structures. Scale bar: 300 μ m (C, F), 700 μ m (D, E), 35 μ m (G), 10 μ m (H, I), 250 μ m (J), 20 μ m (K, L).
doi:10.1371/journal.pone.0042614.g001

S2M–P), consistent with a human stem cell-derived glycinergic neuron. No synaptophysin-positive structures were found to co-label with the motor neuron marker ChAT (**Fig. 1K, L; Fig. S2H, L, P**). Indeed, in the vast majority (>97%) of cases human synaptophysin-positive cells did not contain any differentiated cell marker, indicating a persistent immature phenotype.

Human spinal neural stem cells protect α -motoneurons in grafted segments

In order to assess a possible protective effect of grafted hNSCs on lumbar α -motoneuron survival we performed quantitative histological analyses of persisting lamina IX α -motoneurons in normal, SOD1^{G93A}, SOD1^{G93A}/hNSCs-grafted, and SOD1^{G93A}/media-treated animals in the lumbar (L4 L5) spinal cord segments. Representative half spinal cord images from each animal group are shown in **Fig. 2A–D**. In untreated SOD1^{G93A} animals, there was an average $85 \pm 7\%$ reduction in the number of α -motoneurons per histological section compared to untreated, non-transgenic rats (**Fig. 2I**). While media-treated SOD1^{G93A} rats showed an $80 \pm 9\%$ reduction in the α -motoneuron population, in hNSCs-grafted animals the lateral α -motoneuron pool showed only a $53 \pm 5\%$ decrease relative to normal animals), which was a significantly smaller reduction than the untreated or media-treated SOD1^{G93A} animal groups ($P < 0.001$; one-way ANOVA).

Analysis of α -motoneuron survival in the phrenic nucleus (C5–6) was used to test whether the lumbar cell grafts provided protection in cervical motoneuron pools distant from grafted lumbar segments. Half spinal cord images from untreated normal animals showed an intensely-stained (choline acetyl transferase - ChAT) motoneuron pool in cervical spinal cord (**Fig. 2E**). Untreated SOD1^{G93A} animals at endstage disease developed a dramatic loss in the α -motoneuron population (**Fig. 2F, J**; a $69 \pm 4\%$ reduction compared to age-matched non-transgenic littermates). Media-treated (**Fig. 2G**) and hNSCs-grafted (**Fig. 2H**) SOD1^{G93A} animals had similarly-reduced cervical motor pools ($60 \pm 4\%$ and $65 \pm 4\%$ of normal littermates, respectively).

Grafted human spinal neural stem cells ameliorate lumbar astrogliosis and microglial activation

To test how engraftment of hNSCs affects the astroglial and microglial activation that prominently develop in SOD1^{G93A} rats, region-specific (lamina IX) astrogliosis and microglial activation was assessed by densitometric analysis of glial fibrillary acidic protein (GFAP) and ionized calcium-binding adaptor molecule 1 (Iba1) immunoreactivity, respectively. Untreated normal rats showed minimal GFAP reactivity as expected for wild-type animals, with very thin processes in astrocytes and usually no discernable cell body (**Fig. S3A**). Iba1 immunoreactivity was also comparable to that of wild-type naïve animals, with microglia with long thin processes (**Fig. S3B**). However, by endstage disease, intense reactive astrogliosis (i.e., hypertrophic astrocytes with short, thick processes and enlarged soma) was found in the untreated SOD1^{G93A} rats (**Fig. S3D, M**). Microglial activation in SOD1^{G93A} mutant animals paralleled the reactive astrogliosis with a significant increase in the presence of Iba1+ cells throughout the ventral horn (and concentrated in lamina VIII and IX - **Fig. S3E, M**). While media treatment did not alter development of GFAP or Iba1 reactivity in laminae IX (compared to untreated, mutant SOD1^{G93A} tissue; **Fig. S3I, M**), hNSCs-transplantation reduced the overall immunoreactivity for GFAP and Iba1 (**Fig. S3L, M**). While media-treated tissue had GFAP and Iba1 reactivities 8 ± 0.9 and 6 ± 0.8 fold greater than that in normal animals, both were

reduced [to 4 ± 0.8 fold ($p = 0.04$; one-way ANOVA) and 3.6 ± 0.4 fold ($p = 0.02$; one-way ANOVA)] in hNSCs grafted animals, respectively.

Grafted human spinal neural stem cells migrate extensively and form synapses

To assess the degree of cell migration and synapse formation at extended periods after grafting, we compared non-quantitatively the distribution of grafted (hNUMA+) cells 9 months after transplantation into lumbar spinal cords of immunodeficient rats with the pattern seen in cell-grafted SOD1^{G93A} rats (i.e., around 78 days after cell transplantation). Extensive migration of grafted cells was seen into both white and gray mater (**Fig. 3A, B; Fig. S4A, B**). Double staining of hNUMA+ sections showed that the hNSCs-derived cells localized in white matter acquired only glial phenotypes (**Fig. 3C, D**) [as shown by co-staining with antibodies to neuronal (NeuN, human neural specific enolase - NSE, CHAT) or non-neuronal (GFAP and the mature oligodendrocyte cell marker APC) proteins]. hNSCs-derived cells in the gray matter, on the other hand, had both neuronal and non-neuronal markers (**Fig. 3E**). Electron microscopy confirmed that human synaptophysin (hSYN) immunoreactive axonal terminals had formed synapses with adjacent host neuron-derived dendrites (**Fig. 3F–I**).

Near complete loss of spinally-recorded motor-evoked potentials in non-treated SOD1^{G93A} animals

In order to assess the upper motor neuron connectivity at the spinal level, motor-evoked potentials were recorded in a separate group of endstage SOD1^{G93A} rats with no previous manipulations (i.e. no spinal media or cell injections) and age-matched non-transgenic control animals. Motor-evoked potentials (MEPs) were recorded from the dorsal surface of exposed thoracic T12 segment after electrical stimulation of the motor cortex (**Fig. 4A**). MEPs consist of multiple waves, with the two earliest peaks, N1 and N2, corresponding to the activation of extrapyramidal system [19–21]. In non-transgenic animals, the N1 wave (average amplitude 140.7 ± 39.0 mV; **Table 1**) was recorded at 1.6 ± 0.2 ms and the N2 wave (average amplitude 88.4 ± 51.3 mV) 2.8 ± 0.3 ms after the stimulus, yielding calculated conduction velocities of 52–62 and 28–32 m/s, respectively. In SOD1^{G93A} endstage animals, the N1 amplitude was reduced to 1/6th the normal level (25.5 ± 6.4 mV, $p < 0.05$ compared to normal animals; t-test) and latency was increased by 55% (to 2.5 ± 0.2 ms; $p < 0.05$; t-test) (**Fig. 4B, Table 1**). Similarly, N2 amplitude was reduced to about 30% of normal (to 25.1 ± 9.1 mV) and latency was increased 25% (to 3.5 ± 0.5 ms, $p < 0.05$; t-test) (**Fig. 4B, Table 1**).

Loss of large, descending myelinated axons in spinal white matter of mutant SOD1^{G93A}

Histological analysis of the integrity of descending motor tract degeneration in cervical and lumbar spinal cord was determined in terminal SOD1^{G93A} rats which were previously used for MEPs recording. Silver impregnation techniques were employed to detect the presence and distribution of axo-dendritic disintegration, which is marked by silver deposition [22–25]. While lumbar sections from the normal animals had minimal silver deposition (**Fig. 5A**), similar sections from SOD1^{G93A} animals had numerous degenerating α -motoneurons and interneurons that stained intensely (**Fig. 5B, C**) and an abundant number of fragmented fibers coursing throughout laminae IV–X (**Fig. 5D**). Numerous argyrophilic punctate structures were also prominent in most white matter regions, particularly in the lateral and ventral columns. Using a less sensitive silver method (de Olmos aminocupric silver

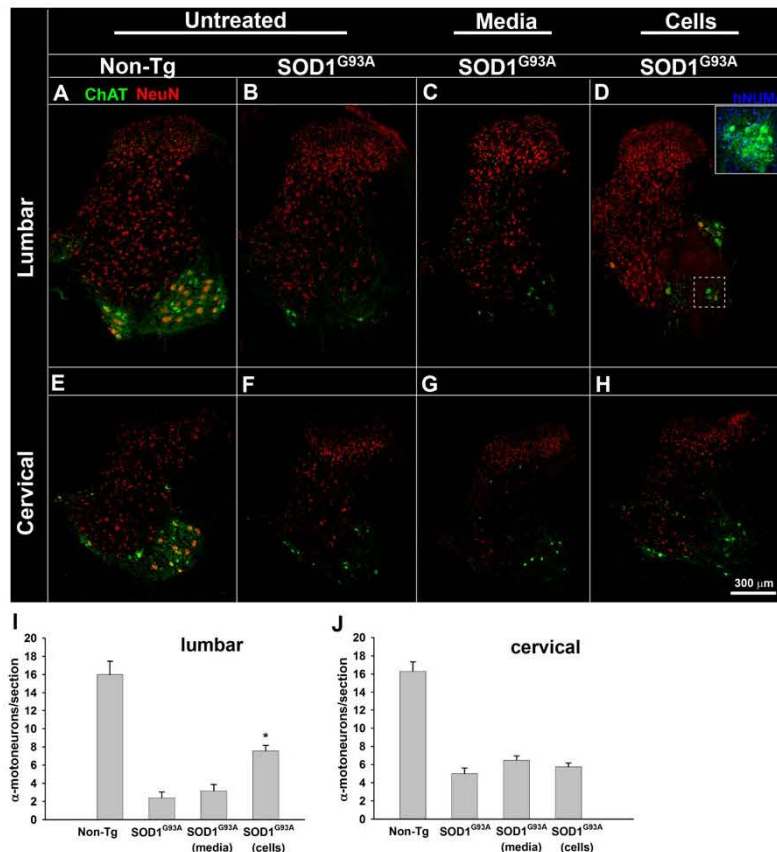


Figure 2. SOD1^{G93A} rats receiving lumbar grafts of human spinal neural stem cells show higher α -motoneuron survival at the lumbar but not cervical spinal segments. Lumbar transverse spinal cord sections from untreated, non-transgenic (Non-Tg; A) and untreated SOD1^{G93A} transgenic (SOD1^{G93A}; B) animals, as well as SOD1^{G93A} animals treated with media (SOD1^{G93A} media; C) or human spinal neural stem cell grafts (SOD1^{G93A} cells; D) were double immunostained to identify all mature neurons (NeuN) and cholinergic cells (α -motoneurons, ChAT). While a dramatic reduction in ChAT-IR cells was noted in all SOD1^{G93A} animals, regardless of treatment, quantitative analysis (I) of persisting α -motoneurons showed a significant increase in the α -motoneuron pool in the cell-grafted animals (D, I). Using adjacent histological sections, inset (D) shows an example of a group of transplanted cells (positive for human nuclear matrix antigen; hNUMA) near a pool of surviving α -motoneurons. Sections taken from the same animals but from the cervical level (C5/6) also show a dramatic reduction in the motoneuron pool but with no apparent protective effect afforded by the lumbar cell grafts (E–H, J). Scale bar: 300 μ m. * $P < 0.001$ compared to non-transgenic, $P = 0.03$ compared to the media-treated group; one-way ANOVA.

doi:10.1371/journal.pone.0042614.g002

impregnation), massive axo-dendritic degeneration (compare the tissue from normal animals [Fig. 5E–G] with that from SOD1^{G93A} animals [Fig. 5H–K]) was identified in several areas in the cervical, thoracic and lumbar spinal cord segments including: i) the lateral and ventral white matter, ii) laminae IV IX within the gray matter, and iii) to a lesser degree in the dorsal columns (Fig. 5H–K).

The total number of remaining axons and their calibers (0.5–2, 2–5, 5–14 μ m in diameter) were determined in the lateral and ventral funiculi [using semi-automated image analysis of osmium-treated 1 μ m plastic sections taken from lumbar spinal cord of normal ($n = 2$; Fig. 5L–N) and SOD1^{G93A} ($n = 2$) endstage animals with no previous manipulations (i.e. no spinal media or cell injections; Fig. 5O–Q)]. In normal tissue, axons of varied caliber were clearly-outlined with myelin (Fig. 5M, N). On the other hand, an easily recognizable reduction in the number of large caliber myelinated axons was found in endstage tissue from SOD1^{G93A} animals (compare Fig. 5M, N to P, Q). Axonal loss

in the lateral funiculus averaged 19% for 0.5–2 μ m caliber axons, 40% for 2–5 μ m caliber axons, and 57% of axons 5–14 μ m in diameter (Table 2). Numerous medium sized (10–15 μ m) and large (15–25 μ m) vacuoles, likely evolving at sites of previous axonal degeneration and phagocytic activity (Fig. 5O, P, arrows), were prominent in lumbar white matter of the SOD1^{G93A} animals. In addition, frequent osmium-dense deposits that were likely macrophages and activated microglia were consistently identified (Fig. 5O, P, arrowheads).

Transient retention in neurologic and reflex activity from grafting of human spinal neural stem cells, but no effect on survival of SOD1^{G93A} animals

Development and progression of ALS-like disease in SOD1^{G93A} was followed after lumbar grafting of hNSCs of presymptomatic (60–65 days old) SOD1^{G93A} rats (Fig. 1A). Disease onset, defined as the peak animal body weight (Fig. 6A), in grafted animals was not different from untreated animals (109 \pm 2d, 111 \pm 2, and

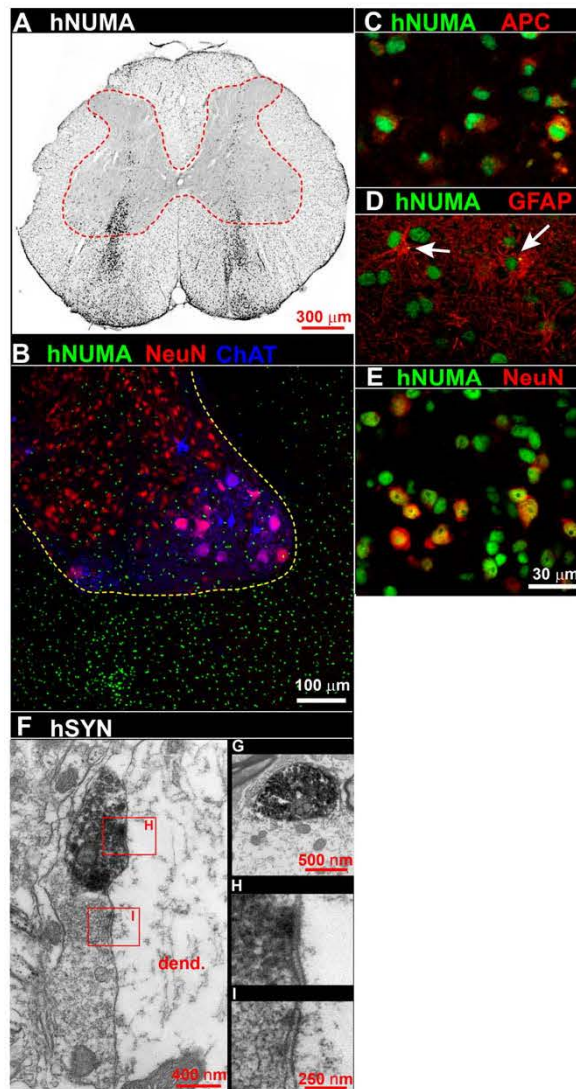


Figure 3. Effective re-population of lumbar gray and white matter by human spinal neural stem cells nine months after lumbar transplantation in immunodeficient rats. When human spinal neural stem cells (same cell line as were used in the grafting experiments in Fig. 1, 2 and Fig. S2, S3) were transplanted into the lumbar spinal cord of immunodeficient rats, histological sections taken after nine months of survival revealed a near homogenous distribution of human cells (hNUMA; A, B) in both gray and white matter. In white matter hNUMA-IR cells were primarily oligodendrocytes (adenomatous polyposis coli; APC; C) or astrocytes (GFAP; D) while in gray matter a neuronal phenotype (NeuN; E) was identified. Electron microscopy revealed axon terminals, enriched with human synaptophysin immunoreaction product (F, G), forming synapses with host neurons or dendrites (F, H, I). Scale bar: 300 μ m (A), 100 μ m (B), 30 μ m (C–E), 400 nm (F), 500 nm (G), 250 nm (H, I). doi:10.1371/journal.pone.0042614.g003

108 \pm 3 for grafted animals, media-injected and untreated SOD1^{G93A} animals; $p=0.41$; t-test). Grafting also produced no statistically significant effect on progression to an early disease point (identified by the age at which the animal had lost 10% of its body weight from denervation-induced muscle atrophy; Fig. 6B)

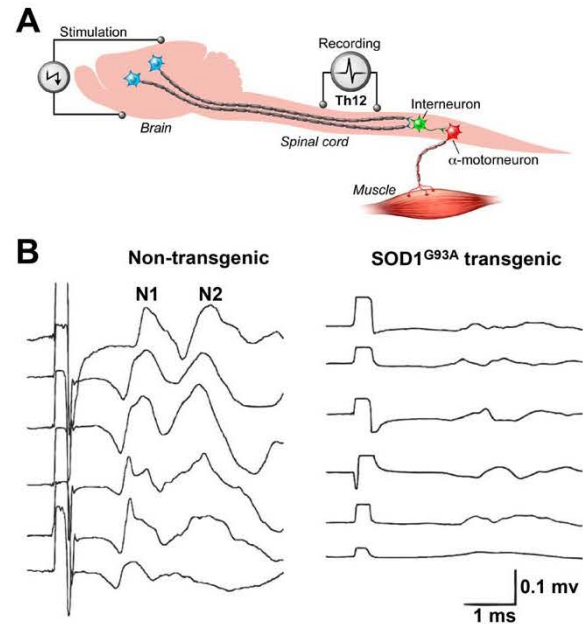


Figure 4. Motor-evoked potentials recorded from the dorsal surface of T12 spinal cord are near completely lost in endstage SOD1^{G93A} rats. To identify the conductivity of descending motor axons MEPs were elicited by electrical stimulation of motor cortex and extra-pyramidal system and responses recorded from exposed T12 spinal segments (A). Recordings in 6 non-transgenic animals showed consistent compound action potentials consisting of N1 and N2 waves with an average latencies of 1.6–2.8 ms respectively (B). In contrast, recording in 6 transgenic SOD1^{G93A} endstage animals showed near complete loss of N1 and N2 waves. doi:10.1371/journal.pone.0042614.g004

between hNSCs-grafted animals and those that received media only (123 \pm 2d versus 127 \pm 2d, respectively; $P=0.122$; t-test). Overall survival was also not significantly affected between the hNSCs-grafted or media-injected animals (136 \pm 3d and 142 \pm 3d, $p=0.18$; t-test) (Fig. 6C). Analyzing males and females separately failed to reveal any significant difference in any disease index (data not shown).

On the other hand, neurological function (using a well-established BBB scoring scale measured from each animal every 3–4 days) was significantly preserved at age 135–142d in the cell-grafted animals compared with the media-treated group (Fig. 6D; $p<0.05$; t-test). Similarly, at the same age (Fig. 6E) recording of Hoffmann reflex revealed a higher average H-wave amplitude for

Table 1. Analysis of motor-evoked potentials recorded from the dorsal surface of the T12 spinal cord segment in non-transgenic and endstage transgenic SOD1^{G93A} rats.

	Amplitude (mV \pm SD)		Latency (ms \pm SD)	
	N1	N2	N1	N2
Non-Tg	140.7 \pm 39.0	88.4 \pm 51.3	1.6 \pm 0.2	2.8 \pm 0.3
SOD1 ^{G93A}	25.5 \pm 6.4*	25.1 \pm 9.1*	2.5 \pm 0.2*	3.5 \pm 0.5*

The amplitudes and latencies of the N1 and N2 waves were calculated and averaged from 6 non-tg and 6 SOD1^{G93A} endstage animals. (* $P<0.05$). doi:10.1371/journal.pone.0042614.t001

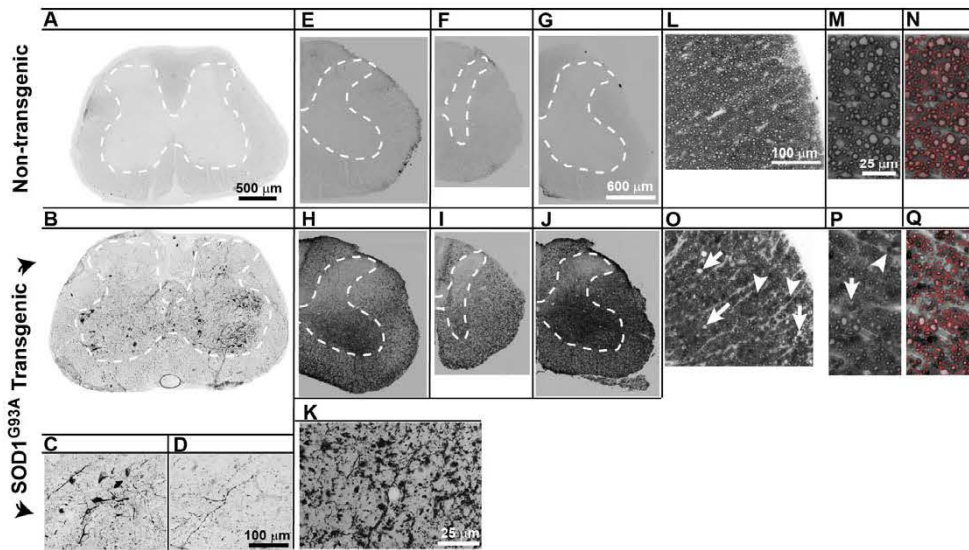


Figure 5. Significant degeneration of descending medium-, and large-size myelinated axons in lumbar segments in endstage SOD^{G93A} rats. Using the Gallyas silver impregnation technique, degenerating neurons were detected mostly within the ventral horn, although reactive cells were often noted in upper lamina (A- non-transgenic, B- SOD^{G93A} endstage). Closer examination shows fragmented cells and fibers not only within the grey matter, but also in the adjacent white matter (C, D). The de Olmos modified cupric-silver stain was used to help detect degenerating axons and dendrites; non-transgenic tissue showed no appreciable staining (E – cervical, F-thoracic, G – lumbar), while SOD^{G93A} tissue reacted intensely, not only in the ventral horns but throughout the gray matter, sparing only lamina I–III (H–J). Closer examination of the white matter showed argyrophilic punctate structures corresponding to silver deposits in disintegrated axons (K). Semithin (1 μm) plastic-embedded tissue sections were used to quantify changes in the axonal population in the lateral and ventral columns. While clearly-delineated axons of varied caliber were readily-outlined by the osmium-stained myelin in non-transgenic animals (L–N), tissue from endstage SOD^{G93A} animals had an easily recognizable reduction of large caliber myelinated axons (O–Q). Lumbar white matter in SOD^{G93A} endstage animals also contained numerous vacuoles (O, P, arrows) and frequent osmium-dense deposits (O, P, arrowheads). Scale bar: 500 μm (A, B), 100 μm (C, D), 600 μm (E–J), 25 μm (K), 100 μm (L, O), 25 μm (M, N, P, Q). doi:10.1371/journal.pone.0042614.g005

the hNSCs-grafted group compared to the media-treated animals (3.5±0.6 vs. 1.1±0.3 mV; p<0.05; t-test), indicating functional preservation between sensory Ia afferent, α-motoneuron and motor plate.

Discussion

Our results show that human fetal spinal neural stem cells (hNSCs) grafted into the lumbar ventral horn in SOD^{G93A} rats provides a region-specific neuroprotective effect in the vicinity of the grafted cells, including a higher number of surviving α-

Table 2. Quantification of lateral and ventral funiculi axons in lumbar spinal cord segments of non-transgenic and endstage transgenic SOD^{G93A} rats.

Lateral Funiculus				
	Total axons	0.5–2.0 μm	2.0–5.0 μm	5.0–14 μm
Non-Tg	45681	31982	11529	2079
Non-Tg	62656	43444	16782	2299
SOD ^{G93A}	40422	30943	8411	994
SOD ^{G93A}	39729	30315	8467	881
Ventral Funiculus				
	Total axons	0.5–2.0 μm	2.0–5.0 μm	5.0–14 μm
Non-Tg	14330	8764	4433	1087
Non-Tg	16500	9830	5382	1247
SOD ^{G93A}	11532	8037	2984	489
SOD ^{G93A}	14002	10285	3153	536

Quantification of the axonal population in the lateral and ventral columns showed an easily recognizable reduction of large caliber myelinated axons. doi:10.1371/journal.pone.0042614.t002

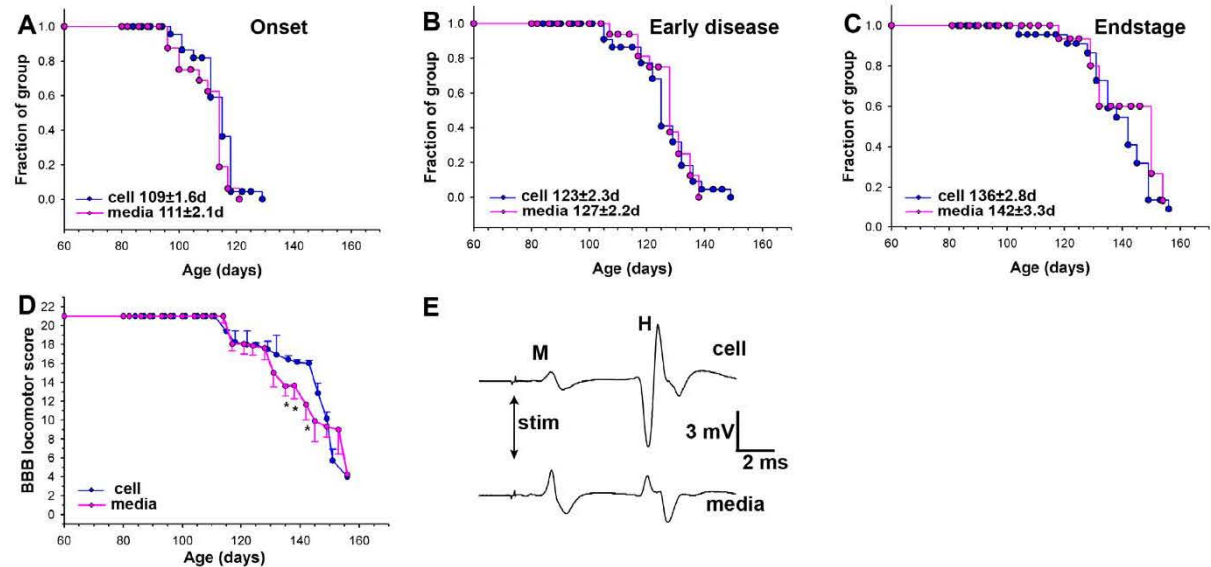


Figure 6. SOD1^{G93A} rats receiving lumbar grafts of human spinal neural stem cells showed transient protection of hindlimb motor function and Hoffmann reflex. Population analyses of media-treated and cell-grafted animals showed no difference in: disease onset - defined as peak body weight (A), early disease progression - defined as the age at which animals had lost 10% body weight (B), or survival (C). Hindlimb motor function assessed by BBB neurological score (D) showed a significantly better score in hNSCs-grafted animals between ages 135–142 d. Similarly, Hoffmann reflex recorded in cell-grafted animals during that time period had significantly higher average amplitudes than those from the media-treated group (E), (* $P < 0.05$).
doi:10.1371/journal.pone.0042614.g006

motoneurons, transient improvement in ambulatory function, corresponding preservation of H-reflex activity, and decreased inflammatory responses. Our findings add to earlier evidence that reported i) preservation of α -motoneurons in lumbar spinal cord in SOD1^{G93A} rats after unilateral grafting of human neural stem cells genetically modified to produce glial cell line-derived neurotrophic factor (GDNF) [26] and ii) functional improvement (as assessed by extended survival and disease duration, improved forelimb motor and respiratory functions) and corresponding decrease in α -motoneuron degeneration in SOD1^{G93A} rats receiving cervical grafts of rat astrocyte precursors [12].

Despite initial reports 18 and 9 years ago, respectively, of SOD1^{G93A} mutant mouse and rat transgenic models [5,27], there is only one characterization of the degree of upper motor neuron degeneration in one mouse model [28] and none in the rat. To this, our current MEPs data show that in symptomatic animals there is a near complete loss of descending motor tract conductivity measured directly from the dural surface of the exposed Th12 spinal segment (Fig. 4). This functional loss corresponds with massive axonal degeneration in the white matter particularly affecting large caliber myelinated axons in the anterior and lateral funiculi (Fig. 5). This is consistent with a classical picture of spinal histopathological changes in ALS patients which, in addition to spinal α -motoneuronal loss, is characterized by upper motor neuron lesion and degeneration involving the entire corticospinal tract [29–32]. Interestingly, in contrast to humans, preferential degeneration of axons in lateral and ventral funiculus was seen in symptomatic SOD1^{G93A} rats while relatively spared axonal populations were seen in the dorsal funiculus (i.e., the region of corticospinal tract in rats). Whether or not it is the result of species specificity is not known, however, one important functional distinction between the organization of the different

motor systems involved in voluntary motor function exists between human and rodents. It has been demonstrated that after complete transection of the pyramidal tract in rats a considerable amount of motor function persists [33]. It is believed that the activity of the extrapyramidal system (such as rubrospinal tract which descend in lateral funiculi in the rat) plays a more dominant role in the initiation and maintenance of voluntary movement in rats. We speculate that a more pronounced axonal loss seen in the lateral funiculi in symptomatic SOD1^{G93A} rats can thus be attributed to a specific motor circuitry-controlling function of descending motor axons residing in this region.

Based on these histopathological and functional data demonstrating an extensive loss of descending motor system in SOD1^{G93A} rats it is readily apparent that unless the functional integrity of all components of the motor neuraxis is maintained (or restored) by a given treatment, only local and/or time-limited functional protection can be achieved, just what we have produced with hNSCs grafts.

We found no survival benefit versus our control media-injected group, despite transient local improvement. This was not unexpected, since for humane reasons survival in this animal model is defined by a loss of righting reflex (i.e., the ability of the animal to right itself). An intact righting reflex requires coordinated hindlimb and forelimb motor function and continuing functional coupling of the upper and lower motor neuron system. In deficits which include upper and lower motor neuron degeneration (such as seen in SOD1^{G93A} rats), region-restricted treatments (as achieved after spinal segmental cell grafting) is not expected to significantly modify upper motor neuron degeneration and loss and the associated progressive decline in righting reflex. Nevertheless, using lumbar spinal grafting of human spinal neural stem cells similar to those of our current study, Xu et al. (2006) [16] previously reported an apparent lifespan extension of

SOD1^{G93A} rats of 11 days (average 149 days) compared to control animals receiving injection of dead cells (average 138 days). Similar to our study a significantly higher number of persisting lumbar α -motoneurons was found in treated animals. More recently, Xu et al. (2011) reported a lifespan extension of SOD1^{G93A} rats by 17 days after dual cervical (C4 C5) and lumbar (L4 L5) transplantation of the same human spinal neural stem cell line as used in our current study [34]. Given the robust graft survival, cell differentiation and migration seen in our study, we speculate that the differences between ours and these prior studies may reflect the occurrence of natural drift in the onset of disease between different cohorts of animals (a feature that has been argued to necessitate >25 animals per group in order to draw statistically valid conclusions) [35] and/or difference in the design of the control groups (i.e., injections of dead cells vs. media only) and potentiation of local neuronal degeneration in dead cell-injected animals.

Several differential characteristics between rodent models and human ALS patients need to be considered when predicting the potential value of spinal cell replacement therapies in human patients. First is a significantly different time course of disease progression in rodents and human patients. In SOD1^{G93A} rodent models the average duration of disease from the initiation of denervation-induced weight loss to terminal stage is 60–70 days in mice [5,27,36,37] and is around 27 days in rat [38]. In human ALS patients it can range between months to several years [1,32]. Such differences have a fundamental impact on the degree of engraftment, maturation and migration of grafted cells, and can ultimately define the degree of expected neuroprotection. In our current experimental design, SOD1^{G93A} rats were implanted at age ~65 days (i.e., on average ~44 days prior to disease onset) and had an average survival time of 75 days after cell grafting (an average of ~140 days to endstage). While robust neuronal differentiation was noted in grafted animals, only limited cell migration was seen in the short term to areas distant from cell-injected regions. Cell migration at 9 months post-grafting in naive, immunodeficient rats, a time period comparable to that expected in human patients receiving spinal grafts, was determined. In contrast to short times post-grafting, much more robust cell migration was seen, with a homogenous distribution of grafted cells identified in white and gray matter (Fig. 3). Cells found in white matter showed near-exclusive differentiation towards astrocytes and oligodendrocytes. These findings support the likelihood that comparable spinal cell repopulation can be expected in human patients postgrafting and that this can be associated with a more relevant functional-protective effect. Combined cell grafting strategies targeted in parallel to spinal and supraspinal motor centers can be anticipated, therefore, to provide a substantial degree of neuroprotection measured both behaviorally as well as by using combined motor and somatosensory-evoked recording.

A second important component in achieving optimal therapeutic benefit in cell replacement therapies is the selection of cell lines (e.g., neural, neuronal or glial-restricted) to be used for spinal/supraspinal grafting. The primary selection criteria should reflect the disease stage and targeted cell population to be replaced, that is, cells whose damage drives early or late disease phases. Since one of the well documented mechanisms contributing to disease progression is the release of toxic factors from SOD1 mutant astrocytes and resultant neuronal degeneration [8,9,11,39], the use of wild type astrocyte precursors for grafting may appear to be an attractive choice. Data from the Maragakis' group [12] demonstrated a region specific therapeutic effect when cells were grafted into the cervical gray matter in presymptomatic SOD1^{G93A} rats.

However, the absolute number of spinal (and also brain) astrocytes may not be static and there is a continued proliferation of glial precursors in the intact adult CNS [40]. In addition, there is increased astrocyte proliferation after injury such as spinal trauma or focal brain ischemia [41,42]. More recent studies using *in vivo* BrdU incorporation assay have shown that, while the primary cellular contribution to spinal cord gliosis seen in symptomatic and endstage SOD1 mutant (G93A) mice is derived from oligodendrocyte-committed NG2+ precursors (up to 49–55%), between 4–5% of BrdU-labeled cells are GFAP-immunoreactive astrocytes [43,44]. These data show modest but continuing proliferation of mutated SOD1 astrocytes throughout the disease progression. Thus, there may be a competitive interaction between replication of the host mutated astrocytes and grafted wild-type astrocyte precursors.

Moreover, from a clinical perspective, one of the limitations in using a lineage restricted precursor population is the potential that it may be targeted for damage and potentially replaced by endogenous mutant astrocyte population. In experimental rodent studies, cells are typically grafted at pre-symptomatic stages while the clinical patient population will primarily be composed of symptomatic patients, with existing upper and/or lower motoneuron/interneuron degeneration. Because there is no evidence of neurogenesis in adult naive or trauma injured spinal cord [40,45], the primary goal in cell replacement therapies that employ glial-restricted precursors will therefore be to stabilize or slow neural degeneration. Second, given the large number of astrocytes compared to neurons in the adult CNS, there is a limited likelihood of achieving significant astrocyte repopulation using cells lines with little or no mitotic/migratory activity, so an important characteristic of astrocyte-restricted lines for grafting is their continuing proliferative/migratory capacity after transplantation. Our current data using 9 month surviving cell-grafted immunodeficient rats demonstrate widespread grafted cell migration with no detectable tumor formation. More recently, we have observed comparable cell migration and safety of human embryonic stem cell (H9)-derived neural stem cells at 5–6 months after spinal grafting in immunodeficient rats (unpublished observations). Nonetheless, a detailed long-term safety/tumorigenicity profile will need to be established for each individual cell line before clinical use.

Finally, our evidence highlights that the use of human fetal spinal cord-derived neural stem cells which can generate astrocytes but mostly neurons *in vivo* have a limited, local therapeutic effect. Therefore, an optimal cell line will likely produce a mixture of glial and neuronal stem cells having both proliferative (at least for the astrocyte-restricted subpopulation) and migratory properties. As demonstrated in our current study, human fetal spinal cord-derived neural stem cells have such properties to a certain extent, albeit a higher ratio of astrocyte precursors in the grafted cell population might be preferable. It now remains to be determined whether human embryonic stem cells-derived neural stem cells will show a distinct differentiation ratio and more rapid migration in an ALS environment after *in vivo* grafting in humans.

In any event, cell replacement therapies should target both spinal and supraspinal components of motor neuraxis. Because the multi-site delivery of therapeutic cells is clearly technically more challenging, additional safety data as well as the development of less invasive cell delivery techniques will be required before this potentially more effective multi-site cell delivery treatment approach can successfully be introduced into clinical practice.

Methods

Ethics Statement and Institutional Animal Care and Use Committee approvals

This study was approved by the University of California, San Diego (UCSD) Internal Review Board (IRB), approval ID#101323.

All animal studies were carried out under protocols approved by the Institutional Animal Care and Use Committee at University of California (approval IDs # S01193 and S07016) San Diego and were in compliance with *The Association for Assessment of Laboratory Animal Care* guidelines for animal use. All studies were performed in such a manner as to minimize group size and animal suffering.

Derivation of the human fetal spinal neural stem cells (hNSCs)

Human fetal spinal neural stem cells (hNSCs) were prepared from the cervical upper thoracic region of spinal cord tissue obtained from a single 8-week human fetus after an elective abortion. The fetal tissue was donated by the mother in a manner fully compliant with the guidelines of NIH and FDA and approved by an outside independent review board. The spinal cord tissue was removed of meninges and dorsal root ganglia and dissociated into a single cell suspension by mechanical trituration in serum-free, modified N2 media. The modified N2 media was composed of: 100 mg/l human plasma apo-transferrin, 25 mg/l recombinant human insulin, 1.56 g/l glucose, 20 nM progesterone, 100 μ M putrescine, and 30 nM sodium selenite in DMEM/F12. For growth of the hNSCs, 10 ng/ml bFGF as the sole mitogen was added to the modified N2 media (growth media). The initial culture was serially expanded as a monolayer culture in precoated flasks (T-175) or plates [46]. Briefly, the precoated vessels were prepared by incubating them for 1 h at room temperature with 100 μ g/ml poly-D-lysine in 10 mM Hepes buffer at 0.165 ml/cm². The vessels were washed three times with water and allowed to completely dry aseptically in the hood. They were then further incubated with 100 μ g/ml fibronectin/PBS for 5 min or alternatively 25 μ g/ml fibronectin/PBS for 1 h. The fibronectin solution was aspirated and the vessels were used immediately without drying. Approximately 6.1×10^6 total cells were obtained upon the initial dissociation of the spinal cord tissue. All of the cells were plated onto one 150 mm plate in 20 ml of the growth media.

The growth medium was changed every other day and in the alternate days, 10 ng/ml of bFGF was directly added to the culture. The first passage was conducted 16 days after plating. At this point, the culture was composed mostly of post-mitotic neurons and mitotic hNSCs. The mitotic cells were harvested by brief treatment with trypsin (0.05% in 0.53 mM EDTA). Trypsin was stopped by addition of soybean trypsin inhibitor to 0.05% final concentration. The cell suspension was triturated with a pipette to obtain a single cell suspension and centrifuged at 1400 rpm for 5 min. The cell pellet was resuspended in growth media and the cells were replated in new pre-coated plates at 1.2×10^6 cells in 20 ml of growth media per 150 mm plate. The cells were harvested at approximately 75% confluence, which occurred in 5–6 days. This process was repeated for 20 passages. At various passages, the cells were frozen in the growth medium plus 10% DMSO at 5×10^6 – 10×10^6 cells/ml using a programmable freezer. The frozen cells were stored in liquid nitrogen. Upon thawing, the overall viability and recovery was typically 80–95%. The resulting cell line, which was produced by epigenetic means only, using bFGF as the sole mitogen, was named “566RSC.” A cell bank of passage 16 cells was prepared and used for this study.

Preparation of hNSCs for implantation

One day prior to each surgery day, one cryopreserved vial of the previously prepared passage 16 cell bank was thawed, washed, concentrated in a hibernation buffer, and shipped from the cell preparation site (Neuralstem, Inc., Rockville, MD, USA) to the surgery site (UCSD, San Diego, CA, USA) at 2–8°C by overnight delivery. Upon receipt the following day, the cells were used directly for implantation without further manipulation. Before and after implantation the viability of cells was measured with Trypan blue (0.4%; Sigma). On average a 75–85% viability rate was recorded.

Experimental groups

Before cell grafting, SOD1^{G93A} transgenic rats were randomly divided into 3 experimental groups: no treatment (untreated SOD1^{G93A}), media-treated SOD1^{G93A}, and cell-grafted SOD1^{G93A}; non-transgenic littermates were used as control animals and received no treatment. A total of 24 animals (12 males, 12 females) were assigned to the cell-grafted SOD1^{G93A} group, while 16 animals (8 males, 8 females) were assigned to receive media only. Immunosuppressive treatment with Prograf (FK506; 3 mg/kg/day subcutaneous; Astellas Pharma, Deerfield, IL) and Cellcept (mycophenolate mofetil; 30 mg/kg/day intraperitoneal; Roche Pharmaceuticals, Nutley NJ) were initiated 2 d before transplantation. Cellcept continued to 7 d post-surgery, while Prograf was changed to 1 mg/kg/day at 14 d post-op and continued until the study end. A separate group of athymic rats (CrI:NIH-Foxn1^{tmu}; n = 12; Charles River) was used for a subset of experiments but underwent no immunosuppression.

Motor-evoked potentials were recorded from the dorsal surface of the lumbar spinal cord (see Motor-evoked potentials recording) in a separate group of endstage SOD1^{G93A} animals (n = 6) and non-transgenic controls (n = 6) which did not undergo any treatment or spinal injections. The same animals were then used for qualitative and quantitative analysis of axonal degeneration/loss of spinal descending motor tracts using silver impregnation techniques and plastic-embedded semithin sections (see Plastic embedding and Silver degeneration staining).

Spinal cord implantation of hNSCs

Animals (60–65 d old) were anesthetized with isoflurane (1.5–2% maintenance; in room air), placed into a spinal clamp apparatus (Stoelting, Wood Dale, IL, USA) and a partial T12–L1 laminectomy was performed using a dental drill (exposing the dorsal surface of L2–L6 segments). Using a glass capillary (tip diameter 80–100 μ m) connected to a microinjector (Kopf Instruments, Tujunga, CA), rats were injected with 0.5 μ l (10,000 cells per injection) of the hNSCs in hibernation buffer, or only the hibernation buffer as control (media). The duration of each injection was 60 s followed by 30 s pause before capillary withdrawal. The center of the injection was targeted into the intermediate zone and ventral horn (distance from the dorsal surface of the spinal cord at L3 level: 1.1–1.2 mm), [47]. Injections were made every 700–900 μ m, rostral-caudally, on each side of the lumbar spinal cord targeting L2–L5 segments. The total number of injections ranged between 9–13 injections per side. After injections, the incision was cleaned with penicillin-streptomycin solution and sutured in two layers. Athymic rats were transplanted in an identical fashion.

Assessment of neurological function and disease progression

Motor function was evaluated using the 21-point open field BBB locomotor scale [48]. Animals were observed for 4–5 min and scored by an experimenter blinded to the treatment groups. *Disease onset* was defined as the age of maximum body weight; *Early disease* was defined as the point at which the animal lost 10% of peak body weight; *Endstage* was defined as when an animal could not right itself after 30 s of being placed on its side [38].

Hoffman reflex (H-reflex) recording

H-reflex was recorded as previously described [49,50]. Under ketamine anesthesia (100 mg/kg/hr, i.m.) the right hind limb of the animal was secured and a pair of stimulating needle electrodes was transcutaneously inserted into the surroundings of the tibial nerve. For recording a pair of silver needle electrodes was placed into the interosseous muscles between the fourth and the fifth or the first and the second metatarsal right foot muscles. The tibial nerve was stimulated using square pulses with increasing stimulus intensity (0.1–10 mA in 0.5 mA increments, 0.1 Hz, 0.2 ms; WPI; Isostim A320) and responses were recorded with an A/C-coupled differential amplifier (Model DB4; DPI, Sarasota, FL).

Motor-evoked potential recording

Under isoflurane anesthesia (1.5–2% maintenance; in room air), terminal SOD1^{G93A} rats (n=6 or age-matched controls, n=6) without any previous treatment (i.e., no spinal injections) were mounted into a stereotaxic frame and the scalp over motor cortex was cut open to expose the skull. Stimulation was done using a pair of stimulating electrodes consisting of a stainless steel screw placed into the skull over the motor cortex and stainless steel needle inserted into the hard palate behind the upper incisors. Previous data show that such placement of stimulating electrodes provides consistent activation of pyramidal and extrapyramidal system [19–21].

A dental drill was used to perform a laminectomy of T11 vertebra exposing the T12 spinal segment. Evoked responses were recorded by a pair of flexible silver ball electrodes placed on the dura surface of the exposed T12 spinal segment. A reference silver-chloride disc electrode was placed subcutaneously on the contralateral side of the recording. After electrode placement, animals were injected with ketamine (100 mg/kg/h, I.M.) and isoflurane anesthesia was discontinued. Stimulation pulses were 0.2 ms long with amplitudes ranging from 0.5 to 8 mA (Isostim A320R, World Precision Instruments, Florida, USA). Signals from recording electrodes were filtered by 10 kHz low pass filter, amplified by differential amplifier (TDT DB4 amplifier with HS4 preamplifier, Tucker-Davis Technologies, Florida, USA), digitized in 30 kHz sampling frequency and stored for further analysis.

Immunohistochemistry

At endstage disease, rats were deeply anesthetized with pentobarbital and phenytoin and transcardially perfused with 200 ml of heparinized saline followed by 250 ml of 4% paraformaldehyde in PBS. The spinal cords were dissected and postfixed in 4% formaldehyde in PBS overnight at 4°C and then cryoprotected in 30% sucrose PBS until transverse sections (30 μm thick) were cut on a cryostat and stored in PBS. Sections for brightfield immunohistochemical staining were pretreated with 3% H₂O₂ in PBS for 15 min, washed 3× in PBS and were then placed in primary antibody similar as sections for fluorescent staining: overnight at 4°C with primary human specific (h) or non-specific antibodies made in PBS with 0.2% Triton-X100; mouse

anti-human nuclear matrix protein/h-nuc (hNUMA; 1:100; Millipore, Temecula, CA, USA); goat anti-doublecortin (DCX; 1:1000; Millipore, Temecula, CA); mouse anti-human neuron specific enolase (hNSE; 1:200, Vector Laboratories Inc., Burlingame, CA); rabbit anti-gliabryllary acidic protein (GFAP; 1:1000, Sigma-Aldrich Corp. St. Louis, MO); goat anti-choline acetyltransferase (ChAT; 1:100; Millipore, Temecula, CA); biotinylated mouse anti-NeuN (Millipore, Temecula, CA); mouse anti-adenomatous polyposis coli (APC; 1:500; EMD Chemicals Inc., Gibbstown, NJ); chicken anti-beta III tubulin (TUJ1; 1:1000; Aves Labs Inc, Tigard, OR); rabbit anti-ionized calcium binding adaptor molecule 1 (Iba1; 1:1000; Wako Chemicals USA, Inc., Richmond, VA); mouse anti-human synaptophysin (hSYN; 1:1000; Millipore, Temecula, CA); guinea pig anti-vesicular glutamate transporter (VGluT1- 1:2500; VGluT2 1:2500; VGluT3 1:5000; Millipore, Temecula, CA); guinea pig anti-glycine transporter 2 (GlyT2; 1:2000; Millipore, Temecula, CA); rabbit anti-growth associated protein 43 (GAP43; 1:500; Millipore, Temecula, CA); rabbit anti-glutamate decarboxylase 65 (GAD65; 1:2000; Millipore, Temecula, CA).

After incubation with primary antibodies, sections were washed 3× in PBS and incubated with fluorescent-conjugated secondary antibodies raised in donkey (Alexa 488, 546; 647; 1:250; Invitrogen Corp., Carlsbad, CA, USA) and DAPI for general nuclear staining. In cases where 2 mouse antibodies were required for multi-labeling, one was biotinylated using a Zenon mouse IgG labeling kit according to the manufacturer's instructions (Invitrogen Corp., Carlsbad, CA, USA). Once staining was complete, sections were mounted on slides, dried at room temperature and covered with Prolong anti-fade kit (Invitrogen Corp., Carlsbad, CA, USA). Sections for brightfield were washed after primary antibody, placed in biotinylated secondary antibody (goat anti-mouse; 1:500; Vector Laboratories, Burlingame, CA) for 2 h at room temperature. Those sections were again washed, placed in avidin-biotin complex (ABC kit, Vector Laboratories, Burlingame, CA) for 2 h at room temperature. Finally, the sections were washed, developed with 3,3'-diaminobenzidine (DAB; Vector Laboratories, Burlingame, CA), mounted on silane-coated slides, air-dried, dehydrated and coverslipped. Images were captured using a Leica DMLB microscope with a Zeiss Axiocam MRm monochrome camera. Some images were captured using a Leica SP2 confocal microscope. Any image post-processing was done with Adobe CS3 (Adobe Systems, Inc., San Jose, CA) with equal changes to any images being compared.

Plastic embedding

For plastic embedding, spinal cord blocks (2–3 mm thick) were postfixed in 0.3% glutaraldehyde for 1 day at 4°C. Tissue was rinsed 3×5 min in 0.1 M phosphate buffer (pH 7.4), and stored in phosphate buffer overnight at 4°C. Secondary postfixation was performed using 0.1% osmium tetroxide in 0.1 M phosphate buffer for 12 hours, followed by rinsing in phosphate buffer. This was followed by progressive alcohol dehydration according to standard procedures up to 100% ethanol, with the addition of further dehydration in a 1:1 solution of ethanol/propylene oxide, and lastly 100% propylene oxide. Dehydrated blocks were then prepared for resin infiltration by incubation in a 1:1 solution of resin/propylene oxide overnight. The resin included: Eponate 12, Araldite 502, Dodecyl Succinic Anhydride (DDSA), and 2,4,6-Tri[Dimethylaminomethyl]phenol (DMP-30) (Ted Pella Inc), mixed in ratios of 10:10:25:1 respectively. Blocks were then transferred to 100% resin for subsequent overnight infiltration on a rotator. Finally, tissue blocks were embedded using fresh resin in multi-chamber silicone rubber molds (Ted Pella). The mold was

placed in an oven (60°C) for 2 days to facilitate resin polymerization. Semithin (1 µm) transverse sections were then cut using a Leica (DM-40) microtome with glass knives. Sections were mounted to slides from distilled water and allowed to dry on slide warmer. Prior to staining, slides were incubated at 60°C in an oven for 10–15 minutes, and then contrast-stained with 4% paraphenylenediamine (PPD).

Silver degeneration staining

De Olmos aminocupric silver impregnation. Neurodegeneration was assessed using the de Olmos aminocupric silver histochemical technique as previously described [23,25]. Following the vendor's instructions (Neuroscience Associates, TN, USA), SOD1^{G93A} endstage rats and non-transgenic age-matched littermates were transcardially perfused with cacodylate-modified PBS followed by cacodylate-modified paraformaldehyde and brain and spinal cord tissue shipped to Neuroscience Associates for processing.

Gallyas silver impregnation [22]. Paraformaldehyde-fixed spinal cord tissue was embedded in paraffin wax and 12 µm thick sections were cut and mounted directly on slide. After dewaxing in xylene and progressive rehydration to water, the slides were placed in fresh 0.3% magnesium permanganate and subsequently rinsed in tap water for 10 minutes. Further magnesium permanganate clearing was done in 2% oxalic acid for 3 min. Background suppression was facilitated by incubation in fresh 0.004% lanthanum nitrate/0.02% sodium acetate solution for 60 minutes. Following wash, slides were placed into a silver iodide solution for 2 minutes, and then neutralized by three washes in 0.5% acetic acid. The intensity of silver impregnated structures was amplified with immersion in a 1:1 ratio of two physical developer solutions: A: ammonium nitrate, silver nitrate, tungstosilic acid, and formaldehyde; and B: 5% anhydrous sodium carbonate solution. Slides were then quickly washed in 0.5% acetic acid, and placed into a 0.5% gold chloride solution for 5–10 minutes. Slides were rinsed in distilled water, placed in 2% sodium sulfate (2 minutes) and rewashed in distilled water before they were progressively dehydrated to xylene and cover slipped in DPX.

Immuno-electron microscopy

Transverse spinal cord sections (50 µm thick) were prepared from lumbar spinal cords of immunodeficient rats at 9 months after hNSCs grafting. Sections were cut on a vibratome and cryoprotected with glycerol dimethylsulfoxide mixture. After cryoprotection, the sections were frozen and thawed four times and treated with 1% sodium borohydride. To reduce nonspecific binding, the sections were treated with 0.3% H₂O₂ 10% methanol in TBS (100 mM Tris-HCl and 150 mM NaCl, pH 7.6) and 3% NGS 1% bovine serum albumin in TBS. Sections were reacted overnight with mouse anti-human-specific synaptophysin (1:1000; Chemicon). Bound antibody was detected using biotinylated donkey anti-mouse IgG (1:500; GE Healthcare, Little Chalfont, UK), the ABC Elite kit (Vector Laboratories, Burlingame, CA), and diaminobenzidine (DAB) as the chromogen. After DAB detection, some sections were processed by an additional antibody labeling cycle using the same method and antibody as above. This staining strategy enhanced the signal-to-background ratio while the background labeling was kept to minimal. Immunoreacted sections were postfixed in buffered 2% OsO₄, rinsed and stained in 1% uranyl acetate, and then dehydrated and embedded in Epon. Ultrathin sections were contrasted with uranyl acetate and analyzed under a Zeiss EM-10 electron microscope operated at 60–80 kV. Electron microscopic negatives were scanned and processed by Adobe Photoshop CS2 (Adobe Systems).

Quantitative immunohistochemistry

GFAP/Iba1 densitometry. Immunohistochemical staining was performed using the same antibody solution for all free-floating sections and processed as described above. Randomly selected four sections (from L4 and L5 spinal cord segments) were analyzed from each animal. Using identical camera settings, images were obtained from lamina IX on both sides of each section. Using the pixel histogram generated for each original image by Image-Pro Plus (v.6.2.0.424; Media Cybernetics Inc., Bethesda, MD), the product of the pixel number and pixel intensity value (0–255) was computed and summed for the entire image. This provides a composite measure of changes in both immunoreactive area and intensity.

Neuronal bouton analyses. Bouton analyses were performed as previously described, [51–54]. The investigator was blinded during analyses. Using immunofluorescence-stained sections and identical microscope settings, 3 images (75 µm×75 µm) were captured from lamina IX (adjacent to a CHAT+ α-motoneuron surrounded by hSYN staining) of each section using a Leica SP2 confocal microscope; at least 3 sections (300 µm separation) were used from each of 5 animals. Image-Pro Plus (v.6.2.0.424; Media Cybernetics Inc., Bethesda, MD) was used to count the total number of human synaptophysin-immunoreactive objects using the same limits for pixel intensity and structure size. The image was then overlaid onto another image from the identical field but stained for other neuronal phenotype markers (VGluT1/2/3, GAD65, GlyT2). The total number of double-positive structures was then identified by Image-Pro Plus. The number of hSYN+ punctata identified on each α-motoneuron ranged between 30–80 per α-motoneuron.

α-motoneuron quantification. Alpha-motoneuron quantification was performed as previously described [55] except using fluorescent-stained (ChAT) tissue sections. The investigator was blinded during all analyses. Five sections taken from C5–C6 or L4–L5 segments, each separated by minimum of 300 µm, were selected from each animal (n = 18 for the cell-grafted group and n = 16 for the media-injected group; i.e., a total of 90 and 80 sections, respectively) and were identically immunostained for ChAT. Sections from grafted animals had graft presence confirmed by additional hNUMA staining. A single 20× image was then captured (focused in the center of the section thickness) from each lamina IX and analyzed with Image-Pro Plus (v.6.2.0.424; Media Cybernetics Inc., Bethesda, MD) to determine CHAT+ α-motoneurons with surface area >700 µm and a staining intensity that was at least 2-fold over background (same threshold used for all α-motoneuron analyses) [56]. Cells identified by Image-Pro Plus were then examined and those with distinct nucleoli, as defined by clearly detectable lack of CHAT immunoreactivity in the nucleoli, were counted (see Fig. S 4C for details).

Graft phenotype characterization (NeuN, GFAP, APC, DCX). To determine the phenotype of the grafted human cells, tissue sections from the L4–L5 engrafted region were double-stained with hNUMA and either NeuN, GFAP, APC, or DCX, as described above. Using identical microscope settings, a z-stack of optical images (0.5-µm-thick; 20× objective) were captured from identified hNUMA+ grafts using a Leica SP2 confocal microscope; at least 3 sections (300 µm separation) were used from each of the 5 animals. Image-Pro Plus (v.6.2.0.424; Media Cybernetics Inc., Bethesda, MD) was then used to identify positive cells in one overlaid optical image (0.5-µm-thick) using identical thresholds for all images. All images were examined by a blinded observer.

Axonal Quantification

The total number of remaining axons was determined in the lateral and ventral funiculi using semi-automated image analysis of osmium-treated 1- μm plastic sections taken from the lumbar spinal cord of normal ($n = 2$) and SOD1^{G93A} ($n = 2$) endstage animals with no previous manipulations (i.e., no spinal media or cell injections).

High resolution mosaic images were obtained using Zeiss Observer software with Multidimensional Acquisition MosiaX (Z1 microscope system with 20 \times objective fitted with a Zeiss MRm camera, AxioVision v4.7). Using the same pixel threshold to identify axons in all images, Image-Pro Plus (v.6.2.0.424; Media Cybernetics Inc., Bethesda, MD) was used to objectively count axons. Further measurement parameters such as area/box and size (length) were applied to discriminate and exclude non-axonal objects. Employment of the size (length) parameter allowed for further axonal analysis in which axons were divided into empirically derived caliber sizes of small, medium, and large axons (0.5–2.0 μm , 2.01–5.0 μm , and 5.01–14.0 μm respectively).

Statistical analysis

Two-way comparisons were performed by student t-test. Multiple comparisons were performed using one-way analysis of variance (ANOVA) followed by Student-Newman-Keuls test. All results are shown as mean \pm standard error of mean (SEM) unless indicated. $P < 0.05$ was considered to be statistically significant.

Supporting Information

Figure S1 Grafted human spinal neural stem cells show expression of several neuronal markers. Histological sections taken from regions containing human spinal neural stem cell transplants were immunostained with neuronal cells markers TUJ1, DCX and GAP43. Human cells were identified by the presence of human-specific nuclear matrix antigen (hNUMA), (A, D). Cell grafts were typically concentrated in the deeper lamina (VII IX) and frequently extended into the adjacent white matter. Regions stained for hNUMA were also strongly stained for betatubulin III (TUJ1; B), doublecortin (DCX; E), and growth-associated protein 43 (GAP43; F). Scale bar (G) is 300 μm for all panels. (TIF)

Figure S2 Grafted, terminally differentiated human neural spinal stem cells-derived neurons develop putative synaptic contact with persisting α -motoneurons in SOD1^{G93A} rats. Human synaptophysin (hSYN) was detected throughout the cell grafts, often found in axonal-like structures with typical varicosities (B insert) and in the vicinity of persisting α -motoneurons (ChAT; choline acetyltransferase) in lamina IX and extending into the adjacent white matter (A D). Single optical layer confocal images of surviving α -motoneurons show hSYN-IR bouton-like structures adjacent to the outer membrane of the soma (E, F), occasionally expressing the GABAergic cell marker

References

- Mulder DW, Kurland LT, Offord KP, Beard CM (1986) Familial adult motor neuron disease: amyotrophic lateral sclerosis. *Neurology* 36: 511–517.
- Cudkovic ME, McKenna-Yasek D, Sapp PE, Chin W, Geller B, et al. (1997) Epidemiology of mutations in superoxide dismutase in amyotrophic lateral sclerosis. *Ann Neurol* 41: 210–221.
- Rothstein JD, Martin LJ, Kuncl RW (1992) Decreased glutamate transport by the brain and spinal cord in amyotrophic lateral sclerosis. *N Engl J Med* 326: 1464–1468.
- Bruijn LI, Becher MW, Lee MK, Anderson KL, Jenkins NA, et al. (1997) ALS-linked SOD1 mutant G85R mediates damage to astrocytes and promotes

glutamate decarboxylase (GAD65), (G, H). Human glutamatergic boutons were located by identifying specific glutamate vesicular transporters 1/2/3 (VGluT) and similarly showed only rare boutons also reactive for hSYN (I L). Glycinergic boutons were identified by the neuronal-specific glycine transporter 2 (GlyT2), (M P). Arrows show examples of double-immunoreactive structures. Scale bar: 300 μm (A D), 25 μm (E P). (TIF)

Figure S3 Spinal grafts of human spinal neural stem cells reduced astrogliosis and microglial activation in SOD1^{G93A} rats. Quantitative densitometry was performed on lumbar (L4 and L5) spinal cord sections immunostained for astrocytes (GFAP) and microglia (Iba1). Lamina IX images were captured from non-transgenic (A C), untreated SOD1^{G93A} (D F), media-treated SOD1^{G93A} (G I), and cell-grafted SOD1^{G93A} (J L) animals. All three SOD1^{G93A} groups show signs of strong astrogliosis and microglia infiltration/activation, with a marked increase in the number of GFAP-IR hypertrophic astrocytes and dense Iba1-immunoreactivity (IR). Based on densitometric analyses, lamina IX GFAP-IR and Iba1-IR in SOD1^{G93A} and media-treated groups were significantly increased over the non-transgenic group (M). Reduced GFAP-IR and Iba1-IR was measured in the cell-grafted group (M). Scale bar: 80 μm . (* significantly increased over non-transgenic; $P < 0.05$; one-way ANOVA); ** significantly increased over non-transgenic but decreased from media-treated; $P < 0.05$; one-way ANOVA). (TIF)

Figure S4 Migration of grafted human fetal spinal neural stem cells in lumbar spinal cord in SOD1^{G93A} rats at 78 days after grafting or in immunodeficient rats at 9 months after grafting. By comparing the spread of hNUMA+ cells in SOD1^{G93A} rats at 78 days after grafting (A) with that seen in immunodeficient rats at 9 months (B), wide spread of grafted cells in both the gray matter and white matter was seen at 9 months (A, B; compare red asterisks in the dorsal and lateral funiculi). To quantify α -motoneurons, CHAT immunofluorescence-stained sections were used. Cells to be counted were identified by surface area ($> 700 \mu\text{m}^2$) and by the presence of nucleoli as evidenced by an easily identifiable lack of CHAT staining in the center of nucleus (C; red arrows). (TIF)

Acknowledgments

This work was supported by the California Institute for Regenerative Medicine (RC1-00131-1-M.M.) and by Taubman Foundation (M.M., E.F., M.H.).

Author Contributions

Conceived and designed the experiments: MM MH EF DWC. Performed the experiments: MH OK SM CS GS JG RN MHP. Analyzed the data: MH MM JG RN. Contributed reagents/materials/analysis tools: KJ GS. Wrote the paper: MM MH.

- rapidly progressive disease with SOD1-containing inclusions. *Neuron* 18: 327–338.
- Howland DS, Liu J, She Y, Goad B, Maragakis NJ, et al. (2002) Focal loss of the glutamate transporter EAAT2 in a transgenic rat model of SOD1 mutant-mediated amyotrophic lateral sclerosis (ALS). *Proc Natl Acad Sci U S A* 99: 1604–1609.
 - Clement AM, Nguyen MD, Roberts EA, Garcia ML, Boillee S, et al. (2003) Wild-type nonneuronal cells extend survival of SOD1 mutant motor neurons in ALS mice. *Science* 302: 113–117.

7. Yamanaka K, Boillee S, Roberts EA, Garcia ML, McAlonis-Downes M, et al. (2008) Mutant SOD1 in cell types other than motor neurons and oligodendrocytes accelerates onset of disease in ALS mice. *Proc Natl Acad Sci U S A* 105: 7594–7599.
8. Nagai M, Re DB, Nagata T, Chialazonitis A, Jessell TM, et al. (2007) Astrocytes expressing ALS-linked mutated SOD1 release factors selectively toxic to motor neurons. *Nat Neurosci* 10: 615–622.
9. Marchetto MC, Muotri AR, Mu Y, Smith AM, Cezar GG, et al. (2008) Non-cell-autonomous effect of human SOD1 G37R astrocytes on motor neurons derived from human embryonic stem cells. *Cell Stem Cell* 3: 649–657.
10. Di Giorgio FP, Carrasco MA, Siao MC, Maniatis T, Eggan K (2007) Non-cell autonomous effect of glia on motor neurons in an embryonic stem cell-based ALS model. *Nat Neurosci* 10: 608–614.
11. Di Giorgio FP, Boulting GL, Bobrowicz S, Eggan KC (2008) Human embryonic stem cell-derived motor neurons are sensitive to the toxic effect of glial cells carrying an ALS-causing mutation. *Cell Stem Cell* 3: 637–648.
12. Lepore AC, Rauck B, Dejea C, Pardo AC, Rao MS, et al. (2008) Focal transplantation-based astrocyte replacement is neuroprotective in a model of motor neuron disease. *Nat Neurosci* 11: 1294–1301.
13. Boillee S, Yamanaka K, Lobsiger CS, Copeland NG, Jenkins NA, et al. (2006) Onset and progression in inherited ALS determined by motor neurons and microglia. *Science* 312: 1389–1392.
14. Ralph GS, Radcliffe PA, Day DM, Carthy JM, Leroux MA, et al. (2005) Silencing mutant SOD1 using RNAi protects against neurodegeneration and extends survival in an ALS model. *Nat Med* 11: 429–433.
15. Miller TM, Kaspar BK, Kops GJ, Yamanaka K, Christian LJ, et al. (2005) Virus-delivered small RNA silencing sustains strength in amyotrophic lateral sclerosis. *Ann Neurol* 57: 773–776.
16. Xu L, Yan J, Chen D, Welsh AM, Hazel T, et al. (2006) Human neural stem cell grafts ameliorate motor neuron disease in SOD-1 transgenic rats. *Transplantation* 82: 865–875.
17. Xu L, Ryugo DK, Pongstaporn T, Johe K, Koliatsos VE (2009) Human neural stem cell grafts in the spinal cord of SOD1 transgenic rats: differentiation and structural integration into the segmental motor circuitry. *J Comp Neurol* 514: 297–309.
18. Lee MK, Tuttle JB, Rebhun LI, Cleveland DW, Frankfurter A (1990) The expression and posttranslational modification of a neuron-specific beta-tubulin isotype during chick embryogenesis. *Cell Motil Cytoskeleton* 17: 118–132.
19. Fehlings MG, Tator CH, Linden RD, Piper IR (1987) Motor evoked potentials recorded from normal and spinal cord-injured rats. *Neurosurgery* 20: 125–130.
20. Fehlings MG, Tator CH, Linden RD, Piper IR (1988) Motor and somatosensory evoked potentials recorded from the rat. *Electroencephalogr Clin Neurophysiol* 69: 65–78.
21. Zappulla RA, Hollis P, Ryder J, Moore FM, Adamson J, et al. (1988) Noncortical origins of the spinal motor evoked potential in rats. *Neurosurgery* 22: 846–852.
22. Braak H, Braak E, Ohm T, Bohl J (1988) Silver impregnation of Alzheimer's neurofibrillary changes counterstained for basophilic material and lipofuscin pigment. *Stain Technol* 63: 197–200.
23. de Olmos JS, Beltramino CA, de Olmos de Lorenzo S (1994) Use of an aminocupric-silver technique for the detection of early and semiacute neuronal degeneration caused by neurotoxins, hypoxia, and physical trauma. *Neurotoxicol Teratol* 16: 545–561.
24. Hall ED, Sullivan PG, Gibson TR, Pavel KM, Thompson BM, et al. (2005) Spatial and temporal characteristics of neurodegeneration after controlled cortical impact in mice: more than a focal brain injury. *J Neurotrauma* 22: 252–265.
25. Switzer RC, 3rd (2000) Application of silver degeneration stains for neurotoxicity testing. *Toxicol Pathol* 28: 70–83.
26. Suzuki M, McHugh J, Tork C, Shelley B, Klein SM, et al. (2007) GDNF secreting human neural progenitor cells protect dying motor neurons, but not their projection to muscle, in a rat model of familial ALS. *PLoS One* 2: e689.
27. Gurney ME, Pu H, Chiu AY, Dal Canto MC, Polchow CY, et al. (1994) Motor neuron degeneration in mice that express a human Cu,Zn superoxide dismutase mutation. *Science* 264: 1772–1775.
28. Ozdinler PH, Bann S, Yamamoto TH, Guzel M, Brown RH, Jr., et al. (2011) Corticospinal motor neurons and related subcortical projection neurons undergo early and specific neurodegeneration in hSOD1G(9)(3)A transgenic ALS mice. *J Neurosci* 31: 4166–4177.
29. Cosottini M, Giannelli M, Siciliano G, Lazzarotti G, Michelassi MC, et al. (2005) Diffusion-tensor MR imaging of corticospinal tract in amyotrophic lateral sclerosis and progressive muscular atrophy. *Radiology* 237: 258–264.
30. da Rocha AJ, Oliveira AS, Fonseca RB, Maia AC, Jr., Buainain RP, et al. (2004) Detection of corticospinal tract compromise in amyotrophic lateral sclerosis with brain MR imaging: relevance of the T1-weighted spin-echo magnetization transfer contrast sequence. *AJNR Am J Neuroradiol* 25: 1509–1515.
31. Davidson CD (1941) Amyotrophic lateral sclerosis: origin and extent of the upper motor neuron lesion. *Arch Neurol* 46: 1039–1056.
32. Brownell B, Oppenheimer DR, Hughes JT (1970) The central nervous system in motor neurone disease. *J Neurol Neurosurg Psychiatry* 33: 338–357.
33. Castro AJ (1972) Motor performance in rats. The effects of pyramidal tract section. *Brain Res* 44: 313–323.
34. Xu L, Shen P, Hazel T, Johe K, Koliatsos VE (2011) Dual transplantation of human neural stem cells into cervical and lumbar cord ameliorates motor neuron disease in SOD1 transgenic rats. *Neurosci Lett* 494: 222–226.
35. Scott S, Kranz JE, Cole J, Lincecum JM, Thompson K, et al. (2008) Design, power, and interpretation of studies in the standard murine model of ALS. *Amyotroph Lateral Scler* 9: 4–15.
36. Dal Canto MC, Gurney ME (1997) A low expressor line of transgenic mice carrying a mutant human Cu,Zn superoxide dismutase (SOD1) gene develops pathological changes that most closely resemble those in human amyotrophic lateral sclerosis. *Acta Neuropathol* 93: 537–550.
37. Dal Canto MC, Gurney ME (1995) Neuropathological changes in two lines of mice carrying a transgene for mutant human Cu,Zn SOD, and in mice overexpressing wild type human SOD: a model of familial amyotrophic lateral sclerosis (FALS). *Brain Res* 676: 25–40.
38. Smith RA, Miller TM, Yamanaka K, Monia BP, Condon TP, et al. (2006) Antisense oligonucleotide therapy for neurodegenerative disease. *J Clin Invest* 116: 2290–2296.
39. Yamanaka K, Chun SJ, Boillee S, Fujimori-Tonou N, Yamashita H, et al. (2008) Astrocytes as determinants of disease progression in inherited amyotrophic lateral sclerosis. *Nat Neurosci* 11: 251–253.
40. Horner PJ, Power AE, Kempermann G, Kuhn HG, Palmer TD, et al. (2000) Proliferation and differentiation of progenitor cells throughout the intact adult rat spinal cord. *J Neurosci* 20: 2218–2228.
41. Zai LJ, Wrathall JR (2005) Cell proliferation and replacement following contusive spinal cord injury. *Glia* 50: 247–257.
42. Takasawa K, Kitagawa K, Yagita Y, Sasaki T, Tanaka S, et al. (2002) Increased proliferation of neural progenitor cells but reduced survival of newborn cells in the contralateral hippocampus after focal cerebral ischemia in rats. *J Cereb Blood Flow Metab* 22: 299–307.
43. Kang SH, Fukaya M, Yang JK, Rothstein JD, Bergles DE (2010) NG2+ CNS glial progenitors remain committed to the oligodendrocyte lineage in postnatal life and following neurodegeneration. *Neuron* 68: 668–681.
44. Magnus T, Carmen J, Deleon J, Xue H, Pardo AC, et al. (2008) Adult glial precursor proliferation in mutant SOD1G93A mice. *Glia* 56: 200–208.
45. Mothe AJ, Tator CH (2005) Proliferation, migration, and differentiation of endogenous ependymal region stem/progenitor cells following minimal spinal cord injury in the adult rat. *Neuroscience* 131: 177–187.
46. Johe KK, Hazel TG, Muller T, Duglich-Djordjevic MM, McKay RD (1996) Single factors direct the differentiation of stem cells from the fetal and adult central nervous system. *Genes Dev* 10: 3129–3140.
47. Kakinohana O, Cizkova D, Tomori Z, Hedlund E, Marsala S, et al. (2004) Region-specific cell grafting into cervical and lumbar spinal cord in rat: a qualitative and quantitative stereological study. *Exp Neurol* 190: 122–132.
48. Basso DM, Beattie MS, Bresnahan JC, Anderson DK, Faden AL, et al. (1996) MASCIS evaluation of open field locomotor scores: effects of experience and teamwork on reliability. Multicenter Animal Spinal Cord Injury Study. *J Neurotrauma* 13: 343–359.
49. Schwarz M, Block F, Pergande G (1994) N-methyl-D-aspartate (NMDA)-mediated muscle relaxant action of flupirtine in rats. *Neuroreport* 5: 1981–1984.
50. Kakinohana O, Hefferan MP, Nakamura S, Kakinohana M, Galik J, et al. (2006) Development of GABA-sensitive spasticity and rigidity in rats after transient spinal cord ischemia: a qualitative and quantitative electrophysiological and histopathological study. *Neuroscience* 141: 1569–1583.
51. Mackie M, Hughes DI, Maxwell DJ, Tillakaratne NJ, Todd AJ (2003) Distribution and colocalisation of glutamate decarboxylase isoforms in the rat spinal cord. *Neuroscience* 119: 461–472.
52. Todd AJ, Hughes DI, Polgar E, Nagy GG, Mackie M, et al. (2003) The expression of vesicular glutamate transporters VGLUT1 and VGLUT2 in neurochemically defined axonal populations in the rat spinal cord with emphasis on the dorsal horn. *Eur J Neurosci* 17: 13–27.
53. Hughes DI, Mackie M, Nagy GG, Riddell JS, Maxwell DJ, et al. (2005) P-boutons in lamina IX of the rodent spinal cord express high levels of glutamic acid decarboxylase-65 and originate from cells in deep medial dorsal horn. *PNAS* 102: 9038–9043.
54. Kakinohana O, Hefferan MP, Miyanohara A, Nejime T, Marsala S, et al. (2012) Combinational Spinal GAD65 Gene Delivery and Systemic GABA-Mimetic Treatment for Modulation of Spasticity. *PLoS One* 7: e30561.
55. Suzuki M, McHugh J, Tork C, Shelley B, Klein SM, et al. (2007) GDNF secreting human neural progenitor cells protect dying motor neurons, but not their projection to muscle, in a rat model of familial ALS. *PLoS One* 2: e689.
56. Suzuki M, McHugh J, Tork C, Shelley B, Hayes A, et al. (2008) Direct muscle delivery of GDNF with human mesenchymal stem cells improves motor neuron survival and function in a rat model of familial ALS. *Mol Ther* 16: 2002–2010.

5.4. Evaluation of neural stem cell replacement therapy in a rat model of acute lumbar spinal cord injury

in publication

Amelioration of motor/sensory dysfunction and spasticity in a rat model of acute lumbar spinal cord injury by human neural stem cell transplantation

van Gorp S, Leerink M, Kakinohana O, Platoshyn O, Santucci C, Galik J, Joosten Ea, **Hruska-Plochan M**, Goldberg D, Marsala S, Johe K, Marsala M.

Manuscript was accepted for publication in journal "Stem cell research & Therapy"

IF (2012): 3.212; 5-year IF (2012): 3.212

Declaration of co-authors

"I hereby declare that Marián Hruška-Plochán was adequately involved (30%) in the study design, experiments, interpretation of results and writing of this manuscript."

San Diego, April 29 2013



Martin Maršala, Prof. MD.

Amelioration of motor/sensory dysfunction and spasticity in a rat model of acute lumbar spinal cord injury by human neural stem cell transplantation.

SEBASTIAAN van GORP^{1,2} (sfjvangorp@outlook.com)

MARJOLEIN LEERINK¹ (mleerink@med-ic.nl)

OSAMU KAKINOHANA¹ (oskakinohana@ucsd.edu)

OLEXANDR PLATOSHYN¹ (oplatoshyn@ucsd.edu)

CAMILA SANTUCCI¹ (csantucci@ucsd.edu)

JAN GALIK^{3,4} (galik@saske.sk)

ELBERT A. JOOSTEN² (b.joosten@maastrichtuniversity.nl)

MARIAN HRUSKA-PLOCHAN^{1,6,7} (mhruskaplochan@ucsd.edu)

DANIELLE GOLDBERG¹ (dsgoldbe@ucsd.edu)

SILVIA MARSALA¹ (smarsala@ucsd.edu)

KARL JOHE⁵ (kjohe@neuralstem.com)

MARTIN MARSALA^{1,3} (mmarsala@ucsd.edu)

- 1- Department of Anesthesiology, University of California, San Diego, La Jolla, CA, USA;
- 2- Department of Anesthesiology, School for Mental Health and Neuroscience, Maastricht University Medical Center, The Netherlands;
- 3- Institute of Neurobiology, Slovak Academy of Sciences, Kosice, Slovakia;
- 4- Institute of Biology and Ecology, Faculty of Science, Pavol Jozef Safarik University, Košice, Slovakia;
- 5- Neuralstem, Inc., Rockville, MD, USA;
- 6 - Institute of Animal Physiology and Genetics, Czech Academy of Sciences, Rumburska 89, 277 21 Libechov, Czech Republic;
- 7 - Department of Cell Biology, Faculty of Science, Charles University in Prague, Prague, Czech Republic

Correspondence:

Martin Marsala, M.D.
Neuroregeneration Laboratory
Department of Anesthesiology
University of California - San Diego
Sanford Consortium for Regenerative Medicine
2880 Torrey Pines Scenic Drive

La Jolla, CA 92037, USA
Office: 858-822-3805
Lab: 858-534-7380
FAX: 858-822-3249

Abstract

Introduction: Intraspinal grafting of human neural stem cells represents a promising approach to promote recovery of function after spinal trauma. Such a treatment may serve to: i) provide trophic support to improve survival of host neurons, ii) improve structural integrity of spinal parenchyma by reducing syringomyelia and scarring in trauma-injured regions, and iii) provide neuronal populations to potentially form relays with host axons, segmental interneurons, and/or α -motoneurons. Here we characterized the effect of intraspinal grafting of clinical grade human fetal spinal cord-derived neural stem cells (**HSSC**) on recovery of neurological function in a rat model of acute lumbar (L3) compression injury.

Methods: Three-month-old female Sprague-Dawley rats received L3 spinal compression injury. Three days post-injury, animals were randomized and received intraspinal injections of either **HSSC**, media-only, or no injections. All animals were immunosuppressed with tacrolimus, mycophenolate mofetil, and methylprednisolone acetate from the day of cell grafting and survived for 8 weeks. Motor and sensory dysfunction was periodically assessed using open field locomotion scoring, thermal/tactile pain/escape thresholds and myogenic motor evoked potentials. The presence of spasticity was measured by gastrocnemius muscle EMG response during computer-controlled ankle rotation. At end-point, gait (CatWalk), ladder climbing, and single frame analyses were also assessed. Syringe size, spinal cord dimensions, and extent of scarring were measured by MRI. Differentiation and integration of grafted cells in the host tissue were validated with immunofluorescence staining using human-specific antibodies.

Results: Intraspinal grafting of **HSSC** led to a progressive and significant improvement in lower extremity paw placement, amelioration of spasticity, and normalization in thermal and tactile pain/escape thresholds at 8 weeks post-grafting. **No significant differences were detected**

in other CatWalk parameters, motor evoked potentials, open field locomotor (BBB) score or ladder climbing test. MRI volume reconstruction and immunofluorescence analysis of grafted cell survival showed near complete injury-cavity-filling by grafted cells and development of putative GABA-ergic synapses between grafted and host neurons.

Conclusions: Peri-acute intraspinal grafting of HSSC can represent an effective therapy which ameliorates motor and sensory deficits after traumatic spinal cord injury.

Keywords: spinal cord injury, human neural stem cells, spinal grafting, functional recovery, rat

Introduction

Extensive experimental and clinical data show that the mechanisms leading to a clinically-defined loss of neurological function after spinal trauma can in general be considered in two categories. First is the pathology and corresponding functional loss resulting from a direct mechanical injury of axons at the injury epicenter, and second is a progressive appearance of secondary changes (local edema, hematoma, excitotoxicity and ischemia) which can evolve over hours to weeks after the initial impact (for review see Hagg & Oudega [1]). Consistent with our current knowledge of the mechanism which leads to the development of secondary post-injury cascade, the current experimental and clinical treatment strategies primarily focus on: i) improvement of local metabolism and blood flow (e.g., through decompression therapy and hypothermia) [2, 3], and ii) modulation of local inflammatory response (e.g., with methylprednisolone) [4-7]. A separate group of experimental treatment modalities are aimed at improving the local neurotrophic activity at and around the injury epicenter with the primary goal of increasing the survival of partially injured axons and/or neurons. In this category of experimentation, besides the use of locally delivered trophic factors (such as BDNF-, GDNF-, and FGF-peptides or growth factors-gene-encoding vectors) [8], regionally grafted fetal or embryonic stem cell-derived neuronal precursors are frequently used [9-18].

Recently, well-defined protocols were developed which permit the isolation and long-term stable expansion of (non-immortalized) human fetal brain or spinal cord tissue-derived neural stem cells [19-24]. Using these protocols, continuing neurogenic potential, as evidenced by neuronal differentiation and the ability of differentiated neurons to generate action potentials *in vitro*, was documented at even high (>20) passage numbers [24, 25]. Some of these lines were successfully used for: i) generation of GMP-grade clonally-derived cell lines, ii) extensive pre-clinical evaluation using a variety of neurodegenerative small and large animal models, and iii)

subsequently used successfully in Phase I human clinical trials [26-28].

In our previous studies, we have extensively characterized the *in vivo* treatment effect after spinal grafting of cGMP-grade human fetal spinal cord-derived stem cells (NSI-566RSCs line) using a spinal ischemia model in rats and transgenic rat model of ALS (SOD1^{G93A}). In those studies, we have shown that: i) grafting of NSI-566RSCs into lumbar spinal cord of adult Sprague-Dawley (SD) rats with previous spinal ischemic injury is associated with a progressive improvement of ambulatory function which correlates with long-term grafted cell survival and extensive neuronal differentiation [29], and ii) bilateral lumbar grafting of NSI-566RSCs in pre-symptomatic SOD1^{G93A} rats provides a transient functional benefit and suppression of α -motoneuron degeneration, i.e., a protective effect which was absent in media-injected animals [30]. Using the same cell line, we have also demonstrated the optimal dosing regimen and safety after grafting into the lumbar spinal cord of immunosuppressed minipigs [29]. The dosing design defined in this pre-clinical minipig study was then subsequently used in a recently completed Phase I human clinical trial in ALS patients receiving lumbar and cervical grafts of NSI-566RSCs [27, 31]. In a more recent study using an immunodeficient rat model of complete spinal cord Th3 transection, it was shown that NSI-566RSCs or rat embryonic neural precursor cells, embedded in a fibrin matrix with trophic factors and grafted one week after injury, were able to form functional relays. The formation of functional relays was validated behaviorally (BBB locomotor score), electrophysiologically (spinal cord evoked potentials), and histologically (host on graft and graft on host synapses) [32].

The goal of our present study was to characterize the effect of NSI-566RSCs grafted spinally in a clinically relevant L3 spinal compression model in continuously immunosuppressed adult SD rats. The presence of treatment effect was assessed by analysis of i) motor and sensory function, ii) myogenic motor evoked potentials (MEPs), iii) spasticity response during computer-

controlled ankle rotation, and iv) qualitative analysis of grafted cell survival and maturation.

Material and Methods

Animals and surgeries

All animal studies were approved by the University of California, San Diego Institutional Animal Care and Use Committee. The study design is outlined in Fig. 1. Twelve-week-old Female Sprague-Dawley rats were used. **The rationale for choosing female rats was based on our previous experience which demonstrates better tolerability of female rats to spinal trauma-related side effects such as urinary retention.** Animals were anesthetized with isoflurane (5% induction, 1.5-2% maintenance; in room air) and placed into a Lab Standard Stereotaxic frame (Stoelting, Cat# 51600, Wood Dale, IL, USA). The animal was elevated 2 cm by placing it on a homeothermic heating blanket (set at 37°C with feedback from the rectal thermometer, Harvard Apparatus, Cat# 507214, Holliston, MA, USA) which sits on a plastic rectangular block. The animal was then placed in Spine Adaptors (Stoelting, Cat# 51695, Wood Dale, IL, USA) and a wide Th13 laminectomy was performed using an air-powered dental drill and binocular microscope (exposing the dorsal surface of spinal segment L3). An acrylic rod (Ø 2.9 mm, length 15 cm; 35 g) was then slowly lowered on the exposed L3 segment until it slightly touched the spinal cord but without inducing any compression. The laminectomy site was then filled with mineral oil in which the tip of a small thermocouple (Physitemp, Cat# IT-14, Clifton, NJ, USA) was submerged and touched the dura. The light from the two fiber optic light pipes of the surgical light (Fiber-Lite, Cat# MI-150 & BGG1823M, Dolan-Jenner, Boxborough, MA, USA) were focused on the surgical site (and directly illuminating the temperature probe). Next, the light intensity was manually regulated so that the spinal cord/mineral oil was warmed to 37°C and remained at $37 \pm 0.3^\circ\text{C}$. If necessary, a 100W infrared lamp was used to gradually adjust and maintain the animal's core temperature at 37°C (rectal). When both temperatures (i.e., paraspinal

and rectal) were at $37 \pm 0.3^{\circ}\text{C}$ for at least 5 min, the rod was slowly lowered until its weight fully rested, perpendicularly, onto the spinal cord. The rod was kept in place for 15 min, while both temperatures were maintained at $37 \pm 0.3^{\circ}\text{C}$. After spinal compression, the rod and mineral oil was removed and the wound sutured in anatomical layers.

Post-surgical care

Buprenorphine (0.05 mg/kg, s.c., Reckitt Benckiser, Richmond, VA, USA), 5 mL of lactated ringer's, 10 mg/kg of Cefazolin (Novaplus/Sandoz, Holzkirchen, Germany), and standard triple antibiotic ointment to cover the incision site (Bacitracin, Neomycin, Polymyxin B) was given after every surgery. Bladders were manually emptied twice daily (if full). Sulfamethoxazole and Trimethoprim USP oral suspension (200 mg & 40 mg per 250 mL drinking water, Hi-Tech Pharmacal, Amityville, NY, USA) was given for at least 10-14 days after SCI or until autonomic bladder voiding occurred and for 1-2 days after any other surgery (sham or grafting). Food was provided by placing it at the bottom of cage and water bottles with an elongated drinking tube were used, until regular overhead supplies could be reached by the animal. Animals diagnosed with bacterial infections throughout the study were treated with Sulfamethoxazole (as above), 10 mg/kg/day of Cefazolin, and lactated ringer's 5 mL/0.5 day.

Cell derivation and preparation

The cells, named "NSI-566RSC", were produced by Neuralstem Inc. (Rockville, MD, USA), as described before [33]. Briefly, human spinal cord neural precursors (HSSC) were prepared from the cervical-upper thoracic region obtained from a single eight week fetus. Meninges and dorsal root ganglia were removed and dissociated into a single cell suspension by mechanical trituration in serum-free, modified N2 media (human plasma apo-transferrin, recombinant human insulin, glucose, progesterone, putrescine, and sodium selenite in DMEM/F12). For growth of

the HSSC, 10 ng/ml basic fibroblast growth factor (bFGF) was added to the modified N2 media and expanded serially as a monolayer culture on poly-D-lysine and fibronectin [34]. Approximately 6.1×10^6 total cells were obtained upon the initial dissociation of the spinal cord tissue. The growth medium was changed every other day. The first passage was conducted 16 days after plating. At this point, the culture was composed mostly of post-mitotic neurons and mitotic HSSC. Mainly the mitotic cells were harvested through brief treatment with trypsin and subsequent use of soybean trypsin inhibitor. The cells were harvested at approximately 75% confluence, which occurred every 5-6 days (20 passages). At various passages, the cells were frozen in the growth medium plus 10% dimethyl sulfoxide at $5-10 \times 10^6-10$ cells/ml. The frozen cells were stored in liquid nitrogen. Upon thawing, the overall viability and recovery was typically 80-95%. A cell bank of passage 16 cells was prepared and used for this study.

For the production of GFP-labeled NSI-566RSC, a Lentiviral vector was constructed containing the human Ubiquitin C promoter driving expression of enhanced green fluorescent protein. Viral particles produced by infected 293FT cells were collected after overnight incubation, then concentrated by centrifugation and stored frozen. Neural stem cell cultures were infected by overnight incubation in growth medium supplemented with viral supernatant. Infected stem cells were washed with PBS and cultured as described above. After multiple passages, >90% of cells were EGFP positive (assessed after immunohistochemical staining). A cell bank of passage 17 cells was prepared and used for this study.

One day prior to each grafting day, one cryopreserved vial of the previously prepared cells was thawed, washed, concentrated in hibernation buffer, and shipped from the cell preparation site (Neuralstem, Inc., Rockville, MD, USA) to the surgery site (University of California, San Diego, CA, USA) at 2-8°C by overnight delivery. Upon receipt the following day, the cells were used directly for implantation without further manipulation. Before and after implantation, the

viability of cells was measured with trypan blue (0.4%; Sigma). Typically, a >85% viability rate was recorded.

Inclusion and exclusion criteria, randomization and blinding

Three days following SCI and prior to grafting, animals were randomly divided into three groups: the vehicle-injected group, non-injected group, or the HSSC-injected group. SCI animals with an open-field locomotion score of ≤ 1 and appearing healthy enough were included. Animals found moribund or automutilating at any point during the study were excluded and euthanized. A total of 42 animals were employed and divided into 6 experimental groups, as follows:

Group A (n=14): SCI animals-NSI-566RSC-grafted,

Group B (n=10): SCI animals-vehicle-injected,

Group C (n=8): SCI animals-non-injected,

Group D (n=6): sham operated (laminectomy only),

Group E (n=6): naïve animals (no surgical manipulation)

Group F (n=2): SCI athymic animals-ubiquitin.eGFP⁺ NSI-566RSCs-grafted.

One animal was excluded in Group A because of automutilation of the hind paw; two animals were excluded in Group C, one because of automutilation of the hind paw and 1 because of bacterial infection. Six animals had been replaced before dosing/randomization, 5 due to inadequate injuries and 1 because of bacterial infection.

Grafting procedure

For the intraparenchymal injections, the animals were placed in the stereotactic frame as described above. The L3 spinal cord (i.e., the dura mater) was then re-exposed at the previous laminectomy site. Injections were performed using a 33 gauge beveled needle and 100 μ L

Nanofil syringe (World Precision Instruments, Cat# NF33BV & Nanofil-100, Sarasota, FL, USA) connected to a microinjection unit (Kopf Instruments, Cat# 5000 & 5001, Tujunga, CA, USA). The duration of each injection was ≥ 45 sec followed by a ≥ 30 sec pause before slow needle withdrawal. The center of the injection was targeted intermediate of the ventral and dorsal horn and close to the lateral funiculus (distance from the dorsal surface of the spinal cord at L3 level: 0.80 mm). Twelve injections (20,000 cells/ μ L) were done; four injections (0.5 μ L each, 0.8-1.0 mm apart, rostrocaudally) at each lateral boundary of the injury (8 in total), plus two (bilateral) injections (0.5 μ L each) 1.5 mm caudal from the previous, most caudal injections, and two injections at the core of the epicenter (1 μ L at each side of the dorsal vein, bilaterally; see diagram in **Fig. 1**). After the injections, the incision was cleaned with penicillin-streptomycin solution and sutured in two layers.

Immunosuppression

Two days after injury (i.e., 1 day before grafting), a methylprednisolone acetate (Depo-Medrol, 10 mg/kg, i.m.) was given, which was repeated thereafter 3 times with 1 mg/kg/week i.m. Starting directly after grafting, all animals received 1.5 mg/kg/BID s.c. of Tacrolimus (Prograf/FK506, Astellas, Deerfield, IL, USA) until the end of the study. For post-transplant days 0-10, the animals also received 30 mg/kg/day s.c. of Mycophenolate mofetil (CellCept, Genentech, CA, USA). Immunosuppression was also given to the non-grafted Sprague-Dawley animals (i.e., the naïve, sham operated, and all SCI-control animals).

Open field locomotion testing

Locomotion recovery after spinal cord contusion injury was monitored using a modified Basso, Beattie, Bresnahan (BBB) open field locomotion rating scale [35]. The BBB score was modified to reflect the distinct locomotor recovery stages observed after L3 SCI. The modified

score entailed 8 well-defined degrees of locomotor recovery: **0-1:** are identical to the BBB-score, **2:** is cumulative score of 2 and 3 of the BBB score, **3:** is cumulative score of 4, 5 and 6 of the BBB score, **4:** is cumulative score of 7 and 8 of the BBB score, **5:** reflects weight support with poor paw clearance, **6:** is broadened and/or shortened stepping, and **7:** is normal walking. In the present study, the locomotor score was obtained before grafting and weekly after injury until the end of the study (i.e., 8.5 weeks post-injury). In addition to a modified BBB score, a regular full 21 scale BBB score was periodically assessed.

Gait analysis

The CatWalk apparatus (CatWalk 7.1, Noldus Technology, The Netherlands) was used to quantify gait parameters during walkway crossings (e.g., paw positioning, base of support, stride length, front limb vs. hind limb coordination) by footprint analysis [36]. Animals had to walk down a horizontal glass walkway ($109 \times 15 \times 0.6$ cm, L×W×H), of which the glass is illuminated along the long edge. At the end of the walkway, animals had access to their home cage and were given a treat upon arrival (Certified Supreme Mini-Treats™, Cat# F05472-1, Frenchtown, NJ, USA). The light only enters the (side of the) glass and reflects merely internally (when the glass is bordered by air). As an animal walks on the glass walkway, light reflects off of the animal's paws, producing a series of bright footprints when viewed through the glass, from below the walkway. The illuminated footprints were then recorded by a video camera with a wide-angle objective that was located underneath the elevated glass walkway. In order to get an optimal contrast between the paws and the surroundings, the test was performed in a room that was totally darkened. The animals were trained for smooth walkway crossing on the 5 days prior to the video acquisitions. To obtain accurate and meaningful data, the following criteria concerning walkway crossings needed to be met: (1) the animal needed to walk uninterrupted across the walkway, at a constant pace, and (2) a minimum of three such crossings per animal were

required. Animals without bilateral paw clearance could not be analyzed (n=4 control-SCI animals, and 3 HSSC-treated animals). Digital data analysis consisted of assigning labels (left-fore, left-hind, right-fore, or right-hind) to the animal's paw prints in a recorded walkway crossing, using dedicated CatWalk software. Next, the software calculated gait parameters. Data from the three proper crossings was averaged for statistical analysis.

Inclined ladder test

The inclined ladder test was performed as described before [37, 38]. Using an inclined ladder (55°) with twenty 120 mm wide rungs (diameter: 1/4"), spaced at equal intervals (60 mm), and having 150 mm-high side walls was used. The rats were trained for this test so that smooth runs were recorded. At the end of the ladder, the animals had access to their home cage and received a treat (as above). The rats were placed at the bottom, and in front, of the ladder. The bottom of the ladder was placed on a 20 cm elevated platform. Climbing was video recorded from a position below the ladder, so that the ventral aspect of the animal is recorded. All animals were able to climb up the ladder. The correct placing of a hind paw and sustained position until its next forward move was counted over 18 rungs (placement on first and last rung not counted).

Single frame hind limb motion analysis

Two parameters were measured in bilateral video captures of animals crossing a runway: the foot-stepping angle (FSA) and the rump-height index (RHI), as described before [37, 38]. The FSA is the angle at which the hind paw is placed on the ground just after the swing phase. The angle is defined by a line parallel to the dorsal surface of the paw and a horizontal line behind the paw. Four to six measurements were made for each hind limb (a total of 8 to 12 step cycles). The RHI was defined as the highest point of the base of the tail during the (recorded part of the) run. The values for the left and right paw of each animal were averaged. The elevated runway bar was

made of a wooden plate/beam (1500 × 150 × 20 mm, L×W×H). The animals were trained to smoothly walk the beam. Once more, at the end of the beam the animals had access to their home cage and received a treat (as above). The videos (i.e., the selected frames) were selected and analyzed using the video tool VirtualDub 1.9.11 (Written by Avery Lee, <http://www.virtualdub.org>) and the on-screen measurement tool Screen Ruler V1.0.1a (<http://www.caveworks.net>).

Myogenic motor evoked potentials

Animals were anesthetized with ketamine (80 mg/kg i.p., Ketaset, Fort Dodge Animal Health, Overland Park, KS, USA). Myogenic Motor Evoked Potentials (MEPs) were elicited by transcranial electrical stimulation (with a pulse duration of 1 ms at 7 mA using a DS3 constant current isolated stimulator (Digitimer LTD., Welwyn Garden City, UK)) of the motor cortex using two percutaneously placed 30G stainless steel stimulation electrodes. Responses were recorded from the gastrocnemius muscle using 30G platinum transcutaneous needle electrodes (distance between recording electrodes ~1 cm; Grass Technologies, Astro-Med, Inc., West Warwick, RI, USA). Recording electrodes were connected to an active headstage (3110W Headstage, Warner Instruments LLS) and signal amplified using DP-311 differential amplifier (Warner Instruments LLS). Amplified signal was acquired by the PowerLab 8/30 data acquisition system (AD Instruments, Inc., Colorado Springs, CO) at sampling frequency of 20 kHz, digitized and stored in PC for analysis. MEPs were measured until three to five highest (stable) recorded potentials were similar. Those traces were averaged per animal and multiplied by one thousand (μV ; all values >1). Next, for data normalization, a logarithmical transformation was applied for further analysis (amplitudes of MEP traces tended to vary much more in animals with higher MEPs amplitudes).

Measurement of muscle spasticity

At 1.5 weeks and 2 months post-injury, the presence of muscle spasticity in the lower extremities was measured using a previously described system [39]. Briefly, fully awake animals were placed in a restrainer and a hindpaw was taped to a rotational metal plate driven by a computer-controlled stepping motor. The metal plate is interconnected loosely to the “bridging” digital force transducer (LCL454G, 0–454 g range; Omega, Stamford, CT, USA). The resistance of the ankle to dorsiflexion was measured during stepping motor-driven ankle dorsiflexion (40°; MDrive 34 with onboard electronics; microstep resolution to 256 microsteps/full step; Intelligent Motion Systems, Marlborough, CT, USA) at 3 different ankle-rotational velocities (40, 60 or 80°/sec). The EMG signal was recorded from the ipsilateral gastrocnemius muscle during the same time frame. To record EMG activity, a pair of tungsten electrodes was inserted percutaneously into the gastrocnemius muscle 1 cm apart. EMG signals were bandpass filtered (100 Hz to 10 kHz) and recorded before, during, and after ankle dorsiflexion. EMG responses were recorded with an alternating current-coupled differential amplifier (model DB4; World Precision Instruments, Sarasota, FL, USA). EMG was recorded concurrently with ankle resistance measurements, both with a sample rate of 1 kHz. Both muscle resistance and EMG data were collected directly to the computer using custom software (Spasticity version 2.01; Ellipse, Kosice, Slovak Republic). Each recorded value was the average of three repetitions. The presence of spasticity response was identified as an increased ankle resistance and concurrent increase in recorded EMG activity during computer-controlled ankle dorsiflexion. To measure the contribution of “mechanical” component in measured resistance (i.e., caused by ankle ankylosis in chronically paraplegic animals), animals were anesthetized with isoflurane at the end of each recording session and the relative contribution of neurogenic (i.e., isoflurane-sensitive) and mechanical (i.e., isoflurane non-sensitive) component identified. The magnitude of

anti-spasticity effect was then expressed as the maximum possible anti-spasticity effect measured under isoflurane anesthesia minus the value of the mechanical component.

Sensory testing

Recovery of sensory function was assessed through quantification of supraspinal “above-level” escape response (AL-ER; i.e., an escape or escape-attempt with incorporation of the forelimbs) thresholds to 1) a gradually increasing force to the hind paws (using the Analgesy-Meter, no disc weights added; Cat# 37215, Ugo-Basile, Collegette, PA, USA), and 2) AL-ER latencies to a constant heat stimulus (intensity 17, cut-off at 30 sec) to the hind paws (using a constant infrared heat source; Cat# 37360, Ugo-Basile, Collegette, PA, USA). The hind paw tested was gently restrained by the investigator to prevent withdrawal. For the heat perception test the apparatus was switched on ≥ 15 min prior to testing, to allow it to warm up.

For the AL-ER tests, both hind paws were tested four times, alternately, for each test, with a testing interval of ≥ 1 hour. No more than four measurements per day were performed, rendering two testing days per test. Maximum cut-off values for the stimuli or latency were at approximately two times that of response threshold of uninjured animals, to prevent tissue damage. Prior to (one week) and during the experimental period, the animals are extensively habituated to the experimenter so that the animals can be held upright (loosely) during all sensory assessments. Habituation consists of picking the animal up and holding/handling it twice daily for ≥ 3 minutes. Subsequently, in absence of a stimulus, animals did only rarely show escape behavior when held for the time it would take to reach cut-off values. We measured the AL-ER thresholds/latencies before injury (baseline) and every 2nd week after injury. The final measurement was done at eight weeks post-injury. Two or less (out of the total of eight, bilateral) measurements could manually be assigned as outliers and be excluded per time point (done while blinded for time point, animal, and treatment group). In addition, individual scores were log

transformed before analysis and we calculated the Maximal Possible Effect, using these log scores, as previously suggested [40]. Hence, we used the standard formula to calculate the Maximal Possible Effect, and assuming a logarithmic relation between stimulus intensity and perceived intensity:

$$100 \times \frac{\log(x_{final}) - \log(\bar{x}_{final \text{ of SCCI control animals}})}{\log(\bar{x}_{baseline \text{ of SCCI animals}}) - \log(\bar{x}_{final \text{ of SCCI control animals}})}$$

Here, x_y is the average AL-ER threshold of an individual animal at time point y (either for a thermal or mechanical stimulus).

Magnetic resonance imaging

Eight weeks after cell grafting, rats were deeply anesthetized with 2 mg pentobarbital and 0.25 mg phenytoin (0.5 mL of Beuthanasia-D, Intervet/Schering-Plough Animal Health Corp., Union, NJ, USA) and transcardially perfused with 200 ml of heparinized saline followed by 250 ml of 4% paraformaldehyde (PFA) in PBS. A 3 cm piece of the vertebral column (Th8-L1) was placed in a tight small latex container filled with 4% PFA to prevent the formation of air bubble/tissue interface artifacts. Samples were scanned using Magnetic Resonance Imaging (MRI). Images were acquired using a 7T Bruker (Bruker Biospin Billerica, MA) horizontal bore small animal magnet, and a 2.5 cm imaging volume transmit/receive coil. A 3D turboRARE sequence was used with the following imaging parameters: Echo time/Repetition time 45/1500 ms, Flip angle 180 degrees, field of view $16 \times 16 \times 16$ mm, matrix $256 \times 256 \times 70$ with a resulting voxel size of $62 \times 62 \times 229$ microns. The imaging time was 84 min per sample.

Volume reconstructions and calculations were done using Amira software (Visage Imaging GmbH, Berlin, Germany).

Axon counting in plastic semi-thin sections

After MRI imaging, spinal cords were dissected from the spine and transverse (1.5-mm-thick) spinal cord block cut from the injury epicenter and prepared for plastic embedding as previously described [41]. Briefly, dissected tissue blocks were treated with 0.1% osmium tetroxide in 0.1 M non-saline phosphate buffer (pH 7.4) for 12 h, followed by adequate rinsing in non-saline phosphate buffer. This was followed by progressive alcohol dehydration according to standard procedures up to 100% ethanol, with the addition of further dehydration in a 1:1 solution of ethanol/propylene oxide, and lastly in 100% propylene oxide. Dehydrated blocks were then prepared for resin infiltration by incubation in a 1:1 solution of resin/propylene oxide on a rotator in a fume hood overnight. The resin solution used consisted of: Eponate 12, Araldite 502, dodecyl succinic anhydride, and 2,4,6-tri [dimethylamino-methyl] phenol (DMP-30; Ted Pella, Inc., Redding, CA), mixed in ratios of 10:10:25:1, respectively. The blocks were then transferred to 100% resin for subsequent overnight infiltration on a rotator. Finally, the tissue blocks were embedded using fresh resin in multi-chamber silicone rubber molds made from a Silastic® E RVT Silicone Rubber Kit (Dow Corning Corp., Midland Township, MI). The molds with embedded sections were placed in an oven at 60°C for 1 day to facilitate resin polymerization. Semi-thin (1 µm) transverse sections were then cut using a microtome (Leica Supercut RM 2065) with a 8-mm diamond knife (Histo Diamond Knife, Cat# LM 7045, DiATOME, Hatfield, PA, USA). The sections were mounted on slides with distilled water and allowed to dry on a slide warmer. Prior to staining, the slides were incubated at 60°C in an oven for 10-15 min, and then contrast-stained with 4% para-phenylene-diamine (PPD).

Mosaic images were taken of two sections per animal at 20X using a Zeiss Imager.M2 fitted with a Zeiss MRm camera (Carl Zeiss Microscopy, Thornwood, NY, USA), a BioPrecision2 stage (Cat# 96S100, Ludl Electronic Products, Hawthorne, NY, USA), and Stereo Investigator

software (MBF Biosciences, Williston, VT, USA). Complete mosaic images were loaded into ImageJ 1.45s. Axonal quantification involved manual definition of pixel threshold (0-255, grayscale; using the Triangle method). Next, ImageJ's Analyze Particles option was used to find particles with a size of 0.20-250 μm^2 and a circularity of 0.5 to 1.0 (which corresponded to axons). All acquisition and analysis values were held consistent throughout the study. Final measurements acquired were the minimal diameter (Feret's) of each particle (and particle counts). Particles with a minimum diameter $>10 \mu\text{m}$ were excluded. Employment of this parameter allowed for further axonal analysis, in which axons were divided into empirically-derived caliber sizes of small, medium, and large axons (0.3–1.0 μm , 1.0–2.5 μm , and 2.5–10 μm , respectively). Data was acquired per spinal region (i.e., dorsal, ventral, and lateral funiculi).

Immunofluorescence staining

After removing the 1.5 mm block from the spinal cord at the injury epicenter, the remaining caudal and rostral parts of the spinal cord (± 1 cm each) were placed in 30% sucrose for cryoprotection for a minimum of 5-7 days. Transverse spinal cord sections were then prepared from the L6 segment. The segment(s) in between the L6 and the injury epicenter and the one rostral to the injury epicenter were sectioned coronally and used for identification of grafted human cells. All sections were cut on a cryostat and stored free-floating in PBS with thimerosal (0.05 wt%). Sections were stained overnight at 4°C with primary human-specific (h) or non-specific antibodies in PBS with 0.2% Triton X-100: mouse anti-Nuclear Mitotic Apparatus (hNUMA, 1:100; Millipore, Billerica, MA, USA), mouse anti-Neuron Specific Enolase (hNSE, 1:500; Vector Labs, Burlingame, CA, USA), mouse anti-Synaptophysin (hSyn, 1:2,000; Millipore), rabbit anti-Glial Fibrillary Acidic Protein (hGFAP, 1:500; Origene, Rockville, MD, USA), mouse anti-Neuronal Nuclei (NeuN, 1:1,000; Millipore), chicken anti-Green Fluorescent Protein (GFP, 1:1,000; Aves Labs,), rabbit anti-Anti-Glutamate Decarboxylase 65 & 67

(GAD65&67; 1:300; Millipore), mouse anti-GFAP (Cy3-labeled; 1:500; Sigma-Aldrich; St. Louis, MO, USA), rabbit anti-Ki67 antibody (mitotic marker, 1:100; Abcam), and rat anti human axonal neurofilament antibody (hHO14; 1:100; gift from Dr. Virginia Lee; University of Pennsylvania). Mouse anti-Growth Associated Protein 43 (GAP43, 1:16,000; Millipore), rabbit anti-Calcitonin Gene-Related Peptide (CGRP, 1:1,000; Biotrend, Destin, FL, USA), and rabbit anti-Ionized calcium Binding Adaptor molecule 1 (Iba1, 1:1,000; Wako, Richmond, VA, USA), were used on the L6 transverse sections. Following washing in PBS 3·5 min, sections were incubated with fluorescent-conjugated secondary donkey antibodies (Alexa® Fluor 488 & 647; 1:500; Jackson Immuno Research, West Grove, PA, USA; & Alexa® Fluor 555, 1:500; Invitrogen). Sections were then mounted on slides, dried at room temperature, and covered with Prolong anti-fade kit (Invitrogen Corp., Carlsbad, CA, USA).

Confocal images (1024 × 1024 pixels) were captured with a Fluoview FV1000 microscope (Olympus, Center Valley, PA, USA) with a 20X or 40X objective, optical section spacing of 0.5 μm, and pulse speed of 20 μsec/pixel. Other images were taken using the Zeiss Imager.M2 setup as described above, using a 10, 20 or 63X magnification. CGRP, GAP43, and Iba1 stainings on L6 transverse sections were quantified using densitometry measurements of the main dorsal horn region (Laminae I through IV; area as marked in **Fig. 7B**). ImageJ software was used for quantification by using the Background Subtraction function.

Statistical analyses

Behavioral data were analyzed using ANOVA (one-way, or two-way group × time repeated measures, using a fixed-effect model, and a Bonferroni *post hoc* test for multiple comparisons). A *P* value of 0.05 was considered significant. Unequal variances were explored prior to using ANOVA analyses using the Bartlett's test, but were not identified. *Post hoc* tests were only calculated if overall group differences were found. Results are expressed as means with the

standard error of the mean (SEM). To analyze differences between the two groups (e.g., vehicle injected vs. non-injected SCI animals), we used Student's t-tests (unequal variances were explored with the F-test, but not found) or repeated measures ANOVA. Naïve and sham operated animals were grouped (and named "non-injured") in all outcomes besides the sensory tests. All statistical analyses were done using GraphPad Prism (La Jolla, CA, USA), SPSS statistics 17 (for K-Means clustering; IBM, Armonk, NY, USA), or STATA 12 (for precise post-hoc test *P*-value calculations; StataCorp LP, College Station, TX, USA) and performed two-tailed.

Results

General animal health and survival of animals during long-term immunosuppression

From the total of 35 SCI Sprague-Dawley rats employed in this study, 32 survived until planned sacrifice while continuously immunosuppressed; 14 NSI-566RSC-injected (1 excluded; because of automutilation of hind paw on day two post-injury), 10 vehicle-injected, 8 non-injected (2 excluded; 1 because of automutilation of hind paw on day 7 post-injury & 1 because of excessive BW loss on post-injury day 18 (likely related to immunosuppression-related toxicity)). In four surviving animals, lower extremity ulcers developed but were effectively treated with local standard triple antibiotic ointment (Bacitracin, Neomycin, and Polymyxin B) and cohesive bandages. In most animals, the Crede's maneuver needed to be performed for 3-5 days after spinal trauma (exceptions: 3 animals in NSI-566RSC-injected group and 2 animals in non-injected SCI-control group, of which one died due to health issues; see above). No additional worsening (i.e., a lowering in open-field locomotor scores at one day post-grafting, compared to pre-grafting values) was noted in intraspinal media- or cell-injected animals.

Spinal injection procedure did not alter neurological outcome in previously L3-contused rats

In order to define the effect of spinal injection itself in modulating the functional recovery profile (i.e., potential worsening in neurological outcome) in L3-injured animals, we have first compared the effect of spinal media injection only with spinal injury animals which received no injections (10 vehicle-injected and 8 non-injected SCI animals). No significant differences were found between these two groups in any of neurological or electrophysiological outcome measures used in this study (repeated measures ANOVA for open field locomotor scores; Student's *t*-test for others). Based on these data, which showed no significant differences between both control groups, these two groups were then pooled into one control group and used for subsequent comparison with HSSC-grafted animals.

Assessment of motor function

Gait analysis showed significant improvement in hind paw placement in SCI-HSSC-grafted animals

Gait analysis was conducted at 8 weeks after grafting (or corresponding time point in controls) using the CatWalk apparatus [42]. The following parameters were analyzed: i) runway crossing time, ii) rostral-caudal hindpaw positioning, iii) hind paws base of support, iv) regularity index/coordination, v) stride length, and vi) phase dispersions.

Rostro-caudal hindpaw positioning (RCHPP): In control non-injured animals, the RCHPP was 0 ± 1.7 mm (i.e., the animals are able to achieve a near complete overlap in the hindpaw positioning relative to the last ipsilateral frontpaw print; full rostral-caudal overlap is represented by a value of "0"). Rats receiving spinal HSSC grafts showed significantly better RCHPP, when compared to control SCI animals (-9.0 ± 1.9 vs. -18.2 ± 3.1 mm, respectively, **Fig. 2A**; Bonferroni: $P=0.04$). Examples of the paw positioning are shown in **Fig. 2B** for a non-injured control, SCI control, and a HSSC-treated SCI animal (**Fig. 2-B1**, **-B2**, and **-B3**, respectively).

No significant differences were detected in other CatWalk parameters (runway crossing time, hind paws base of support, regularity index/coordination, stride length, phase dispersions), myogenic motor evoked potentials, or behavioral motor tests (open field locomotor score (modified BBB score, and regular BBB scores), single-frame motion analysis or ladder climbing test) (Suppl. Fig. 1 A-D).

Effective suppression of muscle spasticity in HSSC-grafted SCI animals

To identify the presence of spasticity (i.e., potentiation in muscle stretch-evoked EMG activity) in animals after SCI, a computer-controlled ankle-rotational force was applied on the right or left paw in fully awake restrained animals and resulting change in EMG activity in the gastrocnemius muscle and correlative ankle resistance was measured [39].

Independent of SCI group (control or HSSC-injected), two quantitatively different EMG patterns and corresponding resistance response (EMG/RES) patterns were recorded in spinally-injured animals. First, if compared to control non-injured animals, little or no change in EMG/RES response was seen at 1.5 weeks after SCI. Second, SCI induced an increased spasticity response in a portion of the animals at 1.5 weeks after injury. A K-Means clustering method was used to group all 44 (SCI and non-injured) animals into 2 groups based on magnitude of resistance to ankle rotation at 1.5 weeks post-injury (or equivalent time point in non-injured animals). Seven animals of each SCI group (i.e., control or HSSC-injected) were found to be clustered in the high “spasticity” group (HIGH), which had a 31.7 ± 3.9 g increase in measured muscle resistance during ankle rotation, compared to the low “spasticity” group (LOW) showing 8.9 ± 1.5 g resistance (Student’s *t*-test: $P < 0.0001$). No difference in the incidence of this high “spasticity” response was noted between SCI control vs. cell-treated groups (incidence: χ^2 : $P = 0.53$; extend: Student’s *t*-test: $P = 0.24$). No naïve or sham operated animals were found to be clustered into the HIGH group. Resistance to ankle rotation measured 8 weeks

after treatment (and expressed as relative change from 1.5 weeks post-injury values) showed a significant decrease in the HSSC-injected HIGH resistance group when compared to HIGH resistance animals from the control SCI group (**Fig. 2C**; i.e., decline of 24.8 ± 6.4 g in HSSC-injected animals and 4.8 ± 6.3 in control SCI animals; Bonferroni: $P=0.048$).

Fig. 2D shows an example of raw data depicting a post injury EMG response (red channel) and corresponding increase in muscle resistance (black channel) during ankle rotation in a SCI-control (**Fig. 2-D1-3**) and a HSSC-injected animal (**D4-6**) at 7 days after treatment and at the end of the 8-week survival. Clear suppression of potentiated EMG response and muscle resistance can be seen in HSSC-treated animals (compare **D4** to **D6**). To identify and dissociate neurogenic (i.e., isoflurane-sensitive) versus mechanical (i.e., isoflurane non-sensitive) components, muscle resistance was re-measured after isoflurane anesthesia and the relative contribution of mechanical component calculated. The induction of isoflurane anesthesia near completely blocked the ankle rotation-evoked EMG response and resulting increase in muscle resistance (**D2, D5**).

Assessment of sensory functions

Analysis of mechanical and thermal sensory function was performed by comparing hindpaw thresholds improvements of evoked above-level/supra-spinal withdrawal responses (i.e., an escape response in which the frontlimbs and/or vocalizations are used) between experimental groups over several time points. Groups consisted of naïve control, sham operated control, SCI-control, or SCI-HSSC-injected animals. Response thresholds were measured before injury and every second week thereafter. No differences were measured between naïve and sham-operated animals at any time point in response thresholds to both mechanical and thermal stimuli (repeated measures ANOVA).

HSSC treatment led to a significant improvement in the supraspinal perception to mechanical stimuli evoked below the level of injury

Prior to injury, no differences in mechanical thresholds to trigger escape responses were measured between all four experimental groups (on average 92 ± 2 g). After SCI, the thresholds increased significantly in both SCI-control and SCI-HSSC-injected animals compared to control non-injured groups, at all time points (Bonferroni; $P < 0.001$). From 4 weeks post injury, SCI-HSSC-injected animals displayed a trend towards progressive improvement in response thresholds if compared to SCI controls (at eight weeks: 177 ± 10 g and 216 ± 10 g, respectively; **Fig. 3A**; repeated measures ANOVA: $P = 0.14$). This resulted in a significant higher percentage of the Maximal Possible Effect for improvement of mechanical stimulus perception in SCI-HSSC-injected animals compared to SCI-control animals (**Fig. 3C**; Student's *t*-test: $P = 0.03$).

Treatment with HSSC was associated with significant recovery of supraspinal heat perception evoked below the level of injury

Prior to SCI, measurement of thermal (infrared) stimulus-evoked paw withdrawal threshold showed no significant differences between all experimental groups (17.3 ± 0.3 sec; one-way ANOVA). At two weeks post SCI, significant increase in paw withdrawal latencies in both the control SCI group and in SCI animals receiving spinal HSSC grafts were measured, when compared to control non-injured (sham operated and naive) groups (26.1 ± 0.7 sec in SCI-control animals and 26.5 ± 0.7 sec in HSSC-grafted animals vs. 18.3 ± 0.2 sec in control non-injured animals; **Fig. 3B**; Bonferroni: $P < 0.001$).

From four weeks after treatment a trend towards a progressive normalization in response threshold was seen in HSSC-treated animals if compared to SCI controls (at eight weeks: 24.0 ± 0.9 sec in SCI-control and 21.4 ± 0.9 sec in HSSC-injected animals, respectively; repeated measures ANOVA: $P = 0.09$). This resulted in a significantly higher percentage of the Maximal

Possible Effect for the improvement of thermal stimuli in SCI-HSSC-injected animals compared to SCI-control animals (**Fig. 3C**; Student's *t*-test: $P=0.02$).

Postmortem spinal cord MRI showed cavity-filling effect by grafted cells in HSSC-injected animals

For lesion volume analyses, a 2 cm long portion of the fixed spinal column was dissected out, kept in 4% paraformaldehyde, and imaged using a 7 TESLA MRI magnet. The primary goal of this analysis was to generate quantitative data on the cavity-filling effect by grafted cells and to assess the extent of rostro-caudal cavitation in vehicle-injected vs. HSSC-injected animals using quantitative volume analysis (**Fig. 4**). In vehicle-injected animals, the presence of fluid-filled cavities was readily identified as the presence of homogenous white areas and scarring as black areas (**Fig. 4B1**; compare with non-injured: **Fig. 4C**). In contrast, in animals receiving cell injection, the cavity was partially or completely filled with grafted cells as evidenced by the presence of low density tissue masses (**Fig. 4A1**). The identity/presence of grafted cells in the “low density tissue masses” was further validated by analysis of semi-thin plastic sections taken from the same region (compare **Fig. 4A2** which depicts the presence of cell grafts vs. extensive cavity in **4B2**). **Fig. 4A** shows a 3D reconstruction image of a cell-injected animal (areas identified as grafted cells are labeled green). **Fig. 4B** shows a SCI-control (media-injected) animal with cavity labeled in light-green-yellow.

Quantification of the cavity volume showed a significantly larger injury-induced cavity in SCI-control animals than in HSSC-injected animals ($3\pm 0.4 \text{ mm}^3$ vs. $0.6\pm 0.2 \text{ mm}^3$, respectively; **Fig. 4D**; Student's *t*-test: $P<0.0001$). Similarly, the scar volume seen in SCI-control animals was larger than in cell-injected animals ($3.3\pm 0.3 \text{ mm}^3$ vs. $1.9\pm 0.3 \text{ mm}^3$, respectively; Student's *t*-test: $P<0.001$).

To assess the potential excessive grafted cell proliferation and resulting spinal cord tissue

expansion, we next compared the total volume (i.e., the volume of the remaining spinal cord, scar, cavity, and/or grafted cells) of cell-grafted spinal cord segments with corresponding segments of control animals. The measured volumes were: $71.8 \pm 3.2 \text{ mm}^3$ in non-injured control animals, $54.6 \pm 2.8 \text{ mm}^3$ in SCI-control animals, and $59.0 \pm 2.2 \text{ mm}^3$ in SCI-HSSC-injected animals (Student's *t*-test: $P=0.27$; SCI-control vs. SCI-HSSC-injected animals).

Survival, maturation and integration of grafted HSSC

To identify the presence of human cells in the rodent spinal cord tissue, two different immunostaining/analytical methods were used. First, GFP-tagged grafted cells were identified by the presence of GFP autofluorescence/immunoreactivity and then co-stained with neuronal and non-neuronal markers. Second, a set of human-specific antibodies was first used to validate the presence of human cells and then combined with other human-non-specific neuronal or non-neuronal antibodies.

Staining with anti-GFP, -NeuN (neuronal marker) and -human-specific synaptophysin antibody showed a near complete repopulation of compression-induced lesion cavity by grafted GFP+ cells (**Fig. 5A**-yellow dotted area). A comparable spinal injury-cavity filling by grafted cells was seen after grafting with GFP or non-labeled HSSC as evidenced by the presence of dense hNUMA-immunoreactive grafts (**Fig. 5A** inserts). Analysis of axo-dendritic sprouting from grafted GFP+ cells showed extensive rostro-caudal neurite sprouting particularly well-developed in the lateral white matter (**Fig. 5B**). In addition, numerous GFP+ axons branching from innervated lateral funiculi and projecting towards α -motoneurons and interneurons was identified (**Fig. 5B**;insert). Triple staining with NeuN, hSYN and GFP antibody showed a high density of hSYN punctata in GFP+ innervated regions (**Fig. 5C**-yellow arrows) as well in the vicinity of endogenous NeuN+ neurons. Staining with hNUMA, hNSE and DCX antibody revealed that the majority of hNUMA+ grafted cells were DCX or DCX/hNSE immunoreactive

(**Fig. 5A-insert; Fig. 5D**). Probing for glial phenotype in grafted cells by double staining with hNUMA and hGFAP or hNUMA and Olig2 antibody revealed well-developed groups of hGFAP+ astrocytes. These GFAP+ cell populations were primarily found in the white matter or at the periphery of individual DCX/hNSE+ grafts (**Fig. 5E**). Less than 2% of hNUMA+ cells showed Olig2 immunoreactivity (**Fig. 5F**; yellow arrows). To assess the presence of mitotically active grafted cells, sections were double-stained with hNUMA and Ki67 antibody. An estimated 0.5-1% of hNUMA+ cells were Ki67 positive. These double hNUMA/Ki67+ cells were regularly distributed throughout the grafted regions but no cluster(s)-like formations of hNUMA/Ki67+ cells were seen in any animal (**Fig. 5G**; yellow arrows).

Confocal analysis of spinal cord sections triple-stained with hSYN, GFP and NeuN antibodies showed numerous hSYN punctata colocalizing with GFP+ processes. Several hSYN punctata were found to reside in the vicinity of interneuronal and/or α -motoneuronal membranes (**Fig. 6A; inserts; white arrows**). Probing for the presence of GAD65/67+ terminals derived from grafted neurons by using triple stained GAD(65/67)/GFP/NeuN sections and confocal microscopy showed the presence of GFP/GAD65/67+ terminals in the vicinity of α -motoneuronal membranes (**Fig. 6B; white arrows**).

Normalization of CGRP expression in L6 dorsal horns in SCI-HSSC-treated animals

To analyze changes in the spinal expression of putative central pain neuromodulators/indicators, including CGRP, GAP43 and Iba-1 [43, 44], we next stained transverse L6 sections (i.e., below-injury-level region) with respective antibodies at 8 weeks after treatment (**Fig. 7 A, B, C**). Densitometry analysis showed that CGRP immunoreactivity was significantly reduced in SCI-HSSC-treated animals (**Fig. 7A2**) when compared to SCI-controls (**Fig. 7A1**; Student's *t*-test: $P=0.04$). We did not find significant group differences in IHC

staining intensities of either GAP43 or Iba1 (**Fig. 7B, C**; Student's *t*-test: $P=0.58$ and $P=0.24$, respectively).

Quantitative assessment of axonal survival in the epicenter of injury using semi-thin plastic sections

For quantitative analysis of axonal survival, a transverse spinal cord block taken from the injury epicenter was used. Using osmium/p-phenylenediamine-stained semi-thin (1- μm -thick) plastic sections, the total number of axons (divided in 3 subgroups based on the axonal caliber; 0.3–1.0, 1.0–2.5, and 2.5–10 μm in diameter) was then counted using ImageJ software.

Systematic quantification of the total number of myelinated axons counted bilaterally in a control naïve animal showed 281,352 axons (**Suppl. Fig. 2A**). Thirty-three percent was represented by small caliber axons, 57% by medium caliber axons and 10% by large caliber axons. In SCI-control animals, the total number of axons was on average $55,137 \pm 5,168$ and was $55,340 \pm 5,650$ in HSSC-injected animals (Student's *t*-test: $P=0.98$; **Suppl. Fig. 2B-D**). Intergroup statistical analysis of the axons at specific diameter (i.e., 0.3–1.0, 1.0–2.5, and 2.5–10 μm) showed *P*-values of 0.88, 0.84, and 0.51 (Student's *t*-tests) between SCI-control and SCI-HSSC-grafted animals, respectively. Intergroup statistical analysis of the axons at specific funiculi (i.e., dorsal, lateral, and ventral funiculi) showed *P*-values of 0.73, 0.82, and 0.72 (Student's *t*-tests) between SCI-control and SCI-HSSC-grafted animals, respectively (**Suppl. Fig. 2D**). Additional intergroup analyses of axon survival categorized by both size and location/funiculus did not show significant differences between SCI-control and SCI-HSSC-grafted animals ($P > 0.36$; Student's *t*-tests) (**Suppl. Fig. 2D**).

Discussion

In the present study, we investigated the treatment effect of spinally grafted GMP-grade human fetal spinal cord-derived neural stem cells (**HSSC**) in a L3 spinal compression injury (SCI) model in rats.

HSSC were grafted into and around the epicenter of the contusion-injured L3 spinal segment at 3 days after spinal trauma in continuously immunosuppressed Sprague-Dawley rats. In comparison to control SCI animals with no treatment or receiving intraspinal injections of media only, the intraspinal grafting of **HSSC** led to a progressive and significant improvement in: i) gait/paw placement, ii) muscle stretch-induced spasticity, and iii) mechanical and thermal sensitivity. These behavioral benefits were associated with robust graft survival and near complete injury-cavity-filling effect with grafted cells and corresponding lack of syringomyelia otherwise seen in control SCI cell-non-treated animals. In addition, the development of putative GABA-ergic synapses between grafted neurons and interneurons and/or α -motoneurons of the host were identified. These data demonstrate that intraspinal grafting of **HSSC** into an injured spinal cord segment in the acute phase of injury represents a safe and effective treatment modality. This cell-replacement therapy was effective in providing qualitatively- and quantitatively-defined functional benefits and also led to significant and long-term improvement in the structural integrity of previously trauma-injured spinal cord segments.

Rat L3 spinal compression injury model

In our current study, a lumbar spinal injury was induced by a static 35 g pressure exerted on the dorsal surface of the L3 spinal segment by using a stainless steel-Teflon rod (2.9 mm in diameter). In our preliminary “survey” study, we have found that in this model the 35g spinal cord compression needs to be maintained for a minimum of 15 min to produce a reproducible degree of functional and histopathologically-defined injury. These data indicate that the

pathophysiological mechanism leading to neuronal/axonal degeneration in this model is primarily related to the ischemia-induced changes. However, interestingly, the histopathological changes in this model are characterized by the development of a well-delineated cavity found just below the compression site. It is in contrast to the “pure” ischemia-reperfusion-induced spinal injury seen in aortic balloon occlusion models in which a selective loss of inhibitory interneurons is seen in previously ischemia-exposed spinal segments in the absence of cavity(s) formation [45, 46]. In this respect, our current model appears to be similar to high velocity (weight drop model) impact injury models which show comparable cavity formation in chronic L2 or L3/4 segment-injured rats [47, 48]. Similarly as demonstrated in the rat “weight drop” contusion models [49], the development of spinal hyper-reflexia, as evidenced by the presence of exacerbated muscle activity evoked by computer-controlled ankle rotation, was seen in a subpopulation of injured animals in our current study. Importantly, spinal cavity formation and muscle spasticity is frequently observed in human patients with a high-velocity-impact-induced traumatic SCI. [50, 51]

Rationale for early spinal cell-replacement therapy after spinal trauma

Both experimental and clinical data show that the spinal pathological processes following acute spinal injury are in part characterized by continuing axonal/neuronal degeneration, which can then continue for months to years after injury [1, 52-55]. It is believed that such an ongoing axonal degeneration is in part the result of the lack of local trophic support associated with loss of neurons/glia cells at and around the injury epicenter. Thus, the use of treatment strategies which can replace or supplement the loss of the local neurotrophic activity and are initiated during this acute period should thus lead to a measurable treatment effect. Previous studies have demonstrated that neural stem cells of mouse, rat or human origin are a rich source of extracellularly released trophic factors (such as NGF, BDNF, GDNF, EGF, IGF-1, and VEGF) in

in vitro cultured cells and that these cell populations retain a high level of neurotrophin expression after *in vivo* grafting in naïve animals and in a variety of neurodegenerative models including spinal injury and transgenic amyotrophic lateral sclerosis (ALS) models [56-61]. In addition, using long-term post-grafting survival periods, it was shown that *in vivo* grafting of neural precursors with neurogenic potential into either the spinal cord at 9 days post spinal cord injury, the brain at 3 days post ischemic insult, or the CNS (brain or spinal cord) of adult or developing rats, there is the development of functionally and morphologically-defined synaptic contacts between grafted neurons and the neurons of the host [62-64].

Based on these characteristics of neural precursors (NPCs), the use of NPCs for acute spinal cord grafting after trauma serves three purposes. First, it serves to provide local trophic support in the areas of previous injury (provided that grafted cells are able to home and survive long-term once grafted into the injured spinal cord milieu) and to minimize or halt the process of progressive axonal/neuronal degeneration. Second, it serves to provide a cavity-filling effect by replacing previously injured-degenerated necrotic tissue and thus prevent the long-term (or progressive) formation of rostro-caudal cavitations (i.e., syringomyelia) [55]. Third, by the development of synaptic contact with the host axons/neurons above and below the injury level it can potentially lead to formation of a functional relay through the injury site.

Effect of spinal grafting of HSSC on the recovery of motor function and muscle spasticity

In our current study, a combination of several motor performance tests were employed including open field modified BBB scoring, CatWalk gait analysis, inclined ladder climbing, single frame hind limb motion analysis, and myogenic motor evoked potentials to identify the degree of motor function recovery after cell grafting. The changes in muscle spasticity in lower extremities (i.e., below the level of injury) were also measured using a computer-controlled ankle rotational system [39]. The CatWalk gait analysis showed significantly improved paw placement in HSSC-

injected SCI animals when compared to control SCI animals. In addition, a significant suppression of otherwise exacerbated muscle spasticity response measured during ankle rotation was seen in cell-treated animals. However, no improvements in other functional CatWalk parameters (runway crossing time, hind paws base of support, regularity index/coordination, stride length, phase dispersions), MEPs, BBB score, single-frame motion analysis or ladder climbing test) were seen. Consistent with our current data, several other studies from different laboratories have demonstrated a variable degree of motor function recovery after spinal grafting of rodent or human fetal, adult or embryonic stem-cells derived neural precursors using a variety of spinal injury models in mice and rat [14, 29, 32, 65-72]. Importantly, these data jointly suggest that a some degree of therapeutic effect can also be achieved once cells are grafted during the early post-injury period (i.e., 3-7 days after spinal trauma).

Effect of spinal grafting of HSSC on the recovery of sensory function

In our study, we assessed the sensory function below the level of injury (hind paws) by measuring the mechanical and thermal thresholds for supraspinally mediated escape behavior. **Using this method (in contrast to hindpaw withdrawal reflex methods) we did *not* observe SCI-induced hyperalgesia at the hindpaws (below-level), which is in line with observations reported from other laboratories. [73, 74] We did, however, find significant improvement of both SCI-induced mechanical and thermal hypoesthesia.** It is important to note that the sensory thresholds did not yet plateau at the end of the 2-month survival period. We speculate that an additional quantitative and qualitative improvement in the sensory function would likely be seen should a longer post-grafting interval be studied. In addition to sensory tests, quantitative analysis of spinal parenchymal markers indicative of developing (spinal) hypersensitivity (i.e., CGRP/GAP43, an indicator of aberrant sprouting of primary sensory neurons [43, 70], and Iba1 staining, a marker of microglia activation [44]) were studied and showed a significant decrease

in CGRP staining intensities in HSSC-treated animals if compared to SCI controls. This suggests that the recovery/decrease in sensory thresholds observed in our study is not a result of aberrant sprouting or microglia activation. Consistent with the observations from our study, previous studies from other laboratories have demonstrated similar functional and histopathologically-defined (i.e. decrease in CGRP staining around the injury site) improvements after spinal grafting of fetal-tissue derived human or rodent neural or glial-restricted precursors in several mouse or rat spinal injury models [65, 66, 68-70, 72, 73].

Differentiation of grafted cells and mechanism of HSSC-mediated therapeutic action

In our current study, near pure population of nestin⁺ human fetal spinal stem cells were grafted intraspinally at 3 days after contusion-induced spinal cord injury. Analysis of the graft survival at 2 months after grafting showed a dense population of grafted hNUMA⁺ cells in grafted previously trauma-injured regions. In addition, numerous hNUMA⁺ cells which migrated out of the graft in distances ranging between 2-3 mm were also seen. Using human-specific antibodies against NSE and synaptophysin (markers of mature neurons), we have also shown that a majority of grafted cells developed into a neuronal phenotype. Many human specific synaptophysin⁺ boutons were found to reside in the vicinity of host neurons.

Quantitative analysis of the host axon survival in the injury epicenter showed no significant sparing effect in HSSC-grafted SCI animals vs. medium-injected or untreated SCI animals. These data suggest that **i)** the majority if not all axons which succumb to pathological processes resulting from secondary changes post injury such as edema, ischemia were already lost or irreversibly damaged at 3 days after trauma (i.e., the time point when the cells were grafted), or **ii)** regional cell grafting is not therapeutically effective in providing acute neuroprotection.

Analysis of the neurotransmitter phenotype in grafted cells showed the development of putative inhibitory GABA-ergic synapses with host neurons. These data show that the restoration

of the local functional inhibitory circuitry by grafted cells can in part lead to the observed functional improvements. While under specific pathological conditions (such as inflammatory or neuropathic pain) the spinal GABA can have excitatory effects due to reduced expression of the potassium-chloride exporter KCC2) [75, 76], systematic experimental but also clinical studies have demonstrated a potent anti-spasticity effect after intrathecal treatment with GABA_B receptor agonist baclofen, suggesting continuing inhibitory GABA_B receptor-mediated action [77, 78]. In addition, we have recently demonstrated an effective anti-spastic effect after spinal parenchymal GAD65 (glutamate decarboxylase) upregulation if combined with systemic tiagabine (GABA uptake inhibitor) treatment in animals with spinal ischemia-induced muscle spasticity [79]. Jointly, these data suggest the anti-spasticity effect observed in our current study can be mediated by a synaptically coupled GABA-inhibitory effect. Accordingly, in our previous study using the same cell line, we have demonstrated the development of putative GABA-ergic synaptic contacts between grafted neurons and persisting α -motoneurons of the host in a rat spinal ischemia model. In the same animals, a significant amelioration of spasticity was measured [29]. In a recent study using EM analysis, we have confirmed the development of synaptic contacts with the host neurons at 9 months after intraspinal grafting of HSSC in normal non-injured immunodeficient rats [30]. Similarly, in a more recent study, the development of functional contacts and restoration of axon potential conductivity across the region of complete Th3 spinal transection by grafted HSSC was seen [32].

In addition to restoration of the local motor circuitry, significant amelioration of otherwise increased spinal CGRP expression seen in non-treated SCI animals was measured in SCI animals receiving spinal injections of HSSC. Consistent with this observation, previous studies have demonstrated that improvement of local spinal GABA-ergic tone, as achieved by subcutaneous inoculation of a replication-incompetent herpes simplex virus (HSV) encoding GAD67 gene in a

Th13 spinal cord hemisection model, led to a similar decrease in otherwise increased CGRP expression [80]. Second, previous studies have shown that spinally grafted **HSSC** show the expression of several trophic factors (GDNF, BDNF, and VEGF) at 2 months after grafting in SOD+ rats [60]. We speculate that the release of these trophic factors can potentiate the sprouting of persisting axons of the host below and above the injury and accelerate the development of new synaptic contacts particularly at longer post-grafting intervals.

Finally, we have demonstrated a near complete injury-cavity filling effect by the grafted cells at 2 months after grafting when the cells were grafted at 3 days after injury. This was in contrast to media-injected animals which showed consistent and extensive rostro-caudal spinal cord cavitation. These data suggest that early post injury cell grafting is desirable as it can effectively block the formation of the spinal cavity and its expansion and related long-term secondary spinal cord degeneration. A comparable cavity-filling effect and prevention in the progression of syringomyelia has been shown after spinal grafting of human embryonic or fetal SSCs in human patients with progressive post-traumatic syringomyelia [54, 55, 81].

It is important to note that the cavity-filling effect demonstrated in our current study was achieved without the use of any supporting matrices or additional topical growth factor(s) delivery. In our preliminary study, we have determined that while the density of grafted cells is relatively low to fill the cavity-forming region, the grafted cells continue to proliferate after grafting to the point when a cavity is near completely filled with grafted cells [unpublished data]. The cell proliferation is inhibited once the cavity is filled and after that the cells differentiate normally. That the cells do not develop into pre-neoplastic or neoplastic cells has been assessed in a 9-month tumorigenicity study with nude rats whose Th9 spinal cord segment was first injured by contusion (manuscript in preparation). Similarly, using the same cell line as used in our current study, we have previously reported a comparable low level of mitotic activity in

grafted cells at 6 weeks to 9 months after grafting in naïve immunodeficient rats or immunosuppressed minipigs [82].

Conclusions

In our current study, we demonstrate a functionally-defined treatment effect after spinal grafting of human GMP-grade fetal spinal stem cells in immunosuppressed SD rats with previous L3 contusion injury. This treatment effect was expressed as a significant improvement in motor and sensory function (gait/paw placement, stretch-induced muscle spasticity, and, mechanical and thermal sensitivity). **No significant differences were detected in other CatWalk parameters, motor evoked potentials, open field locomotor (BBB) score or ladder climbing test.** In addition, an effective filling of trauma-induced spinal cavity with grafted cells was seen in HSSC-treated animals at 2 months after grafting. Jointly, these data demonstrate that the use of this clinical grade NSI-566RSC cell line with already established favorable clinical safety profile represent a potential cell candidate for cell replacement therapy in patients with previous spinal traumatic injury.

Competing interest: Karl Johe, PhD is an employee of and receives salary from Neuralstem, Inc, which provided the cells used in this study. This study was in part funded by Neuralstem, Inc.

Authors' contribution: SvG carried out or participated in all *in vivo* work, statistical analysis, and was involved in drafting the manuscript and the design of the study. ML carried out immunohistochemistry and participated in behavioral assays. OK participated in spasticity assessments. OP and JG carried out myogenic motor evoked potential recordings. CS participated in animal surgeries and post-operative care. EA helped draft the manuscript. MH

and DG participated in immunohistochemistry and microscopy. SM carried out cell preparation and viability testing before grafting. KJ provided the cells used in this study and participated in the design of the study. MM conceived the study, participated in its design, and draft the manuscript. All authors read and approved the final manuscript.

Acknowledgements: We thank Sandee Nguyen who provided assistance with the care of the animals, Ronald Deumens who provided us with supervision and advice and Amber Millen for editorial assistance.

Figure Legends

Figure 1A-E: Schematic diagram of experimental design.

A: To induce spinal cord injury, a 35 g circular rod was placed on the exposed L3 spinal segment and spinal cord compressed in dorso-ventral direction for 15 min. **B:** Three days after injury, animals were randomly assigned to experimental groups and received spinal graft of HSSC or media only. A total of 12 injections were performed targeting the injury epicenter and adjacent areas (see Spinal Injection Map). **C:** After spinal injections, animals survived for 2 months while being continuously immunosuppressed and periodically tested for recovery of motor/sensory functions, changes in motor evoked potentials (MEPs) and gastrocnemius muscle spasticity response evoked by computer-controlled ankle rotation. **D:** At 2 months after treatment, animals were perfusion fixed with 4% paraformaldehyde and spinal cord MRI-imaged *in situ* before histological processing. **E:** After MRI imaging, spinal cords were dissected from the spinal column and spinal blocks prepared for plastic embedding (injury epicenter region) or cryostat sectioning and used for immunofluorescence staining (the regions just above and below the injury epicenter).

Figure 2A-D: Improvement in hind paw positioning and amelioration of muscle spasticity in SCI animals grafted with HSSC.

A: The CatWalk gait analysis of hind paw positioning was performed at 2 months after treatment. In comparison to SCI control animals, a significant improvement was seen in HSSC-grafted animals. **B1-B3:** An example of the sequence of paw step images taken from the CatWalk software in naïve (**B1**) SCI-control (**B2**) and SCI-HSSC-treated animals (**B3**). Note a

near complete paw footprint overlap between the front and the hind paws in naïve animals (**B1**) but a substantial dissociation in the paw footprint overlap in SCI controls (**B2**). A clearly recognizable improvement in paw footprint placement in SCI-HSSC-treated animals can be seen (**B3**). **C**: Statistical analysis showed significant suppression of spasticity response (expressed as a muscle resistance ratio: values at 2 months vs. 7 days post injury in “HIGH spasticity” HSSC-treated animals if compared to “HIGH spasticity” controls. **D**: To identify the presence of muscle spasticity in fully awake animals, the hind-paw ankle is rotated 40° at a velocity of 80°/sec using computer-controlled ankle-rotational device. The spasticity response is identified by exacerbated EMG activity measured in the gastrocnemius muscle and corresponding increase in muscle resistance measured by digital transducer. In control SCI animals with developed spasticity (i.e., “high spasticity”/HIGH group), no change in spasticity response if compared to 7 days post-vehicle injection was seen at 2 months (compare **D1** to **D3**). In contrast to SCI control animals, a clear decrease in spasticity response was seen in SCI-HSSC-treated animals at 2 months after cell injections (compare **D4** to **D6**). To identify the presence of mechanical resistance, animals are anesthetized with isoflurane at the end of the recording session and the contribution of mechanical resistance (i.e., isoflurane non-sensitive) is calculated. (**D2**, **D5**: data expressed as mean±SEM; one-way ANOVAs).

Figure 3A-C: Amelioration of hypoesthesia in SCI-HSSC-grafted animals.

A & B: Baseline and biweekly assessments of perceptible thresholds for (A) mechanical and (B) thermal stimuli, applied below the level of injury, showed a trend towards progressive recovery in SCI-HSSC-grafted animals. **C**: When expressed as percentages of the Maximal Possible Effect for mechanical and thermal perceptible thresholds improvements, SCI-HSSC-treated animals showed significant improvements in sensory function for both mechanical and thermal

components. (A-C: data expressed as mean±SEM; A-B: repeated measures ANOVAs; C: Student *t*-tests).

Figure 4A-D: Effective cavity-filling effect by transplanted cells in SCI HSSC-injected animals.

At the end of the 2-month post-treatment survival, animals were perfusion fixed with 4% paraformaldehyde, spinal column dissected and MRI-imaged in situ before spinal cord dissection for further histological processing. **A, B:** 3-D MRI images of spinal cord segments in animals with previous traumatic injury and treated with spinal **HSSC (A)** or media (**B**) injections. Note the near complete injected-cells cavity-filling effect in **HSSC-treated animals. A1, A2, B1, B2:** To validate the presence of grafted cells or cavitation at the epicenter of injury, the same region was histologically processed, semi-thin plastic sections prepared and compared to corresponding MRI image (compare A1 to A2 and B1 to B2). **C:** 2-D MRI image taken from naïve-non-injured animal. **D:** Quantification of the cavity and scar volume from serial MRI images showed a significantly decreased cavity and scar volumes in SCI-HSSC-injected animals if compared to media-injected SCI controls. (**D:** data expressed as mean±SEM; Student *t*-tests), (Scale Bars: A, B: 5 mm; A1, A2, B1, B2, C: 3 mm).

Figure 5A-G: Survival, differentiation and extensive axonal outgrowth from spinally grafted HSSC. **A:** Grafted GFP+ or hNUMA-positive cells filling near completely the lesion cavity at 8 weeks after grafting can be seen (yellow dotted area; inserts). **B:** Detail from “A” depicting a dense GFP+ neurite network in the lateral funiculus (LF) and with numerous axons projecting towards α -motoneurons and interneurons in the gray matter (insert). **C:** In areas with a dense GFP+ axodendritic network, clear hSYN immunoreactivity associated with GFP+ processes can be detected (yellow arrows). **D:** The majority of grafted hNUMA+ cells showed

development of the neuronal hNSE/DCX⁺ phenotype. **E, F:** A subpopulation of grafted hNUMA⁺ cells showed the astrocyte (hGFAP⁺) and oligodendrocyte (Olig 2) phenotype (**F**; yellow arrows). **G:** Using mitotic marker Ki67, regularly distributed hNUMA/Ki67⁺ grafted cells were identified (yellow arrows). (Scale Bars: A: 1.5 mm (inserts: 200 μ m); B: 600 μ m (insert: 75 μ m); C: 60 μ m; D: 20 μ m; E-G: 10 μ m).

Figure 6A, B: Development of putative GABA-ergic synaptic contact between HSSC and the host neurons.

A: Confocal analysis of hSYN/GFP/NeuN-stained sections shows numerous hSYN punctata associated with GFP⁺ processes derived from grafted cells. Some of the hSYN/GFP⁺ terminals were found to be in the vicinity of the host interneurons or α -motoneurons (**A**; inserts; white arrows). **B:** Triple staining with GAD65+67/GFP/NeuN antibody showed numerous double-stained GAD65+67/GFP⁺ terminals residing on or in the close vicinity of lumbar α -motoneurons (white arrows). (Scale Bars: A: 150 μ m (inserts: 30 μ m); B: 20 μ m).

Figure 7A-C: Significant decrease in the dorsal horn CGRP immunoreactivity caudal to the injury epicenter in SCI-HSSC-treated vs. SCI-control animals.

A-C: CGRP- (**A**), GAP-43- (**B**), and Iba1- (**C**) immunoreactivity in the dorsal horns (DH) caudal of the injury epicenter at 2 months after L3 SCI. The region of interest (ROI) was defined as outlined in **B and C** (left panels, red dotted line). **A:** The quantitative densitometry analysis of CGRP-immunostained images in the dorsal horns of SCI-HSSC-treated animals (**A2**) showed significantly decreased CGRP expression when compared to SCI-control animals (**A1**). **B, C:** The dorsal horn GAP-43 or IB1 immunoreactivity was not significantly different between experimental groups. (**A-C:** data expressed as mean \pm SEM; student *t*-tests). (Scale Bars: A - C: 500 μ m).

Supplemental Figures Legends

Supplemental Figure 1A-D: Effect of spinal HSSC grafting on locomotor function (BBB), foot stepping angle, ladder climbing test and motor evoked potentials. **A:** Weekly measurement of the BBB scores modified for the L3 injuries (left y-axis) and regular BBB scores (right y-axis) showed progressive recovery in both HSSC-grafted and control SCI animals. While there was a trend toward better motor performance in HSSC-grafted-animals, this effect was not significant for both scoring systems. **B:** Single Frame Analysis showed a tendency towards regaining normal foot stepping angles between the paw and floor (measured at stance-phase initiation; see insert/drawing in **B**) in SCI-HSSC-treated animals. However, the angles were not significantly improved if compared to SCI controls. **C:** Using the ladder climbing test, we found a significant decrease in number of correct steps in SCI animals if compared to naïve controls. No significant difference was seen between SCI-control and SCI-HSSC-treated animals if analyzed at 2 months after treatments. **D:** Motor Evoked Potentials recorded at baseline (i.e., before injury) and at 8 weeks post injury showed a significant decrease only for the SCI-control animals. No significant difference between HSSC-grafted and control SCI animals was detected.

Supplemental Figure 2A-D: Quantitative analysis of axonal survival in the epicenter of injury showed no significant differences between SCI-control and SCI-HSSC-treated animals.

A: Schematic diagram of the axon counting design used in our current study. Axons were counted in plastic osmium-stained sections in the dorsal, lateral and ventral funiculi using ImageJ

software. An example of the detection threshold to identify individual axons in a selected field is shown in A2 and A3. **B:** Transverse plastic section depicting a bilaterally distributed graft (red dashed line) and completely filling the cavity created by previous spinal compression. Note that the fusion of the graft with the host tissue is so advanced that the border between the previous injury-evoked cavity and the graft is difficult to delineate (red asterisks). **C:** An example of transverse spinal cord section taken from an animal receiving media injection. An extensive cavity occupying near completely the region of previous gray matter can be seen. **D:** Quantification of axons in SCI-control and SCI-HSSC-treated animals showed no significant differences if analyzed in dorsal, lateral or ventral funiculi or if sub-divided into axons of different caliber (S=small=0.3–1.0 μm ; M=medium=1.0–2.5 μm ; L=large=2.5–10 μm). (Scale Bars: A-C: 500 μm).

References

1. Hagg T, Oudega M: Degenerative and spontaneous regenerative processes after spinal cord injury. *Journal of neurotrauma* 2006, 23:264-280.
2. Jones CF, Cripton PA, Kwon BK: Gross Morphological Changes of the Spinal Cord Immediately After Surgical Decompression in a Large Animal Model of Traumatic Spinal Cord Injury. *Spine* 2012, 37:E890-E899.
3. Oudega M: Molecular and cellular mechanisms underlying the role of blood vessels in spinal cord injury and repair. *Cell and tissue research* 2012, 349:269-288.
4. Bracken MB: Steroids for acute spinal cord injury. *Cochrane Database Syst Rev* 2012, 1:CD001046.
5. Fleming JC, Norenberg MD, Ramsay DA, Dekaban GA, Marcillo AE, Saenz AD, Pasquale-Styles M, Dietrich WD, Weaver LC: The cellular inflammatory response in human spinal cords after injury. *Brain : a journal of neurology* 2006, 129:3249-3269.
6. David S, Kroner A: Repertoire of microglial and macrophage responses after spinal cord injury. *Nature reviews Neuroscience* 2011, 12:388-399.
7. Ankeny DP, Popovich PG: Mechanisms and implications of adaptive immune responses after traumatic spinal cord injury. *Neuroscience* 2009, 158:1112-1121.
8. Lu P, Tuszynski MH: Growth factors and combinatorial therapies for CNS regeneration. *Experimental neurology* 2008, 209:313-320.
9. Sahni V, Kessler JA: Stem cell therapies for spinal cord injury. *Nature reviews Neurology* 2010, 6:363-372.
10. Llado J, Haenggeli C, Maragakis NJ, Snyder EY, Rothstein JD: Neural stem cells protect against glutamate-induced excitotoxicity and promote survival of injured motor neurons through the secretion of neurotrophic factors. *Molecular and cellular neurosciences* 2004, 27:322-331.
11. Bonner JF, Connors TM, Silverman WF, Kowalski DP, Lemay MA, Fischer I: Grafted neural progenitors integrate and restore synaptic connectivity across the injured spinal cord. *The Journal of neuroscience : the official journal of the Society for Neuroscience* 2011, 31:4675-4686.
12. White TE, Lane MA, Sandhu MS, O'Steen BE, Fuller DD, Reier PJ: Neuronal progenitor transplantation and respiratory outcomes following upper cervical spinal cord injury in adult rats. *Experimental neurology* 2010, 225:231-236.
13. Magnuson DS, Zhang YP, Cao QL, Han Y, Burke DA, Whittemore SR: Embryonic brain precursors transplanted into kainate lesioned rat spinal cord. *Neuroreport* 2001, 12:1015-1019.
14. Boido M, Garbossa D, Vercelli A: Early graft of neural precursors in spinal cord compression reduces glial cyst and improves function. *Journal of neurosurgery Spine* 2011, 15:97-106.
15. Erceg S, Ronaghi M, Oria M, Rosello MG, Arago MA, Lopez MG, Radojevic I, Moreno-Manzano V, Rodriguez-Jimenez FJ, Bhattacharya SS, et al: Transplanted oligodendrocytes and motoneuron progenitors generated from human embryonic stem cells promote locomotor recovery after spinal cord transection. *Stem Cells* 2010, 28:1541-1549.
16. Hendricks WA, Pak ES, Owensby JP, Menta KJ, Glazova M, Moretto J, Hollis S, Brewer KL, Murashov AK: Predifferentiated embryonic stem cells prevent chronic pain behaviors and restore sensory function following spinal cord injury in mice.

- Mol Med* 2006, 12:34-46.
17. Donnelly EM, Lamanna J, Boulis NM: Stem cell therapy for the spinal cord. *Stem cell research & therapy* 2012, 3:24.
 18. Willerth SM: Neural tissue engineering using embryonic and induced pluripotent stem cells. *Stem cell research & therapy* 2011, 2:17.
 19. Ferrari D, Binda E, De Filippis L, Vescovi AL: Isolation of neural stem cells from neural tissues using the neurosphere technique. *Current protocols in stem cell biology* 2010, Chapter 2:Unit2D 6.
 20. Svendsen CN, ter Borg MG, Armstrong RJ, Rosser AE, Chandran S, Ostenfeld T, Caldwell MA: A new method for the rapid and long term growth of human neural precursor cells. *Journal of neuroscience methods* 1998, 85:141-152.
 21. Carpenter MK, Cui X, Hu ZY, Jackson J, Sherman S, Seiger A, Wahlberg LU: In vitro expansion of a multipotent population of human neural progenitor cells. *Experimental neurology* 1999, 158:265-278.
 22. Yan J, Xu L, Welsh AM, Chen D, Hazel T, Johe K, Koliatsos VE: Combined immunosuppressive agents or CD4 antibodies prolong survival of human neural stem cell grafts and improve disease outcomes in amyotrophic lateral sclerosis transgenic mice. *Stem Cells* 2006, 24:1976-1985.
 23. Uchida N, Buck DW, He D, Reitsma MJ, Masek M, Phan TV, Tsukamoto AS, Gage FH, Weissman IL: Direct isolation of human central nervous system stem cells. *Proceedings of the National Academy of Sciences of the United States of America* 2000, 97:14720-14725.
 24. Vescovi AL, Parati EA, Gritti A, Poulin P, Ferrario M, Wanke E, Frolichsthal-Schoeller P, Cova L, Arcellana-Panlilio M, Colombo A, Galli R: Isolation and cloning of multipotential stem cells from the embryonic human CNS and establishment of transplantable human neural stem cell lines by epigenetic stimulation. *Experimental neurology* 1999, 156:71-83.
 25. Guo X, Johe K, Molnar P, Davis H, Hickman J: Characterization of a human fetal spinal cord stem cell line, NSI-566RSC, and its induction to functional motoneurons. *Journal of tissue engineering and regenerative medicine* 2010, 4:181-193.
 26. Clinical Trials with 'huCNS-SC'; NLM database search results
[\[http://www.clinicaltrials.gov/ct2/results?term=hucns-sc\]](http://www.clinicaltrials.gov/ct2/results?term=hucns-sc)
 27. A Phase I, Open-label, First in Human, Feasibility and Safety Study of Human Spinal Cord Derived Neural Stem Cell Transplantation for the Treatment of Amyotrophic Lateral Sclerosis - Identifier: NCT01348451
[\[http://www.clinicaltrial.gov/ct2/show/NCT01348451\]](http://www.clinicaltrial.gov/ct2/show/NCT01348451)
 28. Jacobs Y, Selden N, Al-Uzri A, Koch T, Vogel H, Huhn S, Uchida N, Dalma-Weiszhausz D, Tsukamoto A, Steiner R: Long-term Survival and Migration of Allogeneic Human Central Nervous System Stem Cells following Intracerebral Transplantation in Neuronal Ceroid Lipofuscinosis. In *Book Long-term Survival and Migration of Allogeneic Human Central Nervous System Stem Cells following Intracerebral Transplantation in Neuronal Ceroid Lipofuscinosis* (Editor ed.^eds.). City; June 2011.
 29. Cizkova D, Kakinohana O, Kucharova K, Marsala S, Johe K, Hazel T, Hefferan MP, Marsala M: Functional recovery in rats with ischemic paraplegia after spinal grafting of human spinal stem cells. *Neuroscience* 2007, 147:546-560.
 30. Hefferan MP, Galik J, Kakinohana O, Sekerkova G, Santucci C, Marsala S, Navarro R, Hruska-Plochan M, Johe K, Feldman E, et al: Human neural stem cell replacement therapy for amyotrophic lateral sclerosis by spinal transplantation.

- PLoS one* 2012, 7:e42614.
31. Boulis NM, Federici T, Glass JD, Lunn JS, Sakowski SA, Feldman EL: Translational stem cell therapy for amyotrophic lateral sclerosis. *Nature reviews Neurology* 2011, 8:172-176.
 32. Lu P, Wang Y, Graham L, McHale K, Gao M, Wu D, Brock J, Blesch A, Rosenzweig ES, Havton LA, et al: Long-distance growth and connectivity of neural stem cells after severe spinal cord injury. *Cell* 2012, 150:1264-1273.
 33. Hefferan MP, Johe K, Hazel T, Feldman EL, Lunn JS, Marsala M: Optimization of immunosuppressive therapy for spinal grafting of human spinal stem cells in a rat model of ALS. *Cell transplantation* 2011, 20:1153-1161.
 34. Johe KK, Hazel TG, Muller T, Dugich-Djordjevic MM, McKay RD: Single factors direct the differentiation of stem cells from the fetal and adult central nervous system. *Genes & development* 1996, 10:3129-3140.
 35. Basso DM, Beattie MS, Bresnahan JC: A sensitive and reliable locomotor rating scale for open field testing in rats. *Journal of neurotrauma* 1995, 12:1-21.
 36. Deumens R, Koopmans GC, Honig WM, Maquet V, Jerome R, Steinbusch HW, Joosten EA: Limitations in transplantation of astroglia-biomatrix bridges to stimulate corticospinal axon regrowth across large spinal lesion gaps. *Neuroscience letters* 2006, 400:208-212.
 37. Semler J, Wellmann K, Wirth F, Stein G, Angelova S, Ashrafi M, Schempf G, Ankerne J, Ozsoy O, Ozsoy U, et al: Objective measures of motor dysfunction after compression spinal cord injury in adult rats: correlations with locomotor rating scores. *Journal of neurotrauma* 2011, 28:1247-1258.
 38. Apostolova I, Irintchev A, Schachner M: Tenascin-R restricts posttraumatic remodeling of motoneuron innervation and functional recovery after spinal cord injury in adult mice. *The Journal of neuroscience : the official journal of the Society for Neuroscience* 2006, 26:7849-7859.
 39. Marsala M, Hefferan MP, Kakinohana O, Nakamura S, Marsala J, Tomori Z: Measurement of peripheral muscle resistance in rats with chronic ischemia-induced paraplegia or morphine-induced rigidity using a semi-automated computer-controlled muscle resistance meter. *Journal of neurotrauma* 2005, 22:1348-1361.
 40. Mills C, Leblond D, Joshi S, Zhu C, Hsieh G, Jacobson P, Meyer M, Decker M: Estimating efficacy and drug ED50's using von Frey thresholds: impact of weber's law and log transformation. *The journal of pain : official journal of the American Pain Society* 2012, 13:519-523.
 41. Navarro R, Juhas S, Keshavarzi S, Juhasova J, Motlik J, Johe K, Marsala S, Scadeng M, Lazar P, Tomori Z, et al: Chronic spinal compression model in minipigs: a systematic behavioral, qualitative, and quantitative neuropathological study. *Journal of neurotrauma*, 29:499-513.
 42. Koopmans GC, Deumens R, Honig WM, Hamers FP, Steinbusch HW, Joosten EA: The assessment of locomotor function in spinal cord injured rats: the importance of objective analysis of coordination. *Journal of neurotrauma* 2005, 22:214-225.
 43. Ondarza AB, Ye Z, Hulsebosch CE: Direct evidence of primary afferent sprouting in distant segments following spinal cord injury in the rat: colocalization of GAP-43 and CGRP. *Experimental neurology* 2003, 184:373-380.
 44. Hains BC, Waxman SG: Activated microglia contribute to the maintenance of chronic pain after spinal cord injury. *The Journal of neuroscience : the official journal of the Society for Neuroscience* 2006, 26:4308-4317.
 45. Taira Y, Marsala M: Effect of proximal arterial perfusion pressure on function,

- spinal cord blood flow, and histopathologic changes after increasing intervals of aortic occlusion in the rat. *Stroke; a journal of cerebral circulation* 1996, 27:1850-1858.
46. Marsala M, Yaksh TL: Transient spinal ischemia in the rat: characterization of behavioral and histopathological consequences as a function of the duration of aortic occlusion. *Journal of cerebral blood flow and metabolism : official journal of the International Society of Cerebral Blood Flow and Metabolism* 1994, 14:526-535.
 47. Collazos-Castro JE, Soto VM, Gutierrez-Davila M, Nieto-Sampedro M: Motoneuron loss associated with chronic locomotion impairments after spinal cord contusion in the rat. *Journal of neurotrauma* 2005, 22:544-558.
 48. Magnuson DS, Lovett R, Coffee C, Gray R, Han Y, Zhang YP, Burke DA: Functional consequences of lumbar spinal cord contusion injuries in the adult rat. *Journal of neurotrauma* 2005, 22:529-543.
 49. Bose P, Parmer R, Thompson FJ: Velocity-dependent ankle torque in rats after contusion injury of the midthoracic spinal cord: time course. *J Neurotrauma* 2002, 19:1231-1249.
 50. Bunge RP, Puckett WR, Becerra JL, Marcillo A, Quencer RM: Observations on the pathology of human spinal cord injury. A review and classification of 22 new cases with details from a case of chronic cord compression with extensive focal demyelination. *Adv Neurol* 1993, 59:75-89.
 51. Adams MM, Hicks AL: Spasticity after spinal cord injury. *Spinal cord* 2005, 43:577-586.
 52. Ek CJ, Habgood MD, Callaway JK, Dennis R, Dziegielewska KM, Johansson PA, Potter A, Wheaton B, Saunders NR: Spatio-temporal progression of grey and white matter damage following contusion injury in rat spinal cord. *PloS one* 2010, 5:e12021.
 53. Bramlett HM, Dietrich WD: Progressive damage after brain and spinal cord injury: pathomechanisms and treatment strategies. *Progress in brain research* 2007, 161:125-141.
 54. Falci S, Holtz A, Akesson E, Azizi M, Ertzgaard P, Hultling C, Kjaeldgaard A, Levi R, Ringden O, Westgren M, et al: Obliteration of a posttraumatic spinal cord cyst with solid human embryonic spinal cord grafts: first clinical attempt. *Journal of neurotrauma* 1997, 14:875-884.
 55. Wirth ED, 3rd, Reier PJ, Fessler RG, Thompson FJ, Uthman B, Behrman A, Beard J, Vierck CJ, Anderson DK: Feasibility and safety of neural tissue transplantation in patients with syringomyelia. *Journal of neurotrauma* 2001, 18:911-929.
 56. Hawryluk GW, Mothe A, Wang J, Wang S, Tator C, Fehlings MG: An In Vivo Characterization of Trophic Factor Production Following Neural Precursor Cell or Bone Marrow Stromal Cell Transplantation for Spinal Cord Injury. *Stem cells and development* 2012.
 57. Yan J, Welsh AM, Bora SH, Snyder EY, Koliatsos VE: Differentiation and tropic/trophic effects of exogenous neural precursors in the adult spinal cord. *The Journal of comparative neurology* 2004, 480:101-114.
 58. Lu P, Jones LL, Snyder EY, Tuszynski MH: Neural stem cells constitutively secrete neurotrophic factors and promote extensive host axonal growth after spinal cord injury. *Experimental neurology* 2003, 181:115-129.
 59. Yan J, Xu L, Welsh AM, Hatfield G, Hazel T, Johe K, Koliatsos VE: Extensive neuronal differentiation of human neural stem cell grafts in adult rat spinal cord. *PLoS medicine* 2007, 4:e39.

60. Xu L, Yan J, Chen D, Welsh AM, Hazel T, Johe K, Hatfield G, Koliatsos VE: Human neural stem cell grafts ameliorate motor neuron disease in SOD-1 transgenic rats. *Transplantation* 2006, 82:865-875.
61. Fagerlund M, Estrada CP, Jaff N, Svensson M, Brundin L: Neural Stem/Progenitor Cells Transplanted to the Hypoglossal Nucleus Integrates with the Host CNS in Adult Rats and Promotes Motor Neuron Survival. *Cell transplantation* 2011.
62. Rota Nodari L, Ferrari D, Giani F, Bossi M, Rodriguez-Menendez V, Tredici G, Delia D, Vescovi AL, De Filippis L: Long-term survival of human neural stem cells in the ischemic rat brain upon transient immunosuppression. *PloS one* 2010, 5:e14035.
63. Lepore AC, Neuhuber B, Connors TM, Han SS, Liu Y, Daniels MP, Rao MS, Fischer I: Long-term fate of neural precursor cells following transplantation into developing and adult CNS. *Neuroscience* 2006, 142:287-304.
64. Cummings BJ, Uchida N, Tamaki SJ, Anderson AJ: Human neural stem cell differentiation following transplantation into spinal cord injured mice: association with recovery of locomotor function. *Neurological research* 2006, 28:474-481.
65. Hofstetter CP, Holmstrom NA, Lilja JA, Schweinhardt P, Hao J, Spenger C, Wiesenfeld-Hallin Z, Kurpad SN, Frisen J, Olson L: Allodynia limits the usefulness of intraspinal neural stem cell grafts; directed differentiation improves outcome. *Nature neuroscience* 2005, 8:346-353.
66. Mitsui T, Shumsky JS, Lepore AC, Murray M, Fischer I: Transplantation of neuronal and glial restricted precursors into contused spinal cord improves bladder and motor functions, decreases thermal hypersensitivity, and modifies intraspinal circuitry. *The Journal of neuroscience : the official journal of the Society for Neuroscience* 2005, 25:9624-9636.
67. McDonald JW, Liu XZ, Qu Y, Liu S, Mickey SK, Turetsky D, Gottlieb DI, Choi DW: Transplanted embryonic stem cells survive, differentiate and promote recovery in injured rat spinal cord. *Nature medicine* 1999, 5:1410-1412.
68. Alexanian AR, Svendsen CN, Crowe MJ, Kurpad SN: Transplantation of human glial-restricted neural precursors into injured spinal cord promotes functional and sensory recovery without causing allodynia. *Cytotherapy* 2011, 13:61-68.
69. Davies JE, Proschel C, Zhang N, Noble M, Mayer-Proschel M, Davies SJ: Transplanted astrocytes derived from BMP- or CNTF-treated glial-restricted precursors have opposite effects on recovery and allodynia after spinal cord injury. *Journal of biology* 2008, 7:24.
70. Macias MY, Syring MB, Pizzi MA, Crowe MJ, Alexanian AR, Kurpad SN: Pain with no gain: allodynia following neural stem cell transplantation in spinal cord injury. *Experimental neurology* 2006, 201:335-348.
71. Davies JE, Huang C, Proschel C, Noble M, Mayer-Proschel M, Davies SJ: Astrocytes derived from glial-restricted precursors promote spinal cord repair. *Journal of biology* 2006, 5:7.
72. Jin Y, Neuhuber B, Singh A, Bouyer J, Lepore A, Bonner J, Himes T, Campanelli JT, Fischer I: Transplantation of human glial restricted progenitors and derived astrocytes into a contusion model of spinal cord injury. *Journal of neurotrauma* 2011, 28:579-594.
73. Bastrup C, Maersk-Moller CC, Nyengaard JR, Jensen TS, Finnerup NB: Spinal-, brainstem- and cerebrally mediated responses at- and below-level of a spinal cord contusion in rats: evaluation of pain-like behavior. *Pain* 2010, 151:670-679.
74. Hofstetter CP, Schweinhardt P, Klason T, Olson L, Spenger C: Numb rats walk - a

- behavioural and fMRI comparison of mild and moderate spinal cord injury. *The European journal of neuroscience* 2003, 18:3061-3068.
75. Anseloni VC, Gold MS: Inflammation-induced shift in the valence of spinal GABA-A receptor-mediated modulation of nociception in the adult rat. *The journal of pain : official journal of the American Pain Society* 2008, 9:732-738.
 76. Coull JA, Boudreau D, Bachand K, Prescott SA, Nault F, Sik A, De Koninck P, De Koninck Y: Trans-synaptic shift in anion gradient in spinal lamina I neurons as a mechanism of neuropathic pain. *Nature* 2003, 424:938-942.
 77. Rawlins PK: Intrathecal baclofen therapy over 10 years. *The Journal of neuroscience nursing : journal of the American Association of Neuroscience Nurses* 2004, 36:322-327.
 78. Kakinohana O, Hefferan MP, Nakamura S, Kakinohana M, Galik J, Tomori Z, Marsala J, Yaksh TL, Marsala M: Development of GABA-sensitive spasticity and rigidity in rats after transient spinal cord ischemia: a qualitative and quantitative electrophysiological and histopathological study. *Neuroscience* 2006, 141:1569-1583.
 79. Kakinohana O, Hefferan MP, Miyahara A, Nejime T, Marsala S, Juhas S, Juhasova J, Motlik J, Kucharova K, Strnadel J, et al: Combinational spinal GAD65 gene delivery and systemic GABA-mimetic treatment for modulation of spasticity. *PloS one* 2012, 7:e30561.
 80. Liu J, Wolfe D, Hao S, Huang S, Glorioso JC, Mata M, Fink DJ: Peripherally delivered glutamic acid decarboxylase gene therapy for spinal cord injury pain. *Molecular therapy : the journal of the American Society of Gene Therapy* 2004, 10:57-66.
 81. Biyani A, el Masry WS: Post-traumatic syringomyelia: a review of the literature. *Paraplegia* 1994, 32:723-731.
 82. Usvald D, Vodicka P, Hlucilova J, Prochazka R, Motlik J, Kucharova K, Johe K, Marsala S, Scadeng M, Kakinohana O, et al: Analysis of dosing regimen and reproducibility of intraspinal grafting of human spinal stem cells in immunosuppressed minipigs. *Cell transplantation* 2010, 19:1103-1122.

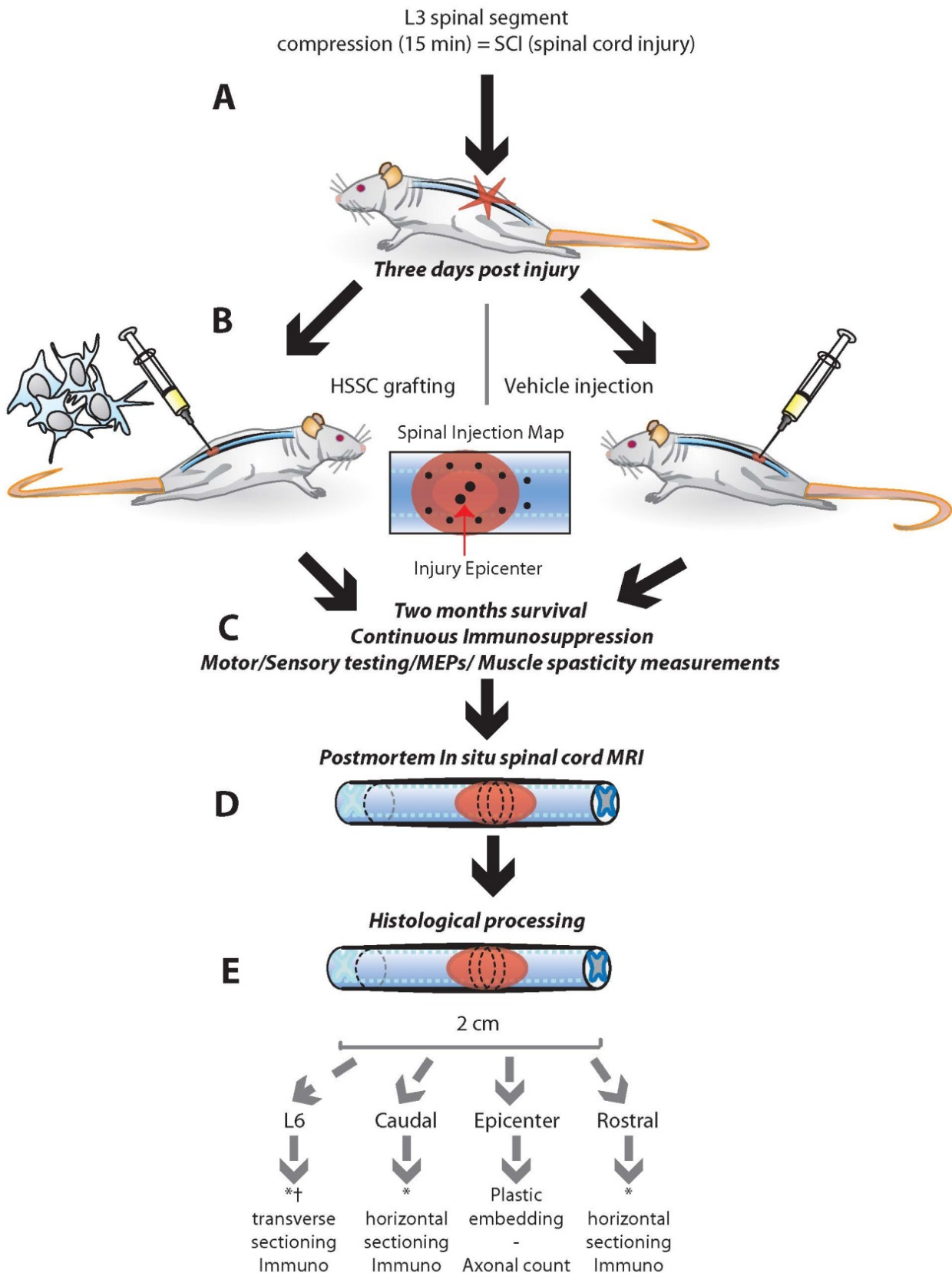


Fig.1 A-E

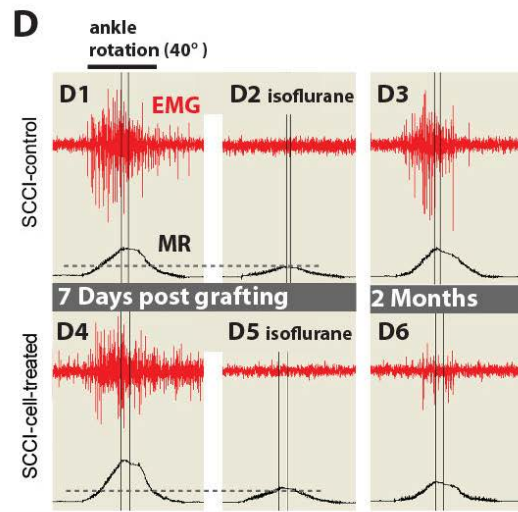
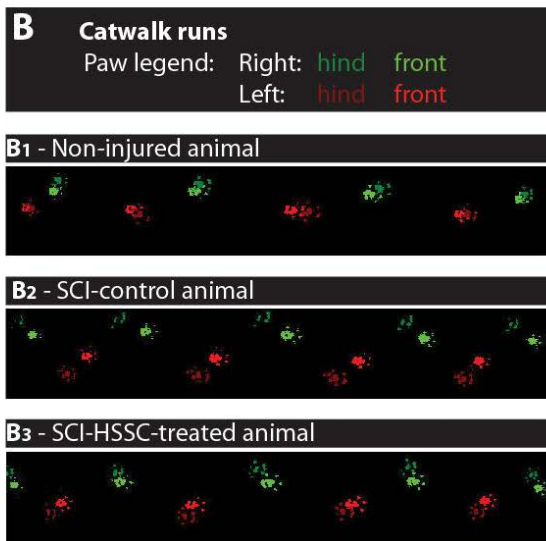
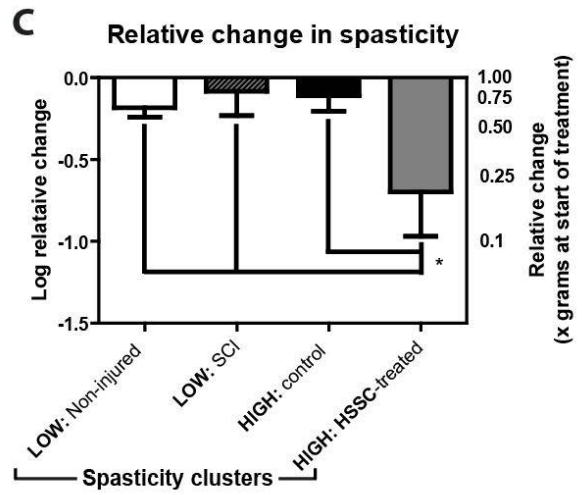
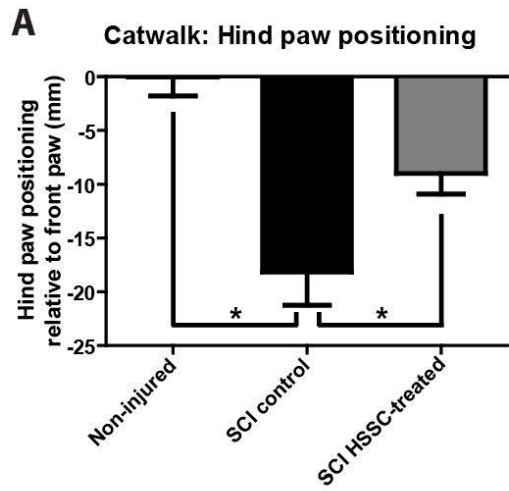


Fig.2 A-D
Figure 2

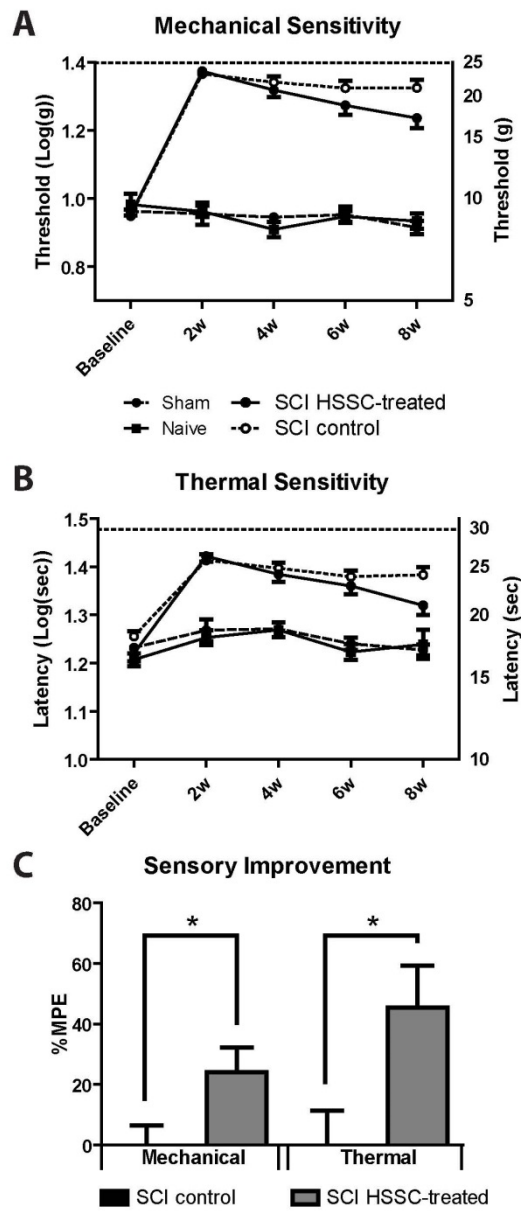


Fig.3 A-C

Figure 3

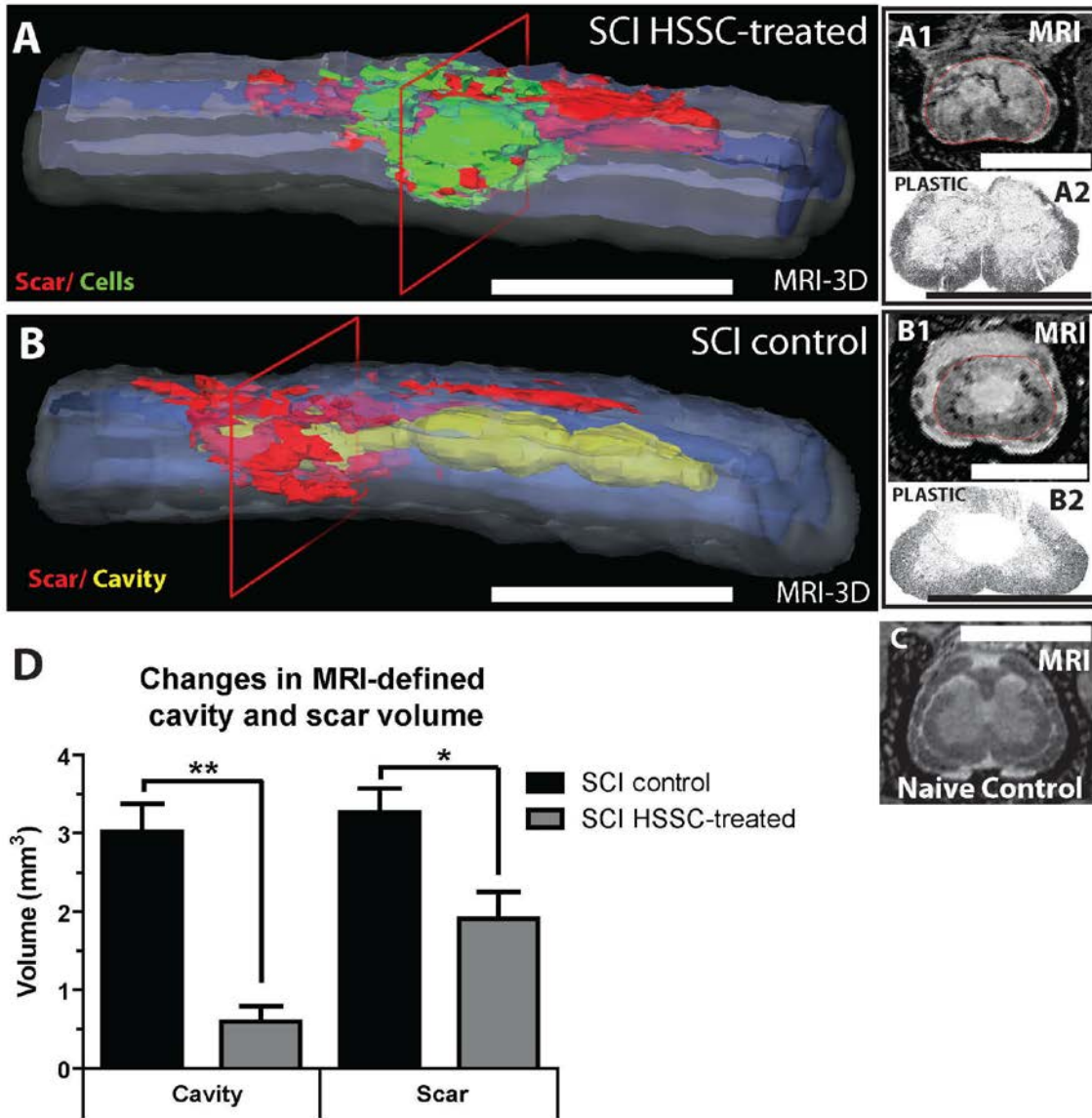


Fig.4 A-D

Figure 4

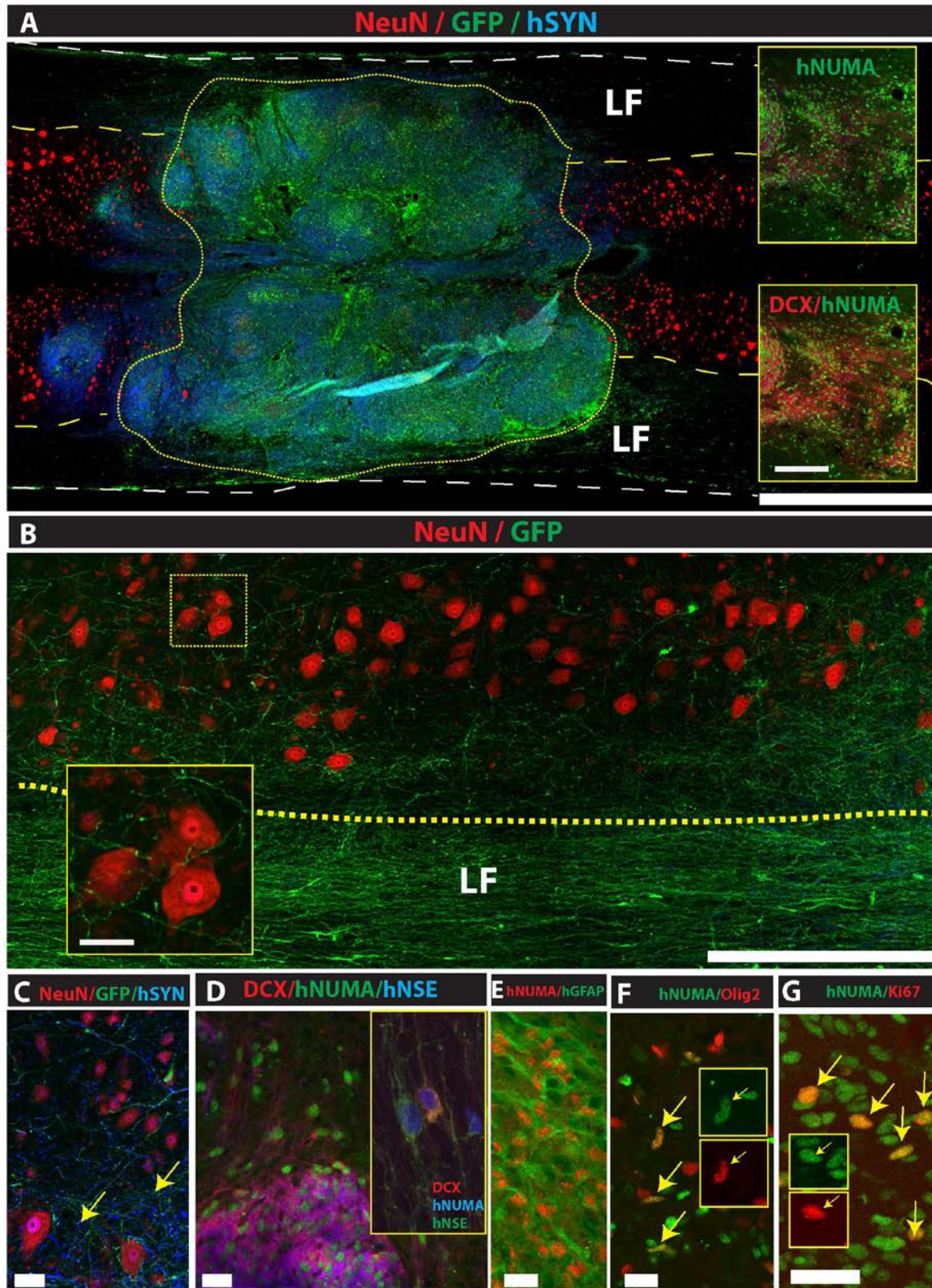


Fig.5 A-G

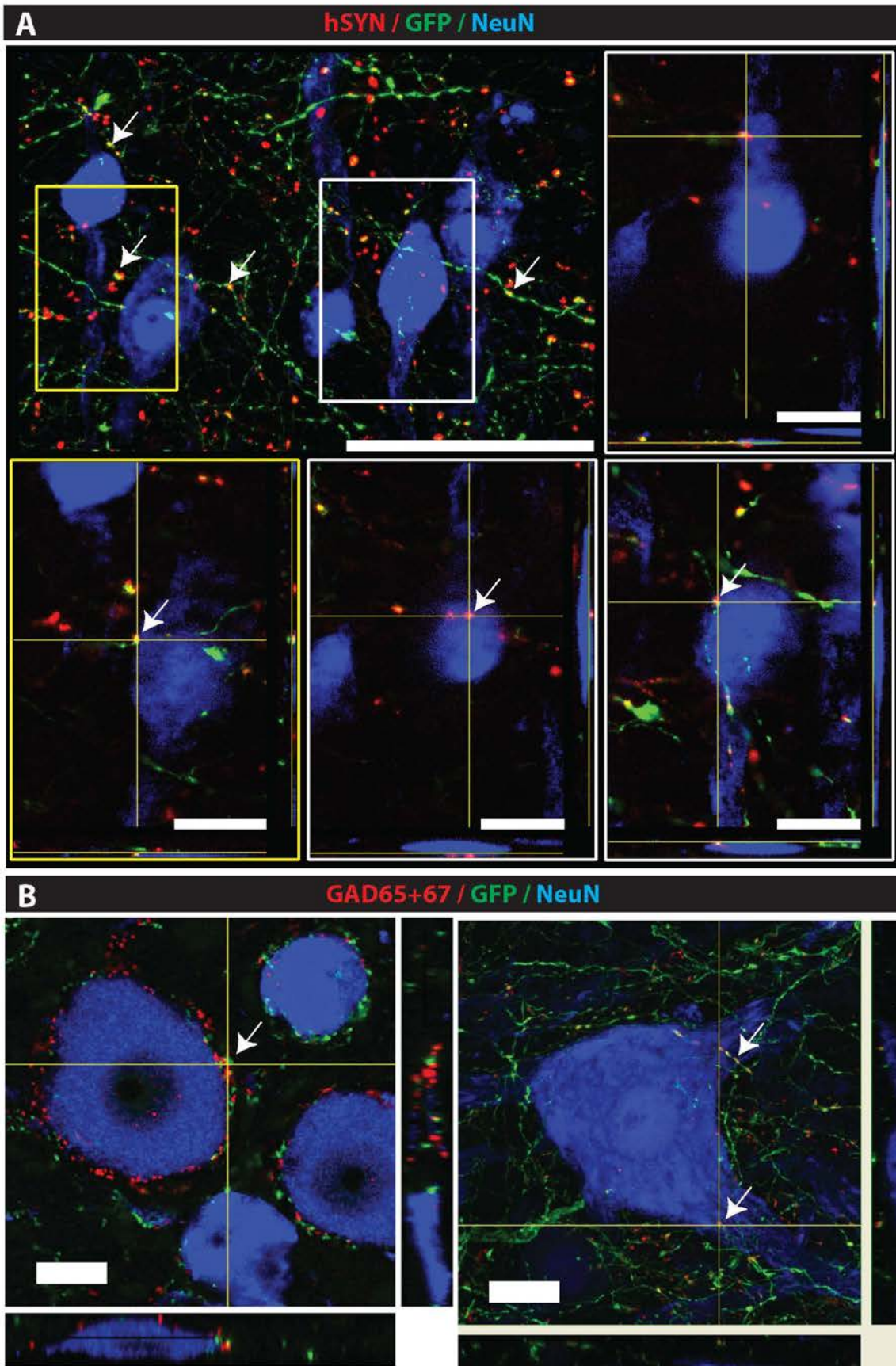


Fig.6A, B
Figure 6

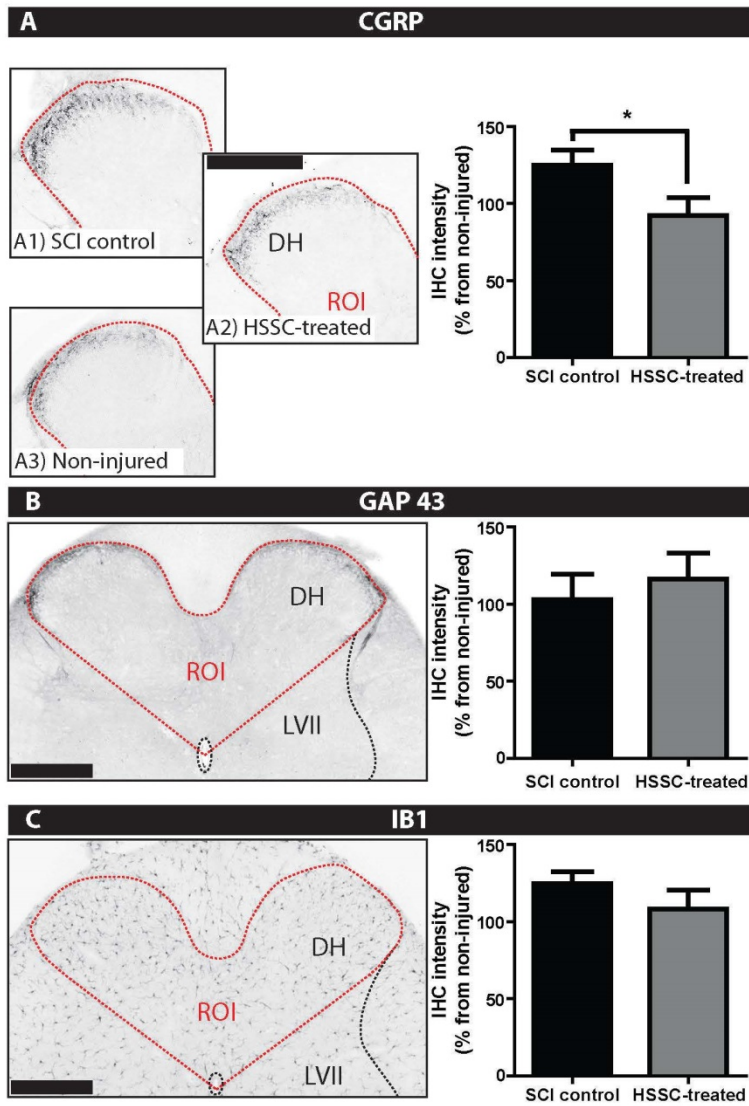


Fig.7

Figure 7

Additional files provided with this submission:

Additional file 1: Suppl Fig.1.tif, 805K

<http://stemcellres.com/imedia/3307253092017684/supp1.tif>

Additional file 2: Suppl Fig.2.tif, 1356K

<http://stemcellres.com/imedia/4937860192017684/supp2.tif>

Additional file 3: Competing interests-completed-marsala.docx, 93K

<http://stemcellres.com/imedia/3754864092317435/supp3.docx>

5.5. Evaluation of Tacrolimus-loaded releasable pellets as an alternative and effective immunosuppression protocol in rat spinal cord transplantation studies

in publication

Effective long-term immunosuppression in rats by subcutaneously implanted sustained-release tacrolimus pellet: effect on spinally grafted human neural precursors survival.

Sevc J, Goldberg D, van Gorp S, Leerink M, Juhas S, Juhasova J, Marsala S, **Hruska-Plochan M**, Hefferan MP, Motlik J, Rypacek F, Machova L, Kakinohana O, Santucci C, Johe K, Lukacova N, Yamada K, Bui JD, Marsala M.


Manuscript in revision in journal "Experimental Neurology"

IF (2012): 4.699; 5-year IF (2012): 4.416

Declaration of co-authors

"I hereby declare that Marián Hruška-Plochán was adequately involved (30%) in the study design, experiments, interpretation of results and writing of this manuscript."

San Diego, April 29 2013


Martin Maršala, Prof. MD.

Effective long-term immunosuppression in rats by subcutaneously implanted sustained-release tacrolimus pellet: effect on spinally grafted human neural precursors survival.

^{1,2}Juraj Sevc, ¹Danielle Goldberg, ³Sebastiaan van Gorp, ¹Marjolein Leerink, ⁴Stefan Juhas, ⁴Jana Juhasova, ¹Silvia Marsala, ^{1,4,5}Marian Hruska-Plochan, ⁷Michael P Hefferan, ⁴Jan Motlik, ⁶Frantisek Rypacek, ⁶Ludka Machova, ¹Osamu Kakinohana, ¹Camila Santucci, ⁷Karl Johe, ⁸Nadezda Lukacova, ⁹Kazuhiko Yamada, ¹⁰Jack D Bui, ¹Martin Marsala

(1) Neuroregeneration Laboratory, Department of Anesthesiology,
University of California - San Diego, La Jolla, CA, USA;

(2) Institute of Biology and Ecology, Faculty of Science, P.J. Safarik University, Moyzes street
11, 040 01 Kosice, Slovakia;

(3) Department of Anesthesiology, Maastricht University Medical Center, Maastricht 6202 AZ,
Netherlands;

(4) Institute of Animal Physiology and Genetics, Czech Academy of Sciences, Rumburska 89,
277 21 Libechov, Czech Republic;

(5) Department of Cell Biology, Faculty of Science, Charles University in Prague, Prague, Czech
Republic;

(6) Institute of Macromolecular Chemistry, Academy of Sciences of the Czech Republic,
Heyrovsky Sq 2, 162 06 Prague 6, Czech Republic;

(7) Neuralstem, Inc., 9700 Great Seneca Highway, Rockville, MD 20850 USA;

(8) Institute of Neurobiology, Slovak Academy of Sciences, Soltesovej 6, Kosice, Slovakia;

(9) Transplantation Biology Research Center, Massachusetts General Hospital, Boston,
Massachusetts 02129, USA;

(10) Department of Pathology, University of California - San Diego, La Jolla, CA, USA

Corresponding author:

Martin Marsala, M.D.

UCSD

Neuroregeneration Laboratory

Department of Anesthesiology

Sanford Consortium for Regenerative Medicine

2880 Torrey Pines Scenic Drive

La Jolla, CA 92037

Ph (office): 858-822-3805

Ph (lab) 858-534-7380

Fax: 858-822-3249

Abstract

Achievement of effective, safe and long-term immunosuppression represents one of the challenges in experimental allogeneic and xenogeneic cell and organ transplantation. The goal of the present study was to develop a reliable, long-term immunosuppression protocol in Sprague-Dawley (SD) rats by: 1) comparing the pharmacokinetics of four different subcutaneously delivered/implanted tacrolimus (TAC) formulations, including: i) castor oil/saline solution, ii) unilamellar or multilamellar liposomes, iii) biodegradable microspheres, and iv) biodegradable 3-month lasting pellets; and 2) defining the survival and immune response in animals receiving spinal injections of human neural precursors at 6 weeks to 3 months after cell grafting. In animals implanted with TAC pellets (3.4 mg/kg/day), a stable 3-month lasting plasma concentration of TAC averaging 19.1 ± 4.9 ng/ml was measured. Analysis of grafted cell survival in SOD⁺ or spinal trauma-injured SD rats immunosuppressed with 3-month lasting TAC pellets (3.4-5.1 mg/kg/day) showed the consistent presence of implanted human neurons with minimal or no local T-cell infiltration. These data demonstrate that the use of TAC pellets can represent an effective, long-lasting immunosuppressive drug delivery system that is safe, simple to implement and is associated with a long-term human neural precursor survival after grafting into the spinal cord of SOD⁺ or spinal trauma-injured SD rats.

Key words: immunosuppression, xenograft, human neural precursors, spinal grafting, Sprague-Dawley rat, T-lymphocyte, tacrolimus pellet

Introduction

One of the essential requirements for successful translation of experimentally-defined cell-based replacement therapies which utilize the allogeneic or xenogeneic cell grafts into clinical practice is the development of safe and effective immunosuppression protocols that will permit long-term survival and maturation of grafted cells. Current clinical and experimental immunosuppression protocols typically use single or combined immunosuppressive drug regimens with drugs delivered orally, intraperitoneally, intravenously or subcutaneously in a single daily dose or divided into multiple daily doses [see reviews (Barraclough, et al., 2011, Halloran, 1996, MacGregor and Bradley, 1995, Wente, et al., 2006)]. While in human clinical settings a targeted plasma concentration of a variety of immunosuppressant drugs can effectively be achieved by a drug dose titration, to accomplish comparable consistency in targeted plasma levels in animal studies remains a major challenge.

Besides cyclosporines, mycophenolate mofetil (MFF), rapamycin or prednisolone, TAC (FK-506, Prograf) represents an immunosuppressant of choice and is frequently used as a solo therapy or in combination with other immunosuppressive drugs (i.e., MFF) (Hefferan, et al., 2011, Reis, et al., 1998, Xu, et al., 2010) [see reviews (Lama, et al., 2003, Su, et al., 2011)]. TAC couples with immunophilins, proteins termed FK-506 binding proteins (FKBPs) (Siekierka, et al., 1989, Thomson, et al., 1995). The formation of a pentameric complex comprised of TAC, FKBPs, calcineurins A and B and calmodulin results in the inhibition of the phosphatase activity of calcineurin (Halloran, 1996, McKeon, 1991). The action of transcription factors requiring dephosphorylation for transport to the cell nucleus is inhibited and leads to suppression of T-cell proliferation and function (Thomson, et al., 1995).

In human clinical allogeneic organ transplantation, the recommended concentration of TAC in blood is in the range of 10-20 ng/ml (Pirsch, et al., 1997, Przepiorka, et al., 1999, Staatz and Tett, 2004) and is effective in maintaining long-term survival of transplanted solid organs (such as kidney, bone marrow or liver) with tolerable side effects typically presented as nephrotoxicity, neurotoxicity, gastrointestinal toxicity or drug-induced diabetes (Vicari-Christensen, et al., 2009). In experimental allograft or xenograft animal studies that use rodents (mice, rats) or minipigs as recipients, TAC is typically administered using a chronically implanted intravenous catheter, intraperitoneally or subcutaneously, with doses ranging from 0.05-3 mg/kg/24 hrs (Gold, et al., 1995, Hefferan, et al., 2011, Saxena, et al., 2007, Tze, et al., 1992, Usvald, et al., 2010). However, despite the use of such aggressive immunosuppressive protocols, experimental xenograft studies are frequently hampered by inconsistent graft survival particularly seen in long-term survival studies. It is believed that the oscillation in plasma drug concentrations and/or

insufficient target plasma levels may in part account for inconsistent graft survival. In addition, the requirements of BID injections in order to achieve satisfactory TAC levels and to minimize toxicity make this approach i) labor intensive, ii) frequently associated with side effects resulting from repetitive animal injections (such as local inflammatory changes and infection), and iii) associated with systemic side effects such as nephrotoxicity and hepatotoxicity [see reviews (Finn, 1999, Gijzen, et al., 2010, Teh, et al., 2011)].

To extend the half-life of administered drugs in general, several longer-releasing formulations were developed. **First**, the use of TAC-loaded liposomes has been shown to provide moderate prolongation of the TAC half-life in the whole blood of naïve rats in comparison with conventional i.v. injections of TAC diluted in saline (Ko, et al., 1994, McAlister, 1998). **Second**, the use of biodegradable microspheres was shown to provide a relatively stable level of TAC in whole blood for up to 10-21 days after single s.c. administration (Miyamoto, et al., 2004, Wang, et al., 2004). **Third**, the use of implantable biodegradable pellets has been successfully used to deliver a variety of synthetic drugs or hormones in human patients and in animal experimental models and showed up to 3-6 months of stable drug release after a single pellet implantation (Jockenhover, et al., 1996, Packard, 1992, Srinivasan, et al., 2002, Studd and Magos, 1987). To our knowledge, no immunosuppressive pellet formulation has been reported to be successfully used in rodent or other animal models of xenogeneic neural precursor transplantation.

Accordingly, the goal of the present study was two-fold. First we characterized the pharmacokinetics of four different subcutaneously delivered/implanted TAC formulations, including: i) castor oil/saline solution, ii) unilamellar or multilamellar liposomes, iii) biodegradable microspheres, and iv) biodegradable 3-month lasting pellets. The optimal TAC formulation, as defined by simplicity of Tac delivery and stable/predictable blood Tac concentration was then selected and used in the second component of our study. The primary goal of the second part of the study was to validate the level of functionally effective immunosuppression in a separate group of SOD1^{G93A} transgenic or spinal trauma-injured SD rats implanted with 3-month lasting TAC pellets and grafted spinally with human fetal spinal stem cells (hSSC) or human ES-derived neural precursors (ES-NPC). The survival of grafted cells was determined at 1-3 months after grafting using human-specific antibodies and confocal microscopy.

In addition, the potency of TAC pellet-induced immunosuppression was validated by quantitative analysis of the circulating T-cell population (CD45, CD4, CD8) and by qualitative and quantitative analysis of the infiltrating T-lymphocytes (CD45, CD4, CD8) in cell-grafted spinal cord regions.

Our results indicate that s.c. implanted 3-month lasting biodegradable TAC pellets represent an effective, safe and simple method to achieve long lasting and effective immunosuppression as evidenced by i)

consistent xenograft survival and cell maturation, ii) near complete suppression of grafted site T-cell infiltration, and iii) suppression of circulating blood T-cell concentration.

Material and Methods

All procedures were approved by the Institutional Animal Care and Use Committees by the University of California, San Diego and by the Czech Academy of Sciences. Adult Sprague-Dawley albino rats (Velaz Praha, Czech Republic and Harlan Industries, Indianapolis) and SOD1^{G93A} ALS rats (SOD+) (UCSD colony, Dr. D. W. Cleveland, San Diego, California; 49–57 days old) were used in experiments. Animals were housed in standard cages with free access to food and water.

Animal experimental groups were divided into 2 principal studies: i) TAC pharmacokinetic study, and ii) spinal grafting of human neural precursors in TAC pellet-immunosuppressed animals.

TAC pharmacokinetic study:

Four different TAC (Prograf®, Astellas Pharma, Deerfield, Illinois, USA) vehicle-delivery systems were used and delivered into the subcutaneous space (see Table 1 for summary).

1) TAC castor oil/saline solution (Groups No. 1 and No. 2):

Because the hydrophobic nature of TAC powder and its poor solubility in water solutions (e.g., saline) (Kino, et al., 1987), TAC powder was dissolved in a mixture of 100% ethanol (8% of total volume), castor oil (2% of total volume) and sterile saline for injections (90% of total volume; **Fig.1 G**). Two dosing designs were studied. In the first dosing design, animals (n=4; Grp. No. 1) received 3 mg/kg of TAC in 24-hr intervals for a total of 5 days. Blood samples for TAC measurement were collected at 2, 9, 24, 72 and 120 hrs. At 24 and 72 hrs the blood samples were collected just before subsequent TAC injection. In the second dosing design, animals (n=4; Grp. No. 2) received 1.5 mg/kg of TAC in 12-hr intervals for a total of 5 days. Blood samples for TAC measurements were collected at 2, 12, 14, 24 and 120 hrs. At 12 and 24 hrs the blood samples were collected just before subsequent TAC injections.

2) TAC liposomes (Groups No. 3 and No. 4):

Two structurally different liposome designs (unilamellar or multilamellar; **Fig.1 I, J**) were used (Encapsula NanoSciences LLC, TN). In the first group, TAC-loaded unilamellar liposomes (n=4; 3 mg/kg; Grp. No. 3) were used. In the second group, TAC-loaded multilamellar liposomes (n=4; 3 mg/kg; Grp. No. 4) were

used. In both groups, TAC liposomes were injected as a single bolus. Blood samples for TAC measurements were collected at 2, 12, 24, 48 and 72 hrs.

3) TAC microspheres (Groups No. 5 and No. 6):

TAC-containing microspheres were prepared from tacrolimus powder and poly (D,L-lactide-coglycolide) copolymer (Resomer LG 503H, Aldrich) adopting the procedure previously described (Wang, et al., 2004). The tacrolimus content in the resulting dry TAC microspheres was 45 mg TAC/g of microspheres as determined by HPLC. Rats were injected with a single bolus of TAC-containing microspheres at a dose of 10 mg/kg (n=3; Grp. No. 5) or 20 mg/kg (n=3; Grp. No. 6). Blood samples for TAC measurements were collected at 2, 9, 24 hrs and at 2, 4, 7, 10, 13, 16, 19, and 22 days.

4) TAC releasable pellets (Groups No. 7, No. 8 and No. 9):

TAC-containing 3-month releasable pellets (45, 65 or 90 mg/pellet; Innovative Research of America, FL, USA or Tacropellet, MD, USA; **Fig. 1H**) were implanted subcutaneously in the interscapular region of the neck in isoflurane (2%)-anesthetized rats. Animals with three different body weight ranges (120-350 g) were employed resulting into 3 different dosing groups releasing 1.8 mg/kg/24 hrs (n=4; Gr. No. 7), 3.4 mg/kg/24 hrs (n=3; Grp. No. 8) and 5.1 mg/kg/24 hrs (n=6; Grp. No. 9) of TAC. Blood samples for TAC measurements were collected periodically between 5-140 days after TAC pellet implant (see Table 1 for details).

Blood collection and TAC analysis:

In all experimental groups, blood samples were collected from the saphenous vein in fully awake restrained animals. The lateral aspect of the hind leg was shaved, cleaned with 70% EtOH and disinfected with Chlorhexidine. The leg was immobilized in the extended position by applying gentle downward pressure immediately above the knee joint. Petroleum jelly was applied on the site in order to visualize the saphenous vein and to optimize the blood flow. A 20 gauge needle was used to puncture the vein. We first punctured the vein proximal to the ankle and then moved up if additional punctures were necessary (no more than three needle punctures were attempted in any of blood collection sessions). A maximum of 200 µl of blood was collected per time point. Blood was collected into EDTA tubes and kept at -20°C until analysis using 2 equivalent validated assays: chemiluminescent microparticle immunoassay (CMIA) and liquid chromatography/mass spectrometry (LC/MS/MS).

Chemiluminescent microparticle immunoassay (CMIA). CMIA – ARCHITECT TAC (Abbot Architect, Chicago, Illinois, USA) assay was used according to the manufacturer's protocol. The detection limits of quantification for this method were 2 ng/ml (min) and 30 ng/ml (max), respectively. If the concentration of

TAC in the sample exceeded the 30 ng/ml limit, blood was diluted with saline (in a 1:1 ratio) and the measurement repeated. The CMIA method was used for quantification in groups 1, 2, 3, 4 and 8.

High performance liquid chromatography – mass spectrometry (LC/MS/MS).

A guard column C18, 4 x 2.0 mm (Phenomenex, Torrance, California, USA) equipped with ABI 4000 QTrap linear ion trap mass spectrometer (AB Sciex, Concord, Canada) was used. Whole blood samples were prepared as follows: 40 µl of sample (EDTA whole blood) was mixed with 140 µl protein precipitation solution (conc. ascomycin and zinc sulfate dissolved in methanol). After centrifugation (17,000 x g for 5 min.), 40 µl of the supernatant was transferred to autosampler vials for injection into the LC/MS/MS system. Guard column C18 was washed for 1 min. (isocratic flow rate, 600 µl/min.) with a mixture of methanol containing 2.5 mM/l ammonium acetate and distilled water containing 2.5 mM/l ammonium acetate (ratio 75:25). Thereafter, the mobile phase was changed to 2.5 mM ammonium acetate dissolved in methanol (100% of the volume, flow rate 600 µl/min., time 1.50 min) and TAC/ascomycin were eluted to the detector. The column was reconditioned with methanol containing 2.5 mM/l ammonium acetate (75% of the volume, flow rate 600 µl/min., time 1.50 min). MS/MS analysis was performed in multiple reactions monitoring mode using transitions m/z 821.6>768.5 for TAC and m/z 809.5>756.5 for ascomycin. System control and data acquisition were performed using Analyst 1.2 software (Applied Biosystems/MDS Sciex) for automated data processing. The detection limits of quantification for this method were 2 ng/ml (min) and 50 ng/ml (max), respectively. LC/MS/MS method was also used for determination of concentration of the TAC in whole blood in groups 5, 6, 7 and 9.

Assessment of Tacrolimus pellets – induced side effects:

Animals were evaluated daily for the presence of motor dysfunction (upper extremity motor function assessment was used in paraplegic spinal trauma animals), agitation, jumpiness, and tactile allodynia. In addition, animals were monitored for the presence of other potentially Tac-treatment-related signs of toxicity including: scruffy coat, porphyrin (an indicator of stress, known as “red tears”, often mistaken as blood), weight loss, hypothermia, pale eyes (a reliable indicator of anemia), soft stool, diarrhea, lethargy, vocalization, and swollenness of the pellet implanted subcutaneous site (potential indicator of a local cyst formation).

Spinal cord grafting of human fetal tissue-derived stem cells or embryonic cell line-derived neural precursors:

To assess the effectiveness of immunosuppression in TAC pellet-immunosuppressed rats, human fetal spinal cord derived stem cells (hSSC) or human embryonic cell line (HUES-7)-derived neural precursors (HUES7-NPC) were employed for intraspinal grafting in transgenic SOD+, (n=10) rats or in SD rats with previous L3 compression injury (n= 4) (see Table 2 for experimental cell grafting groups).

Derivation of the human fetal spinal stem cells and HUES-7-derived neural precursors: Derivation of both cell lines was described in detail in our previous studies (Johe, et al., 1996, Kakinohana, et al., 2012, Usvald, et al., 2010, Yuan, et al., 2011). Briefly, human fetal spinal stem cells (Neuralstem, Inc., Rockville, Maryland, USA) were derived from the cervical-upper thoracic region of spinal cord tissue obtained from a single 8-week human fetus after an elective abortion. One day prior to each surgery day, one cryopreserved vial of the previously prepared neural precursors was washed, concentrated in hibernation buffer, and shipped from the cell preparation site (Neuralstem, Inc., Rockville, MD, USA) to the surgery site (UCSD, San Diego, CA, USA) at 2-8°C by overnight delivery. Upon receipt the following day, the cells were used directly for implantation without further manipulation. Before and after implantation, the viability of cells was measured with trypan blue (0.4%; Sigma). On average, 88-93% viability was seen.

Second, the human embryonic stem cells (hESCs; HUES-7 line; Melton Laboratory, Harvard University, Massachusetts, USA), were cultured on a mitomycin C-treated mouse embryonic fibroblast (MEF) feeder layer in HUES hESC medium. Columnar rosettes were manually isolated from induced embryoid bodies and passaged every 3 days to remove contaminating cells. In this stage, NPC were harvested and FAC-sorted and CD184+, CD44-, CD271-, CD24+ cell populations further expanded on PLO/L- coated plates using modified N2 media. For cell growth, 10 ng/ml bFGF as the sole mitogen was added. NPC were expanded for 10-20 passages and frozen aliquots prepared from passage 15-20. On surgery day, one cryopreserved vial of the previously prepared passage was thawed, washed and concentrated in hibernation buffer. Before and after implantation, the viability of cells was measured with trypan blue (0.4%; Sigma). On average, 85-95% viability was seen.

Spinal cord cell-grafting procedure:

SOD+ rats: animals weighing 267±20.9 g (Group No. 7, age 57 days; n=4; Table 1 and Table 2) and 203.6±44 g (Group No. 9, age 49-52 days; n=6; Table 2) received spinal grafts of hSSC or HUES7- NPC at 13 days after TAC pellet implantation. To implant cells, the previously described technique was used (Kakinohana, et al., 2004). Rats were anesthetized with isoflurane (2% maintenance in room air), placed

into a spinal unit apparatus (Stoelting, Wood Dale, Illinois, USA) and a partial Th12–L1 laminectomy was performed using a dental drill (exposing the dorsal surface of L2–L5 segments). Using a 33-gauge needle connected to a microinjector (Kopf Instruments, Tujunga, California, USA), the spinal cord was injected with 1 μ l (approx. 15,000 cells per injection) of the hSSC or HUES7- NPC cells in hibernation buffer. The duration of each injection was 60 s followed by a 30 s pause before needle withdrawal. The center of the injection was targeted into the base of the ventral horn. 10 injections (approx. 800 μ m rostrocaudally apart) were made on the left side of the lumbar spinal cord. After injections, the incision was cleaned with penicillin-streptomycin solution and sutured in two layers. Animals were injected with analgesics and antibiotics and were allowed to recover. For the first 14 days after transplantation, additional immunosuppression was performed as previously described (Hefferan, et al., 2011) with daily injection of mycophenolate mofetil (MMF, Cellcept, Roche Pharmaceutical, Nutley, New Jersey, USA, dose 30 mg/kg). Animals were allowed to survive until they reached the endstage of the disease (Group 7; 33-77 days after cell grafting, for details see Table 2) or until they lost 10% of their bodyweight caused by the progression of the disease (Group 9; 32-70 days after cell grafting, for details see Table 2).

Spinal cord (L3) contused rats: four female SD rats (n=4; Group No.10; BW: 205 \pm 11.9 g) were anesthetized with isoflurane (2% maintenance in room air), placed into a spinal unit apparatus (Stoelting, Wood Dale, Illinois, USA) and a partial Th13 laminectomy was performed using a dental drill (exposing the dorsal surface of L3 spinal segment). Spinal cord compression injury was induced by placing a 3.2 mm acrylic rod (weight=32 g) for 15 min on the dorsal surface of the exposed L3 segment. After compression, the incision was cleaned with penicillin-streptomycin solution and sutured in two layers. Animals were injected with Depomedrol (methylprednisolone, 10 mg/kg) and antibiotics (Cefazoline, 10 mg/kg) and were allowed to recover. Three days after injury animals were re-anesthetized, previously injured L3 spinal segment exposed and received spinal grafts (total of 5 injections; 1 μ l per injection, approx. 400 μ m rostrocaudally apart) of HUES7-NPC targeted into the epicenter and just above and below the injury. The following immunosuppression protocol was used: for the initial 14 days after cell grafting, animals received combined immunosuppression composed of daily single s.c. injection of MMF (30 mg/kg) and BID injections of TAC (1.5 mg/kg/12 hrs). At 14 days, animals were implanted with TAC pellets delivering the TAC dose of 4.9 \pm 0.27 mg/kg/day. Because our initial PK study showed that on average 10-15 days is required to achieve a targeted plasma TAC concentration (i.e., above 15 ng/ml), animals continued to receive BID injections of TAC (1.5 mg/kg/12 hrs) for an additional 12 days. **MFF treatment (30 mg/kg/day; s.c.) was only used for the initial 14 days after cell grafting.** In this experimental group, animals survived 105 days after cell grafting (for details see Table 2).

Naïve non-immunosuppressed SD rats: four female SD rats (n=4; Group No.11; BW: 367 ±14 g) received lumbar spinal grafts of hSSC (total of 5 injections; 1 µl per injection, approx. 400 µm rostrocaudally apart; approx. 15,000 cells per injection) as described. No immunosuppression was performed and animals survived for 14 days.

Perfusion, fixation and immunofluorescence staining of spinal cord sections

Rats were deeply anesthetized with pentobarbital and phenytoin and transcardially perfused with 200 ml of heparinized saline followed by 250 ml of 4% paraformaldehyde in PBS. The spinal cords were dissected and post-fixed in 4% formaldehyde in PBS overnight at 4°C and then cryoprotected in 30% sucrose PBS until transverse or longitudinal sections (40-µm-thick) were cut on a cryostat and stored in PBS. Sections were immunostained overnight at 4°C with the following primary human-specific (h) or non-specific antibodies made in PBS with 0.2% Triton X-100: mouse anti-nuclear matrix protein/h-nuc (hNUMA; 1:100; Millipore, Temecula, California, USA), rabbit anti-human neuron-specific enolase (hNSE, 1:500, Chemicon), mouse anti-human synaptophysin (hSYN, Chemicon; 1:2000), rabbit anti-human glial fibrillary acidic protein (hGFAP, 1:500, Origene, Rockville, Maryland, USA), goat anti-doublecortin (DCX; 1:1000; Millipore), goat anti-choline acetyltransferase (CHAT, 1:50, Chemicon), mouse anti neuronal nuclei antigen (NeuN, 1:1000, Chemicon), mouse anti-CD4 and anti-CD8 antibodies (1:500; AbD Serotec, Raleigh, North Carolina, USA), mouse anti-CD3 and anti-CD45 antibodies (1:1000, e-Bioscience, San Diego, California, USA), rabbit anti-Iba1 (1:1000, Wako, Richmond, Virginia, USA), mouse anti-RT1B (MHC class II) (1:500, BD Biosciences, San Diego, California, USA), mouse anti CD11b (1:200, BD Biosciences, San Diego, California, USA) and donkey anti-rat IgG (1:500, Invitrogen). After incubation with primary antibodies, sections were washed three times in PBS and incubated with fluorescent-conjugated secondary donkey anti-mouse, donkey anti-rabbit or donkey anti-goat antibodies (Alexa Fluor 488, 546 or 647, 1:250, Invitrogen) and DAPI for general nuclear staining. Sections were then mounted on slides, dried at room temperature and covered with a Prolong anti-fade kit (Invitrogen).

Fluorescent microscopy and leukocyte quantification

Fluorescence-stained sections were analyzed using a Leica DMLB Microscope with a Zeiss Axiocam MRm monochrome camera and Olympus FV1000 confocal deconvolution microscope. Images were captured and analysed using Stereo Investigator software (MBF Bioscience, Williston, Vermont, USA) and Olympus Fluoview FV10-ASW (Olympus Corporation, Tokyo, Japan). Z-stacks, three-dimensional, and orthogonal views were generated in Volocity High Performance 3D Imaging Software. All image

manipulations were limited to brightness/contrast, and were performed in a standardized manner for all images. Images were assembled into figures using Adobe Illustrator (Adobe Systems, Inc., San Jose, CA).

Semi-quantitative evaluation of grafted spinal cord tissue infiltration with different types of leukocytes in animals immunosuppressed using TAC biodegradable 3-month lasting pellets was performed using 40- μ m-thick coronal sections. Quantification was performed in 5 sections per animal in TAC dose groups of 1.8 mg/kg/day and 5.1 mg/kg/day (see Table 1, Groups No. 7 and No. 9; n=3 for each group).

The number of different classes of leukocytes positive for CD45, CD8/CD45, CD4/CD45, RT1B/CD45 and CD11B were counted and analyzed separately with respect to the location of positive cells in: i) the core of the graft; ii) the pial surface of the graft, and iii) the spinal cord parenchyma outside of the graft. The degree of leucocyte infiltration was graded as follows: 0- absence of immune cells, *- 1-10 cells, **- 11-50 cells, *** >51 cells per section.

Quantitative analysis of grafted cell survival

Quantitative analysis of grafted cell survival was performed in animals immunosuppressed with 1.8 mg/kg/day of Tac or 5.1 mg/kg/day of Tac (Tac pellet groups No. 7 and 9; see Table 1 and 2) and grafted with HUES7-NSCs or hSCC (n=2 for each Tac dose and cell line).

For quantification, 5 transverse spinal cord sections were selected (minimum 500 μ m apart) from the cell-grafted segments from each rat. An image of virtual tissue of the whole hNUMA-stained section was captured at 10X using Olympus Imager M2 microscope equipped with MBF Stereo Investigator System. The total number of NUMA+ nuclei was then counted using ImageJ "Analyze Particles" plug-in function after setting an identical detection threshold for all analyzed sections. The number of counted cells was then averaged and expressed as number of cells counted per section for each Tac dose and grafted cell line analyzed.

All images used for quantification (i.e., leucocyte-stained and hNUMA+ stained sections) were examined by a blinded observer.

Flow cytometry

Peripheral blood from rats (saphenous vein) was collected into microtainer EDTA tubes (BD Biosciences, San Jose, CA, USA). Red blood cells were lysed using RBC lysis buffer (Sigma-Aldrich, St. Louis, MO, USA). The lysed blood was stained with antibodies directed to rat CD4, CD8, CD45, and CD3 (Biosciences, San Diego, CA, USA). A minimum of 10,000 live events (defined by FSC and 7-AAD) was acquired on a six-color BD FACSC. Analysis was done using FACSDiva software. CD4+ and CD8+ cell

percentages was measured using a T cell lineage gate defined by 7AAD- CD45+ CD3+ small lymphocytic cells.

Results

Pharmacokinetic profile after subcutaneous TAC delivery (Fig. 1)

Four different TAC vehicle-delivery systems were used for subcutaneous delivery (see Table 1 for details).

1) TAC-containing castor oil/saline solution: the whole blood TAC concentration in animals receiving a single bolus of TAC (3 mg/kg) was on average 39.5 ng/ml at 9 hrs after injection and decreased to 9 ng/ml at 24 hrs. With continuing daily injections at the same dose (i.e., 3 mg/kg), the plasma concentration of TAC was 12.2 and 7.2 ng/ml at 72 and 120 hrs, respectively (i.e., at 24 hrs after the previous injection) (**Fig. 1A**); the whole blood TAC concentration in animals receiving a single bolus of TAC (1.5 mg/kg/BID) was 11.9 ng/ml at 12 hrs after injection. With continuing injections every 12 hrs at the same dose (i.e., 1.5 mg/kg), the blood concentration of TAC was on average 13.5 and 14.9 ng/ml at 24 and 120 hrs, respectively (i.e., at 12 hrs after the previous injection delivered at 12 hrs and 108 hrs, respectively) (**Fig. 1B**). **2) TAC-containing unilamellar or multilamellar liposomes:** the blood TAC concentration in animals receiving a single bolus of unilamellar or multilamellar liposomes-containing TAC (3 mg/kg) was on average 52.9 (unilamellar liposomes) and 52 ng/ml (multilamellar liposomes) at 12 hrs and decreased to 6.1 (unilamellar) and 3.6 ng/ml (multilamellar) at 72 hrs, respectively (**Fig. 1C**). **3) TAC-containing microspheres:** the whole blood TAC concentration in animals receiving a single bolus of TAC-containing microspheres (20 mg/kg or 10 mg/kg) showed a biphasic TAC release profile. The first peak was measured at 4 days after delivery and was 19.6 (20 mg/kg dose) and 6.4 ng/ml (10 mg/kg dose), respectively. The second peak was measured at 12 days after delivery and was 12.6 (20 mg/kg dose) and 8.3 ng/ml (10 mg/kg dose), respectively. The TAC concentration at 19 days after delivery was on average 1.5 and 1.7 ng/ml in 20 mg/kg and 10 mg/kg group, respectively (**Fig. 1D**). **4) TAC-containing pellets:** groups of animals were implanted with 3-month releasable TAC pellets releasing TAC at 1.9, 3.4 or 5.1 mg/kg/day. In the 1.9 mg/kg group (n= 4) the peak value of 11.1 ng/ml was measured 13 days after pellet implantation and then gradually decreased to 2.8 ng/ml at 90 days. In the 3.4 mg/kg group (n=3) the peak TAC concentration was measured at 38 days after pellet implantation and was on average 29.4 ng/ml. At 3 months the TAC levels were 19.1 ng/ml. In the 5.1 mg/kg group (n=6) the peak of TAC concentration was detected at 27 days and was 46 ng/ml. At 53 days the TAC concentration was 41.7 ng/ml (**Fig. 1E, F**). **Macroscopical and microscopical images of all Tac formulations used in this study including castor oil-saline, 90 mg pellet, unilamellar or multilamellar liposomes and microspheres is shown in Fig.1 G-K.**

Tolerability of SD rats to long-term TAC pellet-induced immunosuppression

Animals implanted with 3-month releasable pellets (dose 1.9 mg/kg/day) showed good tolerability for up to 3 months after pellet implantation and no detectable clinically-defined side effects were noted.

In the animal group implanted with 3.4 mg/kg/day TAC pellets, good tolerability was seen for up to 3 months without any prophylactic antibiotic treatment. Three animals were allowed to survive for an additional 2 months while a progressively decreasing TAC blood concentration was monitored. At the end of 5 months, 2 animals succumbed to infection, which was determined to be of gastrointestinal origin.

In the animal group receiving the highest TAC dose (5.1 mg/kg/day), good tolerability was seen for up to 6-7 weeks after pellet implantation. From the total number of 60 animals so far tested in our laboratory with this dose, 3 animals showed nephrotoxicity at 7-8 weeks. Clinically, these animals showed increased agitation and tactile allodynia. In all 3 animals plasma TAC levels were higher than 60 ng/ml. Once these symptoms were identified, the animals usually died within 2-3 days. Postmortem necropsy showed clear kidney atrophy and the presence of blood in the urine (i.e., hematuria). An additional 4 animals were found dead without any pre-clinical signs of toxicity between 3-8 weeks after pellet implantation. In 6 of 44 implanted animals, a cyst partially filled with serous fluid and surrounding the pellet implanted-subcutaneous region was identified.

Survival and maturation of spinally grafted human fetal spinal cord stem cells (hSSC) or human ES-derived neural precursors (HUES7-NPC) in SOD+ rats and TAC-dose dependent suppression of T-cell infiltration (Figs. 2, 3)

To validate the effectiveness of TAC pellet-induced immunosuppression in an experimental xenograft design, transgenic SOD+ rats were implanted with TAC pellets and then received spinal grafts of hSSC or HUES7-NPC 13 days after TAC pellet implantation. Based on the initial pharmacokinetic study, 3 groups of transgenic SOD+ rats previously implanted with TAC pellets delivering either 1.9 mg/kg/day, 3.4 mg/kg/day or 5.1 mg/kg/day of TAC were used for cell grafting. In addition, a group of SD rats with previous L3-4 compression injury were used. Spinal trauma animals were grafted with HUES7-NPC. Animals in all experimental groups survived between 32-105 days after cell grafting (see

Table 2 for experimental groups). In general, independent of the TAC dose group and grafted cell line, comparable long-term engraftment and maturation of grafted cells was seen in SOD+ animals.

In the **1.9 mg/kg/day** TAC group (SOD+ rats) grafted with HUES7-NPC, triple-staining with human-specific nuclear marker (hNUMA), early postmitotic neuronal marker DCX and human-specific GFAP antibody (hGFAP) of transverse spinal cord sections taken from grafted spinal segments showed well engrafted hNUMA+ cell populations composed of DCX+ neurons and hGFAP astrocytes at 77 days after grafting (**Fig. 2A-D**). Double-staining with NeuN (neuronal nuclei antigen) and hNUMA showed that the majority of hNUMA+ cells in the gray matter acquired NeuN immunoreactivity (**Fig. 2E; insert**). Confocal analysis of DCX/hSYN (synaptophysin)/NeuN-stained sections showed a dense population of hSyn+ terminals residing in the vicinity of ventral α -motoneurons and were associated with DCX+ processes (**Fig. 2F, G**).

The degree of T-cell infiltration was probed by staining with CD45, CD4 and CD8 antibodies (see Table 3 for quantitative analysis). High-density CD45+ cell populations were identified typically at the core or at the periphery of cell-grafted regions (**Fig. 2H-J**). In the same areas CD4/8+ lymphocytes surrounded by activated Iba1 immunoreactive microglial cells were seen (**Fig. 2K-M**). Double-staining with CD45 and CD8 antibody showed a clear population of CD45/CD8+ cells in the vicinity of hNUMA+ grafted cells (**Fig. 2N; yellow arrows**).

In the **5.1 mg/kg/day** TAC group (SOD+ rats) grafted with hSSC, double-staining with hNUMA and DCX antibody showed a robust cell engraftment with high population of hNUMA/DCX+ grafted neurons throughout the grafted region and extending from the dorsal horn to ventral gray matter at 70 days after cell grafting (**Fig. 3A**). Numerous solitary hNUMA/DCX+ neurons which migrated from the core of the graft were also identified (**Fig. 3B; inserts**). Staining with human specific synaptophysin antibody showed a wide-spread hSYN punctate-like staining pattern throughout the grafted region (**Fig. 3C**). In the same areas a high density of hGFAP+ astrocytes were also seen (**Fig. 3C-insert**). Double staining with DCX and human-specific NSE antibody (hNSE) showed that in areas with high density of DCX+ processes solitary hNSE+ neurons were also present (**Fig. 3D**).

Quantitative analysis of hNUMA+ cells in 1.9 mg/kg/day TAC group showed on average 2712±320 cells in HUES7-NPC-grafted animals (n=2) and 1772±629 cells in hSSC-grafted group (n=2). In the 5.1 mg/kg/day TAC group on average 2750±527 cells were counted in HUES7-NPC-grafted animals (n=2) and 2164±638 cells were counted in the hSSC-grafted group (n=2).

In both TAC dose groups (3.4 and 5.1 mg/kg/day), staining with CD45, CD4 and CD8 markers showed a similar pattern. The number of CD45+ stained cells was relatively low (if compared to

1.9 mg/kg/day TAC group; see **Table 3** for quantitative analysis) with the majority of CD45+ cells typically found at the periphery of individual grafts (**Fig. 3E-G**). Staining with CD4/8 antibody showed only sporadic presence of CD4/8+ cells (**Fig. 3H-J**) and the majority of CD45+ cells found in grafted DCX+ regions were CD8 negative (**Fig. 3K**; yellow arrows).

Survival and maturation of spinally grafted HUES7-NPC in adult SD rats with previous spinal Th9 contusion (Fig. 4)

To characterize the survival of spinally grafted human ES-derived neural precursors, adult SD rats with previous L3 spinal contusion injury received spinal grafts of HUES7-NPC at 3 days after injury and survived for 3 months. The dose of TAC delivered by implanted TAC pellet was 4.9 mg/kg/day. Immunofluorescence analysis of hNSE/hNUMA/DCX triple-stained sections showed an advanced stage of neuronal maturation as evidenced by an intense hNSE immunoreactivity (**Fig. 4A**; inserts). Numerous double stained hNSE/DCX solitary neurons which migrated outside of the grafts were also identified (**Fig. 4B-D**). Similarly as in SOD+ rats immunosuppressed with a high TAC dose, staining with CD45 antibody revealed only occasional presence of CD45+ cells at the periphery of individual grafts (**Fig. 4E-G**). Co-staining with CD45 and CD8 antibody showed only occasional presence of CD8+ cells (not shown).

Effect of TAC pellet-induced immunosuppression on circulating blood T-cell population and IgG immunoreactivity in spinal human cell-grafted regions (Fig. 5)

To further probe the effect of TAC pellet-induced immunosuppression on T-cell activity, we quantified the density of circulating T-cell population in blood in naïve, SOD+ TAC non-treated and SOD+ TAC-treated (5.1 mg/kg/day) animals. In comparison to TAC non-treated animals, immunosuppressed rats had a significantly decreased number of circulating CD45, CD4 and CD8 cells (**Fig. 5A-C**), ($p < 0.05$; t-test).

To identify the presence of IgG-secreting cells or soluble IgG in cell-grafted spinal cord regions, sections taken from all 3 TAC dosing groups were stained with anti-rat IgG (fluorescence-tagged) and then further stained to detect MHC class II (R1TB) and CD45 to identify B cells. In 1.9 mg/kg/day TAC group numerous IgG+ cells were identified in grafted regions. Similarly as for the CD8 population, the IgG+ cells were typically localized at the periphery of individual grafts. Double staining with anti-rat MHC class II antibody and anti-rat IgG showed the B-lymphocyte phenotype in small subpopulation of IgG+ cells (**Fig. 5D**; yellow arrows). In addition to IgG presence on B-

lymphocytes, an overall increase in the density of IgG staining in cell-grafted regions was seen (**Fig. 5D**; blue dashed area). Since the area had minimal RT1B staining, it is possible that deposited IgG is detected in this area. Similarly, double staining with RT1B and CD45 antibody showed only sporadic presence of RT1B/CD45-double-stained cells in cell-grafted areas (**Fig. 5E**).

Triple staining with macrophage and monocyte marker CD11b, anti-rat IgG and CD45 showed a clear colocalization of CD11b and anti-rat IgG immunoreactivity but with relatively weak CD45 staining pattern in the same CD11b/anti-rat IgG⁺ cells (**Fig. 5F**; yellow arrows).

In 3.4 and 5.1 mg/kg/day TAC groups, only sporadic IgG, RT1B or CD45-stained cells were identified as well as the density of the IgG staining in cell-grafted regions was below detection threshold (**Fig. 5G, H**) and was similar to that seen in control cell-non-grafted animals (not shown).

Rejection of spinally grafted human fetal spinal cord stem cells (hSSC) in the absence of immunosuppression (Fig. 6)

To validate the importance of immunosuppression in providing grafted human cell survival, we next grafted hSSC into lumbar spinal cord in adult SD rats without immunosuppression. Analysis of spinal cord sections at 14 days after cell grafting showed complete grafted cell rejection and intense infiltration of CD4/8 cells at the injection site (**Fig. 6 A, B, C, D**).

Discussion

Experimental and clinical evidence for need of continuing immunosuppression in xenogeneic CNS grafting design

Extensive previous experimental animal but also clinical data show that xenogeneic neural grafts are rapidly rejected in non-immunosuppressed animals and/or human patients. For example, it was demonstrated that grafted porcine dopaminergic neuroblasts (derived from embryonic day 26-27) are rejected within days to weeks after intracerebral grafting in rats in the absence of immunosuppression (Brevig, et al., 2000). It was also demonstrated that the porcine xenografts undergoing rejections are infiltrated with CD8 lymphocytes and are stained positive for IgM and complement component (C3) (Barker, et al., 2000). Similarly, in clinical PD trial, grafting of porcine embryonic dopaminergic neurons showed very poor grafted cell survival at 7 months (one postmortem patient analyzed) after grafting despite continuing immunosuppression with cyclosporine (5 mg/kg) (Deacon, et al., 1997). In the same study, lymphocyte infiltration was also seen in the cell-grafted region. These data are consistent with our previous reports which demonstrate no or poor graft survival after spinal grafting of human spinal stem cells in SOD+ rats or SD rats with previous spinal ischemic injury if animals were immunosuppressed with TAC as a monotherapy (1.5 mg/kg, q12h or 1 mg/kg, qd, respectively) (Hefferan, et al., 2011, Kakinohana, et al., 2012). Similarly, grafted cell rejection was associated with an intense CD4/8 T-lymphocyte infiltration in previously cell-grafted regions. Jointly, these data show that in order to achieve satisfactory and long-term grafted cell survival using xenogeneic grafting design, continuing and aggressive immunosuppression which is effective in suppressing T-cell activity is needed.

Stable and controllable blood TAC concentration and tolerability of SD rats to long-term TAC pellet-induced immunosuppression

In our initial phase of the study, we have compared the plasma kinetics of four different TAC formulations after subcutaneous delivery. Three primary characteristics of the PK data and associated animal manipulations (such as repetitive animal injections) were considered in defining the optimal formulation to be used in the subsequent long-term spinal cell grafting studies and included: i) the stability of plasma TAC concentration over a 24-hr period, ii) required frequency of injections to achieve a targeted plasma TAC concentration, and iii) potential side effects associated with a high plasma TAC concentration or repetitive animal injections.

The rationale for the selection of specific time points for TAC measurements (i.e., more frequent measurements in castor oil/saline, liposomes and microspheres formulations-injected animals and less frequent in TAC pellet-implanted animals; see Table 1 for summary) was based on expected differences in TAC kinetics among all formulation and by the need to identify potential blood toxic TAC levels.

First, in castor oil-saline as a vehicle or liposome (unilamellar or multilamellar) TAC-injected animals, a comparable kinetics profile was seen during the initial 12 hrs after 3 mg/kg TAC injections with the peak concentrations (40-60 ng/ml) measured during 2-12 hrs after injections. In contrast to the castor-oil-saline TAC (3 mg/kg) group in which the TAC levels dropped to 10 ng/ml at 24 hrs after single injection, in liposome-TAC injected animals (3 mg/kg) on average 27 ng/ml TAC was measured at 24 hrs and was still around 11 ng/ml at 48 hrs after injection. In animals injected BID with the castor-oil-saline formulation (1.5 mg/kg/12 hrs) for 5 days, the measured peak TAC concentration was seen at 2 hrs (around 23 ng/ml) and stable levels around 13 ng/ml were then measured between 1-5 days if measured at the end of 12 hrs (i.e., at 12 hrs after previous TAC injection). These TAC pharmacokinetic data are similar as reported from other laboratories using mice or rats (Ko, et al., 1994, McAlister, 1998, Yamauchi, et al., 2004).

From the perspective of conducting long-term immunosuppressive therapy, these data demonstrate that, should a castor-oil vehicle system be used for TAC delivery, the BID delivery regimen has the most favorable safety profile (as defined by the peak concentration) and is relatively stable through TAC levels. While more labor intensive, a stable targeted through TAC levels can be achieved and readily adjusted if needed. The use liposome-TAC formulation provides an extended half life, however, a relatively high peak concentration (i.e., above 50 ng/ml) and the cost (approx. \$1,600/6 animals) to prepare these formulations appears to limit its routine use at present.

Second, TAC microspheres were used and animals received a single subcutaneous injection of either 10 or 20 mg/kg TAC-containing microspheres. In both doses, a biphasic release profile was measured with the first peak seen at 4 days and the second peak at 12 days after injection. In the 20 mg/kg group, the peak measured at 4 days was around 20 ng/ml and the levels were still around 10 ng/ml at 15 days after a single injection. This TAC kinetics profile is similar if not identical as reported in other studies which employed the same TAC microsphere formulation. In contrast to the castor-oil and liposome formulation, no initial TAC plasma concentration “overshoot” was seen at 2 hrs after injection and levels were around 12 ng/ml at 9 hrs after injection (in the 20 mg/kg group). The use of TAC microspheres appears to provide a clear advantage over castor-oil and liposome formulation,

permitting stable TAC plasma levels for up to 15 days after a single subcutaneous injection. Moreover, additional injections can readily be added should a rapid and continuing stable increase in TAC concentration be desired.

Third, TAC pellets containing different concentration of TAC and delivering 1.8 mg/kg, 3.4 mg/kg or 5.1 mg/kg of TAC/day for up to 3 months were used for subcutaneous implantation. In higher concentration groups, a progressive increase in plasma TAC concentration was seen during the initial 30 days after pellet implantation and then remained relatively stable for an additional 1-2 months. While the pellets are designed for 3-month continuing TAC release, we have observed continuing TAC release exceeding 4 months (n=3) with the TAC levels around 13 ng/ml measured at 5 months after pellet implantation.

With respect to toxicity, no detectable side effects were seen in animals receiving 1.9 and 3.4 mg/kg/day doses and surviving between 1-3 months. From a total of 60 animals receiving the 5.1 mg/kg/day TAC dose, 4 animals died from apparent kidney toxicity at 1.5-2 months. These animals showed signs of agitation, tactile hypersensitivity as well as scratching behavior 3-4 days before death. We speculate that these behavioral signs could be the result of progressive kidney failure and increased creatine levels. Increased creatine levels have been reported in patients receiving higher dose of TAC after solid organ transplants (Finn, 1999, Teh, et al., 2011).

Defining the optimal TAC immunosuppressive regimen to permit long-term survival and maturation of spinally grafted human neural precursors in rats

As demonstrated in our current study independent of the daily TAC dose delivered (i.e., 1.9, 3.4 or 5.4 mg/kg/day) in the form of a TAC pellet, consistent survival of grafted ES-derived NPC or human fetal spinal cord stem cells was seen at intervals 30-90 days after grafting. This was expressed as the presence of high density DCX or NSE immunoreactive-grafted neurons in targeted spinal cord regions. In addition, high density neuronal processes derived from grafted human neurons expressing human-specific synaptophysin and projecting toward host interneurons and α -motoneurons were identified. Comparable grafted cell survival and maturation was seen in both SOD+ rats and in SD rats with previous L3 contusion injury. In our previous experiment, we demonstrated consistent xenograft survival three weeks after the transplantation of hSSC into the spinal cord in SOD+ rats treated with daily i.p. injection of TAC (3 mg/kg/day) combined with daily i.p. injection of Mycophenolate mofetil (30 mg/kg) (Hefferan, et al., 2011).

As shown in the present study, the SOD⁺ mutant rats show a significant increase in circulating CD4/8 cells if compared to naïve SD rats and this increase in CD4/8 T-lymphocytes was completely blocked by high dose (5.4 mg/kg/day) TAC treatment (Fig. 5; a-c). In addition, several previous studies have demonstrated significant spinal inflammatory changes in symptomatic SOD⁺ rats characterized by intense activation of microglia and astrocytes in areas of previous α -motoneuron loss (Hall, et al., 1998, Hefferan, et al., 2012). The characteristics of this model and requirement of continuous high dose Tac immunosuppression in order to provide long-term grafted cell survival further emphasize the importance of aggressive immunosuppressive therapy to achieve consistent cell survival in this neurodegenerative model.

Similarly, in our recent study, we demonstrated consistent cell survival for up to 2 months after spinal grafting of HUES7-NPC after using 1 mg TAC/day dose delivered s.c. as a bolus in castor-oil preparation in SD rats with previous spinal ischemic injury. However, no cell survival was seen if animals were allowed to survive for total of 4 months (Kakinohana, et al., 2012). In another study, on average 28-day survival of allogeneic islet grafts in mice after single injection of TAC loaded microspheres (dose 20 mg/kg) or continuing graft survival (>100 days) after repeated injections of TAC loaded microspheres (dose 10 mg/kg; 7-day intervals) was described (Wang, et al., 2004). Jointly, these data show that the TAC dose of around 3 mg/kg/day and divided into two 12-hr doses (if delivered as a bolus s.c injection) or in a form of continuously TAC releasing pellet is required for long-term effective immunosuppression to permit xenograft survival in rats.

Translated to plasma TAC concentration, TAC levels of ≤ 15 ng/ml were measured in 1.5 mg/kg/12 hr (castor-oil formulation) or in 3.42 or 5.1 mg/kg/day (pellet groups), i.e., the TAC dosing regimen which was associated with consistent grafted cell survival for up to 3 months after cell grafting. Comparable TAC plasma levels were shown to be required to permit long-term survival of grafted pancreatic islet cells in mice (Wang, et al., 2004) or to lead to life-long survival of transplanted solid organs in human patients (Pirsch, et al., 1997, Przepiorka, et al., 1999, Stautz and Tett, 2004, Vicari-Christensen, et al., 2009).

TAC dose-dependent suppression of T- and B-lymphocyte activation and proliferation

Quantitative analysis of T-cells (CD8, CD4) in grafted spinal cord regions showed a near complete absence of this cell population in 3.4 and 5.1 mg/kg/day TAC group if analyzed at 77-90 days after cell grafting. Similarly, the analysis of CD8 and CD4 cells in circulating blood showed a significant decrease in the 5.1 mg/kg/day TAC group if compared to non-immunosuppressed SOD⁺ rats. In

contrast to the 3.4 and 5.1 mg/kg/day TAC groups, a clear population of CD4/8 cells was seen in 1.9 mg/kg/day TAC-treated and cell grafted animals. Interestingly, a substantially higher density of CD8 population was seen on the dorsal surface of individual grafts facing the pial membrane. We speculate that the presence of grafted cells in heavily vascularized but BBB-lacking pial arterial system is more susceptible to extravasation of the circulating T-cell population and the resulting T-cell mediated response. We also hypothesize that even if a satisfactory cell survival was seen in the 1.9 mg/kg/day group at 77 days after cell grafting, a progressive grafted cell rejection will likely develop should the same level of low level immunosuppression continue over an extended period of time. We also saw small lymphocytic IgG+ MHC class II+ CD45+ B cells in the graft surface. We speculate that these cells are releasing graft-specific antibodies that are bound the the graft or to CD11b+CD45- microglia cells.

Limitation of subcutaneous TAC pellet-induced immunosuppression

Several technical issues need to be considered once a pellet immunosuppression regimen is going to be implemented into any rat xenograft-immunosuppression study. **1)** Based on our PK study, it takes on average 7-15 days after pellet implant before targeted (≤ 15 ng/ml TAC) plasma levels are achieved in 200-350 g rats. Thus, the TAC pellet needs to be implanted before cells are transplanted and the plasma level of TAC validated. However, because consistent and predictable plasma TAC concentrations were measured in our initial PK study in all 3 TAC pellet dosing groups, we have currently implemented less vigorous TAC plasma monitoring and the TAC concentration is only measured 1-2 times during the course of the 2-3 month post-pellet implantation period. Consistent with our initial PK TAC data, expected TAC concentrations were measured in more than 30 animals. **2)** Should there be a desire to remove already implanted TAC pellets to achieve an abrupt termination of immunosuppression, the tissue surrounding the pellet implanted region needs to be excised in block. From our experience, the pellet identification is substantially obscured as soon as 7-14 days after implantation because of its structural disintegration. **3)** Similarly, should there be a need to increase the dose of delivered TAC, an additional pellet(s) can be implanted. Should this be the case, TAC plasma monitoring is recommended to be performed in 5-7 day intervals for at least 2-3 weeks after additional pellet implant to identify potential unwanted toxic TAC concentrations. However, as shown in our current study, the plasma TAC concentrations up to 45-50 ng/ml were well tolerated for up to 3 months and only a fraction of animals displayed systemic side effects. We are currently testing the tolerability of repetitive TAC

pellet implant (3.5 mg/kg/day dose group) and have not seen any detectable side effects at 4.5 months of continuous immunosuppression at this dose (unpublished observation).

Summary

We demonstrated that by using an implantable 3-month lasting TAC-releasing pellet it is possible to achieve functionally effective immunosuppression in SD rats as defined by long-term survival and maturation of spinally grafted human neural precursors derived from human fetal spinal cord or from embryonic stem cell. Plasma TAC concentration of ≤ 15 ng/ml was found to be required to lead to a near complete suppression of T-cell activity in the human cell-grafted spinal cord region and in circulation blood and was readily achieved by 7-10 days after pellet implantation. Jointly, these data demonstrate that the use of implantable TAC pellets can represent an effective long-lasting immunosuppressive drug delivery system which is technically simple to implement, is safe for an extended period of time (4.5 months) and is associated with consistent and long-term human neural precursor survival after grafting into the spinal cord of SOD+ or spinal trauma-injured SD rats.

Funding/Competing Interests:

This study was funded by CIRM and by Neuralstem Inc. No relationship with Astellas Pharma exists for any of the authors.

References

1. Barker, R. A., Ratcliffe, E., McLaughlin, M., Richards, A., and Dunnett, S. B., 2000. A role for complement in the rejection of porcine ventral mesencephalic xenografts in a rat model of Parkinson's disease. *The Journal of neuroscience : the official journal of the Society for Neuroscience* 20, 3415-3424.
2. Barraclough, K. A., Isbel, N. M., Johnson, D. W., Campbell, S. B., and Staats, C. E., 2011. Once-versus twice-daily tacrolimus: are the formulations truly equivalent? *Drugs* 71, 1561-1577.
3. Brevig, T., Holgersson, J., and Widner, H., 2000. Xenotransplantation for CNS repair: immunological barriers and strategies to overcome them. *Trends in neurosciences* 23, 337-344.
4. Deacon, T., Schumacher, J., Dinsmore, J., Thomas, C., Palmer, P., Kott, S., Edge, A., Penney, D., Kassissieh, S., Dempsey, P., and Isacson, O., 1997. Histological evidence of fetal pig neural cell survival after transplantation into a patient with Parkinson's disease. *Nature medicine* 3, 350-353.
5. Finn, W. F., 1999. FK506 nephrotoxicity. *Renal Failure* 21, 319-329.
6. Gijsen, V. M., de Wildt, S. N., Tibboel, D., and Koren, G., 2010. Tacrolimus-induced nephrotoxicity and genetic variability: A systematic review. *Clinical Pharmacology & Therapeutics* 87, S21-S21.
7. Gold, B. G., Katoh, K., and Stormdickerson, T., 1995. The immunosuppressant FK506 increases the rate of axonal regeneration in rat sciatic nerve. *Journal of Neuroscience* 15, 7509-7516.
8. Hall, E. D., Oostveen, J. A., and Gurney, M. E., 1998. Relationship of microglial and astrocytic activation to disease onset and progression in a transgenic model of familial ALS. *Glia* 23, 249-256.
9. Halloran, P. F., 1996. Molecular mechanisms of new immunosuppressants. *Clinical Transplantation* 10, 118-123.
10. Hefferan, M. P., Galik, J., Kakinohana, O., Sekerkova, G., Santucci, C., Marsala, S., Navarro, R., Hruska-Plochan, M., Johe, K., Feldman, E., Cleveland, D. W., and Marsala, M., 2012. Human neural stem cell replacement therapy for amyotrophic lateral sclerosis by spinal transplantation. *PLoS one* 7, e42614.
11. Hefferan, M. P., Johe, K., Hazel, T., Feldman, E. L., Lunn, J. S., and Marsala, M., 2011. Optimization of immunosuppressive therapy for spinal grafting of human spinal stem cells in a rat model of ALS. *Cell transplantation* 20, 1153-1161.
12. Hefferan, M. P., Johe, K., Hazel, T., Feldman, E. L., Lunn, J. S., and Marsala, M., 2011. Optimization of immunosuppressive therapy for spinal grafting of human spinal stem cells in a rat model of ALS. *Cell transplantation* 20, 1153-1161.
13. Jockenhovel, F., Vogel, E., Kreutzer, M., Reinhardt, W., Lederbogen, S., and Reinwein, D., 1996. Pharmacokinetics and pharmacodynamics of subcutaneous testosterone implants in hypogonadal men. *Clinical Endocrinology* 45, 61-71.
14. Johe, K. K., Hazel, T. G., Muller, T., Dugich-Djordjevic, M. M., and McKay, R. D., 1996. Single factors direct the differentiation of stem cells from the fetal and adult central nervous system. *Genes Dev* 10, 3129-3140.

15. Kakinohana, O., Cizkova, D., Tomori, Z., Hedlund, E., Marsala, S., Isacson, O., and Marsala, M., 2004. Region-specific cell grafting into cervical and lumbar spinal cord in rat: a qualitative and quantitative stereological study. *Experimental neurology* 190, 122-132.
16. Kakinohana, O., Juhasova, J., Juhas, S., Motlik, J., Platoshyn, O., Hefferan, M., Yuan, S. H., Vidal, J. G., Carson, C. T., Galik, J., van Gorp, S., Leerink, M., Lazar, P., Marsala, S., Miyanojara, A., Goldberg, D., Kafka, J., Keshavarzi, S., Ciacci, J. D., and Marsala, M., 2012. Survival and differentiation of human embryonic stem cell-derived neural precursors grafted spinally in spinal ischemia-injured rats or in naive immunosuppressed minipigs: a qualitative and quantitative study. *Cell transplantation*, (in press).
17. Kino, T., Hatanaka, H., Hashimoto, M., Nishiyama, M., Goto, T., Okuhara, M., Kohsaka, M., Aoki, H., and Imanaka, H., 1987. FK-506, a novel immunosuppressant isolated from a streptomyces. 1. fermentation, isolation and physicochemical and biological characteristics. *J. Antibiot.* 40, 1249-1255.
18. Ko, S., Nakajima, Y., Kanehiro, H., Yoshimura, A., and Nakano, H., 1994. The pharmacokinetic benefits of newly developed liposome-incorporated FK506. *Transplantation* 58, 1142-1144.
19. Lama, R., Santos, F., Algar, F. J., Alvarez, A., and Baamonde, C., 2003. Lung transplants with tacrolimus and mycophenolate mofetil: A review. *Transplantation proceedings* 35, 1968-1973.
20. MacGregor, M. S., and Bradley, J. A., 1995. Overview of immunosuppressive therapy in organ-transplantation. *British Journal of Hospital Medicine* 54, 276-&.
21. McAlister, V. C., 1998. Liposomal tacrolimus: Drug migration within blood compartments. *Transplantation proceedings* 30, 1000-1001.
22. McKeon, F., 1991. When worlds collide - Immunosuppressant meet protein phosphatases. *Cell* 66, 823-826.
23. Miyamoto, Y., Uno, T., Yamamoto, H., Li, X. K., Sakamoto, K., Hashimoto, H., Takenaka, H., Kawashima, Y., and Kawarasaki, H., 2004. Pharmacokinetic and immunosuppressive effects of tacrolimus-loaded biodegradable microspheres. *Liver Transplantation* 10, 392-396.
24. Packard, M. J., 1992. Use of slow-release pellets to administer calcitriol to avian embryos - effects on plasma calcium, magnesium and phosphorus. *General and Comparative Endocrinology* 85, 8-16.
25. Pirsch, J. D., Miller, J., Deierhoj, M. H., Vincenti, F., and Filo, R. S., 1997. A comparison of tacrolimus (FK506) and cyclosporine for immunosuppression after cadaveric renal transplantation. *Transplantation* 63, 977-983.
26. Przepiorka, D., Devine, S. M., Fay, J. W., Uberti, J. P., and Wingard, J. R., 1999. Practical considerations in the use of tacrolimus for allogeneic marrow transplantation. *Bone Marrow Transplantation* 24, 1053-1056.
27. Reis, A., Reinhard, T., Sundmacher, R., Braunstein, C., and Godehardt, E., 1998. Effect of mycophenolate mofetil, cyclosporin A, and both in combination in a murine corneal graft rejection model. *British Journal of Ophthalmology* 82, 700-703.
28. Saxena, K., Patro, N., and Patro, I., 2007. FK506 protects neurons following peripheral nerve injury via immunosuppression. *Cellular and molecular neurobiology* 27, 1049-1057.
29. Siekierka, J. J., Hung, S. H. Y., Poe, M., Lin, C. S., and Sigal, N. H., 1989. A cytosolic binding-protein for immunosuppressant FK506 has peptidyl-prolyl isomerase activity but is distinct from cyclophilin. *Nature* 341, 755-757.
30. Srinivasan, V., Pendergrass, J. A., Kumar, K. S., Landauer, M. R., and Seed, T. M., 2002. Radioprotection, pharmacokinetic and behavioural studies in mouse implanted with biodegradable drug (amifostine) pellets. *International Journal of Radiation Biology* 78, 535-543.
31. Staatz, C. E., and Tett, S. E., 2004. Clinical pharmacokinetics and pharmacodynamics of tacrolimus in solid organ transplantation. *Clinical Pharmacokinetics* 43, 623-653.

32. Studd, J., and Magos, A., 1987. Hormone pellet implantation for menopause and premenstrual-syndrome. *Obstetrics and Gynecology Clinics of North America* 14, 229-249.
33. Su, V. C. H., Greanya, E. D., and Ensom, M. H. H., 2011. Impact of mycophenolate mofetil dose reduction on allograft outcomes in kidney transplant recipients on tacrolimus-based regimens: a systematic review. *Annals of Pharmacotherapy* 45, 248-257.
34. Teh, L. K., Dom, S. H. M., Zakaria, Z. A., and Salleh, M. Z., 2011. A systematic review of the adverse effects of tacrolimus in organ transplant patients. *African Journal of Pharmacy and Pharmacology* 5, 764-771.
35. Thomson, A. W., Bonham, C. A., and Zeevi, A., 1995. Mode of action of tacrolimus (FK506) - Molecular and cellular mechanisms. *Therapeutic Drug Monitoring* 17, 584-591.
36. Tze, W. J., Tai, J., Cheung, S. S. C., Ricordi, C., and Starzl, T. E., 1992. FK 506 - An effective immunosuppressant for islet xenotransplantation. *Transplantation proceedings* 24, 2849-2850.
37. Usvald, D., Vodicka, P., Hlucilova, J., Prochazka, R., Motlik, J., Kuchorova, K., Johe, K., Marsala, S., Scadeng, M., Kakihana, O., Navarro, R., Santa, M., Hefferan, M. P., Yaksh, T. L., and Marsala, M., 2010. Analysis of dosing regimen and reproducibility of intraspinal grafting of human spinal stem cells in immunosuppressed minipigs. *Cell transplantation* 19, 1103-1122.
38. Vicari-Christensen, M., Repper, S., Basile, S., and Young, D., 2009. Tacrolimus: review of pharmacokinetics, pharmacodynamics, and pharmacogenetics to facilitate practitioners' understanding and offer strategies for educating patients and promoting adherence. *Progress in Transplantation* 19, 277-284.
39. Wang, Q. X., Uno, T., Miyamoto, Y., Hara, Y., Kitazawa, Y., Lu, F. Z., Funeshima, N., Fujino, M., Yamamoto, H., Takenaka, H., Kawashima, Y., and Li, X. K., 2004. Biodegradable microsphere-loaded tacrolimus enhanced the effect on mice islet allograft and reduced the adverse effect on insulin secretion. *American Journal of Transplantation* 4, 721-727.
40. Wente, M. N., Sauer, P., Mehrabi, A., Weitz, J., Buchler, M. W., Schmidt, J., and Schemmer, P., 2006. Review of the clinical experience with a modified release form of tacrolimus [FK506E (MR4)] in transplantation. *Clinical Transplantation* 20, 80-84.
41. Xu, G. D., Wang, L. Y., Chen, W., Xue, F., Bai, X. L., Liang, L., Shen, X. N., Zhang, M. L., Xia, D. J., and Liang, T. B., 2010. Rapamycin and tacrolimus differentially modulate acute graft-versus-host disease in rats after liver transplantation. *Liver Transplantation* 16, 357-363.
42. Yamauchi, A., Oishi, R., and Kataoka, Y., 2004. Tacrolimus-induced neurotoxicity and nephrotoxicity is ameliorated by administration in the dark phase in rats. *Cellular and molecular neurobiology* 24, 695-704.
43. Yuan, S. H., Martin, J., Elia, J., Flippin, J., Paramban, R. I., Hefferan, M. P., Vidal, J. G., Mu, Y., Killian, R. L., Israel, M. A., Emre, N., Marsala, S., Marsala, M., Gage, F. H., Goldstein, L. S., and Carson, C. T., 2011. Cell-surface marker signatures for the isolation of neural stem cells, glia and neurons derived from human pluripotent stem cells. *PLoS one* 6, e17540.

Figure Legends

Figure 1. Blood TAC pharmacokinetics after subcutaneous injections of four different TAC formulations. **First**, TAC powder was diluted in castor-oil/saline solution and injected every 24 hrs for 5 days (3 mg/kg) (**a**) or every 12 hrs for 5 days (1.5 mg/kg/12 hrs) (**b**). Blood was collected prior to subsequent TAC injection (arrows). **Second**, TAC loaded unilamellar or multilamellar (**c**) liposomes were injected subcutaneously as a single bolus (arrow) (3 mg/kg) and TAC concentration measured periodically for 72 hrs. **Third**, another two groups of animals were injected with single bolus of biodegradable TAC microspheres in the dose 10 mg/kg or 20 mg/kg (**d**). Note the lack of TAC plasma concentration “overshoot” during the first 9 hrs after delivery and a relatively stable plasma TAC concentration for up to 15 days after a single TAC microspheres bolus injection. **Fourth**, the biodegradable 3-month releasable TAC pellets delivering 1.88 mg/kg/day, 3.42 mg/kg/day or 5.1 mg/kg/day of TAC were implanted s.c. and the TAC plasma measured for up to 4.5 months (**e**, **f**). Note a progressive increase in TAC concentration during the initial 3-4 weeks after TAC pellet implantation and then followed by a relatively stable and dose-dependent long-lasting TAC release. Arrows indicate the TAC pellet implantation. Each time point is represented as the mean \pm SD of TAC concentrations. **Macroscopical and microscopical images of different Tac formulations including castor oil-saline (g), 90 mg pellet (h), unilamellar (i) or multilamellar (j) liposomes or microspheres (k).**

Figure 2. Immunofluorescence examination of the presence of grafted human ES-derived neural precursors (HUES7-NPC) and immunological response in the spinal cord tissue of SOD+ rats implanted with 3-month lasting TAC pellet (1.9 mg/kg/day). TAC releasable pellets were implanted subcutaneously in SOD+ rats (n=4; 60-65 days of age) 13 days prior to grafting with HUES7-NPC. After cell grafting, animals were allowed to survive until they reached the endstage of the ALS disease (approx. 77 days after cell implantation). Immunohistochemical staining with human specific antibodies (hNUMA-human nuclear protein, green; hGFAP-human astrocytes, cyan) and doublecortin (DCX, red) revealed consistent presence of well-engrafted cell populations in the spinal parenchyma (**a-d**). Colocalization of hNUMA (red) with NeuN (green) can be seen in a dense population of hNUMA+ grafted cells (**e**). Triple labeling with DCX, hSYN and NeuN antibody showed numerous DCX+ processes projecting towards large α -motoneurons and co-expressing hSYN punctate-like immunoreactivity (**f**, **g**). The

immunosuppressive effect of a given TAC dose (1.9 mg/kg/day) was further tested by identifying the presence of infiltrating T-lymphocytes. A high density leukocyte population (CD45, red) in the vicinity of grafted human cells (hNUMA, green) was observed (**h-j**). Co-staining with markers of T-lymphocytes (CD4 and CD8, red) and microglia (IB1, green) revealed the presence of T-lymphocytes and activated microglia in the areas of grafted cells (**k-m**). The presence of cytotoxic subpopulation of T-lymphocytes in the regions containing hNUMA+ grafted cells (red) was confirmed by colocalization of marker CD8 (green) with general leukocyte marker CD45 (white), (**n**). VH – ventral horn, VF – ventral funiculus. Scale bar a-n: 30 μ m.

Figure 3. Immunohistochemical examination of the presence of grafted human fetal spinal stem cells (hSSC) and immunological response in the spinal cord tissue of SOD+ rats immunosuppressed with 3-month lasting TAC pellet (5.1 mg/kg/day). TAC releasable pellets were implanted subcutaneously in the SOD+ rats (n=6; 60-65 days of age) 13 days prior to grafting with hSSC. Animals were allowed to survive until 10% of bodyweight loss caused by the progression of the ALS disease (i.e., 32-70 days after cell implantation). Immunohistochemical staining with human specific antibody hNUMA (human nuclear protein, green) and doublecortin (DCX, red) revealed consistent presence of high density grafts in the targeted spinal parenchyma in all animals (**a, b**). Double staining with human-specific synaptophysin (hSYN) and GFAP antibody (hGFAP) revealed a dense hSYN punctuate-like immunoreactivity and numerous hGFAP+ grafted astrocytes (**c**). In addition to a dense population of DCX+ grafted neurons the presence of human-specific enolase+ neurons (hNSE; late neuronal marker) can be seen (**d**). The immunosuppressive effect of the administered dose of TAC (5.1 mg/kg/day) was further validated by identifying the presence of T-lymphocytes in human cell-grafted spinal cord sections. Only occasional presence of CD45+ (red) leucocytes was seen; CD45+ elements can preferentially be seen at the periphery of hNUMA+ grafts (**e-g**). Co-staining with CD45 and CD8 antibody shows near complete lack of CD8+ immunoreactivity in CD45+ cells in cell-grafted spinal cord regions and only occasional double stained CD4/CD8/CD45+ cells can be identified (**h-j**), while the majority of CD45+ cells are CD8 negative (**k**; yellow arrows). VH – ventral horn, VF – ventral funiculus. Scale bar a,c: 100 μ m, b,d,e,k: 30 μ m, h:10 μ m

Figure 4. Immunofluorescence examination of the presence of grafted human ES-derived neural precursors (HUES7-NPC) in TAC pellet (4.9 mg/kg/day)-immunosuppressed SD rats with previous L3 contusion injury. Animals (n=4) received spinal grafts of HUES7-NPC at 3 days after spinal injury and were allowed to survive 105 days after the cell grafting. Immunohistochemical staining with antibodies

against human neuronal specific enolase (hNSE, red), human cell nuclei (hNUMA, blue) and doublecortin (DCX, red) on the longitudinally-cut spinal sections revealed continuous graft survival and extensive neuronal differentiation in cell-grafted peri-injury regions (**a-d**). Staining against the general leukocyte marker (CD45, green) and microglia (IB1, red) revealed the absence of leukocytes and the presence of necrotic bodies (non-specific staining, green, yellow arrows) associated with the cytoplasm of microglial cells (**e-g**). cc – central canal, la-lateral, ro-rostral, ca-caudal. Scale bar a: 100 μ m; b-d: 10 μ m; e, f: 30 μ m.

Figure 5. Effect of TAC pellet-induced immunosuppression of circulating T-cells and the spinal infiltration with IgG+ cells, B-cells and granulocyte/monocyte in cell-grafted animals. In TAC pellet-immunosuppressed animals (5.1 mg/kg/day), a significant suppression in the number of circulating blood CD4 and CD8 T-lymphocytes was measured using flow cytometry (**a-c**), (*-p<0.05; T-test). Staining with anti-rat IgG (fluorescence-tagged), anti MHC class II (RT1B) and with anti-CD45 antibody in the 1.9 mg/kg/day TAC group showed a high density of IgG+ cells at the periphery of grafted regions (**d**). In addition, an overall increase in the density of IgG staining in the same areas was seen (**d**; blue dashed area). Triple staining with CD11b, anti-rat IgG and CD45 antibody showed co-expression of CD11b in anti-rat IgG+ cells (**f**; yellow arrows) but no clear colocalization with CD45 marker was detected (**f**; lower panel). In 5.1 mg/kg/day TAC group a near complete lack of anti-rat IgG, RT1B and CD45+ cell was seen (**g**) and only sporadic occurrence of RT1B/CD45+ cells was seen at the periphery of grafted regions (**h**; yellow arrows).

Figure 6. Rejection of spinally grafted hSSC in SD rats in the absence of immunosuppression. Adult SD rats received 10 bilateral injections of hSSC into lumbar spinal cord and survived for 14 days. No immunosuppression treatment was used in any animal. Triple staining of transverse spinal cord sections with DAPI and hNUMA and CD4/8 antibody showed increased cellularity in cell grafted region (**a**; yellow dashed circle) but with no grafted cell survival as evidence by the lack of hNUMA+ cells (**c**). Instead an intense accumulation of CD4/8 cells in previously cell-grafted regions can be seen (**b, d**; yellow arrows). Scale bar a: 100 μ m.

Table

Tab.1 Summary of experimental groups used in tacrolimus PK study.

group	route of tacrolimus	vehicle	dose	frequency	n	time points for detection of Tacrolimus level in blood
No.1	s.c.injection	powder dissolved in castor oil/saline solution	3mg/kg	every 24h	4	2,9,24,72,120 hours
No.2	s.c.injection	powder dissolved in castor oil/saline solution	1.5 mg/kg	every 12h	4	2,12,14,24,120 hours
No.3	s.c.injection	unilamellar liposomes	3mg/kg	once, at beginning	4	2,12,24,48,72 hours
No.4	s.c.injection	multilamellar liposomes	3mg/kg	once, at beginning	4	2,12,24,48,72 hours
No.5	s.c.injection	microspheres	10mg/kg	once, at beginning	3	2,9,24 hours,2,4,7,10,13,16,19, 22 days
No.6	s.c.injection	microspheres	20mg/kg	once, at beginning	3	2,9,24 hours,2,4,7,10,13,16,19, 22 days
No.7	s.c.implantation	3 months lasting pellet	1.8±0.15 mg/kg/day	once, at beginning	4	5,13,20,29,50,56,71,90 days
No.8	s.c.implantation	3 months lasting pellet	3.43±0.21 mg/kg/day	once, at beginning	3	5,7,10,17,26,38,59,74,90 105, 120, 140 days
No.9	s.c.implantation	3 months lasting pellet	5.1±1 mg/kg/day	once, at beginning	6	10,27,42,53 days

Table

Tab.2 Experimental cell grafting groups

rat strain	group	animal ID number	grafted cell line	survival time after cell grafting
SOD1 (ALS)	No.7	4746	HUES7	77
SOD1 (ALS)	No.7	4753	HUES7	33
SOD1 (ALS)	No.7	4750	hSSC	77
SOD1 (ALS)	No.7	4752	hSSC	77
SOD1 (ALS)	No.9	5038	HUES7	40
SOD1 (ALS)	No.9	5081	HUES7	32
SOD1 (ALS)	No.9	5041	hSSC	38
SOD1 (ALS)	No.9	5076	HUES7	32
SOD1 (ALS)	No.9	5095	hSSC	70
SOD1 (ALS)	No.9	5104	hSSC	37
SD (SCCI)	No.10	149	HUES7	105
SD (SCCI)	No.10	153	HUES7	105
SD (SCCI)	No.10	155	HUES7	105
SD (SCCI)	No.10	160	HUES7	105
SD (Naïve)	No.11	1	hSSC	14
SD (Naïve)	No.11	2	hSSC	14
SD (Naïve)	No.11	3	hSSC	14
SD (Naïve)	No.11	4	hSSC	14

SCCI – spinal cord contusion injury

Table

Tab.3 Quantitative/qualitative analysis of leukocyte infiltration in transverse spinal cord sections with identified human cell grafts at 77-90 days after cell grafting.

immunological profile	dose of Tacrolimus		1.8mg/kg/day			5.1mg/kg/day		
	cell type		G-core.	G-pia	SC-par.	G-core.	G-pia	SC-par.
CD45+	leukocytes		***	***	***	*	**	*
CD8+CD45+	cytotoxic T-cells		**	***	*	0	*	0
CD4+CD45+	helper T-cells		***	***	**	*	*	0
RT1B+CD45+	B-lymphocytes		**	***	**	*	*	0
CD11b+	granulocytes+monocytes		**	***	*	*	*	0

0-absence of immune cells, *-1-10 cells, **-11-50 cells, *** >51 cells per section; G-core- core of the graft, G- pial surface of the graft, SC-par. parenchyma of the spinal cord outside of the graft.

Figure
[Click here to download high resolution image](#)

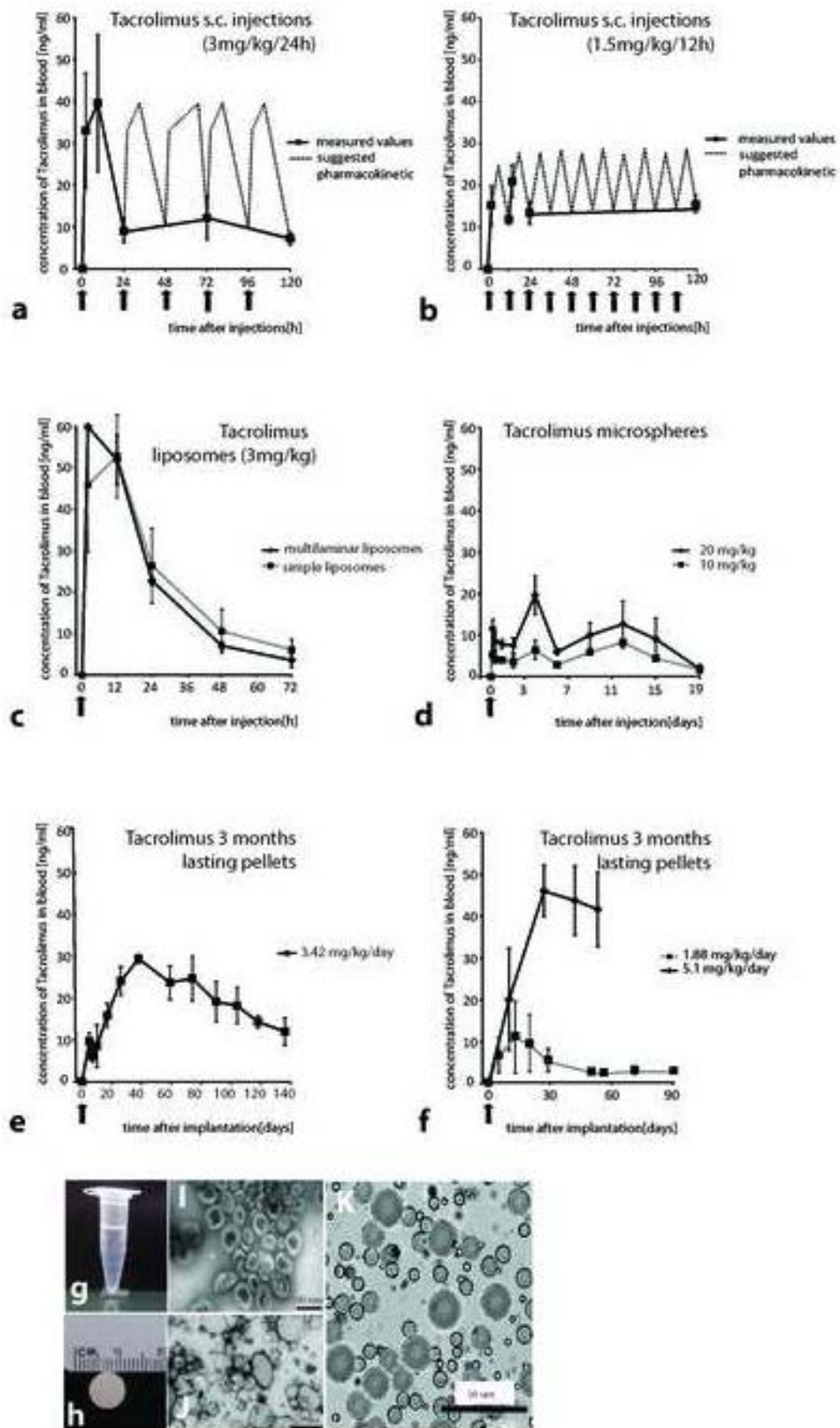


Fig.1 A-K

Figure
[Click here to download high resolution image](#)

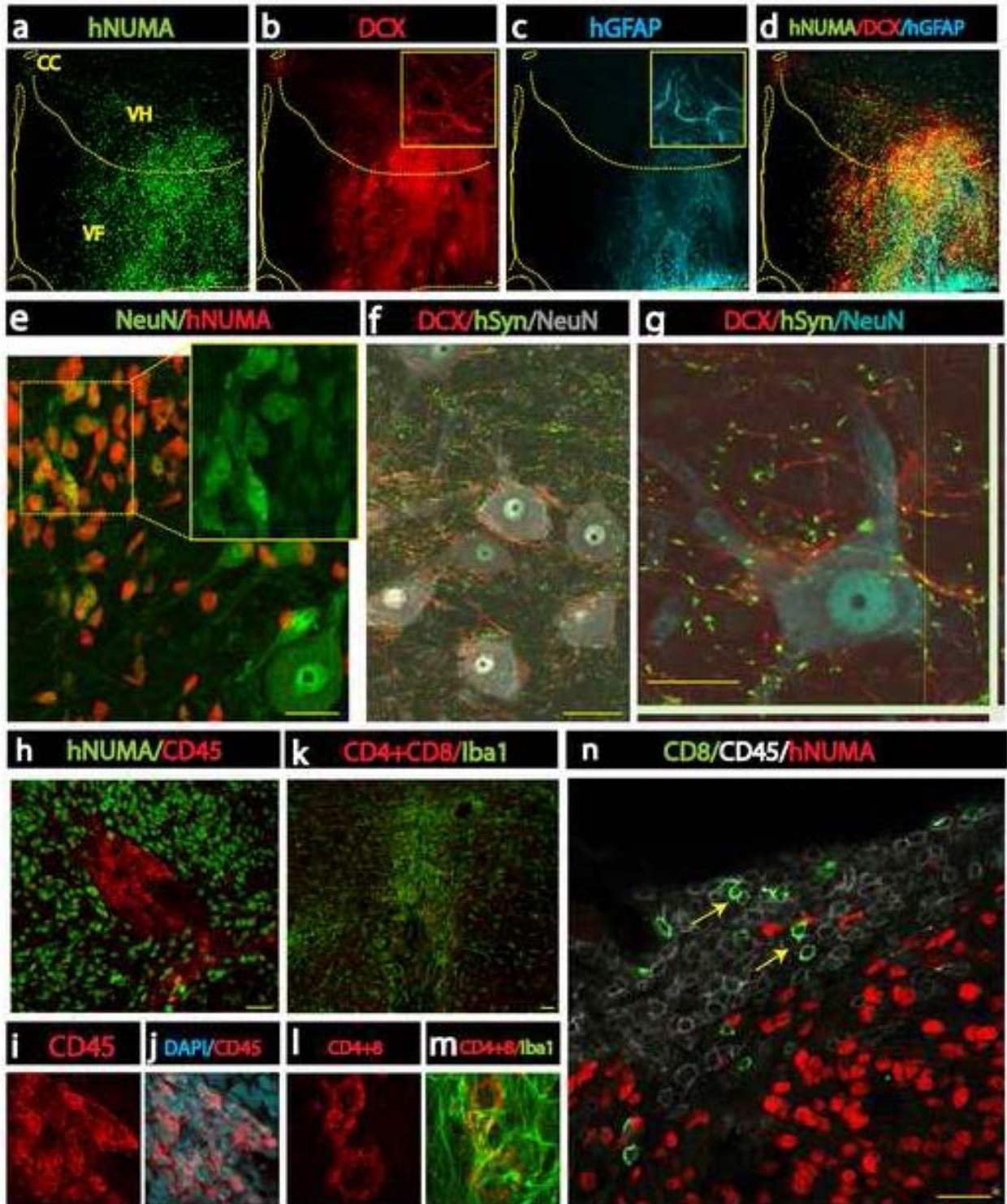


Fig.2 A-N

Figure
[Click here to download high resolution image](#)

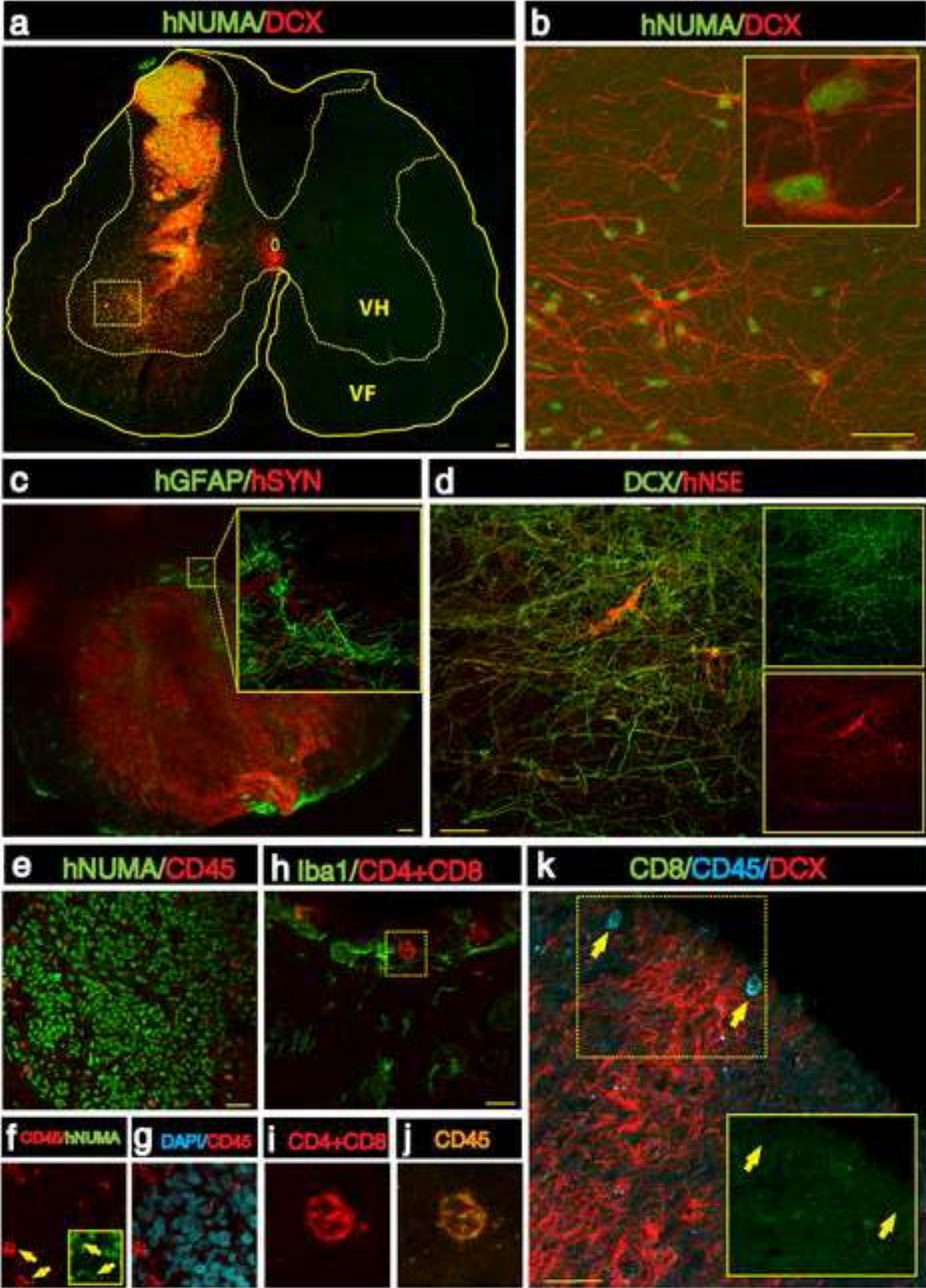


Fig.3 A-K

Figure
[Click here to download high resolution image](#)

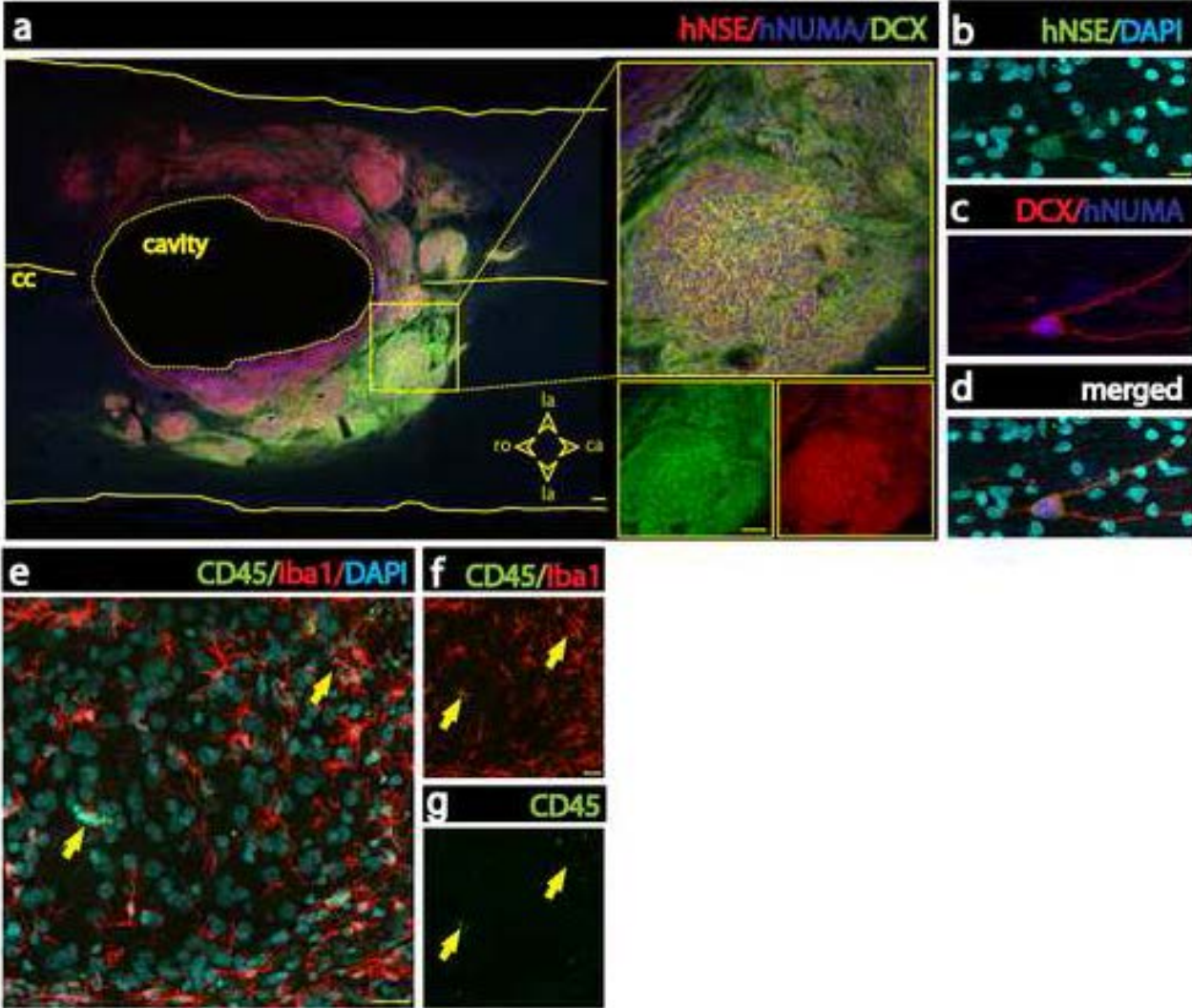


Fig.4 A-G

Figure
[Click here to download high resolution image](#)

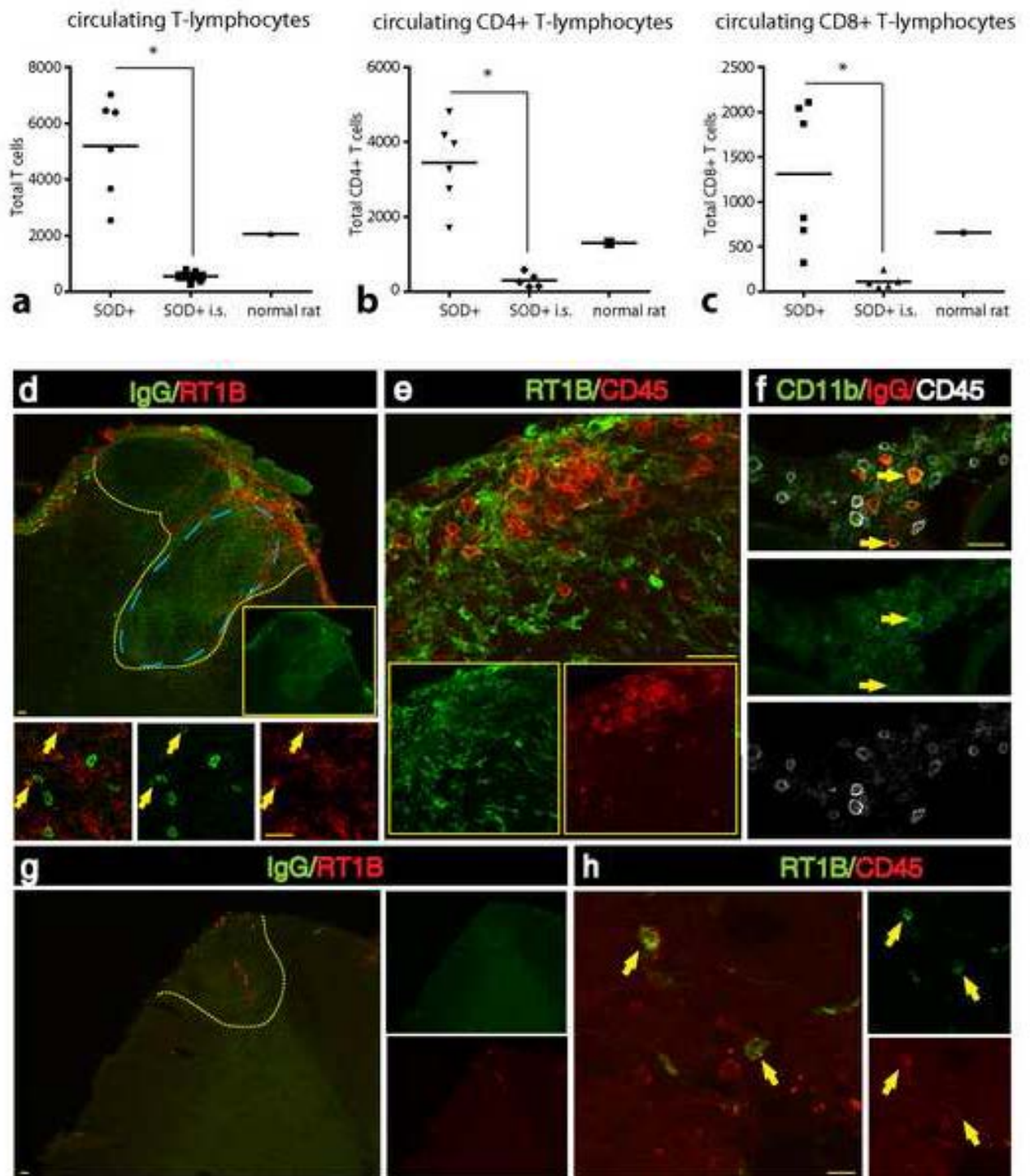


Fig.5 A-H

Figure
[Click here to download high resolution image](#)

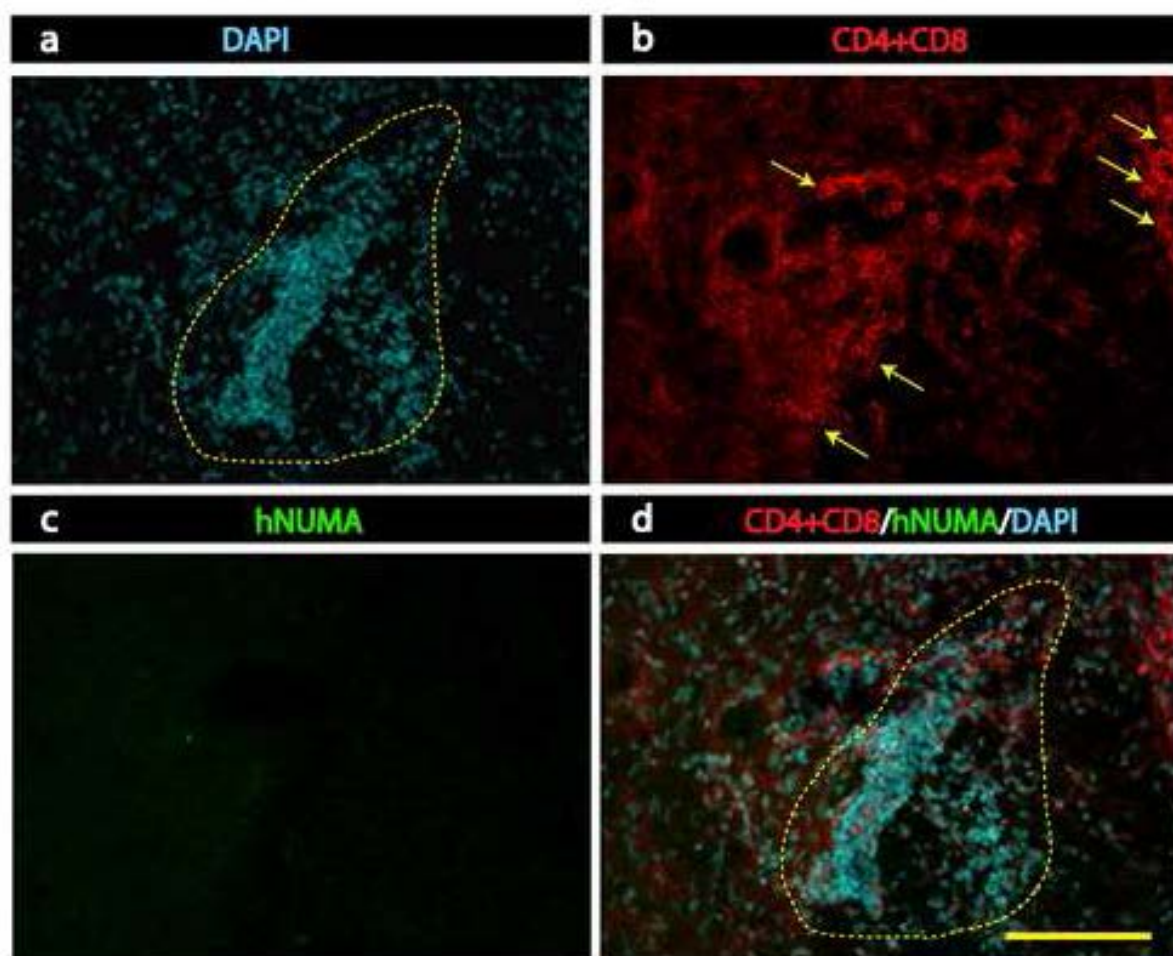


Fig.6 A-D

6. DISCUSSION

6.1. *IN VIVO* MODELING OF HUNTINGTON'S DISEASE

It is undisputable that the rodent genetic models of HD which have been available since 1996 (Mangiarini et al. 1996) provided us with extremely valuable information about huntingtin function, helped us to reveal the complex mechanism of disease pathology, and offered us the first *in vivo* disease environment for validating targets and testing potential therapies (Cattaneo et al. 2005; Zuccato et al. 2010). It is clear, however, that the rodent models of HD have also limitations in modeling of the human disease (Zuccato et al. 2010; Yang and Chan 2011; Morton and Howland 2013). Nevertheless, genetic engineering technology is well advanced in mouse which has allowed generation of great number of mutant and/or knock-out, transgenic and knock-in mouse models which are currently available for neuroscience research (Morton and Howland 2013). And indeed, HD research will always benefit from this incredible choice of mouse models because of the potential of genetics cross-breeding introducing (genetically) manipulated genes of interest into the HD environment to allow us to investigate the mechanisms of the disease, to determine possible therapeutic effects of overexpression of certain wild-type or modulated genes and to specifically “label” certain cell types and/or processes (Zuccato et al. 2010) or allow relatively simple extraction of mRNA from specific cell types directly from the crude lysates (Sanz et al. 2009).

6.1.1. UCHL1 in HD

Benefiting from the great numbers of mouse models available we decided to use the well characterized R6/2 mouse HD model to study the potential involvement of the Ubiquitin Proteasome System (UPS) in HD pathology by crossing it with the *gad* mouse model which lacks the expression of one of the most common protein in the brain – deubiquitinating enzyme UCHL1 which is exclusively expressed in neurons and gametes (Setsuie and Wada 2007; Yi et al. 2007). The histological hallmark of the disease is the formation mutant huntingtin aggregates which are subsequently ubiquitinated (DiFiglia et al. 1997). Aggregates in HD are ubiquitinated (ubiquitinated aggregates present in HD neuronal nuclei are often called inclusion bodies – IBs) and therefore the formation of IBs has always been linked with UPS malfunction.

UCHL1 represents one of the major deubiquitinating enzymes (DUB) in the brain (Cartier et al. 2009) as it is ubiquitously expressed in neurons and because it functions as a deubiquitinating enzyme, ubiquitin ligase and monoubiquitin stabilizer (for review see (Setsuie and Wada 2007)). Mutations of UCHL1 have been linked to several neurodegenerative diseases (for review see (Setsuie and Wada 2007)) and it has been shown that its potentiation can rescue amyloid β protein ($A\beta$) induced pathology by regulating BACE1 protein level, APP processing and $A\beta$ production *in vitro* and *in vivo* (Gong et al. 2006; Zhang et al. 2012).

Early studies of the UPS impairment in HD suggested that polyQ aggregates could directly inhibit the function of 26S proteasome (Bence et al. 2001), that the degradation of polyQ proteins is inefficient (Holmberg et al. 2004) and that the eukaryotic proteasome is not able to

digest polyQ sequences of polyQ-containing proteins (Venkatraman et al. 2004). Conflicting results later showed that the proteasome is fully capable to degrade the expanded polyQ proteins (Michalik and Van Broeckhoven 2004), that the UPS impairment is not caused by direct choking of purified proteasomes but revealed that the UPS impairment is most likely global as detected both in *in vitro* (Bennett et al. 2005) and in *in vivo* studies where the elevated levels of polyUb chains were observed in R6/2 and *Hdh*^{Q150/Q150} mouse models and human post-mortem HD brains (Bennett et al. 2007).

To facilitate the assessment of the UPS activity, recombinant probes typically comprised of enhanced green fluorescent protein appended with a destabilizing modification (degradation signals) which promotes their constitutive degradation by the UPS (“GFPu” UPS reporters) were generated (Bett et al. 2009). In early studies of UPS activity in HD, these artificial reporters of UPS activity were successfully applied in *in vitro* cellular HD models (Bence et al. 2001; Bennett et al. 2005) but when translated into *in vivo* studies using R6/2 mouse model, these reporters failed to accumulate and thus failed to confirm global UPS impairment *in vivo* (Bett et al. 2009; Maynard et al. 2009). Nevertheless, in more recent study fusing of the UPS GFPu reporters to either postsynaptic PSD95 or presynaptic SNAP25 proteins revealed increased levels of GFPu reporters in the synapses of R6/2 and *Hdh*^{Q150} HD mouse models (Wang et al. 2008) which is strikingly similar to what was observed in wild-type hippocampal neurons with inhibited UCHL1 activity (treated with LDN UCHL1 inhibitor) (Cartier et al. 2009). Wang and colleagues also demonstrated that while there is no decrease in proteasomal activity in whole brain lysates of R6/2 mice (Bett et al. 2006; Wang et al. 2008) examination of the chymotrypsin-like proteasomal activity in isolated synaptosomes revealed that proteasomal activity was decreased in synaptosomes isolated from the cortex or striatum of HD mice compared with samples from wild-type. Striatal synaptosomes showed lower proteasomal activity than cortical synaptosomes in both wild-type and HD mice. They also detected an age-dependent decrease in synaptic proteasomal activity in the brain (Wang et al. 2008). These observations suggest that the malfunction of UPS in HD could be region-specific rather than global.

Generation of R6/2 x gad mouse allowed us to examine the effect of the ~50% loss of UCHL1 in the disease environment driven directly by the exon 1 of the mutant huntingtin (Mangiarini et al. 1996; Sathasivam et al. 2013). Interesting functional link between UCHL1 and HD pathology could be found in recent discoveries of UCHL1-dependent regulation of synaptic structure (Cartier et al. 2009) and that UCHL1 is required for maintaining the structure and function of the neuromuscular junction (Chen et al. 2010). UCHL1 is present in spines and postsynaptic densities and the main function of UCHL1 in synapses is most likely free mono-ubiquitin stabilization (Cartier et al. 2009). Our data showed that the reduced UCHL1 expression caused aggregates of mHTT to accumulate more in the neuropil of R6/2 x gad mouse if compared to the R6/2 mouse. We also found that soluble exon 1 mHTT from R6/2 x gad brain lysates migrate faster in the gel (Hruska-Plochan et al. 2013 in review). This suggests that the locally disturbed UPS in synapses in HD mouse models (Wang et al. 2008) could be caused by decreased monoUb-stabilizing and DUB activities and possibly by increased ligation activity of UCHL1 which in turn may lead to deprived free monomeric ubiquitin pools and to accumulation of polyUb chains and increased polyubiquitination of high

molecular weight proteins as detected in previous works *in vivo* (Bennett et al. 2007; Maynard et al. 2009) and in R6/2x*gad* striatum in our experiments (Hruska-Plochan et al. 2013 in review). As a result, less E1mHTT could be targeted to UPS and more E1mHTT could be available for aggregation in R6/2x*gad* brain. It is not clear, however, how mHTT alters UCHL1 function(s) in HD. In our experiments, we observed that UCHL1 co-localized with both soluble mHTT and with aggregated mHTT and with wild-type huntingtin (Hruska-Plochan et al. 2013 in review) (see Fig. 13). We therefore hypothesize that abnormal interaction(s) of UCHL1 with mHTT in HD could lead to impaired UCHL1 functioning or that the UCHL1 could be exhausted due to an ongoing clearance of mHTT by the UPS and autophagy. It has been shown that UCHL1 expression is regulated by the REST/NRSF (for review see (Day and Thompson 2010)) and because mHTT causes a reduction in the transcription of RE1/NRSE neuron-linked genes (Zuccato et al. 2003), mHTT could decrease the levels of UCHL1 indirectly. Another study showed that stimulation of NMDA receptors increases expression of UCHL1 (Cartier et al. 2009) and because the NMDA receptors are over-activated in HD (Young et al. 1988; Zeron et al. 2002; Fan and Raymond 2007; Estrada-Sanchez et al. 2009) this could explain why we did not see decreased levels of UCHL1 protein in R6/2 brain. Finally, recent data suggests that oxidative modification of UCHL1 caused by oxidative stress in neurodegenerative diseases greatly affects UCHL1 activity (for review see (Setsuie and Wada 2007)). More experiments need to be performed to precisely explore the relations between the presence of mHTT aggregates/IBs, neuronal death and UCHL1. It will be important to evaluate UCHL1 enzymatic activities in the presence of exon1 and also full-length mHTT in the complex *in vivo* HD settings as well as in cell-free systems.

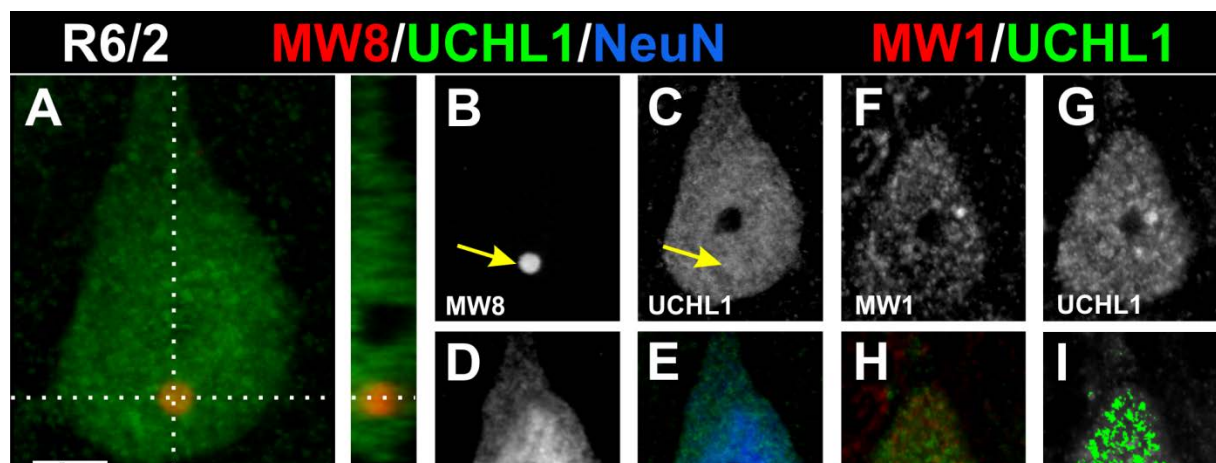


Fig. 13 Confocal microscopy analysis of UCHL1 and mhtt. Fig 6 from author's publication *Partial UCHL1 depletion in R6/2 mouse model of Huntington's Disease accelerates mutant huntingtin aggregation.*

6.1.2. tgHD minipig

Despite their great importance in understanding of the disease mechanisms, the rodent models are relatively short-living animals with small lysencephalic brains and therefore will never accurately resemble human disease conditions (Morton and Howland 2013). The short life span offers just a very limited therapeutic window for the test of new potential therapies and the small size of brain and spinal cord limit the beneficial outcomes of such therapies because they are most of the times invasive (i.e. cell grafting, intraparenchymal vector delivery etc.) thus injuring the CNS just by simple delivery of the therapeutics.

The miniature pig (*Sus scrofa*) has similarities to humans in anatomy, physiology, and metabolism (Vodicka et al. 2005; Lunney 2007; Swindle et al. 2012). The size and structure of pig brain makes it amenable to neurosurgical procedures and non-invasive high resolution neuroimaging methods similar to those performed in humans (such as MRI and PET) (Ishizu et al. 2000; Gizewski et al. 2007; Keereman et al. 2010). The lifespan of minipigs and their sophisticated cognitive and motor abilities also make them useful for long-term studies of learning, memory and behavior (Lunney 2007; Gieling et al. 2011a; Gieling et al. 2011b). There has been recent progress in defining the porcine genome (Jorgensen et al. 2005; Wernersson et al. 2005; Jiang and Rothschild 2007; Archibald et al. 2010), porcine single nucleotide polymorphisms (Ramos et al. 2009), microRNAome (Kim et al. 2008; Reddy et al. 2009; Duff et al. 2010), and improved techniques for genetic modification of pigs (Hofmann et al. 2003; Nagashima et al. 2003; Kurome et al. 2006; Lavitrano et al. 2006). The porcine homologue of the huntingtin gene has a large ORF of 9417 nucleotides encoding 3139 amino acids with a predicted size of 345 kDa (GenBank, Accession No. AB016793). There is a 96 % similarity between the porcine and human huntingtin genes (GenBank, Accession No. AB016794). The number of CAG repeats in the porcine HTT gene is polymorphic, ranging from 8 to 14 units, and falls within the range of the normal human huntingtin gene (Matsuyama et al. 2000). Similar to humans, miniature pig possesses two HTT transcripts of approximately 11 and 13 kb (Lin et al. 1993; Matsuyama et al. 2000). The similarities between porcine and human huntingtin genes and proteins have provided further impetus to use the pig as a model of HD (Aigner et al. 2010; Swindle et al. 2012). Moreover, to our best knowledge, minipig (or pig in general) represents the only large animal with multiple transgenic models already in place and available for broad scientific community at the National Swine Resource and Research Center (NSRRC) (28 models at the time of writing) and at the Exemplar Genetics (ExemplarGenetics) (7 models at the time of writing). Moreover, the availability of different immunodeficient pig models (Ishikawa et al. 2010; Basel et al. 2012) makes pigs ideal for transplantation studies. Pigs are in general established model animals in biomedical research and the use of pigs in preclinical safety research is rapidly increasing (Hagan 2011).

We have therefore decided to generate a minipig transgenic model of HD. Transgenic HD minipigs were generated using lentiviral transduction of porcine zygotes in syngamy, at the onset of embryonic DNA synthesis (Baxa et al. 2013). The precise timing of lentiviral transduction enhances incorporation of the transgene cDNA into embryos. The lentiviral delivery did not cause mosaicism, since the mutant HTT was revealed in all tissues tested in F1 and F2 tgHD minipigs and maintained the same number of glutamines. We found an in-

frame deletion of the expanded CAG/CAA tract such that the integrated transgene encoded 124 glutamines instead of the original 145 glutamines. Importantly, one single copy of exogenous HTT was found in chromosome 1 (1q24-q25) where it was maintained in F1 and F2 offspring. Both female and male transmission of the HD transgene with a Mendelian inheritance was confirmed in our tgHD minipigs. The tgHD minipigs of F0 – F2 generations had two alleles coding endogenous pig HTT and one allele for the N-terminal human mutant HTT. Mutant HTT protein expression was detected in different brain regions including cortex, caudate nucleus and putamen and in a variety of peripheral tissues and confirmed by both Western Blot analysis and TR-FRET. With one exception (hypothalamus in one of the TgHD minipigs), the data from WB and TR-FRET biochemical assays showed a good correspondence for the relative distribution of human mutant HTT in different brain regions and peripheral tissues (Baxa et al. 2013).

Midbrain dopaminergic neurons play a critical role in basal ganglia circuitry and function including coordination of movement. Protein phosphatase 1 regulatory subunit 1B, also known as dopamine- and cAMP-regulated neuronal phosphoprotein (DARPP32), is highly expressed in caudate-putamen medium-sized spiny neurons (Walaas and Greengard 1984; Ouimet and Greengard 1990). Dopamine D1 receptor stimulation enhances cyclic AMP formation, resulting in the phosphorylation of DARPP32 (Walaas and Greengard 1984) at Thr34 by PKA (Hemmings et al. 1984). A loss of DARPP32 levels in medium-sized spiny striatal neurons was observed in several rodent models of HD (Bibb et al. 2000; van Dellen et al. 2000), and in the globus pallidus and putamen of 7 month old HD sheep (Jacobsen et al. 2010) probably as a consequence of degeneration of nigrostriatal projections of dopaminergic neurons in the substantia nigra (Oyanagi et al. 1989; Yohrling et al. 2003). A 16 month old tgHD minipig brain had a reduction compared to WT in the intensity of neuronal labeling for DARPP32 in the caudate nucleus and putamen suggesting that changes in DARPP32 may begin in the tgHD minipig brain at around 16 months of age.

As mentioned earlier, the formation of aggregates is a hallmark of HD pathology. Nuclear and cytoplasmic inclusions of mutant HTT are seen in human postmortem HD brain and in mouse models of HD (Davies et al. 1997; DiFiglia et al. 1997). There was no evidence of aggregates of mHTT protein in the tgHD minipig up to 16 months of age based on biochemical (AGERA, filter retardation) and immunohistochemical assays with antibody to anti-HTT1-17 (AB1) (DiFiglia et al. 1997). This antibody detects mutant HTT inclusions in the human HD brain (DiFiglia et al. 1997). Other antibodies commonly used to detect nuclear inclusions of human HTT fragments in HD mice including MW8 and EM48 produced no staining in the tgHD minipigs. The absence of nuclear inclusions in the tgHD minipigs was consistent with the negative results for aggregation observed using the AGERA and filter retardations assays. Many factors influence the incidence of aggregated mHTT including levels of mutant protein expression, polyglutamine length, the length of the mHTT fragment, and age of the animal (Hackam et al. 1998; Li and Li 1998; Chen et al. 2002).

A surprising finding was evidence for a constant decline in fertility in F1 boars caused by reduced sperm number and penetration rate (see Fig. 14). This phenotype can be easily monitored in the tgHD minipigs and therefore represents a biomarker that can be suitable for therapeutics. Pathology in the germinal epithelium has been documented in human HD and

YAC 128 HD mouse on histological sections where a decreased number of germ cells and reduced seminiferous tubule cross-sectional area have been observed (Van Raamsdonk et al. 2007). The testicular pathology in humans was related to the presence of mutant HTT since severity was greater in patients with longer CAG repeats (Van Raamsdonk et al. 2007). The YAC 128 HD mouse develops testicular pathology between 9 and 12 months prior to significant reduction in testosterone or GnRH levels but coinciding with changes in the brain and the appearance of motor deficits. Unlike the tgHD minipigs, problems with sperm quality and fertility have not yet been reported in HD patients.

Interestingly, reduced number of sperm cells in tgHD minipig boars and their decreased zona pellucida (ZP) penetration capability (Fig. 14) can be directly attributed to reduced activity of the proteasome as the sperm acrosome-borne proteasomes degrade the sperm receptor protein on the ZP that becomes ubiquitinated during oogenesis (Sutovsky 2011; Zimmerman et al. 2011). Moreover, inhibition of proteasomes blocks IVF (Sutovsky 2011) and ubiquitinated sites were identified in all the three protein components of pig ZP, i.e. ZPA, ZPB, and ZPC (Sutovsky et al. 2004; Zimmerman et al. 2011) further confirming the importance of the sperm acrosome-borne proteasomes in fertilization. It is therefore tempting to hypothesize that the decreased impaired penetration rate of ZP by tgHD spermatozoa could be caused by mutant huntingtin-impaired proteasome function. UCHL1 is uniquely expressed in neurons and germ cells (Setsuie and Wada 2007; Yi et al. 2007) and is present in spermatogonia but not in mature spermatozoa where UCHL3 is found and vice versa (Yi et al. 2007). Given the fact that UPS is crucial for sperm quality control (Sutovsky et al. 2001) and that UCHL1 is required for normal spermatogenesis (Kwon et al. 2005), potential aberrant interaction of mutant huntingtin with wild-type UCHL1 in spermatogonia, similar to what we have seen in R6/2x*gad* mouse brain in our experiments (Fig. 13), can help to explain the reduced levels of spermatozoa in tgHD minipig (Fig. 14). On the other side, the complete loss of UCHL1 function in *gad* mice led to decreased apoptosis and increased number of spermatogonia but the weight of epididymis as well as the number of spermatozoa in it was reduced (Kwon et al. 2005). Neurons from *gad* mice were also reported to be apoptosis-resistant (Harada et al. 2004). But, in the case of neurodegenerative diseases (lysosomal storage diseases), downregulation of UCHL1 was observed and overexpression of UCHL1 by plasmid transfection decreased caspase-mediated apoptotic cell death in the disease cell models suggesting anti-apoptotic function of UCHL1 (Bifsha et al. 2007). It has also been previously shown that the inhibition of UCHL1 in pig oocytes led to decrease of free mono-ubiquitin and increased K63-linked polyubiquitin resulting in functional deficits which in this case was demonstrated by polyspermy, thus increased penetration rate through ZP (Susor et al. 2010). It would be therefore interesting to also examine the wild-type minipig sperm penetration rate into the tgHD minipig oocytes with intact ZP once sufficient female tgHD minipigs are available.

As we mentioned earlier, the number of various minipig genetic models which are already available just underline the advantages of this large animal in modeling and research of different diseases. The very recently generated transgenic minipig expressing fluorescently tagged 20S core particles with the EGFP (fused to the proteasomal subunit α -6/ PSMA1 (PSMA1-GFP transgene) (Miles et al. 2013) could be crossed with the tgHD minipig (Baxa et

al. 2013) which would allow better investigation of the proteasome dysfunction not only in the sperm cells but also in the brain.

Several large transgenic models were recently produced and characterized (Morton and Howland 2013). A transgenic non-human primate model (Yang et al. 2008) was generated using a lentiviral construct expressing exon 1 of the human *htt* gene with 84 CAG repeats. Five HD transgenic macaques were generated exhibiting HD neuropathology with rapid onset of an HD like phenotype, though only 2/5 animals survived past 6 months. Two other large animal species were used to generate large animal model in HD in the past years – HD transgenic sheep carrying full-length human *htt* with 73 polyglutamine repeats under the control of the human promoter (Jacobsen et al. 2010) and in addition to our tgHD minipig (Baxa et al. 2013), cloned transgenic HD minipigs bearing N-terminal mutant HTT (208 amino acids and 105Q) have been generated via somatic cell nuclear transfer technology (Yang et al. 2010), but the extremely high expression levels of the transgene led to premature (3 days old) death of three of the 5 born piglets, fourth lived for only 25 days and the fifth founder was still viable at the beginning of 2013 (Morton and Howland 2013). The very short fragment of mutant huntingtin which is expressed in this pig questions its usefulness although no other data were published since the initial report. Considering the “pros” and “cons” of all large animal models which have been generated so far, the primate model of HD (Yang et al. 2008) seems to be less likely to become widely used because of several disadvantages namely the public and ethical issues, the age of sexual maturity and small number of offspring, very high price and need of separate housing etc. Both pigs and sheeps share advantages and disadvantages, but it is clear that the use of just one large animal model will not lead to answer to all the questions we are looking forward to address and thus the full characterization and future use of all currently available large animal model should be pursued (Morton and Howland 2013).

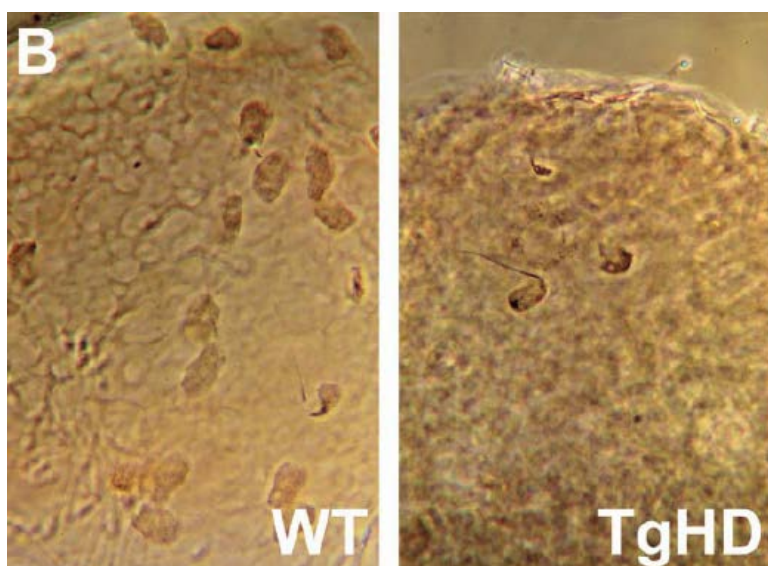


Fig. 14 Failure of reproductive capacity in TgHD boars

Fig. 10 B from author's publication
A Transgenic Minipig Model of Huntington's Disease

6.1.3. HD summary

In summary, we have developed a heterozygote tgHD minipig that expresses a human mutant HTT fragment throughout the CNS and peripheral tissues in a stable fashion through multiple generations (Baxa et al. 2013). The tgHD minipig is healthy at birth and through early development and does not exhibit obvious signs of abnormal movement up to 40 months of age. However, a decline is evident at 16 months in DARPP32 immunoreactivity in the neostriatum, the region most affected in HD. Thus, tgHD minipig should be valuable for testing long term safety of HD therapeutics. We have also have found that UCHL1 is most likely affected in HD as the reduction of UCHL1 expression accelerated mutant huntingtin aggregation and increased the levels of polyUb chains in the striatum of R6/2 HD mouse (Hruska-Plochan et al. 2013 in review). As UCHL1 is present in mutant huntingtin aggregates/IBs and both wild-type huntingtin and soluble mutant huntingtin colocalize with UCHL1 in the R6/2 neurons, and in addition, as the UPS is crucial for sperm quality control and UCHL1 is required for normal spermatogenesis, the tgHD minipig boar's decline in sperm number and ZP penetration rate could therefore be a consequence of aberrant interaction of mutant huntingtin with UCHL1 and strongly suggest UPS impairment in tgHDminipig testes.

6.2. (NEURAL) STEM CELL THERAPY IN SPINAL CORD DISORDERS AND INJURY

Even though the large number of mouse models allows researchers to choose the mouse that is best suitable to address their questions, the small size of mouse CNS greatly complicates and/or hampers the use of mouse models in pre-clinical research where invasive approach is used to deliver therapeutic agents. For that reason the rat disease and injury models are superior to the mouse ones when it comes to cell grafting. In our grafting of human neural stem cells experiments we therefore used i) the already available transgenic rat model of Amyotrophic Lateral Sclerosis which carries human mutant SOD1 protein with G93A point mutation (SOD1 rat) and ii) we established the rat model of acute lumbar (L3) compression injury.

6.2.1. Rationale for spinal cell-replacement therapy after spinal trauma and in ALS

Based on the numerous grafting experiments published in recent years and on the characteristics and properties of neural stem cells (NSCs), the use of NSCs for acute spinal cord grafting after trauma serves three purposes. First, it serves to provide local trophic support in the areas of previous injury (provided that grafted cells are able to home and survive long-term once grafted into the injured spinal cord milieu) and to minimize or halt the process of progressive axonal/neuronal degeneration. Second, it serves to provide a cavity-filling effect by replacing previously injured-degenerated necrotic tissue and thus prevent the long-term (or progressive) formation of rostro-caudal cavitations (i.e., syringomyelia) (Wirth et al. 2001) (Fig. 17). Third, by the development of synaptic contact with the host

axons/neurons above and below the injury level it can potentially lead to formation of a functional relay through the injury site (Fig. 16).

Accordingly, the use of NSCs for intraspinal grafting into the ALS spinal cord serves the following three purposes. First, similarly as in SCI, it serves to provide local trophic support to the motor neurons and to certain extent, minimize neuronal degeneration. Second, it serves to partially replace the host cells which are affected by the mutant SOD1 expression leading to partial clearance of the not yet known toxic factors which are being released by the host diseased astrocytes and/or third, it serves to partially restore the function of the host glial cells – thus, to reuptake of the glutamate from the synaptic cleft and potentially to partial restoration of the myelin insulation of motor neurons. But in the case of ALS, it has to be noted, that the primary outcome of the HSSCs transplantation in human ALS patients is the partial improvement of function and quality of life as the life-extension is not expected based on the aggressive course of the disease and because the majority of the ALS patients will most likely receive the HSSCs grafts after the onset of the disease thus when the progressive motor neuron and oligodendrocyte degeneration, neuroinflammation and toxicity is already on place.

6.2.2 Cell survival and differentiation

In both studies near pure population of nestin+ human fetal spinal stem cells were grafted intraspinally at 3 days after contusion-induced spinal cord injury (van Gorp et al. 2013 in press) or at age ~65 days in SOD1 rat (Hefferan et al. 2012). Analysis of the graft survival at 2 (SCI) or ~2.5 (SOD1) months after grafting showed a dense population of grafted hNUMA+ cells in grafted previously trauma-injured regions or in the central and deep gray matter (laminae VII–IX) with occasional extension into the white matter with slight enlargement of the spinal cord noted typically in the area closest to the graft in SOD1 rats (Hefferan et al. 2012). In addition, numerous hNUMA+ cells which migrated out of the graft in distances ranging between 2-3 mm were also seen in SCI rats (van Gorp et al. 2013 in press) while the migration of HSSC in the spinal cord of SOD1 rats was limited (Hefferan et al. 2012) (even with 25% longer survival after grafting than in SCI animals) which can most likely be explained by space limitation of the relatively “intact” (i.e. without traumatic injury) spinal cord tissue of SOD1 rats.

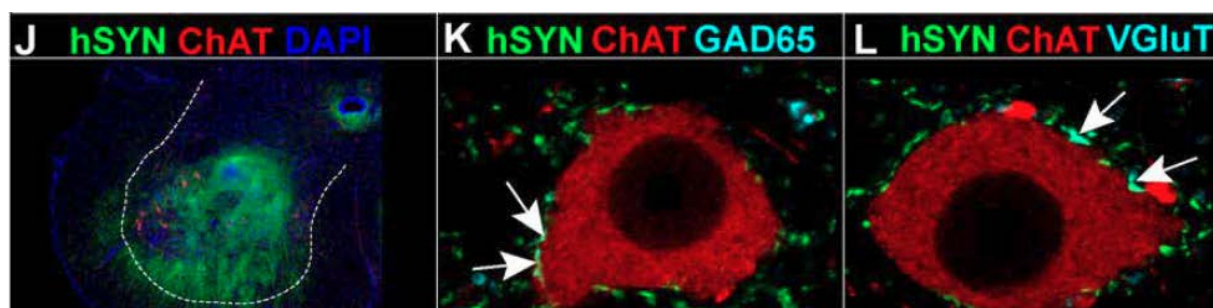


Fig. 15 Human spinal neural stem cells grafted into lumbar spinal cord of SOD1G93A rats show long term survival and preferential neuronal differentiation. Fig 1 J-L from author's publication *Human Neural Stem Cell Replacement Therapy for Amyotrophic Lateral Sclerosis by Spinal Transplantation*

Using human-specific antibodies against NSE and synaptophysin (hNSE; hSyn, respectively - markers of mature neurons), we have also shown that a majority of grafted cells developed into a neuronal phenotype in both studies (Fig. 15). Essentially all structures within the graft core labeled for both hNSE and doublecortin (DCX; early postmitotic neuronal marker which is not present in the parenchyma of adult spinal cord) (Hefferan et al. 2012). In addition, quantitative analysis of the grafts in SOD1 rats demonstrated that $78\pm 6\%$ of hNUMA-positive nuclei were surrounded by a DCX+ cytoskeleton, suggesting that those cells were young, migrating, post-mitotic neurons. Likewise, no cells with DCX were found lacking a hNUMA+ nucleus. Similar to the hNSE staining pattern, fibers with doublecortin were found extending often more than 500 μm radially from the graft core, sometimes crossing through/near lamina X to the opposite side. On average $12.5\pm 1.2\%$ of hNUMA-positive cells expressed the mature neuron marker NeuN (Hefferan et al. 2012). Many hSyn+ boutons were found to reside in the vicinity of host neurons in both studies. Because of the nature of the study, many more hSyn+ bouton-like structures adjacent to the host neuronal cell body and associated processes (even on some persisting α -motoneurons) were found in SOD1 rats (Fig. 15) (Hefferan et al. 2012). By examining specific neurotransmitter phenotype markers in 0.5 μm -thick optical sections, $0.8\pm 0.3\%$ of hSyn+ structures were co-labeled with glutamate decarboxylase 65 (GAD65), a marker for γ -aminobutyric acid (GABA)-producing neurons. Immunostaining for each of the three vesicular glutamate transporters known to exist in the spinal cord (VGluT 1, 2, and 3) revealed that $1.3\pm 0.5\%$ of boutons with hSyn were glutamatergic (Fig. 15). Glycinergic boutons, identified by immunostaining for a glycine transporter, (GlyT2) represented $0.9\pm 0.6\%$ of these boutons. In the vast majority ($>97\%$) of cases hSyn+ cells did not contain any differentiated cell marker, indicating a persistent immature phenotype at 2.5 months after grafting in SOD1 rats (Hefferan et al. 2012).

On the contrary, analysis of the neurotransmitter phenotype in grafted cells in SCI animals showed only the development of putative inhibitory GABA-ergic synapses with host neurons (i.e. GAD65/67+; Fig. 16) (van Gorp et al. 2013 in press). This could be explained by the relatively shorter surviving time of the grafted cells (25%) and by the observed behavior of the HSSCs grafted into the injured lumbar spinal cord – we have determined that while the density of grafted cells is relatively low to fill the cavity-forming region, the grafted cells continue to proliferate after grafting to the point when a cavity is near completely filled with grafted cells (unpublished data). The cell proliferation is inhibited once the cavity is filled and after that the cells differentiate normally. That the cells do not develop into pre-neoplastic or neoplastic cells has been assessed in a 9-month tumorigenicity study with nude rats whose Th9 spinal cord segment was first injured by contusion (manuscript in preparation). Thus the delayed neuronal maturation/differentiation seen in SCI spinal cords was most likely caused by the initial period of proliferation of HSSCs which led to complete filling of the injury-induced cavity.

6.2.3. Effect of spinal grafting of HSSC on the recovery of motor function and muscle spasticity

In our HSSCs transplantation studies, a combination of several motor performance tests were employed including open field modified BBB scoring, CatWalk gait analysis, inclined ladder climbing, single frame hind limb motion analysis, and myogenic motor evoked potentials to identify the degree of motor function recovery after cell grafting. The changes in muscle spasticity in lower extremities (i.e., below the level of injury) were also measured using a computer-controlled ankle rotational system (Marsala et al. 2005). The CatWalk gait analysis showed significantly improved paw placement in HSSC-injected SCI animals when compared to control SCI animals (van Gorp et al. 2013 in press). In addition, a significant suppression of otherwise exacerbated muscle spasticity response measured during ankle rotation was seen in cell-treated SCI animals (van Gorp et al. 2013 in press). In SOD1 animals, Hoffmann reflex spasticity measurements revealed a higher average H-wave amplitude (increase in rate-dependent depression; RDD) for the HSSCs-grafted group compared to the media-treated animals (3.5 ± 0.6 vs. 1.1 ± 0.3 mV; $p, 0.05$; t-test), indicating functional preservation between sensory Ia afferent, α -motoneuron and motor plate (Hefferan et al. 2012). However, no improvements in other functional CatWalk parameters (runway crossing time, hind paws base of support, regularity index/coordination, stride length, phase dispersions), MEPs, BBB score, single-frame motion analysis or ladder climbing test) were seen in the HSSC-treated SCI rats (van Gorp et al. 2013 in press). On the other hand, the BBB score (measured from each animal every 3–4 days) was significantly preserved at age 135–142d in the cell grafted SOD1 animals compared with the media-treated group (Hefferan et al. 2012).

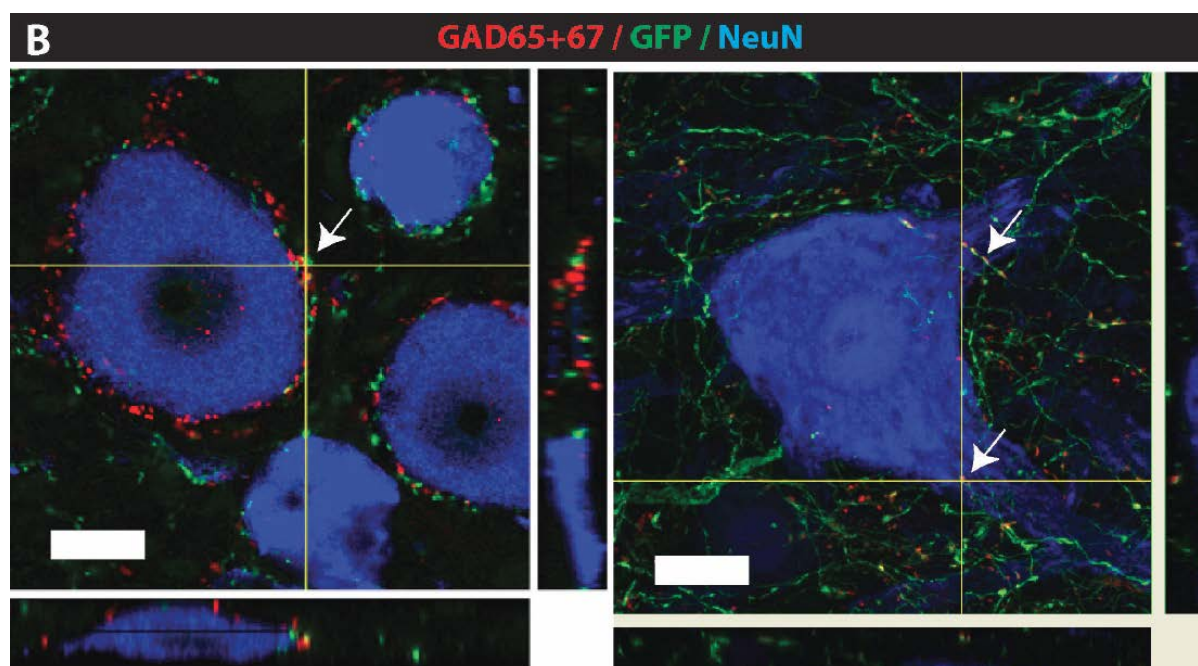


Fig. 16 Development of putative GABA-ergic synaptic contact between HSSC and the host neurons. Fig 6 B from author's publication *Amelioration of motor/sensory dysfunction and spasticity in a rat model of acute lumbar spinal cord injury by human neural stem cell transplantation*.

Consistent with our current data, several other studies from different laboratories have demonstrated a variable degree of motor function recovery after spinal grafting of rodent or human fetal, adult or embryonic stem-cells derived neural precursors using a variety of spinal injury models in mice and rat (McDonald et al. 1999; Hofstetter et al. 2005; Mitsui et al. 2005; Davies et al. 2006; Macias et al. 2006; Cizkova et al. 2007; Davies et al. 2008; Alexanian et al. 2011; Boido et al. 2011; Jin et al. 2011; Lu et al. 2012). Importantly, these data together suggest that some degree of therapeutic effect can be achieved once cells are grafted during the early post-injury period (i.e., 3-7 days after spinal trauma) or in early pre-symptomatic stages of the disease in SOD1 rats (i.e. before the first symptoms can be clinically diagnosed).

6.2.4. Grafted HSSCs into lumbar cord offered no effect on survival of SOD1 rats

Despite the transient improvement of neurological/motor functions and local improvement in motor neuron survival, we found no survival benefit versus our control media-injected group (Hefferan et al. 2012). This was not unexpected, since for humane reasons survival in this animal model is defined by a loss of righting reflex (i.e., the ability of the animal to right itself). An intact righting reflex requires coordinated hindlimb and forelimb motor function and continuing functional coupling of the upper and lower motor neuron system. In deficits which include upper and lower motor neuron degeneration (such as seen in SOD1^{G93A} rats), region-restricted treatments (as achieved after spinal segmental cell grafting) is not expected to significantly modify upper motor neuron degeneration and loss and the associated progressive decline in righting reflex (Hefferan et al. 2012). Nevertheless, using lumbar spinal grafting of human spinal neural stem cells similar to those of our current study, Xu et al. (2006) previously reported an apparent lifespan extension of SOD1^{G93A} rats of 11 days compared to control animals receiving injection of dead cells (Xu et al. 2006) and even longer extension of survival (17 days) was achieved when the HSSCs (in this case, the same cell line as we have used in our study) were grafted into both cervical (C4-C5) and lumbar (L4-L5) segments of the spinal cord (Xu et al. 2011). Similar to our study a significantly higher number of persisting lumbar a-motoneurons was found in HSSCs treated animals in both studies. Given the robust graft survival, cell differentiation and migration seen in our study (Hefferan et al. 2012), we speculate that the differences between ours and these prior studies may reflect the occurrence of natural drift in the onset of disease between different cohorts of animals (a feature that has been argued to necessitate >25 animals per group in order to draw statistically valid conclusions) (Scott et al. 2008) and/or difference in the design of the control groups (i.e., injections of dead cells vs. media only) and potentiation of local neuronal degeneration in dead cell injected animals.

6.2.5. Effect of spinal grafting of HSSC on the recovery of sensory function

In our SCI study, we assessed the sensory function below the level of injury (hind paws) by measuring the mechanical and thermal thresholds for supraspinally mediated escape behavior (van Gorp et al. 2013 in press). Using this method (in contrast to hindpaw withdrawal reflex methods) we did not observe SCI-induced hyperalgesia at the hindpaws (below-level), which is in line with observations reported from other laboratories (Hofstetter et

al. 2003; Baastrup et al. 2010). We did, however, find significant improvement of both SCI-induced mechanical and thermal hypoesthesia. It is important to note that the sensory thresholds did not yet plateau at the end of the 2-month survival period. We speculate that an additional quantitative and qualitative improvement in the sensory function would likely be seen should a longer post-grafting interval be studied (van Gorp et al. 2013 in press).

In addition to sensory tests, quantitative analysis of spinal parenchymal markers indicative of developing (spinal) hypersensitivity (i.e., CGRP/GAP43, an indicator of aberrant sprouting of primary sensory neurons (Ondarza et al. 2003; Macias et al. 2006), and Iba1 staining, a marker of microglia activation (Hains and Waxman 2006)) were studied and showed a significant decrease in CGRP staining intensities in HSSC-treated animals if compared to SCI controls (van Gorp et al. 2013 in press). This suggests that the recovery/decrease in sensory thresholds observed in our study is not a result of aberrant sprouting or microglia activation. Consistent with the observations from our study, previous studies from other laboratories have demonstrated similar functional and histopathologically-defined (i.e. decrease in CGRP staining around the injury site) improvements after spinal grafting of fetal-tissue derived human or rodent neural or glial-restricted precursors in several mouse or rat spinal injury models (Hofstetter et al. 2005; Mitsui et al. 2005; Macias et al. 2006; Davies et al. 2008; Baastrup et al. 2010; Alexanian et al. 2011; Jin et al. 2011).

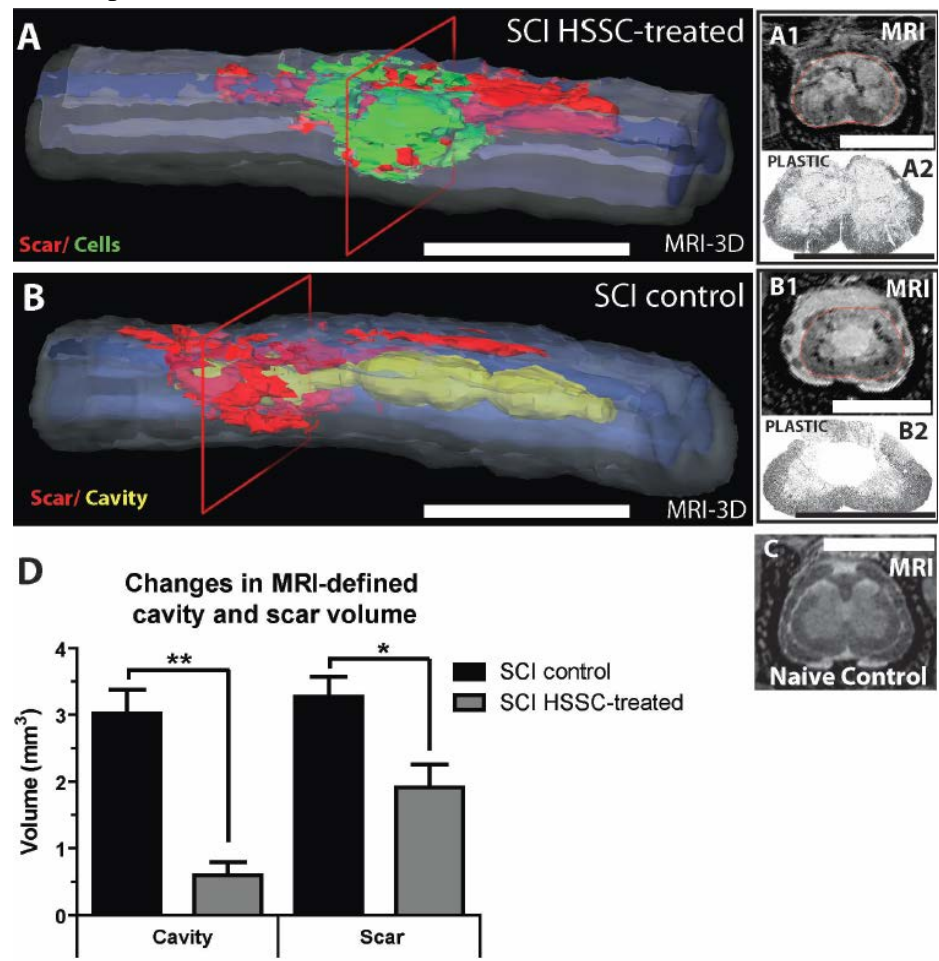


Fig. 17 Effective cavity-filling effect by transplanted cells in SCI HSSC-injected animals. Fig 4 A-D from author's publication *Amelioration of motor/sensory dysfunction and spasticity in a rat model of acute lumbar spinal cord injury by human neural stem cell transplantation.*

6.2.6. Mechanism of HSSC-mediated therapeutic action in SCI and ALS

Quantitative analysis of the host axon survival in the injury epicenter showed no significant sparing effect in HSSC-grafted SCI animals vs. medium-injected or untreated SCI animals. These data suggest that **i**) the majority if not all axons which succumb to pathological processes resulting from secondary changes post injury such as edema, ischemia were already lost or irreversibly damaged at 3 days after trauma (i.e., the time point when the cells were grafted), or **ii**) regional cell grafting is not therapeutically effective in providing acute neuroprotection.

As we mentioned before, transplanted HSSC into the spinal cord both SCI and ALS rat models engrafted and differentiated into neural or glial cells with no extensive proliferation or tumor formation observed (Hefferan et al. 2012) (van Gorp et al. 2013 in press). Analysis of the neurotransmitter phenotype in grafted cells in the SCI model showed the development of putative inhibitory GABA-ergic synapses with host neurons (Fig. 16). These data show that the restoration of the local functional inhibitory circuitry by grafted cells can in part lead to the observed functional improvements (van Gorp et al. 2013 in press). While under specific pathological conditions (such as inflammatory or neuropathic pain) the spinal GABA can have excitatory effects due to reduced expression of the potassium-chloride exporter KCC2) (Coull et al. 2003; Anseloni and Gold 2008), systematic experimental and clinical studies have demonstrated a potent anti-spasticity effect after intrathecal treatment with GABA_B receptor agonist baclofen, suggesting continuing inhibitory GABA_B receptor-mediated action (Rawlins 2004; Kakinohana et al. 2006).

In addition, we have recently demonstrated an effective anti-spastic effect after spinal parenchymal GAD65 (glutamate decarboxylase) upregulation if combined with systemic tiagabine (GABA uptake inhibitor) treatment in animals with spinal ischemia-induced muscle spasticity (Kakinohana et al. 2012a). Jointly, these data suggest that the anti-spasticity effect observed in our current SCI study can be mediated by a synaptically coupled GABA-inhibitory effect. Accordingly, in our previous study using the same cell line, we have demonstrated the development of putative GABA-ergic synaptic contacts between grafted neurons and persisting α -motoneurons of the host in a rat spinal ischemia model. In the same animals, a significant amelioration of spasticity was measured (Cizkova et al. 2007). Similarly, the transient anti-spastic effect of HSSCs-grafted SOD1 expressed by increased RDD of Hoffmann reflex can be at least partially attributed to the development of putative inhibitory GABA-ergic and/or glycinergic synapses (Fig. 15) with host surviving α -motoneurons (Hefferan et al. 2012). This could have been further supported by the partially corrected glutamine uptake from the extracellular space/synaptic cleft by the HSSC-derived glial cells/astrocyte EAAT2 as it was suggested in previous work (Lepore et al. 2008). Furthermore, the temporary improvement of BBB score in the HSSC-treated SOD1 animals can be explained by “dilution” of the yet unknown host astrocyte-secreted toxic factors by the engrafted human neural and glial cells present in the vicinity of host motor neurons which most likely led to their temporary protection. The presence (although small) of the mature human oligodendrocytes could also helped retain the neurological and/or motor function in SOD1 rats by re-myelination of the axons of host motor neurons preserving their conductivity.

The overall improvement in the ventral horn grey matter in the HSSC-treated rats also led to ~50% reduction of neuroinflammation (astrogliosis and microgliosis) as demonstrated by the reduction of total immunoreactivity for GFAP and Iba1 when compared to media treated SOD1 rats (Hefferan et al. 2012). In the same study using EM analysis, we have confirmed the development of synaptic contacts with the host neurons at 9 months after intraspinal grafting of HSSC in normal non-injured immunodeficient rats (Hefferan et al. 2012). Similarly, in a more recent study, the development of functional contacts and restoration of axon potential conductivity across the region of complete Th3 spinal transection by grafted HSSC was seen (Lu et al. 2012). Based on these transplantational experiments, we suggest that ideal cell lineage for spinal cord injury therapy would probably be a certain proportion of oligodendrocytes and neurons (Kim et al. 2007; Sabelstrom et al. 2013), and for ALS it most likely would include delivery of all three neural cell lineages with a high content of astrocyte precursors (Maragakis et al. 2005; Vargas and Johnson 2010).

6.2.7. Defining the optimal TAC immunosuppressive regimen to permit long-term survival and maturation of spinally grafted human neural precursors in rats

Even though we successfully used combinatory immunosuppression protocol which included Prograf (FK506; Astellas Pharma) in combination with Cellcept (mycophenolate mofetil (MFF); Roche Pharmaceuticals) in all our xenografting studies (Cizkova et al. 2007; Usvald et al. 2010; Hefferan et al. 2011b; Hefferan et al. 2012; Kakinohana et al. 2012b) (van Gorp et al. 2013 in press), we have occasionally observed graft rejection. In our HSSCs grafting study in SOD1 rats (Hefferan et al. 2012), hNUMA staining revealed identifiable human grafts in 18/22 animals. Four animals were thus graft-negative as indicated by injection tracks which were clearly visible, but with no human antigen detected. Moreover, in one of our recent studies, we demonstrated consistent cell survival for up to 2 months after spinal grafting of HUES7-NPCs after using 1 mg TAC/day dose delivered s.c. as a bolus in castor-oil preparation in SD rats with previous spinal ischemic injury. However, no cell survival was seen if animals were allowed to survive for total of 4 months (Kakinohana et al. 2012c). Thus, we decided to develop a more consistent and less labor intensive immunosuppression protocol.

In this study, quantitative analysis of T-cells (CD8, CD4) in grafted spinal cord regions showed a near complete absence of this cell population in 3.4 and 5.1 mg/kg/day TAC group if analyzed at 77-90 days after cell grafting (Sevc et al. 2013 in revision). Similarly, the analysis of CD8 and CD4 cells in circulating blood showed a significant decrease in the 5.1 mg/kg/day TAC group if compared to non-immunosuppressed SOD1 rats. In contrast to the 3.4 and 5.1 mg/kg/day TAC groups, a clear population of CD4/8 cells was seen in 1.9 mg/kg/day TAC-treated and cell grafted animals. Interestingly, a substantially higher density of CD8 population was seen on the dorsal surface of individual grafts facing the pial membrane. We speculate that the presence of grafted cells in heavily vascularized but BBB-lacking pial arterial system is more susceptible to extravasation of the circulating T-cell population and the resulting T-cell mediated response (Sevc et al. 2013). We also hypothesize that even if a satisfactory cell survival was seen in the 1.9 mg/kg/day group at 77 days after

cell grafting, a progressive grafted cell rejection will likely develop should the same level of low level immunosuppression continue over an extended period of time.

Independent of the daily TAC dose delivered (i.e., 1.9, 3.4 or 5.4 mg/k/day) in a form of TAC pellet, consistent survival of grafted ES-derived NPCs or HSSCs was seen at intervals 30-90 days after grafting (Sevc et al. 2013 in revision). This was expressed as the presence of high density DCX or hNSE immunoreactive-grafted neurons in targeted spinal cord regions.

In addition, high density neuronal processes derived from grafted human neurons expressing human-specific synaptophysin and projecting toward host interneurons and α -motoneurons were identified. Comparable grafted cell survival and maturation was seen in both SOD1 rats and in SD rats with previous L3 contusion injury (SCI) (Sevc et al. 2013 in revision). In our previous experiment, we demonstrated consistent xenograft survival three weeks after the transplantation of HSSCs into the spinal cord in rats treated with daily i.p. injection of TAC (3 mg/kg/day) combined with daily i.p. injection of Mycophenolate mofetil (30 mg/kg) (Hefferan et al. 2011a).

Together, these data show that the TAC dose of around 3 mg/kg/day and divided into two 12-hr doses (if delivered as a bolus s.c injection) or in a form of continuously TAC releasing pellet is required for long-term effective immunosuppression to permit xenograft survival in rats.

6.2.8. (Neural) stem cell therapy in spinal cord summary

In summary, HSSCs transplanted into the lamina VII of the SOD1 rat lumbar spinal cord (L2-L5) provided local protection to the lamina IX α -motoneurons residing in the close proximity of the grafted cells and showed transient protection of hind-limb motor function and preservation of Hoffman reflex activity and decreased inflammatory responses but offered no protection to α -motoneuronal pools distant from grafted lumbar segments. Using the same GMP-grade HSSC cell line (NSI-566RSC) in immunosuppressed Spreg-Dowley rats with previous L3 contusion injury we demonstrated progressive and significant improvement in motor and sensory function, effective filling of spinal injury/trauma-induced cavity with grafted cells and development of putative GABA-ergic synapses between grafted and host neurons at 2 months after grafting. In addition, we have developed new immunosuppressive tacrolimus-loaded pellets which are now commercially available and provide steady drug release for up to 3 months, making delivery labor efficient, minimally invasive, and producing stabilized blood concentration levels.

It is clear that cell replacement therapies will require effective multi-site delivery and will need to be supplemented by drug and/or gene therapies. Nevertheless our data demonstrated that transplantation of human neural stem cells represent safe and effective potential therapy for both neurodegenerative diseases and acute spinal cord injuries with limitations given by the complexity of the disease and the size of the injury.

6.3. GENERAL CONCLUSION

My doctoral thesis was primarily focused on the animal disease models development and characterization and pre-clinical xenogeneic cell therapies focused on spinal cord disorders and injury. We successfully generated and characterized the first transgenic minipig model of Huntington's disease which carries one copy of the human HTT transgene encoding 124 glutamines integrated into chromosome 1 q24-q25. Our cross-breeding studies revealed possible role of UCHL1 in UPS impairment in HD which could be linked to relative early reproductive problems in tgHD boars which by one year had reduced fertility and fewer spermatozoa per ejaculate. As UPS is crucial for sperm quality control and UCHL1 is required for normal spermatogenesis, the tgHD minipig boar's decline in sperm number and ZP penetration rate could therefore be a consequence of aberrant interaction of mutant huntingtin with UCHL1 and strongly suggest UPS impairment in tgHDminipig testes.

Our human neural stem cells transplantation studies in rat models of ALS and spinal cord injury clearly demonstrated that the engraftment of HSSCs is safe, efficient and offers therapeutic potential which, of course, is limited by the complexity of the disease and the size of the injury. Transplanted HSSCs differentiated mainly into neurons and some astrocytes and oligodendrocytes. In addition, we observed transient protection of α -motoneurons and improvement of neurological/motor functions in HSSCs-treated SOD1 rats and even more apparent motor and sensory function improvement in SCI HSSCs-grafted rats. During our grafting experiments we have also developed a new immunosuppressive protocol based on TAC-loaded pellets which we extensively tested in our lab and which are already available for broad scientific community.

Results of our work helped to expand our understanding on the potential clinical use of cell-replacement therapies in human patients with chronic spinal trauma and ALS. The development of a porcine HD model represent a critical step in large animal HD modeling with the primary utilization of such a model in gene-targeted and cell-replacement therapies.

7. REFERENCES

- (1993). "A novel gene containing a trinucleotide repeat that is expanded and unstable on Huntington's disease chromosomes. The Huntington's Disease Collaborative Research Group." *Cell* **72**(6): 971-983.
- (1996). "Unified Huntington's Disease Rating Scale: reliability and consistency. Huntington Study Group." *Mov Disord* **11**(2): 136-142.
- Ackerley, S., P. Thornhill, A. J. Grierson, J. Brownlee, B. H. Anderton, P. N. Leigh, et al. (2003). "Neurofilament heavy chain side arm phosphorylation regulates axonal transport of neurofilaments." *J Cell Biol* **161**(3): 489-495.
- Aigner, B., S. Renner, B. Kessler, N. Klymiuk, M. Kurome, A. Wunsch, et al. (2010). "Transgenic pigs as models for translational biomedical research." *J Mol Med (Berl)* **88**(7): 653-664.
- Al-Chalabi, A., A. Jones, C. Troakes, A. King, S. Al-Sarraj and L. H. van den Berg (2012). "The genetics and neuropathology of amyotrophic lateral sclerosis." *Acta Neuropathol* **124**(3): 339-352.
- Albin, R. L., A. Reiner, K. D. Anderson, L. S. t. Dure, B. Handelin, R. Balfour, et al. (1992). "Preferential loss of striato-external pallidal projection neurons in presymptomatic Huntington's disease." *Ann Neurol* **31**(4): 425-430.
- Alexanian, A. R., C. N. Svendsen, M. J. Crowe and S. N. Kurpad (2011). "Transplantation of human glial-restricted neural precursors into injured spinal cord promotes functional and sensory recovery without causing allodynia." *Cytotherapy* **13**(1): 61-68.
- All, A. H., F. A. Bazley, S. Gupta, N. Pashai, C. Hu, A. Pourmorteza, et al. (2012). "Human embryonic stem cell-derived oligodendrocyte progenitors aid in functional recovery of sensory pathways following contusive spinal cord injury." *PLoS One* **7**(10): e47645.
- Andersen, P. M., P. Nilsson, V. Ala-Hurula, M. L. Keranen, I. Tarvainen, T. Haltia, et al. (1995). "Amyotrophic lateral sclerosis associated with homozygosity for an Asp90Ala mutation in CuZn-superoxide dismutase." *Nat Genet* **10**(1): 61-66.
- Andersson, M. K., A. Stahlberg, Y. Arvidsson, A. Olofsson, H. Semb, G. Stenman, et al. (2008). "The multifunctional FUS, EWS and TAF15 proto-oncoproteins show cell type-specific expression patterns and involvement in cell spreading and stress response." *BMC Cell Biol* **9**: 37.
- Ankeny, D. P. and P. G. Popovich (2009). "Mechanisms and implications of adaptive immune responses after traumatic spinal cord injury." *Neuroscience* **158**(3): 1112-1121.
- Anseloni, V. C. and M. S. Gold (2008). "Inflammation-induced shift in the valence of spinal GABA-A receptor-mediated modulation of nociception in the adult rat." *J Pain* **9**(8): 732-738.
- Arai, T., M. Hasegawa, H. Akiyama, K. Ikeda, T. Nonaka, H. Mori, et al. (2006). "TDP-43 is a component of ubiquitin-positive tau-negative inclusions in frontotemporal lobar degeneration and amyotrophic lateral sclerosis." *Biochem Biophys Res Commun* **351**(3): 602-611.
- Archibald, A. L., L. Bolund, C. Churcher, M. Fredholm, M. A. Groenen, B. Harlizius, et al. (2010). "Pig genome sequence--analysis and publication strategy." *BMC Genomics* **11**: 438.
- Arenas, J., Y. Campos, R. Ribacoba, M. A. Martin, J. C. Rubio, P. Ablanedo, et al. (1998). "Complex I defect in muscle from patients with Huntington's disease." *Ann Neurol* **43**(3): 397-400.
- Arrasate, M., S. Mitra, E. S. Schweitzer, M. R. Segal and S. Finkbeiner (2004). "Inclusion body formation reduces levels of mutant huntingtin and the risk of neuronal death." *Nature* **431**(7010): 805-810.
- Arundine, M. and M. Tymianski (2003). "Molecular mechanisms of calcium-dependent neurodegeneration in excitotoxicity." *Cell Calcium* **34**(4-5): 325-337.
- Baastrup, C., C. C. Maersk-Moller, J. R. Nyengaard, T. S. Jensen and N. B. Finnerup (2010). "Spinal-, brainstem- and cerebrally mediated responses at- and below-level of a spinal cord contusion in rats: evaluation of pain-like behavior." *Pain* **151**(3): 670-679.
- Bae, B. I., H. Xu, S. Igarashi, M. Fujimuro, N. Agrawal, Y. Taya, et al. (2005). "p53 mediates cellular dysfunction and behavioral abnormalities in Huntington's disease." *Neuron* **47**(1): 29-41.

- Baldo, B., P. Paganetti, S. Grueninger, D. Marcellin, L. S. Kaltenbach, D. C. Lo, et al. (2012). "TR-FRET-based duplex immunoassay reveals an inverse correlation of soluble and aggregated mutant huntingtin in huntington's disease." *Chem Biol* **19**(2): 264-275.
- Bareyre, F. M. and M. E. Schwab (2003). "Inflammation, degeneration and regeneration in the injured spinal cord: insights from DNA microarrays." *Trends Neurosci* **26**(10): 555-563.
- Barker, R. A., E. Ratcliffe, M. McLaughlin, A. Richards and S. B. Dunnett (2000). "A role for complement in the rejection of porcine ventral mesencephalic xenografts in a rat model of Parkinson's disease." *J Neurosci* **20**(9): 3415-3424.
- Barnabe-Heider, F., C. Goritz, H. Sabelstrom, H. Takebayashi, F. W. Pfrieder, K. Meletis, et al. (2010). "Origin of new glial cells in intact and injured adult spinal cord." *Cell Stem Cell* **7**(4): 470-482.
- Barracough, K. A., N. M. Isbel, D. W. Johnson, S. B. Campbell and C. E. Staats (2011). "Once- versus twice-daily tacrolimus: are the formulations truly equivalent?" *Drugs* **71**(12): 1561-1577.
- Basel, M. T., S. Balivada, A. P. Beck, M. A. Kerrigan, M. M. Pyle, J. C. Dekkers, et al. (2012). "Human xenografts are not rejected in a naturally occurring immunodeficient porcine line: a human tumor model in pigs." *Biores Open Access* **1**(2): 63-68.
- Batchelor, P. E., N. F. Kerr, A. M. Gatt, E. Aleksoska, S. F. Cox, A. Ghasem-Zadeh, et al. (2010). "Hypothermia prior to decompression: buying time for treatment of acute spinal cord injury." *J Neurotrauma* **27**(8): 1357-1368.
- Bates, G. (2003). "Huntingtin aggregation and toxicity in Huntington's disease." *Lancet* **361**(9369): 1642-1644.
- Baxa, M., M. Hruska-Plochan, S. Juhas, P. Vodicka, A. Pavlok, J. Juhasova, et al. (2013). "A Transgenic Minipig Model of Huntington's Disease." *J Huntingtons Dis* **2**(1): 47-68.
- Beal, M. F., R. J. Ferrante, S. E. Browne, R. T. Matthews, N. W. Kowall and R. H. Brown, Jr. (1997). "Increased 3-nitrotyrosine in both sporadic and familial amyotrophic lateral sclerosis." *Ann Neurol* **42**(4): 644-654.
- Beckman, J. S., M. Carson, C. D. Smith and W. H. Koppenol (1993). "ALS, SOD and peroxynitrite." *Nature* **364**(6438): 584.
- Behrens, P. F., P. Franz, B. Woodman, K. S. Lindenberg and G. B. Landwehrmeyer (2002). "Impaired glutamate transport and glutamate-glutamine cycling: downstream effects of the Huntington mutation." *Brain* **125**(Pt 8): 1908-1922.
- Belzil, V. V., P. N. Valdmanis, P. A. Dion, H. Daoud, E. Kabashi, A. Noreau, et al. (2009). "Mutations in FUS cause FALS and SALS in French and French Canadian populations." *Neurology* **73**(15): 1176-1179.
- Bence, N. F., R. M. Sampat and R. R. Kopito (2001). "Impairment of the ubiquitin-proteasome system by protein aggregation." *Science* **292**(5521): 1552-1555.
- Benchoua, A., Y. Trioulier, E. Diguët, C. Malgorn, M. C. Gaillard, N. Dufour, et al. (2008). "Dopamine determines the vulnerability of striatal neurons to the N-terminal fragment of mutant huntingtin through the regulation of mitochondrial complex II." *Hum Mol Genet* **17**(10): 1446-1456.
- Benchoua, A., Y. Trioulier, D. Zala, M. C. Gaillard, N. Lefort, N. Dufour, et al. (2006). "Involvement of mitochondrial complex II defects in neuronal death produced by N-terminus fragment of mutated huntingtin." *Mol Biol Cell* **17**(4): 1652-1663.
- Bendotti, C., M. Marino, C. Cheroni, E. Fontana, V. Crippa, A. Poletti, et al. (2012). "Dysfunction of constitutive and inducible ubiquitin-proteasome system in amyotrophic lateral sclerosis: implication for protein aggregation and immune response." *Prog Neurobiol* **97**(2): 101-126.
- Bennett, E. J., N. F. Bence, R. Jayakumar and R. R. Kopito (2005). "Global impairment of the ubiquitin-proteasome system by nuclear or cytoplasmic protein aggregates precedes inclusion body formation." *Mol Cell* **17**(3): 351-365.
- Bennett, E. J., T. A. Shaler, B. Woodman, K. Y. Ryu, T. S. Zaitseva, C. H. Becker, et al. (2007). "Global changes to the ubiquitin system in Huntington's disease." *Nature* **448**(7154): 704-708.

- Bensimon, G., L. Lacomblez and V. Meininger (1994). "A controlled trial of riluzole in amyotrophic lateral sclerosis. ALS/Riluzole Study Group." *N Engl J Med* **330**(9): 585-591.
- Bett, J. S., C. Cook, L. Petrucelli and G. P. Bates (2009). "The ubiquitin-proteasome reporter GFPu does not accumulate in neurons of the R6/2 transgenic mouse model of Huntington's disease." *PLoS One* **4**(4): e5128.
- Bett, J. S., G. M. Goellner, B. Woodman, G. Pratt, M. Rechsteiner and G. P. Bates (2006). "Proteasome impairment does not contribute to pathogenesis in R6/2 Huntington's disease mice: exclusion of proteasome activator REGgamma as a therapeutic target." *Hum Mol Genet* **15**(1): 33-44.
- Bibb, J. A., Z. Yan, P. Svenningsson, G. L. Snyder, V. A. Pieribone, A. Horiuchi, et al. (2000). "Severe deficiencies in dopamine signaling in presymptomatic Huntington's disease mice." *Proc Natl Acad Sci U S A* **97**(12): 6809-6814.
- Bifsha, P., K. Landry, L. Ashmarina, S. Durand, V. Seyrantepe, S. Trudel, et al. (2007). "Altered gene expression in cells from patients with lysosomal storage disorders suggests impairment of the ubiquitin pathway." *Cell Death Differ* **14**(3): 511-523.
- Blair, I. P., K. L. Williams, S. T. Warraich, J. C. Durnall, A. D. Thoeng, J. Manavis, et al. (2010). "FUS mutations in amyotrophic lateral sclerosis: clinical, pathological, neurophysiological and genetic analysis." *J Neurol Neurosurg Psychiatry* **81**(6): 639-645.
- Boido, M., D. Garbossa and A. Vercelli (2011). "Early graft of neural precursors in spinal cord compression reduces glial cyst and improves function." *J Neurosurg Spine* **15**(1): 97-106.
- Boillee, S., C. Vande Velde and D. W. Cleveland (2006a). "ALS: a disease of motor neurons and their nonneuronal neighbors." *Neuron* **52**(1): 39-59.
- Boillee, S., K. Yamanaka, C. S. Lobsiger, N. G. Copeland, N. A. Jenkins, G. Kassiotis, et al. (2006b). "Onset and progression in inherited ALS determined by motor neurons and microglia." *Science* **312**(5778): 1389-1392.
- Bonner, J. F., T. M. Connors, W. F. Silverman, D. P. Kowalski, M. A. Lemay and I. Fischer (2011). "Grafted neural progenitors integrate and restore synaptic connectivity across the injured spinal cord." *J Neurosci* **31**(12): 4675-4686.
- Boston-Howes, W., S. L. Gibb, E. O. Williams, P. Pasinelli, R. H. Brown, Jr. and D. Trotti (2006). "Caspase-3 cleaves and inactivates the glutamate transporter EAAT2." *J Biol Chem* **281**(20): 14076-14084.
- Bourke, S. C., M. Tomlinson, T. L. Williams, R. E. Bullock, P. J. Shaw and G. J. Gibson (2006). "Effects of non-invasive ventilation on survival and quality of life in patients with amyotrophic lateral sclerosis: a randomised controlled trial." *Lancet Neurol* **5**(2): 140-147.
- Bowles, K. R., S. P. Brooks, S. B. Dunnett and L. Jones (2011). "Gene expression and behaviour in mouse models of HD." *Brain Res Bull*.
- Bracken, M. B. (2012). "Steroids for acute spinal cord injury." *Cochrane Database Syst Rev* **1**: CD001046.
- Brevig, T., J. Holgersson and H. Widner (2000). "Xenotransplantation for CNS repair: immunological barriers and strategies to overcome them." *Trends Neurosci* **23**(8): 337-344.
- Britton, J. W., R. J. Uitti, J. E. Ahlskog, R. G. Robinson, B. Kremer and M. R. Hayden (1995). "Hereditary late-onset chorea without significant dementia: genetic evidence for substantial phenotypic variation in Huntington's disease." *Neurology* **45**(3 Pt 1): 443-447.
- Bruening, W., J. Roy, B. Giasson, D. A. Figlewicz, W. E. Mushynski and H. D. Durham (1999). "Up-regulation of protein chaperones preserves viability of cells expressing toxic Cu/Zn-superoxide dismutase mutants associated with amyotrophic lateral sclerosis." *J Neurochem* **72**(2): 693-699.
- Bruijn, L. I., M. F. Beal, M. W. Becher, J. B. Schulz, P. C. Wong, D. L. Price, et al. (1997a). "Elevated free nitrotyrosine levels, but not protein-bound nitrotyrosine or hydroxyl radicals, throughout amyotrophic lateral sclerosis (ALS)-like disease implicate tyrosine nitration as an aberrant in vivo property of one familial ALS-linked superoxide dismutase 1 mutant." *Proc Natl Acad Sci U S A* **94**(14): 7606-7611.

- Bruijn, L. I., M. W. Becher, M. K. Lee, K. L. Anderson, N. A. Jenkins, N. G. Copeland, et al. (1997b). "ALS-linked SOD1 mutant G85R mediates damage to astrocytes and promotes rapidly progressive disease with SOD1-containing inclusions." *Neuron* **18**(2): 327-338.
- Bruijn, L. I., M. K. Houseweart, S. Kato, K. L. Anderson, S. D. Anderson, E. Ohama, et al. (1998). "Aggregation and motor neuron toxicity of an ALS-linked SOD1 mutant independent from wild-type SOD1." *Science* **281**(5384): 1851-1854.
- Burrell, J. R., M. C. Kiernan, S. Vucic and J. R. Hodges (2011). "Motor neuron dysfunction in frontotemporal dementia." *Brain* **134**(Pt 9): 2582-2594.
- Byrne, S., M. Elamin, P. Bede and O. Hardiman (2012). "Absence of consensus in diagnostic criteria for familial neurodegenerative diseases." *J Neurol Neurosurg Psychiatry* **83**(4): 365-367.
- Byrne, S., C. Walsh, C. Lynch, P. Bede, M. Elamin, K. Kenna, et al. (2011). "Rate of familial amyotrophic lateral sclerosis: a systematic review and meta-analysis." *J Neurol Neurosurg Psychiatry* **82**(6): 623-627.
- Cantuti-Castelvetri, I., M. T. Lin, K. Zheng, C. E. Keller-McGandy, R. A. Betensky, D. R. Johns, et al. (2005). "Somatic mitochondrial DNA mutations in single neurons and glia." *Neurobiol Aging* **26**(10): 1343-1355.
- Cao, Q., X. M. Xu, W. H. Devries, G. U. Enzmann, P. Ping, P. Tsoulfas, et al. (2005). "Functional recovery in traumatic spinal cord injury after transplantation of multilineurotrophin-expressing glial-restricted precursor cells." *J Neurosci* **25**(30): 6947-6957.
- Cappuccino, A., L. J. Bisson, B. Carpenter, J. Marzo, W. D. Dietrich, 3rd and H. Cappuccino (2010). "The use of systemic hypothermia for the treatment of an acute cervical spinal cord injury in a professional football player." *Spine (Phila Pa 1976)* **35**(2): E57-62.
- Carter, B. J., P. Anklesaria, S. Choi and J. F. Engelhardt (2009). "Redox modifier genes and pathways in amyotrophic lateral sclerosis." *Antioxid Redox Signal* **11**(7): 1569-1586.
- Cartier, A. E., S. N. Djakovic, A. Salehi, S. M. Wilson, E. Masliah and G. N. Patrick (2009). "Regulation of synaptic structure by ubiquitin C-terminal hydrolase L1." *J Neurosci* **29**(24): 7857-7868.
- Casha, S., W. R. Yu and M. G. Fehlings (2001). "Oligodendroglial apoptosis occurs along degenerating axons and is associated with FAS and p75 expression following spinal cord injury in the rat." *Neuroscience* **103**(1): 203-218.
- Cattaneo, E., C. Zuccato and M. Tartari (2005). "Normal huntingtin function: an alternative approach to Huntington's disease." *Nat Rev Neurosci* **6**(12): 919-930.
- Cha, J. H. (2007). "Transcriptional signatures in Huntington's disease." *Prog Neurobiol* **83**(4): 228-248.
- Chan, E. Y., R. Luthi-Carter, A. Strand, S. M. Solano, S. A. Hanson, M. M. DeJohn, et al. (2002). "Increased huntingtin protein length reduces the number of polyglutamine-induced gene expression changes in mouse models of Huntington's disease." *Hum Mol Genet* **11**(17): 1939-1951.
- Chang-Hong, R., M. Wada, S. Koyama, H. Kimura, S. Arawaka, T. Kawanami, et al. (2005). "Neuroprotective effect of oxidized galectin-1 in a transgenic mouse model of amyotrophic lateral sclerosis." *Exp Neurol* **194**(1): 203-211.
- Cheah, B. C., S. Vucic, A. V. Krishnan and M. C. Kiernan (2010). "Riluzole, neuroprotection and amyotrophic lateral sclerosis." *Curr Med Chem* **17**(18): 1942-1199.
- Chen, F., Y. Sugiura, K. G. Myers, Y. Liu and W. Lin (2010). "Ubiquitin carboxyl-terminal hydrolase L1 is required for maintaining the structure and function of the neuromuscular junction." *Proc Natl Acad Sci U S A* **107**(4): 1636-1641.
- Chen, S., V. Berthelie, J. B. Hamilton, B. O'Nuallain and R. Wetzel (2002). "Amyloid-like features of polyglutamine aggregates and their assembly kinetics." *Biochemistry* **41**(23): 7391-7399.
- Chen, S., X. Zhang, L. Song and W. Le (2012). "Autophagy dysregulation in amyotrophic lateral sclerosis." *Brain Pathol* **22**(1): 110-116.
- Choo, Y. S., G. V. Johnson, M. MacDonald, P. J. Detloff and M. Lesort (2004). "Mutant huntingtin directly increases susceptibility of mitochondria to the calcium-induced permeability transition and cytochrome c release." *Hum Mol Genet* **13**(14): 1407-1420.

- Cizkova, D., O. Kakinohana, K. Kucharova, S. Marsala, K. Johe, T. Hazel, et al. (2007). "Functional recovery in rats with ischemic paraplegia after spinal grafting of human spinal stem cells." Neuroscience **147**(2): 546-560.
- Clement, A. M., M. D. Nguyen, E. A. Roberts, M. L. Garcia, S. Boillee, M. Rule, et al. (2003). "Wild-type nonneuronal cells extend survival of SOD1 mutant motor neurons in ALS mice." Science **302**(5642): 113-117.
- Cloutier, F., M. M. Siegenthaler, G. Nistor and H. S. Keirstead (2006). "Transplantation of human embryonic stem cell-derived oligodendrocyte progenitors into rat spinal cord injuries does not cause harm." Regen Med **1**(4): 469-479.
- Cooper, J. K., G. Schilling, M. F. Peters, W. J. Herring, A. H. Sharp, Z. Kaminsky, et al. (1998). "Truncated N-terminal fragments of huntingtin with expanded glutamine repeats form nuclear and cytoplasmic aggregates in cell culture." Hum Mol Genet **7**(5): 783-790.
- Corrado, L., R. Del Bo, B. Castellotti, A. Ratti, C. Cereda, S. Penco, et al. (2010). "Mutations of FUS gene in sporadic amyotrophic lateral sclerosis." J Med Genet **47**(3): 190-194.
- Couillard-Despres, S., Q. Zhu, P. C. Wong, D. L. Price, D. W. Cleveland and J. P. Julien (1998). "Protective effect of neurofilament heavy gene overexpression in motor neuron disease induced by mutant superoxide dismutase." Proc Natl Acad Sci U S A **95**(16): 9626-9630.
- Coull, J. A., D. Boudreau, K. Bachand, S. A. Prescott, F. Nault, A. Sik, et al. (2003). "Trans-synaptic shift in anion gradient in spinal lamina I neurons as a mechanism of neuropathic pain." Nature **424**(6951): 938-942.
- Crowe, M. J., J. C. Bresnahan, S. L. Shuman, J. N. Masters and M. S. Beattie (1997). "Apoptosis and delayed degeneration after spinal cord injury in rats and monkeys." Nat Med **3**(1): 73-76.
- Cudkovicz, M. E., D. McKenna-Yasek, P. E. Sapp, W. Chin, B. Geller, D. L. Hayden, et al. (1997). "Epidemiology of mutations in superoxide dismutase in amyotrophic lateral sclerosis." Ann Neurol **41**(2): 210-221.
- Cui, L., H. Jeong, F. Borovecki, C. N. Parkhurst, N. Tanese and D. Krainc (2006). "Transcriptional repression of PGC-1alpha by mutant huntingtin leads to mitochondrial dysfunction and neurodegeneration." Cell **127**(1): 59-69.
- Cummings, B. J., N. Uchida, S. J. Tamaki, D. L. Salazar, M. Hooshmand, R. Summers, et al. (2005). "Human neural stem cells differentiate and promote locomotor recovery in spinal cord-injured mice." Proc Natl Acad Sci U S A **102**(39): 14069-14074.
- Dal Canto, M. C. and M. E. Gurney (1995). "Neuropathological changes in two lines of mice carrying a transgene for mutant human Cu,Zn SOD, and in mice overexpressing wild type human SOD: a model of familial amyotrophic lateral sclerosis (FALS)." Brain Res **676**(1): 25-40.
- Dal Canto, M. C. and M. E. Gurney (1997). "A low expressor line of transgenic mice carrying a mutant human Cu,Zn superoxide dismutase (SOD1) gene develops pathological changes that most closely resemble those in human amyotrophic lateral sclerosis." Acta Neuropathol **93**(6): 537-550.
- Damiano, M., A. A. Starkov, S. Petri, K. Kipiani, M. Kiaei, M. Mattiazzi, et al. (2006). "Neural mitochondrial Ca²⁺ capacity impairment precedes the onset of motor symptoms in G93A Cu/Zn-superoxide dismutase mutant mice." J Neurochem **96**(5): 1349-1361.
- Daoud, H., P. N. Valdmanis, E. Kabashi, P. Dion, N. Dupre, W. Camu, et al. (2009). "Contribution of TARDBP mutations to sporadic amyotrophic lateral sclerosis." J Med Genet **46**(2): 112-114.
- David, S. and A. Kroner (2011). "Repertoire of microglial and macrophage responses after spinal cord injury." Nat Rev Neurosci **12**(7): 388-399.
- Davidson, Y., T. Kelley, I. R. Mackenzie, S. Pickering-Brown, D. Du Plessis, D. Neary, et al. (2007). "Ubiquitinated pathological lesions in frontotemporal lobar degeneration contain the TAR DNA-binding protein, TDP-43." Acta Neuropathol **113**(5): 521-533.
- Davies, J. E., C. Huang, C. Proschel, M. Noble, M. Mayer-Proschel and S. J. Davies (2006). "Astrocytes derived from glial-restricted precursors promote spinal cord repair." J Biol **5**(3): 7.

- Davies, J. E., C. Proschel, N. Zhang, M. Noble, M. Mayer-Proschel and S. J. Davies (2008). "Transplanted astrocytes derived from BMP- or CNTF-treated glial-restricted precursors have opposite effects on recovery and allodynia after spinal cord injury." *J Biol* **7**(7): 24.
- Davies, S. J., C. H. Shih, M. Noble, M. Mayer-Proschel, J. E. Davies and C. Proschel (2011). "Transplantation of specific human astrocytes promotes functional recovery after spinal cord injury." *PLoS One* **6**(3): e17328.
- Davies, S. W., M. Turmaine, B. A. Cozens, M. DiFiglia, A. H. Sharp, C. A. Ross, et al. (1997). "Formation of neuronal intranuclear inclusions underlies the neurological dysfunction in mice transgenic for the HD mutation." *Cell* **90**(3): 537-548.
- Day, I. N. and R. J. Thompson (2010). "UCHL1 (PGP 9.5): neuronal biomarker and ubiquitin system protein." *Prog Neurobiol* **90**(3): 327-362.
- De Vos, K. J., A. J. Grierson, S. Ackerley and C. C. Miller (2008). "Role of axonal transport in neurodegenerative diseases." *Annu Rev Neurosci* **31**: 151-173.
- Deacon, T., J. Schumacher, J. Dinsmore, C. Thomas, P. Palmer, S. Kott, et al. (1997). "Histological evidence of fetal pig neural cell survival after transplantation into a patient with Parkinson's disease." *Nat Med* **3**(3): 350-353.
- DeJesus-Hernandez, M., J. Kocerha, N. Finch, R. Crook, M. Baker, P. Desaro, et al. (2010). "De novo truncating FUS gene mutation as a cause of sporadic amyotrophic lateral sclerosis." *Hum Mutat* **31**(5): E1377-1389.
- DeJesus-Hernandez, M., I. R. Mackenzie, B. F. Boeve, A. L. Boxer, M. Baker, N. J. Rutherford, et al. (2011). "Expanded GGGGCC hexanucleotide repeat in noncoding region of C9ORF72 causes chromosome 9p-linked FTD and ALS." *Neuron* **72**(2): 245-256.
- Deng, H. X., Y. Shi, Y. Furukawa, H. Zhai, R. Fu, E. Liu, et al. (2006). "Conversion to the amyotrophic lateral sclerosis phenotype is associated with intermolecular linked insoluble aggregates of SOD1 in mitochondria." *Proc Natl Acad Sci U S A* **103**(18): 7142-7147.
- Devivo, M. J. (2012). "Epidemiology of traumatic spinal cord injury: trends and future implications." *Spinal Cord* **50**(5): 365-372.
- Di Giorgio, F. P., G. L. Boulting, S. Bobrowicz and K. C. Eggan (2008). "Human embryonic stem cell-derived motor neurons are sensitive to the toxic effect of glial cells carrying an ALS-causing mutation." *Cell Stem Cell* **3**(6): 637-648.
- Di Giorgio, F. P., M. A. Carrasco, M. C. Siao, T. Maniatis and K. Eggan (2007). "Non-cell autonomous effect of glia on motor neurons in an embryonic stem cell-based ALS model." *Nat Neurosci* **10**(5): 608-614.
- Dietrich, W. D. (2012). "Therapeutic hypothermia for acute severe spinal cord injury: ready to start large clinical trials?" *Crit Care Med* **40**(2): 691-692.
- Dietrich, W. D., A. Cappuccino and H. Cappuccino (2011a). "Systemic hypothermia for the treatment of acute cervical spinal cord injury in sports." *Curr Sports Med Rep* **10**(1): 50-54.
- Dietrich, W. D., A. D. Levi, M. Wang and B. A. Green (2011b). "Hypothermic treatment for acute spinal cord injury." *Neurotherapeutics* **8**(2): 229-239.
- DiFiglia, M. (1990). "Excitotoxic injury of the neostriatum: a model for Huntington's disease." *Trends Neurosci* **13**(7): 286-289.
- DiFiglia, M., E. Sapp, K. Chase, C. Schwarz, A. Meloni, C. Young, et al. (1995). "Huntingtin is a cytoplasmic protein associated with vesicles in human and rat brain neurons." *Neuron* **14**(5): 1075-1081.
- DiFiglia, M., E. Sapp, K. O. Chase, S. W. Davies, G. P. Bates, J. P. Vonsattel, et al. (1997). "Aggregation of huntingtin in neuronal intranuclear inclusions and dystrophic neurites in brain." *Science* **277**(5334): 1990-1993.
- DiFiglia, M., M. Sena-Esteves, K. Chase, E. Sapp, E. Pfister, M. Sass, et al. (2007). "Therapeutic silencing of mutant huntingtin with siRNA attenuates striatal and cortical neuropathology and behavioral deficits." *Proc Natl Acad Sci U S A* **104**(43): 17204-17209.

- Duff, K., J. Paulsen, J. Mills, L. J. Beglinger, D. J. Moser, M. M. Smith, et al. (2010). "Mild cognitive impairment in prediagnosed Huntington disease." *Neurology* **75**(6): 500-507.
- Duff, K., J. S. Paulsen, L. J. Beglinger, D. R. Langbehn, J. C. Stout and H. D. I. o. t. H. S. G. Predict (2007). "Psychiatric symptoms in Huntington's disease before diagnosis: the predict-HD study." *Biol Psychiatry* **62**(12): 1341-1346.
- Dumas, E. M., S. J. van den Bogaard, M. E. Ruber, R. R. Reilman, J. C. Stout, D. Craufurd, et al. (2012). "Early changes in white matter pathways of the sensorimotor cortex in premanifest Huntington's disease." *Hum Brain Mapp* **33**(1): 203-212.
- Dure, L. S. t., A. B. Young and J. B. Penney (1991). "Excitatory amino acid binding sites in the caudate nucleus and frontal cortex of Huntington's disease." *Ann Neurol* **30**(6): 785-793.
- Dutta, S., M. Mezei, T. D. Lee and V. C. McAlister (1998). "Liposomal tacrolimus and intestinal drug concentration." *Transplant Proc* **30**(6): 2651-2652.
- Duyao, M. P., A. B. Auerbach, A. Ryan, F. Persichetti, G. T. Barnes, S. M. McNeil, et al. (1995). "Inactivation of the mouse Huntington's disease gene homolog Hdh." *Science* **269**(5222): 407-410.
- Ekegren, T., E. Grundstrom, D. Lindholm and S. M. Aquilonius (1999). "Upregulation of Bax protein and increased DNA degradation in ALS spinal cord motor neurons." *Acta Neurol Scand* **100**(5): 317-321.
- Emery, E., P. Aldana, M. B. Bunge, W. Puckett, A. Srinivasan, R. W. Keane, et al. (1998). "Apoptosis after traumatic human spinal cord injury." *J Neurosurg* **89**(6): 911-920.
- Erceg, S., M. Ronaghi, M. Oria, M. G. Rosello, M. A. Arago, M. G. Lopez, et al. (2010). "Transplanted oligodendrocytes and motoneuron progenitors generated from human embryonic stem cells promote locomotor recovery after spinal cord transection." *Stem Cells* **28**(9): 1541-1549.
- Estrada-Sanchez, A. M., T. Montiel, J. Segovia and L. Massieu (2009). "Glutamate toxicity in the striatum of the R6/2 Huntington's disease transgenic mice is age-dependent and correlates with decreased levels of glutamate transporters." *Neurobiol Dis* **34**(1): 78-86.
- ExemplarGenetics. from <http://exemplargenetics.com/>.
- Ezzi, S. A., M. Urushitani and J. P. Julien (2007). "Wild-type superoxide dismutase acquires binding and toxic properties of ALS-linked mutant forms through oxidation." *J Neurochem* **102**(1): 170-178.
- Fan, M. M. and L. A. Raymond (2007). "N-methyl-D-aspartate (NMDA) receptor function and excitotoxicity in Huntington's disease." *Prog Neurobiol* **81**(5-6): 272-293.
- Faulkner, J. and H. S. Keirstead (2005). "Human embryonic stem cell-derived oligodendrocyte progenitors for the treatment of spinal cord injury." *Transpl Immunol* **15**(2): 131-142.
- Faulkner, J. R., J. E. Herrmann, M. J. Woo, K. E. Tansey, N. B. Doan and M. V. Sofroniew (2004). "Reactive astrocytes protect tissue and preserve function after spinal cord injury." *J Neurosci* **24**(9): 2143-2155.
- Fellner, C., C. Menzel, F. A. Fellner, C. Ginthoer, N. Zorger, A. Schreyer, et al. (2010). "BLADE in sagittal T2-weighted MR imaging of the cervical spine." *AJNR Am J Neuroradiol* **31**(4): 674-681.
- Ferraiuolo, L., J. Kirby, A. J. Grierson, M. Sendtner and P. J. Shaw (2011). "Molecular pathways of motor neuron injury in amyotrophic lateral sclerosis." *Nat Rev Neurol* **7**(11): 616-630.
- Ferrante, R. J., M. F. Beal, N. W. Kowall, E. P. Richardson, Jr. and J. B. Martin (1987). "Sparing of acetylcholinesterase-containing striatal neurons in Huntington's disease." *Brain Res* **411**(1): 162-166.
- Ferrante, R. J., N. W. Kowall, M. F. Beal, E. P. Richardson, Jr., E. D. Bird and J. B. Martin (1985). "Selective sparing of a class of striatal neurons in Huntington's disease." *Science* **230**(4725): 561-563.
- Ferrante, R. J., L. A. Shinobu, J. B. Schulz, R. T. Matthews, C. E. Thomas, N. W. Kowall, et al. (1997). "Increased 3-nitrotyrosine and oxidative damage in mice with a human copper/zinc superoxide dismutase mutation." *Ann Neurol* **42**(3): 326-334.
- Finn, W. F. (1999). "FK506 nephrotoxicity." *Ren Fail* **21**(3-4): 319-329.

- Fischer, L. R. and J. D. Glass (2007). "Axonal degeneration in motor neuron disease." Neurodegener Dis **4**(6): 431-442.
- Fitch, M. T., C. Doller, C. K. Combs, G. E. Landreth and J. Silver (1999). "Cellular and molecular mechanisms of glial scarring and progressive cavitation: in vivo and in vitro analysis of inflammation-induced secondary injury after CNS trauma." J Neurosci **19**(19): 8182-8198.
- Fitzmaurice, P. S., I. C. Shaw, H. E. Kleiner, R. T. Miller, T. J. Monks, S. S. Lau, et al. (1996). "Evidence for DNA damage in amyotrophic lateral sclerosis." Muscle Nerve **19**(6): 797-798.
- Fleming, J. C., M. D. Norenberg, D. A. Ramsay, G. A. Dekaban, A. E. Marcillo, A. D. Saenz, et al. (2006). "The cellular inflammatory response in human spinal cords after injury." Brain **129**(Pt 12): 3249-3269.
- Fossale, E., V. C. Wheeler, V. Vrbanac, L. A. Lebel, A. Teed, J. S. Mysore, et al. (2002). "Identification of a presymptomatic molecular phenotype in Hdh CAG knock-in mice." Hum Mol Genet **11**(19): 2233-2241.
- Frank, S. and J. Jankovic (2010). "Advances in the pharmacological management of Huntington's disease." Drugs **70**(5): 561-571.
- Frey, D., C. Schneider, L. Xu, J. Borg, W. Spooren and P. Caroni (2000). "Early and selective loss of neuromuscular synapse subtypes with low sprouting competence in motoneuron diseases." J Neurosci **20**(7): 2534-2542.
- Fulton, B. and A. Markham (1996). "Mycophenolate mofetil. A review of its pharmacodynamic and pharmacokinetic properties and clinical efficacy in renal transplantation." Drugs **51**(2): 278-298.
- Fusco, F. R., Q. Chen, W. J. Lamoreaux, G. Figueredo-Cardenas, Y. Jiao, J. A. Coffman, et al. (1999). "Cellular localization of huntingtin in striatal and cortical neurons in rats: lack of correlation with neuronal vulnerability in Huntington's disease." J Neurosci **19**(4): 1189-1202.
- Gafni, J. and L. M. Ellerby (2002). "Calpain activation in Huntington's disease." J Neurosci **22**(12): 4842-4849.
- Gafni, J., E. Hermel, J. E. Young, C. L. Wellington, M. R. Hayden and L. M. Ellerby (2004). "Inhibition of calpain cleavage of huntingtin reduces toxicity: accumulation of calpain/caspase fragments in the nucleus." J Biol Chem **279**(19): 20211-20220.
- Gafni, J., T. Papanikolaou, F. Degiacomo, J. Holcomb, S. Chen, L. Menalled, et al. (2012). "Caspase-6 activity in a BACHD mouse modulates steady-state levels of mutant huntingtin protein but is not necessary for production of a 586 amino acid proteolytic fragment." J Neurosci **32**(22): 7454-7465.
- Gauthier, L. R., B. C. Charrin, M. Borrell-Pages, J. P. Dompierre, H. Rangone, F. P. Cordelieres, et al. (2004). "Huntingtin controls neurotrophic support and survival of neurons by enhancing BDNF vesicular transport along microtubules." Cell **118**(1): 127-138.
- Gentleman, S. M. (2013). "Review: microglia in protein aggregation disorders: friend or foe?" Neuropathol Appl Neurobiol **39**(1): 45-50.
- Geser, F., N. J. Brandmeir, L. K. Kwong, M. Martinez-Lage, L. Elman, L. McCluskey, et al. (2008). "Evidence of multisystem disorder in whole-brain map of pathological TDP-43 in amyotrophic lateral sclerosis." Arch Neurol **65**(5): 636-641.
- Gieling, E. T., R. E. Nordquist and F. J. van der Staay (2011a). "Assessing learning and memory in pigs." Anim Cogn **14**(2): 151-173.
- Gieling, E. T., T. Schuurman, R. E. Nordquist and F. J. van der Staay (2011b). "The pig as a model animal for studying cognition and neurobehavioral disorders." Curr Top Behav Neurosci **7**: 359-383.
- Gijzen, V. M., P. Madadi, M. P. Dube, D. A. Hesselink, G. Koren and S. N. de Wildt (2012). "Tacrolimus-induced nephrotoxicity and genetic variability: a review." Ann Transplant **17**(2): 111-121.
- Gizewski, E. R., T. Schanze, I. Bolle, A. de Greiff, M. Forsting and T. Laube (2007). "Visualization of the visual cortex in minipigs using fMRI." Res Vet Sci **82**(3): 281-286.

- Glass, J. D., N. M. Boulis, K. Johe, S. B. Rutkove, T. Federici, M. Polak, et al. (2012). "Lumbar intraspinal injection of neural stem cells in patients with amyotrophic lateral sclerosis: results of a phase I trial in 12 patients." *Stem Cells* **30**(6): 1144-1151.
- Goldberg, Y. P., D. W. Nicholson, D. M. Rasper, M. A. Kalchman, H. B. Koide, R. K. Graham, et al. (1996). "Cleavage of huntingtin by apopain, a proapoptotic cysteine protease, is modulated by the polyglutamine tract." *Nat Genet* **13**(4): 442-449.
- Gong, B., Z. Cao, P. Zheng, O. V. Vitolo, S. Liu, A. Staniszewski, et al. (2006). "Ubiquitin hydrolase Uch-L1 rescues beta-amyloid-induced decreases in synaptic function and contextual memory." *Cell* **126**(4): 775-788.
- Gong, B., C. Kielar and A. J. Morton (2012). "Temporal separation of aggregation and ubiquitination during early inclusion formation in transgenic mice carrying the Huntington's disease mutation." *PLoS One* **7**(7): e41450.
- Gong, Y. H., A. S. Parsadanian, A. Andreeva, W. D. Snider and J. L. Elliott (2000). "Restricted expression of G86R Cu/Zn superoxide dismutase in astrocytes results in astrocytosis but does not cause motoneuron degeneration." *J Neurosci* **20**(2): 660-665.
- Goritz, C., D. O. Dias, N. Tomilin, M. Barbacid, O. Shupliakov and J. Frisen (2011). "A pericyte origin of spinal cord scar tissue." *Science* **333**(6039): 238-242.
- Gould, T. W., R. R. Buss, S. Vinsant, D. Prevette, W. Sun, C. M. Knudson, et al. (2006). "Complete dissociation of motor neuron death from motor dysfunction by Bax deletion in a mouse model of ALS." *J Neurosci* **26**(34): 8774-8786.
- Graham, R. K., Y. Deng, E. J. Slow, B. Haigh, N. Bissada, G. Lu, et al. (2006). "Cleavage at the caspase-6 site is required for neuronal dysfunction and degeneration due to mutant huntingtin." *Cell* **125**(6): 1179-1191.
- Gray, M., D. I. Shirasaki, C. Cepeda, V. M. Andre, B. Wilburn, X. H. Lu, et al. (2008). "Full-length human mutant huntingtin with a stable polyglutamine repeat can elicit progressive and selective neuropathogenesis in BACHD mice." *J Neurosci* **28**(24): 6182-6195.
- Groen, E. J., M. A. van Es, P. W. van Vught, W. G. Spliet, J. van Engelen-Lee, M. de Visser, et al. (2010). "FUS mutations in familial amyotrophic lateral sclerosis in the Netherlands." *Arch Neurol* **67**(2): 224-230.
- group, H. s. (1999). "UHDRS'99." from <http://www.huntington-study-group.org/UHDRS/tabid/67/Default.aspx>.
- Gu, M., M. T. Gash, V. M. Mann, F. Javoy-Agid, J. M. Cooper and A. H. Schapira (1996). "Mitochondrial defect in Huntington's disease caudate nucleus." *Ann Neurol* **39**(3): 385-389.
- Gu, X., E. R. Greiner, R. Mishra, R. Kodali, A. Osmand, S. Finkbeiner, et al. (2009). "Serines 13 and 16 are critical determinants of full-length human mutant huntingtin induced disease pathogenesis in HD mice." *Neuron* **64**(6): 828-840.
- Guegan, C., M. Vila, G. Rosoklija, A. P. Hays and S. Przedborski (2001). "Recruitment of the mitochondrial-dependent apoptotic pathway in amyotrophic lateral sclerosis." *J Neurosci* **21**(17): 6569-6576.
- Guegan, C., M. Vila, P. Teismann, C. Chen, B. Onteniente, M. Li, et al. (2002). "Instrumental activation of bid by caspase-1 in a transgenic mouse model of ALS." *Mol Cell Neurosci* **20**(4): 553-562.
- Guo, X., K. Johe, P. Molnar, H. Davis and J. Hickman (2010). "Characterization of a human fetal spinal cord stem cell line, NSI-566RSC, and its induction to functional motoneurons." *J Tissue Eng Regen Med* **4**(3): 181-193.
- Gurney, M. E., H. Pu, A. Y. Chiu, M. C. Dal Canto, C. Y. Polchow, D. D. Alexander, et al. (1994). "Motor neuron degeneration in mice that express a human Cu,Zn superoxide dismutase mutation." *Science* **264**(5166): 1772-1775.
- Gusella, J. F., N. S. Wexler, P. M. Conneally, S. L. Naylor, M. A. Anderson, R. E. Tanzi, et al. (1983). "A polymorphic DNA marker genetically linked to Huntington's disease." *Nature* **306**(5940): 234-238.

- Hackam, A. S., R. Singaraja, C. L. Wellington, M. Metzler, K. McCutcheon, T. Zhang, et al. (1998). "The influence of huntingtin protein size on nuclear localization and cellular toxicity." J Cell Biol **141**(5): 1097-1105.
- Hagan, J. J. (2011). Molecular and Functional Models in Neuropsychiatry, Current Topics in Behavioral Neurosciences 7, Springer-Verlag Berlin Heidelberg.
- Hagg, T. and M. Oudega (2006). "Degenerative and spontaneous regenerative processes after spinal cord injury." J Neurotrauma **23**(3-4): 264-280.
- Haidet-Phillips, A. M., M. E. Hester, C. J. Miranda, K. Meyer, L. Braun, A. Frakes, et al. (2011). "Astrocytes from familial and sporadic ALS patients are toxic to motor neurons." Nat Biotechnol **29**(9): 824-828.
- Hains, B. C. and S. G. Waxman (2006). "Activated microglia contribute to the maintenance of chronic pain after spinal cord injury." J Neurosci **26**(16): 4308-4317.
- Halloran, P. F. (1996). "Molecular mechanisms of new immunosuppressants." Clin Transplant **10**(1 Pt 2): 118-123.
- Hand, C. K., V. Mayeux-Portas, J. Khoris, V. Briolotti, P. Clavelou, W. Camu, et al. (2001). "Compound heterozygous D90A and D96N SOD1 mutations in a recessive amyotrophic lateral sclerosis family." Ann Neurol **49**(2): 267-271.
- Handley, O. J., J. J. Najji, S. B. Dunnett and A. E. Rosser (2006). "Pharmaceutical, cellular and genetic therapies for Huntington's disease." Clin Sci (Lond) **110**(1): 73-88.
- Harada, T., C. Harada, Y. L. Wang, H. Osaka, K. Amanai, K. Tanaka, et al. (2004). "Role of ubiquitin carboxy terminal hydrolase-L1 in neural cell apoptosis induced by ischemic retinal injury in vivo." Am J Pathol **164**(1): 59-64.
- Harper, S. Q., P. D. Staber, X. He, S. L. Eliason, I. H. Martins, Q. Mao, et al. (2005). "RNA interference improves motor and neuropathological abnormalities in a Huntington's disease mouse model." Proc Natl Acad Sci U S A **102**(16): 5820-5825.
- Harrasz, M. M., J. J. Marden, W. Zhou, Y. Zhang, A. Williams, V. S. Sharov, et al. (2008). "SOD1 mutations disrupt redox-sensitive Rac regulation of NADPH oxidase in a familial ALS model." J Clin Invest **118**(2): 659-670.
- Hawryluk, G. W., J. Rowland, B. K. Kwon and M. G. Fehlings (2008). "Protection and repair of the injured spinal cord: a review of completed, ongoing, and planned clinical trials for acute spinal cord injury." Neurosurg Focus **25**(5): E14.
- Hefferan, M. P., J. Galik, O. Kakinohana, G. Sekerkova, C. Santucci, S. Marsala, et al. (2012). "Human neural stem cell replacement therapy for amyotrophic lateral sclerosis by spinal transplantation." PLoS One **7**(8): e42614.
- Hefferan, M. P., K. Johe, T. Hazel, E. L. Feldman, J. S. Lunn and M. Marsala (2011a). "Optimization of immunosuppressive therapy for spinal grafting of human spinal stem cells in a rat model of ALS." Cell transplantation **20**(8): 1153-1161.
- Hefferan, M. P., K. Johe, T. Hazel, E. L. Feldman, J. S. Lunn and M. Marsala (2011b). "Optimization of immunosuppressive therapy for spinal grafting of human spinal stem cells in a rat model of ALS." Cell Transplant **20**(8): 1153-1161.
- Heffernan, C., C. Jenkinson, T. Holmes, H. Macleod, W. Kinnear, D. Oliver, et al. (2006). "Management of respiration in MND/ALS patients: an evidence based review." Amyotroph Lateral Scler **7**(1): 5-15.
- Hemmings, H. C., Jr., P. Greengard, H. Y. Tung and P. Cohen (1984). "DARPP-32, a dopamine-regulated neuronal phosphoprotein, is a potent inhibitor of protein phosphatase-1." Nature **310**(5977): 503-505.
- Heng, M. Y., P. J. Detloff and R. L. Albin (2008). "Rodent genetic models of Huntington disease." Neurobiol Dis **32**(1): 1-9.
- Heng, M. Y., D. K. Duong, R. L. Albin, S. J. Tallaksen-Greene, J. M. Hunter, M. J. Lesort, et al. (2010). "Early autophagic response in a novel knock-in model of Huntington disease." Hum Mol Genet **19**(19): 3702-3720.

- Heng, M. Y., S. J. Tallaksen-Greene, P. J. Detloff and R. L. Albin (2007). "Longitudinal evaluation of the Hdh(CAG)150 knock-in murine model of Huntington's disease." *J Neurosci* **27**(34): 8989-8998.
- Henkel, J. S., J. I. Engelhardt, L. Siklos, E. P. Simpson, S. H. Kim, T. Pan, et al. (2004). "Presence of dendritic cells, MCP-1, and activated microglia/macrophages in amyotrophic lateral sclerosis spinal cord tissue." *Ann Neurol* **55**(2): 221-235.
- Hensley, K., H. Abdel-Moaty, J. Hunter, M. Mhatre, S. Mou, K. Nguyen, et al. (2006). "Primary glia expressing the G93A-SOD1 mutation present a neuroinflammatory phenotype and provide a cellular system for studies of glial inflammation." *J Neuroinflammation* **3**: 2.
- Hersch, S. M. and H. D. Rosas (2011). Biomarkers to Enable the Development of Neuroprotective Therapies for Huntington's Disease. *Neurobiology of Huntington's Disease: Applications to Drug Discovery*. D. C. Lo and R. E. Hughes. Boca Raton (FL).
- Hewitt, C., J. Kirby, J. R. Highley, J. A. Hartley, R. Hibberd, H. C. Hollinger, et al. (2010). "Novel FUS/TLS mutations and pathology in familial and sporadic amyotrophic lateral sclerosis." *Arch Neurol* **67**(4): 455-461.
- Hickey, M. A., A. Kosmalska, J. Enayati, R. Cohen, S. Zeitlin, M. S. Levine, et al. (2008). "Extensive early motor and non-motor behavioral deficits are followed by striatal neuronal loss in knock-in Huntington's disease mice." *Neuroscience* **157**(1): 280-295.
- Hilditch-Maguire, P., F. Trettel, L. A. Passani, A. Auerbach, F. Persichetti and M. E. MacDonald (2000). "Huntingtin: an iron-regulated protein essential for normal nuclear and perinuclear organelles." *Hum Mol Genet* **9**(19): 2789-2797.
- Ho, L. W., R. Brown, M. Maxwell, A. Wytttenbach and D. C. Rubinsztein (2001). "Wild type Huntingtin reduces the cellular toxicity of mutant Huntingtin in mammalian cell models of Huntington's disease." *J Med Genet* **38**(7): 450-452.
- Hodgson, J. G., N. Agopyan, C. A. Gutekunst, B. R. Leavitt, F. LePiane, R. Singaraja, et al. (1999). "A YAC mouse model for Huntington's disease with full-length mutant huntingtin, cytoplasmic toxicity, and selective striatal neurodegeneration." *Neuron* **23**(1): 181-192.
- Hoffner, G., P. Kahlem and P. Djian (2002). "Perinuclear localization of huntingtin as a consequence of its binding to microtubules through an interaction with beta-tubulin: relevance to Huntington's disease." *J Cell Sci* **115**(Pt 5): 941-948.
- Hofmann, A., B. Kessler, S. Ewerling, M. Weppert, B. Vogg, H. Ludwig, et al. (2003). "Efficient transgenesis in farm animals by lentiviral vectors." *EMBO Rep* **4**(11): 1054-1060.
- Hofstetter, C. P., N. A. Holmstrom, J. A. Lilja, P. Schweinhardt, J. Hao, C. Spenger, et al. (2005). "Allodynia limits the usefulness of intraspinal neural stem cell grafts; directed differentiation improves outcome." *Nat Neurosci* **8**(3): 346-353.
- Hofstetter, C. P., P. Schweinhardt, T. Klason, L. Olson and C. Spenger (2003). "Numb rats walk - a behavioural and fMRI comparison of mild and moderate spinal cord injury." *Eur J Neurosci* **18**(11): 3061-3068.
- Holmberg, C. I., K. E. Staniszewski, K. N. Mensah, A. Matouschek and R. I. Morimoto (2004). "Inefficient degradation of truncated polyglutamine proteins by the proteasome." *EMBO J* **23**(21): 4307-4318.
- Horton, T. M., B. H. Graham, M. Corral-Debrinski, J. M. Shoffner, A. E. Kaufman, M. F. Beal, et al. (1995). "Marked increase in mitochondrial DNA deletion levels in the cerebral cortex of Huntington's disease patients." *Neurology* **45**(10): 1879-1883.
- Howland, D. S., J. Liu, Y. She, B. Goad, N. J. Maragakis, B. Kim, et al. (2002). "Focal loss of the glutamate transporter EAAT2 in a transgenic rat model of SOD1 mutant-mediated amyotrophic lateral sclerosis (ALS)." *Proc Natl Acad Sci U S A* **99**(3): 1604-1609.
- Huang, K., A. Yanai, R. Kang, P. Arstikaitis, R. R. Singaraja, M. Metzler, et al. (2004). "Huntingtin-interacting protein HIP14 is a palmitoyl transferase involved in palmitoylation and trafficking of multiple neuronal proteins." *Neuron* **44**(6): 977-986.

- Hurlbert, M. S., W. Zhou, C. Wasmeier, F. G. Kaddis, J. C. Hutton and C. R. Freed (1999). "Mice transgenic for an expanded CAG repeat in the Huntington's disease gene develop diabetes." *Diabetes* **48**(3): 649-651.
- Igaz, L. M., L. K. Kwong, Y. Xu, A. C. Truax, K. Uryu, M. Neumann, et al. (2008). "Enrichment of C-terminal fragments in TAR DNA-binding protein-43 cytoplasmic inclusions in brain but not in spinal cord of frontotemporal lobar degeneration and amyotrophic lateral sclerosis." *Am J Pathol* **173**(1): 182-194.
- Ikedo, K. K., O.; Kawabe, K.; Iwasaki, Y. (2013). "Patient Care and Treatment in Amyotrophic Lateral Sclerosis." *J Neurol Res* **3**(1): 1-11.
- Imarisio, S., J. Carmichael, V. Korolchuk, C. W. Chen, S. Saiki, C. Rose, et al. (2008). "Huntington's disease: from pathology and genetics to potential therapies." *Biochem J* **412**(2): 191-209.
- Ince, P. G., J. R. Highley, J. Kirby, S. B. Wharton, H. Takahashi, M. J. Strong, et al. (2011). "Molecular pathology and genetic advances in amyotrophic lateral sclerosis: an emerging molecular pathway and the significance of glial pathology." *Acta Neuropathol* **122**(6): 657-671.
- Ishiguro, H., K. Yamada, H. Sawada, K. Nishii, N. Ichino, M. Sawada, et al. (2001). "Age-dependent and tissue-specific CAG repeat instability occurs in mouse knock-in for a mutant Huntington's disease gene." *J Neurosci Res* **65**(4): 289-297.
- Ishikawa, Y., A. Hirakata, A. D. Griesemer, J. Etter, S. Moran, J. Weiner, et al. (2010). "Tolerance and long-lasting peripheral chimerism after allogeneic intestinal transplantation in MGH miniature swine." *Transplantation* **89**(4): 417-426.
- Ishizu, K., D. F. Smith, D. Bender, E. Danielsen, S. B. Hansen, D. F. Wong, et al. (2000). "Positron emission tomography of radioligand binding in porcine striatum in vivo: haloperidol inhibition linked to endogenous ligand release." *Synapse* **38**(1): 87-101.
- Iwanami, A., S. Kaneko, M. Nakamura, Y. Kanemura, H. Mori, S. Kobayashi, et al. (2005). "Transplantation of human neural stem cells for spinal cord injury in primates." *J Neurosci Res* **80**(2): 182-190.
- Jaarsma, D., E. D. Haasdijk, J. A. Grashorn, R. Hawkins, W. van Duijn, H. W. Verspaget, et al. (2000). "Human Cu/Zn superoxide dismutase (SOD1) overexpression in mice causes mitochondrial vacuolization, axonal degeneration, and premature motoneuron death and accelerates motoneuron disease in mice expressing a familial amyotrophic lateral sclerosis mutant SOD1." *Neurobiol Dis* **7**(6 Pt B): 623-643.
- Jaarsma, D., E. Teuling, E. D. Haasdijk, C. I. De Zeeuw and C. C. Hoogenraad (2008). "Neuron-specific expression of mutant superoxide dismutase is sufficient to induce amyotrophic lateral sclerosis in transgenic mice." *J Neurosci* **28**(9): 2075-2088.
- Jacobsen, J. C., C. S. Bawden, S. R. Rudiger, C. J. McLaughlan, S. J. Reid, H. J. Waldvogel, et al. (2010). "An ovine transgenic Huntington's disease model." *Hum Mol Genet* **19**(10): 1873-1882.
- Jenkins, B. G., W. J. Koroshetz, M. F. Beal and B. R. Rosen (1993). "Evidence for impairment of energy metabolism in vivo in Huntington's disease using localized ¹H NMR spectroscopy." *Neurology* **43**(12): 2689-2695.
- Jeong, H., F. Then, T. J. Melia, Jr., J. R. Mazzulli, L. Cui, J. N. Savas, et al. (2009). "Acetylation targets mutant huntingtin to autophagosomes for degradation." *Cell* **137**(1): 60-72.
- Jiang, Z. and M. F. Rothschild (2007). "Swine genome science comes of age." *Int J Biol Sci* **3**(3): 129-131.
- Jin, Y., B. Neuhuber, A. Singh, J. Bouyer, A. Lepore, J. Bonner, et al. (2011). "Transplantation of human glial restricted progenitors and derived astrocytes into a contusion model of spinal cord injury." *J Neurotrauma* **28**(4): 579-594.
- Jockenhovel, F., E. Vogel, M. Kreuzer, W. Reinhardt, S. Lederbogen and D. Reinwein (1996). "Pharmacokinetics and pharmacodynamics of subcutaneous testosterone implants in hypogonadal men." *Clin Endocrinol (Oxf)* **45**(1): 61-71.

- Johe, K. K., T. G. Hazel, T. Muller, M. M. Dugich-Djordjevic and R. D. McKay (1996). "Single factors direct the differentiation of stem cells from the fetal and adult central nervous system." Genes Dev **10**(24): 3129-3140.
- Johnson, C. D. and B. L. Davidson (2010). "Huntington's disease: progress toward effective disease-modifying treatments and a cure." Hum Mol Genet **19**(R1): R98-R102.
- Johnson, R. and N. J. Buckley (2009). "Gene dysregulation in Huntington's disease: REST, microRNAs and beyond." Neuromolecular Med **11**(3): 183-199.
- Jones, C. F., P. A. Crompton and B. K. Kwon (2012). "Gross Morphological Changes of the Spinal Cord Immediately After Surgical Decompression in a Large Animal Model of Traumatic Spinal Cord Injury." Spine (Phila Pa 1976) **37**(15): E890-E899.
- Jonsson, P. A., K. Ernhill, P. M. Andersen, D. Bergemalm, T. Brannstrom, O. Gredal, et al. (2004). "Minute quantities of misfolded mutant superoxide dismutase-1 cause amyotrophic lateral sclerosis." Brain **127**(Pt 1): 73-88.
- Jonsson, P. A., K. S. Graffmo, T. Brannstrom, P. Nilsson, P. M. Andersen and S. L. Marklund (2006). "Motor neuron disease in mice expressing the wild type-like D90A mutant superoxide dismutase-1." J Neuropathol Exp Neurol **65**(12): 1126-1136.
- Jorgensen, F. G., A. Hobolth, H. Hornshoj, C. Bendixen, M. Fredholm and M. H. Schierup (2005). "Comparative analysis of protein coding sequences from human, mouse and the domesticated pig." BMC Biol **3**: 2.
- Julien, J. P. (2007). "ALS: astrocytes move in as deadly neighbors." Nat Neurosci **10**(5): 535-537.
- Kabashi, E., P. N. Valdmanis, P. Dion, D. Spiegelman, B. J. McConkey, C. Vande Velde, et al. (2008). "TARDBP mutations in individuals with sporadic and familial amyotrophic lateral sclerosis." Nat Genet **40**(5): 572-574.
- Kakinohana, O., M. P. Hefferan, A. Miyanochara, T. Nejime, S. Marsala, S. Juhas, et al. (2012a). "Combinational spinal GAD65 gene delivery and systemic GABA-mimetic treatment for modulation of spasticity." PLoS One **7**(1): e30561.
- Kakinohana, O., M. P. Hefferan, S. Nakamura, M. Kakinohana, J. Galik, Z. Tomori, et al. (2006). "Development of GABA-sensitive spasticity and rigidity in rats after transient spinal cord ischemia: a qualitative and quantitative electrophysiological and histopathological study." Neuroscience **141**(3): 1569-1583.
- Kakinohana, O., J. Juhasova, S. Juhas, J. Motlik, O. Platoshyn, J. Galik, et al. (2012b). "Survival and differentiation of human embryonic stem cell-derived neural precursors grafted spinally in spinal ischemia-injured rats or in naive immunosuppressed minipigs: a qualitative and quantitative study." Cell Transplant **21**(12): 2603-2619.
- Kakinohana, O., J. Juhasova, S. Juhas, J. Motlik, O. Platoshyn, M. Hefferan, et al. (2012c). "Survival and differentiation of human embryonic stem cell-derived neural precursors grafted spinally in spinal ischemia-injured rats or in naive immunosuppressed minipigs: a qualitative and quantitative study." Cell Transplantation: (in press).
- Kalchman, M. A., R. K. Graham, G. Xia, H. B. Koide, J. G. Hodgson, K. C. Graham, et al. (1996). "Huntingtin is ubiquitinated and interacts with a specific ubiquitin-conjugating enzyme." J Biol Chem **271**(32): 19385-19394.
- Kang, S. H., Y. Li, M. Fukaya, I. Lorenzini, D. W. Cleveland, L. W. Ostrow, et al. (2013). "Degeneration and impaired regeneration of gray matter oligodendrocytes in amyotrophic lateral sclerosis." Nat Neurosci.
- Kanning, K. C., A. Kaplan and C. E. Henderson (2010). "Motor neuron diversity in development and disease." Annu Rev Neurosci **33**: 409-440.
- Keereman, V., Y. Fierens, T. Broux, Y. De Deene, M. Lonneux and S. Vandenberghe (2010). "MRI-based attenuation correction for PET/MRI using ultrashort echo time sequences." J Nucl Med **51**(5): 812-818.

- Kegel, K. B., M. Kim, E. Sapp, C. McIntyre, J. G. Castano, N. Aronin, et al. (2000). "Huntingtin expression stimulates endosomal-lysosomal activity, endosome tubulation, and autophagy." *J Neurosci* **20**(19): 7268-7278.
- Kegel, K. B., A. R. Meloni, Y. Yi, Y. J. Kim, E. Doyle, B. G. Cuiffo, et al. (2002). "Huntingtin is present in the nucleus, interacts with the transcriptional corepressor C-terminal binding protein, and represses transcription." *J Biol Chem* **277**(9): 7466-7476.
- Keirstead, H. S., G. Nistor, G. Bernal, M. Totoiu, F. Cloutier, K. Sharp, et al. (2005). "Human embryonic stem cell-derived oligodendrocyte progenitor cell transplants remyelinate and restore locomotion after spinal cord injury." *J Neurosci* **25**(19): 4694-4705.
- Kieran, D., I. Woods, A. Villunger, A. Strasser and J. H. Prehn (2007). "Deletion of the BH3-only protein puma protects motoneurons from ER stress-induced apoptosis and delays motoneuron loss in ALS mice." *Proc Natl Acad Sci U S A* **104**(51): 20606-20611.
- Kiernan, M. C., S. Vucic, B. C. Cheah, M. R. Turner, A. Eisen, O. Hardiman, et al. (2011). "Amyotrophic lateral sclerosis." *Lancet* **377**(9769): 942-955.
- Kikugawa, K., Nankano, R., Otaku, M., Takashi, I. (2000). "Generation of Mutant SOD1-expressing Mice." *Program for Societas Neurologica Japonica*: 200.
- Kim, B. G., D. H. Hwang, S. I. Lee, E. J. Kim and S. U. Kim (2007). "Stem cell-based cell therapy for spinal cord injury." *Cell Transplant* **16**(4): 355-364.
- Kim, J., I. S. Cho, J. S. Hong, Y. K. Choi, H. Kim and Y. S. Lee (2008). "Identification and characterization of new microRNAs from pig." *Mamm Genome* **19**(7-8): 570-580.
- Kim, M. (2013). "Beta conformation of polyglutamine track revealed by a crystal structure of Huntingtin N-terminal region with insertion of three histidine residues." *Prion* **7**(3).
- Kim, M. W., Y. Chelliah, S. W. Kim, Z. Otwinowski and I. Bezprozvanny (2009). "Secondary structure of Huntingtin amino-terminal region." *Structure* **17**(9): 1205-1212.
- Kim, Y. J., Y. Yi, E. Sapp, Y. Wang, B. Cuiffo, K. B. Kegel, et al. (2001). "Caspase 3-cleaved N-terminal fragments of wild-type and mutant huntingtin are present in normal and Huntington's disease brains, associate with membranes, and undergo calpain-dependent proteolysis." *Proc Natl Acad Sci U S A* **98**(22): 12784-12789.
- Kipnis, J., H. Avidan, R. R. Caspi and M. Schwartz (2004). "Dual effect of CD4+CD25+ regulatory T cells in neurodegeneration: a dialogue with microglia." *Proc Natl Acad Sci U S A* **101** Suppl 2: 14663-14669.
- Klein, S. M., S. Behrstock, J. McHugh, K. Hoffmann, K. Wallace, M. Suzuki, et al. (2005). "GDNF delivery using human neural progenitor cells in a rat model of ALS." *Hum Gene Ther* **16**(4): 509-521.
- Klivenyi, P., R. J. Ferrante, R. T. Matthews, M. B. Bogdanov, A. M. Klein, O. A. Andreassen, et al. (1999). "Neuroprotective effects of creatine in a transgenic animal model of amyotrophic lateral sclerosis." *Nat Med* **5**(3): 347-350.
- Ko, S., Y. Nakajima, H. Kanehiro, A. Yoshimura and H. Nakano (1994). "The pharmacokinetic benefits of newly developed liposome-incorporated FK506." *Transplantation* **58**(10): 1142-1144.
- Kordasiewicz, H. B., L. M. Stanek, E. V. Wancewicz, C. Mazur, M. M. McAlonis, K. A. Pytel, et al. (2012). "Sustained therapeutic reversal of Huntington's disease by transient repression of huntingtin synthesis." *Neuron* **74**(6): 1031-1044.
- Koroshetz, W. J., B. G. Jenkins, B. R. Rosen and M. F. Beal (1997). "Energy metabolism defects in Huntington's disease and effects of coenzyme Q10." *Ann Neurol* **41**(2): 160-165.
- Kostic, V., V. Jackson-Lewis, F. de Bilbao, M. Dubois-Dauphin and S. Przedborski (1997). "Bcl-2: prolonging life in a transgenic mouse model of familial amyotrophic lateral sclerosis." *Science* **277**(5325): 559-562.
- Kurome, M., H. Ueda, R. Tomii, K. Naruse and H. Nagashima (2006). "Production of transgenic-clone pigs by the combination of ICSI-mediated gene transfer with somatic cell nuclear transfer." *Transgenic Res* **15**(2): 229-240.

- Kwiatkowski, T. J., Jr., D. A. Bosco, A. L. Leclerc, E. Tamrazian, C. R. Vanderburg, C. Russ, et al. (2009). "Mutations in the FUS/TLS gene on chromosome 16 cause familial amyotrophic lateral sclerosis." *Science* **323**(5918): 1205-1208.
- Kwon, J., K. Mochida, Y. L. Wang, S. Sekiguchi, T. Sankai, S. Aoki, et al. (2005). "Ubiquitin C-terminal hydrolase L-1 is essential for the early apoptotic wave of germinal cells and for sperm quality control during spermatogenesis." *Biol Reprod* **73**(1): 29-35.
- Lacomblez, L., G. Bensimon, P. N. Leigh, P. Guillet and V. Meininger (1996a). "Dose-ranging study of riluzole in amyotrophic lateral sclerosis. Amyotrophic Lateral Sclerosis/Riluzole Study Group II." *Lancet* **347**(9013): 1425-1431.
- Lacomblez, L., G. Bensimon, P. N. Leigh, P. Guillet, L. Powe, S. Durrleman, et al. (1996b). "A confirmatory dose-ranging study of riluzole in ALS. ALS/Riluzole Study Group-II." *Neurology* **47**(6 Suppl 4): S242-250.
- Laforet, G. A., E. Sapp, K. Chase, C. McIntyre, F. M. Boyce, M. Campbell, et al. (2001). "Changes in cortical and striatal neurons predict behavioral and electrophysiological abnormalities in a transgenic murine model of Huntington's disease." *J Neurosci* **21**(23): 9112-9123.
- Lagier-Tourenne, C. and D. W. Cleveland (2009). "Rethinking ALS: the FUS about TDP-43." *Cell* **136**(6): 1001-1004.
- Lagier-Tourenne, C., M. Polymenidou and D. W. Cleveland (2010). "TDP-43 and FUS/TLS: emerging roles in RNA processing and neurodegeneration." *Hum Mol Genet* **19**(R1): R46-64.
- Lagier-Tourenne, C., M. Polymenidou, K. R. Hutt, A. Q. Vu, M. Baughn, S. C. Huelga, et al. (2012). "Divergent roles of ALS-linked proteins FUS/TLS and TDP-43 intersect in processing long pre-mRNAs." *Nat Neurosci* **15**(11): 1488-1497.
- Lai, S. L., Y. Abramzon, J. C. Schymick, D. A. Stephan, T. Dunckley, A. Dillman, et al. (2011). "FUS mutations in sporadic amyotrophic lateral sclerosis." *Neurobiol Aging* **32**(3): 550 e551-554.
- Lama, R., F. Santos, F. J. Algar, A. Alvarez and C. Baamonde (2003). "Lung transplants with tacrolimus and mycophenolate mofetil: a review." *Transplant Proc* **35**(5): 1968-1973.
- Landles, C., A. Weiss, S. Franklin, D. Howland and G. Bates (2012). "Caspase-6 does not contribute to the proteolysis of mutant huntingtin in the HdhQ150 knock-in mouse model of Huntington's disease." *PLoS Curr* **4**: e4fd085bfc9973.
- Langbehn, D. R., R. R. Brinkman, D. Falush, J. S. Paulsen and M. R. Hayden (2004). "A new model for prediction of the age of onset and penetrance for Huntington's disease based on CAG length." *Clin Genet* **65**(4): 267-277.
- Lanska, D. J., M. J. Lanska, L. Lavine and B. S. Schoenberg (1988). "Conditions associated with Huntington's disease at death. A case-control study." *Arch Neurol* **45**(8): 878-880.
- Lavitrano, M., M. Busnelli, M. G. Cerrito, R. Giovannoni, S. Manzini and A. Vargiolu (2006). "Sperm-mediated gene transfer." *Reprod Fertil Dev* **18**(1-2): 19-23.
- Leavitt, B. R., J. M. van Raamsdonk, J. Shehadeh, H. Fernandes, Z. Murphy, R. K. Graham, et al. (2006). "Wild-type huntingtin protects neurons from excitotoxicity." *J Neurochem* **96**(4): 1121-1129.
- Lee, B. B., R. A. Cripps, M. Fitzharris and P. C. Wing (2013). "The global map for traumatic spinal cord injury epidemiology: update 2011, global incidence rate." *Spinal Cord*.
- Leigh, P. N., H. Whitwell, O. Garofalo, J. Buller, M. Swash, J. E. Martin, et al. (1991). "Ubiquitin-immunoreactive intraneuronal inclusions in amyotrophic lateral sclerosis. Morphology, distribution, and specificity." *Brain* **114 (Pt 2)**: 775-788.
- Lepore, A. C., B. Rauck, C. Dejea, A. C. Pardo, M. S. Rao, J. D. Rothstein, et al. (2008). "Focal transplantation-based astrocyte replacement is neuroprotective in a model of motor neuron disease." *Nat Neurosci* **11**(11): 1294-1301.
- Levine, M. S., G. J. Klapstein, A. Koppel, E. Gruen, C. Cepeda, M. E. Vargas, et al. (1999). "Enhanced sensitivity to N-methyl-D-aspartate receptor activation in transgenic and knockin mouse models of Huntington's disease." *J Neurosci Res* **58**(4): 515-532.
- Lewis, C. A., J. Manning, F. Rossi and C. Krieger (2012). "The Neuroinflammatory Response in ALS: The Roles of Microglia and T Cells." *Neurol Res Int* **2012**: 803701.

- Li, S. H. and X. J. Li (1998). "Aggregation of N-terminal huntingtin is dependent on the length of its glutamine repeats." Hum Mol Genet **7**(5): 777-782.
- Li, X. J., H. Li and S. Li (2010). "Clearance of mutant huntingtin." Autophagy **6**(5).
- Liao, B., W. Zhao, D. R. Beers, J. S. Henkel and S. H. Appel (2012). "Transformation from a neuroprotective to a neurotoxic microglial phenotype in a mouse model of ALS." Exp Neurol **237**(1): 147-152.
- Lievens, J. C., B. Woodman, A. Mahal, O. Spasic-Bosovic, D. Samuel, L. Kerkerian-Le Goff, et al. (2001). "Impaired glutamate uptake in the R6 Huntington's disease transgenic mice." Neurobiol Dis **8**(5): 807-821.
- Lillo, P. and J. R. Hodges (2009). "Frontotemporal dementia and motor neurone disease: overlapping clinic-pathological disorders." J Clin Neurosci **16**(9): 1131-1135.
- Lin, B., J. M. Rommens, R. K. Graham, M. Kalchman, H. MacDonald, J. Nasir, et al. (1993). "Differential 3' polyadenylation of the Huntington disease gene results in two mRNA species with variable tissue expression." Hum Mol Genet **2**(10): 1541-1545.
- Lin, C. H., S. Tallaksen-Greene, W. M. Chien, J. A. Cearley, W. S. Jackson, A. B. Crouse, et al. (2001). "Neurological abnormalities in a knock-in mouse model of Huntington's disease." Hum Mol Genet **10**(2): 137-144.
- Lin, V. W. and C. M. Bono (2010). Spinal cord medicine : principles and practice. New York, Demos Medical.
- Ling, S. C., C. P. Albuquerque, J. S. Han, C. Lagier-Tourenne, S. Tokunaga, H. Zhou, et al. (2010). "ALS-associated mutations in TDP-43 increase its stability and promote TDP-43 complexes with FUS/TLS." Proc Natl Acad Sci U S A **107**(30): 13318-13323.
- Liu, J., J. D. Farmer, Jr., W. S. Lane, J. Friedman, I. Weissman and S. L. Schreiber (1991). "Calcineurin is a common target of cyclophilin-cyclosporin A and FKBP-FK506 complexes." Cell **66**(4): 807-815.
- Llado, J., C. Haenggeli, N. J. Maragakis, E. Y. Snyder and J. D. Rothstein (2004). "Neural stem cells protect against glutamate-induced excitotoxicity and promote survival of injured motor neurons through the secretion of neurotrophic factors." Mol Cell Neurosci **27**(3): 322-331.
- Lo Sardo, V., C. Zuccato, G. Gaudenzi, B. Vitali, C. Ramos, M. Tartari, et al. (2012). "An evolutionary recent neuroepithelial cell adhesion function of huntingtin implicates ADAM10-Ncadherin." Nat Neurosci **15**(5): 713-721.
- Lobsiger, C. S., S. Boillee, M. McAlonis-Downes, A. M. Khan, M. L. Feltri, K. Yamanaka, et al. (2009). "Schwann cells expressing dismutase active mutant SOD1 unexpectedly slow disease progression in ALS mice." Proc Natl Acad Sci U S A **106**(11): 4465-4470.
- Logroscino, G., E. Beghi, S. Zoccolella, R. Palagano, A. Fraddosio, I. L. Simone, et al. (2005). "Incidence of amyotrophic lateral sclerosis in southern Italy: a population based study." J Neuro Neurol Neurosurg Psychiatry **76**(8): 1094-1098.
- Lomen-Hoerth, C., T. Anderson and B. Miller (2002). "The overlap of amyotrophic lateral sclerosis and frontotemporal dementia." Neurology **59**(7): 1077-1079.
- London, E. D., H. I. Yamamura, E. D. Bird and J. T. Coyle (1981). "Decreased receptor-binding sites for kainic acid in brains of patients with Huntington's disease." Biol Psychiatry **16**(2): 155-162.
- Lu, P. and M. H. Tuszynski (2008). "Growth factors and combinatorial therapies for CNS regeneration." Exp Neurol **209**(2): 313-320.
- Lu, P., Y. Wang, L. Graham, K. McHale, M. Gao, D. Wu, et al. (2012). "Long-distance growth and connectivity of neural stem cells after severe spinal cord injury." Cell **150**(6): 1264-1273.
- Lunkes, A., K. S. Lindenberg, L. Ben-Haiem, C. Weber, D. Devys, G. B. Landwehrmeyer, et al. (2002). "Proteases acting on mutant huntingtin generate cleaved products that differentially build up cytoplasmic and nuclear inclusions." Mol Cell **10**(2): 259-269.
- Lunn, J. S., S. A. Sakowski, T. Federici, J. D. Glass, N. M. Boulis and E. L. Feldman (2011). "Stem cell technology for the study and treatment of motor neuron diseases." Regen Med **6**(2): 201-213.
- Lunney, J. K. (2007). "Advances in swine biomedical model genomics." Int J Biol Sci **3**(3): 179-184.

- Luthi-Carter, R., S. A. Hanson, A. D. Strand, D. A. Bergstrom, W. Chun, N. L. Peters, et al. (2002a). "Dysregulation of gene expression in the R6/2 model of polyglutamine disease: parallel changes in muscle and brain." *Hum Mol Genet* **11**(17): 1911-1926.
- Luthi-Carter, R., A. D. Strand, S. A. Hanson, C. Kooperberg, G. Schilling, A. R. La Spada, et al. (2002b). "Polyglutamine and transcription: gene expression changes shared by DRPLA and Huntington's disease mouse models reveal context-independent effects." *Hum Mol Genet* **11**(17): 1927-1937.
- MacDonald, M. E. (2003). "Huntingtin: alive and well and working in middle management." *Sci STKE* **2003**(207): pe48.
- MacGregor, M. S. and J. A. Bradley (1995). "Overview of immunosuppressive therapy in organ transplantation." *Br J Hosp Med* **54**(6): 276-284.
- Machida, Y., T. Okada, M. Kurosawa, F. Oyama, K. Ozawa and N. Nukina (2006). "rAAV-mediated shRNA ameliorated neuropathology in Huntington disease model mouse." *Biochem Biophys Res Commun* **343**(1): 190-197.
- Macias, M. Y., M. B. Syring, M. A. Pizzi, M. J. Crowe, A. R. Alexanian and S. N. Kurpad (2006). "Pain with no gain: allodynia following neural stem cell transplantation in spinal cord injury." *Exp Neurol* **201**(2): 335-348.
- Mackenzie, I. R., E. H. Bigio, P. G. Ince, F. Geser, M. Neumann, N. J. Cairns, et al. (2007). "Pathological TDP-43 distinguishes sporadic amyotrophic lateral sclerosis from amyotrophic lateral sclerosis with SOD1 mutations." *Ann Neurol* **61**(5): 427-434.
- Maier, I. C. and M. E. Schwab (2006). "Sprouting, regeneration and circuit formation in the injured spinal cord: factors and activity." *Philos Trans R Soc Lond B Biol Sci* **361**(1473): 1611-1634.
- Majounie, E., A. E. Renton, K. Mok, E. G. Dopper, A. Waite, S. Rollinson, et al. (2012). "Frequency of the C9orf72 hexanucleotide repeat expansion in patients with amyotrophic lateral sclerosis and frontotemporal dementia: a cross-sectional study." *Lancet Neurol* **11**(4): 323-330.
- Mangiarini, L., K. Sathasivam, M. Seller, B. Cozens, A. Harper, C. Hetherington, et al. (1996). "Exon 1 of the HD gene with an expanded CAG repeat is sufficient to cause a progressive neurological phenotype in transgenic mice." *Cell* **87**(3): 493-506.
- Mantovani, S., S. Garbelli, A. Pasini, D. Alimonti, C. Perotti, M. Melazzini, et al. (2009). "Immune system alterations in sporadic amyotrophic lateral sclerosis patients suggest an ongoing neuroinflammatory process." *J Neuroimmunol* **210**(1-2): 73-79.
- Maragakis, N. J., M. S. Rao, J. Llado, V. Wong, H. Xue, A. Pardo, et al. (2005). "Glial restricted precursors protect against chronic glutamate neurotoxicity of motor neurons in vitro." *Glia* **50**(2): 145-159.
- Marchetto, M. C., A. R. Muotri, Y. Mu, A. M. Smith, G. G. Cezar and F. H. Gage (2008). "Non-cell-autonomous effect of human SOD1 G37R astrocytes on motor neurons derived from human embryonic stem cells." *Cell Stem Cell* **3**(6): 649-657.
- Marden, J. J., M. M. Harraz, A. J. Williams, K. Nelson, M. Luo, H. Paulson, et al. (2007). "Redox modifier genes in amyotrophic lateral sclerosis in mice." *J Clin Invest* **117**(10): 2913-2919.
- Marsala, M., M. P. Hefferan, O. Kakinohana, S. Nakamura, J. Marsala and Z. Tomori (2005). "Measurement of peripheral muscle resistance in rats with chronic ischemia-induced paraplegia or morphine-induced rigidity using a semi-automated computer-controlled muscle resistance meter." *J Neurotrauma* **22**(11): 1348-1361.
- Martin, L. J. (1999). "Neuronal death in amyotrophic lateral sclerosis is apoptosis: possible contribution of a programmed cell death mechanism." *J Neuropathol Exp Neurol* **58**(5): 459-471.
- Martindale, D., A. Hackam, A. Wiczorek, L. Ellerby, C. Wellington, K. McCutcheon, et al. (1998). "Length of huntingtin and its polyglutamine tract influences localization and frequency of intracellular aggregates." *Nat Genet* **18**(2): 150-154.
- Matsuyama, N., S. Hadano, K. Onoe, H. Osuga, J. Showguchi-Miyata, Y. Gondo, et al. (2000). "Identification and characterization of the miniature pig Huntington's disease gene homolog:

- evidence for conservation and polymorphism in the CAG triplet repeat." *Genomics* **69**(1): 72-85.
- Mattiazzi, M., M. D'Aurelio, C. D. Gajewski, K. Martushova, M. Kiaei, M. F. Beal, et al. (2002). "Mutated human SOD1 causes dysfunction of oxidative phosphorylation in mitochondria of transgenic mice." *J Biol Chem* **277**(33): 29626-29633.
- Maucksch, C., E. M. Vazey, R. J. Gordon and B. Connor (2013). "Stem cell-based therapy for Huntington's disease." *J Cell Biochem* **114**(4): 754-763.
- Maynard, C. J., C. Bottcher, Z. Ortega, R. Smith, B. I. Florea, M. Diaz-Hernandez, et al. (2009). "Accumulation of ubiquitin conjugates in a polyglutamine disease model occurs without global ubiquitin/proteasome system impairment." *Proc Natl Acad Sci U S A* **106**(33): 13986-13991.
- McAlister, V. C. (1998). "Liposomal tacrolimus: drug migration within blood compartments." *Transplant Proc* **30**(4): 1000-1001.
- McBride, J. L., S. Ramaswamy, M. Gasmi, R. T. Bartus, C. D. Herzog, E. P. Brandon, et al. (2006). "Viral delivery of glial cell line-derived neurotrophic factor improves behavior and protects striatal neurons in a mouse model of Huntington's disease." *Proc Natl Acad Sci U S A* **103**(24): 9345-9350.
- McDonald, J. W., X. Z. Liu, Y. Qu, S. Liu, S. K. Mickey, D. Turetsky, et al. (1999). "Transplanted embryonic stem cells survive, differentiate and promote recovery in injured rat spinal cord." *Nat Med* **5**(12): 1410-1412.
- McGoldrick, P., P. I. Joyce, E. M. Fisher and L. Greensmith (2013). "Rodent models of amyotrophic lateral sclerosis." *Biochim Biophys Acta*.
- McKeon, F. (1991). "When worlds collide: immunosuppressants meet protein phosphatases." *Cell* **66**(5): 823-826.
- Meehan, C. F., M. Moldovan, S. L. Marklund, K. S. Graffmo, J. B. Nielsen and H. Hultborn (2010). "Intrinsic properties of lumbar motor neurones in the adult G127insTGGG superoxide dismutase-1 mutant mouse in vivo: evidence for increased persistent inward currents." *Acta Physiol (Oxf)* **200**(4): 361-376.
- Meletis, K., F. Barnabe-Heider, M. Carlen, E. Evergren, N. Tomilin, O. Shupliakov, et al. (2008). "Spinal cord injury reveals multilineage differentiation of ependymal cells." *PLoS Biol* **6**(7): e182.
- Menalled, L. B., J. D. Sison, I. Dragatsis, S. Zeitlin and M. F. Chesselet (2003). "Time course of early motor and neuropathological anomalies in a knock-in mouse model of Huntington's disease with 140 CAG repeats." *J Comp Neurol* **465**(1): 11-26.
- Menalled, L. B., J. D. Sison, Y. Wu, M. Olivieri, X. J. Li, H. Li, et al. (2002). "Early motor dysfunction and striosomal distribution of huntingtin microaggregates in Huntington's disease knock-in mice." *J Neurosci* **22**(18): 8266-8276.
- Mestre, T., J. Ferreira, M. M. Coelho, M. Rosa and C. Sampaio (2009). "Therapeutic interventions for symptomatic treatment in Huntington's disease." *Cochrane Database Syst Rev*(3): CD006456.
- Michalik, A. and C. Van Broeckhoven (2004). "Proteasome degrades soluble expanded polyglutamine completely and efficiently." *Neurobiol Dis* **16**(1): 202-211.
- Milanese, M., S. Zappettini, F. Onofri, L. Musazzi, D. Tardito, T. Bonifacino, et al. (2011). "Abnormal exocytotic release of glutamate in a mouse model of amyotrophic lateral sclerosis." *J Neurochem* **116**(6): 1028-1042.
- Miles, E. L., C. O'Gorman, J. Zhao, M. Samuel, E. Walters, Y. J. Yi, et al. (2013). "Transgenic pig carrying green fluorescent proteasomes." *Proc Natl Acad Sci U S A* **110**(16): 6334-6339.
- Miller, J., M. Arrasate, E. Brooks, C. P. Libeu, J. Legleiter, D. Hatters, et al. (2011). "Identifying polyglutamine protein species in situ that best predict neurodegeneration." *Nat Chem Biol* **7**(12): 925-934.
- Miller, R. G., C. E. Jackson, E. J. Kasarskis, J. D. England, D. Forshew, W. Johnston, et al. (2009). "Practice parameter update: the care of the patient with amyotrophic lateral sclerosis: drug, nutritional, and respiratory therapies (an evidence-based review): report of the Quality

- Standards Subcommittee of the American Academy of Neurology." *Neurology* **73**(15): 1218-1226.
- Miller, T. M., A. Pestronk, W. David, J. Rothstein, E. Simpson, S. H. Appel, et al. (2013). "An antisense oligonucleotide against SOD1 delivered intrathecally for patients with SOD1 familial amyotrophic lateral sclerosis: a phase 1, randomised, first-in-man study." *Lancet Neurol*.
- Minguillon, J., B. Morancho, S. J. Kim, M. Lopez-Botet and J. Aramburu (2005). "Concentrations of cyclosporin A and FK506 that inhibit IL-2 induction in human T cells do not affect TGF-beta1 biosynthesis, whereas higher doses of cyclosporin A trigger apoptosis and release of preformed TGF-beta1." *J Leukoc Biol* **77**(5): 748-758.
- Mitchell, J. D. and G. D. Borasio (2007). "Amyotrophic lateral sclerosis." *Lancet* **369**(9578): 2031-2041.
- Mitsui, T., J. S. Shumsky, A. C. Lepore, M. Murray and I. Fischer (2005). "Transplantation of neuronal and glial restricted precursors into contused spinal cord improves bladder and motor functions, decreases thermal hypersensitivity, and modifies intraspinal circuitry." *J Neurosci* **25**(42): 9624-9636.
- Miyamoto, Y., T. Uno, H. Yamamoto, L. Xiao-Kang, K. Sakamoto, H. Hashimoto, et al. (2004). "Pharmacokinetic and immunosuppressive effects of tacrolimus-loaded biodegradable microspheres." *Liver Transpl* **10**(3): 392-396.
- Moffett, J. R., B. Ross, P. Arun, C. N. Madhavarao and A. M. Namboodiri (2007). "N-Acetylaspartate in the CNS: from neurodiagnostics to neurobiology." *Prog Neurobiol* **81**(2): 89-131.
- Moffitt, H., G. D. McPhail, B. Woodman, C. Hobbs and G. P. Bates (2009). "Formation of polyglutamine inclusions in a wide range of non-CNS tissues in the HdhQ150 knock-in mouse model of Huntington's disease." *PLoS One* **4**(11): e8025.
- Mok, K. Y., G. Koutsis, L. V. Schottlaender, J. Polke, M. Panas and H. Houlden (2012). "High frequency of the expanded C9ORF72 hexanucleotide repeat in familial and sporadic Greek ALS patients." *Neurobiol Aging* **33**(8): 1851 e1851-1855.
- Morgenstern, D. A., R. A. Asher and J. W. Fawcett (2002). "Chondroitin sulphate proteoglycans in the CNS injury response." *Prog Brain Res* **137**: 313-332.
- Morimoto, N., M. Nagai, Y. Ohta, K. Miyazaki, T. Kurata, M. Morimoto, et al. (2007). "Increased autophagy in transgenic mice with a G93A mutant SOD1 gene." *Brain Res* **1167**: 112-117.
- Morton, A. J. and D. S. Howland (2013). "Large Genetic Animal Models of Huntington's Disease." *J Huntingtons Dis* **2**(1): 3-19.
- Mu, X., J. He, D. W. Anderson, J. Q. Trojanowski and J. E. Springer (1996). "Altered expression of bcl-2 and bax mRNA in amyotrophic lateral sclerosis spinal cord motor neurons." *Ann Neurol* **40**(3): 379-386.
- Muller, F. L., W. Song, Y. Liu, A. Chaudhuri, S. Pieke-Dahl, R. Strong, et al. (2006). "Absence of CuZn superoxide dismutase leads to elevated oxidative stress and acceleration of age-dependent skeletal muscle atrophy." *Free Radic Biol Med* **40**(11): 1993-2004.
- Munoz, D. G., M. Neumann, H. Kusaka, O. Yokota, K. Ishihara, S. Terada, et al. (2009). "FUS pathology in basophilic inclusion body disease." *Acta Neuropathol* **118**(5): 617-627.
- Nagai, M., M. Aoki, I. Miyoshi, M. Kato, P. Pasinelli, N. Kasai, et al. (2001). "Rats expressing human cytosolic copper-zinc superoxide dismutase transgenes with amyotrophic lateral sclerosis: associated mutations develop motor neuron disease." *J Neurosci* **21**(23): 9246-9254.
- Nagai, M., D. B. Re, T. Nagata, A. Chalazonitis, T. M. Jessell, H. Wichterle, et al. (2007). "Astrocytes expressing ALS-linked mutated SOD1 release factors selectively toxic to motor neurons." *Nat Neurosci* **10**(5): 615-622.
- Nagashima, H., T. Fujimura, Y. Takahagi, M. Kurome, N. Wako, T. Ochiai, et al. (2003). "Development of efficient strategies for the production of genetically modified pigs." *Theriogenology* **59**(1): 95-106.
- Nakamura, M., R. A. Houghtling, L. MacArthur, B. M. Bayer and B. S. Bregman (2003). "Differences in cytokine gene expression profile between acute and secondary injury in adult rat spinal cord." *Exp Neurol* **184**(1): 313-325.

- Naver, B., C. Stub, M. Moller, K. Fenger, A. K. Hansen, L. Hasholt, et al. (2003). "Molecular and behavioral analysis of the R6/1 Huntington's disease transgenic mouse." Neuroscience **122**(4): 1049-1057.
- Nefussy, B. and V. E. Drory (2010). "Moving toward a predictive and personalized clinical approach in amyotrophic lateral sclerosis: novel developments and future directions in diagnosis, genetics, pathogenesis and therapies." EPMA J **1**(2): 329-341.
- Nefussy, B. D., V. E. (2013). Toward a Personalized Approach in Amyotrophic Lateral Sclerosis: New Developments in Diagnosis, Genetics, Pathogenesis and Therapies. Neurodegenerative Diseases: Integrative PPPM Approach as the Medicine of the Future, Advances in Predictive, Preventive and Personalised Medicine 2. S. Mandel, Springer ScienceCBusiness Media Dordrecht 2013. **2**.
- Neumann, M., L. K. Kwong, E. B. Lee, E. Kremmer, A. Flatley, Y. Xu, et al. (2009a). "Phosphorylation of S409/410 of TDP-43 is a consistent feature in all sporadic and familial forms of TDP-43 proteinopathies." Acta Neuropathol **117**(2): 137-149.
- Neumann, M., R. Rademakers, S. Roeber, M. Baker, H. A. Kretzschmar and I. R. Mackenzie (2009b). "A new subtype of frontotemporal lobar degeneration with FUS pathology." Brain **132**(Pt 11): 2922-2931.
- Neumann, M., D. M. Sampathu, L. K. Kwong, A. C. Truax, M. C. Micsenyi, T. T. Chou, et al. (2006). "Ubiquitinated TDP-43 in frontotemporal lobar degeneration and amyotrophic lateral sclerosis." Science **314**(5796): 130-133.
- Neusch, C., M. Bahr and C. Schneider-Gold (2007). "Glial cells in amyotrophic lateral sclerosis: new clues to understanding an old disease?" Muscle Nerve **35**(6): 712-724.
- Neuwald, A. F. and T. Hirano (2000). "HEAT repeats associated with condensins, cohesins, and other complexes involved in chromosome-related functions." Genome Res **10**(10): 1445-1452.
- Nguyen, M. D., R. C. Lariviere and J. P. Julien (2001). "Deregulation of Cdk5 in a mouse model of ALS: toxicity alleviated by perikaryal neurofilament inclusions." Neuron **30**(1): 135-147.
- NIH. (2013). "Safety Study of Human Spinal Cord-derived Neural Stem Cell Transplantation for the Treatment of Chronic SCI." from <http://clinicaltrials.gov/ct2/show/NCT01772810?term=NCT01772810&rank=1>.
- Niwa, J., S. Ishigaki, N. Hishikawa, M. Yamamoto, M. Doyu, S. Murata, et al. (2002). "Dorfin ubiquitylates mutant SOD1 and prevents mutant SOD1-mediated neurotoxicity." J Biol Chem **277**(39): 36793-36798.
- Novak, M. J. and S. J. Tabrizi (2010). "Huntington's disease." BMJ **340**: c3109.
- NSRRC. from <http://www.nsrrc.missouri.edu/>.
- Okamoto, K., Y. Fujita and Y. Mizuno (2010). "Pathology of protein synthesis and degradation systems in ALS." Neuropathology **30**(2): 189-193.
- Okamoto, K., Y. Mizuno and Y. Fujita (2008). "Bunina bodies in amyotrophic lateral sclerosis." Neuropathology **28**(2): 109-115.
- Oliveira, J. M., S. Chen, S. Almeida, R. Riley, J. Goncalves, C. R. Oliveira, et al. (2006). "Mitochondrial-dependent Ca²⁺ handling in Huntington's disease striatal cells: effect of histone deacetylase inhibitors." J Neurosci **26**(43): 11174-11186.
- Ondarza, A. B., Z. Ye and C. E. Hulsebosch (2003). "Direct evidence of primary afferent sprouting in distant segments following spinal cord injury in the rat: colocalization of GAP-43 and CGRP." Exp Neurol **184**(1): 373-380.
- Onders, R. P., A. M. Carlin, M. Elmo, S. Sivashankaran, B. Katirji and R. Schilz (2009). "Amyotrophic lateral sclerosis: the Midwestern surgical experience with the diaphragm pacing stimulation system shows that general anesthesia can be safely performed." Am J Surg **197**(3): 386-390.
- Orr, A. L., S. Li, C. E. Wang, H. Li, J. Wang, J. Rong, et al. (2008). "N-terminal mutant huntingtin associates with mitochondria and impairs mitochondrial trafficking." J Neurosci **28**(11): 2783-2792.

- Oudega, M. (2012). "Molecular and cellular mechanisms underlying the role of blood vessels in spinal cord injury and repair." *Cell Tissue Res* **349**(1): 269-288.
- Ouimet, C. C. and P. Greengard (1990). "Distribution of DARPP-32 in the basal ganglia: an electron microscopic study." *J Neurocytol* **19**(1): 39-52.
- Oyanagi, K., S. Takeda, H. Takahashi, E. Ohama and F. Ikuta (1989). "A quantitative investigation of the substantia nigra in Huntington's disease." *Ann Neurol* **26**(1): 13-19.
- Packard, M. J. (1992). "Use of slow-release pellets to administer calcitriol to avian embryos: effects on plasma calcium, magnesium, and phosphorus." *Gen Comp Endocrinol* **85**(1): 8-16.
- Panov, A. V., C. A. Gutekunst, B. R. Leavitt, M. R. Hayden, J. R. Burke, W. J. Strittmatter, et al. (2002). "Early mitochondrial calcium defects in Huntington's disease are a direct effect of polyglutamines." *Nat Neurosci* **5**(8): 731-736.
- Park, E., A. A. Velumian and M. G. Fehlings (2004). "The role of excitotoxicity in secondary mechanisms of spinal cord injury: a review with an emphasis on the implications for white matter degeneration." *J Neurotrauma* **21**(6): 754-774.
- Pasinelli, P. and R. H. Brown (2006). "Molecular biology of amyotrophic lateral sclerosis: insights from genetics." *Nat Rev Neurosci* **7**(9): 710-723.
- Paulsen, J. S. (2011). "Cognitive impairment in Huntington disease: diagnosis and treatment." *Curr Neurol Neurosci Rep* **11**(5): 474-483.
- Perrin, V., E. Regulier, T. Abbas-Terki, R. Hassig, E. Brouillet, P. Aebischer, et al. (2007). "Neuroprotection by Hsp104 and Hsp27 in lentiviral-based rat models of Huntington's disease." *Mol Ther* **15**(5): 903-911.
- Perutz, M. F., T. Johnson, M. Suzuki and J. T. Finch (1994). "Glutamine repeats as polar zippers: their possible role in inherited neurodegenerative diseases." *Proc Natl Acad Sci U S A* **91**(12): 5355-5358.
- Perutz, M. F., B. J. Pope, D. Owen, E. E. Wanker and E. Scherzinger (2002). "Aggregation of proteins with expanded glutamine and alanine repeats of the glutamine-rich and asparagine-rich domains of Sup35 and of the amyloid beta-peptide of amyloid plaques." *Proc Natl Acad Sci U S A* **99**(8): 5596-5600.
- Petersen, A., K. E. Larsen, G. G. Behr, N. Romero, S. Przedborski, P. Brundin, et al. (2001). "Expanded CAG repeats in exon 1 of the Huntington's disease gene stimulate dopamine-mediated striatal neuron autophagy and degeneration." *Hum Mol Genet* **10**(12): 1243-1254.
- Philips, T., A. Bento-Abreu, A. Nonneman, W. Haecck, K. Staats, V. Geelen, et al. (2013). "Oligodendrocyte dysfunction in the pathogenesis of amyotrophic lateral sclerosis." *Brain* **136**(Pt 2): 471-482.
- Phillips, W., K. M. Shannon and R. A. Barker (2008). "The current clinical management of Huntington's disease." *Mov Disord* **23**(11): 1491-1504.
- Politis, M., N. Pavese, Y. F. Tai, S. J. Tabrizi, R. A. Barker and P. Piccini (2008). "Hypothalamic involvement in Huntington's disease: an in vivo PET study." *Brain* **131**(Pt 11): 2860-2869.
- Polymenidou, M. and D. W. Cleveland (2011). "The seeds of neurodegeneration: prion-like spreading in ALS." *Cell* **147**(3): 498-508.
- Polymenidou, M., C. Lagier-Tourenne, K. R. Hutt, C. F. Bennett, D. W. Cleveland and G. W. Yeo (2012). "Misregulated RNA processing in amyotrophic lateral sclerosis." *Brain Res* **1462**: 3-15.
- Popovich, P. G. (2000). "Immunological regulation of neuronal degeneration and regeneration in the injured spinal cord." *Prog Brain Res* **128**: 43-58.
- Popovich, P. G., P. Wei and B. T. Stokes (1997). "Cellular inflammatory response after spinal cord injury in Sprague-Dawley and Lewis rats." *J Comp Neurol* **377**(3): 443-464.
- Pramatarova, A., J. Laganiere, J. Roussel, K. Brisebois and G. A. Rouleau (2001). "Neuron-specific expression of mutant superoxide dismutase 1 in transgenic mice does not lead to motor impairment." *J Neurosci* **21**(10): 3369-3374.

- Pringsheim, T., K. Wiltshire, L. Day, J. Dykeman, T. Steeves and N. Jette (2012). "The incidence and prevalence of Huntington's disease: a systematic review and meta-analysis." *Mov Disord* **27**(9): 1083-1091.
- Pun, S., A. F. Santos, S. Saxena, L. Xu and P. Caroni (2006). "Selective vulnerability and pruning of phasic motoneuron axons in motoneuron disease alleviated by CNTF." *Nat Neurosci* **9**(3): 408-419.
- Qureshi, M., D. A. Schoenfeld, Y. Paliwal, A. Shui and M. E. Cudkowicz (2009). "The natural history of ALS is changing: improved survival." *Amyotroph Lateral Scler* **10**(5-6): 324-331.
- Rakhit, R., P. Cunningham, A. Furtos-Matei, S. Dahan, X. F. Qi, J. P. Crow, et al. (2002). "Oxidation-induced misfolding and aggregation of superoxide dismutase and its implications for amyotrophic lateral sclerosis." *J Biol Chem* **277**(49): 47551-47556.
- Ramos, A. M., R. P. Crooijmans, N. A. Affara, A. J. Amaral, A. L. Archibald, J. E. Beever, et al. (2009). "Design of a high density SNP genotyping assay in the pig using SNPs identified and characterized by next generation sequencing technology." *PLoS One* **4**(8): e6524.
- Ranen, N. G., O. C. Stine, M. H. Abbott, M. Sherr, A. M. Codori, M. L. Franz, et al. (1995). "Anticipation and instability of IT-15 (CAG)_n repeats in parent-offspring pairs with Huntington disease." *Am J Hum Genet* **57**(3): 593-602.
- Raoul, C., A. G. Estevez, H. Nishimune, D. W. Cleveland, O. deLapeyriere, C. E. Henderson, et al. (2002). "Motoneuron death triggered by a specific pathway downstream of Fas. potentiation by ALS-linked SOD1 mutations." *Neuron* **35**(6): 1067-1083.
- Ravikumar, B., R. Duden and D. C. Rubinsztein (2002). "Aggregate-prone proteins with polyglutamine and polyalanine expansions are degraded by autophagy." *Hum Mol Genet* **11**(9): 1107-1117.
- Ravikumar, B., C. Vacher, Z. Berger, J. E. Davies, S. Luo, L. G. Oroz, et al. (2004). "Inhibition of mTOR induces autophagy and reduces toxicity of polyglutamine expansions in fly and mouse models of Huntington disease." *Nat Genet* **36**(6): 585-595.
- Rawlins, P. K. (2004). "Intrathecal baclofen therapy over 10 years." *J Neurosci Nurs* **36**(6): 322-327.
- Reddy, A. M., Y. Zheng, G. Jagadeeswaran, S. L. Macmil, W. B. Graham, B. A. Roe, et al. (2009). "Cloning, characterization and expression analysis of porcine microRNAs." *BMC Genomics* **10**: 65.
- Reddy, P. H., M. Williams, V. Charles, L. Garrett, L. Pike-Buchanan, W. O. Whetsell, Jr., et al. (1998). "Behavioural abnormalities and selective neuronal loss in HD transgenic mice expressing mutated full-length HD cDNA." *Nat Genet* **20**(2): 198-202.
- Reiner, A., R. L. Albin, K. D. Anderson, C. J. D'Amato, J. B. Penney and A. B. Young (1988). "Differential loss of striatal projection neurons in Huntington disease." *Proc Natl Acad Sci U S A* **85**(15): 5733-5737.
- Reis, A., T. Reinhard, R. Sundmacher, C. Braunstein and E. Godehardt (1998). "Effect of mycophenolate mofetil, cyclosporin A, and both in combination in a murine corneal graft rejection model." *Br J Ophthalmol* **82**(6): 700-703.
- Renton, A. E., E. Majounie, A. Waite, J. Simon-Sanchez, S. Rollinson, J. R. Gibbs, et al. (2011). "A hexanucleotide repeat expansion in C9ORF72 is the cause of chromosome 9p21-linked ALS-FTD." *Neuron* **72**(2): 257-268.
- Reyes, N. A., J. K. Fisher, K. Austgen, S. VandenBerg, E. J. Huang and S. A. Oakes (2010). "Blocking the mitochondrial apoptotic pathway preserves motor neuron viability and function in a mouse model of amyotrophic lateral sclerosis." *J Clin Invest* **120**(10): 3673-3679.
- Rhodes, K. E. and J. W. Fawcett (2004). "Chondroitin sulphate proteoglycans: preventing plasticity or protecting the CNS?" *J Anat* **204**(1): 33-48.
- Rigamonti, D., J. H. Bauer, C. De-Fraja, L. Conti, S. Sipione, C. Sciorati, et al. (2000). "Wild-type huntingtin protects from apoptosis upstream of caspase-3." *J Neurosci* **20**(10): 3705-3713.
- Ringholz, G. M., S. H. Appel, M. Bradshaw, N. A. Cooke, D. M. Mosnik and P. E. Schulz (2005). "Prevalence and patterns of cognitive impairment in sporadic ALS." *Neurology* **65**(4): 586-590.

- Ripps, M. E., G. W. Huntley, P. R. Hof, J. H. Morrison and J. W. Gordon (1995). "Transgenic mice expressing an altered murine superoxide dismutase gene provide an animal model of amyotrophic lateral sclerosis." Proc Natl Acad Sci U S A **92**(3): 689-693.
- Robberecht, W. and T. Philips (2013). "The changing scene of amyotrophic lateral sclerosis." Nat Rev Neurosci **14**(4): 248-264.
- Rockabrand, E., N. Slepko, A. Pantalone, V. N. Nukala, A. Kazantsev, J. L. Marsh, et al. (2007). "The first 17 amino acids of Huntingtin modulate its sub-cellular localization, aggregation and effects on calcium homeostasis." Hum Mol Genet **16**(1): 61-77.
- Rosen, D. R., T. Siddique, D. Patterson, D. A. Figlewicz, P. Sapp, A. Hentati, et al. (1993). "Mutations in Cu/Zn superoxide dismutase gene are associated with familial amyotrophic lateral sclerosis." Nature **362**(6415): 59-62.
- Rosenblatt, A. (2007). "Neuropsychiatry of Huntington's disease." Dialogues Clin Neurosci **9**(2): 191-197.
- Rosenzweig, E. S., G. Courtine, D. L. Jindrich, J. H. Brock, A. R. Ferguson, S. C. Strand, et al. (2010). "Extensive spontaneous plasticity of corticospinal projections after primate spinal cord injury." Nat Neurosci **13**(12): 1505-1510.
- Ross, C. A. and S. J. Tabrizi (2011). "Huntington's disease: from molecular pathogenesis to clinical treatment." Lancet Neurol **10**(1): 83-98.
- Rothstein, J. D. (2009). "Current hypotheses for the underlying biology of amyotrophic lateral sclerosis." Ann Neurol **65** Suppl 1: S3-9.
- Rothstein, J. D., M. Van Kammen, A. I. Levey, L. J. Martin and R. W. Kuncl (1995). "Selective loss of glial glutamate transporter GLT-1 in amyotrophic lateral sclerosis." Ann Neurol **38**(1): 73-84.
- Rutherford, N. J., Y. J. Zhang, M. Baker, J. M. Gass, N. A. Finch, Y. F. Xu, et al. (2008). "Novel mutations in TARDBP (TDP-43) in patients with familial amyotrophic lateral sclerosis." PLoS Genet **4**(9): e1000193.
- Sabatelli, M., A. Conte and M. Zollino (2013). "Clinical and genetic heterogeneity of amyotrophic lateral sclerosis." Clin Genet **83**(5): 408-416.
- Sabelstrom, H., M. Stenudd and J. Frisen (2013). "Neural stem cells in the adult spinal cord." Exp Neurol.
- Sadri-Vakili, G., B. Bouzou, C. L. Benn, M. O. Kim, P. Chawla, R. P. Overland, et al. (2007). "Histones associated with downregulated genes are hypo-acetylated in Huntington's disease models." Hum Mol Genet **16**(11): 1293-1306.
- Saft, C., J. Zange, J. Andrich, K. Muller, K. Lindenberg, B. Landwehrmeyer, et al. (2005). "Mitochondrial impairment in patients and asymptomatic mutation carriers of Huntington's disease." Mov Disord **20**(6): 674-679.
- Sah, D. W. and N. Aronin (2011). "Oligonucleotide therapeutic approaches for Huntington disease." J Clin Invest **121**(2): 500-507.
- Sahni, V. and J. A. Kessler (2010). "Stem cell therapies for spinal cord injury." Nat Rev Neurol **6**(7): 363-372.
- Saigoh, K., Y. L. Wang, J. G. Suh, T. Yamanishi, Y. Sakai, H. Kiyosawa, et al. (1999). "Intragenic deletion in the gene encoding ubiquitin carboxy-terminal hydrolase in gad mice." Nat Genet **23**(1): 47-51.
- Salazar, D. L., N. Uchida, F. P. Hamers, B. J. Cummings and A. J. Anderson (2010). "Human neural stem cells differentiate and promote locomotor recovery in an early chronic spinal cord injury NOD-scid mouse model." PLoS One **5**(8): e12272.
- Sanz, E., L. Yang, T. Su, D. R. Morris, G. S. McKnight and P. S. Amieux (2009). "Cell-type-specific isolation of ribosome-associated mRNA from complex tissues." Proc Natl Acad Sci U S A **106**(33): 13939-13944.
- Sapp, E., C. Schwarz, K. Chase, P. G. Bhide, A. B. Young, J. Penney, et al. (1997). "Huntingtin localization in brains of normal and Huntington's disease patients." Ann Neurol **42**(4): 604-612.

- Sarkar, S. and D. C. Rubinsztein (2008). "Huntington's disease: degradation of mutant huntingtin by autophagy." *FEBS J* **275**(17): 4263-4270.
- Sasaki, S. (2011). "Autophagy in spinal cord motor neurons in sporadic amyotrophic lateral sclerosis." *J Neuropathol Exp Neurol* **70**(5): 349-359.
- Sasaki, S. and M. Iwata (2007). "Mitochondrial alterations in the spinal cord of patients with sporadic amyotrophic lateral sclerosis." *J Neuropathol Exp Neurol* **66**(1): 10-16.
- Sathasivam, K., A. Neueder, T. A. Gipson, C. Landles, A. C. Benjamin, M. K. Bondulich, et al. (2013). "Aberrant splicing of HTT generates the pathogenic exon 1 protein in Huntington disease." *Proc Natl Acad Sci U S A* **110**(6): 2366-2370.
- Sawa, A., G. W. Wiegand, J. Cooper, R. L. Margolis, A. H. Sharp, J. F. Lawler, Jr., et al. (1999). "Increased apoptosis of Huntington disease lymphoblasts associated with repeat length-dependent mitochondrial depolarization." *Nat Med* **5**(10): 1194-1198.
- Scherzinger, E., R. Lurz, M. Turmaine, L. Mangiarini, B. Hollenbach, R. Hasenbank, et al. (1997). "Huntingtin-encoded polyglutamine expansions form amyloid-like protein aggregates in vitro and in vivo." *Cell* **90**(3): 549-558.
- Schilling, B., J. Gafni, C. Torcassi, X. Cong, R. H. Row, M. A. LaFevre-Bernt, et al. (2006). "Huntingtin phosphorylation sites mapped by mass spectrometry. Modulation of cleavage and toxicity." *J Biol Chem* **281**(33): 23686-23697.
- Schilling, G., M. W. Becher, A. H. Sharp, H. A. Jinnah, K. Duan, J. A. Kotzok, et al. (1999). "Intranuclear inclusions and neuritic aggregates in transgenic mice expressing a mutant N-terminal fragment of huntingtin." *Hum Mol Genet* **8**(3): 397-407.
- Scott, S., J. E. Kranz, J. Cole, J. M. Lincecum, K. Thompson, N. Kelly, et al. (2008). "Design, power, and interpretation of studies in the standard murine model of ALS." *Amyotroph Lateral Scler* **9**(1): 4-15.
- Setsuie, R. and K. Wada (2007). "The functions of UCH-L1 and its relation to neurodegenerative diseases." *Neurochem Int* **51**(2-4): 105-111.
- Sharp, J., J. Frame, M. Siegenthaler, G. Nistor and H. S. Keirstead (2010). "Human embryonic stem cell-derived oligodendrocyte progenitor cell transplants improve recovery after cervical spinal cord injury." *Stem Cells* **28**(1): 152-163.
- Shaw, P. J., P. G. Ince, G. Falkous and D. Mantle (1995). "Oxidative damage to protein in sporadic motor neuron disease spinal cord." *Ann Neurol* **38**(4): 691-695.
- Shelbourne, P. F., N. Killeen, R. F. Hevner, H. M. Johnston, L. Tecott, M. Lewandoski, et al. (1999). "A Huntington's disease CAG expansion at the murine Hdh locus is unstable and associated with behavioural abnormalities in mice." *Hum Mol Genet* **8**(5): 763-774.
- Shi, R. and J. D. Pryor (2002). "Pathological changes of isolated spinal cord axons in response to mechanical stretch." *Neuroscience* **110**(4): 765-777.
- Shibata, N., R. Nagai, K. Uchida, S. Horiuchi, S. Yamada, A. Hirano, et al. (2001). "Morphological evidence for lipid peroxidation and protein glycooxidation in spinal cords from sporadic amyotrophic lateral sclerosis patients." *Brain Res* **917**(1): 97-104.
- Shoulson, I. and A. B. Young (2011). "Milestones in huntington disease." *Mov Disord* **26**(6): 1127-1133.
- Siekierka, J. J., S. H. Hung, M. Poe, C. S. Lin and N. H. Sigal (1989). "A cytosolic binding protein for the immunosuppressant FK506 has peptidyl-prolyl isomerase activity but is distinct from cyclophilin." *Nature* **341**(6244): 755-757.
- Sipione, S., D. Rigamonti, M. Valenza, C. Zuccato, L. Conti, J. Pritchard, et al. (2002). "Early transcriptional profiles in huntingtin-inducible striatal cells by microarray analyses." *Hum Mol Genet* **11**(17): 1953-1965.
- Skibinski, G. A. and L. Boyd (2012). "Ubiquitination is involved in secondary growth, not initial formation of polyglutamine protein aggregates in *C. elegans*." *BMC Cell Biol* **13**: 10.

- Slow, E. J., J. van Raamsdonk, D. Rogers, S. H. Coleman, R. K. Graham, Y. Deng, et al. (2003). "Selective striatal neuronal loss in a YAC128 mouse model of Huntington disease." Hum Mol Genet **12**(13): 1555-1567.
- Smith, R., P. Brundin and J. Y. Li (2005). "Synaptic dysfunction in Huntington's disease: a new perspective." Cell Mol Life Sci **62**(17): 1901-1912.
- Sorensen, S. A. and K. Fenger (1992). "Causes of death in patients with Huntington's disease and in unaffected first degree relatives." J Med Genet **29**(12): 911-914.
- Southwell, A. L., N. H. Skotte, C. F. Bennett and M. R. Hayden (2012). "Antisense oligonucleotide therapeutics for inherited neurodegenerative diseases." Trends Mol Med **18**(11): 634-643.
- Sproviero, W., V. La Bella, R. Mazzei, P. Valentino, C. Rodolico, I. L. Simone, et al. (2012). "FUS mutations in sporadic amyotrophic lateral sclerosis: clinical and genetic analysis." Neurobiol Aging **33**(4): 837 e831-835.
- Sreedharan, J., I. P. Blair, V. B. Tripathi, X. Hu, C. Vance, B. Rogelj, et al. (2008). "TDP-43 mutations in familial and sporadic amyotrophic lateral sclerosis." Science **319**(5870): 1668-1672.
- Srinivasan, V., J. A. Pendergrass, Jr., K. S. Kumar, M. R. Landauer and T. M. Seed (2002). "Radioprotection, pharmacokinetic and behavioural studies in mouse implanted with biodegradable drug (amifostine) pellets." Int J Radiat Biol **78**(6): 535-543.
- Stack, E. C., J. K. Kubilus, K. Smith, K. Cormier, S. J. Del Signore, E. Guelin, et al. (2005). "Chronology of behavioral symptoms and neuropathological sequela in R6/2 Huntington's disease transgenic mice." J Comp Neurol **490**(4): 354-370.
- Steffan, J. S., N. Agrawal, J. Pallos, E. Rockabrand, L. C. Trotman, N. Slepko, et al. (2004). "SUMO modification of Huntingtin and Huntington's disease pathology." Science **304**(5667): 100-104.
- Steffan, J. S., L. Bodai, J. Pallos, M. Poelman, A. McCampbell, B. L. Apostol, et al. (2001). "Histone deacetylase inhibitors arrest polyglutamine-dependent neurodegeneration in *Drosophila*." Nature **413**(6857): 739-743.
- Studd, J. and A. Magos (1987). "Hormone pellet implantation for the menopause and premenstrual syndrome." Obstet Gynecol Clin North Am **14**(1): 229-249.
- Sturrock, A. and B. R. Leavitt (2010). "The clinical and genetic features of Huntington disease." J Geriatr Psychiatry Neurol **23**(4): 243-259.
- Su, V. C., E. D. Greanya and M. H. Ensom (2011). "Impact of Mycophenolate Mofetil Dose Reduction on Allograft Outcomes in Kidney Transplant Recipients on Tacrolimus-Based Regimens: A Systematic Review (February)." Ann Pharmacother.
- Sun, Y., A. Savanenin, P. H. Reddy and Y. F. Liu (2001). "Polyglutamine-expanded huntingtin promotes sensitization of N-methyl-D-aspartate receptors via post-synaptic density 95." J Biol Chem **276**(27): 24713-24718.
- Susor, A., L. Liskova, T. Toralova, A. Pavlok, K. Pivonkova, P. Karabinova, et al. (2010). "Role of ubiquitin C-terminal hydrolase-L1 in antipolyspermy defense of mammalian oocytes." Biol Reprod **82**(6): 1151-1161.
- Sutovsky, P. (2011). "Sperm proteasome and fertilization." Reproduction **142**(1): 1-14.
- Sutovsky, P., G. Manandhar, T. C. McCauley, J. N. Caamano, M. Sutovsky, W. E. Thompson, et al. (2004). "Proteasomal interference prevents zona pellucida penetration and fertilization in mammals." Biol Reprod **71**(5): 1625-1637.
- Sutovsky, P., R. Moreno, J. Ramalho-Santos, T. Dominko, W. E. Thompson and G. Schatten (2001). "A putative, ubiquitin-dependent mechanism for the recognition and elimination of defective spermatozoa in the mammalian epididymis." J Cell Sci **114**(Pt 9): 1665-1675.
- Suzuki, M., J. McHugh, C. Tork, B. Shelley, S. M. Klein, P. Aebischer, et al. (2007). "GDNF secreting human neural progenitor cells protect dying motor neurons, but not their projection to muscle, in a rat model of familial ALS." PLoS One **2**(8): e689.
- Swindle, M. M., A. Makin, A. J. Herron, F. J. Clubb, Jr. and K. S. Frazier (2012). "Swine as models in biomedical research and toxicology testing." Vet Pathol **49**(2): 344-356.

- Tabrizi, S. J., M. W. Cleeter, J. Xuereb, J. W. Taanman, J. M. Cooper and A. H. Schapira (1999). "Biochemical abnormalities and excitotoxicity in Huntington's disease brain." Ann Neurol **45**(1): 25-32.
- Tabrizi, S. J., R. Reilmann, R. A. Roos, A. Durr, B. Leavitt, G. Owen, et al. (2012). "Potential endpoints for clinical trials in premanifest and early Huntington's disease in the TRACK-HD study: analysis of 24 month observational data." Lancet Neurol **11**(1): 42-53.
- Tabrizi, S. J., R. I. Scahill, A. Durr, R. A. Roos, B. R. Leavitt, R. Jones, et al. (2011). "Biological and clinical changes in premanifest and early stage Huntington's disease in the TRACK-HD study: the 12-month longitudinal analysis." Lancet Neurol **10**(1): 31-42.
- Takano, H. and J. F. Gusella (2002). "The predominantly HEAT-like motif structure of huntingtin and its association and coincident nuclear entry with dorsal, an NF-kB/Rel/dorsal family transcription factor." BMC Neurosci **3**: 15.
- Talbot, K. (2009). "Motor neuron disease: the bare essentials." Pract Neurol **9**(5): 303-309.
- Tartari, M., C. Gissi, V. Lo Sardo, C. Zuccato, E. Picardi, G. Pesole, et al. (2008). "Phylogenetic comparison of huntingtin homologues reveals the appearance of a primitive polyQ in sea urchin." Mol Biol Evol **25**(2): 330-338.
- Tateishi, T., T. Hokonohara, R. Yamasaki, S. Miura, H. Kikuchi, A. Iwaki, et al. (2010). "Multiple system degeneration with basophilic inclusions in Japanese ALS patients with FUS mutation." Acta Neuropathol **119**(3): 355-364.
- Thakur, A. K., M. Jayaraman, R. Mishra, M. Thakur, V. M. Chellgren, I. J. Byeon, et al. (2009). "Polyglutamine disruption of the huntingtin exon 1 N terminus triggers a complex aggregation mechanism." Nat Struct Mol Biol **16**(4): 380-389.
- Thompson, L. M., C. T. Aiken, L. S. Kaltenbach, N. Agrawal, K. Illes, A. Khoshnan, et al. (2009). "IKK phosphorylates Huntingtin and targets it for degradation by the proteasome and lysosome." J Cell Biol **187**(7): 1083-1099.
- Thomson, A. W., C. A. Bonham and A. Zeevi (1995). "Mode of action of tacrolimus (FK506): molecular and cellular mechanisms." Ther Drug Monit **17**(6): 584-591.
- Tobisawa, S., Y. Hozumi, S. Arawaka, S. Koyama, M. Wada, M. Nagai, et al. (2003). "Mutant SOD1 linked to familial amyotrophic lateral sclerosis, but not wild-type SOD1, induces ER stress in COS7 cells and transgenic mice." Biochem Biophys Res Commun **303**(2): 496-503.
- Trask, B. J. (1991). "DNA sequence localization in metaphase and interphase cells by fluorescence in situ hybridization." Methods Cell Biol **35**: 3-35.
- Trushina, E., R. B. Dyer, J. D. Badger, 2nd, D. Ure, L. Eide, D. D. Tran, et al. (2004). "Mutant huntingtin impairs axonal trafficking in mammalian neurons in vivo and in vitro." Mol Cell Biol **24**(18): 8195-8209.
- Turner, B. J. and K. Talbot (2008). "Transgenics, toxicity and therapeutics in rodent models of mutant SOD1-mediated familial ALS." Prog Neurobiol **85**(1): 94-134.
- Turner, M. R., M. C. Kiernan, P. N. Leigh and K. Talbot (2009). "Biomarkers in amyotrophic lateral sclerosis." Lancet Neurol **8**(1): 94-109.
- Usvald, D., P. Vodicka, J. Hlucilova, R. Prochazka, J. Motlik, K. Kuchorova, et al. (2010). "Analysis of dosing regimen and reproducibility of intraspinal grafting of human spinal stem cells in immunosuppressed minipigs." Cell Transplant **19**(9): 1103-1122.
- Van Damme, P., M. Dewil, W. Robberecht and L. Van Den Bosch (2005). "Excitotoxicity and amyotrophic lateral sclerosis." Neurodegener Dis **2**(3-4): 147-159.
- Van Deerlin, V. M., J. B. Leverenz, L. M. Bekris, T. D. Bird, W. Yuan, L. B. Elman, et al. (2008). "TARDBP mutations in amyotrophic lateral sclerosis with TDP-43 neuropathology: a genetic and histopathological analysis." Lancet Neurol **7**(5): 409-416.
- van Dellen, A., J. Welch, R. M. Dixon, P. Cordery, D. York, P. Styles, et al. (2000). "N-Acetylaspartate and DARPP-32 levels decrease in the corpus striatum of Huntington's disease mice." Neuroreport **11**(17): 3751-3757.

- van den Berg, M. E., J. M. Castellote, I. Mahillo-Fernandez and J. de Pedro-Cuesta (2010). "Incidence of spinal cord injury worldwide: a systematic review." *Neuroepidemiology* **34**(3): 184-192; discussion 192.
- van Duijn, E., E. M. Kingma and R. C. van der Mast (2007). "Psychopathology in verified Huntington's disease gene carriers." *J Neuropsychiatry Clin Neurosci* **19**(4): 441-448.
- Van Raamsdonk, J. M., W. T. Gibson, J. Pearson, Z. Murphy, G. Lu, B. R. Leavitt, et al. (2006). "Body weight is modulated by levels of full-length huntingtin." *Hum Mol Genet* **15**(9): 1513-1523.
- Van Raamsdonk, J. M., Z. Murphy, D. M. Selva, R. Hamidzadeh, J. Pearson, A. Petersen, et al. (2007). "Testicular degeneration in Huntington disease." *Neurobiol Dis* **26**(3): 512-520.
- Vance, C., B. Rogelj, T. Hortobagyi, K. J. De Vos, A. L. Nishimura, J. Sreedharan, et al. (2009). "Mutations in FUS, an RNA processing protein, cause familial amyotrophic lateral sclerosis type 6." *Science* **323**(5918): 1208-1211.
- Vargas, M. R. and J. A. Johnson (2010). "Astrogliosis in amyotrophic lateral sclerosis: role and therapeutic potential of astrocytes." *Neurotherapeutics* **7**(4): 471-481.
- Venkatraman, P., R. Wetzell, M. Tanaka, N. Nukina and A. L. Goldberg (2004). "Eukaryotic proteasomes cannot digest polyglutamine sequences and release them during degradation of polyglutamine-containing proteins." *Mol Cell* **14**(1): 95-104.
- Vodicka, P., K. Smetana, Jr., B. Dvorankova, T. Emerick, Y. Z. Xu, J. Ourednik, et al. (2005). "The miniature pig as an animal model in biomedical research." *Ann N Y Acad Sci* **1049**: 161-171.
- von Horsten, S., I. Schmitt, H. P. Nguyen, C. Holzmann, T. Schmidt, T. Walther, et al. (2003). "Transgenic rat model of Huntington's disease." *Hum Mol Genet* **12**(6): 617-624.
- Vonsattel, J. P. and M. DiFiglia (1998). "Huntington disease." *J Neuropathol Exp Neurol* **57**(5): 369-384.
- Vonsattel, J. P., R. H. Myers, T. J. Stevens, R. J. Ferrante, E. D. Bird and E. P. Richardson, Jr. (1985). "Neuropathological classification of Huntington's disease." *J Neuropathol Exp Neurol* **44**(6): 559-577.
- Vukosavic, S., M. Dubois-Dauphin, N. Romero and S. Przedborski (1999). "Bax and Bcl-2 interaction in a transgenic mouse model of familial amyotrophic lateral sclerosis." *J Neurochem* **73**(6): 2460-2468.
- Vukosavic, S., L. Stefanis, V. Jackson-Lewis, C. Guegan, N. Romero, C. Chen, et al. (2000). "Delaying caspase activation by Bcl-2: A clue to disease retardation in a transgenic mouse model of amyotrophic lateral sclerosis." *J Neurosci* **20**(24): 9119-9125.
- Walaas, S. I. and P. Greengard (1984). "DARPP-32, a dopamine- and adenosine 3':5'-monophosphate-regulated phosphoprotein enriched in dopamine-innervated brain regions. I. Regional and cellular distribution in the rat brain." *J Neurosci* **4**(1): 84-98.
- Wang, J., H. Slunt, V. Gonzales, D. Fromholt, M. Coonfield, N. G. Copeland, et al. (2003). "Copper-binding-site-null SOD1 causes ALS in transgenic mice: aggregates of non-native SOD1 delineate a common feature." *Hum Mol Genet* **12**(21): 2753-2764.
- Wang, J., C. E. Wang, A. Orr, S. Tydlacka, S. H. Li and X. J. Li (2008). "Impaired ubiquitin-proteasome system activity in the synapses of Huntington's disease mice." *J Cell Biol* **180**(6): 1177-1189.
- Wang, J., G. Xu, V. Gonzales, M. Coonfield, D. Fromholt, N. G. Copeland, et al. (2002). "Fibrillar inclusions and motor neuron degeneration in transgenic mice expressing superoxide dismutase 1 with a disrupted copper-binding site." *Neurobiol Dis* **10**(2): 128-138.
- Wang, J., G. Xu, H. Li, V. Gonzales, D. Fromholt, C. Karch, et al. (2005a). "Somatodendritic accumulation of misfolded SOD1-L126Z in motor neurons mediates degeneration: alphaB-crystallin modulates aggregation." *Hum Mol Genet* **14**(16): 2335-2347.
- Wang, Q., T. Uno, Y. Miyamoto, Y. Hara, Y. Kitazawa, F. Z. Lu, et al. (2004). "Biodegradable microsphere-loaded tacrolimus enhanced the effect on mice islet allograft and reduced the adverse effect on insulin secretion." *Am J Transplant* **4**(5): 721-727.
- Wang, Y. L., W. Liu, E. Wada, M. Murata, K. Wada and I. Kanazawa (2005b). "Clinico-pathological rescue of a model mouse of Huntington's disease by siRNA." *Neurosci Res* **53**(3): 241-249.

- Wanker, E. E. (2000). "Protein aggregation and pathogenesis of Huntington's disease: mechanisms and correlations." *Biol Chem* **381**(9-10): 937-942.
- Watanabe, Y., K. Yasui, T. Nakano, K. Doi, Y. Fukada, M. Kitayama, et al. (2005). "Mouse motor neuron disease caused by truncated SOD1 with or without C-terminal modification." *Brain Res Mol Brain Res* **135**(1-2): 12-20.
- Weir, D. W., A. Sturrock and B. R. Leavitt (2011). "Development of biomarkers for Huntington's disease." *Lancet Neurol* **10**(6): 573-590.
- Weiss, A., D. Abramowski, M. Bibel, R. Bodner, V. Chopra, M. DiFiglia, et al. (2009). "Single-step detection of mutant huntingtin in animal and human tissues: a bioassay for Huntington's disease." *Anal Biochem* **395**(1): 8-15.
- Wellington, C. L., L. M. Ellerby, C. A. Gutekunst, D. Rogers, S. Warby, R. K. Graham, et al. (2002). "Caspase cleavage of mutant huntingtin precedes neurodegeneration in Huntington's disease." *J Neurosci* **22**(18): 7862-7872.
- Wellington, C. L., L. M. Ellerby, A. S. Hackam, R. L. Margolis, M. A. Trifiro, R. Singaraja, et al. (1998). "Caspase cleavage of gene products associated with triplet expansion disorders generates truncated fragments containing the polyglutamine tract." *J Biol Chem* **273**(15): 9158-9167.
- Wellington, C. L., R. Singaraja, L. Ellerby, J. Savill, S. Roy, B. Leavitt, et al. (2000). "Inhibiting caspase cleavage of huntingtin reduces toxicity and aggregate formation in neuronal and nonneuronal cells." *J Biol Chem* **275**(26): 19831-19838.
- Wengenack, T. M., S. S. Holasek, C. M. Montano, D. Gregor, G. L. Curran and J. F. Poduslo (2004). "Activation of programmed cell death markers in ventral horn motor neurons during early presymptomatic stages of amyotrophic lateral sclerosis in a transgenic mouse model." *Brain Res* **1027**(1-2): 73-86.
- Wente, M. N., P. Sauer, A. Mehrabi, J. Weitz, M. W. Buchler, J. Schmidt, et al. (2006). "Review of the clinical experience with a modified release form of tacrolimus [FK506E (MR4)] in transplantation." *Clin Transplant* **20 Suppl 17**: 80-84.
- Wernersson, R., M. H. Schierup, F. G. Jorgensen, J. Gorodkin, F. Panitz, H. H. Staerfeldt, et al. (2005). "Pigs in sequence space: a 0.66X coverage pig genome survey based on shotgun sequencing." *BMC Genomics* **6**: 70.
- Wexler, A. (2010). "Stigma, history, and Huntington's disease." *Lancet* **376**(9734): 18-19.
- Wexler, N. S. and U. V. C. Res (2004). "Venezuelan kindreds reveal that genetic and environmental factors modulate Huntington's disease age of onset." *Proceedings of the National Academy of Sciences of the United States of America* **101**(10): 3498-3503.
- Wheeler, V. C., W. Auerbach, J. K. White, J. Srinidhi, A. Auerbach, A. Ryan, et al. (1999). "Length-dependent gametic CAG repeat instability in the Huntington's disease knock-in mouse." *Hum Mol Genet* **8**(1): 115-122.
- Wheeler, V. C., J. K. White, C. A. Gutekunst, V. Vrbanac, M. Weaver, X. J. Li, et al. (2000). "Long glutamine tracts cause nuclear localization of a novel form of huntingtin in medium spiny striatal neurons in HdhQ92 and HdhQ111 knock-in mice." *Hum Mol Genet* **9**(4): 503-513.
- White, T. E., M. A. Lane, M. S. Sandhu, B. E. O'Steen, D. D. Fuller and P. J. Reier (2010). "Neuronal progenitor transplantation and respiratory outcomes following upper cervical spinal cord injury in adult rats." *Exp Neurol* **225**(1): 231-236.
- WHO (2002). "World report on road traffic injury prevention: summary."
- Wiedau-Pazos, M., J. J. Goto, S. Rabizadeh, E. B. Gralla, J. A. Roe, M. K. Lee, et al. (1996). "Altered reactivity of superoxide dismutase in familial amyotrophic lateral sclerosis." *Science* **271**(5248): 515-518.
- Wiedemann, F. R., G. Manfredi, C. Mawrin, M. F. Beal and E. A. Schon (2002). "Mitochondrial DNA and respiratory chain function in spinal cords of ALS patients." *J Neurochem* **80**(4): 616-625.
- Wijeyekoon, R. and R. A. Barker (2011). "The Current Status of Neural Grafting in the Treatment of Huntington's Disease. A Review." *Front Integr Neurosci* **5**: 78.

- Wirth, E. D., 3rd, P. J. Reier, R. G. Fessler, F. J. Thompson, B. Uthman, A. Behrman, et al. (2001). "Feasibility and safety of neural tissue transplantation in patients with syringomyelia." J Neurotrauma **18**(9): 911-929.
- Wong, P. C., C. A. Pardo, D. R. Borchelt, M. K. Lee, N. G. Copeland, N. A. Jenkins, et al. (1995). "An adverse property of a familial ALS-linked SOD1 mutation causes motor neuron disease characterized by vacuolar degeneration of mitochondria." Neuron **14**(6): 1105-1116.
- Woodman, B., R. Butler, C. Landles, M. K. Lupton, J. Tse, E. Hockly, et al. (2007). "The Hdh(Q150/Q150) knock-in mouse model of HD and the R6/2 exon 1 model develop comparable and widespread molecular phenotypes." Brain Res Bull **72**(2-3): 83-97.
- Woulfe, J., D. A. Gray and I. R. Mackenzie (2010). "FUS-immunoreactive intranuclear inclusions in neurodegenerative disease." Brain Pathol **20**(3): 589-597.
- Wu, D. C., D. B. Re, M. Nagai, H. Ischiropoulos and S. Przedborski (2006). "The inflammatory NADPH oxidase enzyme modulates motor neuron degeneration in amyotrophic lateral sclerosis mice." Proc Natl Acad Sci U S A **103**(32): 12132-12137.
- Xia, J., D. H. Lee, J. Taylor, M. Vandelft and R. Truant (2003). "Huntingtin contains a highly conserved nuclear export signal." Hum Mol Genet **12**(12): 1393-1403.
- Xu, G., L. Wang, W. Chen, F. Xue, X. Bai, L. Liang, et al. (2010). "Rapamycin and tacrolimus differentially modulate acute graft-versus-host disease in rats after liver transplantation." Liver Transpl **16**(3): 357-363.
- Xu, L., D. K. Ryugo, T. Pongstaporn, K. Johe and V. E. Koliatsos (2009). "Human neural stem cell grafts in the spinal cord of SOD1 transgenic rats: differentiation and structural integration into the segmental motor circuitry." J Comp Neurol **514**(4): 297-309.
- Xu, L., P. Shen, T. Hazel, K. Johe and V. E. Koliatsos (2011). "Dual transplantation of human neural stem cells into cervical and lumbar cord ameliorates motor neuron disease in SOD1 transgenic rats." Neurosci Lett **494**(3): 222-226.
- Xu, L., J. Yan, D. Chen, A. M. Welsh, T. Hazel, K. Johe, et al. (2006). "Human neural stem cell grafts ameliorate motor neuron disease in SOD-1 transgenic rats." Transplantation **82**(7): 865-875.
- Xu, Z., L. C. Cork, J. W. Griffin and D. W. Cleveland (1993). "Increased expression of neurofilament subunit NF-L produces morphological alterations that resemble the pathology of human motor neuron disease." Cell **73**(1): 23-33.
- Yamamoto, A., M. L. Cremona and J. E. Rothman (2006). "Autophagy-mediated clearance of huntingtin aggregates triggered by the insulin-signaling pathway." J Cell Biol **172**(5): 719-731.
- Yamamoto, A., J. J. Lucas and R. Hen (2000). "Reversal of neuropathology and motor dysfunction in a conditional model of Huntington's disease." Cell **101**(1): 57-66.
- Yamanaka, K., S. Boillee, E. A. Roberts, M. L. Garcia, M. McAlonis-Downes, O. R. Mikse, et al. (2008a). "Mutant SOD1 in cell types other than motor neurons and oligodendrocytes accelerates onset of disease in ALS mice." Proc Natl Acad Sci U S A **105**(21): 7594-7599.
- Yamanaka, K., S. J. Chun, S. Boillee, N. Fujimori-Tonou, H. Yamashita, D. H. Gutmann, et al. (2008b). "Astrocytes as determinants of disease progression in inherited amyotrophic lateral sclerosis." Nat Neurosci **11**(3): 251-253.
- Yan, J., L. Xu, A. M. Welsh, G. Hatfield, T. Hazel, K. Johe, et al. (2007). "Extensive neuronal differentiation of human neural stem cell grafts in adult rat spinal cord." PLoS Med **4**(2): e39.
- Yanai, A., K. Huang, R. Kang, R. R. Singaraja, P. Arstikaitis, L. Gan, et al. (2006). "Palmitoylation of huntingtin by HIP14 is essential for its trafficking and function." Nat Neurosci **9**(6): 824-831.
- Yang, D., C. E. Wang, B. Zhao, W. Li, Z. Ouyang, Z. Liu, et al. (2010). "Expression of Huntington's disease protein results in apoptotic neurons in the brains of cloned transgenic pigs." Hum Mol Genet **19**(20): 3983-3994.
- Yang, S. H. and A. W. Chan (2011). "Transgenic Animal Models of Huntington's Disease." Curr Top Behav Neurosci **7**: 61-85.

- Yang, S. H., P. H. Cheng, H. Banta, K. Piotrowska-Nitsche, J. J. Yang, E. C. Cheng, et al. (2008). "Towards a transgenic model of Huntington's disease in a non-human primate." Nature **453**(7197): 921-924.
- Yi, Y. J., G. Manandhar, M. Sutovsky, R. Li, V. Jonakova, R. Oko, et al. (2007). "Ubiquitin C-terminal hydrolase-activity is involved in sperm acrosomal function and anti-polyspermy defense during porcine fertilization." Biol Reprod **77**(5): 780-793.
- Yohrling, G. J. t., G. C. Jiang, M. M. DeJohn, D. W. Miller, A. B. Young, K. E. Vrana, et al. (2003). "Analysis of cellular, transgenic and human models of Huntington's disease reveals tyrosine hydroxylase alterations and substantia nigra neuropathology." Brain Res Mol Brain Res **119**(1): 28-36.
- Yokoseki, A., A. Shiga, C. F. Tan, A. Tagawa, H. Kaneko, A. Koyama, et al. (2008). "TDP-43 mutation in familial amyotrophic lateral sclerosis." Ann Neurol **63**(4): 538-542.
- Yoon, C. and M. H. Tuszynski (2012). "Frontiers of spinal cord and spine repair: experimental approaches for repair of spinal cord injury." Adv Exp Med Biol **760**: 1-15.
- Young, A. B., J. T. Greenamyre, Z. Hollingsworth, R. Albin, C. D'Amato, I. Shoulson, et al. (1988). "NMDA receptor losses in putamen from patients with Huntington's disease." Science **241**(4868): 981-983.
- Yu, L., S. Metzger, L. Clemens, T. Ott, G. Xiaofeng, M. Gray, et al. (2011). Early cognitive impairment, striatal neurodegeneration and neuronal atrophy in BACHD transgenic rats. 6th CHDI Annual HD Therapeutics Conference, Palm Springs, CA, USA.
- Zeitlin, S., J. P. Liu, D. L. Chapman, V. E. Papaioannou and A. Efstratiadis (1995). "Increased apoptosis and early embryonic lethality in mice nullizygous for the Huntington's disease gene homologue." Nat Genet **11**(2): 155-163.
- Zeron, M. M., O. Hansson, N. Chen, C. L. Wellington, B. R. Leavitt, P. Brundin, et al. (2002). "Increased sensitivity to N-methyl-D-aspartate receptor-mediated excitotoxicity in a mouse model of Huntington's disease." Neuron **33**(6): 849-860.
- Zhang, M., Y. Deng, Y. Luo, S. Zhang, H. Zou, F. Cai, et al. (2012). "Control of BACE1 degradation and APP processing by ubiquitin carboxyl-terminal hydrolase L1." J Neurochem **120**(6): 1129-1138.
- Zhao, C., W. Deng and F. H. Gage (2008). "Mechanisms and functional implications of adult neurogenesis." Cell **132**(4): 645-660.
- Zimmerman, S. W., G. Manandhar, Y. J. Yi, S. K. Gupta, M. Sutovsky, J. F. Odhiambo, et al. (2011). "Sperm proteasomes degrade sperm receptor on the egg zona pellucida during mammalian fertilization." PLoS One **6**(2): e17256.
- Zou, Z. Y., L. Y. Cui, Q. Sun, X. G. Li, M. S. Liu, Y. Xu, et al. (2013). "De novo FUS gene mutations are associated with juvenile-onset sporadic amyotrophic lateral sclerosis in China." Neurobiol Aging **34**(4): 1312 e1311-1318.
- Zuccato, C., A. Ciammola, D. Rigamonti, B. R. Leavitt, D. Goffredo, L. Conti, et al. (2001). "Loss of huntingtin-mediated BDNF gene transcription in Huntington's disease." Science **293**(5529): 493-498.
- Zuccato, C., M. Tartari, A. Crotti, D. Goffredo, M. Valenza, L. Conti, et al. (2003). "Huntingtin interacts with REST/NRSF to modulate the transcription of NRSE-controlled neuronal genes." Nat Genet **35**(1): 76-83.
- Zuccato, C., M. Valenza and E. Cattaneo (2010). "Molecular mechanisms and potential therapeutical targets in Huntington's disease." Physiol Rev **90**(3): 905-981.

8. LIST OF ABBREVIATIONS

- A4V Alanine 4 changed to valine mutation
- AchE Acetylcholinesterase
- ADAM10 A Disintegrin and metalloproteinase domain-containing protein 10
- ALS Amyotrophic Lateral Sclerosis
- BAK Bcl-2 homologous antagonist killer
- BAX Bcl-2-associated X protein
- BBB blood brain barrier or Basso, Beattie, and Bresnahan (BBB) scores (depends on the context)
- BCL-2 B-cell lymphoma 2
- Bdnf Gene for brain derived neurotropic factor
- bFGF Basic fibroblast growth factor
- BID Bis in die
- Biotin-16-dUTP Biotin-16-2'-deoxyuridine-5'-triphosphate, can be used to produce biotinylated DNA probes
- BDNF Brain derived neurotropic factor
- bp Base pairs
- C9ORF72 Chromosome 9 open reading frame 72 mutation
- CAG CAG triplet
- CBP CREB-binding protein
- CD4, CD14 etc. Cluster of differentiation no4, no14 etc.
- CGRP Calcitonin gene related peptide
- ChAT Choline acetyltransferase
- DAPI 4',6-diamidino-2-phenylindole
- Daxx Death-associated protein 6
- E1mHTT Exon 1 of mutant huntingtin
- EAAT2 Excitatory amino-acid transporter
- EGF Epidermal growth factor
- EGF Epidermal growth factor
- EMG Electromyography
- FADD Fas-Associated protein with Death Domain
- FALS Familiar ALS
- Fas FAS receptor (FasR), also known as apoptosis antigen 1 (APO-1 or APT), cluster of differentiation 95 (CD95) or tumor necrosis factor receptor superfamily member 6 (TNFRSF6)
- FDA Food and Drug Administration
- FISH Fluorescence in situ hybridization
- FITC Fluorescein isothiocyanate

- FK506 Tacrolimus (also FK-506 or fujimycin, trade names Prograf, Advagraf, Protopic)
- FKBP5 FK506 binding protein
- FTD Frontotemporal dementia
- FTLD Frontotemporal lobe degeneration
- FUS/TLS FUS (fused in sarcoma) or TLS (translocation in liposarcoma)
- G93A Glycine 93 changed to alanine mutation
- GABA γ -Aminobutyric acid
- GAP43 Growth Associated Protein 43
- GDNF Glial cell-derived neurotrophic factor
- GFP Green fluorescent protein
- GFPu GFP appended with a destabilizing modification (degradation signals) which promotes their constitutive degradation by the UPS
- GLT1 Excitatory amino-acid transporter in rodents
- GMP Good manufacturing practice
- GnRH Gonadotropin-releasing hormone
- H3 Histone H3
- H46R Histidine 46 changed to arginine mutation
- HD Huntington's disease
- Hdh promoter Mouse huntingtin promoter
- HEAT Consensus sequences called huntingtin, elongation factor 3, protein phosphatase 2A, and TOR 1 repeats
- hES-Ops Human embryonic stem cell-derived oligodendrocyte progenitors
- HSSCs Human spinal cord-derived neural stem cells
- i.v. Intravenous
- Iba1 Ionized calcium-binding adapter molecule 1
- IBs Inclusions (polyubiquitinated) of aggregated huntingtin
- IETD Caspase-8 inhibitor peptide
- IGF-1 Insulin-like growth factor 1
- IKK I κ B kinase complex
- IT15 Interesting transcript 15 (HTT)
- K6, K9, K15, K48, K63 Position of lysine in a protein
- KCC2 Chloride potassium symporter 5
- KO Genetic knock-out
- L3 3rd lumbar vertebrae
- LAMP-2A Lysosome-associated membrane protein 2 variant A, receptor for chaperone-mediated autophagy
- LDN LDN-57444 UCHL1 inhibitor
- LMN Lower motor neuron
- MFF Mycophenolate mofetil
- MSNs Medium spiny-sized striatal neurosn

- mTOR Mammalian target of rapamycin
- MVC Motor vehicle collisions
- NADPH Reduced form of Nicotinamide adenine dinucleotide phosphate
- NES Nuclear export signal
- NGF Nerve growth factor
- NLS Nuclear localization signal
- NMDA N-Methyl-D-aspartic acid
- NMDAR N-Methyl-D-aspartic acid receptor
- nNOS Nitric oxide synthase 1 (neuronal)
- NOX2 Subunit of NADPH oxidase
- NR2B Glutamate [NMDA] receptor subunit epsilon-2 also known as N-methyl D-aspartate receptor subtype 2B
- null mutation Mutation of both alleles of one gene
- P/CAF P300/CBP-associated factor, transcriptional coactivator
- P300 E1A binding protein p300
- p38 p38 mitogen-activated protein kinases
- p53 Protein 53 or tumor protein 53; is a tumor suppressor protein
- polyQ Polyglutamine stretch in huntingtin protein
- polyUb Polyubiquitin chain
- PSD95 Postsynaptic density protein 95
- PUMA p53 upregulated modulator of apoptosis
- RE1/NRSE Repressor element 1/ also known as the neuronrestrictive silencer element
- REST/NRSF RE1-silencing transcription factor/ also known as neuronal restrictive silencing factor
- ROS Reactive oxygen species
- s.c. Subcutaneous
- S13, S16, S536 Position of serine in protein
- SALS Sporadic ALS
- SCI Spinal cord injury
- SNAP25 Synaptosomal-associated protein 25
- SOD1 Copper/zinc superoxide dismutase 1
- T12-L1 12th thoracic through 1st lumbar vertebrae
- TAC tacrolymus
- TDP-43 43 kDa TAR DNA-binding protein
- tgHD Huntington's disease transgene
- TKX mixture of Tiletaminum 250 mg, Zolazepamum 250 mg, Ketamine 10 % 3 ml, Xylazine 2 % 3 ml
- TREG CD4+CD25+ regulatory T (lymphocyte) cells
- Ub Ubiquitin
- UMN Upper motor neuron

- UPS Ubiquitin proteasome system
- VEGF Vascular endothelial growth factor
- WT Wild type
- α MN α -motoneuron

9. AUTHOR'S PUBLICATIONS

9.1. Publications in Scientific Journals with IF with relation to Ph.D. thesis

Hefferan MP, Galik J, Kakinohana O, Sekerkova G, Santucci C, Marsala S, Navarro R, **Hruska-Plochan M**, Johe K, Feldman E, Cleveland DW, Marsala M. *Human neural stem cell replacement therapy for amyotrophic lateral sclerosis by spinal transplantation*. PLoS One, 7(8):e42614.

IF (2012): 4,092; 5-year IF (2012): 4.537. Cited by 2 articles.

van Gorp S, Leerink M, Kakinohana O, Platoshyn O, Santucci C, Galik J, Joosten Ea, **Hruska-Plochan M**, Goldberg D, Marsala S, Johe K, Marsala M. *Amelioration of motor/sensory dysfunction and spasticity in a rat model of acute lumbar spinal cord injury by human neural stem cell transplantation*. Stem Cell Research & Therapy (accepted for publication)

IF (2012): 3.212; 5-year IF (2012): 3.212

Hruska-Plochan M, Juhas S, Juhasova J, Wu S, Dumpi J, Weiss A, Marsala M, Motlik J. *Partial UCHL1 depletion in R6/2 mouse model of Huntington's Disease accelerates mutant huntingtin aggregation*. NeuroReport (submitted)

IF (2012): 1.656; 5-year IF (2012): 1.989

Sevc J, Goldberg D, van Gorp S, Leerink M, Juhas S, Juhasova J, Marsala S, **Hruska-Plochan M**, Hefferan MP, Motlik J, Rypacek F, Machova L, Kakinohana O, Santucci C, Johe K, Lukacova N, Yamada K, Bui JD, Marsala M. *Effective long-term immunosuppression in rats by subcutaneously implanted sustained-release tacrolimus pellet: effect on spinally grafted human neural precursors survival*. Experimental Neurology (in revision)

IF (2012): 4.699; 5-year IF (2012): 4.416

9.2. Publications in Scientific Journals without IF with relation to Ph.D. thesis

Baxa M, **Hruska-Plochan M**, Juhas S, Vodicka V, Pavlok A, Juhasova J, Miyanochara A, Nejime T, Klima J, Macakova M, Marsala S, Weiss A, Kubickova S, Musilova P, Vrtel R, Sontag EM, Thompson EM, Schier J, Hansikova H, Howland DS, Cattaneo E, Difiglia M, Marsala M, Motlik J. *A Transgenic Minipig Model of Huntington's Disease*. Journal of Huntington's Disease 2 (2013) 47–68. DOI 10.3233/JHD-130001 (first two authors are joint first authors)

Journal launched in June 2012 and thus does not have an IF yet

9.3. Publications in Scientific Journals with IF without relation to Ph.D. thesis

Kovalská M, **Hruška-Plochán M**, Østrup O, Adamkov M, Lehotský J, Strejček F, Statelová D, Mikušková K, Varg I, Petrovičová I. *The embryonic nucleogenesis during inhibition of major transcriptional activity in bovine preimplantation embryos*. *Biologia* 67/4: 818—825, 2012. DOI: 10.2478/s11756-012-0066-1

IF (2012): 0.557; 5-year IF (2012): 0.630

9.4. Poster presentations

- 5th Plenary Meeting of EHDN in Lisbon, Portugal, September 5-6, 2008.
- IV Meeting on Molecular Mechanisms of Neurodegeneration, Milan, Italy, May 8-10, 2009
- World Congress on Huntington Disease in Vancouver, BC, Canada, September 12- 15, 2009
- 7th Forum of European Neuroscience, Amsterdam, The Netherlands, July 3-7, 2010
- 6th Plenary Meeting of EHDN in Prague, Czech Republic, September 3-5th, 2010
- 6th Annual Huntington's Disease Therapeutics Conference: A Forum for Drug Discovery & Development in Palm Springs, CA, USA, February 07-10, 2011

10. CURRICULUM VITAE

MARIÁN HRUŠKA-PLOCHÁŇ

DATE OF BIRTH: MAY 11 1984

NATIONALITY: SLOVAK

EMAIL: hruska@iapg.cas.cz; hruskamp@gmail.com

EDUCATION

2008 - to date Charles University in Prague, Czech Republic, Faculty of Natural Science, Study program: Cell and Developmental Biology, Ph.D. thesis: "*Huntington's disease modeling and stem cell therapy in spinal cord disorders and injury*"

2003 – 2007 University of Constantine the Philosopher in Nitra, Slovakia, Faculty of Natural Science, Study program: Biology, Diploma thesis: "Inhibition of RNA polymerase I transcription in early bovine embryo"; Adjusted degree: Master of Science (M.Sc.)

FELLOWSHIPS, AWARDS, GRANTS

2010 FENS-IBRO Summer School "Translational research in basal ganglia disorders", Mallorca, Spain September 20-24

2010 Grant Agency of Charles University in Prague (GAUK), grant no. 18410 "UCH-L1 impairment in Huntington's disease" (03/2010 – 03/2012)

2009 EMBO Short-Term Fellowship Award - fellowship no. ASTF 308-2009, University of Aarhus, Denmark: "Generation of a porcine model of Huntington's disease" 01-03/2010

2009 World Congress on Huntington's Disease Scientific Trainee Travel Award, Vancouver, Canada

2007 Slovak Gas Industry Foundation (SPP) - fellowship no. N SPP 20/2007, University of Copenhagen, Denmark: "Embryonal genome activation" 01-02/2007

INTERNATIONAL RESEARCH EXPERIENCE

2011 Visiting Scholar, Massachusetts General Hospital, Massachusetts Institute for Neurodegenerative Diseases, Boston MA, USA, July 2011

2011 Visiting Scholar, University of British Columbia, Faculty of Medicine, Centre for Molecular Medicine and Therapeutics, Vancouver BC, Canada, May 2011

2010 Visiting Scholar, University of California San Diego, CA, USA, 10/2010-06/2013

2010 Visiting Scholar, University of Aarhus, Institute of Anatomy, Aarhus, Denmark, 01-03/2010

2007 Visiting Scholar, University of Copenhagen, Department of Basic Animal and Veterinary Sciences, Copenhagen, Denmark, 01-02/2007

INVITED LECTURES

2011 *Large Animal Models of Neurodegenerative Diseases*, October 23-25, Liblice, CR

2010 *Lexington Conference on Translational Neuroscience*, April 14-16, Kentucky, USA

2009 *Czech and Polish EHDN Investigators Meeting*, February 26-28, Warsaw, Poland

RESEARCH INTEREST

- Gene and stem cell therapy in ALS and Huntington's disease